Radionuclide Sorption in Fine-Grained Barrier Soils for Low-Level Radioactive Waste (LLW) Disposal

by

Erin Leigh Hunter

A dissertation submitted in partial fulfillment of

the requirements for the degree of

Doctor of Philosophy

(Civil Engineering)

at the

UNIVERSITY OF WISCONSIN – MADISON

2014

Date of Final Oral Examination: 02/10/2014

The following members of the Final Oral Committee approve the dissertation:

Craig H. Benson, Professor, Civil and Environmental Engineering
James M. Tinjum, Assistant Professor, Engineering Professional Development
Tuncer B. Edil, Professor Emeritus, Civil and Environmental Engineering
Matthew Ginder-Vogel, Assistant Professor, Civil and Environmental Engineering
Eric E. Roden, Professor, Geoscience

Abstract

Radionuclide Sorption in Fine-Grained Barrier Soils for Low-Level Radioactive Waste (LLW) Disposal

Erin Leigh Hunter

Under the supervision of Professor James M. Tinjum and Professor Craig H. Benson at the University of Wisconsin-Madison

Interactions of soil, radionuclides, and water influence the design and implementation of low-level radioactive waste (LLW) disposal facilities. Uniform assessment of containment strategies for LLW is controlled by the need for further understanding of the transport processes affecting the waste itself, particularly the potential for sorption and diffusion of radionuclides through installed containment barriers. Soils high in clay content offer a variety of benefits for lining disposal sites, specifically their natural abundance and availability and typically low hydraulic conductivity. Additionally, clays have been recognized within the literature for their ability to attenuate pollutants, including heavy metals, actinides, and other trace elements. With the reliance on barrier soils to ideally prevent, but more realistically limit, contamination of the environment surrounding LLW disposal facilities, understanding sorption as a solute transport mechanism through these materials is fundamental for improving disposal systems. Of potential further impact are the geochemical aspects that can alter sorption properties of barrier soils, including pH, ionic strength, calcium content, and carbonate content.

Batch experimentation aims to address sorption interactions through the individual study of a single radionuclide and a synthetic radioactive leachate mixture onto a suite of barrier soils and geosynthetic clay liner-derived bentonites with varying mineralogical properties. Four primary batch sorption experiments were run: (1) control experimentation, (2) kinetics, (3) sorption edges/envelopes, and (4) sorption isotherms.

The acquired results help to parameterize the relationship between radionuclide sorption, solution characteristics, including pH and ionic strength, and the mineralogical characteristics of the selected soils. The proportionality of radionuclide sorption to the exchange capacity of soils, as a function of the type and magnitude of the minerals within the soil column, is investigated. Inclusion of carbonate species shows a decrease in sorption capacity, while the presence of amorphous iron increases sorption. Cross-comparisons between sorption behavior of purified clays and iron minerals within the literature to the study soils show a reliance on multiple portions of the mineralogic soil content to account for demonstrated radionuclide sorption capacity.

Acknowledgements

Many thanks go to my advisors and the members of my PhD committee for the time and thoughts that they have provided: Professors Craig Benson, James Tinjum, Tuncer Edil, Matthew Ginder-Vogel, and Eric Roden. Particular acknowledgments go to my advisors for their guidance throughout the course of my PhD. Additional thanks go to Prof. Tinjum, for his keen editing abilities, and Prof. Ginder-Vogel, for providing additional research insight and advice on all fronts when I needed it most.

Special thanks are extended to Jackie Baster Cooper, as environmental lab manager, and Michael Heiman, my very dependable undergraduate assistant. Additional thanks go to Kuo Tian, my co-student throughout this project.

My unending gratitude is extended to all of the friends I have made due to GLE – GeoFriends are the very best! In particular, thanks to Joe Scalia and Nikki Woodward, Nick and Michelle Howe, Lauren Meyer, and the many iterations of the C&D crew for helping me keep the tradition alive.

Most importantly, I am particularly grateful for the love and support of my parents, James and Beverly Withiam and Randall and Carolyn Hunter. My time in Madison has not always been the easiest, and I would not have made it this far without always having you on my side.

The research described in this document was conducted under the sponsorship of the US Department of Energy under Cooperative Agreement Number DE-FC01-06EW07053 entitled The Consortium for Risk Evaluation with Stakeholder Participation III awarded to Vanderbilt University. The opinions, findings, conclusions, or recommendations expressed herein are solely those of the authors and do not necessarily represent the views of the US Department of Energy.

Table of Contents

List of Figures

List of Tables

Executive Summary

Interactions of soil, radionuclides, and water influence the design, construction, and performance of low-level radioactive waste (LLW) disposal facilities. Development of containment strategies for LLW requires a fundamental understanding of the transport processes affecting the waste itself, particularly the potential for sorption and diffusion of radionuclides through installed containment barriers. With the reliance on barrier soils to ideally prevent, but more realistically limit, contamination of the environment surrounding LLW disposal facilities, understanding sorption as a solute transport mechanism through these materials is fundamental for improving disposal systems. Aspects altering sorption properties of barrier soils include pH, ionic strength, calcium content, and carbonate content.

Three concepts are used to define the disposal of low-level radioactive waste (LLW). First, LLW should be stored in near-surface (<10s of meters below the ground surface), engineered facilities. Second, the waste being disposed must be radioactive, but cannot display high quantities of radioactivity or pose an immediate threat to the surrounding environment and/or human population. Third, LLW must maintain the level of stability outlined by the given regulatory agencies. This particular provision refers to the stability of the waste materials over the course of physical or biological decomposition, as opposed to radioactive stability. These three concepts help to define the federally administrated legislation that constitutes and allocates responsibilities to the Nuclear Regulatory Commission and other agencies to address handling, disposal, and containment of LLW in the US.

Items disposed as LLW are typically radioactive due to contact with radiation or radioactive materials (U.S. NRC 2002). These items include personal protective

equipment and cleaning supplies, in addition to items directly used by radiation workers in various academic, industrial, medical, or research settings (U.S. NRC 2002). Due to the variety of activities producing items classified as LLW, content can vary widely between disposal sites, encompassing everything from water treatment residues from nuclear reactors to animal carcasses from cancer research (U.S. NRC 2002).

Although the content of LLW distinguishes it from municipal solid waste (MSW), design of MSW landfills and LLW disposal facilities is similar. Both types of disposal facilities are typically designed around three main components: a lower liner system, separating the surrounding sub-surface environment from the area designated for containment and serving as a space for collection of leachate generated via flow-through; the waste itself, dictating considerations on containment and monitoring; and a final cover system, for final separation from the prospect of intrusion into the outside environment. One major difference distinguishing LLW from MSW are the precautions put in place to shield workers and the public from radioactive exposure. To address this issue, LLW disposal packaging frequently incorporates steel drums, concrete, lead, or other means beyond standard MSW disposal containers (U.S. NRC 2002). As with MSW, the lower liner systems for LLW can be made from a variety of barrier materials. The barrier materials chosen depend on the location of the disposal site and any applicable regulations, but frequently incorporate natural clay-based soils for creating compacted clay liners and geosynthetic clay liners (GCLs). Soils that are high in clay content offer a variety of benefits for lining disposal sites, specifically their natural abundance and availability and typically low hydraulic conductivity. Additionally, clays have been recognized for their ability to attenuate pollutants, including heavy metals (Abollino et al. 2003, 2008), actinides (Bradbury and Baeyens 2005a), and other trace elements (Brown and Parks 2001). This concept is of particular importance when

considering the need for shielding the environment from potential hazards arising from LLW disposal.

Three working hypotheses for sorption interactions between LLW concentrations of radionuclides and containment soils were considered within this study. They are as follows:

1. Radionuclide sorption is proportional to the exchange capacity of barrier soils, as a function of the minerals present;
2. Competition for sorption sites between radionuclides within mixtures is a function of the speciation of radionuclides present within a given system;
3. Distribution of radionuclide species in the liquid and solid phase can be predicted by the equilibrium geochemistry of a given system.

Batch sorption experimentation addressed these concepts through the study of a single radionuclide and a radioactive synthetic leachate mixture onto a suite of barrier soils with varying mineralogical properties and a complimentary set of geosynthetic clay liner (GCL) –derived bentonites. Four primary types of batch sorption experiments were run: (1) control experimentation, (2) kinetics, (3) sorption edges/envelopes, and (4) sorption isotherms. The results acquired help to parameterize the relationship between radionuclide sorption, solution characteristics (including pH and ionic strength), and the mineralogical characteristics of the selected soils.

The literature contains many studies that have focused on interactions of a single radionuclide with purified, homogenous minerals. As the basis for building thermodynamic databases and laying experimental groundwork, these studies provide implications for the study of more complex natural and man-made geochemical systems. Building from the literature, a series of experiments were designed to investigate the interaction of uranium, as one of the primary radioactive components of LLW, with natural, non-homogeneous soils used as barriers within disposal schemes. A suite of

four soils with typical landfill liner properties was selected for use in this study. Soils *A* (Georgia)*, B* (Texas), and *C* (Wisconsin) have been previously characterized (Benson and Trast 1995; Gurdal et al. 2003; Park et al. 2011) and implemented in MSW systems. Soil *D* (Texas) was used as received and without alteration to composition specifically for this project from a current LLW facility. Collectively, the four materials represent a range of soil classifications that are suitable for use as liner materials (Benson and Trast 1995; Daniel 1987). In addition to these soils, glass beads approximating sand-sized soil particles (passing the #45 and retained on the #60 sieve) were used as a sorption control.

Uranium was chosen as the single radionuclide for the initial round of experimentation due to its predominance at four DOE LLW sites (Section 3 – Tian et al. 2014), in addition to the available information for comparison with sorption to pure minerals found within the literature (Bradbury and Baeyens 2005a; Davis et al. 2004; Schlegel and Descostes 2009). Uranium acetate dihydrate (chemical formula: $UO_2(C_2O_2H_3)_2 \bullet 2\ H_2O$) was used as the uranium source for experimentation. Coupled with single radionuclide experimentation, a radioactive synthetic leachate (RSL) was created to mimic the true leachate composition of the DOE LLW sites and used for a second round of experimentation.

Soil control experimentation confirmed that no dissolution of the soil occurs via end-over-end rotation in either the initial background electrolyte solution or DI water. Comparison of results from solution control experimentation to experimentation with glass beads showed some loss of U to the reaction vessels during both sets of experimentation resulting in an average solution concentration of 710 µg/L. No additional loss to the glass beads was shown in comparison to the solution control experimentation (see Figures 5.3 and 5.6).

Reaction timing, or the chemical kinetics of the chosen soil-U systems, was analyzed through comparison of increasing interaction time between the components. Time periods ranged from 15 min (900 s) to 7 d (604800 s), with the witnessed steady state occurring within approximately 24 h (86400 s).

Comparing the mineralogy of the soils (see Figure 4.2) to the results from single radionuclide kinetics experimentation (see Figure 5.5) provides insight into the influence of different mineral phases on sorption capacity. Soil *A* displays increased sorption as time increases, following typical trends for kinetics experimentation. Soil *C* follows a similar trend to Soil *A*. The concentration trend for both Soils *A* and *C* is partially influenced by the low concentrations of U remaining in solution for both soils, with many points falling below the method detection limit (MDL) in both instances. Soils *A* and *C* have partially opposing mineralogic characteristics. In the case of both soils, the majority of the relative abundance is comprised of quartz. The relative abundance of quartz in Soil *A* is 20% greater than in Soil *C*. As demonstrated by comparison with the glass beads (which are comprised of amorphous silica (SiO_2), making them chemically indistinguishable from quartz), other aspects of the soil column are likely controlling sorption, particularly the presence of clays iron (oxy)(hydr)oxide minerals. Soil *A* contains 14% kaolinite and a total reactive Fe content of 175 µmol/g, while Soil *C* has 29% of its relative abundance comprised of mixed-layer illite/smectite and an amorphous or poorly crystalline Fe content of 13 µmol/g. The capacity of pure kaolinite (Barger and Koretsky 2011; Kremleva et al. 2011), illite (Bradbury and Baeyens 2005a, 2009b), smectite (Bradbury and Baeyens 2005a, 2005b; Galunin et al. 2009, 2010; Schlegel and Descostes 2009), and various iron (oxy)(hydr)oxides (Curtis et al. 2004; Davis et al. 2004; Fox et al. 2006; Powell et al. 2004; Singer et al. 2009, 2012a and b; Singh et al. 2010, 2012; Singh et al. 2009; Stewart et al. 2010; Waite et al. 1994) for sorption of uranium and other actinides has been well documented within the literature. Although

the kaolinite, mixed-layer illite/smectite, and iron (oxy)(hydr)oxide fractions of Soils *A* and *C* do not represent a majority of the soil column, the abundances are great enough to dominate sorption at the investigated $[U]_o$.

Although containing similar percentages of quartz, pure illite, and mixed-layer illite/smectite, Soils *B* and *C* display highly differing trends in sorption quantity and behavior. Soil *B* shows no discernible trend across time. The total concentration of U remaining in solution across all reaction periods for Soil *B* is much higher than the other experimental soils. The variance displayed may be attributable to the presence of calcite ($CaCO_3$, 3%) and dolomite ($(Ca,Mg)(CO_3)_2$, trace %) within Soil *B* and the larger quantity of amorphous/poorly crystalline Fe found in Soil *C*. The presence of carbonate (CO_3^{2-}) and associated species such as calcite can limit sorption of U (Stewart et al. 2010; Yan et al. 2010). Although the attributed quantities of carbonate species are small when compared to the presence of quartz or mixed-layer illite/smectite, the addition of any quantity of carbonate to the U sorption system can alter the overall sorption capacity.

Sorption edges and envelopes (E&E) (see Figure 5.15) depict the amount of a constant initial concentration of a given species of interest sorbed to a given sorbent with changing pH. Both Soils *B* and *D* display behavior that can draw comparisons to U sorption experimentation on purified minerals found within the literature. Soil *D* with its gradual but continuous increase in sorbed U between pH 5 and 9, initially follows the trend Schlegel and Descostes (2009) showed for U sorption on Na-SWy-2, a smectite. The similarities in sorption behavior between Soil *D* and Na-SWy-2 are particularly striking when considered in the context of the relative abundance of smectite within Soil *D* (3% mixed-layer illite/smectite).

The presence of kaolinite in Soil *D* may also influence the U sorption capacity of the soil. Barger and Koretsky (2011) showed a steady increase in U removal between pH 3 and 7, maintaining near 100% U sorption from pH 8 to 9, for K-Ga-1b, pure natural

kaolinite. The behavior displayed by pure kaolinite, similar to the pure smectite, again resembles that of Soil *D*. As Soil *D* has a more significant kaolinite relative abundance (15%), the impact of kaolinite on the sorption behavior of the total soil column is expected to be more significant.

With its more S-shaped appearance, E&E results for Soil *B* show similarities to U sorption to Na-illite du Puy (Bradbury and Baeyens 2005a). Soil *B* has a significant relative abundance of mixed layer illite-smectite (25%), with pure illite representing half of the mixed layers. Aside from the predominance of quartz within the soil column, mixed layer illite-smectite represents the next most abundant faction within Soil *B*. As such, this portion may dominate sorption within Soil *B*, and similarities to the sorption behavior of pure illite may help to confirm this concept.

For both Soils *A* and *C*, comparisons to literature values are more tenuous. The soils show near total sorption across the tested pH range. Within the literature to this point, no individual mineral has shown U removal to the extent displayed by Soils *A* and *C* across the entire pH range (Barger and Koretsky 2011; Bradbury and Baeyens 2005a, 2005b, 2009b; Davis et al. 2004; Galunin et al. 2009; Kremleva et al. 2011; Schlegel and Descostes 2009, amongst others). The near total removal during E&E experimentation may be considered a consequence of the small $[U]_o$ used to mimic DOE leachate concentrations. As such, the higher $[U]_o$ concentrations used for sorption isotherm experimentation provides additional insight to the true capacity of Soils *A* and *C*.

Comparing the results from initial experimentation and soil characterization to the literature shows the impact that various soil properties and minerals with their differing exchange capacities have on the sorption capacity of the total soil column. The presence of calcite results in decreased sorption capacity, as shown by comparing results for Soils *B* and *C*. For Soils *A* and *C*, the presence of kaolinite, mixed layered illite/smectite, and a differing forms of iron (oxy)(hydr)oxides may provide increased sorption capacity, similar

to the values shown within the literature for the pure mineral phases. Soil *D*, with its wider range of minerals in comparison to the other soils, may derive its capacity from the kaolinite and smectite present, although not to the extent shown for Soils *A* and *C*. Additionally, other portions of Soil *D* may be inhibiting further sorption of U.

Building from the basis of the single radionuclide experimentation, a second set of batch sorption experiments were conducted using a radioactive synthetic leachate (RSL) as the solution and both the initial set of barrier soils and a complimentary set of geosynthetic clay liner (GCL) –derived bentonites as the sorbents. Six GCLs were used with varying properties: 2 standard sodium bentonite-based GCLs (*CS* and *GS*), 3 chemical resistant GCLs (*CR*, *CR+*, and *GR*), and a bentonite-polymer composite GCL (*CT*). As with single radionuclide experimentation, uranium acetate served as the primary radionuclide for comparison of sorption capacity amongst the materials, while Ca^{2+}, Na^{+}, and CO_3^{2-} influenced the RSL solution speciation.

As shown through the results of the kinetics and E&E experimentation for RSL, while many of the soils perform well under certain system conditions, none of the tested materials is adept at U retention across all tested situations. This caveat is especially relevant in the context of Soils *A* and *C* and Bentonite CT, which each outperformed the other materials in terms of U sorption at the lowest tested pH ranges, but allowed nearly 100% of the U to remain in solution at the higher pH levels. However, as anticipated by the literature results for similarly speciated systems (Galunin et al. 2009, 2010; Stewart et al. 2010), U sorption is hindered by the presence of Ca and CO_3^{2-} within the RSL system. Due to the basis for RSL creation from within the DOE LLW data sets (Tian et al. 2014; Section 3), the current experimental system conditions are an accurate representation of those that are occurring at LLW sites in the U.S. Consequently, the types of materials readily available and frequently installed as barriers within LLW

systems are unlikely to perform as desired, particularly in the face of long-term regulations.

In the context of the original experimental hypotheses for this study, the chosen barrier materials were shown to rely heavily on their inherent mineralogies, with the Fe fractions dominating sorption capacity for the natural barrier soils, and differences in cation exchange capacity due to both clay and polymer behavior influencing the bentonites. Competition between solution species, particularly in terms of preferential cation replacability, dominated solution behavior within the RSL system. The presence of Ca and CO_3^{2-} in the RSL solution altered both speciation and sorption behavior for U on all tested sorbents. While the demonstrated sorption behaviors differed slightly from those shown within the literature, the complexity of the both the natural soils used within experimentation and the RSL mixture itself lend explanations to those differences. Finally, the measured concentrations of many of the solution species could be directly correlated to their equilibrium geochemical behaviors as modeled through speciation and oversaturation calculations.

Although clay-based soils have been considered a critical material in the construction of barrier systems, real soils behave differently than the purified clay minerals that have been frequently studied to this point in the literature. Cross-comparisons between sorption behavior of purified clays and iron minerals to the study soils show a reliance on multiple portions of the soil column to account for demonstrated radionuclide sorption capacity. Both the physical and chemical properties of natural soils influence uranium sorption, with iron content serving as a critical factor in accounting for soil sorption capacity. As such, development and identification of ideal barrier soils relies on the interaction of multiple mineral properties to account for the desired containment of LLW.

Section 1 - Introduction

From the point of their discovery in the late 19th century, the use of radioactive materials has skyrocketed. As with most anthropogenic goods, production and use of radionuclide-containing products ultimately lead to some form of disposal. Radioactive materials differ from the inert elements found in most products due to radioactive decay. In turn, radioactive decay results in the emission of additional daughter products while reducing the quantity of parent radioactive materials and increasing stability of the residual constituents. Most materials used in radioactive applications are ultimately classified as low-level radioactive waste (LLW) based on regulations for exposure rates, measures of radioactivity, and material composition. A discussion of sorption as related to the practical application of low-level radioactive waste disposal follows.

1.1 Necessity for understanding sorption processes

Design and construction of barriers to prevent radionuclide transport are controlled by two factors. The first controlling factor is composition of the waste form, in terms of which radionuclides are present. The second aspect controlling transport is the composition of the installed barriers. In addition to the two primary controlling factors, the impact of attenuating circumstances on the waste composition and the geochemistry of the system can further control transport. Radionuclide transport is limited by the inherent sorptive capacity of the materials utilized as barriers within disposal systems. With the reliance on barrier soils to ideally prevent, but more realistically limit, contamination of the environment surrounding LLW disposal facilities, understanding sorption as a solute transport mechanism through these materials is fundamental for improving disposal systems. Although playing a primary role in containment theory, knowledge of sorption processes in the context of radionuclide transport is still under development, particularly for mixed suites of mineralogical compounds that are representative of the natural soils

used for containment layers. Of further concern is the potential for inaccurate estimates in quantifying sorption. Potential inaccuracies could result from either overestimation of sorbed species or underestimation in the quantity of dissolved species able to be sorbed within a system (Altmann 2008). Full understanding of the sorption processes affecting radionuclide transport allows for more accurate modeling and development of effective disposal systems.

1.2 Current literature on sorption

The organization of this dissertation begins with Section 2 (Background). To more accurately assess the potential for radionuclides to sorb to barrier materials, the current literature on radionuclide transport in barrier systems is reviewed. Sorption mechanisms, materials currently used and studied for their sorptive capabilities, system geochemistry, and testing methods will each be discussed for their impact on radionuclide sorption.

Coupled systems are complex as a direct result of the difficulties inherent in fully accounting for all influences present in the environment and within man-made constructs. Better understanding can be cultivated from a detailed investigation of the procedures and methodology used in the broader research community and subsequent provision of proper framework for upcoming studies. A single process, specifically pure cation exchange, had been unable to account for experimentally derived sorption behavior (Bradbury and Baeyens 2009b). The potential processes occurring between barrier soil materials and radioactive solutions present a multi-faceted issue for disposal. However, at present little research has focused on the sorption interactions of radionuclides with the types of natural soils used within barriers. Models need to be tailored to every occurrence, using multiple mechanisms to better define exhibited behavior over a wide range of conditions.

1.3 Dissertation Organization

Following Section 2 (Background), Section 3 (Leachate Composition) describes the collected LLW leachates from four DOE sites and accompanying analysis and comparison to MSW leachate. Section 4 (Materials) details the soil characterization used for the outlined experimental approach. Section 5 (Single Radionuclide Experimentation) discusses the experimental results and associated implications of the studied single radionuclide system. Section 6 (LLW Leachate Experimentation) describes experimental results using a radioactive synthetic leachate (RSL) and cross-comparisons to the single radionuclide system. Citations are provided in Section 7 (References). Appendices A and B highlight the abbreviations and elements referenced within the text, respectively. Appendix C discusses the distribution coefficient and provides a calculation example. Appendix D contains the equations and parameters used in fitting sorption isotherms, while Appendix E provides an example and equations for calculating mineral solubility in solutions. Appendix F provides documentation of geochemical modeling conducted using the SpecE8 application with The Geochemist's Workbench. Appendix G contains additional data tables for Section 6. Finally, Appendix H provides comparative figures using pH-variable U concentrations for the RSL Edges and Envelopes experimentation, including K_d values.

Section 2 – Background

Radioactivity is the spontaneous emission of a stream of particles as a consequence of a nuclear reaction, as occurs in the production of nuclear energy, or directly from unstable atomic nuclei. Atomic instability results from the isotopic separation of elements, where two or more forms of the same element contain an equal number of protons, but different numbers of neutrons in their nuclei, giving differing atomic masses to the forms but maintaining the same chemical properties. Isotopes that display these properties are referred to as radionuclides or, more colloquially, emitters. Products formed as a consequence of radioactivity are referred to as daughter products, as they are the offspring of the parent radionuclides.

Radioactive decay, the process by which particles are emitted, can take three primary approaches. Alpha decay involves the loss of 2 protons and 2 neutrons (essentially a He atom), resulting in the daughter product being an isotope of a different element than the parent. Alpha decay has only been shown to occur in elements with atomic number greater than 52 (Te and above). Beta decay occurs in two forms: the release of beta particles (β-), whereby atoms with excess neutrons increase their atomic number, and positron (β+) decay, in which atoms with a deficiency in neutrons decrease their atomic number. Both forms of beta decay act to shift the resulting daughter products to more stable isotopes. Gamma radiation typically accompanies the other decay methods. A γ ray, a photon without mass at rest or charge, is emitted when the nucleus of a daughter product is left in an excited (i.e., charged) state following the primary decay mechanism and spontaneously moves to a lower or the ground state of energy for a given particle. The ground state is the lowest state of energy for a given particle. In addition to single decay modes, combinations of the processes are also common.

Radionuclides are compared to one another using two primary means. The first mechanism used to compare different radionuclides is the half-life ($t_{1/2}$) of a species, or the time required for half of the original radioactive material to decay. Half-lives for radioactive species can range from seconds ($t_{1/2}$ of ^{216}Po = 0.15 s) to billions of years ($t_{1/2}$ of ^{232}Th = 4.45 x 10^{17} s), whereas inert isotopes are assumed to have infinite half-lives. Along with the half-lives of radioactive species, the activity of species (A), or the number of decays per unit of time for a given radioactive sample, is also used for comparison of species. Activity is given in terms of becquerels (Bq), where one Bq is one decay per second. The becquerel is a unit that is derived and accepted by the International System of Units (SI) and replaced the older curie (Ci) unit for activity, defined as the activity of 1 gram of ^{226}Ra. Although use of Ci for defining the activity of species has been discouraged by the National Institute of Standards and Technology, Ci and pCi (picocurie, 1 x 10^{-12} Ci) are commonly used units within Department of Energy (DOE) documentation. Corresponding to the activity of a given species is the specific activity (S_A), or the number of decays per unit time per a given initial amount of the substance, by mass, volume, or moles of the sample. Of importance is the relationship between the half-life of a given species and its corresponding specific activity. Species with very long half-lives typically have lower specific activities. As an example, ^{238}U, with $t_{1/2}$ = 1.41x10^{17} s (4.47 billion years), has a S_A of 12210 Bq/g, while ^{226}Ra, the isotope for which specific activity was originally identified, has a S_A = 3.7 x 10^{10} Bq/g (37 GBq/g) and $t_{1/2}$ = 5.05 x 10^{10} s (1600 years). The half-life and specific activity provide the decay rate and a measure of the radioactivity of a given species.

The agencies charged with the development of nuclear technologies and the subsequent handling and disposal of radioactive materials, including the U.S. Department of Energy (DOE), the U.S. Nuclear Regulatory Commission (NRC), the Nuclear Energy Agency (NEA) of the Organization for Economic Co-operation and

Development (OECD), and the International Atomic Energy Agency (IAEA), characterize radioactive waste by a variety of definitions. The NRC classifies radioactive waste into four categories – low-level waste (LLW), waste incidental to reprocessing (WIR), high-level waste (HLW), and uranium mill tailings – which are readily comparable to the classifications provided by the DOE and IAEA, as shown in Table 2.1. Concern for public health due to heightened toxicity and potential for irradiation by radioactive materials are principal commonalities amongst regulatory definitions. Differences between classifications are characterized by overall radioactivity and total waste composition, in addition to waste form stability of the materials. In summarizing the adjoining policies of the various regulatory agencies, three concepts are used to define LLW. First, LLW must be able to be stored in near-surface (< 10s of meters below the ground surface), engineered facilities. Second, the waste being disposed must be radioactive, but cannot display high quantities of radioactivity or pose an immediate threat to the surrounding environment and/or human population. Third, LLW must maintain the level of stability outlined by the given regulatory agencies. This particular provision refers to the stability of the waste materials over the course of physical or biological decomposition, as opposed to radioactive stability. A “Safety Case” model, similar to that defined by Altmann (2008), highlights the importance for site placement, engineering, and safety feasibility prior to presentation to the general public for final approval and execution. The aspects of LLW policy and the “Safety Case” model define the regulations, the federally administrated legislation that constitutes and allocates responsibilities, used by the NRC and other agencies to address handling, disposal, and containment of LLW in the US.

The allowed contents of LLW can vary between agencies. Items disposed as LLW have typically become radioactive due to contact with radiation or radioactive materials (U.S. NRC 2002). These items include personal protective equipment and cleaning supplies, in addition to items directly used by radiation workers in various

academic, industrial, medical, or research settings (U.S. NRC 2002). Due to the variety of activities producing items classified as LLW, content can vary widely between disposal sites, encompassing everything from water treatment residues from nuclear reactors to animal carcasses from cancer research (U.S. NRC 2002).

Although the content of LLW separates it from municipal solid waste (MSW), design of MSW landfills and LLW disposal facilities is similar. Both types of disposal facilities are typically designed around three main components: a lower liner system, separating the surrounding sub-surface environment from the area designated for containment and serving as a space for collection of leachate generated via flow-through; the waste itself, dictating considerations on containment and monitoring; and a final cover system, for final separation from the prospect of intrusion into the outside environment. One major difference distinguishing LLW from MSW are the precautions put in place to shield workers and the public from radioactive exposure. To address this issue, LLW disposal packaging frequently incorporates steel drums, concrete, lead, or other means beyond standard MSW disposal containers (U.S. NRC 2002). As with MSW, the lower liner systems for LLW can be made from a variety of barrier materials. The barrier materials chosen depend on the location of the disposal site and any applicable regulations, but frequently incorporate natural clay-based soils for creating compacted clay liners. Soils high in clay content offer a variety of benefits for lining disposal sites, specifically their natural abundance and availability and typically low hydraulic conductivity. Additionally, clays have been recognized for their ability to attenuate other pollutants, including heavy metals (Abollino et al. 2003, 2008), actinides (Bradbury and Baeyens 2005a), and other trace elements (Brown and Parks 2001). This concept is of particular importance when considering the need for shielding the environment from potential hazards arising from LLW disposal.

Similarities between waste forms help to identify the degradation processes occurring during active disposal and over the lifetime of LLW. Grambow (2008) identified the need for characterizing the stability of waste forms on a three-fold basis: homogeneity of the waste, low long-term dissolution rates, and low interfacial solution concentrations of mobile radionuclides. Uniform assessment of containment strategies for LLW is controlled by the need for further understanding of the transport processes of the waste itself, particularly the potential for sorption and diffusion of radionuclides through installed containment barriers.

2.1 Radionuclides in LLW

Both inert contaminated materials (which represent the bulk volume of waste) and radionuclides control composition and disposal of LLW. The complexity of disposed waste regulations allows for interactions between a wide variety of radioactive and inert materials. Specific radionuclides are identified by the NRC for their “long-lived” or “short-lived” behavior as related to considerations for their ultimate disposal (10 CFR pt.61.55 2001). In the strictest sense, the radionuclides the NRC classifies as “long-lived” do not necessarily have overtly long half-lives, instead falling well within the typical human life span (see Table 2.2). However, the total decay sequences of the species identified have exceedingly long time frames, on the order of thousands to millions of years, or generate particularly strong emitters as a result of radioactive decay. As such, the time frame for protection against outside intrusion is similar to the species identified as being implicitly “long-lived”. This distinction, specifically with inclusion of ^{241}Pu and ^{242}Cm, differentiates the NRC classification from rulings developed by the DOE and the IAEA, which group these and other transuranic species into singular classifications not intended for near surface disposal. The radionuclide classifications developed by the NRC and other

regulatory agencies additionally identify allowable disposal mechanisms based on half-lives and other characteristics.

A substantial number of radioactive isotopes are eligible for disposal as LLW based on the various regulations. The variety of disposal-eligible radioactive species and the nature of radioactive decay result in differences between deposited species and the resulting leachate at disposal sites. Inyang et al. (2009b) highlighted 13 radionuclides representing the highest activity contribution in deposited LLW from the DOE. From data received from disposal sites around the US, Tian et al. (2014 – Section 3) noted the predominance of U, ^{99}Tc, ^{129}I, ^{3}H, and ^{14}C in leachate from LLW. In addition to the species identified by Inyang et al. (2009b) and Tian et al. (2014 – Section 3), trace concentrations of Cm, Eu, Pu, Ra, Se, and other radionuclides can be present in LLW based on the regulatory agencies' rulings (10 CFR pt. 61.55 2001). Table 2.2 compares the potential radioactive species in LLW as described in Inyang et al. (2009b), Tian et al. (2014 – Section 3), and 10 CFR pt. 61.55 (2001).

The behavior of radionuclides is influenced by speciation and valence state. Wang et al. (2010) differentiated between radionuclides displaying cationic (^{60}Co, ^{137}Cs, and ^{90}Sr) and anionic (^{129}I, ^{79}Se, and ^{99}Tc) tendencies. Earlier research conducted by Morrison and Spangler (1992) showed a strong correlation between U and cationic behavior and Mo and anionic behavior, as demonstrated by their respective adsorption edge and envelope formations. Cationic behavior is characterized by increasing sorption with increasing system pH, forming an adsorption edge, while anionic behavior shows decreasing sorption with increasing system pH, creating an adsorption envelope. The opposing pH tendencies exhibited by various radionuclides create difficulties in finding methods and materials to address full suites of behaviors resulting from mixed waste streams. To this point, many studies choose to focus on the behavior of a single radionuclide or on the comparison of systems with individual radionuclides with vastly

differing chemical and physical properties to isolate the behavior of the materials of interest. Altmann (2008) highlighted the need for further understanding of the reduction chemistry and isotopic dilution processes within barrier systems through use of the ^{129}I and ^{79}Se species. Similarly, Sato and Miyamoto (2004) and Breynaert et al. (2010) explored varying aspects of ^{79}Se speciation in relation to the geochemistry of the surrounding conditions. Although Sato and Miyamoto (2004) and Breynaert et al. (2010) utilized similar speciation sequences, the resulting conclusions regarding Se speciation leading to retardation differ between the studies. Understanding of Pu and Cm transport has been hindered by unknown Pu species resulting from the ^{244}Cm decay sequence under field conditions (Buesseler et al. 2009). ^{60}Co, which decays to ^{60}Ni, and ^{240}Pu, with its long decay chain (extending from ^{240}Pu to ^{208}Pb), were used to compare the efficiency of barrier thickness to barrier density (Inyang et al. 2009b). The ^{244}Cm decay sequence, including daughter product ^{240}Pu, is shown in Figure 2.1. For comparison, the ^{238}U decay sequence is shown in Figure 2.2. These examples highlight a variety of the approaches used in the study of radionuclide transport across disparate fields of study. Although using related isotope sequences, direct comparison and integration between studies remains difficult.

To assess the behavior of a wide variety of species, some authors have implemented the use of analogues for species and isotopes with longer half-lives. Sato and Miyamato (2004) used ^{75}Se as an analogue to ^{79}Se due to a significantly shorter half-life of 114 d versus 327,000 yr. Similarly, Um et al. (2010a) used ^{233}U to determine labile U within the investigated system, based on its ease of distinction from ^{238}U when using liquid scintillation. Non-radioactive lanthanides with similar valence states have been substituted as structural and chemical analogues to radioactive actinides to study sorption complexation and cation exchange under less hazardous experimental conditions (Fernandes et al. 2008; Galunin et al. 2009 and 2010; Geckeis and Rabing

2008; Kautenburger and Beck 2011). As an example, Eu(III) can act as a chemical analogue for all trivalent lanthanides and actinides, in particular serving as an ideal representative ion for Am(III), Cm(III), and Pu(III) due to similar thermodynamic properties and valence state stemming from periodic trends (Fernandes et al. 2008). The use of substitutions provides simplified investigative approaches while continuing to foster broader understanding of the interactions occurring. For analogues to be experimentally effective, the chemical similarities between the species of interest and the analogue must outweigh other differences, particularly regarding molecular size.

2.2 Necessity for understanding sorption processes

Installation of barriers to prevent radionuclide transport by all methods is controlled by two factors. The first controlling factor is composition of the waste form, in terms of which radionuclides are present. The second aspect controlling transport is the composition of the installed barriers. In addition to the two primary controlling factors, the impact of attenuating circumstances on the waste composition and the geochemistry of the system can further control transport. Radionuclide transport is limited by the inherent sorptive capacity of the materials utilized as barriers within disposal systems. With the reliance on barrier soils to ideally prevent, but more realistically limit, contamination of the environment surrounding LLW disposal facilities, understanding sorption as a solute transport mechanism through these materials is fundamental for improving disposal systems. Although playing a primary role in containment theory, knowledge of sorption processes in the context of radionuclide transport is still under development. Of further concern is the potential for inaccurate estimates in quantifying sorption. Potential inaccuracies could result from either overestimation of sorbed species or underestimation in the quantity of dissolved species able to be sorbed within a system

(Altmann 2008). Full understanding of the sorption processes affecting radionuclide transport will allow for more accurate modeling of future disposal systems.

2.3 Current literature on sorption

To more accurately assess the potential for radionuclides to sorb to barrier materials, the current literature on radionuclide transport in barrier systems is reviewed. Sorption mechanisms, materials currently used for their sorptive capabilities, system geochemistry, and testing methods will each be discussed for their impact on radionuclide sorption.

2.3.1 Mechanisms

Sorption involves multiple mechanisms including ion exchange, surface complexation, and precipitation. Ion exchange is the result of substitution of an ion of interest with a cation electrostatically bound to a sorptive surface. The exchanged cations serve to electrostatically charge balance particles within a soil matrix. The negative charge of the soil matrix arises from permanent structural substitutions within clay minerals of either Al^{3+} for Si^{4+} or Fe^{2+} for Al^{3+}, as well as broken or unsatisfied bonds along edges of the structure (Sposito 1989).

Ion exchange is mechanistically different from surface complexation, as surface complexation relies on interactions of particles that occur in addition to the electrostatics of a given system. Sorption via surface complexation can be expressed as three related general processes: adsorption, absorption, and precipitation. All three processes can impact the ability of materials to act as barriers, and as such are critical for prevention and minimization of contaminant movement. Although some investigators opt to holistically view sorption or surface complexation without differentiating between various processes (Rod et al. 2010), many more explicitly define and investigate individual aspects due to the differences between processes.

Adsorption is characterized by the attachment of a species of interest to a two-dimensional surface. For clays and clayey soils, two-dimensional surfaces exist along the outer surface and edges of the mineralogic structure. Conversely, absorption indicates penetration of a species of interest into the three-dimensional matrix of the sorbent. Absorption occurs between the interlayers of a clay structure, connecting layers by binding along multiple surfaces. Adsorption and absorption can be further defined in terms of inner-sphere and outer-sphere complexation. Both types of complexation can occur by either adsorption or absorption. However, Strawn and Sparks (1999) note that outer-sphere complexation primarily occurs at interlayer basal plane sites, marking absorption, while inner-sphere complexation more frequently involves the amphoteric edge sites along the clay surface as during adsorption. Differences in specific properties for ion exchange and specific adsorption are summarized in Table 2.3.

In addition to adsorption and absorption, materials may precipitate directly onto the surface of a sorbent. Adsorption, absorption, and surface precipitation are depicted in the context of montmorillonite in Figure 2.3. Distinguishing between bulk precipitation of the sorbate compound and more specific forms of sorption may be difficult, particularly where multiple species of a radionuclide exist simultaneously in solution, rather than a single dominant species. Depending upon the speciation of the precipitant, the precipitation can result in creating either less or more soluble species, impacting further transport of the contaminant. Precipitated species with high solubility are likely to re-dissolve when placed or remaining in contact with aqueous solutions, resulting in continued movement through a given system. Conversely, low-solubility precipitates aid in preventing undesirable species from transporting out of the containment system.

Radionuclide sorption can occur by any of the mechanisms discussed or through simultaneous processes. Sorption mechanisms may vary by radionuclide speciation and with the incorporation of differing sorbents, as well as with the geochemistry of the bulk

substrate. For the uptake of U on hectorite and montmorillonite, outer-sphere complexes dominated sorption at low ionic strength and pH, while inner-sphere complexes were prevalent on edge sites at circa-neutral pH (Schlegel and Descostes 2009). U(VI) edge surface complexes form on montmorillonite, while hectorite produces positively charged oligomers of U(VI) on the clay basal planes, but knowledge of which binding sites are used is debatable for the investigated interactions (Schlegel and Descostes 2009). Geckeis and Rabing (2008) suggested via spectroscopy that Cm forms inner-sphere complexes with a variety of aluminosilicate materials and predict similar behavior for other trivalent lanthanides and actinides. Conversely, Hartmann et al. (2008) found that Cm^{3+} remains in its original hydration state, suggesting that Cm(III) is not forming any inner-sphere complexes on montmorillonite as compared with other aluminocilicates. With multiple mechanisms displayed for both U and Cm, the complexity of sorption within barrier materials is further emphasized, marking potential difficulties in addressing all processes that may occur.

Sorption of radionuclides can also result from ion exchange with other sorbed species at the sorbent surface in addition to direct surface complexation with soil materials. In clay minerals, this is expressed in the preferential exchange of Na^{+}, K^{+}, Ca^{2+}, Mg^{2+}, or other nuclides via the clay's cation exchange capacity (CEC). Frequently, ion exchange is the result of competition between sorbed species and free ions in solution. Bradbury and Baeyens (2005b) showed that metal ions are not mutually competitive with all potential species in solution, but rather nuclides are selectively competitive based on valence and hydrolysis behavior. Selectivity can affect the exchange of previously sorbed ions with the radionuclides of interest (Bradbury and Baeyens 2005b). Cs adsorption exemplifies this mechanism, with a preferential ion exchange process similar to that of balancing the negative charge of clay minerals and additional influence from steric factors and hydration energy in comparison to other ions

(Cornell 1993). Further, Cs has been shown to display partial fixation, resulting in potential exchange on the clay surface for molecules of higher affinity, like K, and unhindered transport of Cs through barriers (Missana et al. 2004).

Multiple sorption processes can simultaneously affect the behavior of materials in radionuclide systems. Missana et al. (2004) found differentiable Cs sorption occurring on at least two separate site types for montmorillonite, with separate time scales and affinities occurring at various interfaces between the sorbent and sorbate. Similarly, U experiences ion exchange below pH 6 for outer-sphere complexation on montmorillonite, but demonstrates surface complexation resulting in inner-sphere complexation at high pH and ionic strength (Missana et al. 2004). Throughout their work, Bradbury and Baeyens (1997; 1999; 2005a and b; 2009a and b) have advocated the use of a two-site model for accurately describing the evolving sorption mechanisms occurring across a variety of nuclides and sorbents. Additionally, a single process, specifically pure cation exchange, had been unable to account for experimentally derived sorption behavior (Bradbury and Baeyens 2009b). The potential processes occurring between barrier soil materials and radioactive solutions present a multi-faceted issue for disposal. Models need to be tailored to every occurrence, using multiple mechanisms to better define exhibited behavior over a wide range of conditions.

2.3.2 Materials

Barrier soils play a central role in maintaining the separation of waste and its resultant leachate from the surrounding environment in contemporary disposal. Utilization of barrier materials for their sorptive capacity will be increasingly important as disposal of LLW materials garners greater attention by the general populace (Gates et al. 2009). Two generalized categories of barrier soil are commonly investigated within the literature. The first category consists of processed materials, comprised of either

individual clay or iron-based minerals that have been purified and separated from natural composite mixtures, or bentonites or other soil mixtures specifically designed for disposal applications. The second category reflects site-specific materials, collected from locations intended for disposal sites or with previous contamination.

2.3.2.1 Processed Materials – Purified clay minerals

Clay minerals are known for their sorptive capacity derived from their inherent mineralogical structures. Two clay configurations are of importance for their sorptive capacity. 2:1 clay minerals, so named for their two tetrahedral layers to each octahedral layer, derive their sorptive capacity from their ability to uptake water and expand their physical structures. 1:1 clay mineral structures, with one tetrahedral sheet to each octahedral layer, have limited ability to physically expand, but are important for their large surface area, allowing extensive sorption via adsorption. Minerals important for their interactions with radionuclides include montmorillonite, illite, and kaolinite.

Montmorillonite (idealized formula: $(Na,Ca)_{0.3}(Al,Mg)_2Si_4O_{10}(OH)_2 \bullet nH_2O$) frequently appears as a metal and radionuclide sorbent within the literature (Allard and Galas 2009; Bradbury and Baeyens 1997, 1999, 2005a and b; Cornell 1993; Darban et al. 2010; Fernandes et al. 2008; Galunin et al. 2009, 2010; Geckeis and Rabing 2008; Hartmann et al. 2008; Inyang et al. 2009b; Morrison and Spangler 1992; Schlegel and Descostes 2009; Sorieul et al. 2008). While a partial reduction of structural Fe^{3+} to Fe^{2+} was observed under low levels of radiation, structural changes were reversed upon removal from the direct irradiating source, demonstrating the stability of montmorillonite when in contact with radionuclides (Allard and Galas 2009). Sorption on montmorillonite is heavily influenced by the negative surface charge of the clay, resulting from substitutions within the tetrahedral structure that lead to unsatisfied bonds. Due to the 2:1 structure of montmorillonite, multiple sorption mechanisms can occur for differing

radionuclide species. Uranium sorption on montmorillonite is highly pH dependent and characterized by an edge surface complex (Schlegel and Descostes 2009), while Cm binds by an inner-sphere mechanism that differs from other materials (Geckeis and Rabing 2008).

In addition to the focus afforded to montmorillonite for its high activity and large expansion capacity, a variety of other clay minerals have also been investigated due to their abundance in the soil matrix. A number of authors compare the sorption behavior of illite to montmorillonite due to their structural similarities (Bradbury and Baeyens 2009a, b; Cornell 1993; Kim and Kirkpatrick 1997; Krumhansl et al. 2001; Lujaniene et al. 2007). In particular, Cs is heavily influenced by the presence of illite within a mixed clay matrix, and will preferentially sorb to illite over other clay minerals (Lujaniene et al. 2007). Cs retention on illite is influenced by the structural surface charge of the material (Kim and Kirkpatrick 1997) and its ability to replace missing K at exposed interlayer edge sites, reinforcing the illite lattice (Krumhansl et al. 2001). The capacity for kaolinite (Barger and Koretsky 2011; Kautenburger and Beck 2010; Kremleva et al. 2011), attapulgite (Fan et al. 2009), and chlorite (Singer et al. 2009) to sorb radionuclides, particularly U(VI), has also been investigated.

2.3.2.2 Processed Materials – Iron Minerals

Although clay minerals play a role within barrier soils, other minerals are also present. Consequently, the interactions of radionuclides with other fractions of the soil column require additional consideration. Specifically, iron (oxy)(hydr)oxides, in their various forms, often are a critical factor in limiting radionuclide movement. When looking at only gravel-sized fractions of Hanford Site soils, soils with higher iron oxide content showed a greater sorption capacity than soils with larger gravel fractions alone – specifically stemming from the impact of iron oxide coatings in the studied soils (Um et

al. 2009b). Additionally, differences in modeled sorption capacity for U to reacted samples has been related to an increase in Fe from the presence of increased ferrihydrite, acting as the primary sorbent within soil mixtures (Curtis et al. 2004). Studies have focused on the impact to system sorption capacity of goethite, α-FeOOH, (Singh et al. 2010, 2012; Stewart et al. 2010), ferrihydrite, Fe_2O_3, (Curtis et al. 2004; Davis et al. 2004; Fox et al. 2006; Waite et al. 1994), and magnetite, Fe_3O_4 (Powell et al. 2004; Singer et al. 2009, 2012a and b; Singh et al. 2009), both as singular minerals and as fractions of natural soils. In addition to acting as a sorption surface, substitution into inner-sphere type complexes at Fe sites on a variety of mineral surfaces within soils can ideally reduce U(VI) to U(IV), limiting U mobility (Singer et al. 2009). Magnetite in particular has been shown to act a sink for As(V), Cr(VI), and Hg(II), amongst other redox-active metals, demonstrating the potential to behave similarly for transforming U(VI) to U(IV) (Singer et al. 2012a).

Similar to clay minerals, iron (oxy)(hydr)oxides can act as sorption surfaces for radionuclides. For goethite, adsorption has been shown as the primary mechanism for U(VI) removal under most tested system conditions (Singh et al. 2010). Under high initial concentrations where precipitation dominates U(VI) removal by goethite, adsorption acts as a significant secondary mechanism (Singh et al. 2010). Comparable uptake behavior to goethite has been demonstrated for U(VI) removal by magnetite, coupled with concurrent reduction to U(IV) and coprecipitation of UO_2 nanoparticles (Singer et al. 2012a). Further, following nanoparticle formation, U on single-crystal magnetite begins to undergo passivation and development of a single monolayer U layer on accessible basal surfaces (Singer et al. 2012b). Magnetite also has demonstrated extensive sorption capacity for ^{137}Cs, ^{90}Sr, ^{154}Eu, and ^{141}Ce, partially as a result of its negative surface charge above pH 7 (Singh et al. 2009), as well as acting to facilitate coupled sorption and reduction of Pu(V) to Pu(IV) (Powell et al. 2004). Additionally, U(VI)

adsorption is not limited by surface sites on the goethite surface (Singh et al. 2010) and is positively impacted by the presence of structural defects in single crystal magnetite (Singer et al. 2012b). Consequently, the impact on sorption capacity imparted by iron-based minerals within soil mixtures may be amplified when compared to the purified or single crystal minerals. In heterogeneous mixtures, the surface sites and structural defects imparted by the inherent formation processes results in edge properties dominating the nano-scale as compared to single-crystal systems.

2.3.2.3 Processed Materials - Bentonites

Beyond purified minerals, commercially available bentonites are frequently studied sorbents for radionuclides (Arcos et al. 2008; Galunin et al. 2009 and 2010; Holmboe et al. 2010; Iijima et al. 2010; Majdan et al. 2010; Missana et al. 2004 and 2008; Sato et al. 1992; Sato and Miyamoto 2004; Sorieul et al. 2008; Wang et al. 2010). Bentonites have a number of potential uses in radioactive disposal, including use as backfill within and between waste containers and as a primary component in the construction of geosynthetic clay liners (GCLs), which have been proposed for use within LLW disposal. Researchers use these materials as acquired from suppliers (Arcos et al. 2008; Galunin et al. 2009 and 2010; Holmboe et al. 2010; Iijima et al. 2010; Missana et al. 2004 and 2008; Sato et al. 1992; Sato and Miyamoto 2004), as well as following additions and modifications to the bentonite to enhance sorption capacity (Majdan et al. 2010; Sorieul et al. 2008; Wang et al. 2010). The mineralogy of bentonite, with a majority of the material typically montmorillonite or other smectites, dictates its behavior as a sorbent. Although bentonite has a basis in montmorillonite, bentonite contains multiple minerals of varying percentages depending on location of origin, and therefore does not have a fixed molecular formula. Pore water exchange between

bentonite and sorbed materials and the CEC of the clay fraction typically control sorption for systems using bentonite (Arcos et al. 2008).

Galunin et al. (2009; 2010) utilized a suite of bentonites with a mineralogic basis in montmorillonite and purified specialty montmorillonites for comparing the influence of structural features in the sorption of lanthanide analogues. Similarly, Wang et al. (2010) monitored Cs retention on organoclays derived from MX-80, a specific commercial bentonite, which were modified with alkylammonium surfactants to improve sorption of anionic nuclides. The induced hydrophobicity of modified organoclays could allow greater retention of anions via sorption coupled with the initial CEC of bentonites (Majdan et al. 2010), but may reduce the cation retention capacity of the clay fraction (Wang et al. 2010). Alteration of bentonites following installation has also been investigated to account for the barrier soil mixtures resulting during application. Se was strongly retarded under the resultant reducing conditions in bentonite backfill, irrespective of the altered bentonite to silica content ratio of the bentonite backfill (Sato and Miyamoto 2004).

2.3.2.4 Source Materials

Understanding interactions with locally sourced soil is a primary concern in the design and implementation of LLW disposal. A number of authors highlight the interactions of materials at proposed high-level radioactive waste (HLW) disposal sites (Altmann 2008; Breynaert et al. 2010; Van Loon et al. 2009; Wu et al. 2009). Others have investigated the sorption of radionuclides to the surrounding soils at former production facilities and exposure-impacted sites (Bai et al. 2009; Buesseler et al. 2009; Chawla et al. 2010; Cheng and Saiers 2010; Curtis et al. 2004; Davis et al. 2004; Goldstein et al. 2010; Hammond et al. 2011; Hyun et al. 2009; Law et al. 2010; Liu et al. 2009, Lujaniene et al. 2007; Luo and Gu 2009; Omar et al. 2009; Um et al. 2009 a and

b, 2010a; Utsunomiya et al. 2009; Wan et al. 2009; Wellman et al. 2008). Across the various site-specific materials, tracking the impact of both the Fe-oxide and clay content of the soils has proven critical to modeling movement of radionuclides through the studied systems (Barnett et al. 2000; Bostick et al. 2002; Curtis et al. 2004; Davis et al. 2004; Stewart et al. 2010; Um et al. 2009 b). Similarity in Fe-oxide content, in spite of otherwise varying mineralogies, is the dominant factor leading to similar sorption capacity between subsurface sediments from the Oak Ridge, Hanford, and Savannah River Sites (Bostick et al. 2002). Additionally, the presence of Fe-oxide coatings on natural sediments may contribute to kinetic behavior in U(VI) sorption featuring quick initial uptake followed by continued rearrangement over time to reach a "more structurally or energetically favored" interaction between the materials (Barnett et al. 2000).

Characterization of site-based materials provides preliminary knowledge of the radionuclides present at previously contaminated sites and helps to determine consequential courses of action for remediation and siting of potential disposal locations. Calculations on mobility and transport of radioactive wastes should, theoretically, be focused on site-specific calculations and geochemical properties (Grambow 2008), although similarities can be drawn between sites with analogous characteristics for better prediction of potential interactions. For an area of concern, complete equilibrium between phases and speciation of the radionuclide of interest is assumed as a controlling factor, as opposed to having only reached a steady state. Bai et al. (2009) emphasized that sorption and desorption of U(VI) should be determined for all individual sites to find if the "Local Equilibrium Assumption" is reasonable under a given set of environmental conditions, including the pH, flow regime, and soils present. Additionally, porosity and effective porosity are considered the controlling soil properties for transport of radionuclides as investigated by Chawla et al. (2010), factors that are additionally

affected by the geochemistry and equilibrium conditions of the system. Coupled with the physical soil properties of source materials, alterations to the mineralogical content of a soil through the presence of iron oxide coatings on larger particles can lead to greater potential for increased sorption capacity than in unaltered soils (Um et al. 2009b).

2.3.3 System geochemistry

Interactions of soil, radionuclides, and water influence the design and implementation of LLW disposal facilities. Aspects altering sorption properties include pH, ionic strength, calcium content, and carbonate content. Additionally, the presence and interaction of coprecipitants and other materials can have a variety of consequences on the sorption of radionuclides.

"Source-dependent" and "source-independent" speciation behaviors have been shown to influence Pu transport within the soil matrix at the Savannah River Site (Buesseler et al. 2009) and are readily extrapolated to other radionuclides and site conditions. "Source-dependent" mechanisms are the environmental aspects directly connected to the specific source of radionuclides within a system, as with the production of ^{240}Pu from ^{244}Cm (Buesseler et al. 2009). Goldstein et al. (2010) measured effectiveness of barrier soils surrounding the Nopal I Uranium deposit for preventing flow of long-lived U-series daughter products by sorption and other mechanisms – an inherently "source-dependent" behavior. Coinciding with "source-dependent" mechanisms, "source-independent" behaviors are geochemical processes rapid enough to permit speciation to reach a steady state (Buesseler et al. 2009). As an example, precipitates of U(VI) close to the soil surface are slower to release than U(VI) adsorbed to mineral surfaces at deeper depths, controlling the fate and transport of U(VI) across the soil column (Um et al. 2009a). Goldstein et al. (2010) characterized radionuclide transport at 10^3 to 10^7 times slower than the groundwater flow rate in the saturated zone,

decreasing in the order $^{226}Ra \approx {}^{238}U > {}^{239}Pu \approx {}^{230}Th$, due to the influence of the geochemistry of the surrounding system. Across a variety of sites impacted by exposure through either natural deposits or use as disposal locations, these concepts can serve to frame further discussion of the geochemical processes impacting potential radionuclide sorption.

2.3.3.1 System pH

pH is frequently a controlling variable in the sorptive capacity of barrier soil for the interactions of specific radionuclides and the aqueous chemistry of the system. Radionuclides, similar to other metals, can have significant speciation changes with altered pH. The oxidation and reduction behavior of radionuclides can be further influenced by the pH of groundwater or precipitation infiltrating a barrier system. Changes in Pu speciation are expected to result from remedial efforts that alter the pH and other geochemical properties of groundwater in the surrounding soil, resulting in higher concentrations of oxidized ^{240}Pu (Buesseler et al. 2009).

Sorption behavior, presented as K_d, the solid-liquid distribution coefficient, as a function of pH for U, Am, Eu, and Np across a suite of minerals are shown in Figures 2.4 through 2.8. The radionuclides included were chosen for the availability of information regarding sorption to a variety of minerals, using data already presented with or readily transformed to a K_d. A brief discussion of K_d calculations and an example are provided in Appendix C. U sorption (shown for clay minerals in Figure 2.4 and iron minerals in Figure 2.5) is strongly a function of the pH of the surrounding system (Um et al. 2010a), with distinct sorption plateaus documented for montmorillonite and hectorite (Schlegel and Descostes 2009), as well as sediments collected from the Oak Ridge, Savannah River, and Hanford sites (Barnett et al. 2000). Additionally, Bradbury and Baeyens (2009b) and Davis et al. (2004) exhibited comparable trends for U(VI) sorption to illite

and ferrihydrite, respectively. Schlegel and Descostes (2009) explain the decrease of U(VI) sorption beginning around pH 8.5 in both hectorite and montmorillonite as a result of the formation of anionic U complexes. As an alternative explanation, Barnett et al. (2000) suggest that pH-dependent behavior is strongly controlled by the Fe content of soil. U(VI) fixation is only temporary under circa-neutral conditions and can desorb back into solution (Schlegel and Descostes 2009).

Similar to U(VI), Am(III) and Eu(III) display sorption plateaus beginning in the circa-neutral pH range (pH 6 to 8) (Figures 2.6 and 2.7). Unlike the behavior displayed by U(VI), sorption capacity for Am(III) and Eu(III) has not been shown to decrease with increasing pH, remaining relatively constant with the formation of hydroxide species, a factor of the similar valence of the radionuclides (Bradbury and Baeyens 2005b). In deference to the expected changes with valence for pH-dependent sorption behavior, Np(V) sorption (Figure 2.8) is markedly different than the other presented radionuclides, with a significant increase in capacity only above pH 8 and no defined plateau on the tested materials (Bradbury and Baeyens 2009b). With pH and speciation inherently linked, sorption capacity can be directly influenced by changes to the system pH, with equilibrium pH levels in LLW leachate controlling other system components.

2.3.3.2 Ionic Strength

For radionuclides with different valences, the affect of altering the ionic strength of the sorbate matrix has had varied effects. Increasing the ionic strength of a system of interest marginally decreased initial sorption of both Am(III) and Np(V) at low pH on Na-illite (Bradbury and Baeyens 2009b), as shown in Figure 2.6 and Figure 2.8, respectively. Cs adsorption is inversely related to ionic strength (Cornell 1993), which correlates the assertion that Cs adsorption is dominantly via a cation exchange mechanism (Tsai et al. 2009). Barnett et al. (2000) suggest that direct competition

occurs between U(VI) and Na^+ on collected natural sediments as the ionic strength of the system increases from 0.01 to 0.1 M. Alternatively, Singer et al. (2009) reported no impact on uranyl sorption to chlorite from increasing the ionic strength from 0.001 to 0.1 M NaCl. Earlier studies by Bradbury and Baeyens (2005a and b) showed the impact of altering both the total ionic strength and prominent solution ion. Increased ionic strength resulted in less total sorption onto montmorillonite across a suite of nuclides including Eu(III) and Cd(II) (Bradbury and Baeyens 2005b). Although the ionic strength trends between different soil-radionuclide pairs are readily comparable, the extent of impact to any given system is difficult to accurately predict without additional information, as evidenced by the difference for uranyl sorption in Na^+-based solutions.

2.3.3.3 Calcium content

The impact of calcium on the geochemical behavior of radionuclide sorption is a function of the speciation and variety of radionuclides present. The addition of hydrated lime ($Ca(OH)_2 \cdot 2H_2O$) to simulated U tailings fluid lowered U concentrations to then acceptable EPA groundwater levels (1992 EPA standard = 30 pCi/L (1.11 Bq/L), which is approximately 43 µg/L; contemporary EPA standard = 30 µg/L, or approximately 0.762 Bq/L based on the S_A of naturally occurring U at 25.4 Bq/mg) and demonstrated the potential to extract additional metals when combined with sorbent (Morrison and Spangler 1992). Galunin et al. (2009) showed that less total and more readily reversible sorption of La and Lu, acting as actinide analogues, occurred in a 0.02 mol/L calcium-based medium as compared to DI water. Competition arose between Ca from the background water and the sorbates of interest when La, Lu, and Ca have similar starting solution concentrations (Galunin et al. 2010). The concentration of Ca and pH had a large impact on U(VI) adsorption to natural sediments from the Hanford and Oak Ridge sites (Stewart et al. 2010). Maintaining a constant U(VI) concentration while increasing

Ca resulted in a decreased adsorbed concentration of U on goethite-coated sand and a suite of natural sediments (Stewart et al. 2010). ^{90}Sr competes directly with Ca for interactions with organic colloids and carbonate, at concentrations as low as from nuclear testing global fallout (Chawla et al. 2010). As the Ca concentration is typically far greater than the concentration of the sorbent of interest, direct competition between Ca and radionuclides is not the controlling factor decreasing radionuclide sorption when compared to Ca-free systems (Galunin et al. 2009, 2010; Stewart et al. 2010). Instead, Ca tends to sorb to interlayer sites, displacing other sorbed species to less specific sorption sites (Galunin et al. 2009). With its near universal presence, the interaction of Ca remains an integral aspect to understanding radionuclide fate and transport in barrier soils.

2.3.3.4 Carbonate content

Along with the impact of calcium, carbonate content can control the pH and sorptive capacity of other system components, with varying impact depending on the radionuclide of interest. Numerous studies (Davis et al. 2004; Fernandes et al. 2008, 2010; Liu et al. 2009; Stewart et al. 2010; Um et al. 2010a; Wellman et al. 2008) have investigated the impact of carbonate on U(VI) sorption to a variety of soils. Researchers have additionally studied how carbonate can alter sorption mechanisms for lanthanides and other actinides (Fernandes et al. 2008, 2010; Geckeis and Rabing 2008).

The altered speciation of U(VI) in the presence of atmospheric CO_2 levels can be seen Figure 2.9, as compared to a CO_2-free system displayed previously in Figure 2.4. The presence of carbonate species in solution dominates U(VI) speciation, resulting in an increased potential for U(VI) transport through the subsurface towards the groundwater table (Wellman et al. 2008). Modeling U sorption using K_d is strongly influenced by both the pH of the system and the amount of carbonate present in solution

(Um et al. 2010a). Davis et al. (2004) noted that pCO_2, the partial pressure of carbon dioxide in the atmosphere directly affecting carbonate saturation, was a dominant factor in U(VI) sorption and speciation, displaying an inverse proportionality where a higher pCO_2 resulted in a lower quantity of U(VI) sorbed. Specifically, the discrete ranges for sorption and desorption behavior of U(VI) across multiple soil types have been related as a direct function of the carbonate system, where increasing pH at a constant pCO_2 results in higher aqueous carbonate concentrations coupled with increased U(VI)-carbonate complexation (Barnett et al. 2000). The formation of aqueous U(VI)-carbonato species may result in increased competition between surface sites and the aqueous carbonate for the uranyl ions present in solution at higher pH, decreasing the sorption occurring (Waite et al. 1994). Increased CO_2 was shown to impact the degree of sorption on ferrihydrite, but unlike other materials where a higher pCO_2 resulted in a lower quantity of U(VI) sorbed, some masking of the decreased sorption capacity may be occurring due to the high degree of initial sorption (Fox et al. 2006).

The impact of carbonate has also been demonstrated in systems focused on natural sediments. High levels of carbonate within Hanford soils may account for U(VI) entering into solution with groundwater more than 60 years after initial contamination (Wan et al. 2009). Adsorption of U(VI) to natural sediments found at Hanford and Oak Ridge is limited by U(VI) precipitated in carbonate-related species, particularly as the uranyl-calcium-carbonato complexes $Ca_2UO_2(CO_3)_3$ and $CaUO_2(CO_3)_3^{2-}$ (Stewart et al. 2010). Using $Ca_2UO_2(CO_3)_3^0{}_{(aq)}$ as the dominant aqueous species to model groundwater complexity at a mill tailings site, Hyun et al. (2009) note that uranyl species bound only to carbonate may still dominate surface speciation. Singer et al. (2012a) note that the formation of uranyl-calcium-carbonato surface complexes can occur under acidic range pH levels, further impacting sorption and reduction of U(VI). Above pH 8.5, where uranyl-calcium-carbonato complexes fully dominate the solution speciation, adsorption is further

limited by precipitation of U(VI)-bearing carbonate species (Stewart et al. 2010). Additionally, other alkaline earth-uranyl-carbonato species, such as those involving Mg, Sr, or other species, could display similar behavior to the Ca species in regards to U(VI) reduction (Singer et al. 2012a). However, comparing the U(VI)-only and uranyl-carbonate systems on magnetite where reduction to U(IV) readily occurs to the U(VI)-CO_3-Ca system, which had no measurable reduction, showed the potential for the reduction to offer an additional path to sorption or removal from the system (Singer et al. 2012b).

In comparing two zero-valent iron (ZVI) systems (identical except for their bicarbonate content), removal of U(VI) was extremely rapid in the bicarbonate-free system, but increasing the bicarbonate concentration decreased the overall U(VI) removal rate and increased the time needed for removal (S. Yan et al. 2010). Similar to the ZVI systems, U(VI) sorption on chlorite showed solution-composition-specific behavior, with a 50% reduction in uptake in the carbonate-bearing system as compared to the carbonate-free system (Singer et al. 2009). Throughout these systems, the presence of carbonate species results in altered valences for U(VI) complexes. The change in valence, particularly to neutral and higher valence state species that dominate the system, results in reduced sorption of uranyl-carbonato species when compared to the carbonate-free system.

In addition to uranium, carbonate has varying impacts on sorption of other radionuclides. Carbonate eliminates the sorption plateau experienced by the carbonate-free Eu(III) system, resulting in a swift decline in Eu(III) sorbed above pH 8 (Fernandes et al. 2008) (see Figure 2.10). Carbonate has no demonstrated impact on Cm sorption (Geckeis and Rabing 2008). Carbonate interaction with sorbed species may be a result of valence differences between the radionuclides, given the demonstrated differences between U(VI), Eu(III), and Cm within the literature.

2.3.3.5 Interactions with coprecipitants

Interactions with coprecipitants can principally be viewed in respect to competition between radionuclide species. Radionuclide competition is selective based on the valence and hydrolysis behavior of the nuclides in question (Bradbury and Baeyens 2005b). Cation replacability behavior for clay and clayey soil is analogous, where higher valence, smaller size, and greater abundance result in the replacement of cations in a known order (alternatively given as $Li^+ < Na^+ < H^+ < K^+ < NH_4^+ < Mg^{2+} < Ca^{2+} < Cu^{2+} < Al^{3+} < Fe^{3+}$, in order of increasing "replacement power" from Li^+ through Fe^{3+} (Holtz et al. 2011, pg. 137), or $Cs^+ > Rb^+ > K^+ > Na^+ > Li^+$, $Ba^{2+} > Sr^{2+} > Ca^{2+} > Mg^{2+}$, in order of decreasing adsorption affinity for monovalent and divalent cations, respectively (Sposito 1989, pg. 155)). With valence state a primary factor affecting competitive sorption, the control of originating materials on speciation and the consequent pH of a system should be determined to better interpret potential interactions. Due to the complexity of regulations and resulting waste streams at disposal sites, predicting the exact sorption behavior of a mixture of radionuclides can be challenging.

Compatibility amongst suites of radionuclides can also impact simultaneous sorption onto designated materials due to interactions amongst the species in solution. For example, no single additive from a tested group of 24 was able to extract both U and Mo over a pH range similar to those seen in mine tailings degradation (Morrison and Spangler 1992). Cs sorption was affected by the presence of other ions in solution, particularly K^+, but also NH_4^+, due to the similarity in valence state between the ions (Lujaniene et al. 2007). Interactions amongst radionuclides are inevitable in disposal of LLW, barring extensive measures to ensure separation of waste streams. Subsequently, studies modeling direct competition, like Bradbury and Baeyens (2005b), are important for the prediction of sorption behavior in LLW systems.

2.3.3.6 Interactions with other materials

A variety of additional materials relevant to LLW disposal have been scrutinized for their potential impact on radionuclide sorption. Investigated materials include humic and fulvic acids, due to their abundance in the sub-surface environment, and phosphate, a primary component in the production of nuclear fuel. Although humic substances are considered to be capable of dissolving and mobilizing U, their demonstrated capacity has been less than predicted (Luo and Gu 2009). Humic substances are thought to often control sorptive capacity in [Eu - humic substance - mineral surface] systems (Fan et al. 2009), but opposing results contradict this hypothesis. Eu(III) sorption on attapulgite in the presence and absence of fulvic and humic acids shows strong binding at low pH, but reduced sorption at high pH values when compared to the acid-free systems (Fan et al. 2009). Alternatively, ^{154}Eu strongly sorbed to magnetite across all pH values both in the presence and absence of humic acid (Singh et al. 2009). ^{137}Cs and ^{90}Sr have increasing sorption to magnetite above pH 6 both with and without humic acid, with ^{90}Sr reaching 100% sorption at pH 10, while ^{141}Ce experienced near 100% sorption across all pH values (Singh et al. 2009). Despite their environmental prevalence the inclusion of humic and fulvic acids has not been shown at this point to systemically impact the uptake of radionuclides on sorbents.

Other factors can also alter sorptive capacity. Complexes of isosaccharinic and gluconic acids with Th(IV), U(IV), Np(IV), and Pu(IV) may increase actinide mobility, but little is known about the complexes that may form between the radionuclides and acids, or their stability under likely system conditions (Gaona et al. 2008). Bioreduction may play an important role in understanding transuranic reduction within different soil regimes (Law et al. 2010), but the extent of impact remains unproven to this point. The role of other contaminants expected at numerous sites, including Hanford, seems to be less critical than originally proposed, specifically the role of phosphate from leaked waste

(Um et al. 2009a). Any extraneous material present, whether naturally occurring or a consequence of previous site activities, creates the opportunity for unforeseen consequences to the desired radionuclide retention.

2.3.3.7 Colloid formation and transport

An additional issue with the use of bentonite and other clay minerals is the potential for colloid formation of the clay, and subsequent transport along flow paths through a barrier system. Although clay particles typically act to bond to one another in a solid surface formation, under certain conditions smaller groups of particles, called colloids, can separate and disperse away from the larger system. The sorption of radionuclides to separated clay colloids can allow consequent enhanced transport by the same properties intended to limit movement (Missana et al. 2004). The degradation of bentonite into colloidal-sized clay particles as a result of turbulent subsurface flow conditions can drastically alter radionuclide sorption, as more surface area is exposed for interaction with the sorbate of interest (Iijima et al. 2010). Although ^{239}Pu and ^{90}Sr can be bound to the colloidal soil fraction, little transport appears plausible as a result of the soil alone when outside the saturated zone of an aquifer, making colloidal transport a function of aquifer flow conditions (Chawla et al. 2010). Cheng and Saiers (2010) note that colloid transport in less-saline aquifer environments may be important for determining the potential for radionuclide migration within these types of systems, as compared to systems with higher ionic strength. Coupled with the impact of low salinity is the reversibility of radionuclide sorption to clay colloids, allowing for redeposition along transport pathways (Missana et al. 2008). Colloidal radionuclide transport appears to rely on both the system geochemistry and the impact of non-steady-state flow through a given system.

Different colloids interact with actinides in ways that can both increase and decrease mobility through the other materials associated with depositories (Geckeis and Rabing 2008). Colloids formed in association with Cs, U, and Sr at the Nevada Test Site could radically affect transport of the radioactive elements away from the contaminated zone (Utsunomiya et al. 2009). For colloid-facilitated transport of Cs, ionic strength of pore water influenced transient flow, decreasing colloid transport as ionic strength increased (Cheng and Saiers 2010). Pu and Am are noticeably absent in colloid formation, while Tc and I are partitioned into the aqueous phase rather than to colloidal nanoparticles (Utsunomiya et al. 2009). Due to the differences between radionuclide species in colloidal formation, understanding the direct interactions between soil and radionuclides is critical to prevent the transport of colloids in LLW containment systems.

2.4 Experimental methods

In creating an experimental regime to better understand the impact of sorption mechanisms, research has focused on both direct experimentation and modeling processes. As with other systems, practitioners rely on physical experimentation as a background for framing the complexities of creating accurate models of radionuclide-influenced systems. Complexities persist in coupling simultaneous chemical and physical processes and scaling comparisons between bench- and field-scale studies (Miller et al. 2010). Coupled systems are complex as a direct result from the difficulties inherent in fully accounting for all influences present in the environment and within man-made constructs. Better understanding can be cultivated from a detailed investigation of the procedures and methodology used in the broader research community and subsequent provision of proper framework for upcoming studies.

Experimentation for radionuclide sorption investigations has been constrained to bench-top investigations and constrained field-scale installations. While often building

from one another, both aspects have rarely been implemented concurrently to provide an encompassing view of sorption processes. Following physical experimentation, an array of models have been developed and tested for prediction of sorption behavior. A discussion of these methods follows.

2.4.1 Bench-top investigations

A variety of laboratory techniques have been used to better understand the interactions between radionuclides and sorbents. These techniques can be grouped into batch sorption experiments and flow-through investigations.

Batch techniques focus on interactions between a sorbent, solution, and sorbate of known measured starting quantity. Once steady state is achieved, one or more components are removed from the closed system to measure changes in concentration between the sorbent and sorbate. Many researchers use batch experiments to prepare isotherms that measure sorption capacity with increasing initial radionuclide concentration (Bai et al. 2009; Cornell 1993; Galunin et al. 2010; Heberling et al. 2008; Iijima et al. 2010; Omar et al. 2009; Stewart et al. 2010; Tsai et al. 2009). Additionally, sorption capacity for a single sorbate concentration can be compared by measuring the effect of changing pH, in turn creating a sorption envelope for a given radionuclide (Bradbury and Baeyens 2005a and b, 2009a and b). The information garnered from these procedures can provide much of the critical knowledge needed for sorption determinations, including steady-state system kinetics, sorption density across a pH regime, and total sorption capacity as a function of radionuclide concentration.

As an alternative to the use of batch techniques, flow-through experiments rely on steady addition of solution through a sorbent-packed vessel to measure sorption over a specified amount of flow or period of time. Reactor systems and column experiments can be used to simulate solution movement through subsurface systems. Despite

differences among experimental set-ups, the desired results typically identify similar effects between systems. Along these lines, Morrison et al. (2001), Liu et al. (2009), and Goldstein et al. (2010) used differing methodology to relate the sorptive capacity of a variety of materials for U(VI). Morrison et al. (2001) used a series of column experiments under laboratory and field conditions to determine the effectiveness of zero-valence iron in removing U. Liu et al. (2009) used small-scale, stirred-flow cell reactors with synthetic groundwater mixtures and varied the pH, Ca, and CO_3 concentrations to mimic natural variations. Goldstein et al. (2010) modeled U transport in a slug-flow model through a single-tank reactor to represent conditions of the Hanford 132 well while simplifying the geochemical constraints of the system. Constructing systems to accurately simulate vastly different disposal locations is possible with the variety of flow-through experimental techniques available to researchers.

2.4.2 Field-based testing

Given the intent to provide lasting solutions to the long-term issues associated with radionuclide disposal and contamination, field-scale studies are necessary to investigate the effectiveness of potential remediation techniques. Unlike bench-scale experiments, field-scale tests allow for *in situ* environmental conditions that may be difficult to simulate in the laboratory. Conversely, the implementation of field-scale studies requires extensive cooperation amongst researchers and the agencies charged with handling and disposal of radionuclides. Further, the time frame to reach steady-state geochemical and flow conditions for field-scale testing is significantly longer than for bench studies as a function of the scale effect. With these caveats, field-scale testing provides the opportunity to employ sorption solutions on a larger scale prior to full implementation.

Within the literature, one repeated theme in field-scale investigations has been the deployment of permeable reactive barriers (PRB) of zero-valence iron (ZVI or Fe(0)), at a variety of sites throughout the U.S. Reductive precipitation of the Fe(0) may be a dominant process for the removal of U experienced at PRB field sites (Morrison et al. 2001). Due to implementation within a natural environment, field studies of PRB are heavily influenced by the *in situ* geochemistry, resulting in changes that may affect the sorptive capacity. As a PRB of ZVI corrodes over time, pE increases, pH decreases, and carbonates precipitate, resulting in redistribution of the iron redistributes and removal of U and V from solution (Morrison 2003).

Aside from the impact of the surrounding environment on field-scale studies, scale- and location-based practicalities enforce differences between the laboratory and field, even when similar experimental methods are used in both locations. Column experiments with ZVI from PRBs used different atmospheric backgrounds at the field site and laboratory, as well as the use of a bactericide within the laboratory as compared to the natural groundwater used for flushing in the field (Morrison et al. 2001). These differences mark only an example of the differing constraints on these systems. Comparisons of contrasting experimental methods require thorough understanding of the constraints used for field- versus lab-based studies.

2.4.3 Interpretation of Results and Models

Following the execution of experimental techniques, interpretation of the consequent results can further emphasize the nuances of sorption in varying systems. Comparison between isotherm models can allow for better understanding of the sorption mechanisms at work within barrier systems. Comparison of results obtained with similar experimental techniques for radionuclides with differing valences and speciation allows for better system behavioral models to be produced. These goals are most frequently

accomplished using traditional isotherm models, particularly the Linear (Iijima et al. 2010), Freundlich (Bai et al. 2009; Cornell 1993; Galunin et al. 2010; Heberling et al. 2008; Tsai et al. 2009), and Langmuir models (Galunin et al. 2010; Omar et al. 2009; Stewart et al. 2010; Tsai et al. 2009). Additional isotherm models have also been used, such as the Sips model (Galunin et al. 2010; Humelnicu et al. 2011), which combines facets of both Freundlich and Langmuir sorption behavior. The sorption sites present on the sorbent and the valence of the sorbate radionuclides heavily influence which mechanisms accurately depict what interactions are occurring within a given system. Different mechanisms have been shown to accurately depict related sorption systems, such as those with a single constant radionuclide on various materials, by following separate models, as for Cs by Cornell (1993) and Tsai et al. (2009). Further, not all results can be accurately fit by previously defined mechanisms under the conditions used by researchers. Consequently, extrapolations to the literature are required to explain less-understood behaviors of radionuclide sorption (Stewart et al. 2010).

The final major methodological tool used in radionuclide sorption investigations is the development and implementation of models. More so than other methods, accurate models must rely on information generated from physical investigations to better predict system behaviors. Having a basis in the properties of a system of interest, whether at the bench-scale or to simulate a large area, requires a starting set of parameters to serve as a link between the physical experiment and the model. However, including both physical and chemical processes in the modeling of sorption systems doubles the necessary scale range as compared to using physical transport processes alone (Miller et al. 2010). Inaccurate models frequently arise from under-scaling of total phenomena or of the impact of certain aspects involved within systems. Division of plume behavior at the Hanford site in modeled movement predictions exhibits different sets of U behavior, with changes in pH, speciation, mineralization, and the U concentrations between the

sections of the plume affecting predicted overall sorption and transport (Wan et al. 2009). In an effort to overcome similar challenges, during the development of the Geo-Radiological Barrier Gamma Attenuation Model (GRBGAM), Inyang et al. (2009a) accounted for increasing or decreasing barrier density, “build-up” factors for different materials and thicknesses, weathering by both changes to chemical composition and changes to bulk wet density, and variations in γ emitters. Much like the attention paid by Inyang et al. (2009a), Miller et al. (2010) highlight three aspects that affect the ability of models to be accurately applied to a variety of situations: (1) the interaction of the physics and chemistry existing at a site: (2) the relation in scale between a bench-top or field-scale experiment and the full-scale, and (3) the application of laboratory-based findings to the overall environment (Miller et al. 2010).

Although the model developed by Inyang et al. (2009a and b) focuses on the large-scale interaction between an environment and radionuclide transport, similar challenges exist in the application of models to account for atomic-scale sorption behavior. A prominent example of this type of model is the two site protolysis non-electrostatic surface complexation and cation exchange (2 SPNE SC/CE) model developed by Bradbury and Baeyens (1997). The model’s two sites, both representing amphoteric surface hydroxyl groups at clay platelet edges, are designated as strong and weak, with weak sites dominating the system (Bradbury and Baeyens 2005a). By focusing on the small-scale behavior, the 2 SPNE SC/CE model is able to predict a variety of behaviors for a suite of nuclides across numerous clay materials.

2.5 Conclusions

Interactions of radionuclides with minerals commonly found in barrier soils have received considerable attention within the literature. The quantity of information on radionuclide sorption encompasses a wide variety of sorbents, nuclides, and materials

acting as additional factors within these systems. Across all situations, calculations on mobility and transport of radioactive wastes should be focused on site-specific calculations and geochemical properties (Grambow 2008) to determine if the “Local Equilibrium Assumption” is reasonable under a given set of conditions (Bai et al. 2009). Site-specific calculations and experimentation allow for thorough understanding of the material properties inherent to the soils used as barriers against transport in disparate locations. These properties and the water chemistry of the surroundings are essential for establishing the geochemistry of a disposal system, serving as the backdrop for sorption changes.

Radionuclide sorption is heavily influenced by the ionic behavior of the radionuclides in question. Further, the presence of additional materials including calcium, carbonate, organics, and other radionuclides can alter the potential sorption mechanisms. Viable mechanisms affecting sorption may differ between radionuclide and barrier material combinations, but the potential for sorption is primarily controlled by other influencing factors. Truly effective systems must account for all facets affecting sorption within a disposal system in order to understood relational impacts between components.

Building from the basis for research in HLW, much can still be ascertained regarding the interactions of LLW and soil barrier materials. The low concentrations and allowable amounts of radioactivity that characterize LLW as dictated by the regulatory agencies impose separate considerations for transport prevention when compared to HLW. Although combinations of radionuclides are found in HLW, they differ significantly from those in LLW in speciation and interactions.

Research focusing on realistic scenarios is critical for complete understanding of the processes occurring during LLW disposal. In particular, documentation of the

sorption processes occurring between the radionuclides present in LLW and the barrier soils used for their containment will help clarify what interactions are plausible within these systems. Building from information collected from the literature regarding radionuclide sorption on pure minerals and soil-derived materials, batch sorption tests were used to quantify sorption on both natural containment soils and bentonites derived from geosynthetic clay liners (GCLs). The experimental set-up addressed three working hypotheses regarding radionuclide-soil interactions. They are as follows:

1. Radionuclide sorption is proportional to the exchange capacity of barrier soils, as a function of the minerals present;
2. Competition for sorption sites between radionuclides within mixtures is a function of the speciation of radionuclides present within a given system;
3. Distribution of radionuclide species in the liquid and solid phase can be predicted by the equilibrium geochemistry of a given system.

The initial concepts provide the groundwork for fuller understanding of the processes occurring within LLW disposal.

Table 2.1. Comparison of radioactive waste definitions of the DOE, NRC and IAEA.

DOE (U.S. DOE 1999)	NRC (10 CFR pt.61.55 2001)	IAEA (IAEA 2009)
Low-Level Waste (LLW) – By definition, waste that does not fit any of the other categories, but is still radioactive	**Low-Level Waste (LLW)** – Commercial radioactive wastes that are not the other two main categories	**Exempt Waste (EW)** – Waste that meets criteria for clearance, exemption, or expulsion for regulation for radiation
Mixed Low-Level Waste (MLLW) – Waste that is both radioactive and contains RCRA-regulated hazardous constituents	→ The NRC further divides LLW into 3 sub-categories, defined in detail in 10 CFR pt.61.55 (2001): **Class A**, **Class B**, and **Class C**	**Very Short Lived Waste (VSLW)** – Waste that is stored for a limited period of decay for up to a few years and is subsequently cleared for non-radioactive disposal
Transuranic Waste (TRU) – Waste that contains transuranic radionuclides with a half life > 20 years at concentrations > 100 nCi/g	**Waste Incidental to Reprocessing (WIR)**	**Very Low Level Waste (VLLW)** – Waste that isn't EW, but doesn't need a high level of containment and isolation, such as soil and rubble with low activity concentration levels
High-Level Waste (HLW) – Highly radioactive waste material resulting from the reprocessing of spent nuclear fuel	**High-Level Waste (HLW)** – Irradiated nuclear reactor fuel	**Low Level Waste (LLW)** – Waste that may include short lived radionuclides at higher activity concentration levels for long-lived radionuclides at relatively low levels of activity concentration that is able to be stored in the near surface
Mill Tailings – As dictated by the Uranium Mill Tailings Radiation Control Act (UMTRCA); naturally occurring, residual radioactive materials	**Uranium Mill Tailings** – Residues remaining after the processing of natural ore to extract uranium and thorium	**Intermediate Level Waste (ILW)** – Waste that contains long lived radionuclides (including α emitters) with no or limited heat dissipation provisions, that can be stored 10s to 100s of meters below ground
Specifically Not Covered: Spent Nuclear Fuel; Material Stockpile; the Strategic Reserve, Programmatic Reserve, or National Asset Material; Non-radioactive materials		**High Level Waste (HLW)** – Waste that contains high levels of activity concentrations with significant heat dissipation; Must be stored in deep, stable, geologic formations at several 100s of meters or more depth

Note: The DOE and the NRC hyphenate Low-Level and High-Level Waste, while the IAEA does not.

Table 2.2. Radionuclides deposited or measured in leachate from LLW, along with LLW regulated radionuclides.

Deposited Radionuclides (adapted from Inyang et al. 2009b)		Leachate Radionuclides (adapted from Tian et al. 2014 – Section 3)		Regulated Radionuclides (adapted from NRC Regulation 10 CFR pt. 61.55 2001)	
Nuclide	Half-Life (yr)	Nuclide	Half-Life (yr)	Long-Lived	
^{144}Ce	0.779	^{14}C	5730	Nuclide	Half-Life (yr)
^{58}Co	0.194	^{3}H	12.28	^{14}C	5730
^{60}Co	5.271	^{129}I	1.57×10^{7}	^{242}Cm	0.45
^{51}Cr	0.0759	^{99}Tc	2.13×10^{5}	^{129}I	1.57×10^{7}
^{134}Cs	2.062	^{238}U	4.47×10^{9}	^{94}Nb	20300
^{137}Cs	30.17	* Note: Additional radionuclides present - measured as gross α and β radiation		^{59}Ni	75000
^{55}Fe	2.7			^{241}Pu	14.4
^{3}H	12.28			^{99}Tc	2.13×10^{5}
^{54}Mn	0.857			α-Transuranic	> 5
^{95}Nb	0.0958			Short-Lived	
^{63}Ni	100.1			^{60}Co	5.271
^{90}Sr	28.6			^{137}Cs	30.17
^{65}Zn	0.669			^{3}H	12.28
				^{63}Ni	100.1
				^{90}Sr	28.6

Table 2.3. Comparison of ion exchange and specific adsorption.

Property	Ion Exchange	Specific Adsorption
Surface Species	Outer-sphere surface complexes and diffuse ion swarm, due to solution conditions	Inner-sphere surface complexes, due to discrete ligands at the surface and predicted based on charge
Adsorptive Charge versus Surface Charge	Always opposite	Either opposite or the same
Kinetics	Transport control – diffuse ion swarm, where rate is controlled by diffusion	Surface control, due to charge of surface functional groups
Anion Affinity	Increases with absolute value of charge and size of ionic radius	Increases with log K of protonation
Cation Affinity	Increases with charge and ionic radius	Increases with log K for hydrolysis

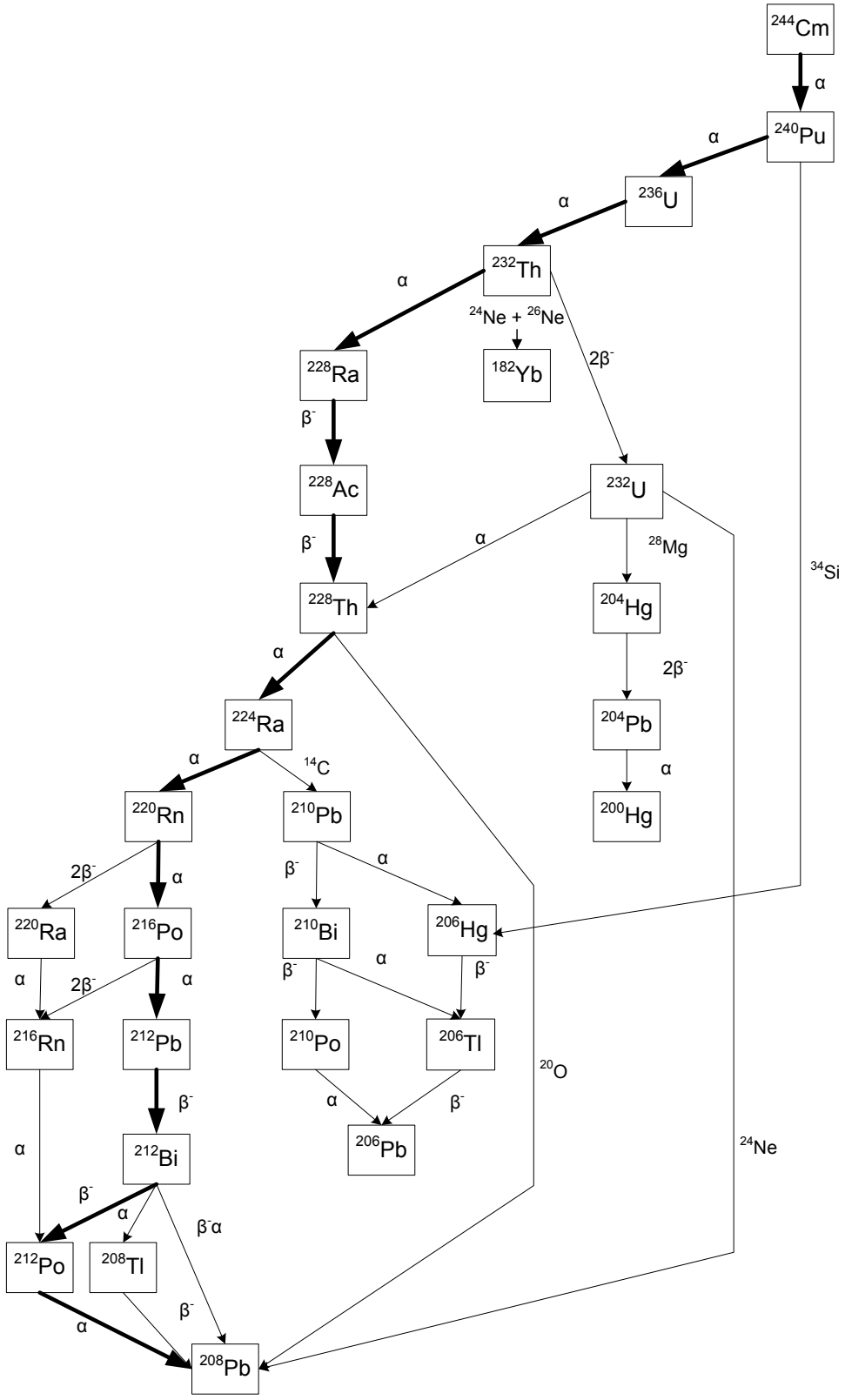

Figure 2.1. ^{244}Cm and ^{240}Pu decay sequence. Bold arrows represent the most likely decay path. (Adapted from Gray 2007a)

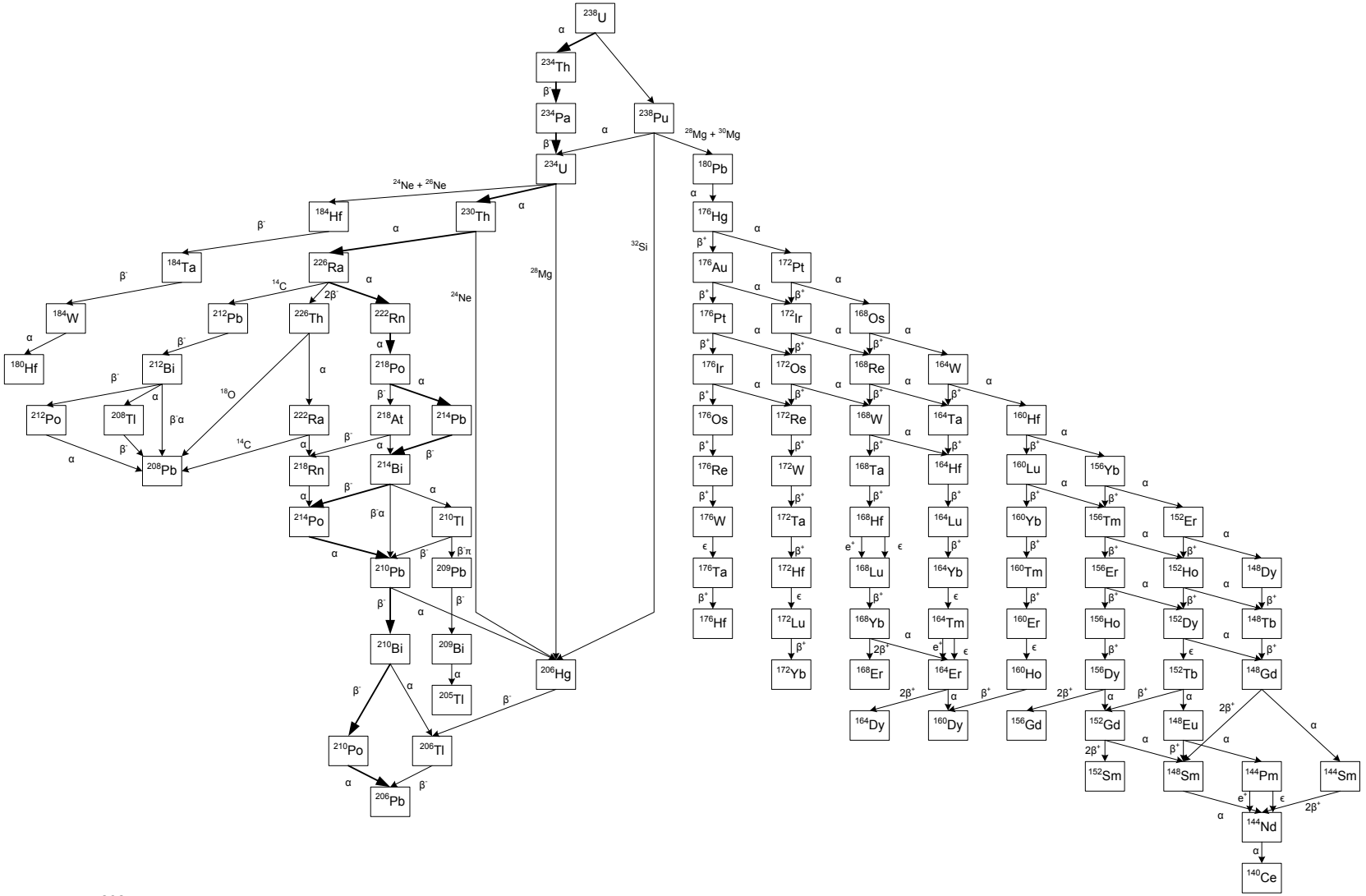

Figure 2.2. ^{238}U decay sequence. Bold arrows represent the most likely decay path. (Adapted from Gray 2007b)

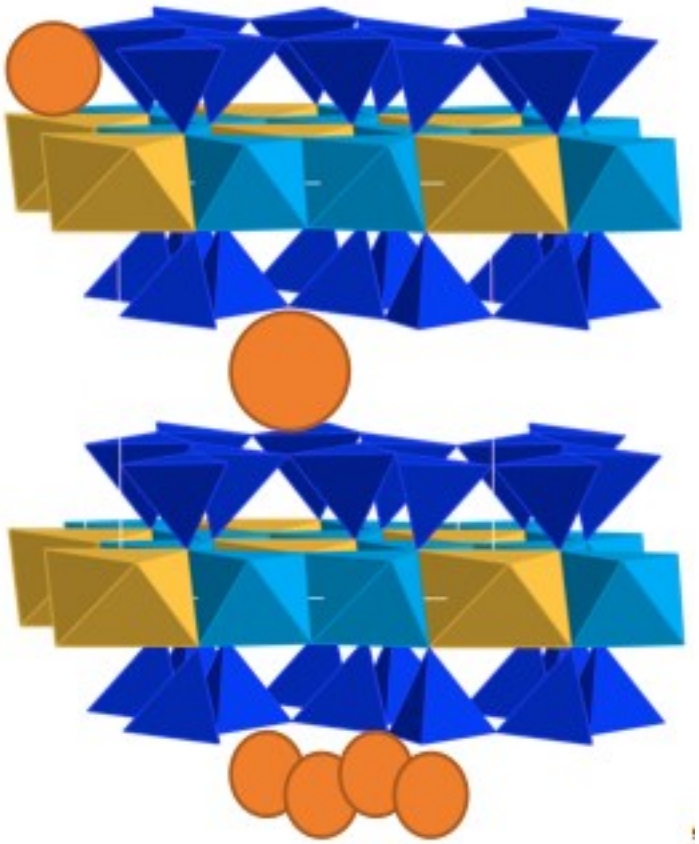

Figure 2.3. Montmorillonite structure depicting adsorption (top), absorption (middle), and surface precipitation (bottom). The montmorillonite structure is depicted by the 2:1 ratio of tetrahedral (dark blue) to octahedral (yellow and light blue) layers, with expansion possible due to the forces acting on the interlayers. Adsorption is the 2-D accumulation of a species on an external surface. Absorption occurs when accumulation enters into a particle, with diffusion into the interlayers of the clay structure. Precipitation is 3-D accumulation on the external surface of the particle.

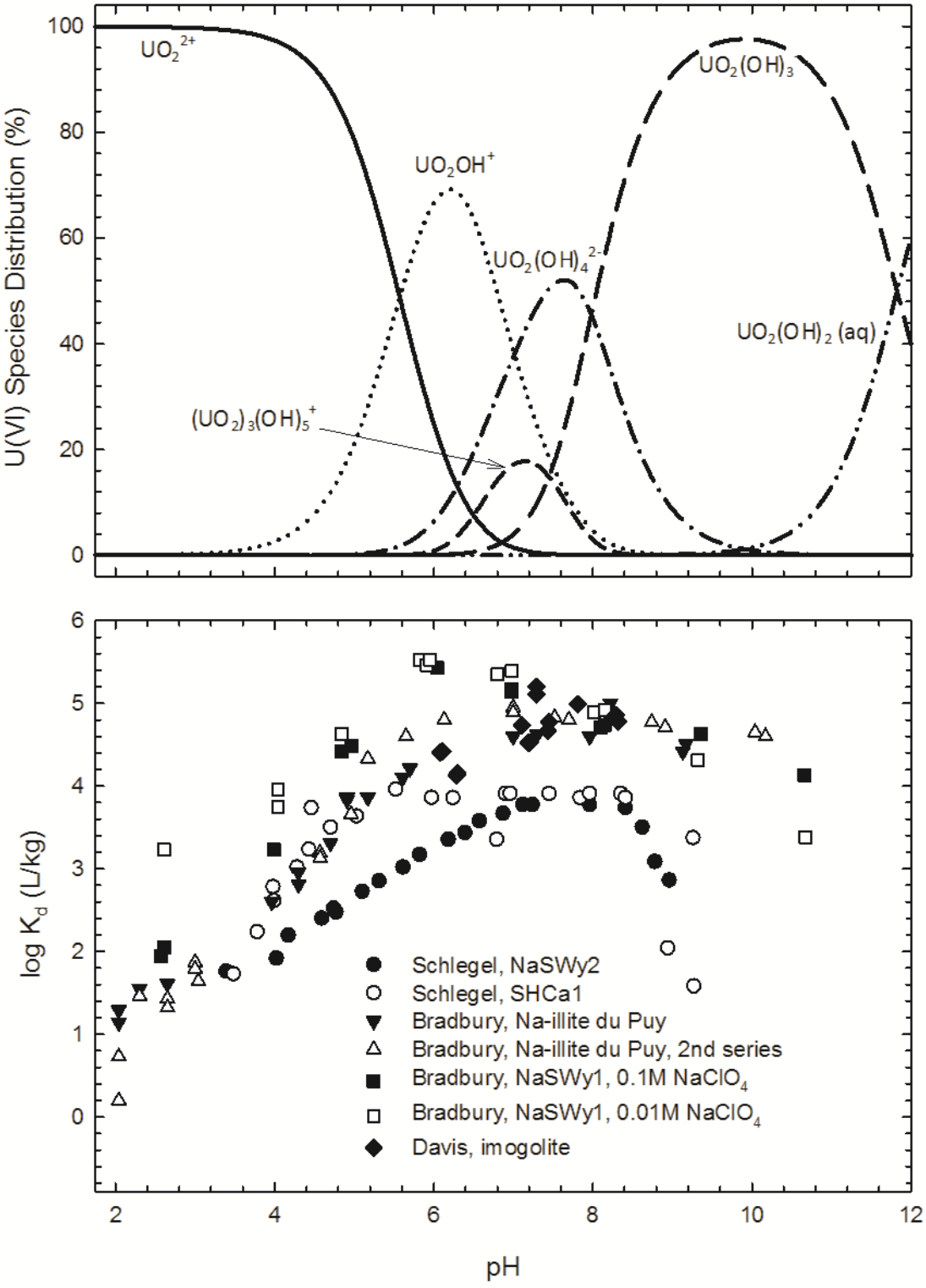

Figure 2.4. Uranium speciation and sorption on clay minerals. (Sources: Bradbury and Baeyens 2005a; Davis et al. 2004; Schlegel and Descostes 2009)

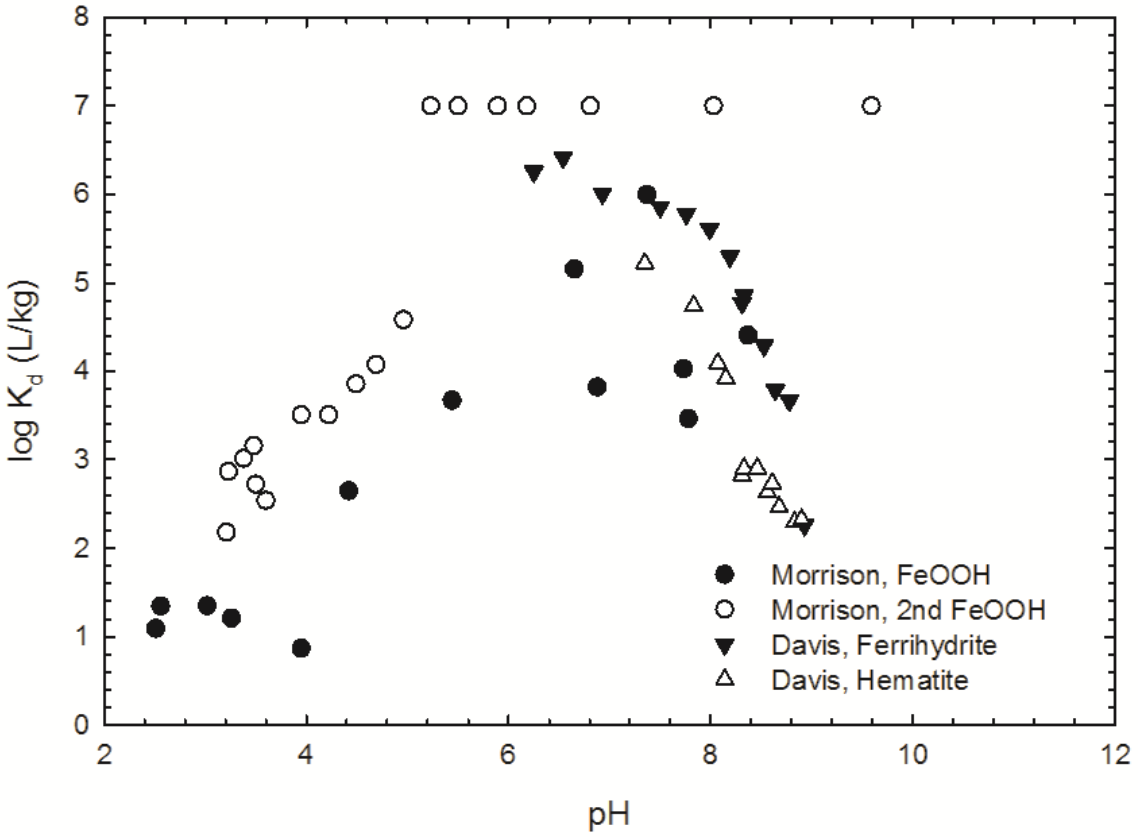

Figure 2.5. Uranium sorption on iron minerals. (Sources: Morrison and Spangler 1992; Davis et al. 2004)

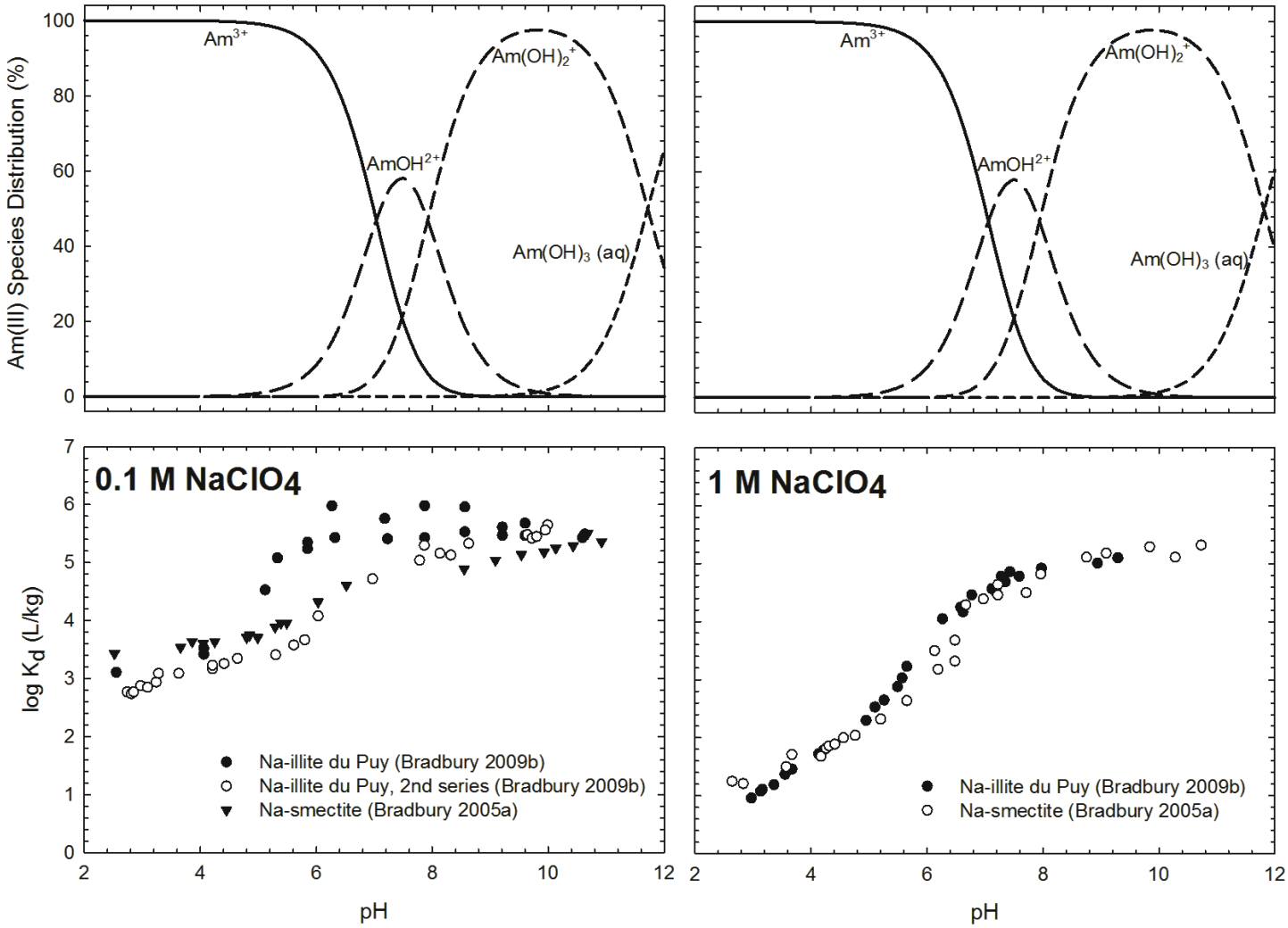

Figure 2.6. Americium speciation and sorption in 0.1 M and 1 M $NaClO_4$. (Sources: Bradbury and Baeyens 2005a and 2009b)

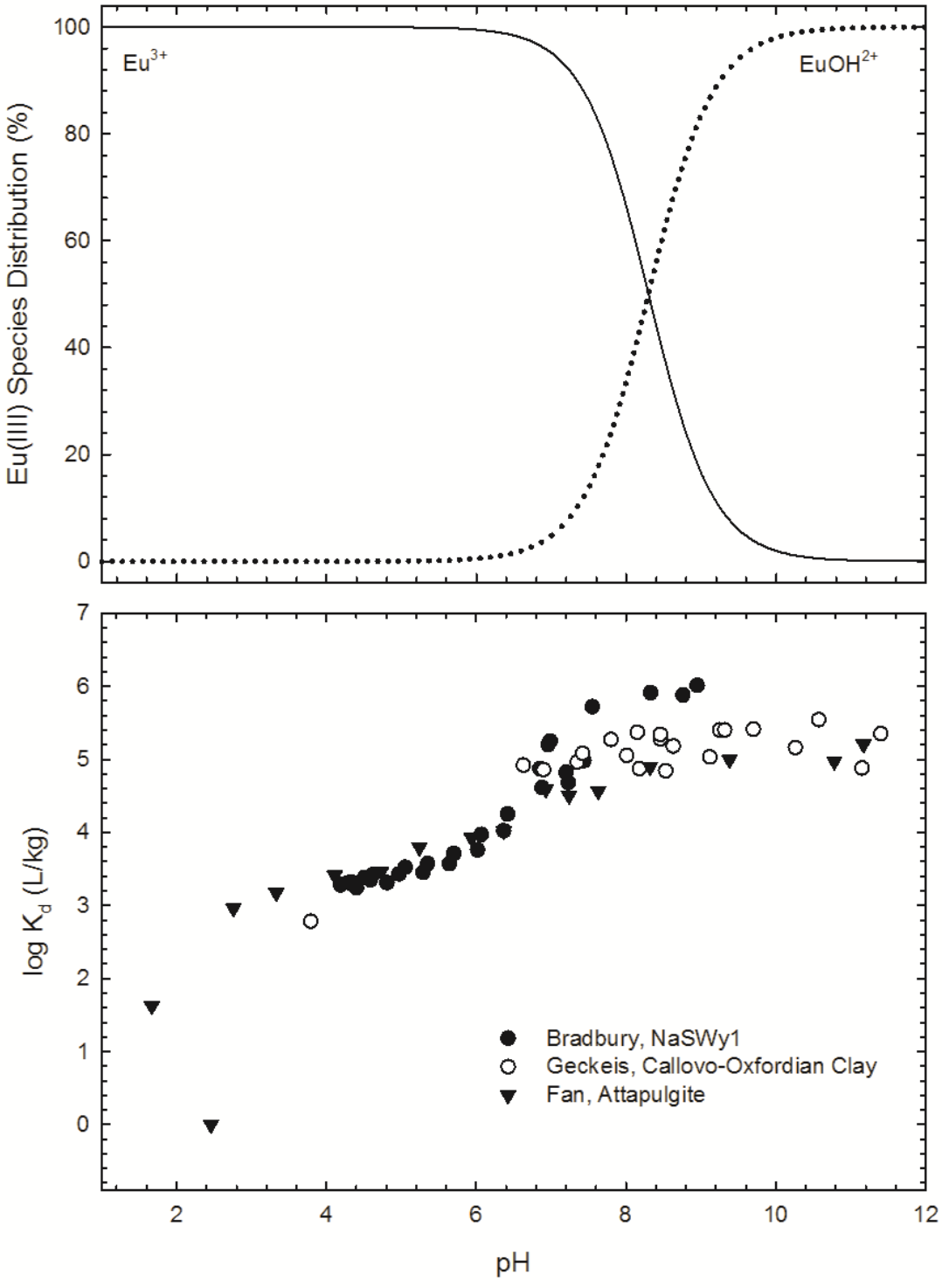

Figure 2.7. Europium speciation and sorption. (Sources: Bradbury and Baeyens 2005b; Fan et al. 2009; Geckeis and Rabing 2008)

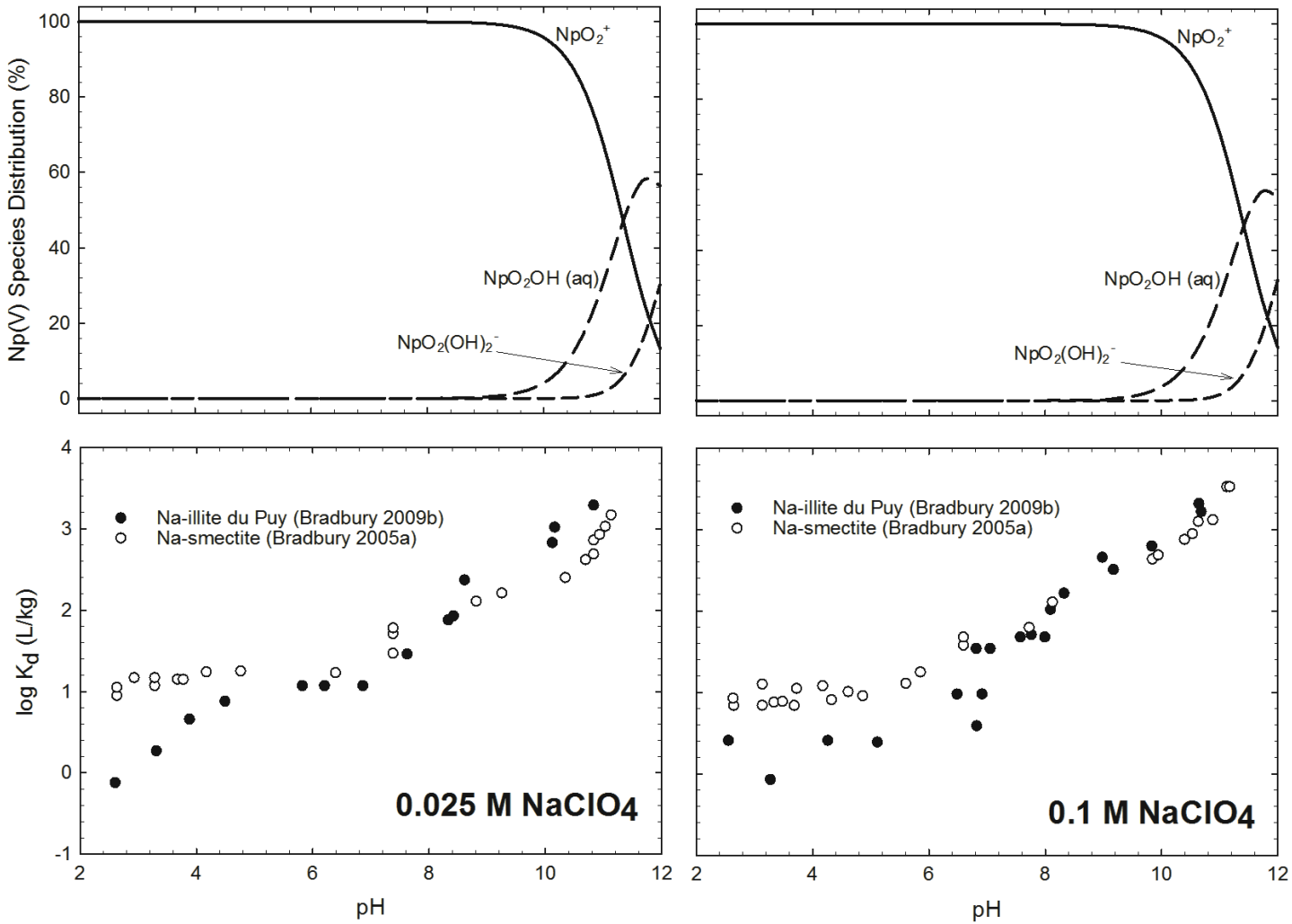

Figure 2.8. Neptunium speciation and sorption in 0.025 M and 0.1 M $NaClO_4$. (Sources: Bradbury and Baeyens 2005a and 2009b)

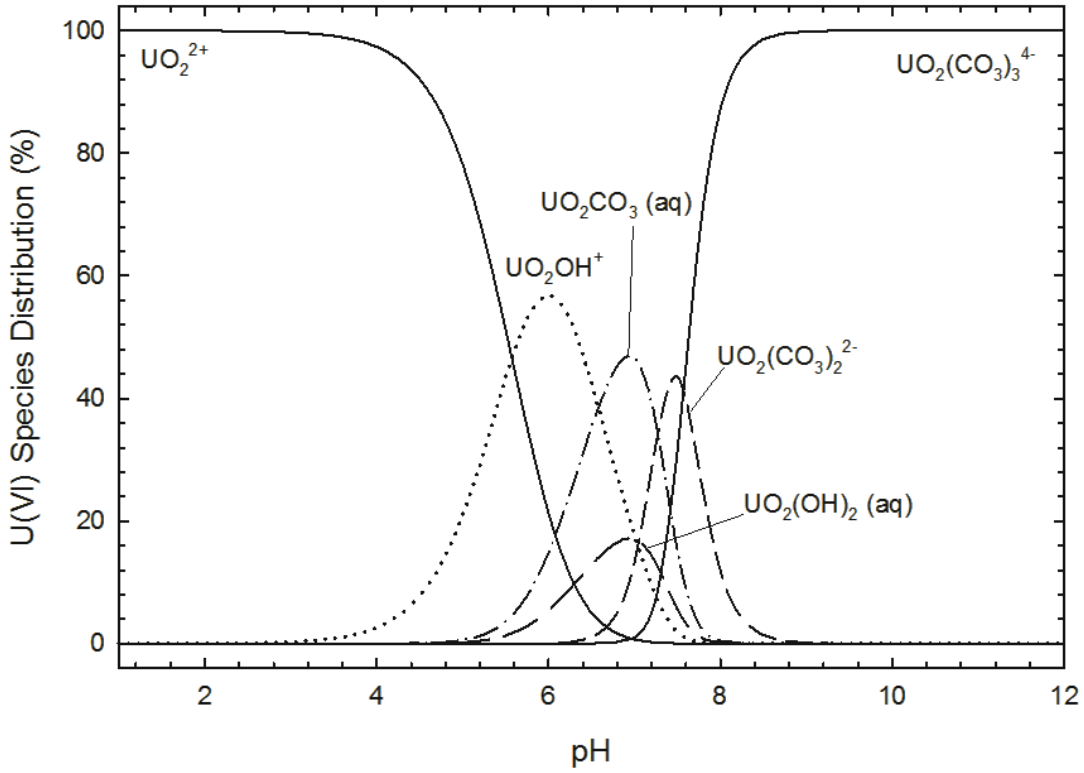

Figure 2.9. U(VI) speciation in the presence of atmospheric CO_2. In addition to the displayed species, four additional species occur at concentrations less than 2.5% of the total U(VI) species distribution: $(UO_2)(OH)_2^{2+}$, $(UO_2)_3(OH)_5^{+}$, $(UO_2)_4(OH)_7^{+}$, and $UO_2(OH)_3^{-}$.

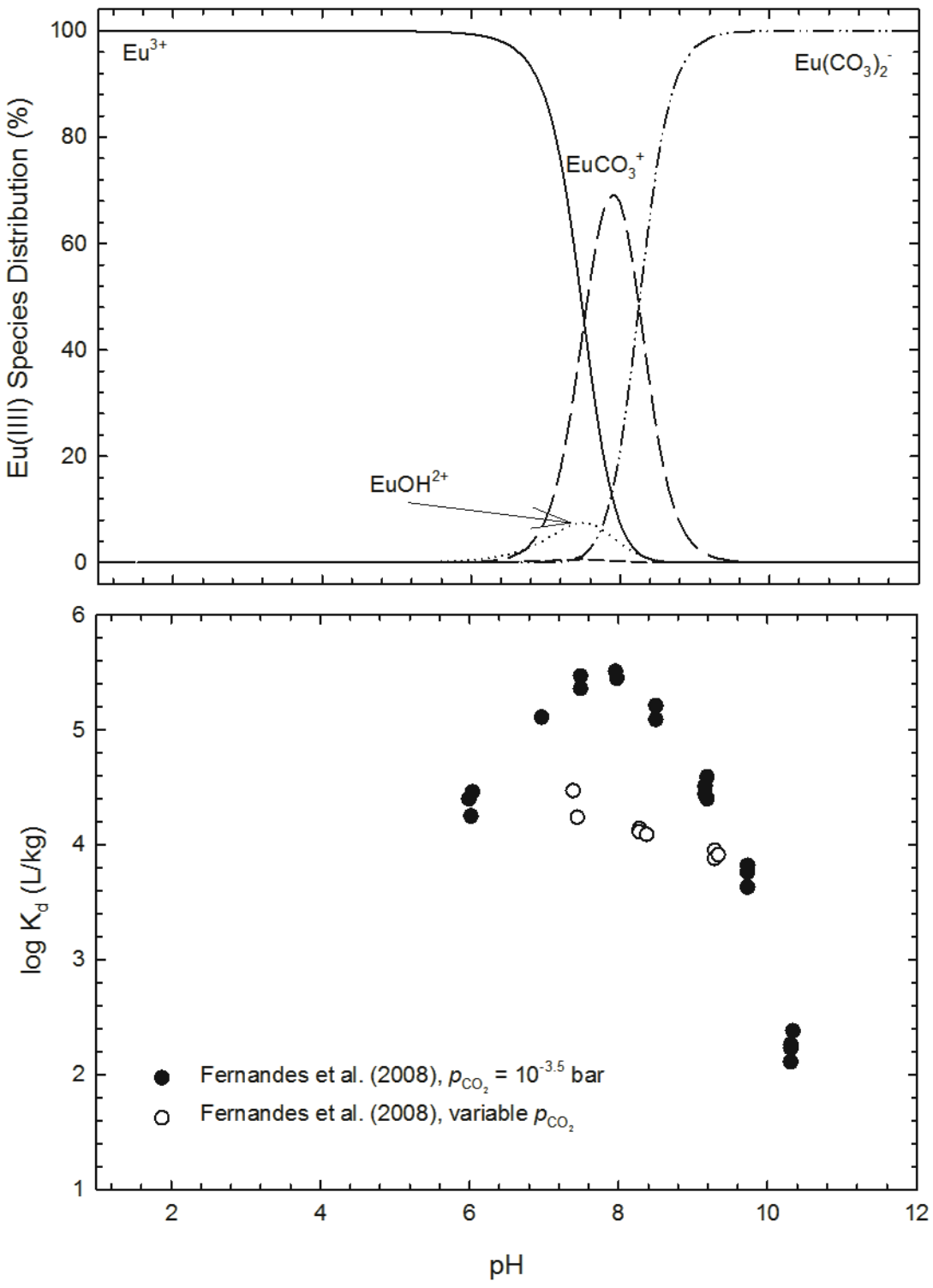

Figure 2.10. Eu(III) sorption in the presence of CO_2 . Note that some species may be missing due to lack of thermodynamic constants within the modeling database. (Source: Fernandes et al. 2008).

Section 3 – Chemical Characteristics of Leachate in Low-Level Radioactive Waste Disposal Facilities

K. Tian, E.L. Hunter, J.M. Tinjum, and C.H. Benson

3.1 Abstract

Leachate from low-level radioactive waste (LLW) is a potential pollutant to groundwater and surface water due to the presence of heavy metals and radionuclides. Many LLW disposal facilities have been built in the U.S.; however few studies have focused on the composition and characteristics of LLW leachate. Leachate data presented in this paper were collected at and analyzed by four LLW disposal facilities associated with the U.S. Department of Energy (DOE). Pollutants in LLW leachate can be categorized into three groups: inorganic macro-components, trace heavy metals, and radionuclides. As municipal solid waste (MSW) leachate has been thoroughly investigated in prior studies, cross-comparison allows more detailed characterization of LLW. LLW leachate contains little organic carbon and concentrations of inorganic macro-components and trace heavy metals that remain relatively constant over time. However, the concentrations of certain radionuclides (total uranium, tritium, technetium-99, and strontium-90) are significant in LLW leachate. Characterization of LLW leachate provides critical base-line information for design of future LLW containment structures.

3.2 Subject Headings

Radioactive wastes, landfills, waste management, leaching

3.3 Introduction

Low-level radioactive waste (LLW) is nuclear waste primarily generated by government facilities, industries, and medical diagnostic processes. LLW is distinguished

from waste materials incidental to processing, high-level waste, and uranium mill tailings (U.S. NRC 2002). LLW typically contains waste items such as contaminated protective shoe covers and clothing, reactor water treatment residues, equipment and tools, luminous dials, medical tubes, and other items incidental to radioactive work (U.S. NRC 2002). LLW, like all radioactive waste, is characterized by radioactive decay, a process in which an unstable atomic nucleus loses energy by emitting ionizing particles. The half-life ($t_{1/2}$), or the time required for half of the original radioactive material to decay, of some radionuclides requires hundreds, or even millions of years. As examples of radionuclides potentially present in LLW, the $t_{1/2}$ of ^{90}Sr is 28.8 years while the $t_{1/2}$ of ^{79}Se is 0.327 million years. The radioactivity of LLW can range from just above natural background levels to highly radioactive levels in certain cases (e.g., parts from inside reactor vessels at nuclear power plants).

LLW is generally disposed in near-surface facilities designed and constructed to prevent contamination to the surrounding environment. A multi-liner system is typically used to isolate LLW. Similar to municipal solid waste (MSW) landfill facilities, multi-layer systems for LLW consist of low permeability liners, a leachate collection system (LCS), a leak detection system (LDS), and a groundwater monitoring system, as shown in Figure 3.1. Additionally, LLW is commonly packaged in steel, concrete, lead, or other encased disposal containers (U.S. NRC 2002). Based on reports from the U.S. Department of Energy (DOE), DOE disposal facilities received over 3.3×10^6 m^3 of LLW through 1997 (U.S. DOE OEM 2000). Further, an estimated 8.1×10^6 m^3 of additional LLW will be disposed in DOE facilities by 2070 (U.S. DOE OEM 2000). DOE disposal facilities include those associated with the Waste Management Program (1.5×10^6 m^3), current Comprehensive Environmental Response, Compensation, and Liability Act (CERCLA) sites (5.4×10^6 m^3), and planned future CERCLA facilities (3.9×10^5 m^3) (US DOE OEM 2000).

The containment and isolation of LLW over a design lifetime that may exceed 1000 years is procedurally different than that of MSW disposal and containment. LLW barrier systems are expected to provide low permeability, low diffusivity, and effective retardation to minimize long-term contaminant migration. Grambow (2008) identified the need for characterizing the stability of radioactive waste forms on a three-fold basis: homogeneity of the waste, low long-term dissolution rates, and low interfacial solution concentrations of mobile radionuclides. These factors can be contextualized in the short-term by evaluating the composition of leachate from LLW disposal facilities.

During the operational life of a LLW facility, leachate originates as precipitation that subsequently travels through the waste layers and the containment system. Solid contaminants dissolve in the infiltrating water through a combination of physical, chemical, and microbial processes and interactions within the waste (Christensen and Kjeldsen 1989). The resulting leachate poses a potential risk to groundwater and surface water, dependent on the chemical composition. Specific radionuclides identified by the NRC Regulation 10 CFR 61.55 (2001), Inyang et al. (2009b), and Kaplan et al (1998) and noted for their inclusion in LLW are highlighted in Table 3.1.

Two main factors control the transport of radionuclides: radionuclide speciation and barrier attenuation processes. Radionuclides can display both cationic (^{60}Co, ^{137}Cs, and ^{90}Sr) and anionic (^{129}I, ^{79}Se, and ^{99}Tc) tendencies as a consequence of speciation (Wang et al. 2010). Cationic behavior, where the species of interest has a positive charge, is typically characterized by increasing sorption with increasing system pH, while anionic species, those with negative charge stemming from excess electrons, have decreasing sorption with increasing system pH. The opposing pH and ionic tendencies exhibited by various radionuclides create difficulties in finding methods and materials to address full suites of behaviors resulting from mixed waste streams. Um and Serne (2005) reported that ^{99}Tc and ^{125}I, acting as anions, had no or little sorption affinity,

respectively, across a range of pH values for sediments from the Hanford LLW disposal facility site, suggesting ease of transport outside of containment. ^{75}Se, although also an anion, demonstrated increased sorption affinity, indicating intermediate retention to the Hanford soils, while ^{90}Sr, acting as a cation, had significant sorption affinity, suggesting strong retention (Um and Serne 2005). The high mobility of ^{99}Tc in soils arises in part from repulsion of its anionic species ($^{99}TcO_4^-$) to the increasing negative surface charge of soils above neutral pH (Zachara et al. 2007a), while ^{90}Sr can be strongly retarded due to having similar chemical properties and behaviors as Ca (Rimstidt et al. 1998). In addition to the influence of speciation on sorption behavior, radionuclides, like other metals, can display multiple sorption mechanisms, often dependent on the pH of the system. As an example, Missana et al. (2004) indicated that Cs sorption typically results from ion exchange for molecules of higher affinity, while U experiences both ion exchange at low pH and surface complexation above pH 6. Consequently, even though many radionuclides may be present in LLW, there is the possibility that some may not be present in LLW leachate due to low initial concentrations and attenuation processes occurring during transport through the waste. Further, the presence of additional materials (such as calcium, carbonate, and organics), coupled with interactions between multiple radionuclides can alter the potential sorption mechanisms. Viable mechanisms affecting sorption may differ between radionuclide and barrier material combinations, but the potential for sorption is primarily controlled by factors influenced directly by the leachate composition and chemistry. Truly effective systems must account for all facets affecting sorption within a disposal system to understand relational impacts between components.

Few studies have been published summarizing the concentration of radionuclides and other chemical components in LLW leachate. Without this baseline information, the impact of LLW leachate on the surrounding environment would be

difficult to estimate in the event of a disposal facility leakage. Moreover, limited information is available in the literature focused on the behavior of barrier system components in contact with LLW leachate, such as the long-term durability of HDPE geomembranes, hydraulic conductivity of geosynthetic clay liners (GCLs), and sorption capacity of barrier soils exposed to LLW leachate. Many studies have evaluated natural and geosynthetic material behavior in containment applications. For example, Rowe et al. (2009) conducted a ten-year study on the durability of HDPE geomembrane in MSW barrier systems through immersion testing with synthetic MSW leachate based on the Keele Valley Landfill leachate, while Gulec et al. (2004) studied the effects of acid mine drainage (AMD) on HDPE geomembrane properties with synthetic AMD leachate. Studies have determined the hydraulic conductivity of GCLs exposed to inorganic salt solutions (Jo et al. 2005), aluminum residue leachate (Benson et al. 2008a), alkaline solutions (Gates and Bouazza 2010), and MSW leachate (Rosin-Paumier and Touze-Foltz 2012), as well as in composite liner systems (Rowe 2005). Compared with these solutions, LLW leachate has an important additional component — radionuclides, where the implication for radiation affects on the long-term behaviors of geosynthetic materials remains unclear.

The primary objective of this paper is thus to analyze the leachate composition from four LLW disposal facilities associated with the DOE, as described in the following section. Based on data from the four disposal facilities, LLW leachate composition was divided into three categories. To better understand the materials present in LLW, LLW leachate was compared to MSW leachate. As MSW leachate has been extensively studied (Christensen and Kjeldsen 1989, 1995; Christensen et al. 1998; Fatta et al. 1999; Saarela 2003; Mor et al. 2006), the range of chemicals present in MSW have been summarized and temporal concentration changes comprehensively discussed. Comparison between LLW and MSW leachates can provide an approach to better

understanding both the inert and radioactive components of LLW leachate. Further, understanding of LLW leachate composition can be used to help predict natural and geosynthetic liner material behavior in LLW disposal facilities.

3.4 Methods

3.4.1 Leachate Data Collection

Leachate was collected at four DOE-operated LLW disposal facilities: the Environmental Restoration Disposal Facility (ERDF) in Hanford, WA; the On-Site Disposal Facility (OSDF) in Fernald, OH; the Idaho CERCLA Disposal Facility (ICDF) in Idaho Falls, ID; and the Environmental Management Waste Management Facility (EMWMF) in Oak Ridge, TN.

Built in 1996, ERDF only accepts LLW generated from environmental restoration activities pertaining to CERCLA requirements at the Hanford site (U.S. DOE 2012). The capacity of ERDF increased to 1.64×10^7 tons of waste with the addition of two disposal cells completed in January 2011. LLW at the site includes contaminated soil, waste, and debris generated from building demolition. Monitoring of the LLW leachate began in 1999.

OSDF was designed for the cleanup of the Fernald, Ohio, site on behalf of the DOE and occupies approximately 36 ha (Powell et al. 2011). OSDF comprises eight individual cells, with the last cell closed in 2006 (Powell et al. 2011). The project was completed in 2006. Approximately 2.25×10^6 m^3 of contaminated soil and foundations were excavated to achieve cleanup levels established by the U.S Environmental Protection Agency (EPA). The leachate data in this paper were collected from 2005 to 2010.

ICDF is a disposal facility accepting both LLW and mixed low-level radioactive waste (MLLW) generated from remediation activities at the Idaho National Laboratory

(Benson et al. 2007). ICDF's first landfill cell and the evaporation pond were completed in September 2003. A second cell began receiving waste in February 2006. The included leachate data represent only the LLW portions of the facility and were collected from 2003 to 2010.

EMWMF, with a total capacity of approximately 1.3×10^6 m^3, is approved for disposal of LLW as defined in Subtitle C of the Resource Conservation and Recovery Act, as well as hazardous wastes defined by the Toxic Substances Control Act (Benson et al. 2008b). Contaminated soils and demolition debris dominate the waste stream at EMWMF. EMWMF began to accept LLW in 2003, and the leachate data discussed covers the years from 2003-2010.

LLW leachate samples are collected from the LCS installed at each of the 4 sites. Samples were collected in plastic or glass bottles that have been cleaned and rinsed with reagent water, following the EPA's SW 846. At OSDF, samples were collected from sample ports at the bottom of the LCS. If the volume of a sample from the discharge lines was insufficient, the samples were collected from LCS tanks using dedicated Teflon bailers.

3.4.2 Leachate Chemical Analysis

Various analytical methods, as deemed appropriate by the separate facilities, were used to determine the chemical composition of the leachates. Table 3.2 lists the specific analytical methods that were used in analyzing the leachate at each site. EPA methods 9060 and 415.1 were used to analyze total organic carbon (TOC) in LLW leachate at the OSDF and EMWMF sites, respectively. Inductively coupled plasma-atomic emission spectrometry (ICP-AES) was used per EPA method 6010C as part of SW-846 to determine metals in solution at all four LLW sites. Sulfate and chloride were measured via ion chromatography through EPA method 300.0.

Standardized methodology was not used for the radiological analyses at all four sites. For uranium, both alpha spectroscopy and relevant methods within EPA SW-846 were used for analysis. Beta-emitting isotopes were detected by liquid scintillation counting at all four sites, and different gamma rays were collected and analyzed by a gamma-ray spectroscopy system.

3.5 Results and Discussion

The concentration of LLW leachate compositions varied significantly between the 4 disposal facilities. In general, LLW leachate components can be grouped into three categories (accompanying tables are listed):

i) Inorganic macro-components including major cations (Ca, Mg, Na, and K) and major anions (Cl, SO_4^{2-}, HCO_3^-, and NO_3^-/NO_2^-) (Table 3.3)

ii) Trace heavy metals, such as Al, As, Ba, Cu, Fe, Li, Mn, Ni, Sr, and Zn (Table 3.3)

iii) Radionuclides (Tables 3.4 and 3.5).

Kjeldsen et al. (2002) divided MSW leachate compositions into four categories: dissolved organic matter, inorganic macro-components, heavy metals, and xenobiotic organic compounds. Two of the three groups are common to both MSW and LLW leachate (namely inorganic macro-components and heavy metals); however, LLW leachate contains higher radionuclide concentrations and lacks xenobiotic organic compounds due to a lack of organic wastes within the overall waste composition. Other elements, such as Se, Hg, Ag, and Co, may be found in LLW leachate, but are generally at concentrations near or below method detection limits (MDLs), and are therefore less important for understanding the overall leachate composition. Volatile organic compounds were also measured at the LLW sites, but concentrations were below MDLs.

Total organic carbon (TOC) is an important MSW leachate parameter dependent on the presence of organic degradation products, as indicated by Kjeldsen et al. (2002) with the inclusion of dissolved organic matter as a MSW leachate category. The decomposition of organic matter generates components with varying molecular weight, ranging from small volatile acids to refractory fulvic- and humic-like compounds (Chian and Dewalle 1977). Low concentrations of total organic carbon were measured at the three reporting LLW sites (ICDF data did not contain TOC measurements), ranging from 0.86 to 48.1 mg/L, with a mean of 7.78 mg/L (Table 3.3). Comparatively, Kjeldsen et al. (2002) reported that the concentration of total organic matter in MSW was between 30 and 29000 mg/L. The very low TOC concentrations in LLW leachate are likely a result of waste composition. As mentioned previously, LLW is generated by government, industries, and medical facilities and contains a high percentage of inorganic components and very little organic matter, due to the significant presence of contaminated soil and debris. Alternatively, MSW waste includes organic rubbish, such as food, yard trimmings, cloth, and leather items (Daskalopoulos et al. 1998). Due to the low concentrations of TOC in LLW, organic matter has been not been considered a significant component of the leachate. Therefore, the composition of LLW leachate is divided into three categories, similar to those described for MSW, with the third category comprised of radionuclides.

Table 3.3 presents the measured leachate parameters based on field data from the four LLW sites as well as comparisons to MSW sites. LLW leachate data from OSDF, ERDF, and ICDF exhibit relatively constant component concentrations over time, while the leachate components at EMWMF temporally vary. Across the 4 sites, LLW leachate contains very low concentrations of organic carbon, low heavy metal concentrations, and concentrations of inorganic macro-components comparable to MSW leachates. The concentrations of all detected radionuclides at the four LLW sites are

shown in Table 3.4; however, only four isotopes are considered to be significant: Uranium, Tritium, Technetium-99, and Strontium-90.

Few studies have focused on the decay processes of LLW leachate, and no clear decomposition phases have been observed. However, the decomposition mechanisms and leachate composition of MSW have been comprehensively studied for several decades (Farquhar and Rovers 1973; Ehrig 1988; Christensen and Kjeldsen 1989; Kjeldsen et al. 2002). Comparisons are made between the chemical composition of LLW leachate and MSW leachate, in order to provide better context to understand LLW leachate composition.

The pH for LLW leachate changes over a relatively small range (5.7-9.1) and most pH data only range from 6-8 (Figure 3.2 (a)). Figure 3.2(b) shows that pH values for LLW leachate did not change with time at any of the four sites. The pH temporal consistency may be due to the lack of organic materials found in LLW, leading to little pH change expected during the waste stabilization process. Zachara et al. (2007a) found that for natural sediments in the Hanford vadose zone the pH range is approximately 7 to 8.5. Since the major waste source at ERDF is contaminated Hanford soil, the pH of the LLW leachate mirrors that of the waste. In contrast, the pH of MSW leachate changes significantly during landfill decomposition, described by Farquhar and Rovers (1973) as involving an aerobic phase, an anaerobic acid phase, an initial methanogenic phase, and a stable methanogenic phase. Ehrig (1988) indicated that pH decreases during the anaerobic acid phase, when easily degradable organic compounds are highly concentrated. In the later stable methanogenic phase, pH increases and the ratio of biological oxygen demand to chemical oxygen demand (BOD/COD) decreases, indicating that the most easily degradable organic carbon has decomposed. Therefore, the concentration of certain inorganic chemical compositions in MSW leachate changes

with landfill decomposition phases. Due to the lack of organic carbon present in LLW, no pH change with decomposition is expected when compared to MSW landfills.

3.5.1 Inorganic Macro-components

The concentrations of inorganic macro-components, including major cations and anions, are listed in Table 3.3 with total concentration ranges and average concentrations based on the collected LLW leachate data. The concentrations of many dissolved inorganic macro-components in LLW leachate could be controlled by dissolution and precipitation of mineral phases from contaminated soils (e.g., Ca^{2+}, Mg^{2+}, and CO_3^{2-} in calcite and dolomite) and sorption and desorption from the surface of clay minerals.

The concentrations of major cations (Ca^{2+}, Mg^{2+}, K^+, and Na^+) are shown in Figure 3.3. Ca^{2+} and Mg^{2+} levels in LLW and MSW leachate are comparable (Figure 3.3 (a) and (b)), while the concentrations of K^+ and Na^+ in LLW are an order of magnitude lower than MSW leachate (Figure 3.3 (c) and (d)). Figure 3.4 presents the change in concentration of major cations with time at the four LLW disposal sites. The concentrations of all major cations are relatively constant at OSDF, ERDF, and ICDF, but vary over time at EMWMF. The concentration of Mg^{2+} at the EMWMF site increases linearly during all recorded years, while the concentration of the other major cations (Ca^{2+}, K^+, and Na^+) increase slowly in the first six years and then sharply for the following four. Since EMWMF is still operating, new disposed waste sources might be influencing the varying trend. The concentrations of Ca^{2+} and Mg^{2+} are much higher at OSDF than at the other three LLW sites. Gravel used to construct the LDS and LCS at OSDF consisted of crushed limestone, making carbonate minerals (such as calcite and dolomite) the dominant solids in contact with atmospheric precipitation at OSDF (U.S. DOE OLM 2008). Moreover, the majority of waste at OSDF is contaminated soils

comprised of glacial tills, which contain 40% to 70% carbonate on average (U.S. DOE OLM 2008). These factors may explain why the leachate from OSDF has higher Ca^{2+} and Mg^{2+} concentrations than the other sites. Christensen et al. (2001) indicated that Ca^{2+} and Mg^{2+} are lower in the methanogenic phase of MSW decomposition due to the higher pH and lower concentration of dissolved organic matter present. However, the pH of LLW leachate is relatively constant over time and the concentration of TOC remains at a low level. Therefore, the concentrations of major cations do not change significantly with time.

Figure 3.5 shows the concentrations of major anions: sulfate (SO_4^{2-}), chloride (Cl^-), and nitrate/nitrite (NO_3^-/NO_2^-). All four LLW sites have higher average concentrations of SO_4^{2-} and NO_3^-/NO_2^- than MSW leachate. The concentrations of Cl^- at the four sites are between one and two orders of magnitude lower than those for MSW leachate. Due to the characteristics of their waste streams, OSDF and ERDF in particular have high concentrations of SO_4^{2-} (Figure 3.5 (a)). At both sites, large amounts of drywall and concrete debris were disposed, which may contribute to the high concentration of SO_4^{2-}. Figure 3.6 demonstrates the concentration change with time for the major anions. In general, similar to the major cations, the concentrations of anions at OSDF, ERDF, and ICDF remain relatively constant, but vary over time at EMWMF. The concentration of sulfate at the EMWMF site increased sharply in the first two recorded years then decreased from the second to fourth year, and finally increased slightly from the fourth through the sixth year. Sulfate's changing trend is additionally mirrored by the concentration of radionuclides in LLW leachate at the EMWMF site.

3.5.2 Trace Heavy Metals

The concentration of heavy metals varies widely at the four LLW sites, but the average trace metal concentrations are very low when compared with MSW leachate

(Figure 3.7). Average concentrations for Al, As, Ba, Cu, Fe, Li, Mn, Sr, and Zn can be found in Table 3.3. Additional elements, including, Co, Cd, and Cr, are also found in LLW leachate, but at concentrations at or below minimum detection levels and are of less relative importance. Figure 3.8 shows the changing concentration of trace metals at each site, in general, no obvious trends are observed

Heavy metal concentrations in LLW leachate can be explained by the limited sources of metal in LLW. Kjeldsen et al. (2002) indicated that Fe and Mn can be considered to be inorganic macro-components in MSW leachate due to their higher concentration level. The high level of Fe in the MSW leachate may be a result of the large amount of iron and steel scrap disposed with MSW. However, while LLW contains potential sources of iron, especially from disposed soils at the ERDF site, the low solubility of Fe(III) in soil controls Fe availability in LLW leachate, leading to low Fe concentrations. In LLW leachate, Fe is still present at high concentrations compared with other trace metals, but significantly lower concentrations than the major cations and anions; thus, Fe is included with the trace heavy metals rather than the inorganic macro-components. Zn and Pb typically have low concentrations in LLW due to a lack of waste sources. High concentrations of Zn in MSW leachate are attributed to the inclusion of waste from batteries and fluorescent lamps (Mor et al. 2006). Similarly, Moturi et al. (2004) indicated that the presence of Pb in MSW leachate is from the disposal of Pb batteries, chemicals for photograph processing, Pb-based paints, and pipes in MSW landfills. LLW sites might receive limited wastes that contain large amounts of Zn and Pb as a consequence of LLW composition. Metal attenuation may be another reason for the low concentrations of metals in LLW. Kjeldsen et al. (2002) indicated that sorption and precipitation are significant mechanisms for metal immobilization in MSW leachate, resulting in fairly low heavy metal concentrations. The same attenuation processes occur at LLW sites due to similar barrier systems used at both of LLW and MSW.

3.5.3 Radionuclides

Many radionuclides could potentially be found in LLW leachate due to varying waste compositions. The composition of LLW was distinct at each of the four sites, leading to multiple potentially present radionuclides in LLW. Table 3.4 lists the specific radionuclides monitored in the LLW leachate at each site. However, most radionuclides are present in concentrations at or below method detection limits. As such, the detectable radionuclides and their corresponding concentrations are listed in Table 3.5. This paper focuses on four specific radionuclides that represent the most widely prevalent and consistently measured species: total Uranium, ^{3}H, ^{90}Sr and ^{99}Tc.

3.5.3.1 Gross Alpha and Beta Activity

Two LLW landfill sites measure the gross alpha and beta activity in leachate (Figure 3.9). Increasing alpha and beta activity are discernible at ERDF for the first ten years of measurement, with a slight decrease in activity during the last two years. At EMWMF, beta activity trends upward with time; however, the alpha activity increases sharply for the first three years, decreases in the following two years, and then increases thereafter. In general, most alpha particles were emitted from uranium, while ^{99}Tc, ^{90}Sr, and ^{3}H are the dominant sources for beta activity. The gross alpha trend corresponded to the change in uranium concentration, while the gross beta trend corresponded to the combined concentrations of ^{99}Tc and ^{90}Sr. The increasing trend of radionuclides in leachate may be a unique characteristic at the ERDF site. Since EMWMF is still operating, the complex variation in activity might be a result of new waste sources actively being disposed.

3.5.3.2 Total Uranium

Uranium is an element found naturally occurring with three isotopes: ^{238}U with $t_{1/2}$ ~ 4.47×10^{9} yr; ^{235}U with $t_{1/2} = 7.04 \times 10^{8}$ yr; and ^{234}U with $t_{1/2} = 2.46 \times 10^{5}$ yr. Uranium

was measured in µg/L at the OSDF, ERDF, and EMWMF sites. The uranium concentration present in natural waters depends upon the surrounding geology (Bakaç and Kumru 2000). Langmuir (1997) indicated that the concentrations of uranium in natural waters range from 0.1 µg/L to 7 µg/L, while concentrations in seawater are higher, ranging from 2 µg/L to 4 µg/L. Another study found that the median concentration of uranium is 20 µg/L in Russian lake water and 41 µg/L in Norwegian lakes (Reimann et al. 1999). Øygard and Gjengedal (2009) found uranium concentrations less than 3.1 µg/L in MSW landfill leachate, similar to concentrations expected for naturally occurring water around the landfill. However, uranium occurs at significantly higher concentrations in LLW leachate (Figure 3.10) as a consequence of the disposed wastes. For example, a significant amount of contaminated soil, waste, and debris were disposed at the OSDF, ERDF and EMWMF sites due to CERCLA cleanup actions. Dong et al. (2005) indicated that uranium (VI) adsorption in a calcite-saturated solution increases as a function of pH from 7.2 to 8.5, and then the adsorption decreases as the pH increase from 8.5 to 10. Since the pH at each of the four LLW sites is close to neutral, retardation of uranium may be limited, particularly below pH 7.2. Additionally, the presence of Ca-carbonate can reduce the sorption of uranium because calcite coatings can block the highly reactive surface sorption sites and a strong aqueous complex ($Ca\text{-}U\text{-}CO_3$) can form in solution (Um et al. 2007). Ca-carbonate occurs in the LLW leachate at all LLW sites, potentially resulting in enhanced U transport through barrier systems. At OSDF and ICDF, the concentrations of uranium are relatively constant (Figure 3.10 (a)); however, uranium concentrations increased from 212 µg/L to 3060 µg/L at ERDF from 1999 to 2009, and then dropped to 1480 µg/L in 2010. The average uranium concentration was 780 µg/L across the four LLW sites.

3.5.3.3 Technetium-99

^{99}Tc is the primary radioactive isotope of technetium with a half-life of 2.11×10^5 years. Another important species of technetium is the metastable isomer ^{99m}Tc, which is used in nuclear medicine, and is produced from molybdenum-99. ^{99m}Tc is a short-lived isotope with a half-life of around 6 h, which decays by isomeric transition to ^{99}Tc. ^{99}Tc is one of the more problematic components of nuclear waste due to its long half-life and significant mobility as an anionic species in the environment. Um and Serne (2005) concluded that ^{99}Tc, as pertechnetate, TcO_4^-, is largely not adsorbed onto Hanford sediments. Consequently, ^{99}Tc is expected to be highly mobile in LLW disposal facilities, making ^{99}Tc a risk for the long-term disposal of LLW. ^{99}Tc ranges from 0.24 Bq/L to over 47.87 Bq/L among the four LLW sites. The OSDF, ERDF, and ICDF sites show a relatively constant concentration of ^{99}Tc. Similar to Uranium, ^{99}Tc concentrations are highest (18.05 Bq/L to 37 Bq/L) at ERDF. EMWMF showed high concentrations of ^{99}Tc at the beginning of data collection (47.88 Bq/L), but decreased to 0.24 Bq/L in the subsequent seven years, potentially due to a limited ^{99}Tc waste source. Much of the original ^{99}Tc was likely washed out by rainwater in a short time period, resulting in the decreased concentration over time.

3.5.3.4 Strontium-90

Natural strontium is nonradioactive, but the ^{90}Sr isotope constitutes a radioactive hazard. ^{90}Sr is a byproduct of nuclear fission and present in significant quantities in spent nuclear fuel and radioactive waste from nuclear reactors. Ion exchange is a dominant mechanism for ^{90}Sr attenuation processes (Zachara et al. 2007a). Rimstidt et al. (1998) indicated that Sr has similar chemical properties to Ca. Both Sr and Ca are divalent cations in solution and have similar atomic radii (1.0 and 1.12 nm for Ca and Sr, respectively). Therefore Sr can substitute for Ca in calcite and aragonite (polymorphs of

$CaCO_3$) to form strontianite ($SrCO_3$) (Faure 2001; Rimstidt et al. 1998). Um and Serne (2005) found a high K_d value for ^{90}Sr on Hanford sediments. The concentration of ^{90}Sr in LLW leachate was monitored at the EMWMF and ICDF sites (Figure 3.10(c)). Figure 3.11(c) shows the change in ^{90}Sr concentration, which is similar to uranium at EMWMF and ICDF. ^{90}Sr increases from 0.03 Bq/L to 12.43 Bq/L at the ICDF site over the observation period. The concentration of ^{90}Sr appears to stabilize at EMWMF with a concentration around 3.7 Bq/L.

3.5.3.5 Tritium (H-3)

Tritium is another major radionuclide found in LLW leachate and is typically produced in nuclear reactors or high-energy accelerators. Figure 3.10(d) shows the concentrations of tritium at three LLW landfill sites as well as 35 MSW landfill sites. U.S. drinking water standards stipulate a maximum contaminant level of 740 Bq/L for tritium. The concentrations of tritium at EMWMF and ICDF are lower than the drinking water standard; however, the limited data for tritium concentrations at ERDF show much higher concentrations, ranging from 3589-4625 Bq/L. The average concentrations of tritium are higher at MSW sites than LLW sites.

3.5.4 Ionic Strength and RMD

The ratio of monovalent to divalent cations (RMD) characterizes the relative abundance of monovalent and multivalent cations in leachate. Kolstad et al. (2004) defined RMD as $M_m/\sqrt{M_d}$, where M_m is the total molarity of monovalent cations in solution and M_d is the total molarity of multivalent cations in solution. Figure 3.12 compares RMD to ionic strength for MSW and LLW leachates. MSW shows a linear relationship between ionic strength and RMD. Three of the LLW leachates display similar behavior of RMD to ionic strength as the MSW leachates. The exception is OSDF, where the lower RMD value is due to high Ca and Mg concentrations.

Additionally, the high sulfate concentration present at OSDF raises the ionic strength at the site. The low concentrations of inorganic macro-components at EMWMF during the earliest measurements and continuous upward growth lead to an increased ionic strength over time.

3.6 Summary

LLW leachate data from four DOE sites display varying compositions in terms of inorganic macro-components, trace heavy metals, and radionuclides. Dissolved organic matter concentrations in LLW leachate are a non-critical leachate component when compared with MSW leachate. Concentrations of inorganic macro-components are similar between LLW and MSW leachate. For major cations, the concentrations of Ca and Mg are similar at LLW and MSW sites, while K and Na concentrations are higher at MSW landfill sites. For major anions, the sulfate concentration is much higher at LLW sites, particularly OSDF and ERDF, due to large amounts of disposed drywall and concrete debris. Trace heavy metals in LLW leachate show relatively lower concentrations compared with MSW leachate. The concentration of heavy metals is relatively constant over time at OSDF, ERDF, and ICDF. At EMWMF, the trace heavy metal concentration began to increase after 6 years of data collection.

Many radionuclides are measured at the analyzed LLW sites, but the concentrations for most are near or below method detection limits. Exceptions are the concentrations of uranium, technetium-99, strontium-90, and tritium. Different radionuclide concentrations show varying trends at different LLW sites. The leachate from ERDF has the highest uranium and ^{99}Tc concentrations among the four sites. The uranium concentration has increased sharply over time at ERDF. The concentration of ^{90}Sr at EMWEF and ICDF has also increased over time. Total alpha and beta activity in

leachate increases with time at ERDF and EMWMF. In summary, the measured radioactivity of the analyzed LLW leachate is increasing with time.

3.7 Acknowledgments

The research described in this document was conducted under the sponsorship of the US Department of Energy under Cooperative Agreement Number DE-FC01-06EW07053 entitled The Consortium for Risk Evaluation with Stakeholder Participation III awarded to Vanderbilt University. The opinions, findings, conclusions, or recommendations expressed herein are solely those of the authors and do not necessarily represent the views of the US Department of Energy.

Table 3.1. Radionuclides classified for low-level radioactive waste.

NRC 10 CFR 61.55	Inyang et al. (2009b)	Kaplan et al (1998)
^{90}Sr	**^{90}Sr**	**^{90}Sr**
^{137}Cs	**^{137}Cs**	**^{137}Cs**
^{99}Tc		**^{99}Tc**
^{129}I		**^{129}I**
^{60}Co	**^{60}Co**	
^{3}H	**^{3}H**	
^{63}Ni	**^{63}Ni**	
^{14}C	^{144}Ce	^{90}Se
^{242}Cm	^{58}Co	^{237}Np
^{59}Ni	^{51}Cr	U
^{94}Nb	^{134}Cs	
^{241}Pu	^{55}Fe	
Alpha emitting transuranic nuclides with half-life greater than 5 years	^{54}Mn	
	^{95}Nb	
Total of all nuclides with less than 5 year half-life	^{65}Zn	

Note: Bold species are common across multiple sources, while undifferentiated species are unique to a specific ruling or source.

Table 3.2. Analytical methods used in collection and analysis of LLW, based on information provided by the DOE.

Parameter	OSDF	ERDF	EMWMF	ICDF
Radionuclides				
Technetium-99	Liquid Scint.[a]	N.A.	Liquid Scint.[a]	Liquid Scint.[a]
Tritium	Liquid Scint.[a]	N.A.	N.A.	E906.0
Uranium	SW-846[b]	N.A.	SW-846[b]	ALPHASPEC
Strontium-90			N.A.	N.A.
Inorganic Cations				
Aluminum	SW-846[b]	SW-846[b]	SW-846[b]	SW-846[b]
Arsenic				
Barium				
Boron				
Calcium				
Cobalt				
Copper				
Iron				
Lithium				
Magnesium				
Manganese				
Nickel				
Potassium				
Selenium				
Sodium				
Vanadium				
Zinc				
General Chemistry				
Total Organic Halogens	9020B[b]	N.A.	N.A.	N.A.
Total Organic Carbon	9060[b]	Blank	415.1[c]	N.A.
Chloride	325.2[c], 300(all)[c]	300[c]	300[c]	300[c]
Nitrate/Nitrite	353.1[c],353.2[c], 4500D[d],4500E[d]	353.2[c]	353.2[c]	353.2[c]
Sulfate	375.2[c], 300.0[c], 4500E[d]	300.0[c]	300.0[c]	300.0[c]
Total Dissolved Solids	160.1[c], 2540C[d]	160.1[c]	N.A.	N.A.
Total Alkalinity	310.1[c], 2320B[d]	N.A.	N.A.	N.A.

Notes:

[a] Performance-based analytical specifications for these parameters are provided in Fernald Preserve Quality Assurance Project Plan. (Liquid Scint. = Liquid Scintillation)

[b] Test Methods for Evaluating Solid Waste, Physical/Chemical Methods (EPA 1998).

[C] Methods for Chemical Analysis of Water and Wastes (EPA 1983).

[d] Standard Methods for Analysis of Water and Wastewater, 17th edition (APHA 1989).

[e] Industry standard method, laboratory-specific, based on acceptance by Washington Closure Hanford.

Table 3.3. Measured parameters of LLW leachate.

Parameters	Sites	No. of Meas.	Ave.	Range	COV
pH	OSDF	42	6.87	6.07-7.86	0.06
	ERDF	36	7.57	7.1-8.2	0.04
	EMWMF	84	7.32	5.69-9.13	0.08
	ICDF	160	7.08	6.11-8.51	0.05
Oxidation Reduction Potential (mv)	OSDF	228	72.09	-94.4-321.1	1.08
	ERDF	-	-	-	-
	EMWMF	102	144.52	14-252.3	0.38
	ICDF	126	128.05	-193-344	1.06
Total Organic Carbon (mg/L)	OSDF	32	4.75	1.9-22.9	1.37
	ERDF	20	14.17	4.1-48.1	0.81
	EMWMF	31	4.28	0.86-10.4	0.52
	ICDF	-	-	-	-
	MSW[a]			30-29000	

Inorganic Macro-components (mM)

Parameters	Sites	No. of Meas.	Ave.	Range	COV
Ca	OSDF	73	12.2	1.64-24.9	0.28
	ERDF	33	5.06	3.95-6.5	0.14
	EMWMF	97	3.27	0.77-8.05	0.59
	ICDF	33	5.28	1.26-10.05	0.37
	MSW	201[b]	5.02	0.0035- 346.82	
Mg	OSDF	74	11.2	0.913-30.2	0.49
	ERDF	22	2.85	1.99-3.74	0.21
	EMWMF	97	0.89	0.20-1.43	0.31
	ICDF	33	3.03	0.84-6.33	0.38
	MSW	211[b]	6.72	0.0012-204.93	
Na	OSDF	74	1.85	0.40-4.17	0.51
	ERDF	33	7.31	8.52-14.1	0.12
	EMWMF	97	1.08	0.19-3.08	0.62
	ICDF	33	10.85	4.87-38.13	0.51
	MSW	198[b]	49.48	0.00053-1926.23	
K	OSDF	74	0.58	0.13-1.94	0.43
	ERDF	33	0.61	0.43-0.72	0.13
	EMWMF	82	0.12	0.04-0.28	0.41
	ICDF	33	0.22	0.11-0.36	0.25
	MSW	173[b]	10.05	0.00036-1458.17	

Sulfate	OSDF	74	18.5	1.52-29.6	0.36
	ERDF	49	5.26	3.38-8.65	0.19
	EMWMF	30	1.88	0.39-7.20	0.89
	ICDF	32	2.79	1.10-15.4	0.87
	MSW	193[b]	2.16	0.0021-82.23	
Chloride	OSDF	74	2.04	0.33-6.17	0.55
	ERDF	47	7.31	4.93-14	0.23
	EMWMF	31	0.54	0.12-0.97	0.42
	ICDF	32	8.9	1.71-19.27	0.47
	MSW	189[b]	22.81	0.036-236.38	
Nitrate/ Nitrite	OSDF	74	0.0766	0.000048-1.20	2.43
	ERDF	49	5.26	2.02-8.65	0.28
	EMWMF	30	0.012	0.0019-0.024	0.52
	ICDF	33	0.35	0.15-0.88	0.38
	MSW	44	0.057	0.00032-1.77	
Alkalinity	OSDF	31	3.99	2.19-5.57	0.2
	ERDF	-	-	-	-
	EMWMF	2	1.35	1.31-1.39	0.05
	ICDF	48	4.91		

Trace Metals (mM)

Parameters	**Sites**	**No. of Meas.**	**Ave.**	**Range**	**COV**
Al	OSDF	74	0.0766	0.000048-1.20	2.43
	ERDF	22	0.0014	0.00046-0.0025	0.47
	EMWMF	97	0.0088	0.00078-0.087	1.48
	ICDF	19	3.3E-05	0.0000041-0.00012	1.08
	MSW	50[b]	0.37	0.0037-33.3	
As	OSDF	18	0.00027	0.000033-0.00189	1.75
	ERDF	45	0.00012	0.000067-0.00021	0.31
	EMWMF	-	-	-	-
	ICDF	33	9.3E-05	0.00002-0.00029	0.49
	MSW	187[b]	0.00086	0.000013-0.068	
Ba	OSDF	74	0.00037	0.00016-0.00075	0.41
	ERDF	49	0.00067	0.00047-0.00093	0.17
	EMWMF	97	0.0057	0.00021-0.0033	0.52
	ICDF	19	0.0016	0.00029-0.0032	0.46
	MSW	145[b]	0.0077	0.000065-3.46	

Cu	OSDF	72	0.00019	0.000039-0.00054	0.54
	ERDF	22	0.00011	0.000039-0.00016	0.34
	EMWMF	76	3.5E-05	0.0000064-0.000085	0.62
	ICDF	19	9.1E-05	0.000023-0.00023	0.46
	MSW	172[b]	0.001	0.0000173-0.11	
Fe	OSDF	74	0.119	0.0022-1.02	1.73
	ERDF	8	0.0005	0.00022-0.000893	0.55
	EMWMF	97	0.0041	0.000204-0.043	1.49
	ICDF	17	0.0056	0.00023-0.034	1.71
	MSW	120[b]	0.25	0.0018-10.92	
Li	OSDF	58	0.029	0.0010-0.139	1.2
	ERDF	-	-	-	
	EMWMF	82	0.0007	0.00009-0.0022	0.68
	ICDF	-	-	-	-
	MSW	6[b]	0.092	0.0076-0.29	
Mn	OSDF	74	0.023	0.000091-0.132	1.51
	ERDF	-	-	-	-
	EMWMF	97	0.0015	0.000016-0.024	2.7
	ICDF	33	0.00011	0.000022-0.00074	1.2
	MSW	131[b]	0.043	0.00023-2.73	
Sr	OSDF	42	0.028	0.00279-0.055	0.43
	ERDF	-	-	-	-
	EMWMF	97	0.0036	0.00092-0.026	0.94
	ICDF	5	0.015	0.012-0.019	0.22
	MSW	7[b]	0.021	0.00083-0.051	
Zn	OSDF	68	0.00048	0.000074-0.0023	1.01
	ERDF	49	0.00015	0.0000077-0.00054	0.76
	EMWMF	97	0.00015	0.0000081-0.0015	1.18
	ICDF	33	0.00043	0.000031-0.0026	1.1
	MSW	207[b]	0.013	0.000061-3.82	

Notes: '-' means not measured at the site

'ND' means not detected

[a] Data from Kjeldsen et al., 2002.

[b] Values represent the number of MSW sites sampled.

Table 3.4. Radionuclides measured at study LLW sites.

OSDF	ERDF	ICDF		EMWMF			
U	U	U	^{54}Mn	U	^{251}Cf	^{237}Np	^{226}Ra
^{99}Tc	^{99}Tc	^{99}Tc	^{237}Np	^{99}Tc	^{252}Cf	^{59}Ni	^{228}Ra
	^{129}I	^{129}I	^{95}Nb	^{129}I	^{135}Cs	^{63}Ni	^{108m}Ag
	^{3}H	^{3}H	^{238}Pu	^{3}H	^{137}Cs	^{94}Nb	^{89}Sr
	^{14}C	^{14}C	^{239,240}Pu	^{14}C	^{36}Cl	^{236}Pu	^{227}Th
	^{40}K	^{90}Sr	^{226}Ra	^{90}Sr	^{60}Co	^{238}Pu	^{228}Th
	^{60}Co	^{241}Am	^{103}Ru	^{225}Ac	^{242}Cm	^{239,240}Pu	^{229}Th
	^{137}Cs	^{125}Sb	^{106}Ru	^{227}Ac	^{245}Cm	^{241}Pu	^{230}Th
	^{152}Eu	^{144}Ce	^{108m}Ag	^{26}Al	^{246}Cm	^{242}Pu	^{232}Th
	^{154}Eu	^{134}Cs	^{110m}Ag	^{241}Am	^{247}Cm	^{244}Pu	^{234}Th
	^{155}Eu	^{137}Cs	^{65}Zn	^{243}Am	^{248}Cm	^{210}Po	^{126}Sn
	^{226}Ra	^{58}Co	^{95}Zr	^{126}Sb	^{152}Eu	^{40}K	^{90}Y
	^{228}Ra	^{60}Co		^{133}Ba	^{154}Eu	^{231}Pa	
	^{228}Th	^{152}Eu		^{207}Bi	^{155}Eu	^{234m}Pa	
	^{232}Th	^{154}Eu		^{249}Cf	^{210}Pb	^{223}Ra	
	^{241}Am	^{155}Eu		^{250}Cf	^{212}Pb	^{225}Ra	

Table 3.5. Detectable radionuclides at study LLW sites.

Radionuclides	Site	No. of Meas. (Above MDL/ Total)	Ave. (Bq/L)	Range (Bq/L)		COV
				Low	High	
U (µg/L)	OSDF	74/74	121.2	35.2	285	0.41
	ERDF	38/38	1488.7	212	3060	0.55
	EMWMF	104/104	69.52	6.4	388	1.45
	ICDF	31/31	67	10.26	387	0.93
^{99}Tc	OSDF	27/27	0.591	0.254	1.991	0.88
	ERDF	37/38	27.701	18.056	37	0.18
	EMWMF	94/107	2.452	0.152	47.88	2.87
	ICDF	15/33	0.297	0.163	0.577	0.39
^{3}H	ERDF	10/10	4266.1	3589	4625	0.11
	EMWMF	101/106	71.991	13.109	341.69	0.95
	ICDF	19/31	40.204	0.74	75.85	0.75
	MSW	33[a]	682.28	0.017	7955	
^{90}Sr	EMWMF	108/108	3.837	0.109	17.427	0.91
	ICDF	31/33	2.194	0.03	12.432	1.2
^{225}Ac	EMWMF	8/28	0.017	0.006	0.053	0.97
^{227}Ac	EMWMF	11/105	0.015	0.006	0.036	0.62
^{26}Al	EMWMF	1/64	0.272			
^{241}Am	EMWMF	22/108	0.012	0.004	0.054	0.87
^{249}Cf	EMWMF	2/30	0.006	0.003	0.009	0.38
^{250}Cf	EMWMF	1/30	0.002			
^{251}Cf	EMWMF	3/30	0.007	0.005	0.011	0.48
^{36}Cl	EMWMF	69/105	0.427	0.093	2.802	1.01
^{60}Co	EMWMF	4/85	0.261	0.13	0.345	0.35
^{245}Cm	EMWMF	19/75	0.011	0.004	0.017	0.24
^{246}Cm	EMWMF	19/76	0.011	0.004	0.017	0.24
^{247}Cm	EMWMF	6/76	0.01	0.003	0.019	0.68
^{248}Cm	EMWMF	22/105	0.01	0.001	0.036	0.26
^{152}Eu	EMWMF	1/85	1.606			
^{129}I	EMWMF	17/107	0.094	0.014	0.474	1.1
	ICDF	56/110	0.149	0.016	0.308	0.48
^{210}Pb	EMWMF	9/55	0.043	0.025	0.084	0.43
^{237}Np	EMWMF	14/108	0.016	0.014	0.084	1.05
^{59}Ni	EMWMF	2/30	7.659	7.4	7.918	0.048
^{63}Ni	EMWMF	5/75	3.45	3.45	10.804	1.2
^{236}Pu	EMWMF	1/62	0.013			

Radionuclides	Site	No. of Meas. (Above MDL/ Total)	Ave. (Bq/L)	Range (Bq/L)		COV
				Low	High	
^{238}Pu	EMWMF	2/88	0.006	0.004	0.009	0.61
	ICDF	2/33	0.006	0.001	0.011	1.14
^{239,240}Pu	EMWMF	4/108	0.009	0.003	0.014	0.51
	ICDF	1/15	0.005			
^{241}Pu	EMWMF	1/74	1.11			
^{242}Pu	EMWMF	36/74	0.013	0.004	0.04	0.58
^{244}Pu	EMWMF	5/74	0.006	0.004	0.01	0.46
^{210}Po	EMWMF	4/28	0.013	0.009	0.021	0.46
^{40}K	EMWMF	9/73	2.715	1.226	6.771	0.59
^{234m}Pa	EMWMF	105/106	1.149	0.14	5.779	1.22
^{223}Ra	EMWMF	1/35	0.007			
^{225}Ra	EMWMF	8/35	0.017	0.006	0.053	0.97
^{226}Ra	EMWMF	21/93	0.016	0.004	0.043	0.65
^{228}Ra	EMWMF	30/92	0.09	0.016	0.337	1.05
^{89}Sr	EMWMF	1/29	0.992			
^{227}Th	EMWMF	7/78	0.01	0.006	0.017	0.4
^{228}Th	EMWMF	9/105	0.021	0.003	0.108	1.54
^{229}Th	EMWMF	12/73	0.07	0.006	0.655	2.65
^{230}Th	EMWMF	73/105	0.024	0.004	0.131	0.89
^{232}Th	EMWMF	26/106	0.021	0.004	0.206	1.82
^{234}Th	EMWMF	56/74	0.545	0.14	5.18	1.71
^{90}Y	EMWMF	74/74	4.751	0.182	17.427	0.67

Notes:

"MDL" means: Method Detection Limit

Table only presents detectable radionuclides at each site – not all measured.

[a] Data from Kjeldsen et al., 2002.

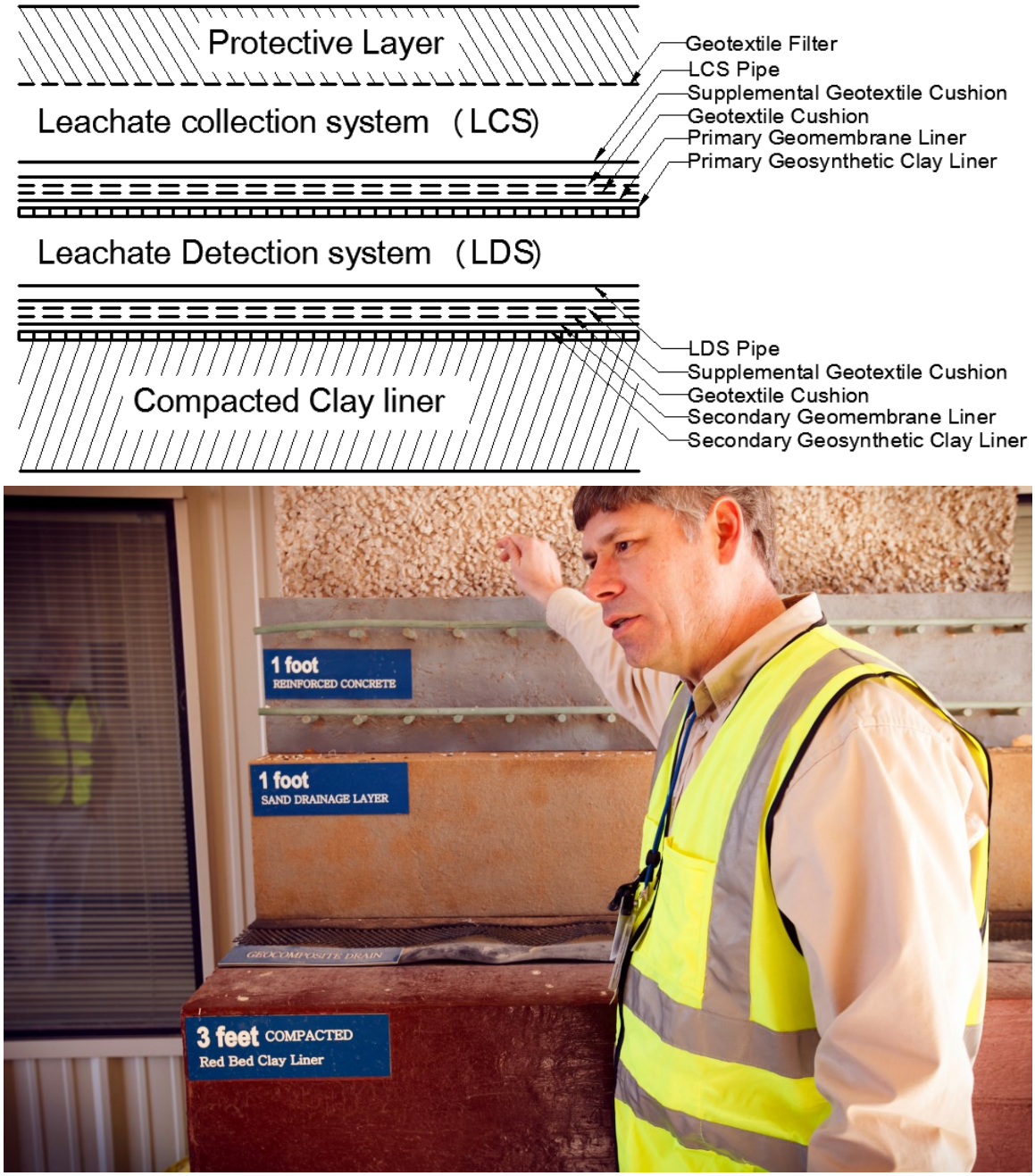

Figure 3.1. Top panel: Typical lower layer cross-section for LLW disposal facilities. (Modified from Powell et al. 2011). Lower panel: Rodney A. Baltzer, president of Waste Control Specialists, with a model of the installed barrier system at the Andrews, TX LLW facility (Stravato 2014).

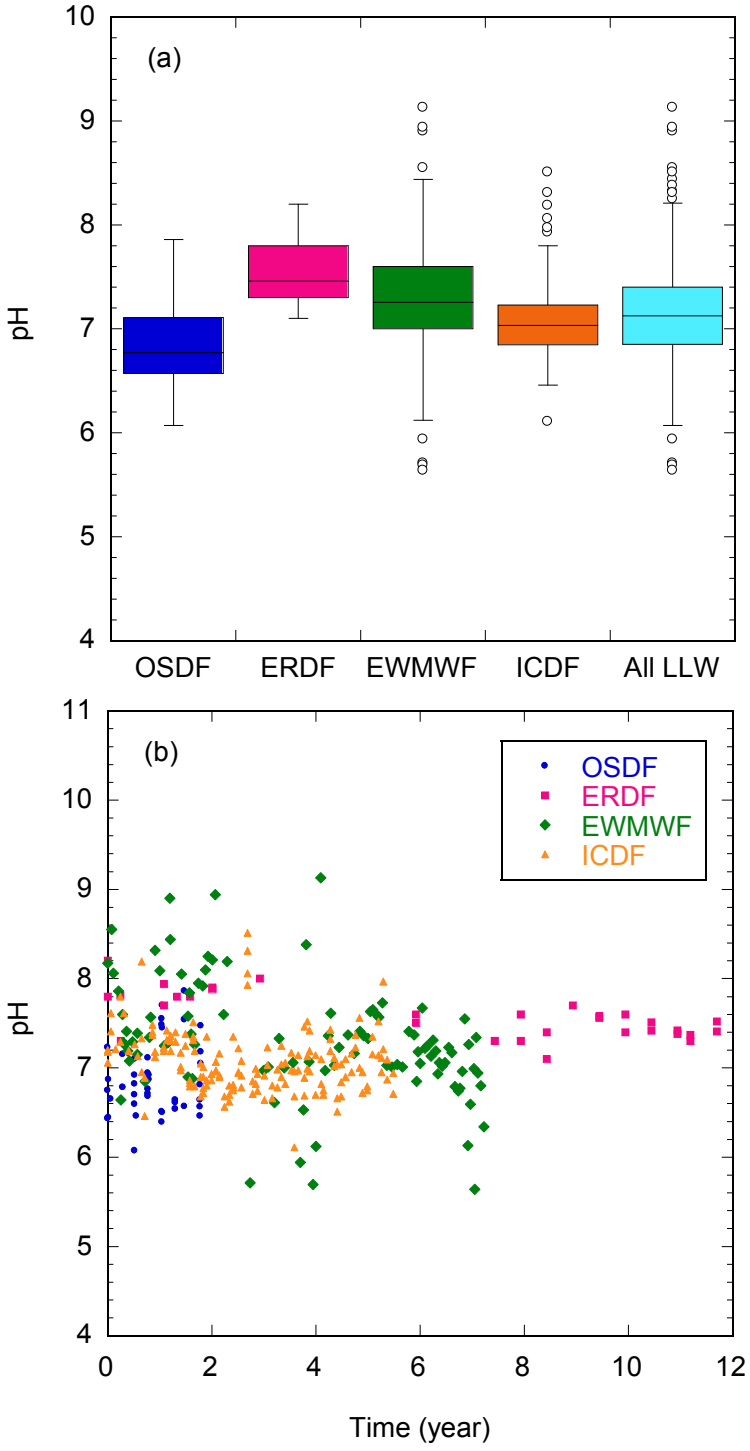

Figure 3.2. Comparison of (a) pH values across LLW sites and (b) pH variation with time. (ERDF: the Environmental Restoration Disposal Facility at Hanford, WA; OSDF: the On Site Disposal Facility at Fernald, OH; ICDF: the Idaho CERCLA Disposal Facility at Idaho Falls, ID; EMWMF: Environmental Management Waste Management Facility at Oak Ridge; All LLW contains data for all four LLW sites)

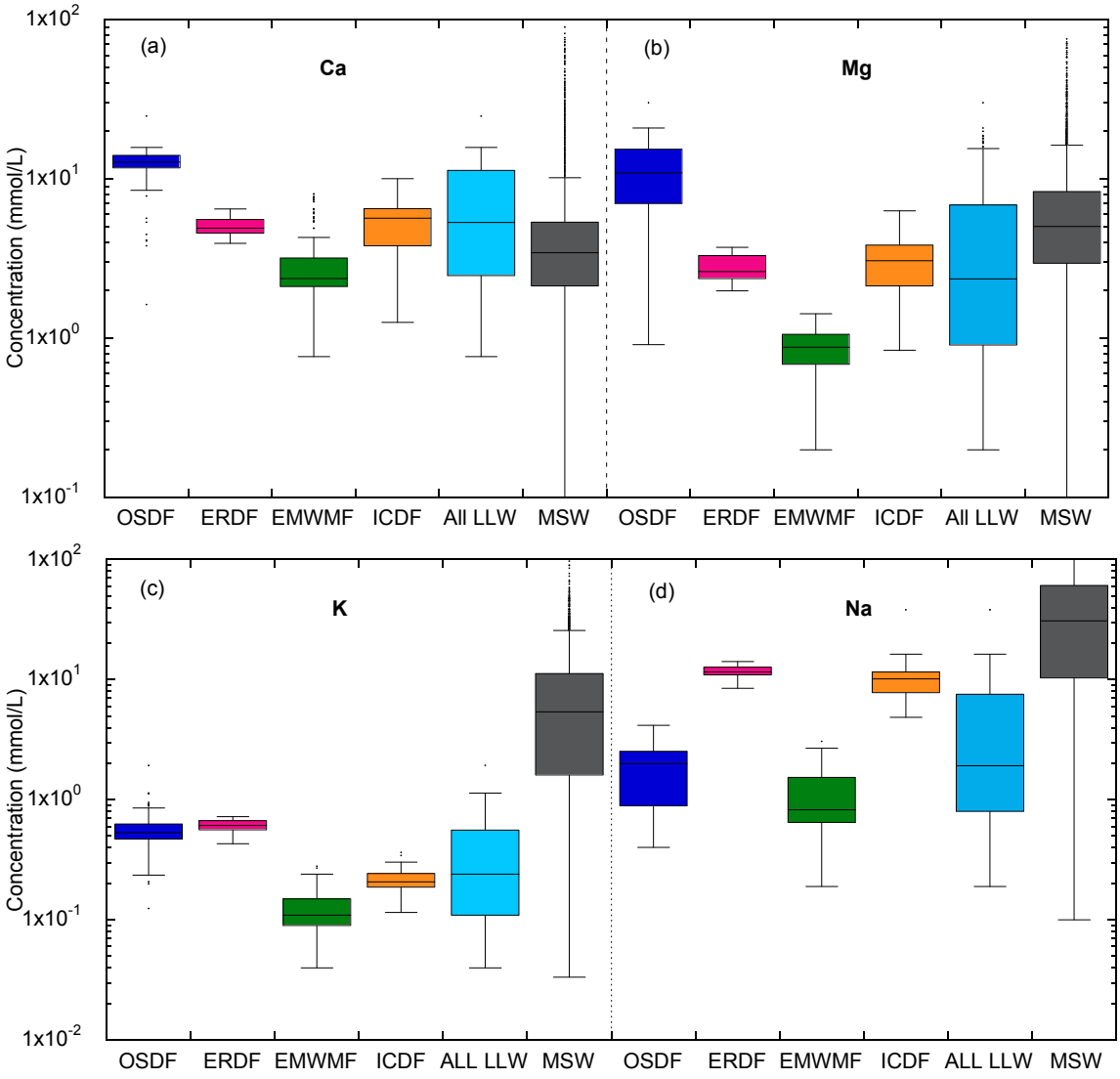

Figure 3.3. Comparison of major cation concentrations at LLW sites. LLW concentrations of calcium, Ca (a), magnesium, Mg (b), potassium, K (c), and sodium, Na (d), are compared to MSW concentrations.

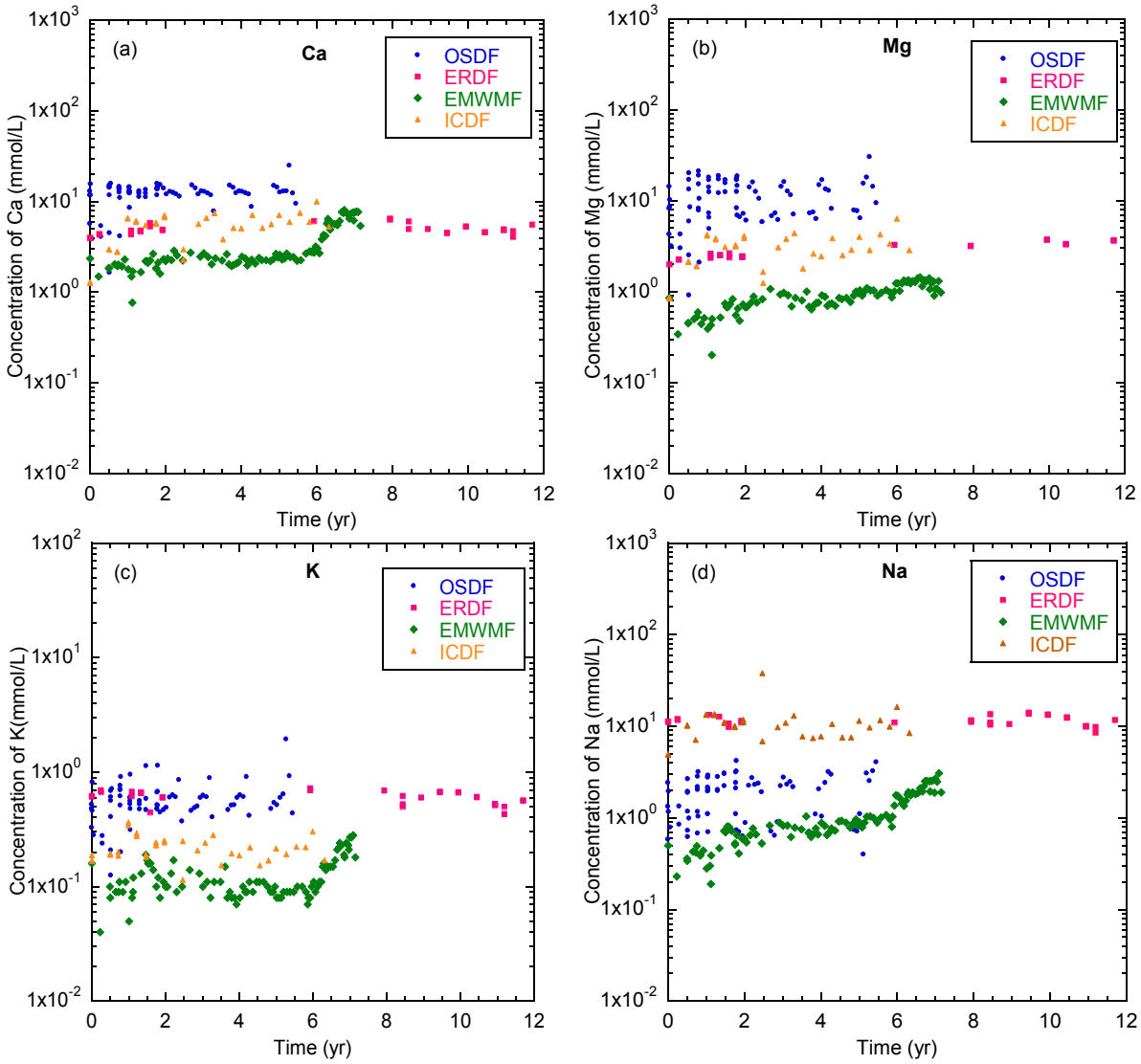

Figure 3.4. Major cation concentrations over time: (a) calcium, Ca; (b) magnesium, Mg; (c) potassium, K; and (d) sodium, Na.

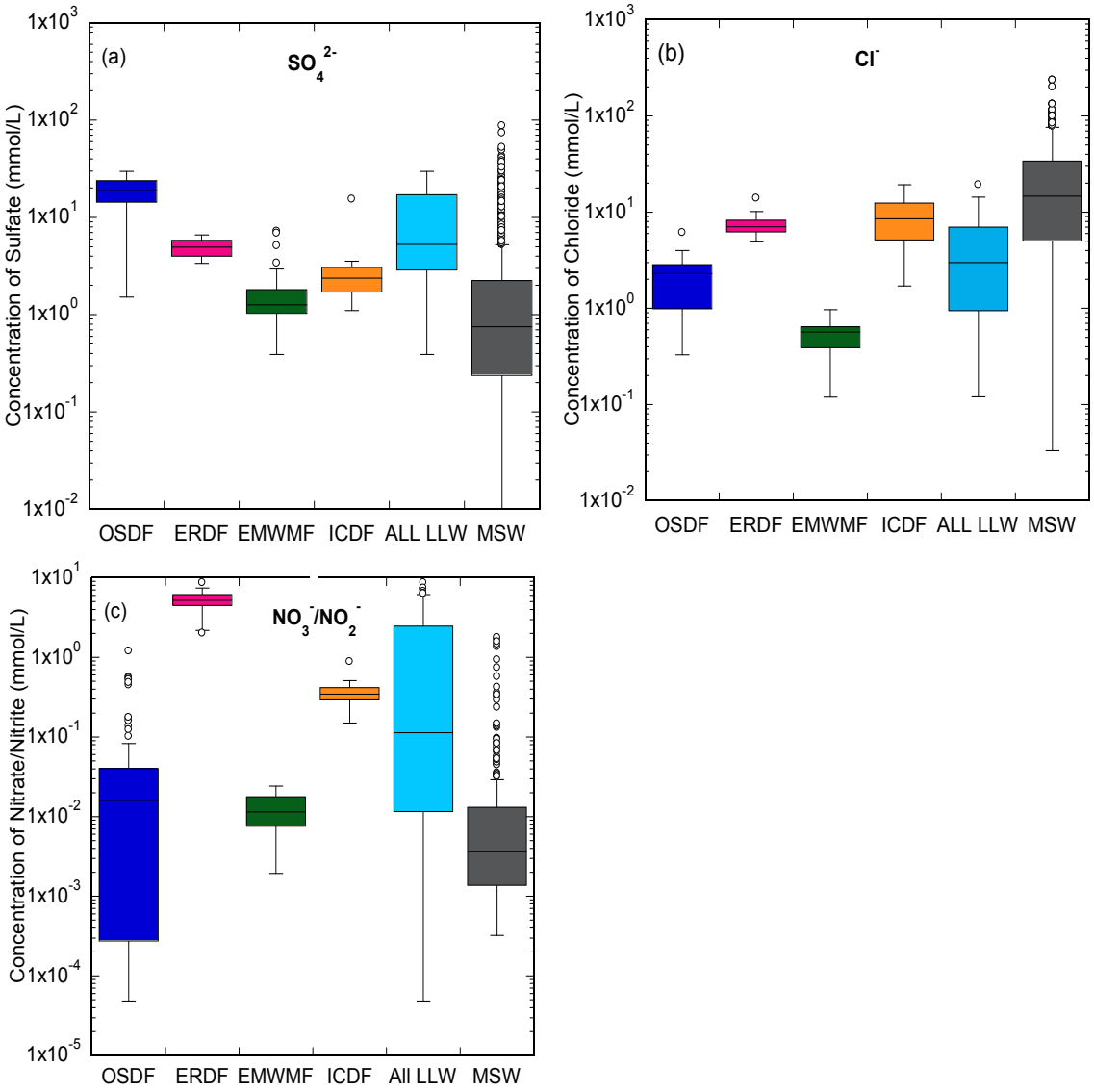

Figure 3.5. Comparison of major anion concentrations in LLW and MSW leachates: (a) sulfate, SO_4^{2-}; (b) chloride, Cl^-; and (c) nitrate/nitrite, NO_3^-/NO_2^-.

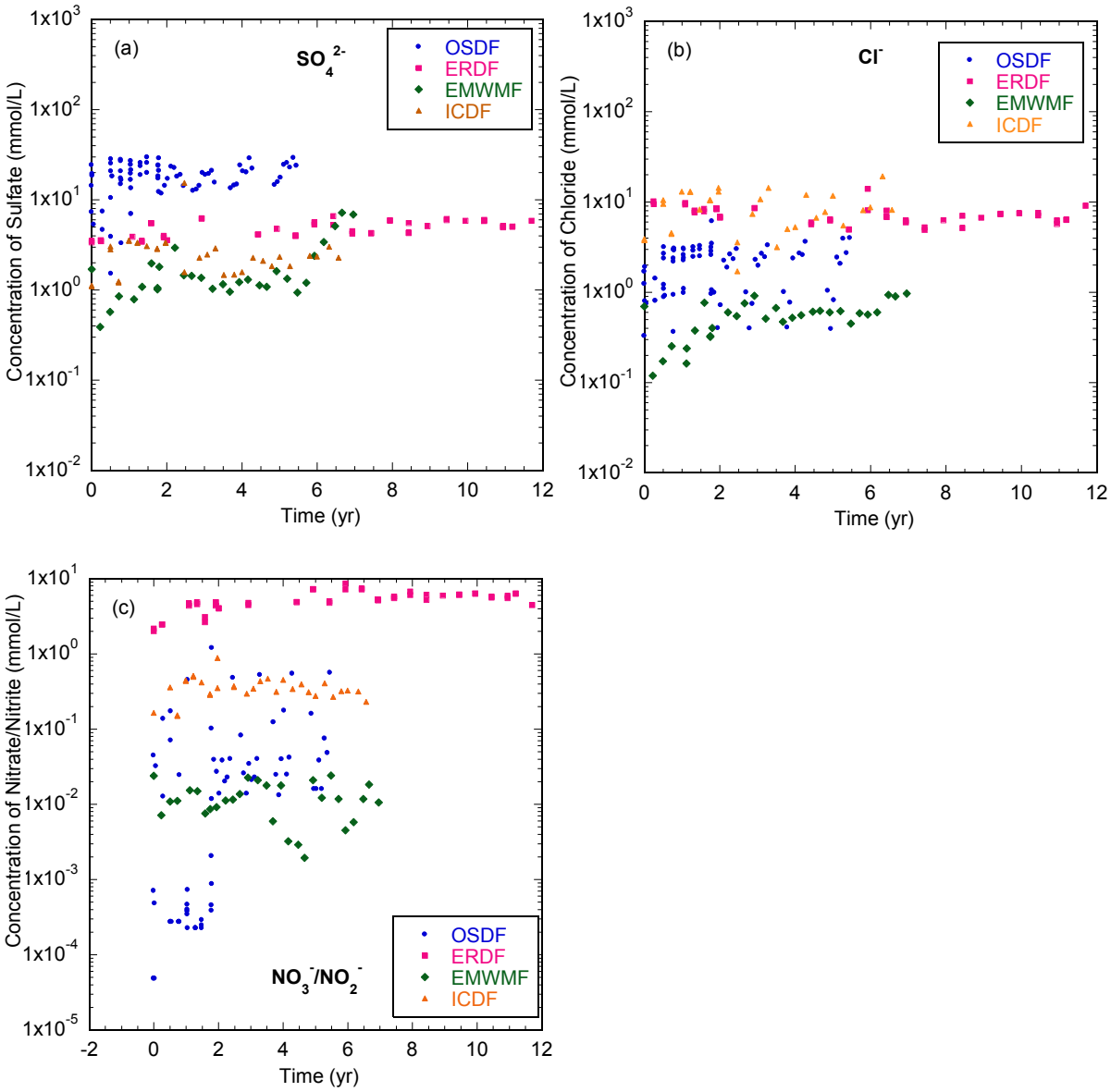

Figure 3.6. Changes in major anion concentrations with time: (a) sulfate, SO_4^{2-}; (b) chloride, Cl^-; and (c) nitrate/nitrite, NO_3^-/NO_2^-.

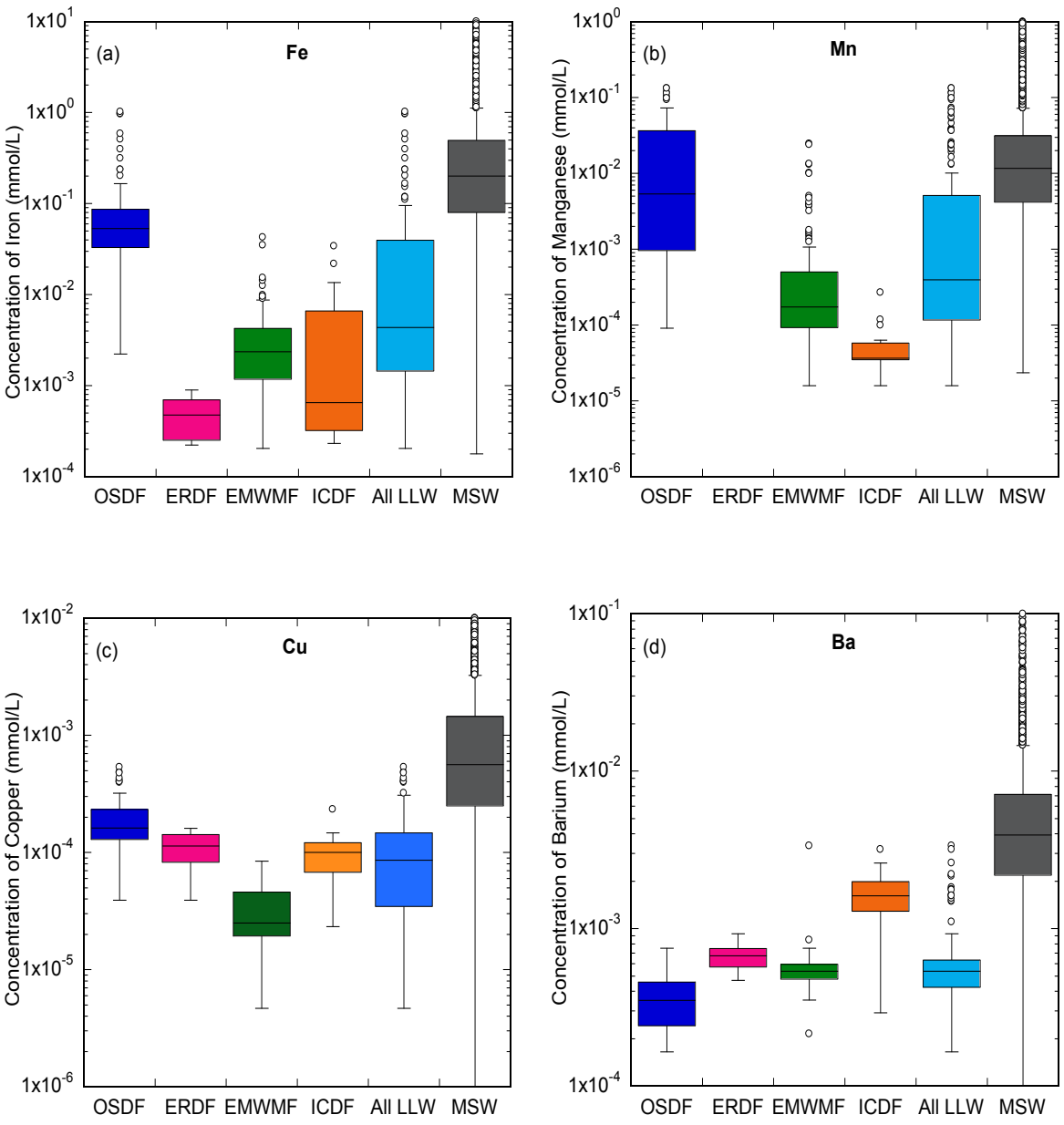

Figure 3.7. Comparison of trace heavy metal concentrations in LLW and MSW leachates: (a) iron, Fe; (b) manganese, Mn; (c) copper, Cu; and (d) barium, Ba.

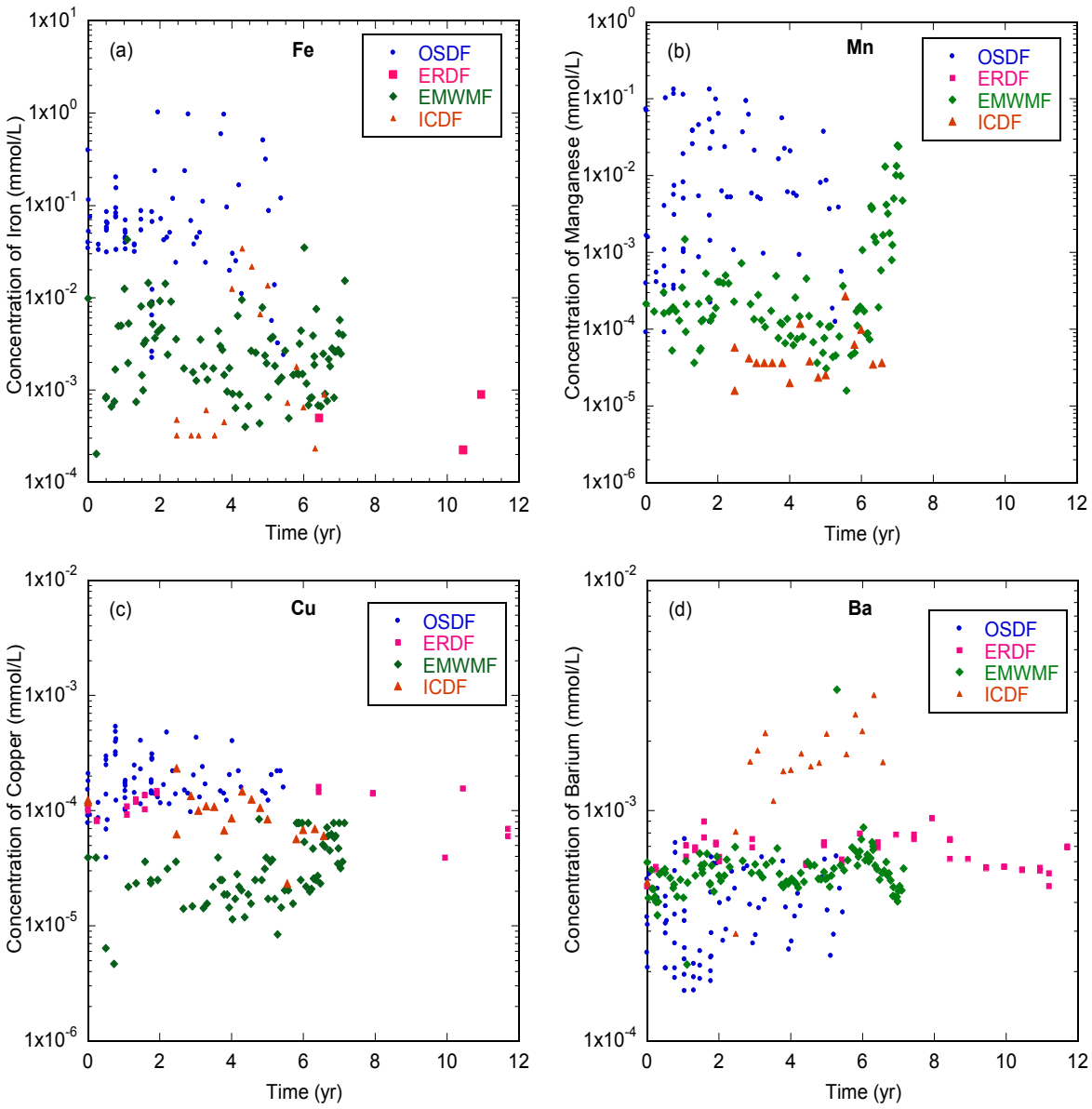

Figure 3.8. Change of trace heavy metal concentrations with time: (a) iron, Fe; (b) manganese, Mn; (c) copper, Cu; and (d) barium, Ba.

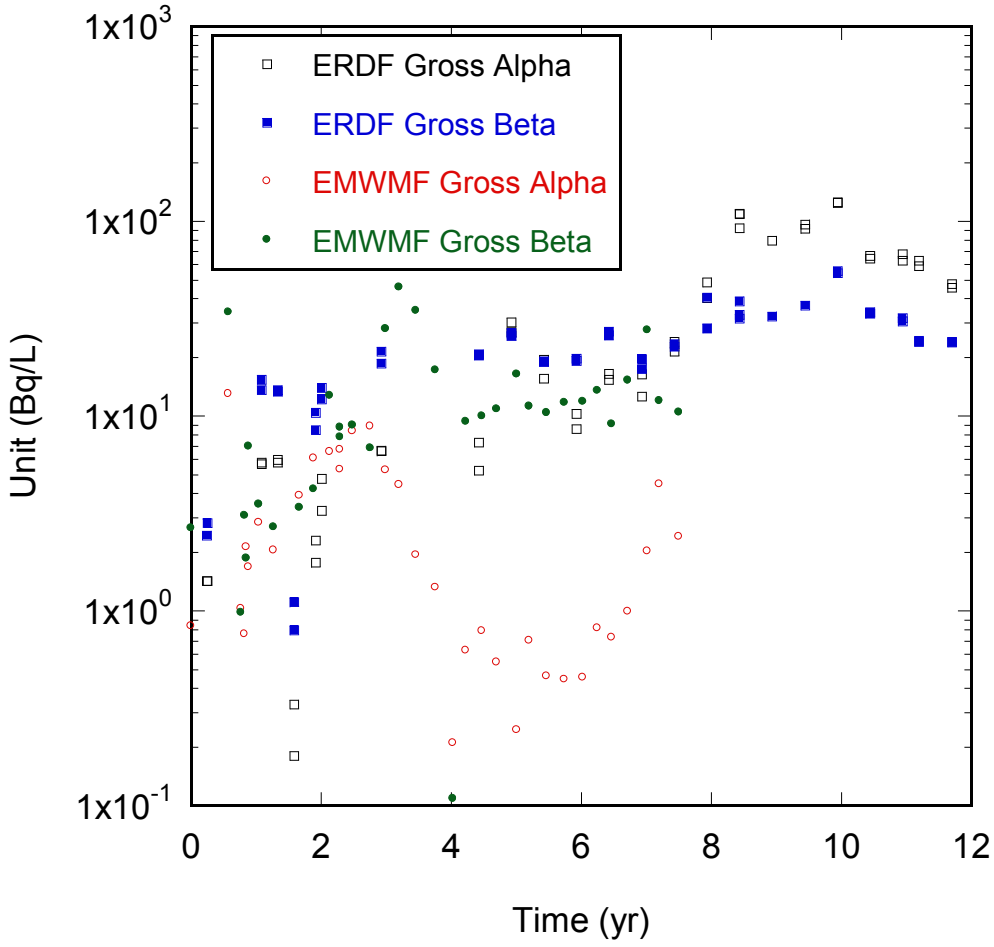

Figure 3.9. Gross alpha and beta activity (in Bq/L) versus time.

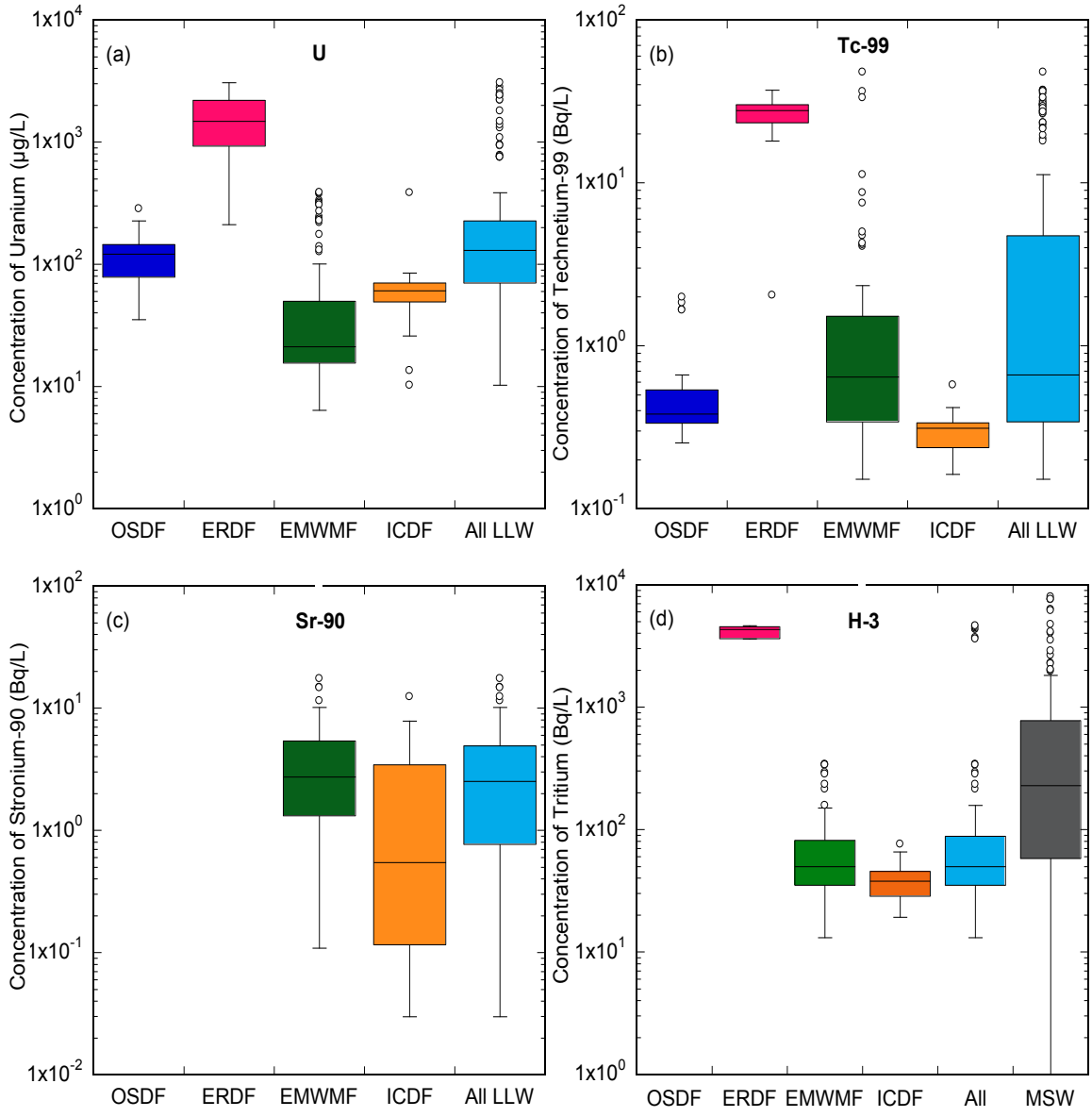

Figure 3.10. Comparison of specific radionuclide concentrations across LLW sites and in MSW, where applicable: (a) Total Uranium, U; (b) Technetium-99, ^{99}Tc; (c) Strontium-90, ^{90}Sr; and (d) Tritium, ^{3}H.

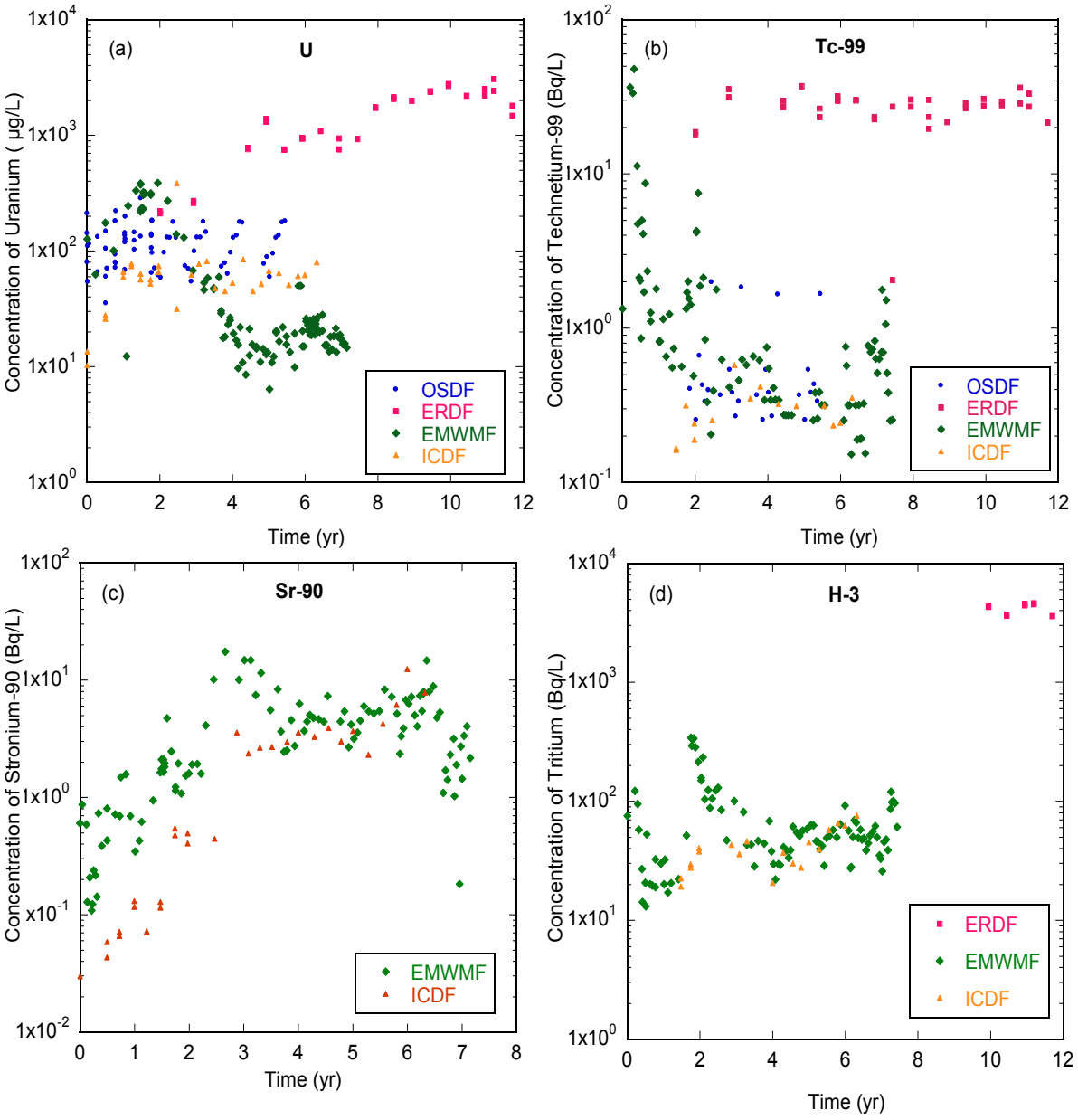

Figure 3.11. Change in concentration for specific radionuclides with time: (a) Total Uranium, U; (b) Technetium-99, ^{99}Tc; (c) Strontium-90, ^{90}Sr; and (d) Tritium, ^{3}H.

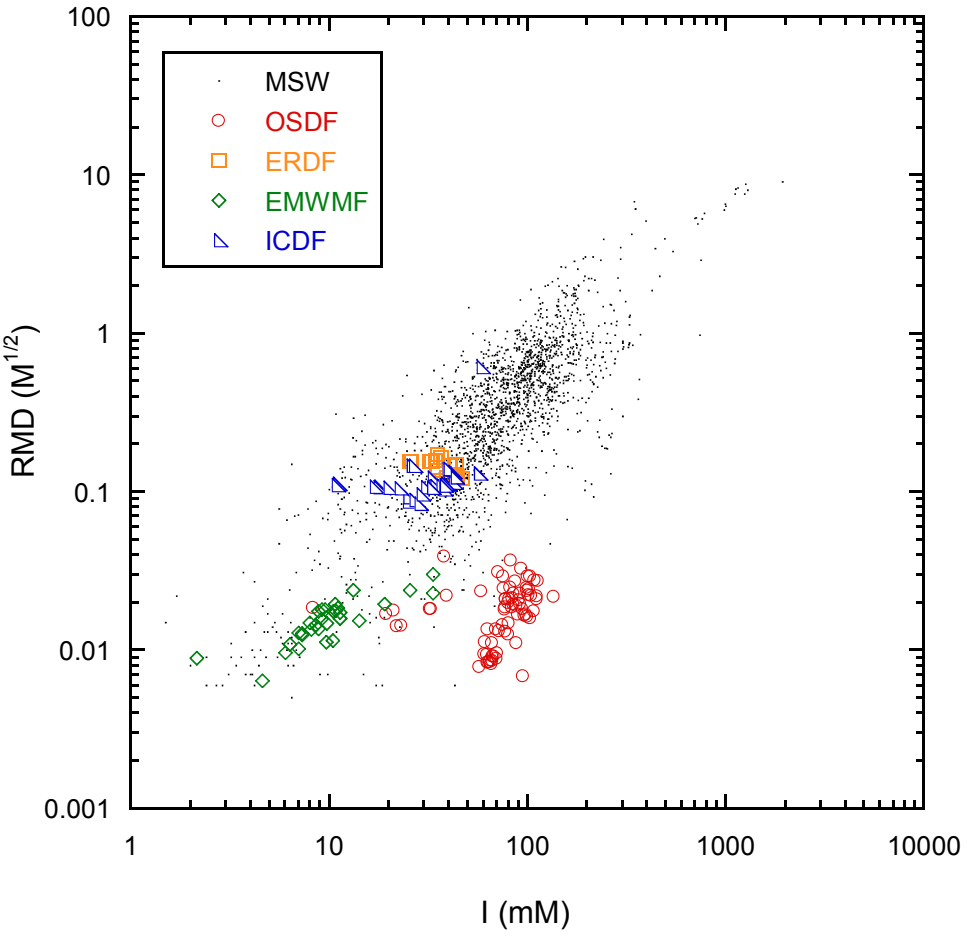

Figure 3.12. Comparison of RMD to Ionic Strength (I) for LLW and MSW leachates.

Section 4 – Materials

During this study, caution was exercised to prevent radiation exposure from use of radioactive materials. Due to the low quantities of radioactive materials used to simulate the concentrations found in LLW, prevention was accomplished mainly through rigorous use of personal protective equipment (PPE), coupled with safe laboratory practices and careful handling of materials. PPE for this project was stipulated by the Office of Radiation Safety at the University of Wisconsin-Madison and included lab coats, goggles, and gloves. Bench covers were routinely replaced and the laboratory was monitored for residual radiation.

4.1 Soils

A suite of four soils with typical landfill compacted clay liner properties was selected for use in this study. Soil identified as *WCS Andrews* (subsequently Soil *D* throughout) was used as received and without alteration to composition from the Waste Control Specialists LLW site in Andrews, Texas. Soils *Albany Red* (Albany, Georgia), *Houston Brown* (Houston, Texas), and *Kamm Clay* (Dane County, Wisconsin) – subsequently Soils *A*, *B*, and *C*, respectively - have been previously characterized (Benson and Trast 1995; Gurdal et al. 2003; Park et al. 2011) and implemented in MSW systems. All soils were analyzed for particle size distribution (ASTM D 422 2007), specific gravity (ASTM D 854 2010), and Atterberg limits (ASTM D 4318 2010), and classified based on the Unified Soil Classification System (ASTM D 2487 2006). The clay activity, defined by Skempton (1953) as the plasticity index divided by the clay fraction of a soil, was calculated using the values obtained during other soil characterization analyzes. The bulk and clay mineralogy of the soil was determined using X-Ray Diffraction (XRD) by Mineralogy, Inc., Tulsa, OK. Additionally, ASTM D 4373 (2007) was used for comparing general carbonate content of the soils to the values

obtained from XRD. The carbonate values from both XRD and the calcimeter testing (ASTM D 4373 2007) were found to be in agreement with one another. Selected properties of the soils are summarized in Tables 4.1 and 4.2, including previously published values where applicable. The grain size distributions for the soil suite are shown in Figure 4.1, with indications to the transition between methods displayed. Figure 4.2 compares the relative abundance of various mineral fractions found within the study soils. Collectively, the four materials represent a range of soil classifications that are suitable for use as liner materials (Benson and Trast 1995; Daniel 1987). In addition to these soils, glass beads approximating sand-sized soil particles (passing the US #45 (0.354 mm) and retained on the US #60 (0.251 mm) sieve) were used as a sorption control.

In addition to the geotechnical characterization of the study soils, further analyses were conducted to determine additional properties potentially consequential to soil sorption capacity. The soluble cation (SC) and bound cation content (BC) and cation exchange capacity (CEC) of the soils was analyzed using ASTM D 7503 (2010). The total reactive (C/D) and amorphous (or poorly crystalline) (HCl) iron content of the four soils was determined using methods described by Jackson et al. (1986). Specific surface area (SSA) of the study soils was analyzed by the ethylene glycol monoethyl ether (EGME) (Carter et al. 1986) and water vapor-BET methods. Soil pH for the soils was determined using both water and $CaCl_2$-based solutions, as stipulated by ASTM D 4972 (2007). Results of these measurements are found in Table 4.3. Element-specific SC and BC measurements are provided in Table 4.4. Graphical comparison of various properties can be found in Figures 4.3 to 4.6.

Prior to batch experimentation, each of the selected soils were air-dried and ground using a mortar and pestle to < 1 mm. Note from the grain size distribution (Figure 4.1) that more than 90% of each of the soils passed this size point prior to crushing,

allowing separation to be focused on conglomerated particle aggregates. Particles with diameters above 6.35 mm were scalped from the sample.

4.2 Solutions

For single radionuclide batch sorption, sodium perchlorate ($NaClO_4$) was used as the background electrolyte for the solution-based chemistry. Sodium was chosen due to its significant presence within the leachate chemistry of the four DOE sites discussed by Tian et al. (2014 – Section 3) in addition to its naturally occurring presence and importance in clay mineralogy. Although providing a higher quantity of sodium than measured in the LLW leachate chemistry, (Table 4.5; range: 0.0008 M to 0.0126 M) (Tian et al. 2014 – Section 3), the 0.05 M final concentration was chosen for comparison with the ionic strengths used for other radionuclide sorption experimentation to purified clay minerals within the literature (Table 4.6; range: 0.01 M to 0.5 M). Additionally, the 0.05 M concentration is similar in magnitude as the combined concentrations of the four major cations (Na, Mg, K, and Ca) within the LLW leachate, allowing a single background electrolyte to act as a comparison to the total system.

Selection of radionuclides for experimentation was based on those species with measured and reported leachate concentrations at four DOE LLW sites in the United States, as summarized in Tables 4.7 and 4.8 (after Tian et al. 2014 – Section 3). Uranium was chosen for the first part of this study for its predominance at all four sites, in addition to the available information for comparison with sorption to pure minerals found within the literature (Bradbury and Baeyens 2005a; Davis et al. 2004; Schlegel and Descostes 2009). Uranium acetate dihydrate (chemical formula: $UO_2(C_2O_2H_3)_2 \bullet 2\ H_2O$; alternatively $UO_2(OCOCH_3)_2 \bullet 2\ H_2O$ or $UO_2(CH_3COO)_2 \bullet 2\ H_2O$ (hereafter referred to as uranium acetate)) was used as the uranium source for experimentation. Uranium acetate was received in powder form derived from yellowcake uranium, with a MSDS-

listed specific activity of 0.28 μCi/g (SI units: 1.04 x 10^4 Bq/g), from the Office of Radiation Safety at the University of Wisconsin-Madison. Two separate solutions of uranium acetate and DI water were prepared for use during experimentation. The first solution, for use throughout most of the experimentation, had a uranium acetate concentration of 79600 μg/L for an activity of 824.7 Bq/L (22288 pCi/L). The second solution, created for the sorption isotherm experimentation only, had a uranyl acetate concentration of 42800 μg/L for an activity of 443.4 Bq/L (11984 pCi/L). The first solution was used to represent 20.35 Bq/L (550 pCi/L) within the experimentation for the first solution (20.62 Bq/L (557 pCi/L) as executed based on the actual concentration of U added to the solution). A range of 6 to 6000 μg/L for the isotherm experimentation (0.11 to 111 Bq/L (3.0 to 3000 pCi/L)) was created from the second solution.

Table 4.1. Soil characteristics, including USCS classification, particle size distributions, and liquid limit (LL), plastic limit (PL), plasticity index (PI), and clay activity (A) values for the project soils. Previously published soil characteristics, compiled from Benson and Trast (1995), Gurdal et al. (2003), and Park et al. (2011), are provided in italics for comparison.

Soil Identifier	Location	USCS		Particle Size Distribution (USCS)				LL	PL	PI	A
		Group Symbol	*Group Name*	*% Gravel*	*% Sand*	*% Fines*	*% 2-μm Clay*				
A	Albany, GA	SC *(SC-SM)*	Clayey sand *(Silty clayey sand)*	3.3 *(4.8)*	58.8 *(67.7)*	37.9 *(31.5)*	64.1 *(23.2)*	30 *(25.8)*	16 *(16.3)*	14 *(9.5)*	0.25
B	Houston, TX	CL *(CH)*	Lean clay *(Fat clay)*	1.2 *(0)*	16.3 *(12)*	82.5 *(88)*	42.8 *(63)*	44 *(53)*	12 *(12)*	32 *(41)*	0.74
C	Madison, WI	CL *(CL)*	Lean clay *(Lean clay)*	1.0 *(0)*	15.0 *(0)*	84.0 *(96)*	30.0 *(41)*	49 *(48)*	21 *(21)*	28 *(27)*	0.91
D	Andrews, TX	CH	Fat clay	0.0	2.6	97.4	54.1	50	18	32	0.60

Table 4.2. Soil mineralogy of the project soils as determined by XRD.

Soil	Quartz (%)	Plagioclase Feldspar (%)	K Feldspar (%)	Calcite (%)	Dolomite (%)	Magnetite (%)	Hematite (%)	Goethite (%)	Kaolinite (%)	Chlorite (%)	Illite/Mica (%)	Mixed-Layer Illite/Smectite (%) (% illite layers)	Total (%)
A	75	---	---	---	---	---	---	9	14	1	1	---	100
B	65	3	2	3	Trc.	---	---	---	1	Trc.	1	25 (50)	100
C	54	9	5	---	---	---	---	---	1	Trc.	2	29 (25)	100
D	57	Trc.	2	Trc.	---	8	4	4	15	2	5	3 (70)	100

Note: Trc. indicates trace levels detected.

Table 4.3. Soluble cation and bound cation content, cation exchange capacity, total reactive and poorly crystalline Fe content, specific surface area (SSA), and soil pH measurements for study soils.

Soil Name	Soluble Cations (cmol+/kg)	Bound Cations (cmol+/kg)	Cation Exchange Capacity (cmol+/kg)	C/D		HCl		SSA (m^2/g)		Soil pH	
				Total Reactive Fe (µmol/g)	std.dev.	Poorly Crystalline Fe (µmol/g)	std.dev.	EGME	Water Vapor	DI Water	0.01 M $CaCl_2$
A	2	2.5	7.6	174.79	18.74	1.44	0.1	43	32	7.86	7.7
B	2.1	34.8	32.2	107.59	11.19	2.33	0.1	145	90	8.52	7.67
C	0.8	17.5	26.3	97.91	11.87	12.98	0.38	145	84	7.72	7.36
D	2.2	9.9	17.6	180.62	18.59	0.8	0.06	118	71	8.06	7.73

Table 4.4. Measured soluble and bound cations separated by base cation.

Soil Name	Soluble Cations (cmol+/kg)	Bound Cations (cmol+/kg)	
A	1.47	2.40	**Ca**
B	0.64	26.31	
C	0.20	9.36	
D	0.71	7.24	
A	0.14	0.00	**K**
B	0.20	0.32	
C	0.12	0.21	
D	0.27	0.17	
A	0.30	0.06	**Mg**
B	0.37	6.80	
C	0.34	7.67	
D	0.42	2.46	
A	0.09	0.07	**Na**
B	0.91	1.37	
C	0.13	0.30	
D	0.76	0.00	

Table 4.5. Sodium (Na) and major cation (Na, Mg, K, and Ca) average concentrations reported for 4 DOE LLW disposal sites by Tian et al. (2014 – Section 3), along with the overall average values across all 4 sites.

Site Name	Na (mol/L)	Combined Na, Mg, K, and Ca (mol/L)
OSDF	0.0020	0.03
ERDF	0.0126	0.02
EMWMF	0.0008	0.004
ICDF	0.0102	0.02
Average	*0.006*	*0.02*

Table 4.6. Clay types used as sorbents and sodium (Na) concentrations representing system ionic strengths for other uranium sorption studies within the literature.

Author	Clay	Na (mol/L)
Bradbury and Baeyens (2005a)	Na-Illite du Puy	0.1
Bradbury and Baeyens (2005a)	Na-Illite du Puy (alternate series)	0.1
Bradbury and Baeyens (2005a)	Na-SWy-1	0.1
Bradbury and Baeyens (2005a)	Na-Swy-1 (alternate series)	0.01
Davis et al. (2004)	Imogolite	Variable (artificial groundwater solutions)
Schlegel and Descostes (2009)	Na-Swy-2	0.5
Schlegel and Descostes (2009)	S-Hca-1	0.5

Table 4.7. Average, minimum, and maximum measured concentrations of radioisotopes and gross radioactivity at 4 DOE sites. All concentrations are given in pCi/L, except for the italicized Total U concentrations, which are reported in µg/L. Values marked as N/R, for not reported, were neither measured or recorded at the corresponding sites. Presented concentrations are derived from raw data received from Tian et al. (2014 – Section 3).

	C14			H3			I126			Tc99		
Location	***Average***	***Minimum***	***Maximum***	***Average***	***Minimum***	***Maximum***	***Average***	***Minimum***	***Maximum***	***Average***	***Minimum***	***Maximum***
ERDF	47.9	-3.0	118.0	111530.0	97000.0	125000.0	N/R	N/R	N/R	731.9	55.4	1000.0
EMWMF	6.3	-5.4	77.1	1864.9	132.0	9234.9	0.9	-1.2	12.8	58.8	1.7	1294.1
ICDF	0.9	-6.1	4.2	741.2	20.0	2050.0	N/R	N/R	N/R	4.7	-2.3	15.6
OSDF	N/R	N/R	N/R	N/R	N/R	N/R	N/R	N/R	N/R	16.0	6.9	53.8

	U238			Total U			Gross α Activity			Gross β Activity		
Location	***Average***	***Minimum***	***Maximum***	***Average***	***Minimum***	***Maximum***	***Average***	***Minimum***	***Maximum***	***Average***	***Minimum***	***Maximum***
ERDF	N/R	N/R	N/R	*1522.8*	*212.0*	*3060.0*	N/R	N/R	N/R	N/R	N/R	N/R
EMWMF	N/R	N/R	N/R	*275.2*	*219.0*	*383.0*	74.5	0.9	350.8	311.8	2.8	1240.0
ICDF	8.3	1.4	34.4	22.5	3.5	130.1	N/R	N/R	N/R	N/R	N/R	N/R
OSDF	N/R	N/R	N/R	*121.2*	*35.2*	*285.0*	N/R	N/R	N/R	N/R	N/R	N/R

Table 4.8. Same as Table 4.7, but with values converted to the SI units of Bq/L, except where noted previously. Note: 1 Ci = 3.7 x 10^{10} Bq; 1 Ci = 1 x 10^{12} pCi.

	C14			H3			I126			Tc99		
Location	***Average***	***Minimum***	***Maximum***	***Average***	***Minimum***	***Maximum***	***Average***	***Minimum***	***Maximum***	***Average***	***Minimum***	***Maximum***
ERDF	1.8	-0.1	4.4	4126.6	3589.0	4625.0	N/R	N/R	N/R	27.1	2.0	37.0
EMWMF	0.2	-0.2	2.9	69.0	4.9	341.7	0.0	0.0	0.5	2.2	0.1	47.9
ICDF	0.0	-0.2	0.2	27.4	0.7	75.9	N/R	N/R	N/R	0.2	-0.1	0.6
OSDF	N/R	N/R	N/R	N/R	N/R	N/R	N/R	N/R	N/R	0.6	0.3	2.0

	U238			Total U			Gross α Activity			Gross β Activity		
Location	***Average***	***Minimum***	***Maximum***	***Average***	***Minimum***	***Maximum***	***Average***	***Minimum***	***Maximum***	***Average***	***Minimum***	***Maximum***
ERDF	N/R	N/R	N/R	*1522.8*	*212.0*	*3060.0*	N/R	N/R	N/R	N/R	N/R	N/R
EMWMF	N/R	N/R	N/R	*275.2*	*219.0*	*383.0*	2.8	0.0	13.0	11.5	0.1	45.9
ICDF	0.3	0.1	1.3	0.8	0.1	4.8	N/R	N/R	N/R	N/R	N/R	N/R
OSDF	N/R	N/R	N/R	*121.2*	*35.2*	*285.0*	N/R	N/R	N/R	N/R	N/R	N/R

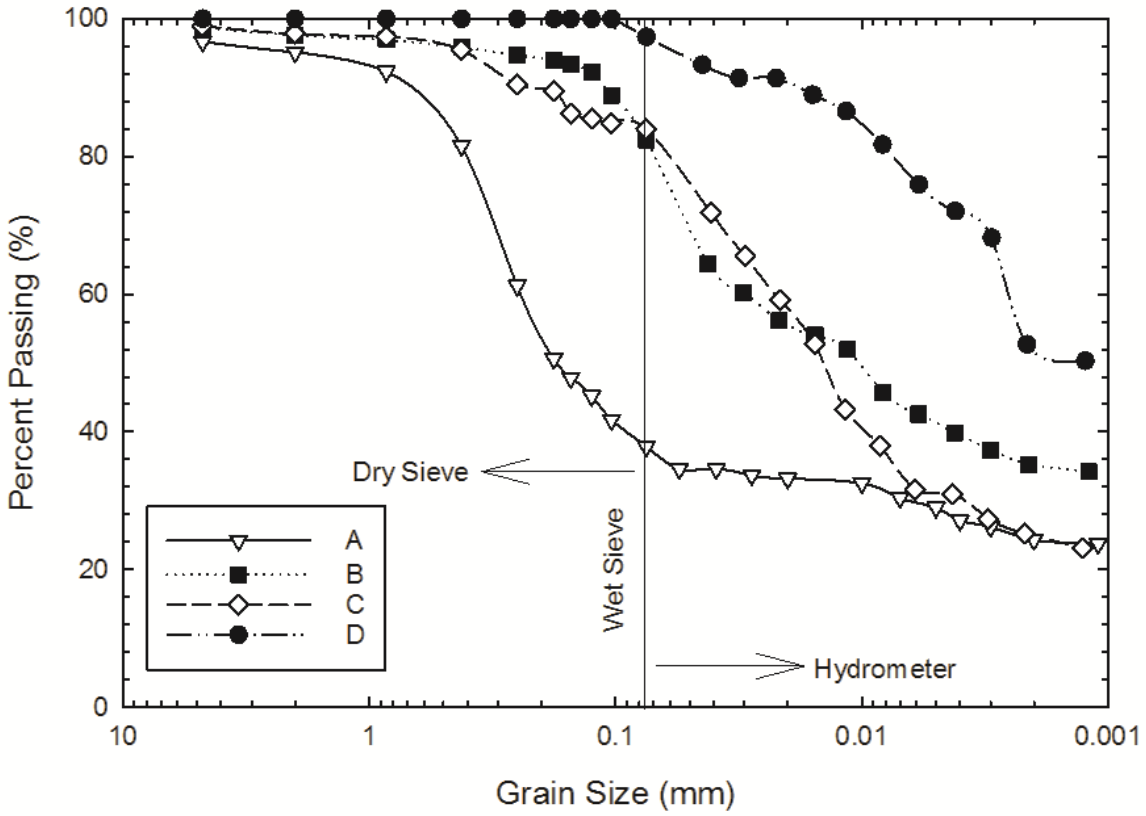

Figure 4.1. Grain size distribution for the four study soils. The solid line represents the sieve size used during wet sieve separation of the soils. Soil passing the wet sieve (to the right of the line) was analyzed for particle size by hydrometer, while soil to the left of the line was classified by dry sieve.

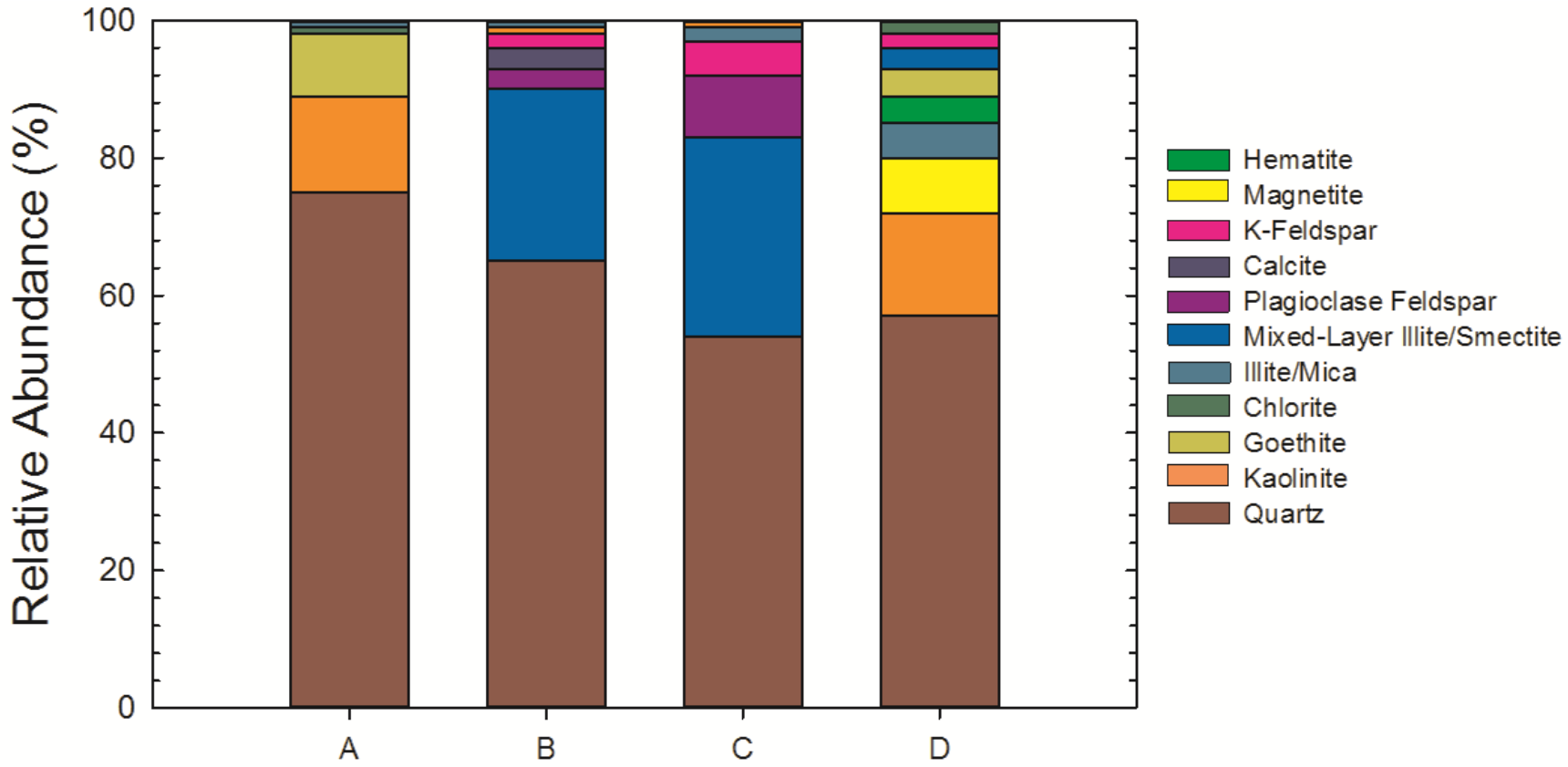

Figure 4.2. Comparison of the various crystalline minerals found in the four study soils through XRD testing.

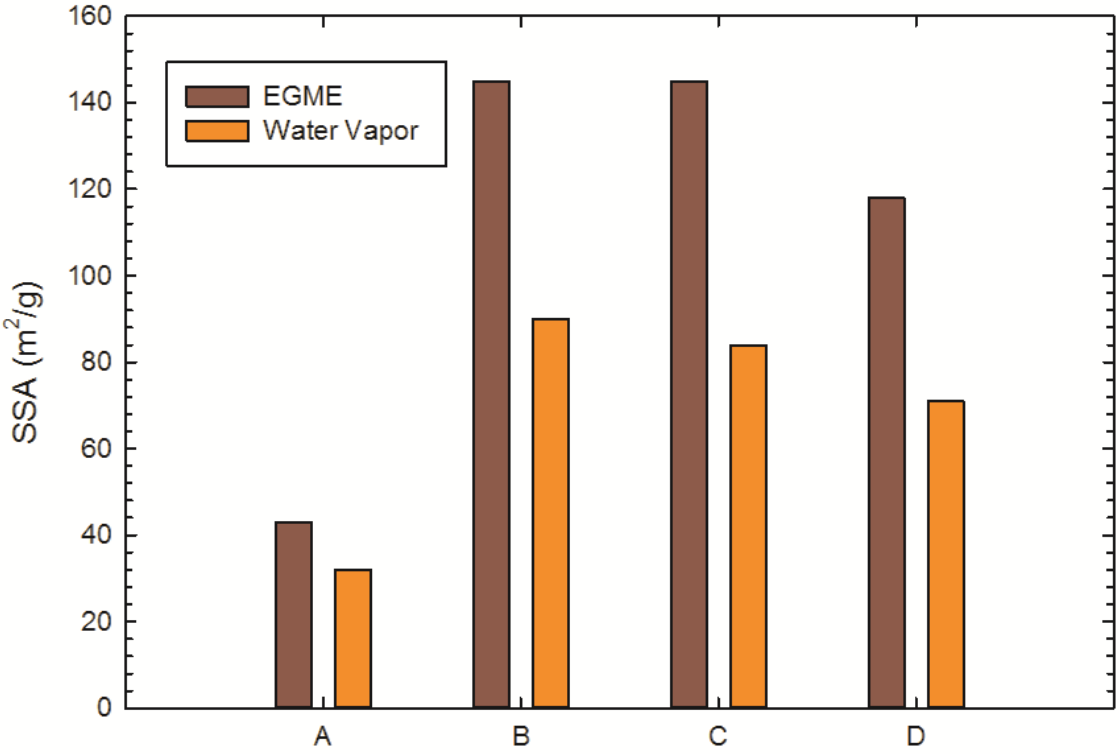

Figure 4.3. Specific surface area (SSA, in m^2/g) of the four study soils as determined by the EGME and water vapor methods.

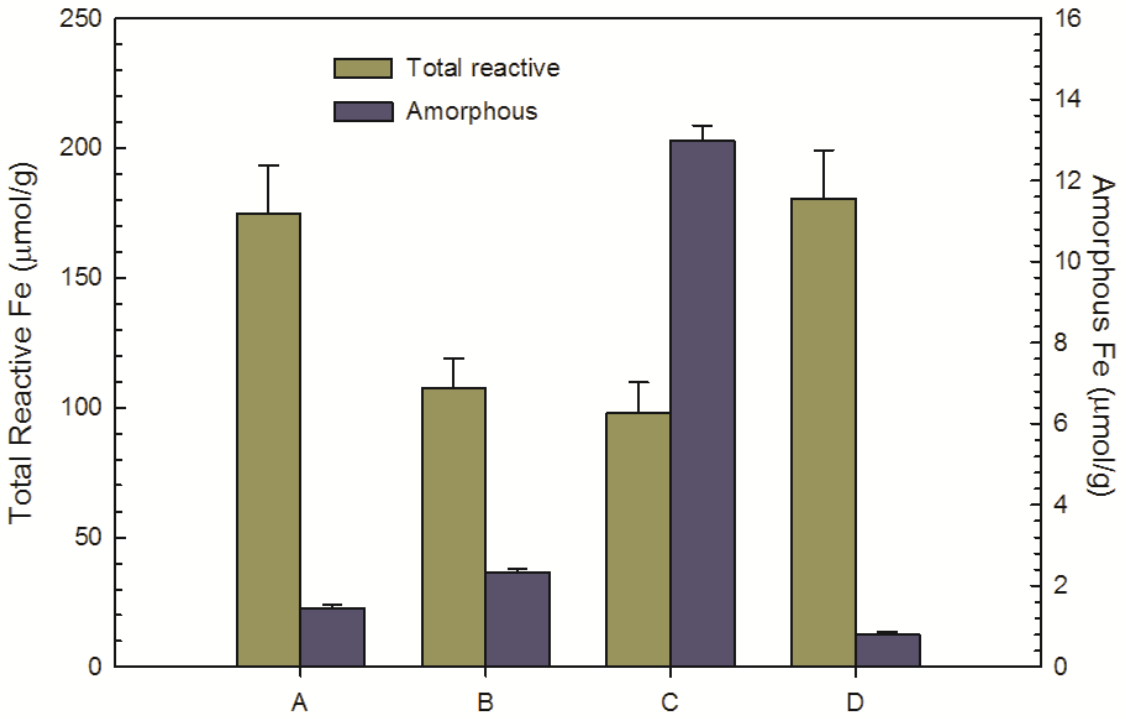

Figure 4.4. Comparison of the total reactive and amorphous/poorly crystalline iron content of the four study soils as determined using the citrate/sodium dithionite and hydrochloric acid methods.

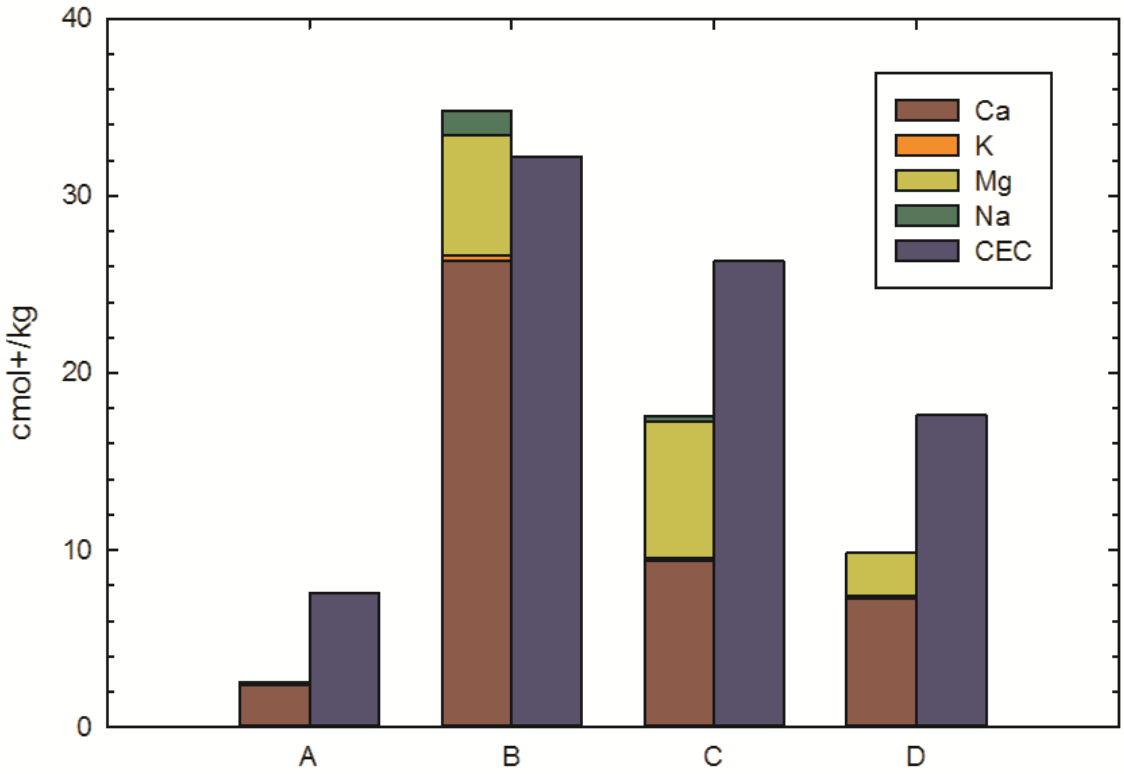

Figure 4.5. Comparison of bound cations and cation exchange capacity for the four study soils.

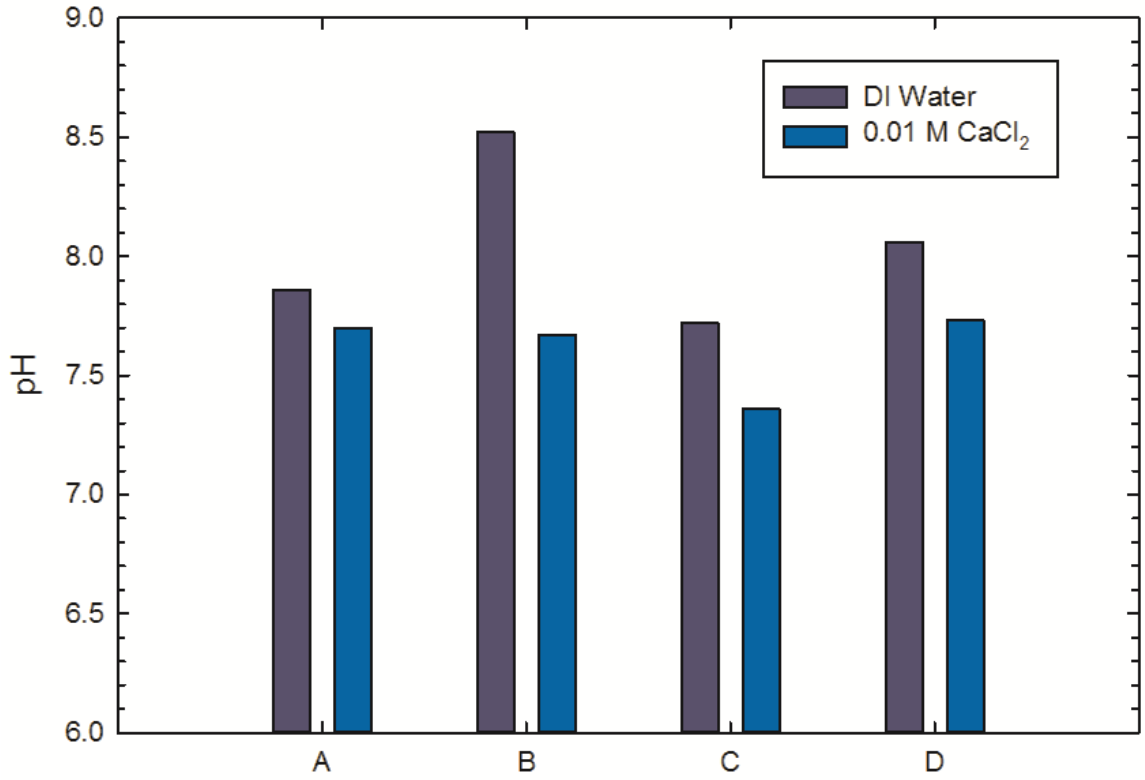

Figure 4.6. Comparison of measured pH values for the soil suite from both solutions used for soil pH measurement following ASTM D 4972.

Section 5 – U Sorption to Natural, Fine-Grained Barrier Materials

The literature contains many studies that have focused on interactions of a single radionuclide with purified, homogenous minerals. As the basis for building thermodynamic databases and laying experimental groundwork, these studies provide implications for the study of more complex natural and man-made geochemical systems. Building from the literature, a series of experiments were designed to investigate the interaction of uranium, as one of the primary radioactive components of LLW, with natural, non-homogeneous soils used as barriers within disposal schemes.

5.1 Methods

Batch sorption was conducted to analyze the single radionuclide sorption capacity of the chosen soil materials. Four primary batch sorption experiments were run: (1) control experimentation, (2) kinetics, (3) sorption edges/envelopes, and (4) sorption isotherms.

Experimentation was conducted in triplicate using 50-mL capped polypropylene reaction tubes. A total volume of 40 mL of solution, 10 mL less than the reaction tube size, was used during batch sorption for two reasons. First, experimentation was conducted under ambient atmospheric conditions, namely the inclusion of atmospheric levels of carbon dioxide during sample preparation. The remaining headspace within the reaction tubes allowed for continued inclusion of CO_2, as opposed to sparging with nitrogen under glovebox conditions. The inclusion of CO_2 within the system alters the potential solution chemistry of U, as uranyl-carbonate species dominate U speciation above pH 7 (Barnett et al. 2000). Second, in addition to atmospheric conditions, the additional headspace was critical for both end-over-end tumbling during reaction

experimentation and centrifugation following reaction timing to minimize potential pressure build-up within the tubes. Although the experimental issues could have been eliminated with less headspace than the allowed 10 mL, using 40 mL as the reaction volume provided additional ease of calculations and set-up during experimentation. Solution speciation for U(VI) open to atmospheric CO_2 was shown in Figure 2.9, and mirrors the described experimental system conditions and anticipated experimental speciation.

Within experimentation, 0.4 g of soil were added to the 40 mL of solution, providing a solid-to-liquid (S:L) ratio of 10 g to 1 L (10:1). This ratio was chosen to allow substantial interaction between the sorbent and sorbate, resulting in full saturation. Additionally, this S:L is readily comparable to other literature on radionuclide sorption studies (Bradbury and Baeyens 2005a).

Throughout experimentation, 0.05 M $NaClO_4$ served as the final ionic strength of the solutions. The pH of the solutions during batch sorption experimentation was adjusted using microliter (average addition: less than 4 µL) quantities of sodium hydroxide (NaOH) and hydrochloric acid (HCl) between initial experimental pH values of 5 and 9 in 0.5 pH unit increments. This range mirrors the complete pH range found within the collected DOE LLW leachates (Tian et al. 2014 – Section 3).

Two sets of controls were used for comparison and assurance of proper execution of the chosen experimental set-up. The first set of control experimentation paired each soil with the chosen background electrolyte to measure for any natural concentration of the radionuclide occurring within the soils. Additionally, the first set of experimentation allowed for documentation of cation leaching from soil solely in the presence of the background electrolyte. The second set of control experimentation paired the radionuclide in solution with the background electrolyte to account for any sorption occurring to the reaction containers.

Batch experimentation to determine the kinetics of the system was conducted at pH 7 to replicate the median leachate pH value across all DOE sites (data derived from Tian et al. 2014 – Section 3). A series of increasing reaction times from 15 min to 7 d was used to find the time necessary to reach steady state. A single radionuclide concentration was used throughout kinetics experimentation.

Sorption edges and envelopes were run via batch experimentation to characterize the sorption behavior on each of the soils. A single radionuclide concentration (20.62 Bq U/L (557 pCi U/L), or approximately 710 µg U/L) was used in creating the sorption edges/envelopes. The concentration of the solution (20.62 Bq/L) was chosen at a slightly greater concentration than the median value documented across the 4 DOE sites (Tables 4.7 and 4.8; Tian et al. 2014 – Section 3) to ensure sorption capacity beyond the documented maximum concentrations for most of the sites.

Sorption capacity of the soils was analyzed through the creation of sorption isotherms. Seven radionuclide concentrations, ranging from 6 to 6000 µg U/L (approximately 0.11 to 111 Bq/L (3.0 to 3000 pCi U/L)), were used to document sorption capacity within the soils. Sorption isotherms were conducted at initial pH values of 5, 7, and 9 to represent the boundary and mean pH values measured within leachate conditions. The range of U concentrations used for isotherm experimentation and stemming from the second solution (6 to 6000 µg/L or 0.11 to 111 Bq/L) were chosen to fully encompass and extend beyond the measured concentrations of both ^{238}U and Total Uranium in the leachate at all 4 DOE sites, within the measurable limitations of the ICP-OES (Tables 4.7 and 4.8; Tian et al. 2014 – Section 3).

Reaction time for experimentation was monitored during end-over-end rotation on ThermoScientific Labquake rotators, with continuous rotation of 8 rpm (rotations per minute). Following lab timing, samples were centrifuged at 5000 rpm for 10 min to separate the soil solids from solution. After centrifugation, sample aliquots were filtered

below 0.2 μm with polypropylene membrane filters and acidified below pH 2 with HNO_3 for storage prior to further analysis.

For all batch sorption experimentation, specimens were analyzed for changes to the concentrations of major cations (Na, Mg, K, and Ca) and structural components of the soils (Al, Fe, and Si) in solution via inductively coupled plasma optical emission spectrometry (ICP-OES). U was additionally measured via ICP-OES, in contrast to the more commonly used quantification methods involving ICP-MS. ICP-OES is not typically considered the most ideal spectroscopy for the measurement of U due to low wavelength intensities, signal interferences with Fe and OH^- groups, and the potential need for chemical separation (dos Reis et al. 2009). Contrastingly, ICP-MS provides measurement of U at ng/L concentrations with few elemental interferences (El Himri et al. 2000). However, as other aspects of the solution chemistry are easily and readily analyzed with ICP-OES, inclusion of U measurement for comparison was beneficial.

Measurement of radionuclides in solution can occur via multiple experimental methods. Specific quantification of uranium in solution is commonly executed using either liquid scintillation or ICP-MS. ASTM D 6239 details methodology for analyzing uranium concentrations by alpha-liquid scintillation spectrometry (α-LS). Sensitivity for the α-LS standard is listed for 0.037 Bq/L (1 pCi/L) or greater concentrations of U in waters. Comparatively, EPA Method 200.8 (EPA 1994) describes methodology for measurement of uranium and a suite of other dissolved elements in waters by ICP-MS. Typical method detection limits for U by Method 200.8 are given as 0.1 μg/L (aqueous) or 0.05 mg/kg (solids) total recoverable concentrations in scanning mode and 0.01 μg/L (aqueous) for both total recoverable and direct analysis concentrations in selection ion monitoring mode. Alternatively, minimum detection limits (MDL) for multiple U wavelengths via ICP-OES were shown to be 10 μg/L or less. For the given range of initial U concentrations used within the sorption experimentation, final solution

concentrations at the low end of the isotherm spectrum may decrease below the detection sensitivity for ICP-OES following sorption, but were anticipated to remain measurable for most samples at concentration levels well above the specified MDL.

5.2 Control Experimentation

Batch sorption control experimentation compares the interaction of two of the three system components used, namely radionuclides or soils with the matrix ionic strength solutions. For the soil control experimentation, a known quantity of each of the four soils or the glass beads was mixed with the designated volume of sodium perchlorate (the background electrolyte chosen for the system) as described in Section 4 (Materials), and allowed to react for a given time period. No uranium acetate was included in the solutions for the soil control experimentation. Alternatively, for the uranium control experimentation, a known concentration of uranium acetate was mixed with the designated volume of sodium perchlorate (40 mL total of solution) and allowed to react for the designated time period, with no mass of soil added. Control experimentation was conducted for both 24-h and 7-d reaction periods. Following the given reaction period, the concentrations of eight elements were measured via ICP-OES. The elements analyzed were Na, Mg, K, and Ca (representing the base cations typically satisfying cation exchange capacity in clays and clay-rich soils); Fe, Al, and Si (structural components of the soils); and U. The triplicate averages of the measured concentrations for Na, Mg, K, Ca, Fe, Al, and Si are listed in Table 5.1, while those for U are reported in Table 5.2. The EPA (40 CFR pt.136 2003) states that data collected via ICP-OES should initially be rounded to the thousandth decimal place (i.e. 0.001) following averaging of points. Additionally, all results should be reported in mg/L up to three (3) significant figures (40 CFR pt. 136 2003). The EPA approach has been applied to data reported for Na, Mg, K, Ca, Fe, Al, and Si. While the same rounding approach

has been applied to the corresponding data collected for U, quantities are reported in µg/L due to the significantly lower initial concentrations of U within the experimentation.

Only subtle differences in measured concentrations were observed between the 24-h and 7-d reaction periods amongst the analyzed and interpreted values for the measured elements. Figure 5.1 shows the measured concentrations of Na, K, Si, and U in the Soil *D* control experimentation between pH 5 and 9 for both reaction periods. Na concentrations are controlled by the addition of the 0.05 M $NaClO_4$ background electrolyte solution, resulting in substantially higher Na concentrations as compared to the other measured elements. K (representing the base cations) and Si (representing the structural components) concentrations in solution are consistent across both the pH range and the increased reaction period. For both the base cations and structural component elements, relative consistency in measured values for the increased reaction periods confirms that no dissolution of the soil is occurring via end-over-end rotation with the background electrolyte solution. Additionally, the longer reaction period displays no undue influence to the soil. Consistency between concentrations was anticipated and confirmation helps to provide baseline information on the experimental system.

Measured U concentrations in the soil control experimentation show some variability between pH levels, but are similar between the 24-h and 7-d reaction periods. The measured U concentrations are very close to the minimum detection level (MDL) for the ICP-OES U 263.553-nm wavelength, determined via the procedure described by the EPA in Appendix B of 40 CFR pt.136 (2003) to be 10 µg/L (or 10 ppb). Concentrations reported below this value can be interpreted as having negligible measured U. As such, the measured concentrations of U originating in the soil is minimal, and fall within or below the expected range of U in natural soils, at 0.7 to 11 ppm (Emsley 2011).

Uranium concentrations remaining in solution for the solution control experimentation across the tested pH range for the 24-h and 7-d reaction periods are

shown in Figure 5.2. Similar to the solution control experimentation shown in Figure 5.2, Figure 5.3 provides results for additional solution control experimentation at pH 7, with time frames ranging from 15 min (900 s) to 7 d (604800 s), to mimic the time frames investigated during kinetics experimentation. The points for 24 h and 7 d mirror the pH 7 points for the same reaction periods in Figure 5.2. Accompanying Figure 5.3, Figure 5.4 compares the measured final pH at each of the kinetics time frames to the measured U concentrations during solution control experimentation.

The starting uranium solution concentration of 20.62 Bq/L (557 pCi/L) corresponded to 1990 µg/L of uranyl acetate, and 1117 µg/L of uranium based on the uranyl acetate chemical formula. Given the initial added U concentration of 1117 µg/L throughout experimentation, the amount of uranium remaining in solution across the entire pH range suggests that some sorption to the solution storage containers was a factor during experimentation. Barger and Koretsky (2011) noted loss to reaction vessels of up to 90% of initial U(VI) concentrations. The concentration of U removed from solution during control experimentation ranges from 19 to 40% of the starting concentration (209 to 443 µg/L) during the 24-h reaction period and 35 to 60% of the starting concentration (395 to 669 µg/L) during the 7-d reaction period, as measured on the U 263.553-nm wavelength via ICP-OES. Consequently, while sorption to the storage vessels most likely occurred, a readily measurable and consistent quantity of U remained in solution prior to the inclusion of the sorbents of interest, allowing for quantification and comparison during experimentation. In deference to these factors, two lines are shown on Figure 5.2. The dashed line, at 749 µg/L, represents the average concentration of U in solution across all pH levels for both the 24-h and 7-d control experimentation. The solid line, at 710 µg/L, represents the average U solution concentration for the time frames used for kinetics experimentation.

Across the time frames used for kinetics experimentation, 24 h appears to be an outlier from the other points. For the time periods between 15 min and 4 h as well as the 7-d time period, 36% to 42% of the starting uranium concentration was removed from solution (400 to 465 µg/L), while only 20% of the starting uranium concentration (221 µg/L) was removed at the 24-h reaction period. The reasoning behind this discrepancy amongst the time frames is likely the consequence of the experimental execution order. As shown in Figure 5.2, [U] is consistent for the series of 24-h reaction period experiments across the pH range, all of which were conducted at a single time, earlier than either the 7-d experiments or those used to mirror the time frames for kinetics experimentation. The only exception occurs at pH 9 for both the 24-h and 7-d reaction periods. The lower measurements at the highest pH may be a consequence of the anticipated change in speciation at higher pH, as shown in the speciation diagram for the system (Figure 2.9). Based on these findings, the 710 µg/L value was chosen as the reference $[U]_o$, or initial concentration value, for use throughout kinetics and edge and envelope experimentation.

As found during both the kinetics and E&E experimentation, solution control issues influenced sorption isotherm control experimentation. As addressed in Section 4.2, Solutions, a separate uranium acetate solution was created for use during isotherm experimentation from that for the rest of the single radionuclide experimentation. The 42800 µg/L of uranium acetate were added to the stock solution for an activity of 443.4 Bq/L (11984 pCi/L) based on the MSGS-listed activity. Within isotherm experimentation, a range of 6 to 6000 µg/L (0.11 to 111 Bq/L (3.0 to 3000 pCi/L)) was anticipated through serial dilution of the stock solution. Some differences were noted in the measured concentrations of the solution control experimentation and values based on the added uranium acetate, as shown in Table 5.3. However, the anticipated range provides the most logical concentrations for comparison in the context of the values measured in

solution during experimentation with the soils (discussed in detail in Section 5.5, Isotherm Experimentation). For that reason, calculations for isotherm experimentation have used the range of 6 µg/L to 6000 µg/L. The values measured during isotherm solution control experimentation are provided solely for comparison.

5.3 Kinetics Experimentation

Reaction timing, or the chemical kinetics of the chosen soil-U systems, was analyzed through comparison of increasing interaction time between the components. Time periods ranged from 15 min (900 s) to 7 d (604800 s). The same elements and methods of analysis used during control experimentation were again used for comparison of the experimental interactions. Tables 5.4 and 5.5 list the triplicate averages for the seven other elements and U, respectively.

Figures 5.5 through 5.14 show the comparison of aqueous U concentrations remaining in solution, or [U], in µg/L, over the time periods measured from the kinetics experimentation. Figure 5.5 compares the four study soils and the glass bead sorption control to one another. Figures 5.6 through 5.14 display the individual soils and the calculated standard deviation at each time step for the triplicate experimentation. All data points in Figures 5.6 through 5.14 represent the calculated mean from the three triplicate experiments. Concentrations are taken from ICP-OES measurements using the U 263.553-nm wavelength, with measurements calibrated above the MDL of 10 ppb (10 µg/L). The starting U concentration, $[U]_o$, for all kinetics experimentation was 710 µg/L.

Kinetics experimentation ideally allows interpretation of the time necessary to reach steady state between the experimental soils and U solution. The witnessed steady state of the system serves as a representative environment for equilibrium conditions under a time scale appropriate to laboratory-based investigations. Research within the literature has often focused on significantly longer time frames for investigating U

kinetics, up to 18 weeks (Bai et al. 2009; Missana et al. 2004). However, Bai et al. (2009) note that greater than 85% of the initial U concentration reached what the authors term “equilibrium” within 72 h of initial experimentation. The “equilibrium” described by Bai et al. (2009) is the apparent steady state of the investigated system. Consequently, the shorter time frame indicated for study within the documented experimentation should still allow for investigation of steady state interactions between the U solution and sorbents of interest.

Analysis of the trend displayed by the glass beads (Figure 5.6), included experimentally to serve as a control “soil” against which no or little U sorption is expected to occur, is important for understanding interactions of the active sorbents and the solution control experimentation. Comparing the values across the glass bead kinetics experimentation shows that, while more U remains in solution at the 15-min time frame for the glass beads than the solution control experiment, likely a consequence of earlier experimentation, a substantial amount of additional U is removed by the 7-d time frame. The 7-d solution control U concentrations (Figure 5.3) are directly comparable to the 7-d glass beads kinetics data, with approximately 650 µg/L of U remaining in solution for both experimental sets. Differences between time periods are readily attributable to the storage containers and order of experimentation. As glass beads kinetics experimentation occurred prior to the solution control kinetics experimentation, cross comparison to the 24-h solution control experimentation, executed at the same time, shows similar concentrations to the glass beads. Consequently, the glass beads serve as a reasonable control to the other soils used within experimentation, showing no additional sink for U sorption to occur.

Looking at the individual soils, varying trends emerge over the course of kinetics experimentation. Soil *A* (Figures 5.7 and 5.8) displays increased sorption as time increases, following typical trends for kinetics experimentation. The concentration of U

remaining in solution with Soil *A* falls below the MDL (10 µg/L) after 1 h of reaction time. Although the measured concentrations at the 24 h reaction period are higher than the MDL, the concentrations remaining in solution across all time periods show near total sorption of the initial U concentration. The amount of U remaining in solution for the Soil *B* soil (Figures 5.9 and 5.10) shows similar U concentrations at the shortest (15 min or 900 s) and longest (7 d or 604800 s) reaction times, with points with both increased and decreased sorption in the intermediate reaction times, for no discernible trend across time. The total concentrations of U remaining in solution across all reaction periods for Soil *B* are much higher than the other experimental soils. Soil *C* (Figures 5.11 and 5.12) follows a similar trend to Soil *A* and other traditional sorption kinetics experimentation, with a higher concentration remaining in solution at the shorter time frames, and slowly decreasing solution concentration as steady state is approached. The concentration trend for both Soil *A* and Soil *C* is partially influenced by the low concentrations of U remaining in solution for both soils, with many points falling below the MDL in both instances. As shown by Figures 5.8, 5.10, and 5.12 for Soils *A*, *B*, and *C*, respectively, no consistent correlation can be drawn between the final measured experimental pH and [U]. For Soil *D*, the amount of U remaining in solution increases as reaction time increases (Figures 5.13 and 5.14), suggesting decreased total sorption with increased reaction time. Due to the experimental set-up used for determining reaction kinetics, decreased sorption onto the sorbent surface and actual U desorption off of the sorbent is indistinguishable. However, as shown in Figure 5.14, as final pH of the experiments using Soil *D* increased, so did [U], suggesting that the system may be more heavily influenced by the impact of system speciation (see Figure 2.9 for the corresponding U system speciation).

5.4 Sorption Edges and Envelopes Experimentation

Sorption edges and envelopes (E&E) depict the amount of a constant initial concentration of a given species of interest sorbed to a given sorbent with changing pH. Edges and envelopes describe two of the characteristic shapes taken by this type of experimentation. Sorption edges depict behavior where a small quantity of the sorbate is sorbed at low pH, while the sorbed concentration increases with increasing pH, typically to a plateau. Sorption envelopes depict the opposite behavior – large quantities of a sorbate sorbed at low pH, with an initial platform, and a decrease in the quantity sorbed as pH increases. Tables 5.6 and 5.7 list the triplicate averages for the sorption edge and envelope experimentation, for the seven other elements and U, respectively.

Figures 5.15 through 5.25 compare the collected U concentration data for all sorption edge and envelope experimentation. Figure 5.15 compares the four study soils in addition to the glass bead sorption control across the studied pH range. Figures 5.16 through 5.25 display U concentrations for the glass beads and the individual soils along with the calculated standard deviation at each initial pH. All data points in Figures 5.16 through 5.25 represent the calculated mean from the three triplicate experiments. Reported concentrations are taken from ICP-OES measurements using the U 263.553 nm wavelength, with measurements calibrated above the MDL of 10 ppb (10 µg/L), accounting for the EPA reporting stipulations described in Section 4.2. The starting U concentration, $[U]_o$, for sorption edge and envelope experimentation was 710 µg/L. Figure 5.26 compares the collected U concentration data for all sorption edge and envelope experimentation of the 4 study soils across both in the studied initial pH range and the final measured pH range. Final pH measurements from experimentation show approximately a 0.75 to 1 pH unit range for the 4 soils (right panel of Figure 5.26) as a consequence of the soil buffering capacity and initial soil pH values.

Glass beads serve as a sorption control in the sorption edge and envelope experimentation, as with the kinetics experimentation. Figures 5.16 and 5.17 depict the change in U concentration between pH 5 and pH 9 in 0.5 pH unit increments for the glass bead control. Figure 5.17 compares the U remaining in solution to the U sorbed as a function of the starting concentration ($[U]_o$ = 710 µg/L), as well as the percentage sorbed and/or removed from the initial glass bead solution. Comparing results of the glass beads E&E experimentation to the solution control experimentation over the same 24-h reaction period (Figure 5.2) shows a slight reduction in the amount of U remaining in solution across the entire pH range. As discussed in Section 5.2, between pH 5 and 9 the 24-h solution control experimentation showed 19% to 40% (209 µg/L to 443 µg/L) of the starting concentration (1117 µg/L) removed from solution. For an identical starting concentration (1117 µg/L), initial pH range, and time frame, the glass bead E&E control had 37% to 51% (411 µg/L to 571 µg/L) removal of the starting concentration from solution. However, adjusting to the reference $[U]_o$, 710 µg/L, as shown in Figure 5.17, shows little difference between the glass beads and solution control experimentation, suggesting that the glass beads again serve as a consistent control surface for the system.

One primary difference between the solution control and glass bead E&E experimentation is the apparent trend across the initial measured pH range. While the trend for [U] displayed by the solution control experimentation is relatively consistent between pH 5 and 8.5, with a sharp drop-off in [U] at pH 9 (Figure 5.2), the glass bead E&E experimentation shows a significantly higher [U] at pH 5, with a steady reduction in [U] occurring between pH 5.5 and 8, and a similar sharp drop-off in [U] from pH 8.5 to 9 (Figures 5.16 and 5.17). The change in magnitude of [U] from pH 5 to 9 for both sets of experimentation is similar, on the order of a difference of approximately 160 µg/L between the lowest and highest pH values for both experiments. Overall, the trends

displayed by both sets are similar, although more pronounced in the glass beads experimentation, and mirror anticipated trends from the system speciation (Figure 2.9). Further, differences in the overall [U] for both sets of experimentation are a consequence of the experimental timing, resulting in the reference $[U]_o$ serving as a good indicator of the true initial concentration during the glass beads E&E experimentation.

Results for E&E experimentation for Soil *A* over the 24-h reaction period, shown in Figures 5.18 and 5.19, are similar to those from kinetics experimentation, with near total removal of U – more than 99% $[U]_o$, 710 µg/L - is shown for all initial pH levels. Figure 5.19 compares [U] to the concentration of U sorbed, along with providing the % of U sorbed from $[U]_o$, across the tested pH range. All ICP-OES results, accounting for standard deviation between the triplicated experiments, fall below the MDL level of 10 µg/L, suggesting very little U remains in solution.

As shown in Figures 5.20 and 5.21, Soil *B* displays a decrease in [U] between pH 5 and 9, assuming an S-curve shape reminiscent of more traditional sorption edge configurations. Although showing similar behavior to the glass beads, Soil *B* displays greater total sorption, with 24 to 76% $[U]_o$ removed.

Figures 5.22 and 5.23 display results for E&E experimentation using Soil *C*. As with Soil *A,* at least 99% $[U]_o$ was removed from solution across all initial pH values by Soil *C*. Consequently, no distinctions can currently be drawn regarding the influence of pH on sorption in the experimental range for Soil *C*.

Figures 5.24 and 5.25 show the E&E experimentation for Soil *D* for the 24-h reaction period between pH 5 and 9, with $[U]_o$ = 710 µg/L. For Soil *D*, the concentration of U remaining in solution steadily decreases between pH 5 and 9, without reaching an uptake plateau over the initial pH range. Between 75 and 83% $[U]_o$ is removed over the tested pH range.

5.5 Sorption Isotherm Experimentation

Sorption isotherm experimentation is designed to investigate the sorption capacity for a given sorbent at a single constant temperature, pH, and reaction time period for an increasing range of initial sorbate concentrations. Three separate initial pH levels were employed during experimentation: pH 5, 7, and 9. The chosen initial pH range encompasses the measured pH range for LLW leachate from four DOE LLW sites (Tian et al. 2014 – Section 3), as well as the mean measured value across all LLW sites. Tables 5.8 and 5.9 provide the triplicate average measured concentrations for the seven additional elements and U for the sorption isotherm experimentation.

Results for isotherm experimentation for the four study soils are shown in Figures 5.27 to 5.42. Figures 5.27 to 5.30 contain results for Soil *A*, while results for Soil *B* are found in Figures 5.31 to 5.37. Results for Soil *C* and Soil *D* are shown in Figures 5.38 to 5.41 and 5.42 to 5.45, respectively. The figures for all sorption isotherm experimentation compare the steady-state concentration, or C, of U, on the x-axis in µg/L, to the concentration of U sorbed to the soil surface, or X, on the y-axis, which represents the maximum U sorption in µg of U sorbed per mg of soil solid. The values of $[U]_o$ used throughout isotherm experimentation (termed C_o for original concentration in information corresponding to isotherm data) correspond to the entire intended experimental range, as described in Section 4.2, Solutions. Additionally, all figures include points that mirror $[U]_o$ for both the kinetics and E&E experimentation, at 710 µg/L.

Isotherm fitting parameters for the four soils are reported in Tables 5.10 to 5.14. The equations and parameters used for isotherm fitting are explained in Appendix D. The ubiquitous nature of liquid-solid interactions and their consequential impact on the environment highlight the importance of accurate isotherm modeling and prediction (Limousin et al. 2007). As discussed in Section 2.4.3 (Interpretation of Results and Methods), the literature on contaminant sorption contains a variety of modeling

mechanisms that have been applied to systems with varying sorbates and sorbents (Bai et al. 2009; Cornell 1993; Galunin et al. 2010; Heberling et al. 2008; Humelnicu et al. 2011; Iijima et al. 2010; Omar et al. 2009; Stewart et al. 2010; Tsai et al. 2009). Three prominent and commonly used fitting mechanisms were applied throughout the following discussion of the experimental results, and describe the change in affinity between the U sorbate and the various soil sorbents employed. While many other fitting mechanisms have been derived within the literature at large and described in detail by Foo and Hameed (2010) and Limousin et al. (2007), the models used in describing the experimental system's behavior are those most commonly used for geochemical systems, allowing ease of comparison to behavior documented within the literature.

The employed fitting mechanisms are distinct from another based on both their derived equations and the system behavior they are intended to most closely model. The Linear model describes sorbent behavior where as more sorbate is added to a system, the affinity of the sorbent for the sorbate continues to increase. Typically the Linear model works best when sorption is particularly efficient, characterized by a system where there are low concentrations of sorbate sorbing to a small number of available surface sites on a sorbent. The Freundlich model builds off of the Linear model, but accounts for a slowing rate of sorption at higher sorbate concentrations through the inclusion of an exponential variable. Of importance is the Freundlich isotherm model's ability to describe sorption occurring in multiple layers at the sorbent surface, as well as its application to non-uniform sorbate and sorbent distributions (Foo and Hameed 2010).

The Langmuir model is the most frequently used isotherm across sorption studies and specifically for radionuclides. The Langmuir model assumes that sorption occurs at sites with specific surface areas in a single, uniform layer on a sorbent surface. Sorption behavior that is accurately modeled by the Langmuir equation represents saturation of a monolayer system (Galunin et al. 2010). Important to note for the

Langmuir model is that differences in sorption are a result of sorbent-sorbate interactions, with no inclusion of lateral interactions of the sorbate at the sorbent surface. Additionally, for all three of the employed isotherm models, the described interactions in no way act to detail the actual, physical sorption mechanisms occurring at the sorbent surface. Instead, they serve to describe witnessed, measured interactions between solution concentrations of sorbate between the sorbent and solution during steady-state interactions.

The average final pH values for each initial pH increment are provided in Table 5.15. Although compression of the intended pH range occurs for all 4 study soils due to soil buffering, the resultant final pH values remain distinct from one another, allowing each to represent an individual isotherm. To simplify descriptions of the distinctions occurring between the various isotherms for individual study soils throughout the text, descriptions and figure captions for the experimental results will refer to the initial tested pH levels, rather than the steady-state pH values provided in Table 5.15. Due to the divergence in final steady-state pH measurements from the initial pH adjustments, cross-comparisons between the different study soils will be based only on those isotherms with similar final pH measurements.

5.5.1 Soil A Isotherm Results

The experimental sorption isotherm results for Soil *A* are found in Figures 5.27. to 5.30. Figure 5.27 shows a comparison of the three tested initial pH levels for Soil *A*. All three isotherms assume a L-curve shape, due to the high affinity of Soil *A* for U within the given system constraints. The L-curve isotherm shape is indicative of “progressive saturation” of the soil sorbent, as described by Limousin et al. (2007). As shown in Figure 5.27, Soil *A* shows a slight decrease in sorption affinity for U with increasing pH, indicated by the shift towards higher C values at approximately equal X values for both

pH 7 and pH 9 when compared to results from pH 5. However, the differences are marginal between the 3 initial pH values, particularly when viewed in the light of the similar variance as expressed by the Total Sum of Squares (indicated in Table 5.10) in the experimental results across all 3 initial pH values. The experimental results suggest that the sorption affinity of Soil *A* for U under the given experimental conditions is not reliant upon pH of the system for the tested C_o values.

Results for Soil *A* at initial pH 5, pH 7, and pH 9 are shown in Figures 5.28, 5.29, and 5.30, respectively, with the related fitting parameters found in Table 5.10. Comparing the fitting parameters for each individual plot, the Linear, Freundlich, and Langmuir isotherm models all provide a significant level of accuracy in fitting the data, as shown by the r^2 values. The r^2 values for all three fitting mechanisms across the 3 tested initial pH values all are greater than 0.95. At initial pH 5 and initial pH 7, the Langmuir model shows the most accurate fitting of the experimental data across all C_o values, as indicated by both the highest r^2 values amongst the three models (0.979 and 0.986, respectively – Table 5.10) and the plotted comparisons shown in Figures 5.28 and 5.29. Although the Langmuir model also very accurately fits the data for initial pH 9 (r^2 = 0.990, Table 5.10), the Freundlich model has a slightly higher r^2 value (0.992, Table 5.10), derived in part from a more accurate fit through the lower C_o values, as shown in Figure 5.30. The high r^2 values for Soil *A* suggest the system sorbs U in a single layer, with a level of pH dependence indicated by the variability between the isotherms and in the incorporation of K_L.

As with all isotherm fitting, the accuracy of each model is influenced by a variety of factors, specifically the variance of the experimental data and the behavior that data displays. Further, in the case of Soil *A*, the small solution concentrations of U measured following interaction with the soil sorbent, at less than 1% of C_o remaining in solution for the upper 4 C_o values (see Table 5.9), make accurate fitting and prediction of expanded

trends more difficult. The extremely high affinity of Soil *A* for U under the tested concentration levels and given experimental conditions suggest that within the investigated system, a true sorption plateau – where fewer sites remain open for sorption to occur as a higher concentration of sorbate is added to the system – has not been reached. As indicated by Limousin et al. (2007), differentiation of L-curve isotherms with clearly defined sorption plateaus versus gentle curves, similar to the behavior of Soil *A*, is frequently difficult based solely on a single set of experimental data. The lack of a sorption plateau is further exemplified by the calculated values for X_{max}, the maximum sorbate loading calculated based on the experimental data, within the Langmuir model for each of the initial pH values. Across all 3 pH levels, the calculated X_{max} values range from 3 to more than 10 times the experimentally-derived X values, indicating the potential for greater sorption loading on Soil *A* under the given conditions.

5.5.2 Soil B Isotherm Results

Figures 5.31 through 5.37 provide experimental results for sorption isotherm experimentation using Soil *B.* Figure 5.31 compares the results for the three initial pH levels. In opposition to the results for Soil *A*, the three initial pH levels show distinct behavior from one another for Soil *B*. As the initial pH of the experimental system increases, Soil *B* shows increasing sorption affinity for U, as characterized by increasing X values with decreasing corresponding C values. This is particularly highlighted in the difference between the isotherms for initial pH 5 and pH 9. While the isotherm from the initial pH 5 data suggests the approach towards a sorption plateau, the pH 9 isotherm continues to trend upwards, acting as an indicator of the increased sorption affinity at the higher pH level.

Figures 5.32 through 5.37 show the experimental results and isotherm models for Soil *B* at initial pH values of 5, 7, and 9, with the corresponding isotherm fitting

parameters provided in Table 5.11. Experimental results for the initial pH 5 sorption isotherm show a clear divergence from the Linear isotherm model, as shown by Figure 5.32 and the significantly lower r^2 value (0.721, Table 5.11). The Soil *B* initial pH 5 isotherm approaches a true sorption plateau, such as that exemplified by the Langmuir model with a finite X_{max} value representing the maximum sorption loading. Of importance in comparing the various isotherm models and their accompanying accuracy is the presence of a distinct outlier amongst the initial pH 5 data. Although the point that mirrors the C_o concentration used for kinetics and E&E experimentation in theory should have C and X values that fall between those for the 600 and 3000 µg/L C_o concentrations, the corresponding X value for C_o = 710 µg/L falls far below that of its neighbors. The accuracy of the model across modeled C_o values for both the Freundlich and Langmuir models is lower than what would be expected from the assumed isotherm shape of the data points created via serial dilution. Consequently, although both models show a relatively high level of accuracy (with r^2 values > 0.92), modeling of only the data resulting from serial dilution of the solution specifically created for the isotherm experimentation shows a near perfect fit to Langmuir model behavior (r^2 = 0.999, adjusted parameters shown in Table 5.12, and displayed in Figure 5.35). The discrepancy between the mirrored kinetics and E&E points could be attributed to a number of variables within the system, including the points having final pH values outside of the standard deviation of the total set, alterations to the assumed constant solution concentration of U or $NaClO_4$, or undue influence of the natural soil heterogeneity.

The initial pH 7 data for Soil *B* assumes a L-curve isotherm, similar to that of the initial pH 5 data (Figure 5.32 and Figure 5.33 for pH 5 and pH 7, respectively). Consequently, both the Freundlich and Langmuir isotherm models have high r^2 values (0.978 and 0.984, respectively – Table 5.11) reflective of the similarity present between

the two models and the experimental data. The initial pH 7 data does not appear to approach as defined a plateau as the initial pH 5 data, as evidenced by the both the higher r^2 value for the Linear model (Figure 5.33 and Table 5.11) and the continued upward trend of the data across the upper C_o values, particularly when compared to the same points for initial pH 5. This suggests that the initial pH 7 data may be closer to the initial H-curve mechanism indicative of high affinity sorption with low C_o values, or the initial behavior of high affinity systems prior to more complete solution concentration saturation. Although the 710 µg/L C_o again appears as a potential outlier influencing the variance and accuracy of the fitted models, unlike with the initial pH 5 data the differences between inclusion and exclusion of the mirrored points is marginal, only serving to further bolster the application of Langmuir model behavior to the displayed experimental findings.

Figure 5.34 depicts the experimental data and fitted models for the initial pH 9 data for Soil B. As shown in the comparison to the other initial pH levels found in Figure 5.31, the affinity of Soil *B* for U increases with increasing pH, most noted at pH 9. In opposition to the other two initial pH levels, the initial pH 9 data is most closely modeled by the Freundlich model (r^2 = 0.994, Table 5.11), suggesting a closer approximation to the exponential form indicating a slowing rate of sorption at higher sorbate concentrations implied by the Freundlich equation. However, all three models closely fit the experimental data set (all r^2 > 0.97, Table 5.11). As such, the initial pH 9 data is shown to take a H-curve shape, indicative of the increased sorption affinity of Soil *B* at the higher pH and suggestive of further sorption capacity for U at the higher pH.

Figures 5.36 and 5.37 provide a similar comparison of the serial dilution isotherm behavior at pH 7 and 9 to complement the data in Table 5.12 and the pH 5 results shown in Figure 5.35.

5.5.3 Soil C Isotherm Results

Sorption isotherm experimentation for Soil *C* is depicted in Figures 5.38 to 5.41, with the accompanying isotherm fitting parameters listed in Table 5.13. Figure 5.38 provides a comparison of the three initial pH levels for Soil *C*. In comparing the 3 initial pH isotherms of Soil *C*, similarities can be drawn to the behavior displayed by both Soil *A* and Soil *B*. As with Soil *B*, Soil *C* shows an increase in sorption affinity with increased pH at the highest C_o values. However, for the low C_o values, the behavior of Soil *C* is more similar to that of Soil *A*, with little displayed difference across the changing pH levels. Although showing little alteration in behavior between the pH levels, each isotherm takes a L-curve shape, indicative of the high affinity of Soil *C* for U under the given experimental conditions across all pH levels.

Figures 5.39 to 5.41 show the sorption isotherms and models for initial pH 5, 7, and 9, respectively. The experimental data for initial pH 5 (shown in Figure 5.39) is relatively well modeled by the three isotherm models, as evidenced by the respective r^2 values (all $r^2 > 0.95$, Table 5.13). For the three isotherms for Soil *C*, the initial pH 5 experimental data assumes the most defined L-curve shape of the set. Consequently the initial pH 5 data is most closely modeled by the Langmuir model ($r^2 = 0.982$, Table 5.13), which assumes sorption occurs in a single, uniform monolayer across the surface of the sorbent and approaches a finite maximum surface loading.

Figures 5.40 and 5.41 depict the data for initial pH 7 and pH 9. While all three models are depicted on the accompanying figures for the higher initial pH values for Soil *C*, the Linear and Langmuir models are indistinguishable from one another within the figures. The similarity is further emphasized by the identical r^2 values for the models at each pH (Table 5.13). For the experimental data for both initial pH 7 and 9, the Freundlich model most accurately models the displayed behavior ($r^2 = 0.971$ and 0.938 for initial pH 7 and 9, respectively, Table 5.13). Both data sets show little resolution into

the typical characteristic shapes found for traditional isotherms, as exemplified by the dispersion of points at the low C_o values for both pH levels. This dispersion is likely a further consequence of the low C values falling near or below the indicated MDL level for the selected ICP-OES wavelength, making resolution of the accompanying data less than ideal. The same reasons influence the accuracy of the various isotherm models for modeling the data set, and result in r^2 values lower than those for initial pH 5 with its more defined behavior (see Table 5.13 and Figures 5.39 to 5.41 for initial pH 5 to 9, respectively).

5.5.4 Soil D Isotherm Results

Sorption isotherm experimental data for Soil *D* is shown in Figures 5.42 to 5.45. For all sorption isotherm experimentation for Soil D, an additional C_o value was included at a lower concentration than those used for the other 3 soils. The additional value was eliminated from the experimentation from the other soils due to the expectation of the initial C_o value falling below the well-defined MDL limit for U via ICP-OES, making steady-state solution measurements less than ideal. Figure 5.42 displays the average values for the 3 initial pH levels tested for Soil *D*. Soil *D* displays C values for each pH level that are well defined and distinct from one another, similar to the behavior of Soil *B*. As shown in Figure 5.42, Soil *D* shows an increase in sorption affinity for U with increasing pH, indicated by the shift towards lower C values and higher X values by both initial pH 7 and pH 9 when compared to results from initial pH 5.

Figures 5.43 to 5.45 contain the experimental results and isotherm fits for Soil *D* at initial pH values of 5, 7, and 9, respectively. In the case of all 3 pH levels, the various isotherm models provide accurate fits to the experimental data, with r^2 values above 0.92 for each respective data set. Amongst the models used, the Freundlich isotherm model most closely represents the behavior of each set of experimental data, a noted contrast

from the Langmuir model employed as the most accurate fit for a majority of the other soil data sets. Congruently, the Freundlich model has the lowest sum of squares at each pH level, representing the smallest amount of divergence from the data set, jointly confirming the r^2 values (see Figures 5.43 to 5.45 and Table 5.14).

The divergence of the Soil *D* isotherms from Langmuir model behavior is influenced in part by the assumed shape of the experimental data. Unlike the other study soils, the sorption isotherm data for Soil *D*, particularly for initial pH 7 and 9, trends towards a S-curve isotherm shape, indicative of a lower affinity system. The S-curve isotherm takes a sigmoidal shape with a differentiated inflection point, typically located at the solution concentration where sorption begins to outcompete complexation of the sorbate metal by solution ligands (Limousin et al. 2007). S-curve isotherms are characteristic of materials where fewer sites open on the sorbent surface as sorbate loading increases and original surface sites become filled.

5.5.5 Isotherm Discussion

Modeling of sorption isotherms relies on relatively simple equations to describe and interpret complex behaviors. As noted by Shackelford (1991), sorption behavior for most metal species is non-linear at the concentrations found within landfill leachates. Although LLW leachate differs from MSW leachate as discussed in depth within Section 3, the sorption behavior of radionuclides is still anticipated to be non-linear within most liner materials due to the leachate concentrations. Highlighting the complexity present within the given systems are the data sets where multiple models accurately represent the experimental results, as shown for the initial pH 9 isotherm for Soil *A*. Within the literature, other systems have demonstrated similar behavior to that shown experimentally for Soil *A*, such as the modeling of Cs sorption on crushed granite by

Tsai et al. (2009), where both the Freundlich and Langmuir models approached unity (i.e. $r^2 = 1.00$).

Some authors have suggested that the transition between models represent changes as a consequence of concentration increases. Baeyens and Bradbury (1997) found both Linear and Freundlich model behavior for Ni on Na-montmorillonite as a result of increasing concentration due to the experimental set-up of using serial dilution through batch sorption. Dong et al. (2005) demonstrated a similar relationship between Linear and Freundlich model behavior for increasing concentrations of U(VI) on Hanford soils to that of Baeyens and Bradbury (1997) for Ni. Similarly, Volchek et al. (2011) showed a transition from Langmuir to Freundlich behavior for Cs on cement mortar, suggesting a move from a monolayer system to multi-layer behavior due to increased potential for interactions with the interior of the solid structure with increasing sorbate/sorbent saturation, echoing the 2 distinct sorption behaviors Poinssot et al. (1999) found for Cs on illite. Within the experimental data, use of multiple sorption models to explain variations or transitions in sorption behavior could account for some of the differences found over the course of serial dilution, particularly as found for Soil *B* (see Figure 5.31 and 5.35).

Across all 4 soils, differences in sorption behavior are found for relatively small differences in pH (see Table 5.14 for final pH across each isotherm set). Baeyens and Bradbury (1997) noted that differences for sorption of Ni on Na-montmorillonite were highly pH-dependent under conditions using similar experimental conditions to those used within this study. Further, Chen and Lu (2008) found that small pH changes affected the overall system for radio-Co on montmorillonite, attributed in part to the formation of inner-sphere type complexes between the sorbate and sorbent. Singer et al. (2009) further connected sorption behavior at different concentrations to system pH for

U(VI) on chlorite, where the solution speciation at different pH levels was shown to have a direct connection to both U removal from the system and isotherm model accuracy.

Throughout the experimental system, U sorption on each of the four study soils is shown to be non-linear, split between Langmuir and Freundlich behavior dependent on both the soil and pH in question. U behavior within the literature has also been shown to be mostly non-linear, with a few notable exceptions. Within the major findings report regarding uranium geochemistry at the Hanford site, Zachara et al. (2007b) state that U(VI) sorption is expected to be linear on most sediments found at Hanford for concentrations below saturation of available sorption sites, defined in the context of the report as 1 mg/L of U. The dependence on Linear behavior within the report differs from other literature studying U behavior on Hanford soils (Bai et al. 2009; Barnett et al. 2000; Stewart et al. 2010; Um et al. 2010b), including that of Dong et al. (2005), whose findings are highlighted and substantiated within the Zachara et al. (2007b) report. However, the argument for Linear behavior as expressed by Zachara et al. (2007b) encapsulates the difficulty in using K_d values, as the critical variable within the Linear isotherm model (see Appendix D) in addition to a commonly used parameter for cross comparisons of materials (see Appendix C), in describing sorption behavior, particularly for U. Linear isotherm behavior results in a single K_d value across changing concentrations. As noted by Curtis et al. (2004), when isotherm behavior is non-linear, the resulting K_d values are non-constant – a critical observation in assessing changes to behavior in the U(VI) system due to its variability in solution state and the variety of mechanisms that can result in attachment to solid phases. Davis et al. (2004) delineated the two sides of the single K_d argument as the push for increased computational efficiency through use of a constant value versus more accurate modeling through use of other non-linear isotherm models and despite the development of appropriate thermodynamic models for U(VI). Consequently, while the Zachara et al. (2007b) report

has implications for work at Hanford and in regards to leachate and sorption behavior occurring at the ERDF at Hanford elsewhere within this dissertation, the non-linear sorption behavior of U is contextually acceptable for both other reports within the literature and the experimental results of this study.

A few studies have specific implications for the experimental results described within the previous sections. Within the experimental system, three main aspects shape the behavior of the sorbate/sorbent interactions: U, acting as the sorbate of interest; the role of carbonate due to the inclusion of atmospheric levels of carbon dioxide and the concurrent impact on U speciation; and the mineralogic heterogeneity within the natural barrier soils. The study of U sorption on ferrihydrite by Waite et al. (1994) serves as a basis for much of the information found within the literature in the intervening 20 years. Of importance within the Waite et al. (1994) study is the characteristically non-linear, Freundlich-type sorption behavior of U on ferrihydrite. Additionally, Waite et al. (1994) showed a shift of edge behavior to a lower pH range in the alkaline region as U(VI) concentrations increased, indicative of the increasing surface coverage by U for the ferrihydrite sorption sites. Barnett et al. (2000) created non-linear U sorption isotherms on natural sediments collected at the Oakridge, Savannah River, and Hanford sites. The authors assert that the high r^2 values ($r^2 > 0.98$ for all three isotherms) emphasize the well-characterized behavior of the material interactions (Barnett et al. 2000). Fernandes et al. (2012) compared the U sorption behavior in poorly-buffered systems under atmospheric levels of CO_2 to more highly-buffered systems with greater included carbonate concentrations, finding non-linear behavior through both systems. The similarities of the literature to the experimental results emphasize the influence of the various system impacts on the overall documented behavior.

As a general comparison, Figures 5.46 through 5.48 contrast the isotherm behavior of each of the study soils at the initial pH. Due to the divergence in final pH

from the initial system pH (final pH values can be found in Table 5.15), these figures serve solely as an overview of the documented experiments. Realistic comparisons of the system must be based on the final measured system pH, indicating similar solution conditions between the various experimental sets. In this vein, Figures 5.49 and 5.50 compare only Soils *A* and *C* at approximately pH 7.90 and pH 8.50, respectively. The two chosen pH levels correspond to the initial pH 7 and pH 9 data for the two soils. As shown in Table 5.15, the initial pH 7 experiments for Soil *A* converged to a final pH of 7.91 ± 0.17, while for Soil *C* the average value was 7.94 ± 0.08. Similarly, the initial pH 9 experimentation resulted in an average pH of 8.47 ± 0.23 for Soil *A* and 8.51 ± 0.12 for Soil *C*. Turning again to Table 5.15, the average final pH values for the other two soils make cross-comparison more difficult, due to the wider variation.

Looking specifically at Figures 5.49 and 5.50, Soils *A* and *C* appear to have similar affinity to U across experimentation. Within both figures, Soil *A* shows more defined behavior for the lower C values, as indicated by the reduced scatter amongst the data points and their resolution towards a more characteristic isotherm shape. Within Figure 5.50, at pH 8.5 (stemming from the initial pH 9 data for the two soils), Soil *C* has increased affinity for the two highest C_o values, as compared to Soil *A*. As shown in Figure 5.49, affinity between the two soils is more similar. The reasoning behind the difference is not immediately apparent. As discussed previously, the affinity of both Soil *A* and *C* for U in the context of the experimental concentration levels makes complete behavioral resolution difficult to fully assess due to the extremely small percentage of U remaining in solution.

5.6 Influence of Mineralogy on Sorption

Comparing the mineralogy of the soils (results summarized in Table 4.2 and Figure 4.2) to the preliminary results from kinetics experimentation provides initial insight

into the differences between the samples. Although containing similar percentages of quartz, pure illite, and mixed-layer illite/smectite, Soils *B* and *C* display highly differing trends in sorption quantity and behavior. The variance displayed may be attributable to the presence of calcite ($CaCO_3$, 3% relative abundance of the measured soil fraction) and dolomite ($(Ca,Mg)(CO_3)_2$, trace percentages) within Soil *B*. The presence of carbonate (CO_3^{2-}) and associated species such as calcite can limit sorption of U (Stewart et al. 2010; S. Yan et al. 2010). Although the attributed quantities of carbonate species are small when compared to the presence of quartz or mixed-layer illite/smectite, the addition of any quantity of carbonate to the U sorption system can alter the overall sorption capacity. The formation of aqueous U(VI)-carbonato species, such as those resulting from interaction with atmospheric conditions, may result in increased competition between surface sites and the aqueous carbonate for the uranyl ions present in solution at higher pH, decreasing the sorption occurring (Waite et al. 1994). Consequently, the open solution system combined with the carbonate species present in *B* could combine to further limit sorption than either mechanism individually, similar to the behavior shown for subsurface sediments by Barnett et al. (2000).

Soils *A* and *C*, which each display near total sorption of $[U]_o$ during kinetics and sorption edge and envelope experimentation across the tested pH range, have partially opposing mineralogic characteristics. Within the literature to this point, no individual clay mineral has shown removal to the extent displayed by *A* and *C* across the entire pH range (Barger and Koretsky 2011; Bradbury and Baeyens 2005a, 2005b, 2009b; Davis et al. 2004; Kremleva et al. 2011; Schlegel and Descostes 2009). While the near total removal may be a consequence of the small $[U]_o$, the combination of minerals present in both *A* and *C* influence the total sorption capacity. Although the majority of both soils is comprised of quartz, with *A* having 20% greater relative abundance than *C*, other aspects of the soil column are likely controlling sorption. The glass beads, which as

amorphous silica (SiO_2) are chemically indistinguishable from quartz, serve as evidence for other aspects of the soil column likely controlling sorption. *A* contains 14% kaolinite and 9% goethite, versus 1% kaolinite and no detected presence of goethite in *C*. Alternatively, *C* has 29% of its relative abundance comprised of mixed-layer illite/smectite and a greater quantity of amorphous Fe than the other study soils (see Table 4.3). The capacity of kaolinite (Barger and Koretsky 2011; Kremleva et al. 2011), goethite (Singh et al. 2010; Stewart et al. 2010), illite (Bradbury and Baeyens 2005a, 2009b), montmorillonite, or smectite more generally (Bradbury and Baeyens 2005a, 2005b; Schlegel and Descostes 2009), and amorphous iron oxide content (Barnett et al. 2000; Um et al. 2009) to impact sorption of uranium and other actinides has been well documented within the literature. Although the aforementioned fractions of *A* and *C* do not represent a majority of the soil column, the combination of minerals at the present abundances may be great enough to dominate sorption at the investigated $[U]_o$ during experimentation.

Both Soils *D* and *B* display behavior that can draw comparisons to U sorption experimentation on purified minerals found within the literature (see Figure 2.4; Barger and Koretsky 2011; Bradbury and Baeyens 2005a; Davis et al. 2004; Schlegel and Descostes 2009). Soil *D*, with its gradual but continuous upward trend between pH 5 and 9, initially follows the trend Schlegel and Descostes (2009) showed for U sorption on Na-SWy-2, a Wyoming sodium montmorillonite, similar to the mixed-layer illite/smectite present (3%, Figure 1). An important difference between the sorption behaviors of the materials is the plateau between pH 7 and 8.5, followed by a sharp decrease in sorption to pH 9, for Na-SWy-2 (Schlegel and Descostes 2009). The decrease in sorption above pH 8.5 is attributed to the formation of anionic U complexes in solution (Schlegel and Descostes 2009). While similar complexes are expected in the uranium acetate solution, particularly the emergence of anionic uranyl carbonates, no decrease in sorption is

noted for Soil *D*. Coupled with the smectitic behavior, Barger and Koretsky (2011) showed a steady increase in U removal between pH 3 and 7, maintaining near 100% sorption from pH 8 to 9, for K-Ga-1b, pure natural kaolinite. The behavior displayed by the pure kaolinite mineral closely resembles that of Soil *D*. As *D* has a more significant kaolinite relative abundance (15%, Figure 4.2), the impact of kaolinite on the sorption behavior of the total soil column is expected to be more significant than that of smectite.

With its more S-shaped appearance, Soil *B* shows similarities to U sorption on Na-illite du Puy (Figure 2.4; Bradbury and Baeyens 2005a). Soil *B* has a significant relative abundance of mixed layer illite-smectite (25%), with pure illite representing half of the total layers, in addition to having a small portion of illite/mica (1%; see Table 4.2 and Figure 4.2). Aside from the predominance of quartz within the soil column, mixed layer illite-smectite represents the next most abundant faction within soil. As such, this portion may dominate sorption within Soil *B*, and similarities to the sorption behavior of pure illite may help to confirm this concept.

5.7 Conclusions

Figure 5.51 compares the distribution calculated distribution coefficients (K_d) for U across the initial pH range for each of the four natural barrier soils. A brief discussion of K_d calculations and an example are provided in Appendix C. For further understanding of the values derived from experimentation in terms of the literature, Figure 5.52 cross-compares literature values derived from purified clays and iron minerals.

Although clay-based soils have been considered a critical material in the construction of barrier systems, real soils behave differently than the purified clay minerals that have been frequently studied to this point in the literature. Cross-comparisons between sorption behavior of purified clays and iron minerals to the study soils show a reliance on multiple portions of the soil column to account for demonstrated

radionuclide sorption capacity. Both the physical and chemical properties of natural soils influence uranium sorption, with iron content serving as a critical factor in accounting for soil sorption capacity. Correspondingly, Table 5.16 provides a comparison of a number of characterized traits of each of the four study soils as they compare to the measured U sorption behavior within the context of this study. Multiple behaviors combine to make Soil A and Soil C the best U sorption performers within the study set. As such, development and identification of ideal barrier soils will also rely on the interaction of multiple mineral properties to account for the desired containment of LLW over the course of extended interactions.

Table 5.1. Measured concentrations (in mg/L) of selected analytes across the pH range of interest for control experimentation. Reported ICP-OES wavelengths (in nm) for each selected analyte are listed. Numerical values represent average of three triplicate experiments, except for italicized values, which represent the average of two experiments.

Soil	Reaction Time	Analyte (via ICP-OES)	pH								
			5	5.5	6	6.5	7	7.5	8	8.5	9
D - WCS Andrews	24 h	Na 589.592	679	677	679	677	673	676	672	665	664
		Mg 285.213	3.07	2.93	2.89	2.82	2.92	2.83	2.84	2.75	2.75
		K 766.491	5.14	5.19	3.89	2.67	2.75	2.40	2.48	2.30	2.63
		Ca 422.673	25.0	23.3	22.6	22.0	21.1	20.8	20.6	19.9	19.7
		Fe 238.204	-0.017	-0.018	-0.017	-0.015	-0.015	-0.011	-0.015	-0.016	-0.017
		Al 396.152	0.011	0.013	0.014	0.025	0.012	0.012	0.012	0.014	0.014
		Si 251.611	1.22	1.17	1.20	1.19	0.895	0.875	0.857	0.865	0.902
	7 days	Na 589.592	642	647	643	646	642	642	644	645	634
		Mg 285.213	3.00	2.95	2.82	2.87	2.72	2.66	2.62	2.70	2.57
		K 766.491	4.93	3.12	3.51	2.93	5.78	2.71	5.68	2.77	5.29
		Ca 422.673	26.9	26.4	24.2	25.9	23.5	22.4	22.3	22.6	21.9
		Fe 238.204	-0.057	-0.054	-0.056	-0.058	-0.058	-0.058	-0.058	-0.058	-0.053
		Al 396.152	0.008	0.009	0.009	0.009	0.011	0.012	0.012	0.011	0.013
		Si 251.611	1.10	1.08	1.06	1.08	1.07	1.08	1.07	1.10	1.11
A - Albany Red	24 h	Na 589.592	674	676	663	671	670	678	675	664	653
		Mg 285.213	1.09	0.922	0.878	0.871	0.833	0.724	0.551	0.646	0.557
		K 766.491	0.953	0.907	0.901	1.44	0.974	1.51	0.765	0.978	0.831
		Ca 422.673	12.5	15.0	12.6	12.4	11.9	11.9	10.2	12.0	12.2
		Fe 238.204	-0.017	-0.017	-0.014	-0.015	-0.016	-0.013	-0.016	-0.026	-0.046
		Al 396.152	0.003	0.005	0.006	0.006	0.006	0.020	0.011	0.010	0.015
		Si 251.611	0.646	0.512	0.475	0.498	0.476	0.429	0.343	0.421	0.399
	7 days	Na 589.592	650	645	642	642	652	645	654	644	651
		Mg 285.213	1.17	1.08	1.07	0.948	0.830	0.786	0.766	0.678	0.658
		K 766.491	2.94	2.57	2.38	2.29	4.07	3.14	3.58	2.52	5.75
		Ca 422.673	14.2	13.6	13.6	13.1	13.0	13.0	12.6	12.9	12.5
		Fe 238.204	-0.057	-0.058	-0.058	-0.058	-0.058	-0.055	-0.057	-0.057	-0.057
		Al 396.152	0.003	0.003	0.003	0.004	0.006	0.006	0.007	0.012	0.012
		Si 251.611	0.961	0.892	0.874	0.781	0.665	0.646	0.634	0.605	0.587

Table 5.1. (continued).

Soil	Reaction Time	Analyte (via ICP-OES)	pH								
			5	5.5	6	6.5	7	7.5	8	8.5	9
B - Houston Brown	24 h	Na 589.592	639	636	652	641	663	642	643	640	641
		Mg 285.213	5.64	5.21	4.87	4.59	4.14	3.94	3.93	3.85	3.67
		K 766.491	1.78	1.20	1.74	1.21	1.17	1.04	1.20	1.01	1.09
		Ca 422.673	73.1	59.6	49.8	44.9	30.8	31.8	30.7	29.7	26.5
		Fe 238.204	-0.056	-0.056	-0.053	-0.057	-0.017	-0.056	-0.051	-0.054	-0.054
		Al 396.152	0.016	0.014	0.014	0.013	0.016	0.015	0.015	0.017	0.017
		Si 251.611	1.36	1.22	1.15	1.11	1.02	0.995	1.00	1.00	0.979
	7 days	Na 589.592	637	637	637	631	628	633	629	628	625
		Mg 285.213	4.75	4.62	4.12	4.39	4.30	4.13	4.02	3.94	3.84
		K 766.491	2.86	1.72	11.3	5.16	3.01	2.17	1.56	1.46	1.29
		Ca 422.673	49.3	45.1	35.3	36.2	35.4	32.5	30.6	29.6	28.3
		Fe 238.204	-0.057	-0.058	-0.057	0.016	-0.014	-0.014	-0.014	-0.014	-0.014
		Al 396.152	0.012	0.011	0.013	0.022	0.017	0.018	0.018	0.019	0.020
		Si 251.611	1.48	1.47	1.34	1.41	1.40	1.37	1.36	1.36	1.36
C - Kamm Clay	24 h	Na 589.592	635	644	634	707	653	702	710	708	713
		Mg 285.213	6.83	6.61	6.30	5.79	5.91	5.76	5.71	5.64	5.46
		K 766.491	1.13	1.60	1.03	1.11	3.46	0.993	0.989	1.08	0.976
		Ca 422.673	20.3	19.8	19.0	18.5	16.5	18.3	18.3	18.2	17.8
		Fe 238.204	-0.037	-0.040	-0.037	-0.058	0.006	-0.053	-0.057	-0.058	-0.058
		Al 396.152	0.028	0.024	0.029	0.006	0.029	0.006	0.007	0.008	0.010
		Si 251.611	1.74	1.54	1.49	0.977	1.26	0.991	0.956	0.936	0.917
	7 days	Na 589.592	634	627	630	653	693	691	689	691	692
		Mg 285.213	7.37	7.42	6.97	6.81	6.90	6.60	6.50	6.42	6.24
		K 766.491	2.56	1.69	1.47	2.42	1.79	1.45	0.991	1.08	0.976
		Ca 422.673	21.4	21.6	205	20.4	21.0	20.4	20.1	20.0	19.6
		Fe 238.204	0.017	-0.012	-0.012	-0.014	-0.013	-0.014	-0.008	-0.007	-0.012
		Al 396.152	0.009	0.008	0.008	0.009	0.011	0.011	0.012	0.012	0.013
		Si 251.611	1.74	1.72	1.59	1.55	1.52	1.32	1.34	1.29	1.24

Table 5.1. (continued)

Soil	Reaction Time	Analyte (via ICP-OES)	pH								
			5	5.5	6	6.5	7	7.5	8	8.5	9
Glass Beads	24 h	Na 589.592	711	719	717	712	742	714	718	717	715
		Mg 285.213	0.017	0.016	0.015	0.096	0.023	0.017	0.018	0.017	0.023
		K 766.491	0.208	0.106	0.035	0.123	0.049	0.094	0.039	0.072	0.041
		Ca 422.673	0.162	0.155	0.177	0.282	0.327	0.155	0.160	0.169	0.222
		Fe 238.204	-0.057	-0.058	-0.055	-0.056	-0.017	-0.057	-0.058	-0.058	-0.058
		Al 396.152	-0.001	-0.001	-0.001	-0.001	0.003	-0.001	-0.001	-0.001	-0.001
		Si 251.611	0.051	0.056	0.054	0.084	0.103	0.105	0.118	0.174	0.751
	7 days	Na 589.592	703	694	696	696	693	695	698	695	693
		Mg 285.213	0.022	0.024	0.021	0.022	0.022	0.023	0.026	0.027	0.043
		K 766.491	0.320	0.046	0.201	0.080	0.078	0.044	0.144	0.053	0.084
		Ca 422.673	0.177	0.181	0.174	0.176	0.186	0.180	0.220	0.206	0.270
		Fe 238.204	-0.009	-0.013	-0.014	-0.010	-0.014	-0.010	-0.013	-0.014	-0.013
		Al 396.152	0.000	-0.001	0.000	-0.001	0.000	0.000	0.000	-0.001	0.000
		Si 251.611	0.190	0.230	0.250	0.324	0.441	0.503	0.650	0.784	1.912
No Soil	24 h	Na 589.592	690	690	690	687	683	687	686	684	688
		Mg 285.213	0.001	0.001	0.001	0.001	0.001	0.001	0.009	0.028	0.001
		K 766.491	0.234	0.039	0.057	0.034	0.067	0.029	0.052	0.041	0.029
		Ca 422.673	0.046	0.048	0.045	0.046	0.047	0.055	0.086	0.059	0.072
		Fe 238.204	-0.014	-0.009	-0.011	-0.012	-0.013	-0.014	-0.010	-0.010	-0.014
		Al 396.152	-0.001	0.001	0.000	-0.001	-0.001	-0.001	-0.001	-0.001	-0.001
		Si 251.611	0.000	0.007	0.002	0.001	-0.001	-0.001	0.001	0.001	-0.002
	7 days	Na 589.592	1750	1740	1730	1750	1740	1740	170	1640	1600
		Mg 285.213	0.007	-0.013	-0.012	-0.008	-0.013	-0.012	-0.013	-0.012	-0.012
		K 766.491	0.541	*0.079*	*0.173*	0.098	*0.114*	0.104	*0.101*	*0.118*	0.071
		Ca 422.673	-0.040	-0.044	-0.044	-0.043	-0.044	-0.045	-0.046	-0.042	-0.044
		Fe 238.204	-0.030	-0.031	-0.031	-0.029	-0.030	-0.030	-0.031	-0.031	-0.031
		Al 396.152	-0.029	-0.029	-0.029	-0.029	-0.029	-0.028	-0.029	-0.029	-0.029
		Si 251.611	-0.057	-0.057	-0.058	-0.058	-0.057	-0.058	-0.058	-0.056	-0.056

Table 5.2. Measured concentrations (in µg/L) of U by ICP-OES across the pH range of interest for control experimentation. Numerical values represent the average of three triplicate experiments. OES measurements are reported on the U 263.553 nm wavelength.

Soil	Reaction Time	Analysis Technique	Initial pH								
			5	5.5	6	6.5	7	7.5	8	8.5	9
D - WCS Andrews	24 h	OES	14.4	1.36	19.3	4.09	11.1	8.77	12.5	8.83	10.4
	7 days	OES	10.7	10.5	5.12	12.2	21.3	17.4	17.8	13.6	6.28
A - Albany Red	24 h	OES	9.33	11.0	0.733	2.86	5.92	2.77	-0.150	5.80	1.19
	7 days	OES	13.1	17.0	-1.24	2.11	26.7	11.8	10.2	8.70	3.56
B - Houston Brown	24 h	OES	1.01	11.8	14.5	6.38	4.94	13.1	2.07	11.5	-1.41
	7 days	OES	15.8	15.1	10.4	7.62	0.067	8.93	12.5	10.9	15.6
C - Kamm Clay	24 h	OES	12.6	10.1	15.1	11.3	2.50	15.2	19.1	4.73	19.4
	7 days	OES	14.6	7.23	7.32	2.63	11.9	5.28	11.9	7.23	4.67
Glass Beads	24 h	OES	0.231	13.1	9.43	12.0	3.73	12.4	4.74	0.727	12.4
	7 days	OES	-0.857	4.21	7.48	5.13	10.2	-1.25	9.71	6.21	1.19
U Only - No Soil	24 h	OES	843	902	847	908	896	875	865	880	674
	7 days	OES	722	708	665	654	652	654	641	650	448

Table 5.3. Comparison of calculated uranium concentrations in the sorption isotherm experimentation (in µg/L, based on serial dilution of the stock solution) to values anticipated based on the measured values from kinetics and E&E experimentation and the actual measured concentrations from isotherm solution control experimentation.

Anticipated Final Conc. – Uranium (based on added uranium acetate)	Estimate of Final (based on estimations from E&E and Kinetics)	Average Measured Final Conc.	Standard Deviation of Final Conc.
µg/L	µg/L	µg/L	µg/L
6.00	3.82	2.24	1.43
30.02	19.09	12.59	4.64
60.05	38.18	18.78	5.08
300.24	190.88	160.08	5.17
600.48	381.76	396.79	12.76
3002.39	1908.79	2897.36	87.39
6004.78	3817.59	2393.34	649.50

Table 5.4. Measured concentrations (in mg/L) of selected analytes across the pH range of interest for kinetics experimentation. Numerical values represent average of three triplicate experiments, except for italicized values, which represent the average of two experiments.

Soil	pH	Analyte (via ICP-OES)	Reaction Time						
			15 min	30 min	1 h	2 h	4 h	24 h	7 days
D - WCS Andrews	7	Na 589.592	669	664	679	2280	2270	673	668
		Mg 285.213	2.89	2.91	2.95	3.37	3.20	2.84	2.95
		K 766.491	3.14	4.60	2.83	4.29	2.97	3.31	2.37
		Ca 422.673	19.2	19.8	20.5	20.5	21.1	23.3	24.0
		Fe 238.204	-0.011	-0.013	-0.014	0.015	-0.025	-0.014	-0.014
		Al 396.152	0.008	0.009	0.010	0.015	-0.019	0.013	0.013
		Si 251.611	0.225	0.273	0.334	0.467	0.545	0.784	0.981
A - Albany Red	7	Na 589.592	673	2280	684	2260	2260	668	667
		Mg 285.213	0.687	0.803	0.686	0.801	0.802	0.713	0.807
		K 766.491	*0.901*	*0.879*	0.706	*0.846*	*0.843*	*0.823*	0.789
		Ca 422.673	11.3	11.3	11.5	11.5	11.9	12.1	12.9
		Fe 238.204	-0.008	-0.027	-0.014	-0.027	-0.026	-0.010	-0.013
		Al 396.152	0.006	-0.022	0.006	-0.025	-0.024	0.007	0.008
		Si 251.611	0.142	0.129	0.190	0.198	0.274	0.386	0.571
B - Houston Brown	7	Na 589.592	659	2250	663	*2280*	2240	669	665
		Mg 285.213	3.96	4.52	4.01	*4.59*	4.53	4.06	4.04
		K 766.491	1.47	*1.24*	1.05	1.46	1.60	1.62	1.15
		Ca 422.673	28.9	28.5	29.8	*29.2*	29.3	31.1	30.7
		Fe 238.204	-0.013	-0.027	-0.014	-0.021	-0.024	-0.010	-0.014
		Al 396.152	0.016	-0.017	0.016	-0.019	-0.016	0.017	0.018
		Si 251.611	0.425	0.445	0.540	*0.677*	0.754	0.942	1.17

Table 5.4. (continued)

Soil	pH	Analyte (via ICP-OES)	Reaction Time						
			15 min	30 min	1 h	2 h	4 h	24 h	7 days
C - Kamm Clay	7	Na 589.592	664	2220	668	2230	2220	2230	661
		Mg 285.213	5.60	6.30	5.47	6.51	6.36	6.80	6.30
		K 766.491	*1.21*	*1.18*	*1.36*	1.31	*1.13*	1.20	0.952
		Ca 422.673	17.7	17.1	17.4	17.6	17.3	18.4	19.5
		Fe 238.204	-0.012	-0.027	-0.013	-0.027	-0.027	-0.028	-0.014
		Al 396.152	0.007	-0.025	0.007	-0.025	-0.019	-0.023	0.009
		Si 251.611	0.350	0.409	0.439	0.541	0.707	0.992	1.25
Glass Beads	7	Na 589.592	675	*2310*	676	2290	2250	2280	678
		Mg 285.213	0.013	*0.002*	0.017	0.004	0.007	0.016	0.032
		K 766.491	*0.340*	*0.101*	*0.392*	*0.131*	*0.224*	*0.136*	0.087
		Ca 422.673	0.152	*0.042*	0.143	0.037	0.052	0.183	0.190
		Fe 238.204	-0.014	-0.028	-0.010	-0.024	-0.026	-0.027	-0.013
		Al 396.152	-0.001	-0.030	-0.001	-0.030	-0.030	-0.029	-0.001
		Si 251.611	0.009	-0.032	0.012	-0.027	-0.012	0.024	0.237
No Soil	7	Na 589.592	1580	1600	1610	1600	1600	683	1740
		Mg 285.213	-0.012	-0.010	-0.010	-0.007	-0.010	0.001	-0.013
		K 766.491	0.550	0.282	0.252	0.212	0.385	0.067	0.219
		Ca 422.673	-0.045	-0.042	-0.042	-0.040	-0.038	0.047	-0.044
		Fe 238.204	-0.029	-0.031	-0.029	-0.030	-0.030	-0.013	-0.030
		Al 396.152	-0.029	-0.029	-0.029	-0.029	-0.029	-0.001	-0.029
		Si 251.611	-0.057	-0.056	-0.056	-0.057	-0.056	-0.001	-0.057

Table 5.5. Measured concentrations (in µg/L) of U by ICP-OES across the pH range of interest for kinetics experimentation.

Soil	pH	Analysis Technique	Reaction Time						
			15 min	30 min	1 h	2 h	4 h	24 h	7 days
A - WCS Andrews	7	OES	66.4	65.3	89.8	105	143	209	192
B - Albany Red	7	OES	23.9	16.0	8.06	6.84	5.17	21.1	-3.02
C - Houston Brown	7	OES	347	327	375	338	309	377	346
D - Kamm Clay	7	OES	16.4	6.00	12.4	7.19	5.42	9.35	6.68
Glass Beads	7	OES	898	819	805	830	794	795	628
No Soil	7	OES	704	716	717	713	695	896	652

Table 5.6. Measured concentrations (in mg/L) of selected analytes across the pH range of interest for sorption edge and envelope experimentation. Numerical values represent average of three triplicate experiments, except for italicized values, which represent the average of two experiments.

Soil	Reaction Time	Analyte (via ICP-OES)	pH					
			5		5.5		6	
			550	0	550	0	550	0
D - WCS Andrews	24 h	Na 589.592	2140	679	2130	677	*2130*	679
		Mg 285.213	3.41	3.07	3.21	2.93	*3.18*	2.89
		K 766.491	2.96	5.14	2.73	5.19	*2.87*	3.89
		Ca 422.673	24.0	25.0	23.0	23.3	*22.4*	22.6
		Fe 238.204	-0.027	-0.017	-0.027	-0.018	-0.028	-0.017
		Al 396.152	-0.021	0.011	-0.020	0.013	-0.023	0.014
		Si 251.611	0.787	1.22	0.782	1.17	*0.776*	1.20
A - Albany Red	24 h	Na 589.592	*2190*	674	2170	676	2160	663
		Mg 285.213	*1.03*	1.09	0.925	0.922	0.907	0.878
		K 766.491	*1.18*	0.953	1.23	0.907	1.56	0.901
		Ca 422.673	*13.3*	12.5	12.5	15.0	12.4	12.6
		Fe 238.204	-0.027	-0.017	-0.025	-0.017	-0.026	-0.014
		Al 396.152	-0.026	0.003	-0.024	0.005	-0.024	0.006
		Si 251.611	0.513	0.646	0.457	0.512	0.447	0.475
B - Houston Brown	24 h	Na 589.592	2090	634	1570	636	1570	652
		Mg 285.213	5.13	5.64	4.39	5.21	4.23	4.87
		K 766.491	1.50	1.78	1.35	1.20	1.36	1.74
		Ca 422.673	43.6	73.1	32.6	59.6	30.4	49.8
		Fe 238.204	-0.026	-0.056	-0.027	-0.056	-0.029	-0.053
		Al 396.152	-0.018	0.016	-0.015	0.014	-0.014	0.014
		Si 251.611	1.14	1.36	1.73	1.22	1.70	1.15
C - Kamm Clay	24 h	Na 589.592	1560	635	*1620*	644	1570	634
		Mg 285.213	6.41	6.83	*6.31*	6.61	6.14	6.30
		K 766.491	1.94	1.13	*1.11*	1.60	1.27	1.03
		Ca 422.673	17.0	20.3	*16.7*	19.8	16.5	19.0
		Fe 238.204	-0.029	-0.037	-0.030	-0.040	-0.029	-0.037
		Al 396.152	-0.023	0.028	-0.024	0.024	-0.010	0.029
		Si 251.611	2.11	1.74	*1.96*	1.54	1.89	1.49
Glass Beads	24 h	Na 589.592	1790	711	1780	719	1760	717
		Mg 285.213	0.032	0.017	0.018	0.016	0.017	0.015
		K 766.491	*0.172*	0.208	*0.301*	0.106	*0.186*	0.035
		Ca 422.673	0.092	0.162	0.072	0.155	0.069	0.177
		Fe 238.204	-0.018	-0.057	-0.031	-0.058	-0.031	-0.055
		Al 396.152	-0.017	-0.001	-0.029	-0.001	-0.029	-0.001
		Si 251.611	0.078	0.051	0.025	0.056	0.033	0.054

Table 5.6. (continued)

Soil	Reaction Time	Analyte (via ICP-OES)	pH					
			6.5		7		7.5	
			550	0	550	0	550	0
D - WCS Andrews	24 h	Na 589.592	2150	677	2130	673	2160	676
		Mg 285.213	3.19	2.82	3.13	2.92	3.16	2.83
		K 766.491	2.67	2.67	2.71	2.75	2.74	2.40
		Ca 422.673	22.3	22.0	22.2	21.1	22.1	20.8
		Fe 238.204	-0.027	-0.015	-0.024	-0.015	-0.027	-0.011
		Al 396.152	-0.019	0.025	-0.018	0.012	-0.017	0.012
		Si 251.611	0.799	1.19	0.802	0.895	0.816	0.875
A - Albany Red	24 h	Na 589.592	2160	671	2150	670	2150	678
		Mg 285.213	0.859	0.871	0.830	0.833	0.820	0.724
		K 766.491	1.26	1.44	1.38	0.974	1.69	1.51
		Ca 422.673	12.8	12.4	13.3	11.9	13.1	11.9
		Fe 238.204	-0.027	-0.015	-0.027	-0.016	-0.027	-0.013
		Al 396.152	-0.023	0.006	-0.022	0.006	-0.022	0.020
		Si 251.611	0.428	0.498	0.421	0.476	0.411	0.429
B - Houston Brown	24 h	Na 589.592	*1580*	641	1590	663	1580	642
		Mg 285.213	3.45	4.59	4.13	4.14	4.06	3.94
		K 766.491	1.12	1.21	1.40	1.17	1.35	1.04
		Ca 422.673	*28.6*	44.9	28.2	30.8	27.2	31.8
		Fe 238.204	-0.029	-0.057	-0.029	-0.017	-0.029	-0.056
		Al 396.152	-0.015	0.013	-0.011	0.016	-0.011	0.015
		Si 251.611	1.45	1.11	1.77	1.02	1.73	0.995
C - Kamm Clay	24 h	Na 589.592	1550	707	1550	653	1730	702
		Mg 285.213	5.91	5.79	5.82	5.91	6.20	5.76
		K 766.491	1.28	1.11	1.23	3.46	1.59	0.993
		Ca 422.673	16.0	18.5	15.9	16.5	17.0	18.3
		Fe 238.204	-0.029	-0.058	-0.029	0.006	-0.029	-0.053
		Al 396.152	-0.020	0.006	-0.020	0.029	-0.021	0.006
		Si 251.611	1.80	0.977	1.77	1.26	1.58	0.991
Glass Beads	24 h	Na 589.592	1760	712	1750	742	1760	714
		Mg 285.213	0.017	0.096	0.017	0.023	0.016	0.017
		K 766.491	*0.137*	0.123	*0.174*	0.049	*0.273*	0.094
		Ca 422.673	0.071	0.282	0.071	0.327	0.071	0.155
		Fe 238.204	-0.031	-0.056	-0.031	-0.017	-0.031	-0.057
		Al 396.152	-0.029	-0.001	-0.029	0.003	-0.029	-0.001
		Si 251.611	0.047	0.084	0.049	0.103	0.057	0.105

Table 5.6. (continued)

Soil	Reaction Time	Analyte (via ICP-OES)	pH					
			8		8.5		9	
			550	0	550	0	550	0
D - WCS Andrews	24 h	Na 589.592	2130	672	2140	665	2140	664
		Mg 285.213	3.08	2.84	3.10	2.75	3.09	2.75
		K 766.491	2.89	2.48	2.76	2.30	3.08	2.63
		Ca 422.673	21.7	20.6	22.0	19.9	21.5	19.7
		Fe 238.204	-0.027	-0.015	-0.027	-0.016	-0.027	-0.017
		Al 396.152	-0.017	0.012	-0.017	0.014	-0.016	0.014
		Si 251.611	0.837	0.857	0.843	0.865	0.874	0.902
A - Albany Red	24 h	Na 589.592	*2180*	675	2170	664	2140	653
		Mg 285.213	*0.792*	0.551	0.771	0.646	0.699	0.557
		K 766.491	0.999	0.765	1.29	0.978	1.36	0.831
		Ca 422.673	*12.4*	10.2	12.3	12.0	11.8	12.2
		Fe 238.204	-0.027	-0.016	-0.027	-0.026	-0.025	-0.046
		Al 396.152	-0.022	0.011	-0.021	0.010	-0.019	0.015
		Si 251.611	0.344	0.343	0.403	0.421	0.391	0.399
B - Houston Brown	24 h	Na 589.592	1570	643	1570	640	1560	641
		Mg 285.213	3.94	3.93	3.88	3.85	3.71	3.67
		K 766.491	1.33	1.20	1.44	1.01	1.39	1.09
		Ca 422.673	26.0	30.7	25.3	29.7	23.6	26.5
		Fe 238.204	-0.028	-0.051	-0.029	-0.054	-0.029	-0.054
		Al 396.152	-0.009	0.015	-0.008	0.017	-0.006	0.017
		Si 251.611	1.73	1.00	1.73	1.00	1.75	0.979
C - Kamm Clay	24 h	Na 589.592	1720	710	*1750*	708	1740	713
		Mg 285.213	6.14	5.71	*6.10*	5.64	6.07	5.46
		K 766.491	1.46	0.989	*1.44*	1.08	1.35	0.976
		Ca 422.673	16.9	18.3	*16.9*	18.2	16.9	17.8
		Fe 238.204	-0.030	-0.057	-0.030	-0.058	-0.030	-0.058
		Al 396.152	-0.021	0.007	-0.022	0.008	-0.018	0.010
		Si 251.611	1.59	0.956	*1.57*	0.936	1.56	0.917
Glass Beads	24 h	Na 589.592	1750	718	1750	717	1740	715
		Mg 285.213	0.016	0.018	0.016	0.017	0.021	0.023
		K 766.491	*0.153*	0.039	*0.156*	0.072	*0.119*	0.041
		Ca 422.673	0.068	0.160	0.070	0.169	0.085	0.222
		Fe 238.204	-0.029	-0.058	-0.030	-0.058	-0.031	-0.058
		Al 396.152	-0.029	-0.001	-0.029	-0.001	-0.029	-0.001
		Si 251.611	0.075	0.118	0.115	0.174	0.873	0.751

Table 5.7. Measured concentrations (in µg/L) of U by ICP-OES across the pH range of interest for sorption edge and envelope experimentation.

Soil	Reaction Time	Analysis Technique	pH 5		pH 5.5		pH 6	
			550	0	550	0	550	0
D - WCS Andrews	24 h	OES	175	14.4	163	1.36	157	19.3
A - Albany Red	24 h	OES	1.84	9.33	6.16	11.0	3.09	0.733
B - Houston Brown	24 h	OES	542	1.01	402	11.8	363	14.5
C - Kamm Clay	24 h	OES	6.03	12.6	*7.20*	10.1	8.94	15.1
Glass Beads	24 h	OES	706	0.231	655	13.1	638	9.43

Soil	Reaction Time	Analysis Technique	pH 6.5		pH 7		pH 7.5	
			550	0	550	0	550	0
D - WCS Andrews	24 h	OES	144	4.09	149	11.1	141	8.77
A - Albany Red	24 h	OES	2.61	2.86	4.43	5.92	5.18	2.77
B - Houston Brown	24 h	OES	*316*	6.38	291	4.94	274	13.1
C - Kamm Clay	24 h	OES	6.37	11.3	6.13	2.50	8.77	15.2
Glass Beads	24 h	OES	642	12.0	623	3.72	613	12.4

Soil	Reaction Time	Analysis Technique	pH 8		pH 8.5		pH 9	
			550	0	550	0	550	0
D - WCS Andrews	24 h	OES	132	12.5	128	8.83	119	10.4
A - Albany Red	24 h	OES	2.17	-0.150	4.03	5.80	3.36	1.19
B - Houston Brown	24 h	OES	238	2.07	223	11.5	174	-1.41
C - Kamm Clay	24 h	OES	8.90	19.1	*6.005*	4.73	5.70	19.4
Glass Beads	24 h	OES	611	4.73	576	0.727	546	12.4

Table 5.8. Measured concentrations (in mg/L) of selected analytes across the pH range of interest for sorption isotherm experimentation. Numerical values represent average of three triplicate experiments, except for italicized values, which represent the average of two experiments.

Soil	pH	Analyte (via ICP-OES)	Starting Solution Concentration of U (µg/L)							
			0	6	30	60	300	600	3000	6000
D - WCS Andrews	5	Na 589.592	679	3230	3220	1720	1710	1710	3210	3210
		Mg 285.213	3.07	3.75	3.83	3.03	3.01	3.06	3.79	3.91
		K 766.491	5.14	28.5	35.7	3.16	2.90	3.53	30.5	40.1
		Ca 422.673	25.0	25.7	26.4	22.5	22.2	22.9	26.0	27.6
		Fe 238.204	-0.017	-0.007	-0.031	-0.031	-0.031	-0.029	-0.027	-0.029
		Al 396.152	0.011	-0.002	-0.007	-0.019	-0.018	-0.019	0.001	-0.006
		Si 251.611	1.22	1.47	1.35	1.34	1.33	1.33	1.34	1.37
	7	Na 589.592	673	2840	3220	1820	1820	1830	3180	3190
		Mg 285.213	2.92	3.45	3.76	2.95	2.97	3.04	3.79	3.90
		K 766.491	2.75	45.1	34.3	2.82	3.34	3.50	63.8	65.1
		Ca 422.673	21.1	23.3	27.3	21.4	21.5	21.9	25.3	25.9
		Fe 238.204	-0.015	-0.030	-0.032	-0.030	-0.030	-0.031	-0.017	-0.025
		Al 396.152	0.012	-0.004	-0.003	-0.016	-0.016	-0.016	-0.003	-0.003
		Si 251.611	0.895	1.48	1.40	1.33	1.344	1.37	1.37	1.36
	9	Na 589.592	664	2830	3240	1830	1810	1810	3180	3210
		Mg 285.213	2.75	3.28	3.69	2.94	2.94	2.95	3.54	3.59
		K 766.491	2.63	39.6	57.4	3.27	3.36	3.53	35.1	52.2
		Ca 422.673	19.7	22.1	24.1	21.0	20.8	20.9	23.7	23.9
		Fe 238.204	-0.017	-0.028	-0.032	-0.031	-0.031	-0.029	-0.030	-0.029
		Al 396.152	0.014	0.000	-0.003	-0.014	-0.015	-0.014	-0.001	0.000
		Si 251.611	0.902	1.54	1.42	1.42	1.40	1.40	1.40	1.37

Table 5.8. (continued)

Soil	pH	Analyte (via ICP-OES)	Starting Solution Concentration of U (µg/L)						
			0	30	60	300	600	3000	6000
A - Albany Red	5	Na 589.592	674	2470	1790	1800	1810	2840	2830
		Mg 285.213	1.09	1.07	0.885	1.01	1.05	1.48	1.39
		K 766.491	0.953	0.925	1.48	1.97	1.29	30.7	23.6
		Ca 422.673	12.5	12.0	12.0	13.1	12.5	13.9	13.8
		Fe 238.204	-0.017	-0.003	-0.030	-0.029	-0.030	-0.030	-0.017
		Al 396.152	0.003	-0.003	-0.023	-0.023	-0.024	-0.013	-0.013
		Si 251.611	0.646	0.767	0.757	0.868	0.933	1.36	1.31
	7	Na 589.592	670	2420	2410	2430	2410	2830	2840
		Mg 285.213	0.833	0.719	0.786	*0.792*	0.778	0.865	0.956
		K 766.491	0.974	0.848	0.873	0.783	0.821	27.2	24.6
		Ca 422.673	11.9	11.6	11.0	11.2	11.3	12.3	12.7
		Fe 238.204	-0.016	-0.012	-0.012	0.023	0.048	-0.026	-0.029
		Al 396.152	0.006	0.002	-0.001	0.001	0.001	-0.007	-0.009
		Si 251.611	0.476	0.558	0.597	*0.598*	0.595	0.756	0.827
	9	Na 589.592	653	2410	2420	2420	2380	2840	2850
		Mg 285.213	0.557	0.560	0.584	0.561	0.613	0.715	0.756
		K 766.491	0.831	0.793	0.739	0.802	1.70	40.4	39.4
		Ca 422.673	12.2	10.5	10.9	10.8	10.7	12.2	12.3
		Fe 238.204	-0.046	-0.010	-0.014	0.019	-0.008	-0.030	-0.030
		Al 396.152	0.015	0.024	0.009	0.011	0.006	-0.001	-0.001
		Si 251.611	0.399	0.523	0.523	0.525	0.581	0.686	0.713

Table 5.8. (continued)

Soil	pH	Analyte (via ICP-OES)	Starting Solution Concentration of U (µg/L)						
			0	30	60	300	600	3000	6000
B - Houston Brown	5	Na 589.592	639	2740	2780	2770	1980	1970	1980
		Mg 285.213	5.64	5.33	5.31	5.26	12.4	12.5	12.5
		K 766.491	1.78	1.20	1.23	1.21	1.79	1.87	1.79
		Ca 422.673	73.1	45.8	44.9	45.1	53.3	57.3	59.1
		Fe 238.204	-0.056	0.019	-0.006	-0.010	-0.053	-0.042	-0.049
		Al 396.152	0.016	0.007	0.006	0.006	-0.008	-0.007	-0.007
		Si 251.611	1.36	1.70	1.49	1.46	1.88	1.99	2.00
	7	Na 589.592	663	2760	2760	2780	2770	1970	1980
		Mg 285.213	4.14	4.45	4.41	4.51	4.43	10.5	10.5
		K 766.491	1.17	1.09	1.11	1.12	1.11	1.67	1.66
		Ca 422.673	30.8	30.5	29.0	30.7	30.1	23.6	25.3
		Fe 238.204	-0.017	-0.013	0.026	-0.015	-0.019	-0.053	0.121
		Al 396.152	0.016	0.010	0.010	0.010	0.010	0.001	0.001
		Si 251.611	1.02	1.44	1.42	1.42	1.38	1.82	1.84
	9	Na 589.592	641	2750	2760	2750	2710	1570	1570
		Mg 285.213	3.67	4.31	4.20	4.12	4.24	5.14	5.08
		K 766.491	1.09	1.59	1.31	1.35	1.40	2.10	1.92
		Ca 422.673	26.5	26.8	26.7	26.4	26.9	33.8	33.8
		Fe 238.204	-0.054	-0.035	-0.042	-0.043	-0.043	-0.050	-0.059
		Al 396.152	0.017	0.012	0.011	0.013	0.012	-0.005	-0.006
		Si 251.611	0.979	1.60	1.46	1.42	1.44	1.10	1.01

Table 5.8. (continued)

Soil	pH	Analyte (via ICP-OES)	Starting Solution Concentration of U (µg/L)						
			0	30	60	300	600	3000	6000
C - Kamm Clay	5	Na 589.592	635	2700	2710	2730	2720	2690	2700
		Mg 285.213	6.83	7.59	7.20	7.15	7.23	7.25	7.56
		K 766.491	1.13	1.61	1.38	1.31	1.36	1.31	1.37
		Ca 422.673	20.3	19.3	18.9	18.5	18.7	18.2	13.7
		Fe 238.204	-0.037	-0.014	-0.039	-0.041	-0.044	-0.002	-0.015
		Al 396.152	0.028	-0.005	-0.005	-0.005	-0.005	0.005	-0.002
		Si 251.611	1.74	1.89	1.76	1.72	1.71	2.06	1.89
	7	Na 589.592	653	2810	2810	2820	2810	2710	2710
		Mg 285.213	5.91	6.70	6.64	6.67	6.74	6.71	6.84
		K 766.491	3.46	1.76	1.59	1.60	1.50	1.72	1.76
		Ca 422.673	16.5	17.8	17.6	17.7	17.9	17.6	17.4
		Fe 238.204	0.006	-0.003	-0.011	-0.012	-0.012	-0.015	0.006
		Al 396.152	0.029	0.003	0.002	0.002	0.003	0.005	0.008
		Si 251.611	1.26	1.63	1.41	1.42	1.39	1.53	1.49
	9	Na 589.592	713	2850	2770	2730	2760	*2690*	2650
		Mg 285.213	5.46	6.25	6.09	5.84	6.13	*6.07*	6.04
		K 766.491	0.976	1.55	1.40	1.37	1.40	*1.51*	1.51
		Ca 422.673	17.8	17.5	16.9	16.4	16.9	*16.4*	16.3
		Fe 238.204	-0.058	0.031	-0.005	-0.006	-0.011	0.010	-0.011
		Al 396.152	0.010	0.015	0.011	0.017	0.011	0.012	0.015
		Si 251.611	0.917	1.24	1.29	1.27	1.29	1.39	1.35

Table 5.9. Measured concentrations (in µg/L) of U by ICP-OES across the pH range of interest for sorption isotherm experimentation. Key to reported values: x – not prepared. Numerical values represent average of three triplicate experiments, except for italicized values, which represent the average of two experiments.

Soil	pH	Analysis Technique	Starting Solution Concentration of U (µg/L)							
			0	**6**	**30**	**60**	**300**	**600**	**3000**	**6000**
D - WCS Andrews	5	OES	14.4	5.12	4.37	6.98	28.9	74.3	915	1960
	7	OES	11.1	1.98	2.44	4.32	18.7	54.3	1010	1410
	9	OES	10.4	2.28	3.64	5.14	12.9	41.3	536	898
A - Albany Red	5	OES	9.33	x	2.91	2.37	2.91	2.57	19.1	55.2
	7	OES	5.92	x	2.27	3.04	1.09	1.53	22.6	56.4
	9	OES	1.19	x	1.13	0.291	0.851	2.17	28.7	57.1
B - Houston Brown	5	OES	1.01	x	8.86	20.8	112	273	2150	5020
	7	OES	4.94	x	4.85	5.94	52.1	115	1120	3060
	9	OES	-1.41	x	0.268	5.67	30.0	70.7	957	2120
C - Kamm Clay	5	OES	12.6	x	1.89	1.94	1.26	5.37	17.8	59.5
	7	OES	2.50	x	5.07	5.03	4.18	10.8	22.9	51.7
	9	OES	19.4	x	7.08	4.25	6.56	10.5	16.7	38.5

Table 5.10. Initial data and fitting parameters for Soil *A* isotherms. A correlation of the fit to the data, the r^2 value, is listed for each fitting mechanism and provides a measure of the accuracy. Further, the r^2 value is based on the ratio between the sum of squares for each individual fitting parameter and the total sum of squares derived from the variance of the measured values.

Fitting Parameter	pH 5	pH 7	pH 9
Total Sum of Squares	291000	291000	291000
Linear Sum of Squares	12400	7030	3180
K_d	11.3	10.9	10.5
Linear r^2	0.957	0.976	0.989
Freundlich Sum of Squares	8190	4920	2260
K_F	22.5	18.8	17.6
n	0.821	0.859	0.866
Freundlich r^2	0.972	0.983	0.992
Langmuir Sum of Squares	6050	4130	3020
X_{max}	1510	2020	6270
K_L	0.012	0.007	0.002
Langmuir r^2	0.979	0.986	0.99

Table 5.11. Initial data and fitting parameters for Soil *B* isotherms. A correlation of the fit to the data, the r^2 value, is listed for each fitting mechanism and provides a measure of the accuracy. Further, the r^2 value is based on the ratio between the sum of squares for each individual fitting parameter and the total sum of squares derived from the variance of the measured values.

Fitting Parameter	pH 5	pH 7	pH 9
Total Sum of Squares	9240	74300	122000
Linear Sum of Squares	2580	7610	3160
K_d	0.023	0.105	0.19
Linear r^2	0.721	0.898	0.974
Freundlich Sum of Squares	725	1640	743
K_F	1.62	2.24	1.42
n	0.49	0.611	0.731
Freundlich r^2	0.922	0.978	0.994
Langmuir Sum of Squares	658	1180	1680
X_{max}	132	469	1100
K_L	6.75×10^{-4}	5.60×10^{-4}	2.55×10^{-4}
Langmuir r^2	0.929	0.984	0.986

Table 5.12. Data and fitting parameters for Soil *B* isotherms using only data derived from serial dilution. A correlation of the fit to the data, the r^2 value, is listed for each fitting mechanism and provides a measure of the accuracy. Further, the r^2 value is based on the ratio between the sum of squares for each individual fitting parameter and the total sum of squares derived from the variance of the measured values.

Fitting Parameter	pH 5	pH 7	pH 9
Linear Sum of Squares	2560	7480	2740
K_d	0.023	0.105	0.189
Linear r^2	0.71	0.897	0.977
Freundlich Sum of Squares	260	375	630
K_F	2.99	4	1.86
n	0.419	0.538	0.695
Freundlich r^2	0.971	0.995	0.995
Langmuir Sum of Squares	5.6	313	1620
X_{max}	111	401	1190
K_L	1.62×10^{-3}	8.58×10^{-4}	2.28×10^{-4}
Langmuir r^2	0.999	0.996	0.986

Table 5.13. Initial data and fitting parameters for Soil *C* isotherms. A correlation of the fit to the data, the r^2 value, is listed for each fitting mechanism and provides a measure of the accuracy. Further, the r^2 value is based on the ratio between the sum of squares for each individual fitting parameter and the total sum of squares derived from the variance of the measured values.

Fitting Parameter	pH 5	pH 7	pH 9
Total Sum of Squares	291000	292000	293000
Linear Sum of Squares	14200	11500	31000
K_d	10.6	11.4	14.5
Linear r^2	0.951	0.96	0.894
Freundlich Sum of Squares	8620	8580	18100
K_F	22.1	6.32	4.74
n	0.811	1.16	1.33
Freundlich r^2	0.97	0.971	0.938
Langmuir Sum of Squares	5170	11500	31000
X_{max}	1410	2580000	5480000
K_L	0.013	4.40×10^{-6}	2.64×10^{-6}
Langmuir r^2	0.982	0.96	0.894

Table 5.14. Data and fitting parameters for Soil *D* sorption isotherms. A correlation of the fit to the data, the r^2 value, is listed for each fitting mechanism and provides a measure of the accuracy. Further, the r^2 value is based on the ratio between the sum of squares for each individual fitting parameter and the total sum of squares derived from the variance of the measured values.

Fitting Parameter	pH 5	pH 7	pH 9
Total Sum of Squares	142000	177000	226000
Linear Sum of Squares	2460	13400	4130
K_d	0.284	0.284	0.541
Linear r^2	0.983	0.924	0.982
Freundlich Sum of Squares	828	6750	3410
K_F	1.08	1.05×10^{-5}	0.153
n	0.78	2.43	1.19
Freundlich r^2	0.994	0.962	0.985
Langmuir Sum of Squares	1550	13400	4140
X_{max}	1450	417000	499000
K_L	1.94×10^{-4}	6.80×10^{-7}	1.09×10^{-6}
Langmuir r^2	0.989	0.924	0.982

Table 5.15. Comparison of the average measured final pH values and their consequent standard deviation to the initial pH values used during sorption isotherm experimentation for the four study soils.

	pH		
Soil	**5**	**7**	**9**
A	7.63 ± 0.30	7.91 ± 0.17	8.47 ± 0.23
B	8.26 ± 0.06	8.89 ± 0.06	9.15 ± 0.04
C	7.25 ± 0.09	7.94 ± 0.08	8.51 ± 0.10
D	9.05 ± 0.09	9.31 ± 0.07	9.45 ± 0.06

Table 5.16. Comparison of impact of various soil properties on barrier performance.

Soil	SSA	BC	CEC	Amorphous Fe	Total Reactive Fe	Carbonate	Best Sorbent
A					*		*
B	*	*	*			*	
C	*			*			*
D					*		

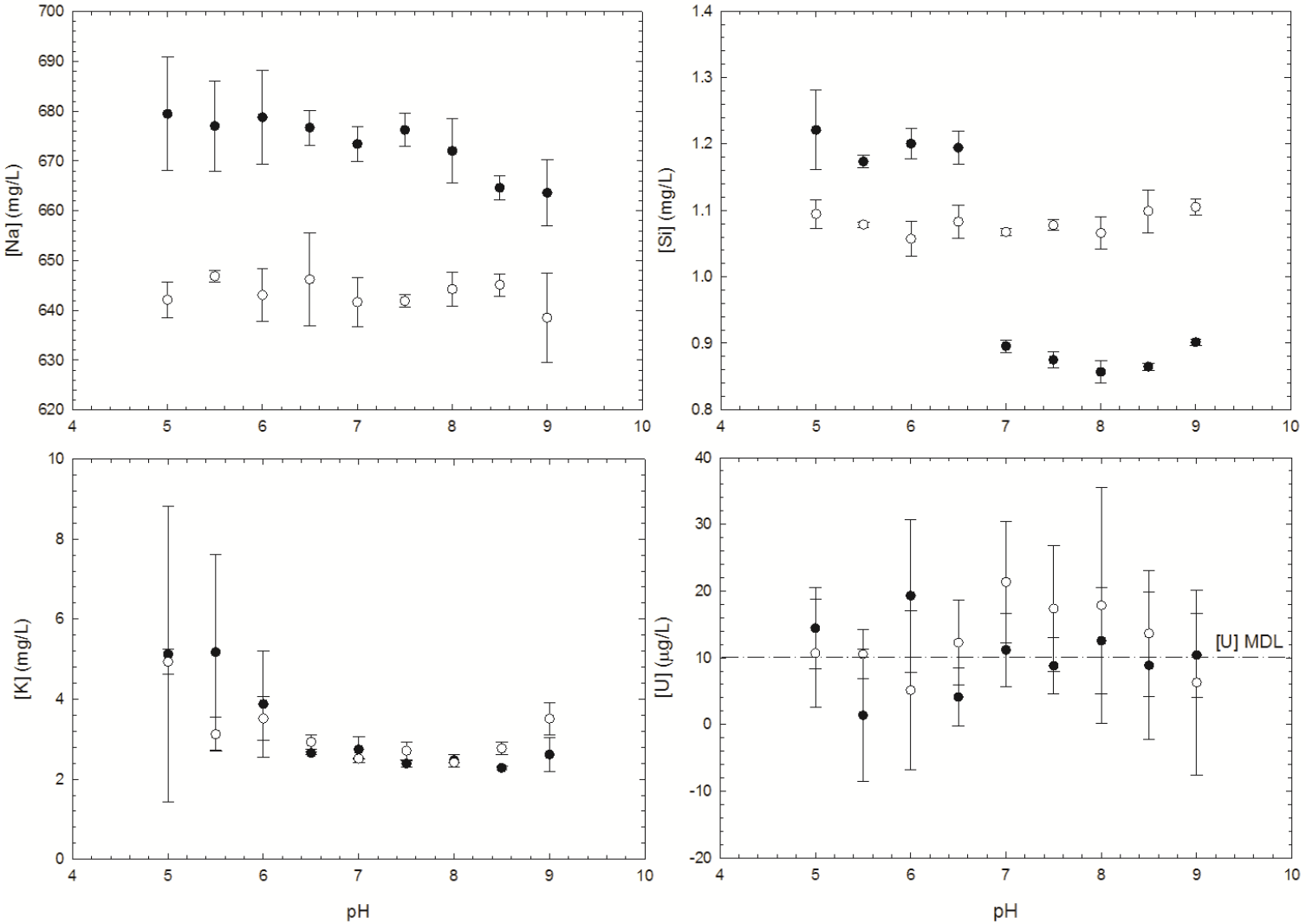

Figure 5.1. Solution control experimentation data for the WCS Andrews soil – Na, Si, and K (concentrations in mg/L) and U (µg/L) over the 24-h (filled symbols) and 7-d (open symbols) reaction periods between pH 5 and 9 in 0.5 pH units.

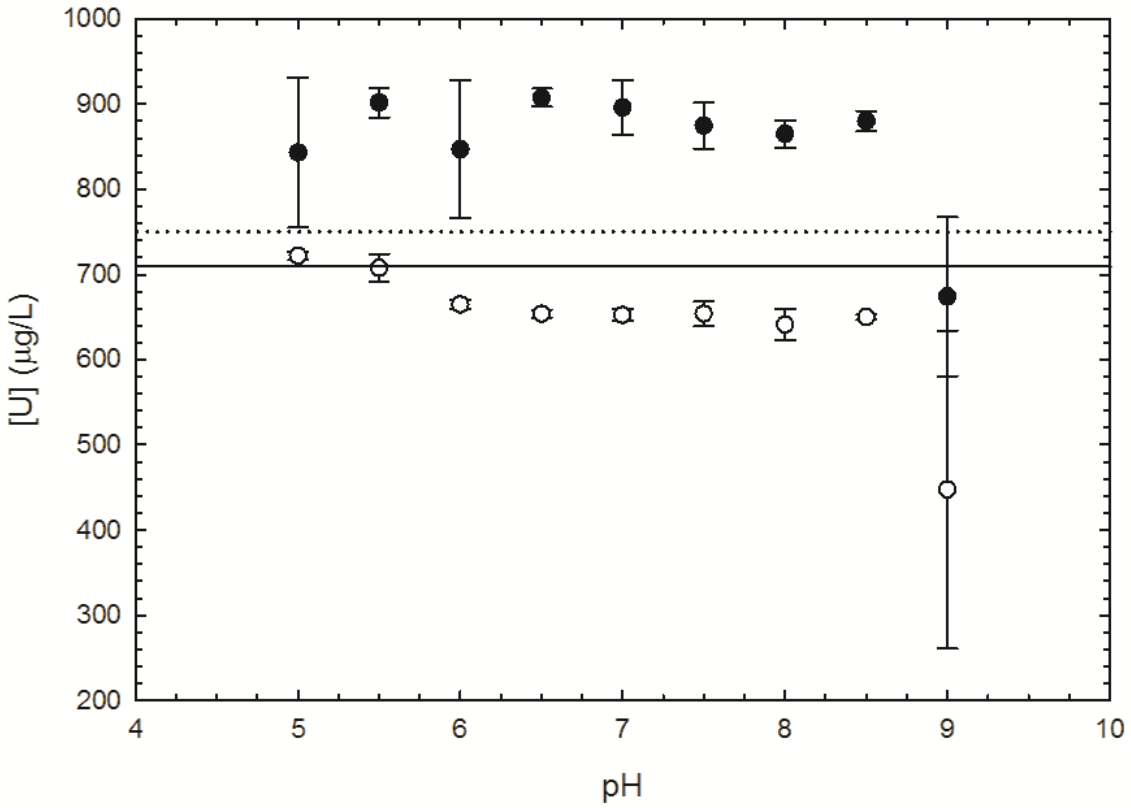

Figure 5.2. Change in concentration of uranium remaining in solution with pH for solution control experimentation over the 24-h (filled symbols) and 7-d (open symbols) reaction periods. Points represent the average of three triplicate experiments for each 0.5 pH increment between pH 5 and pH 9, as measured by the U 263.553 nm wavelength by ICP-OES. Error bars indicate the standard deviation between triplicated samples.

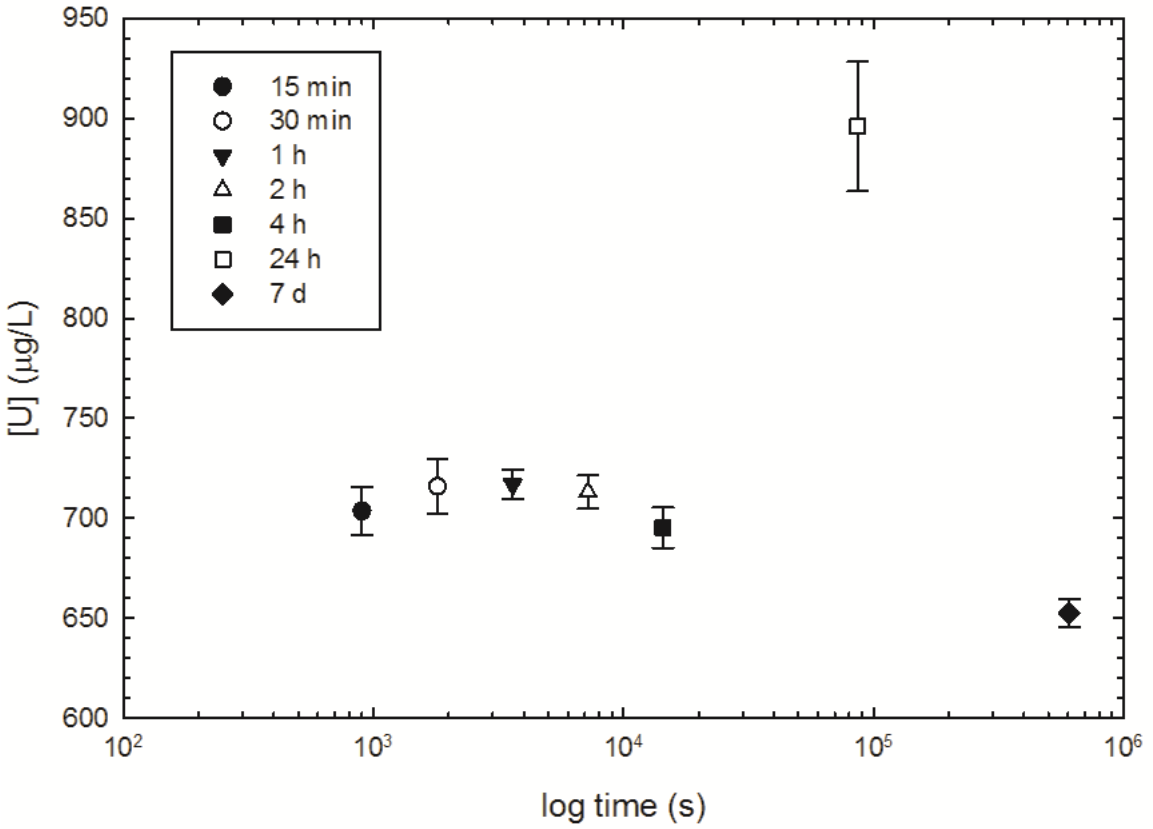

Figure 5.3. Comparison of U concentrations measured in solution during solution control kinetics experimentation. Measured time frames ranged from 15 min (900 s) to 7 d (604800 s). The initial U concentration across all experimentation was averaged to 710 µg/L. Measurements at 24 h represent potential outliers from other time frames.

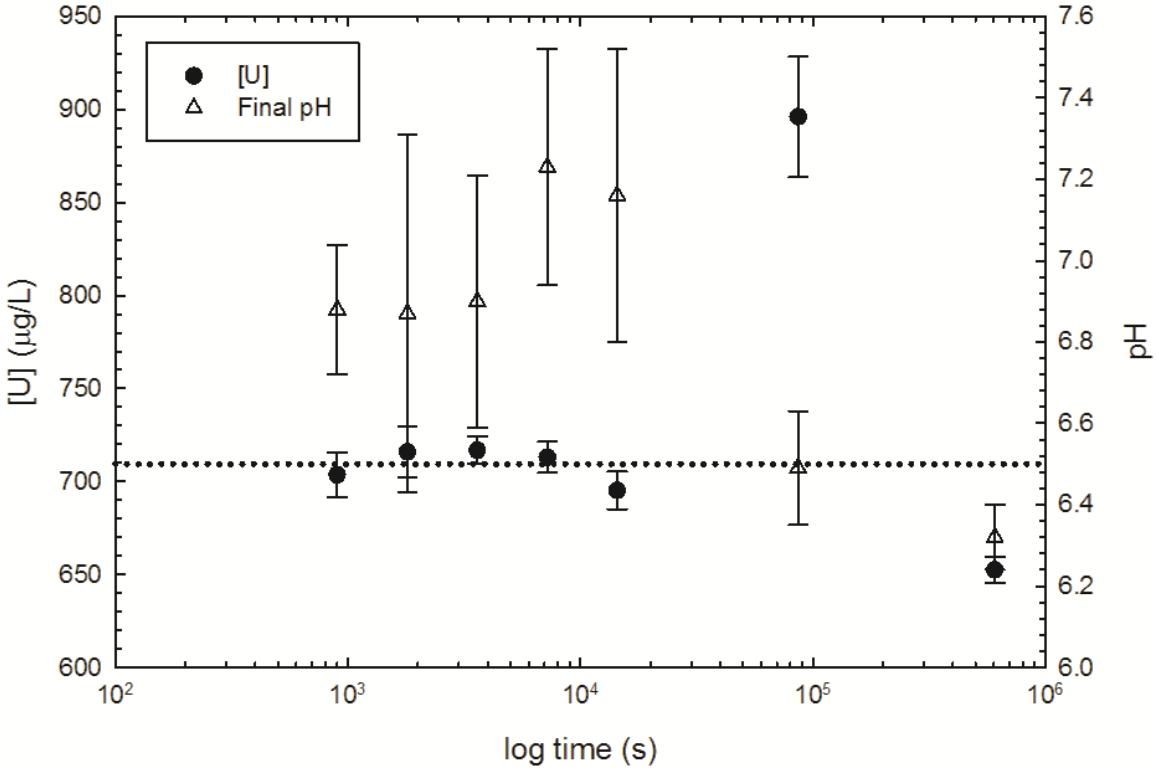

Figure 5.4. Comparison of measured U concentrations (in µg/L) and final measured pH levels across kinetics solution control experimentation. The measured 710 µg U/L (2.98 µM U) is 64% of the expected 1117 µg U/L (4.69 µM U).

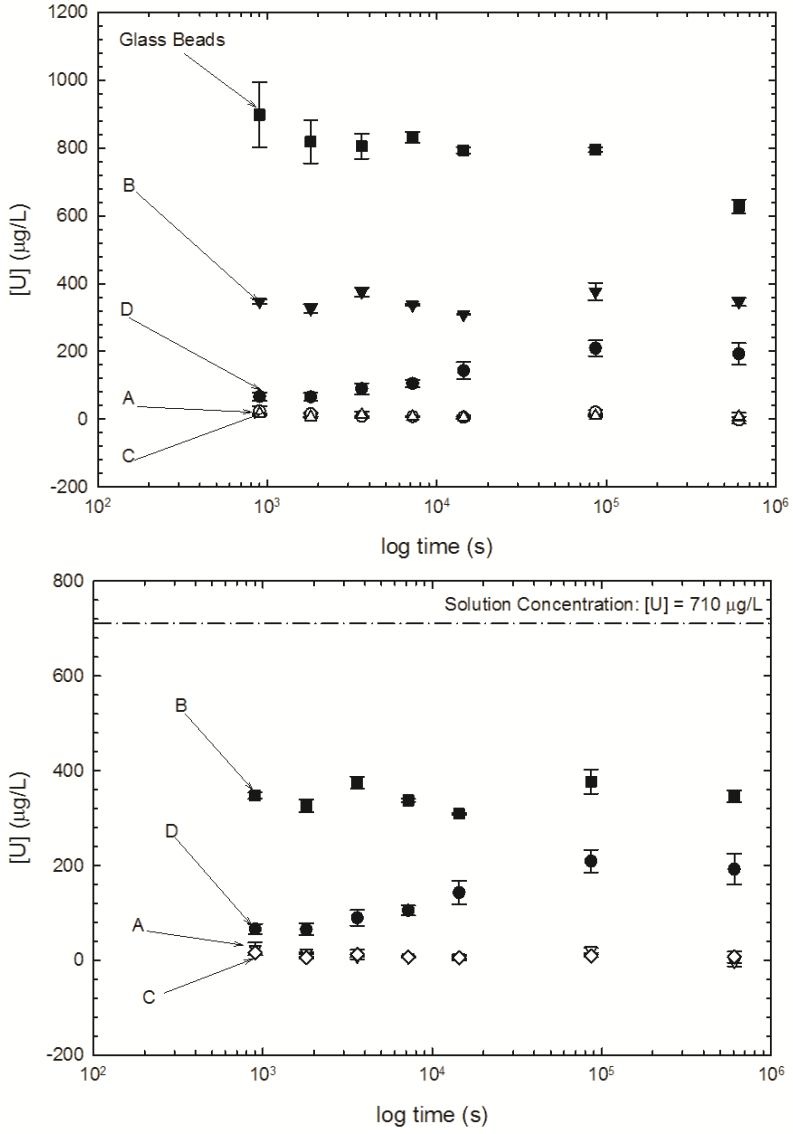

Figure 5.5. Comparison of U concentrations measured in solution during kinetics experimentation for the four study soils and the glass bead sorption control. Measured time frames ranged from 15 min (900 s) to 7 d (604800 s). The initial U concentration across all experimentation was 710 µg/L.

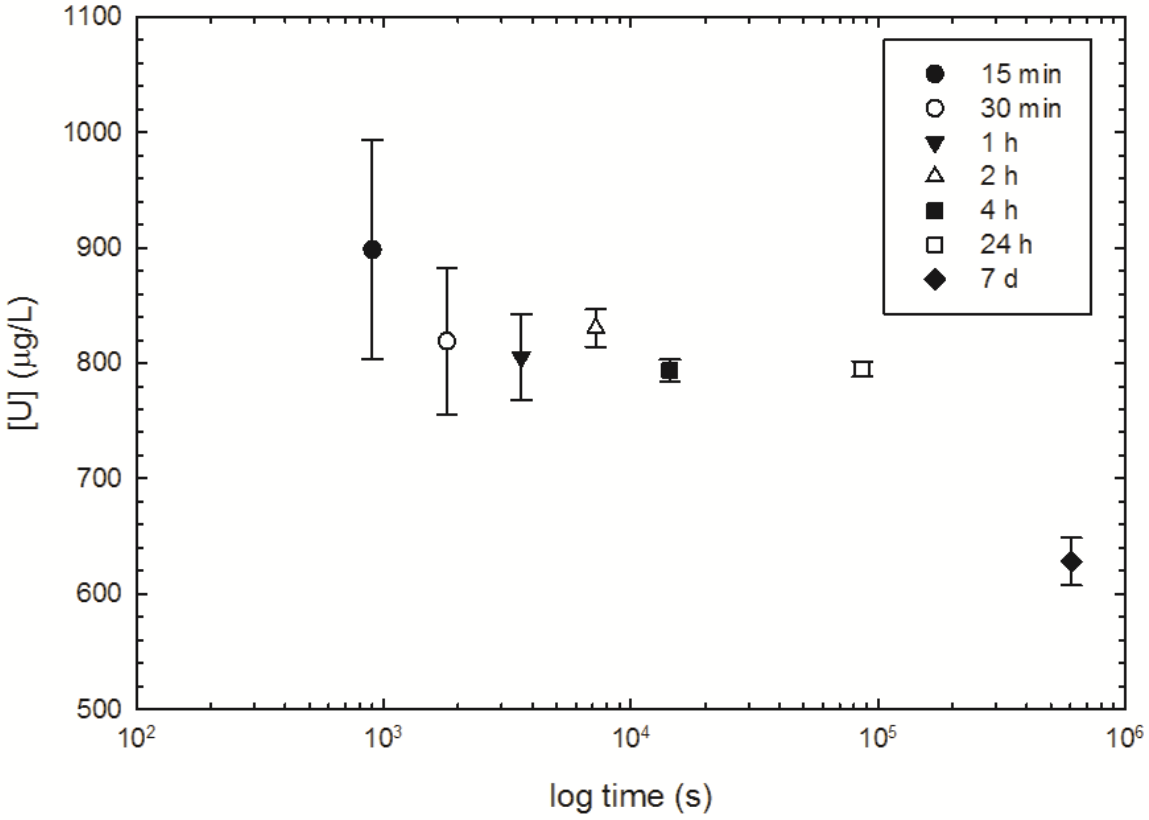

Figure 5.6. Comparison of U concentrations measured in solution during kinetics experimentation for the glass bead sorption control.

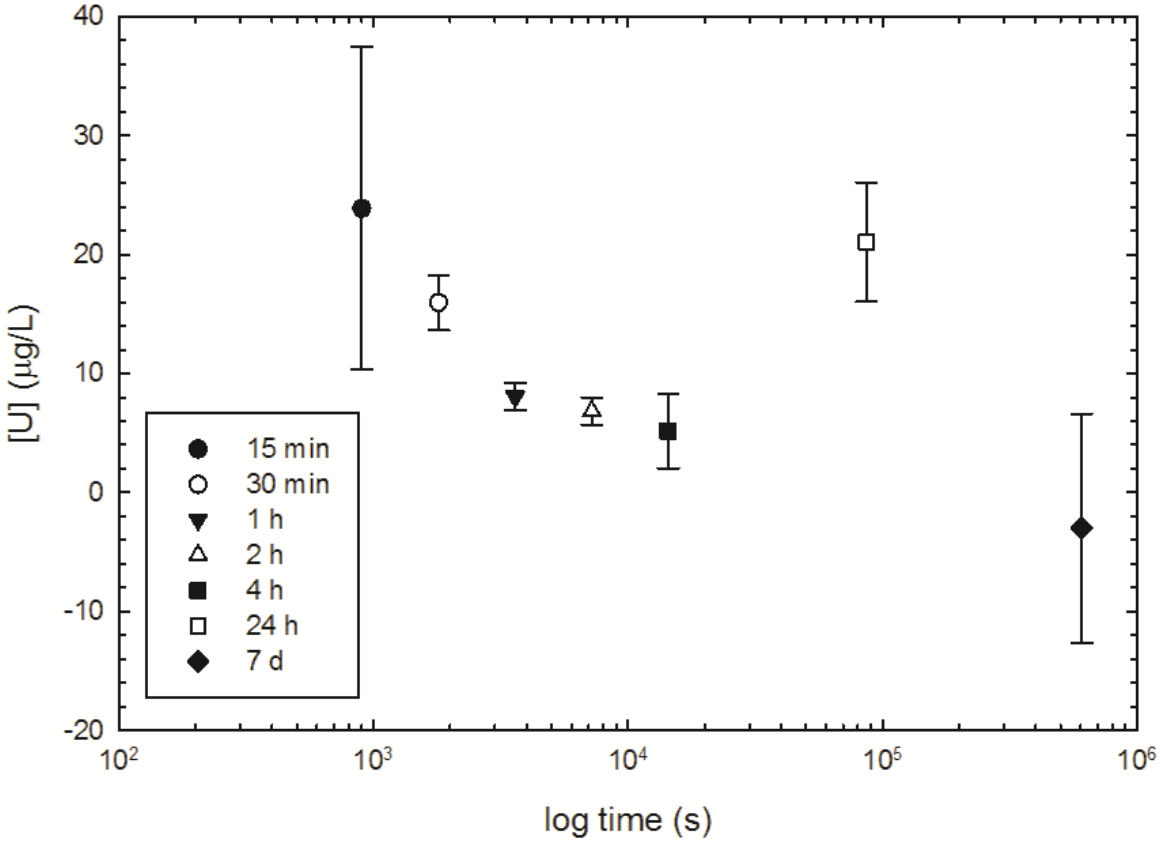

Figure 5.7. Comparison of U concentrations measured in solution during kinetics experimentation for Soil *A*.

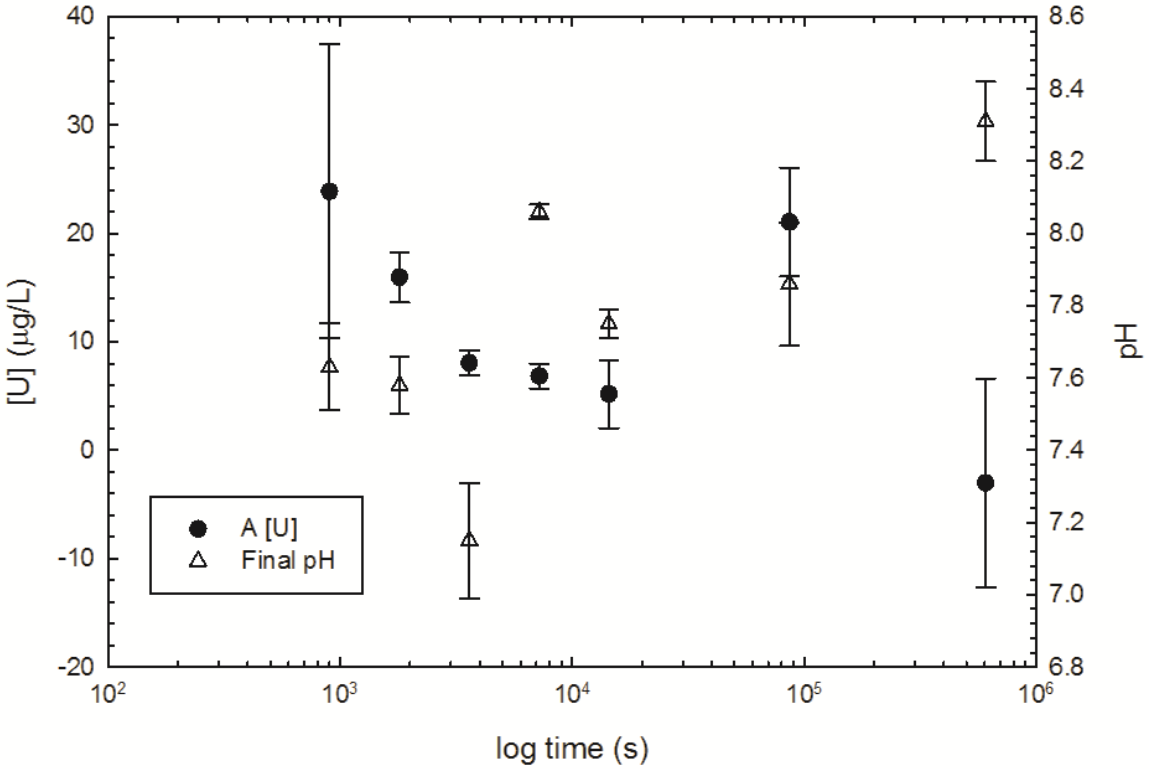

Figure 5.8. Comparison of U concentrations to final pH during kinetics experimentation for Soil *A*.

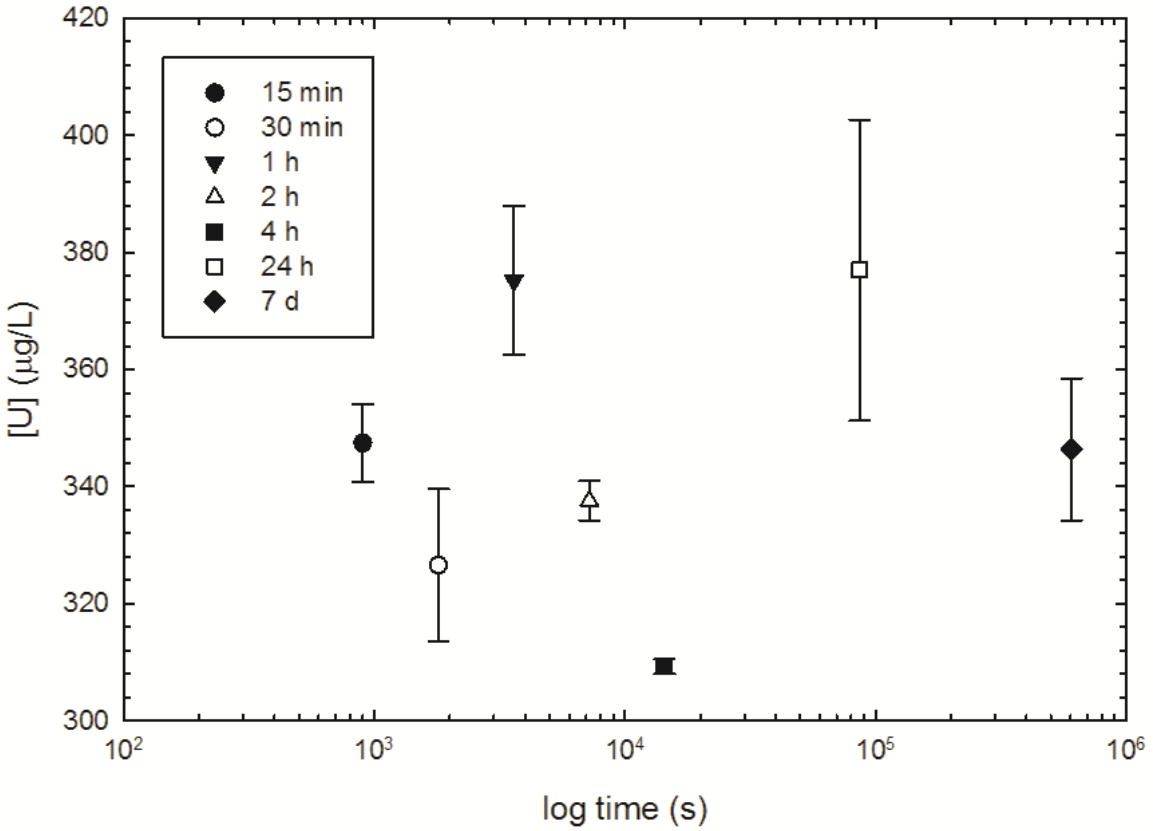

Figure 5.9. Comparison of U concentrations measured in solution during kinetics experimentation for Soil *B*.

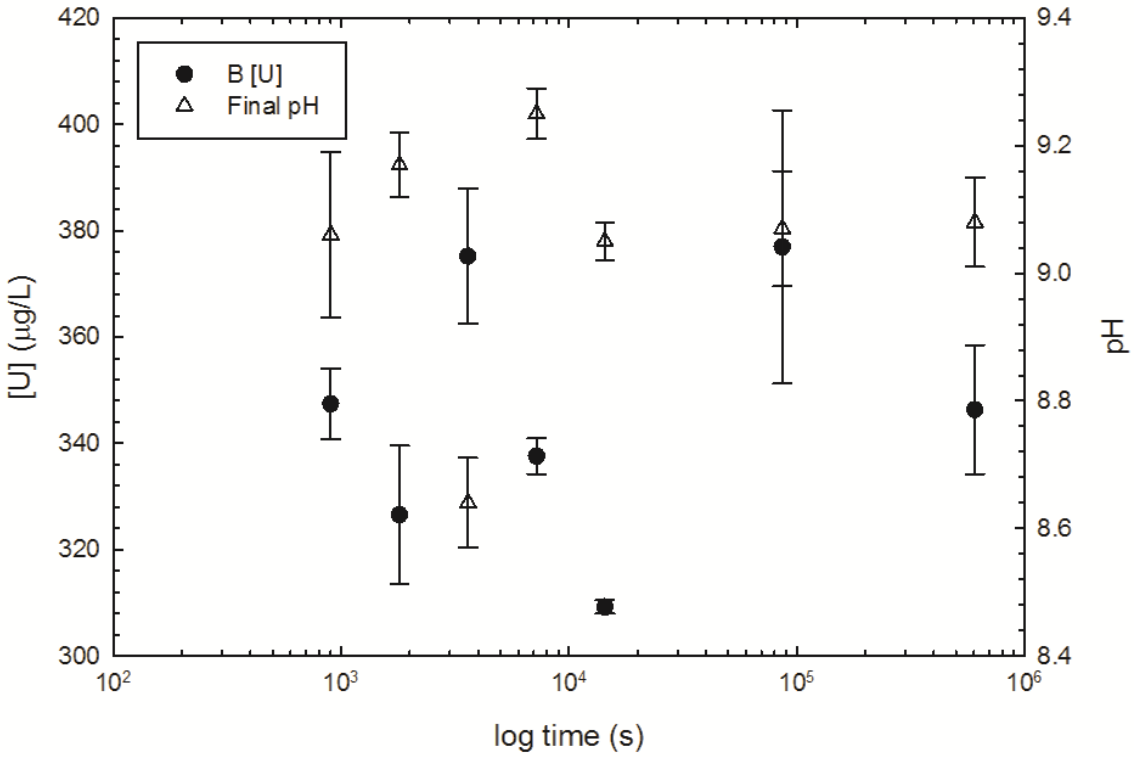

Figure 5.10. Comparison of U concentrations to final pH during kinetics experimentation for Soil *B*.

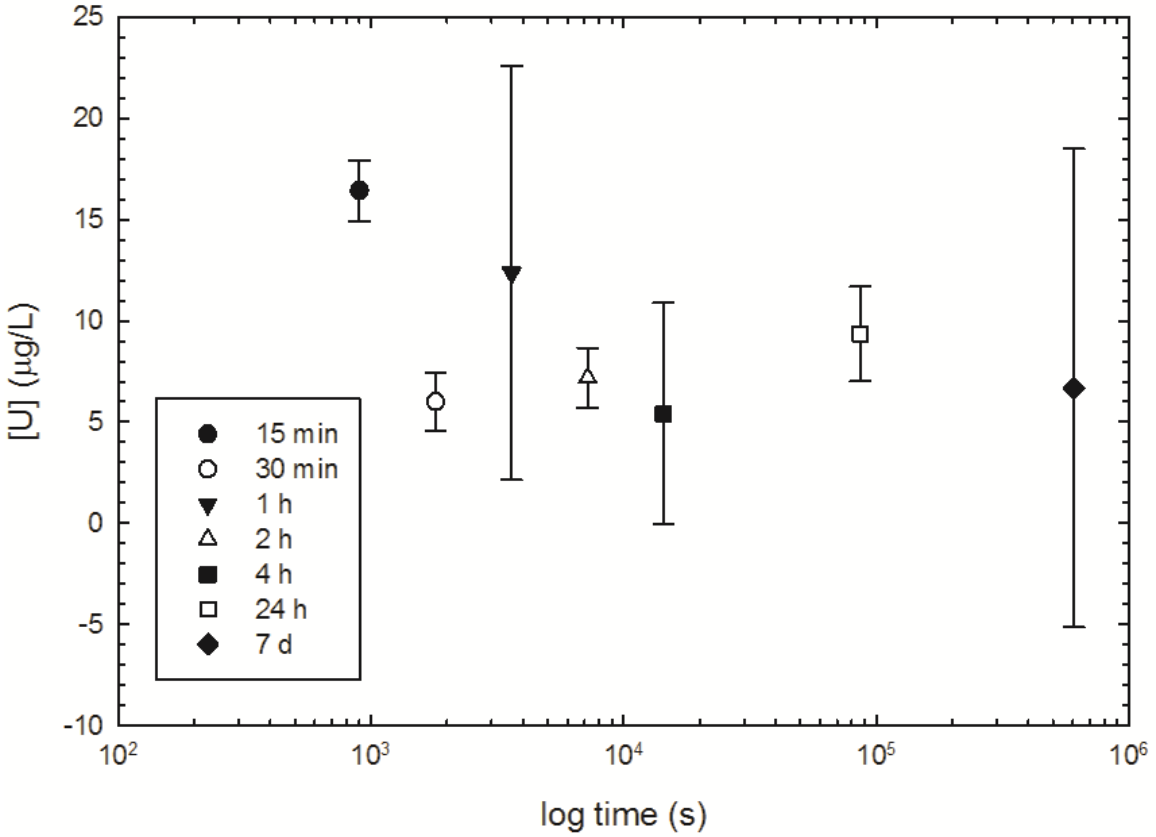

Figure 5.11. Comparison of U concentrations measured in solution during kinetics experimentation for Soil *C*.

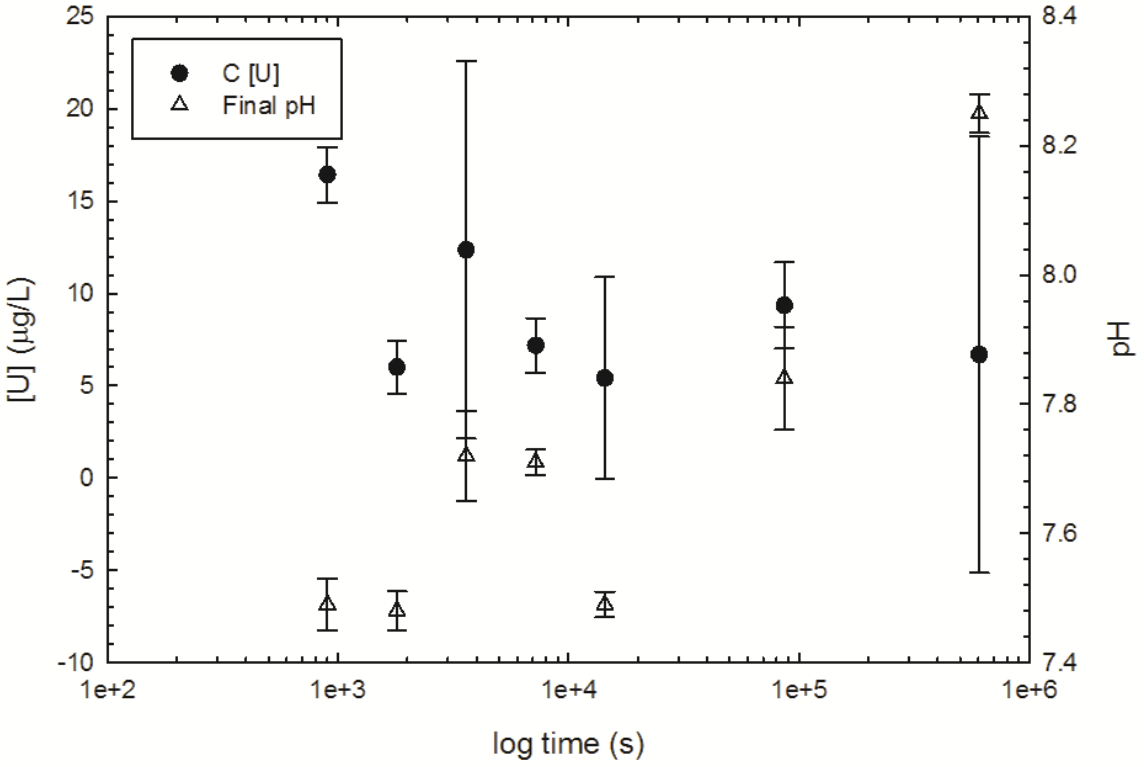

Figure 5.12. Comparison of U concentrations to final pH during kinetics experimentation for Soil *C*.

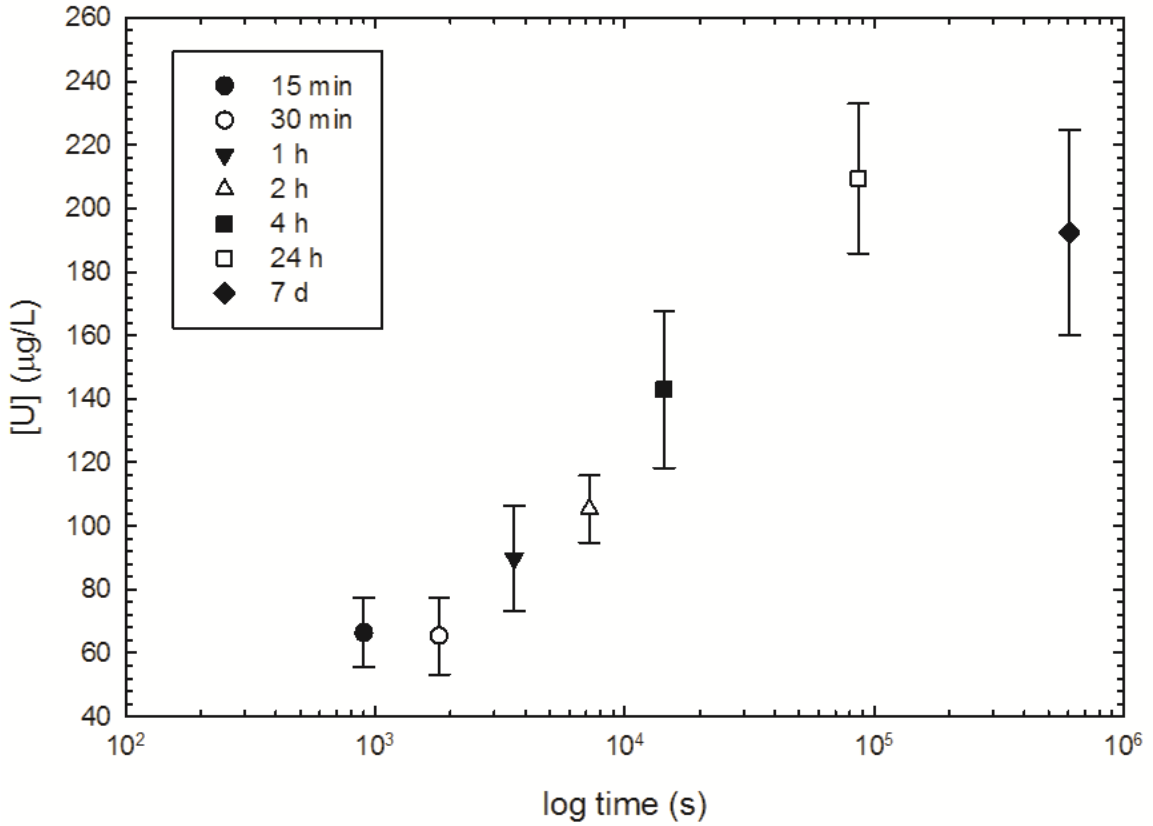

Figure 5.13. Comparison of U concentrations measured in solution during kinetics experimentation for Soil *D*.

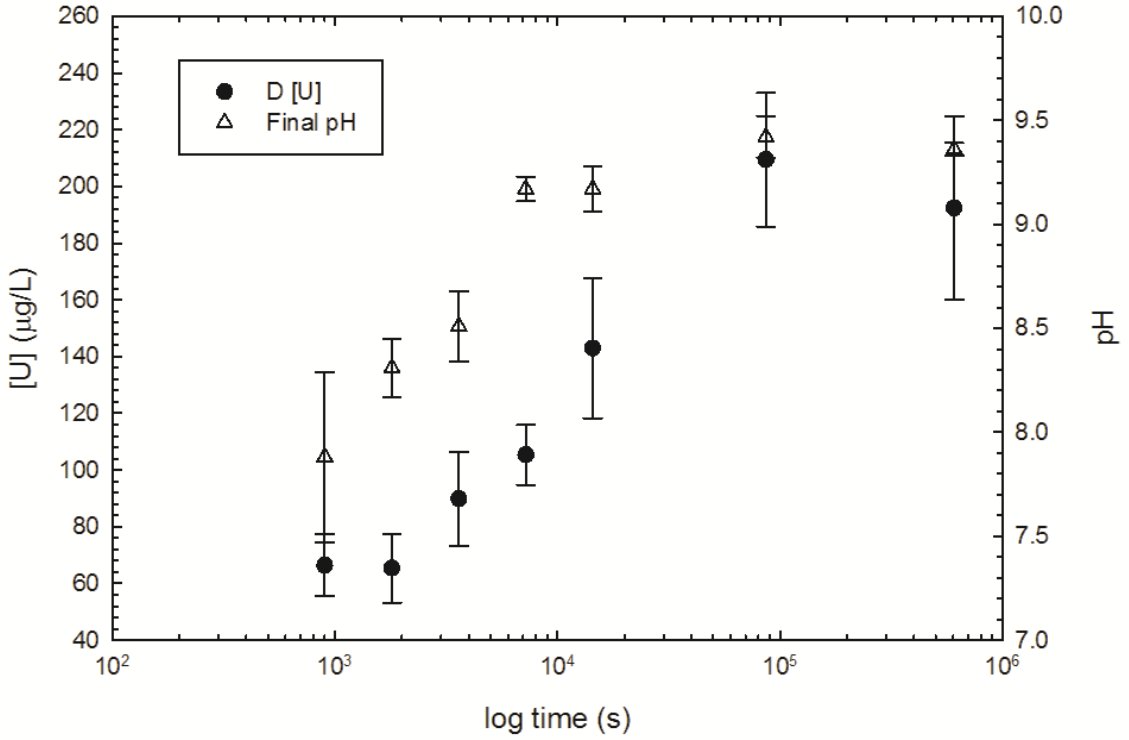

Figure 5.14. Comparison of U concentrations to final pH during kinetics experimentation for Soil *D*.

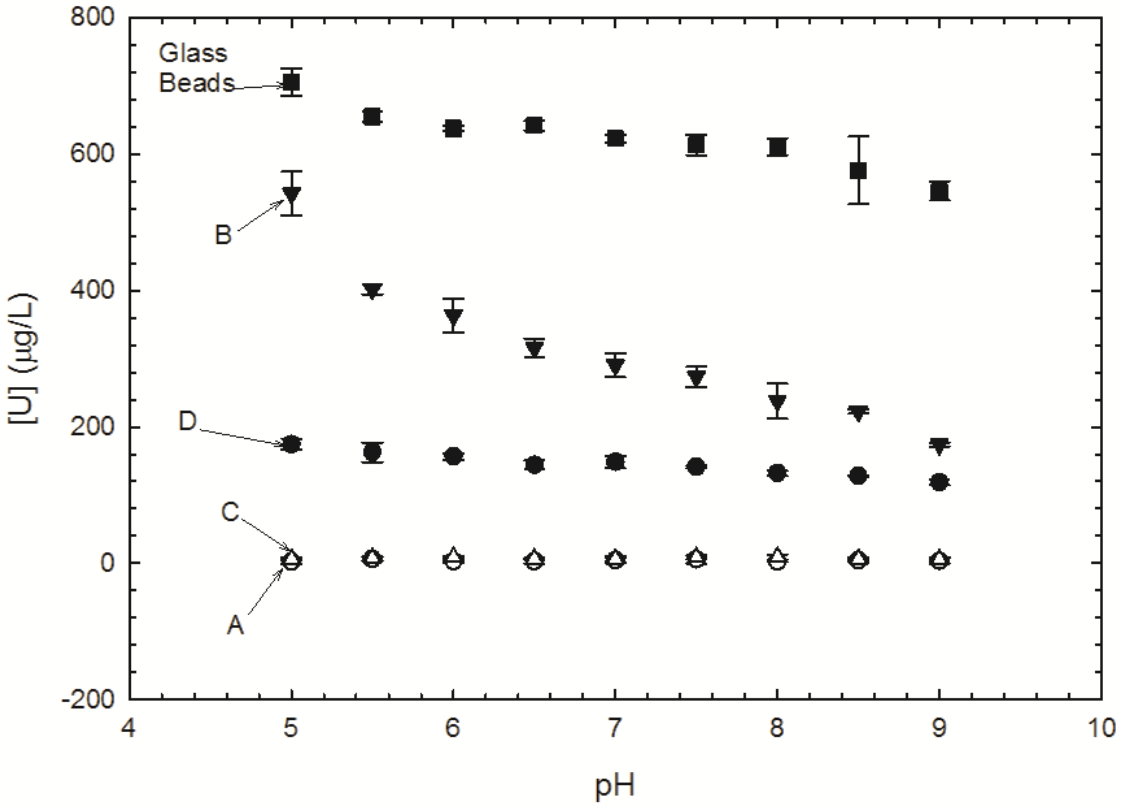

Figure 5.15. Comparison of U concentrations measured in solution between pH 5 and 9 during sorption edge and envelope experimentation for the four study soils and the glass bead sorption control. The initial U concentration across all experimentation was 710 µg/L.

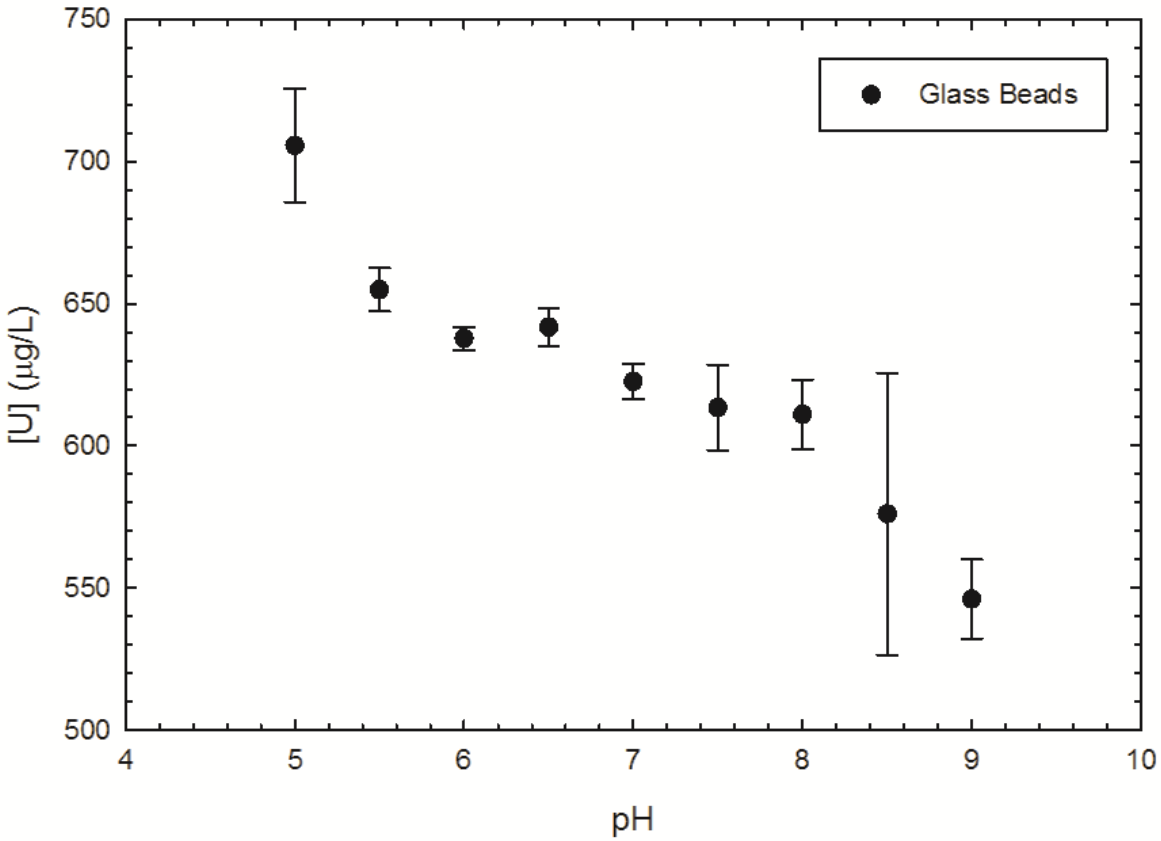

Figure 5.16. Comparison of U concentrations measured in solution during sorption edge and envelope experimentation for the glass beads sorption control, between pH 5 and 9.

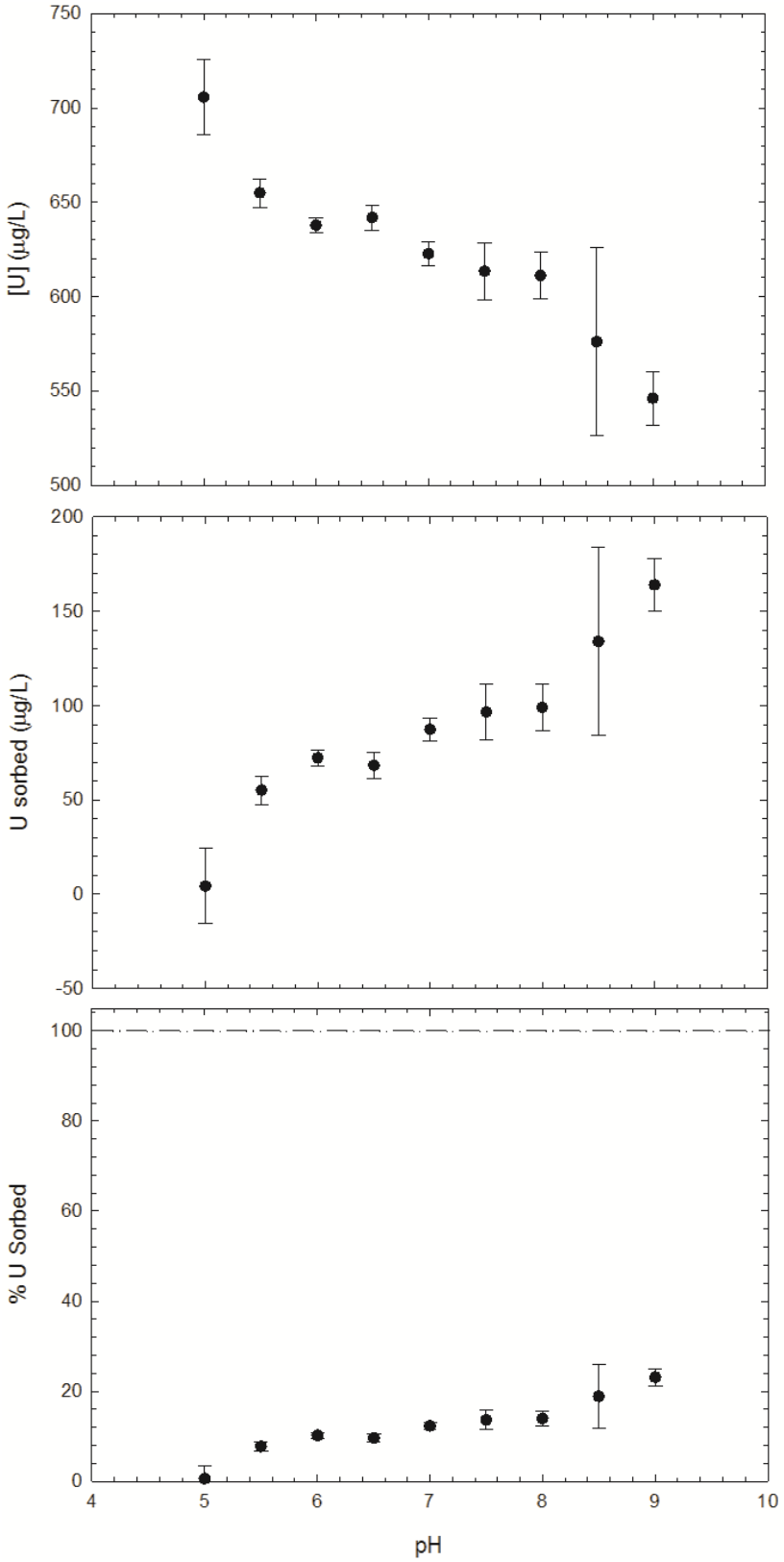

Figure 5.17. Comparison of U concentrations measured in solution during sorption edge and envelope experimentation for the glass beads sorption control, between pH 5 and 9.

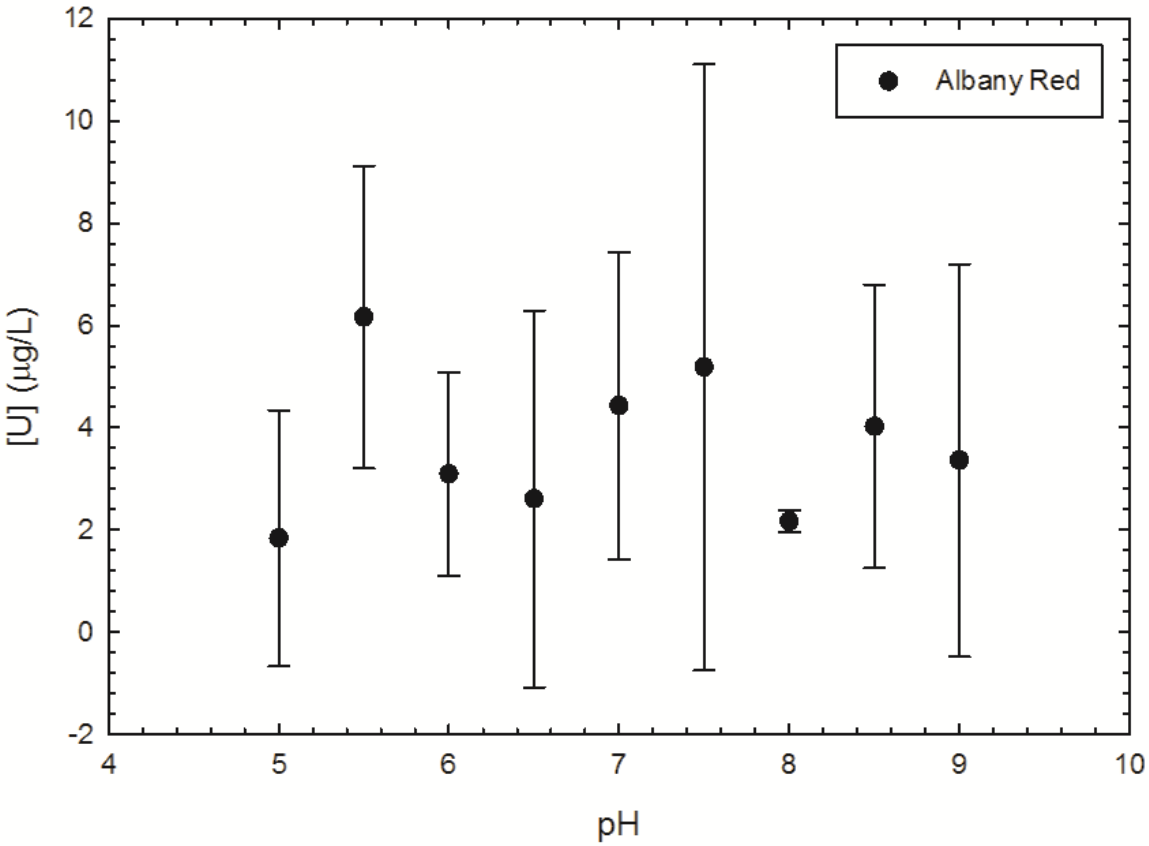

Figure 5.18. Comparison of U concentrations measured in solution following sorption edge and envelope experimentation for Soil *A*, between pH 5 and 9.

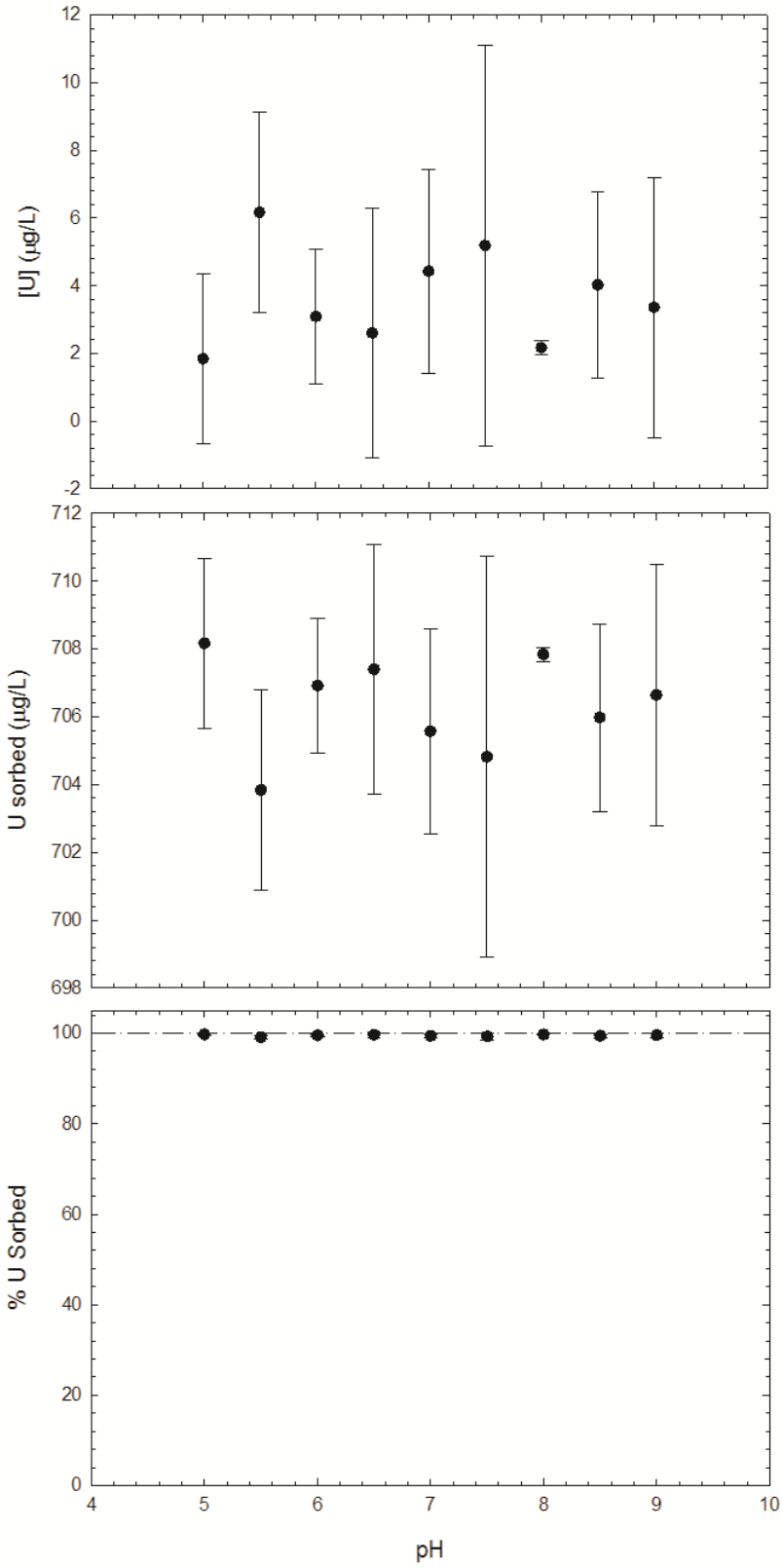

Figure 5.19. Comparison of U concentrations measured in solution following sorption edge and envelope experimentation for Soil *A*, between pH 5 and 9.

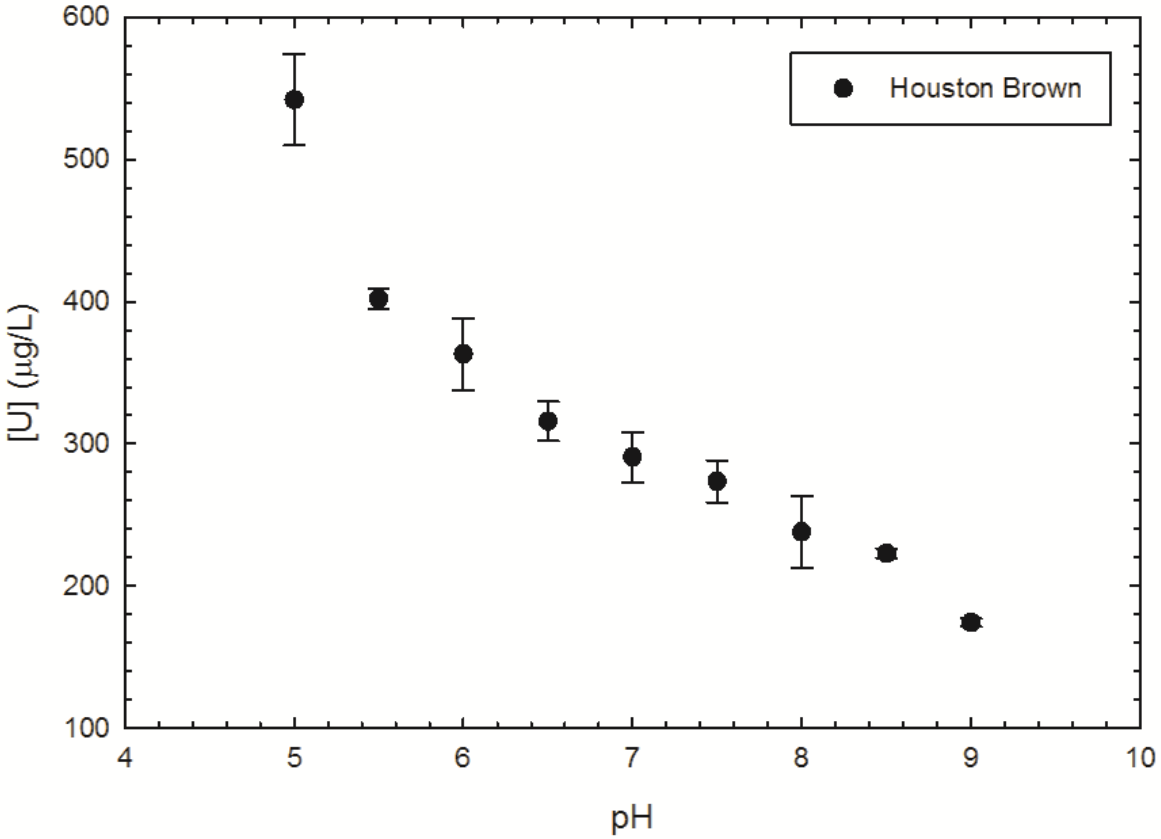

Figure 5.20. Comparison of U concentrations measured in solution following sorption edge and envelope experimentation for Soil *B*, between pH 5 and 9.

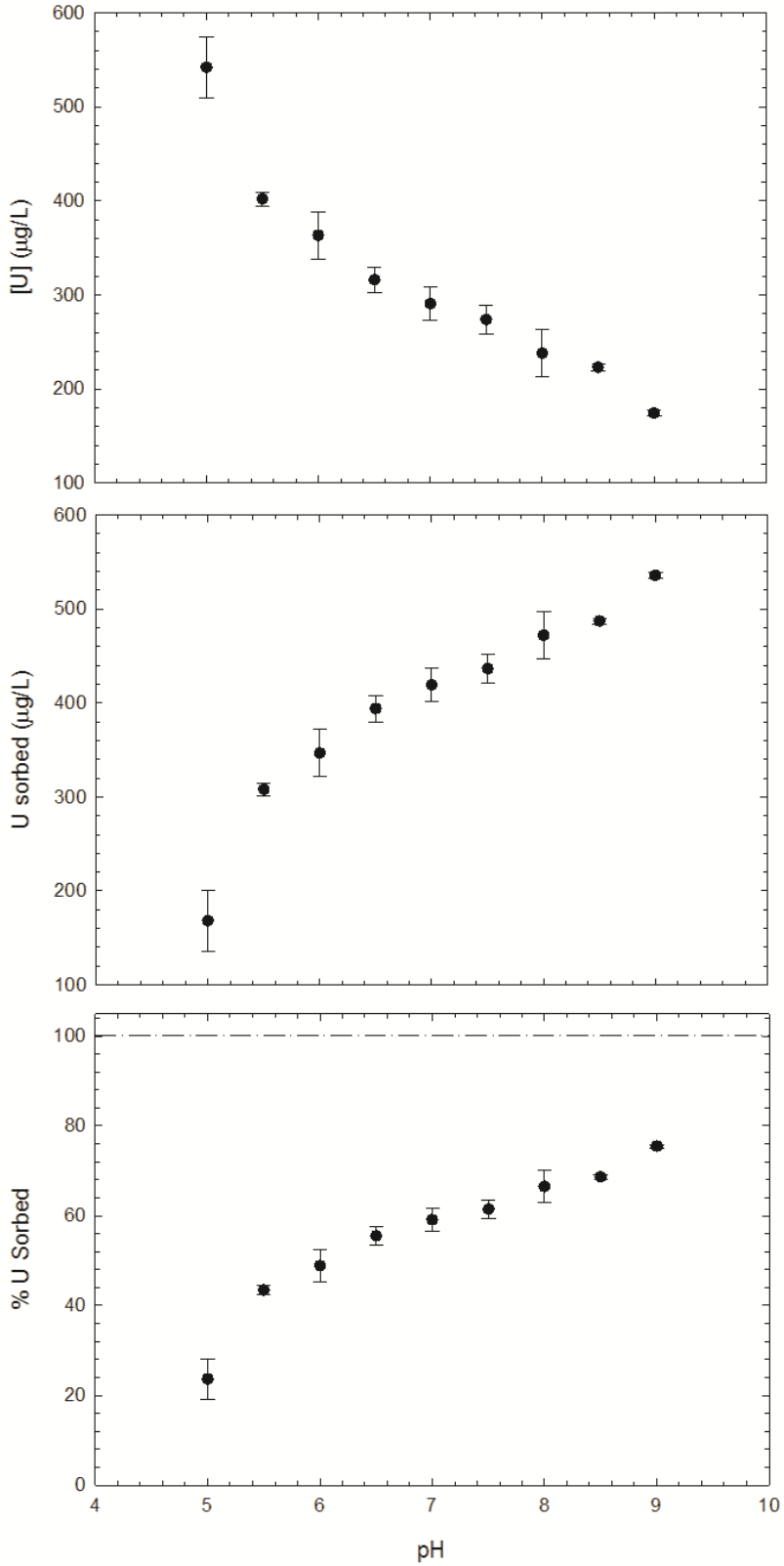

Figure 5.21. Comparison of U concentrations measured in solution following sorption edge and envelope experimentation for Soil *B*, between pH 5 and 9.

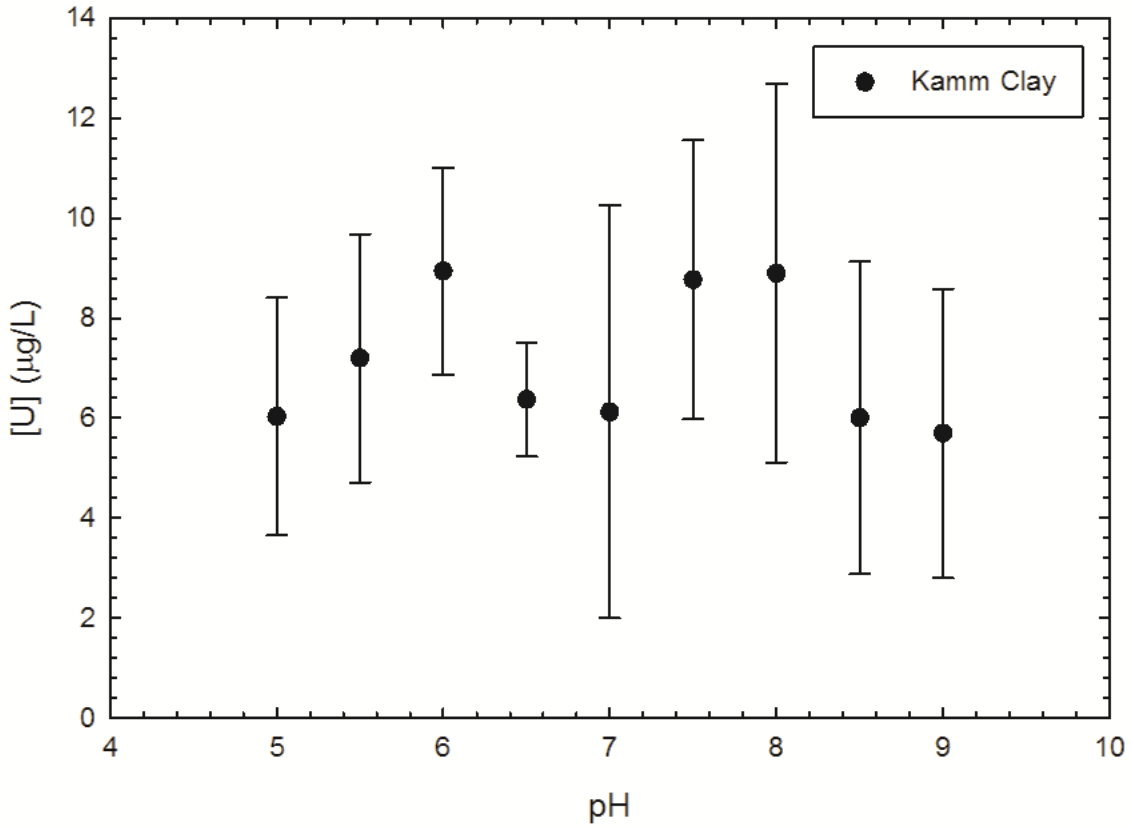

Figure 5.22. Comparison of U concentrations measured in solution following sorption edge and envelope experimentation for Soil *C*, between pH 5 and 9.

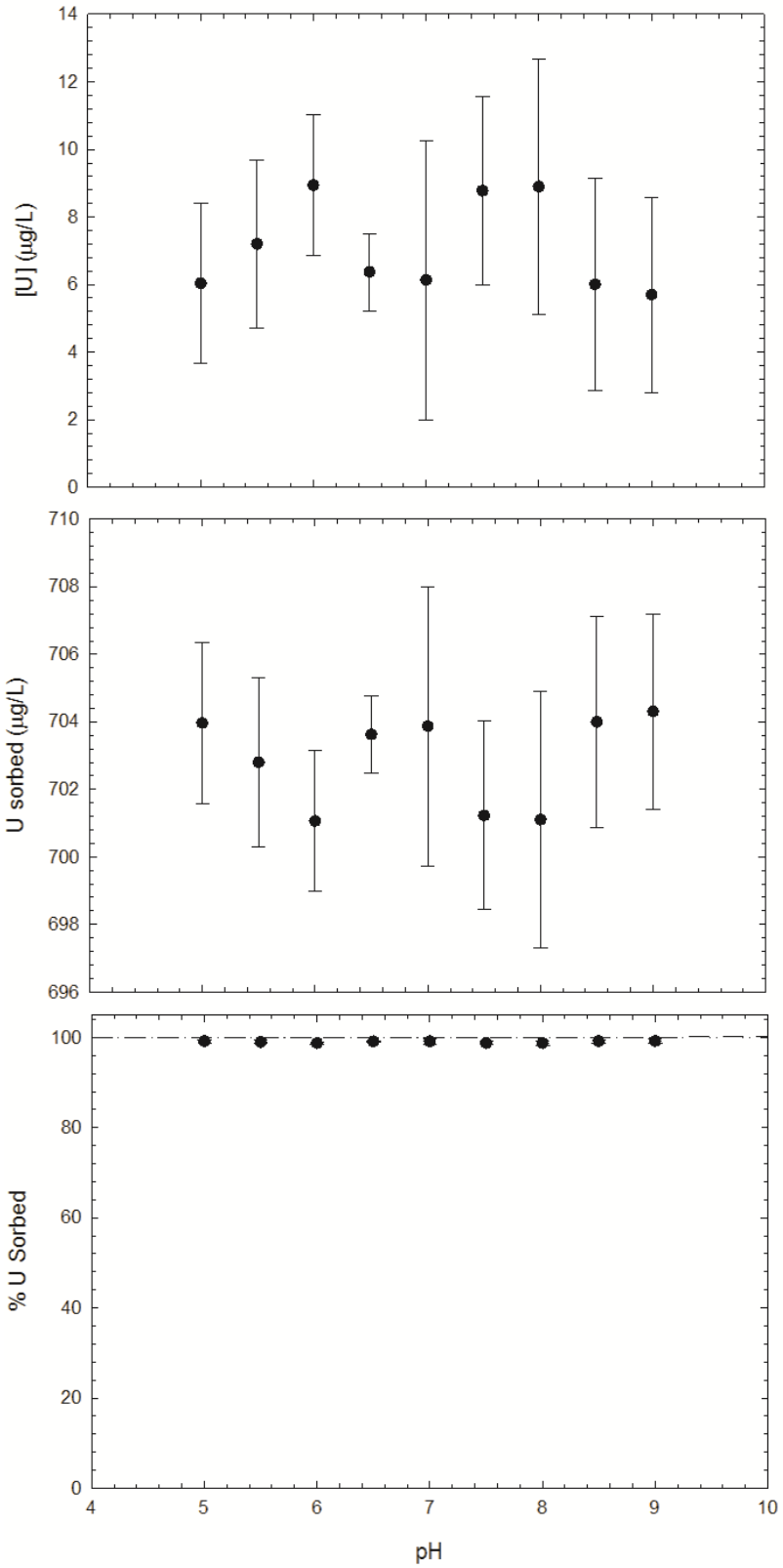

Figure 5.23. Comparison of U concentrations measured in solution following sorption edge and envelope experimentation for Soil *C*, between pH 5 and 9.

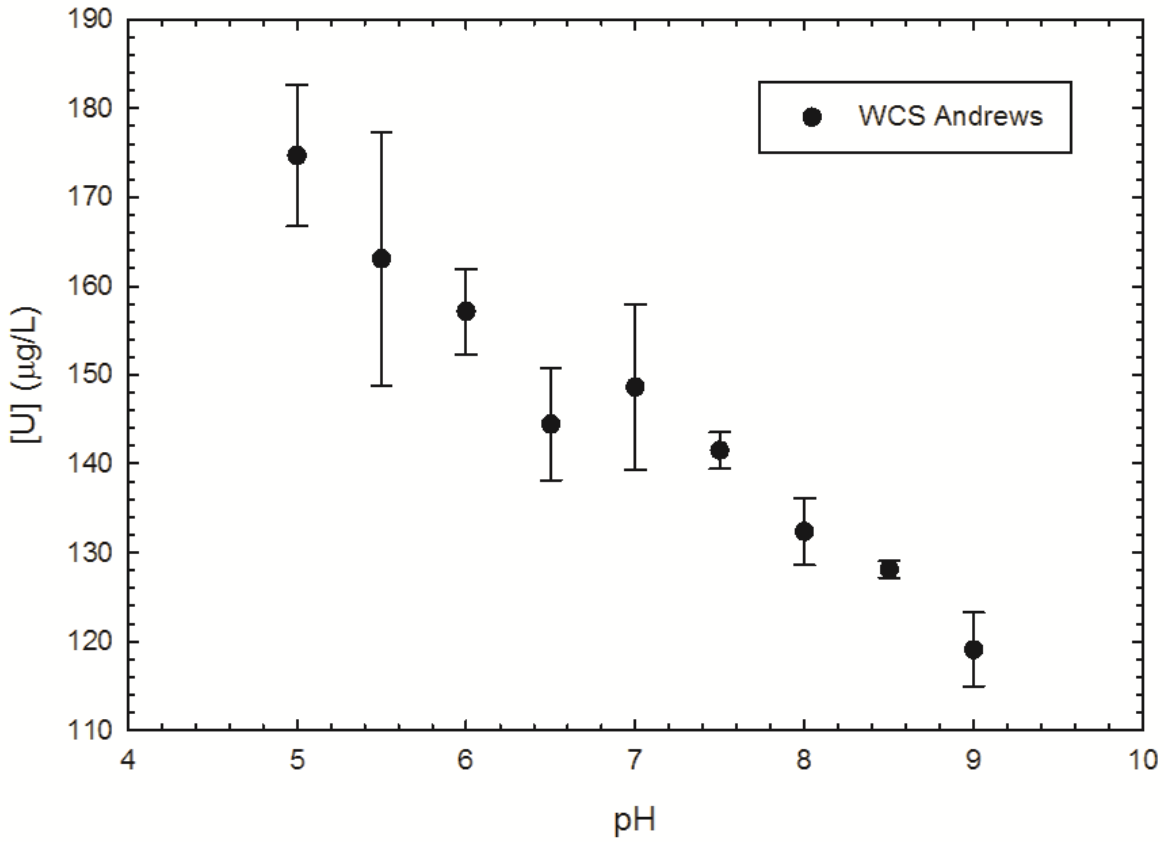

Figure 5.24. Comparison of U concentrations measured in solution following sorption edge and envelope experimentation for Soil *D*, between pH 5 and 9.

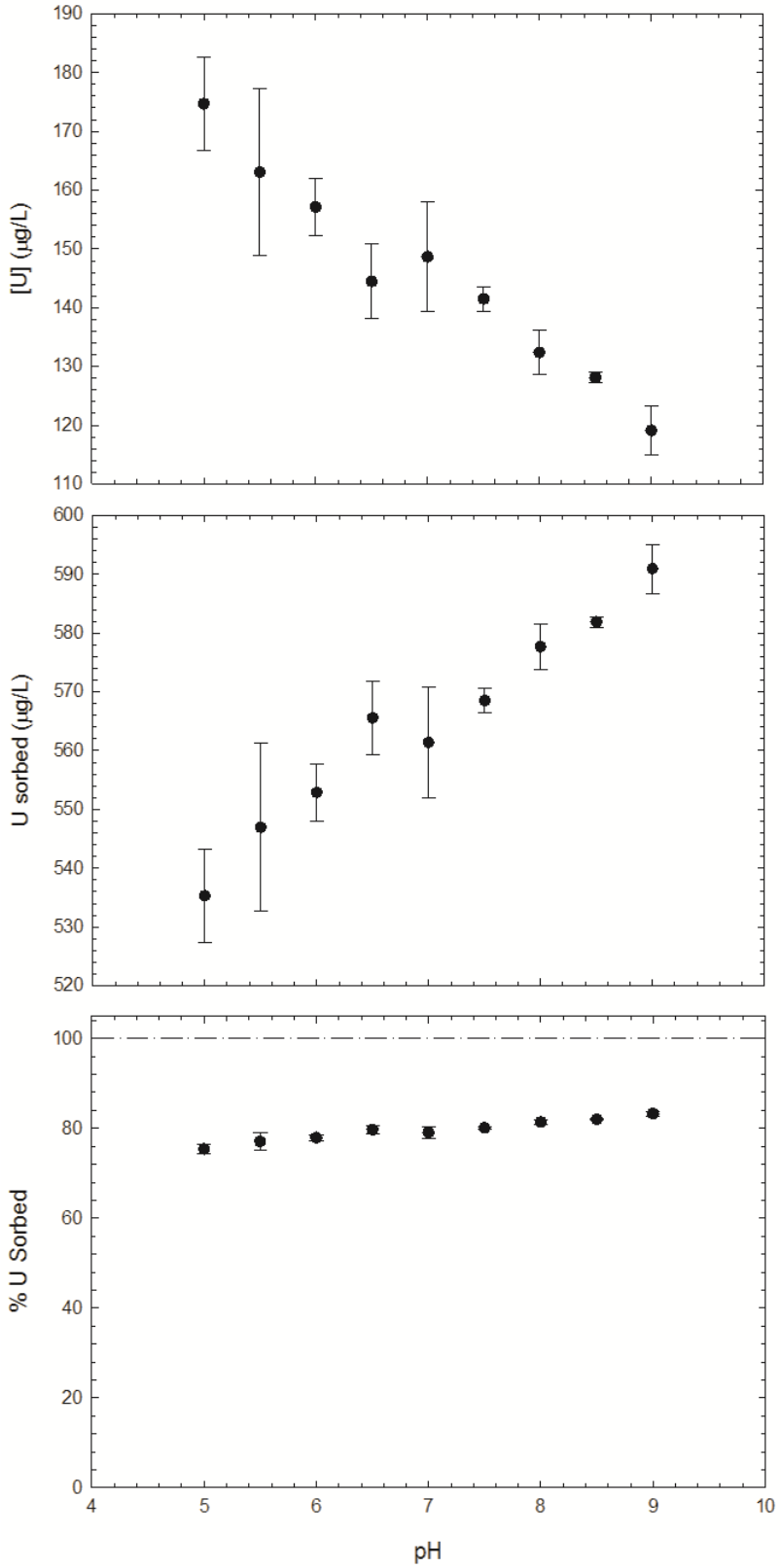

Figure 5.25. Comparison of U concentrations measured in solution following sorption edge and envelope experimentation for Soil *D*, between pH 5 and 9.

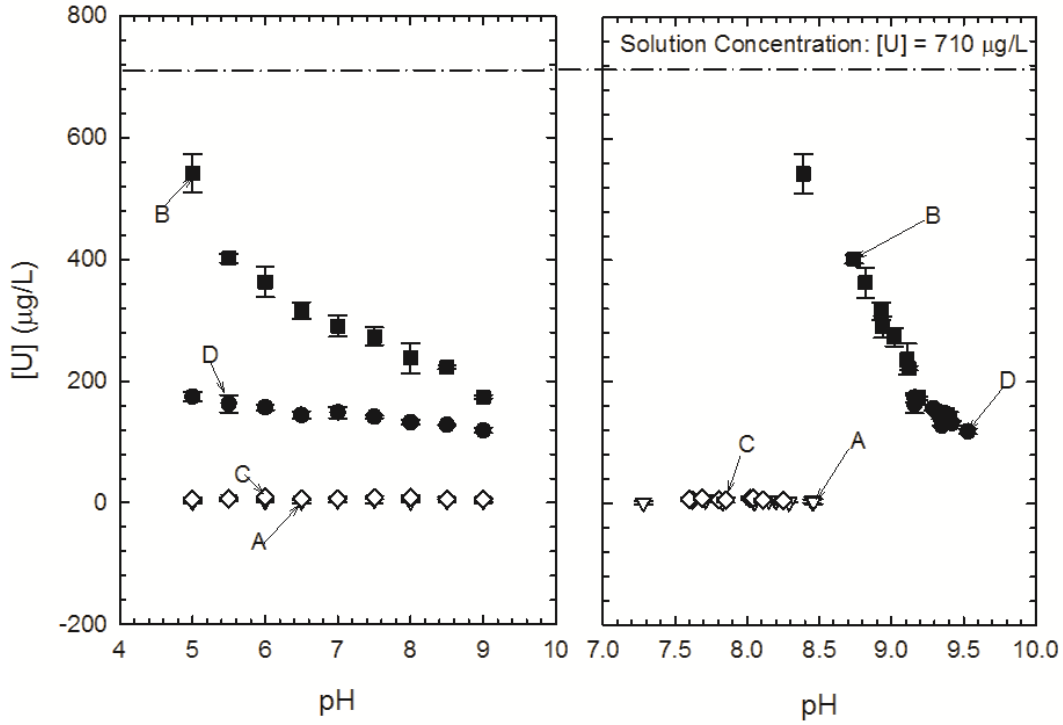

Figure 5.26. Comparison of U concentrations measured in solution between pH 5 and 9 during sorption edge and envelope experimentation for the four study soils. Initial pH is shown in the left panel, and final pH in the right panel. The initial solution concentration, $[U]_o$, across all experimentation was 710 µg/L.

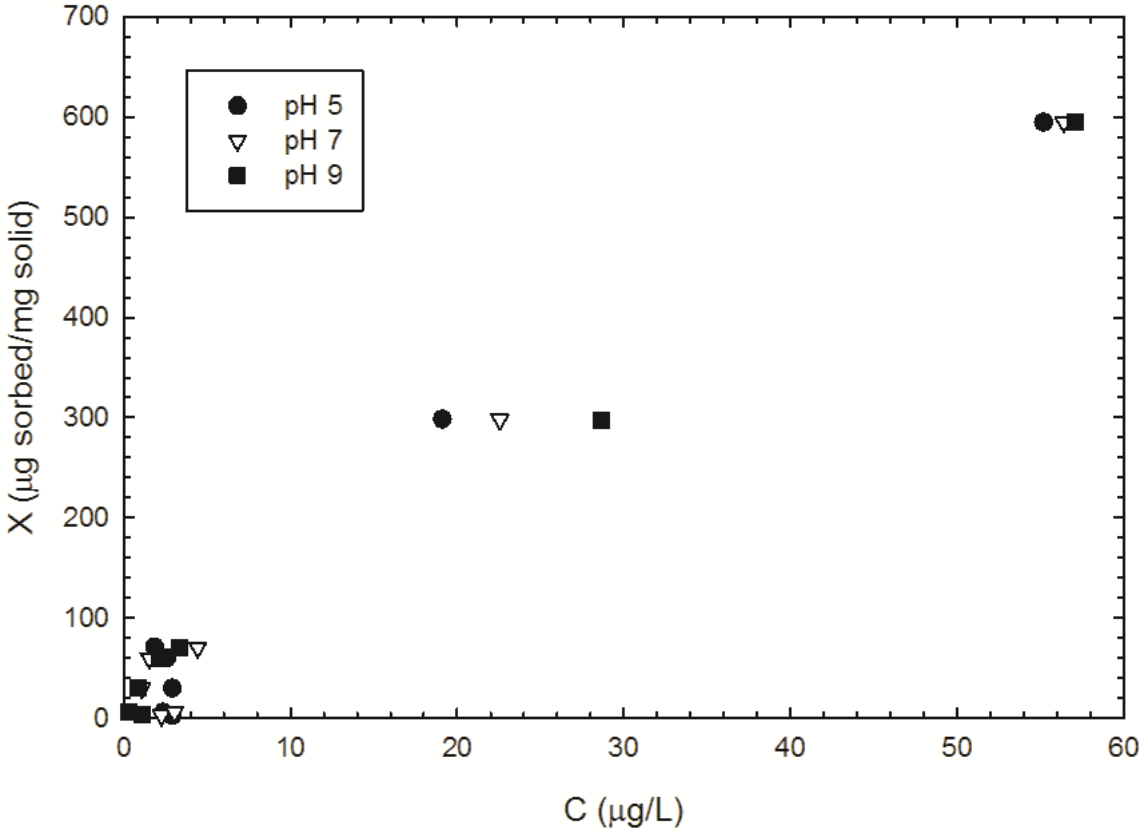

Figure 5.27. Isotherm experimentation results for Soil *A* at initial pH values of 5, 7, and 9, respectively. Original concentration, or C_o, values ranged from 30 to 6000 µg/L. The equilibrium concentration, or C, of U, is shown on the x-axis in µg/L, while X represents the maximum U sorption in µg of U sorbed per mg of soil solid.

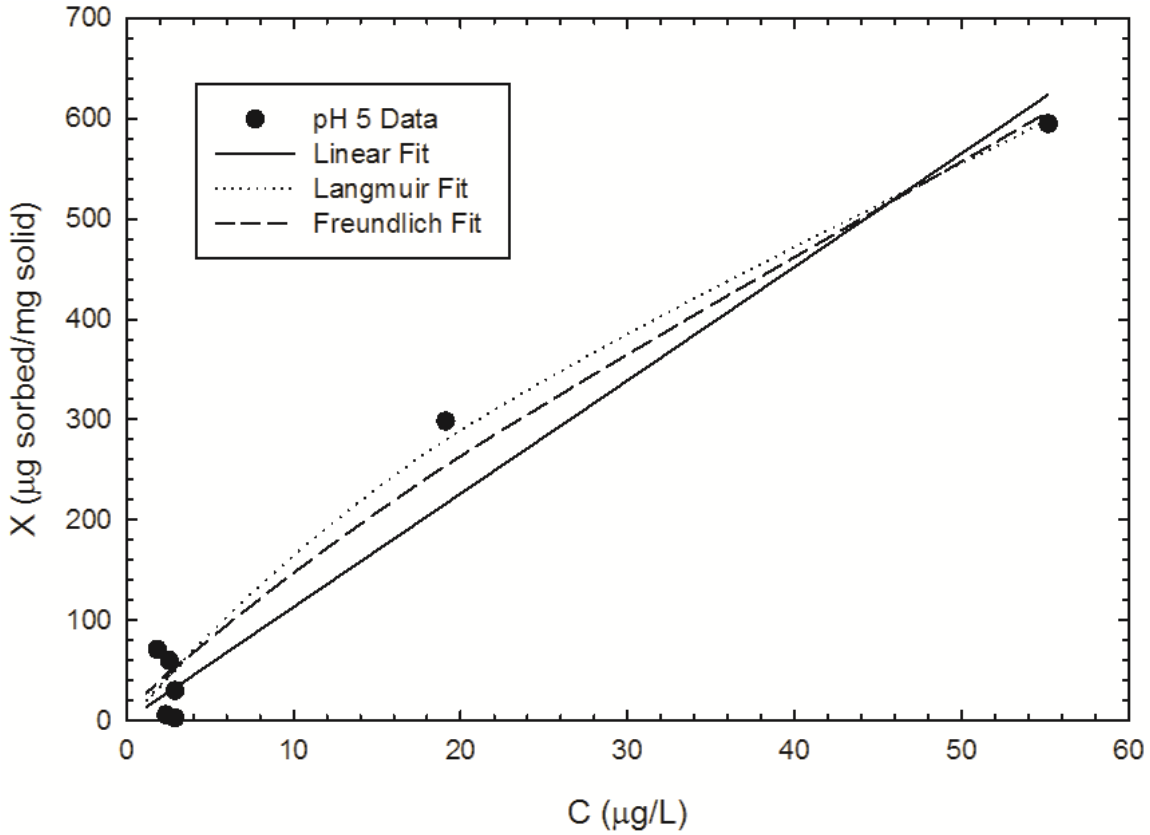

Figure 5.28. Isotherm experimentation results for Soil *A* at initial pH 5. Original concentration, or C_o, values ranged from 30 to 6000 µg/L. The equilibrium concentration, or C, of U, is shown on the x-axis in µg/L, while X represents the maximum U sorption in µg of U sorbed per mg of soil solid.

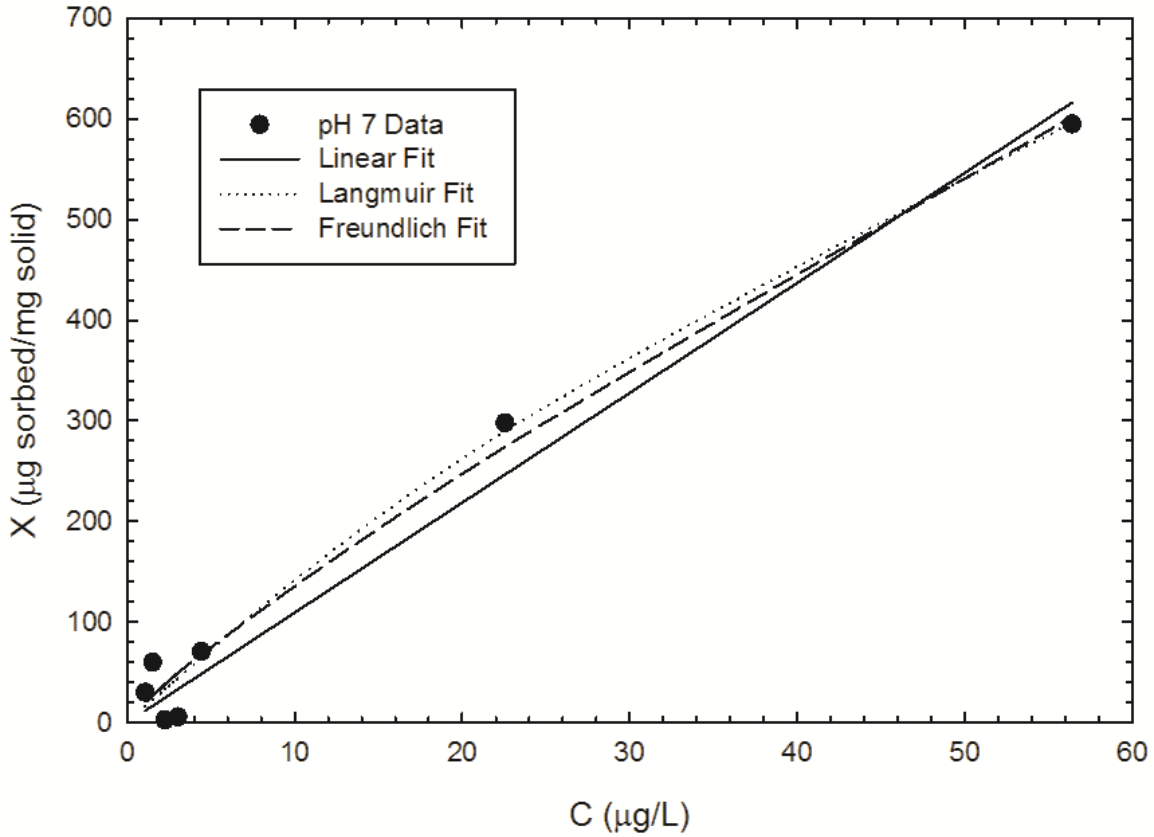

Figure 5.29. Isotherm experimentation results for Soil *A* at initial pH 7. Original concentration, or C_o, values ranged from 30 to 6000 µg/L. The equilibrium concentration, or C, of U, is shown on the x-axis in µg/L, while X represents the maximum U sorption in µg of U sorbed per mg of soil solid.

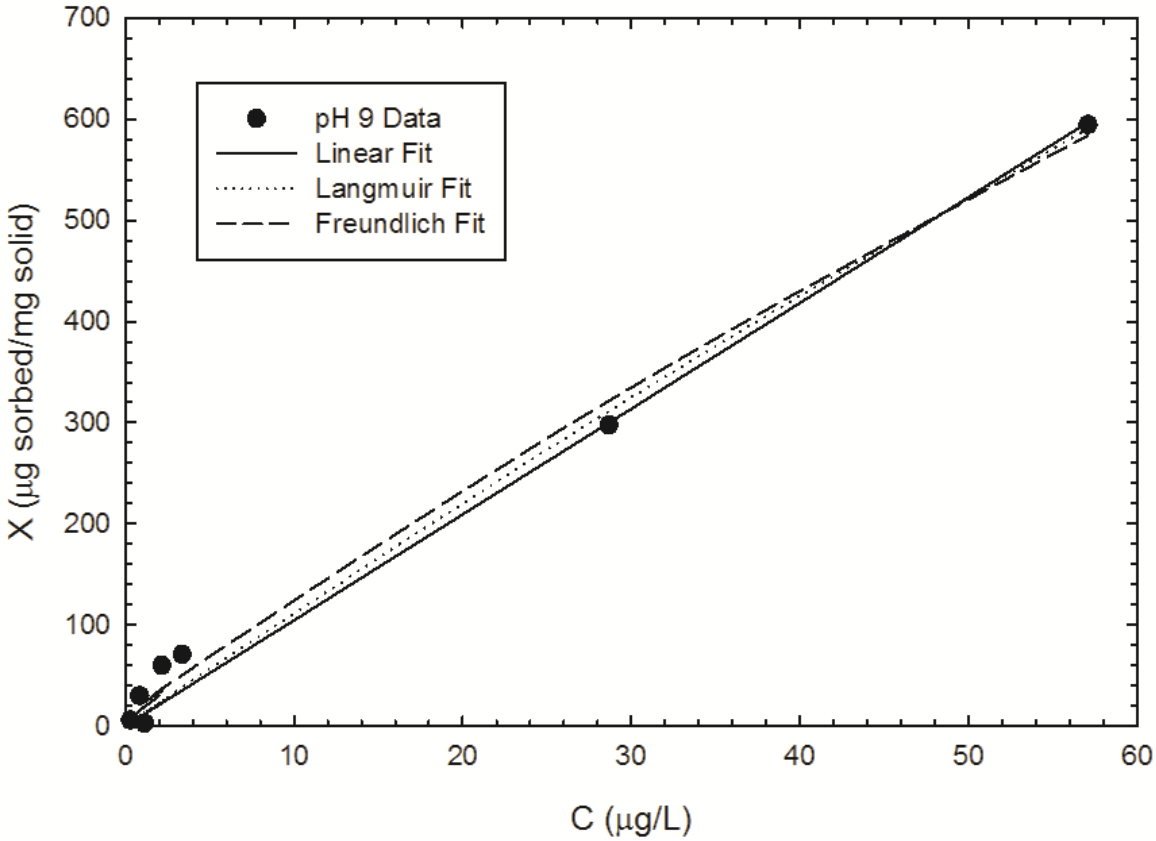

Figure 5.30. Isotherm experimentation results for Soil *A* at initial pH 9. Original concentration, or C_o, values ranged from 30 to 6000 µg/L. The equilibrium concentration, or C, of U, is shown on the x-axis in µg/L, while X represents the maximum U sorption in µg of U sorbed per mg of soil solid.

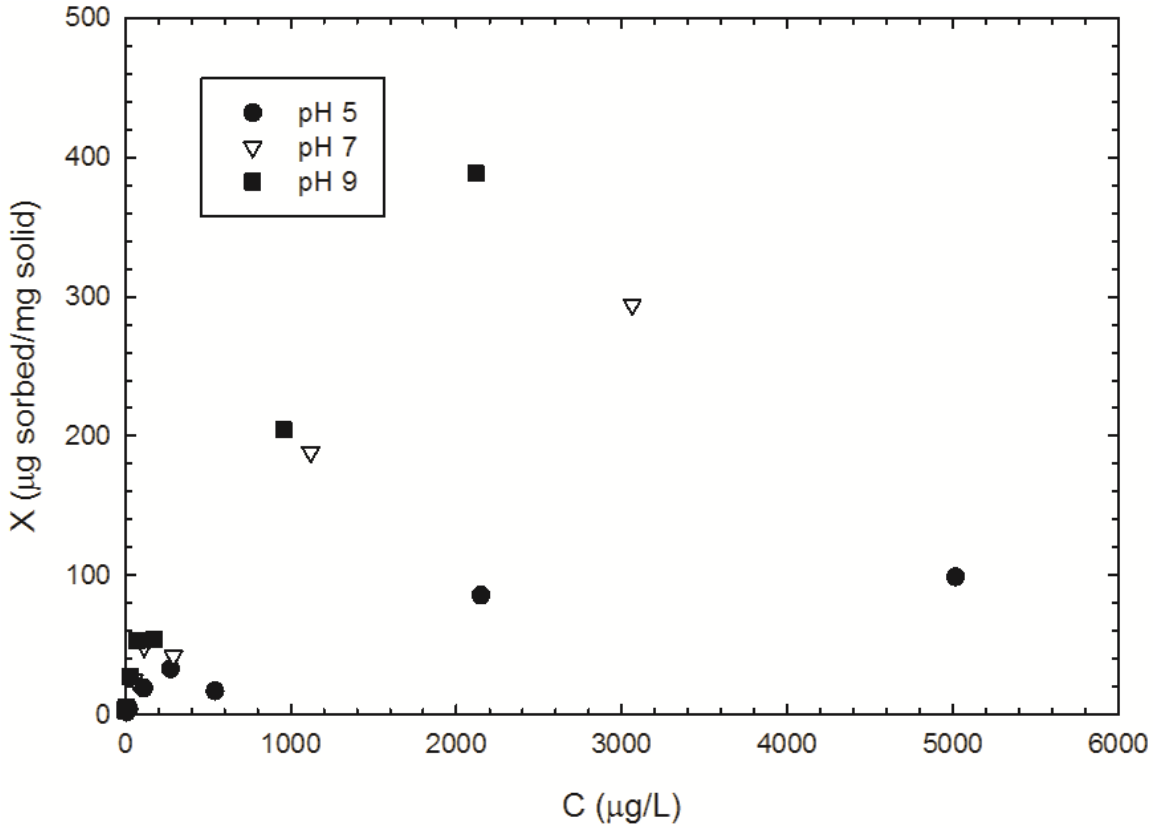

Figure 5.31. Isotherm experimentation results for Soil *B* at initial pH values 5, 7, and 9, respectively. Original concentration, or C_o, values ranged from 30 to 6000 µg/L. The equilibrium concentration, or C, of U, is shown on the x-axis in µg/L, while X represents the maximum U sorption in µg of U sorbed per mg of soil solid.

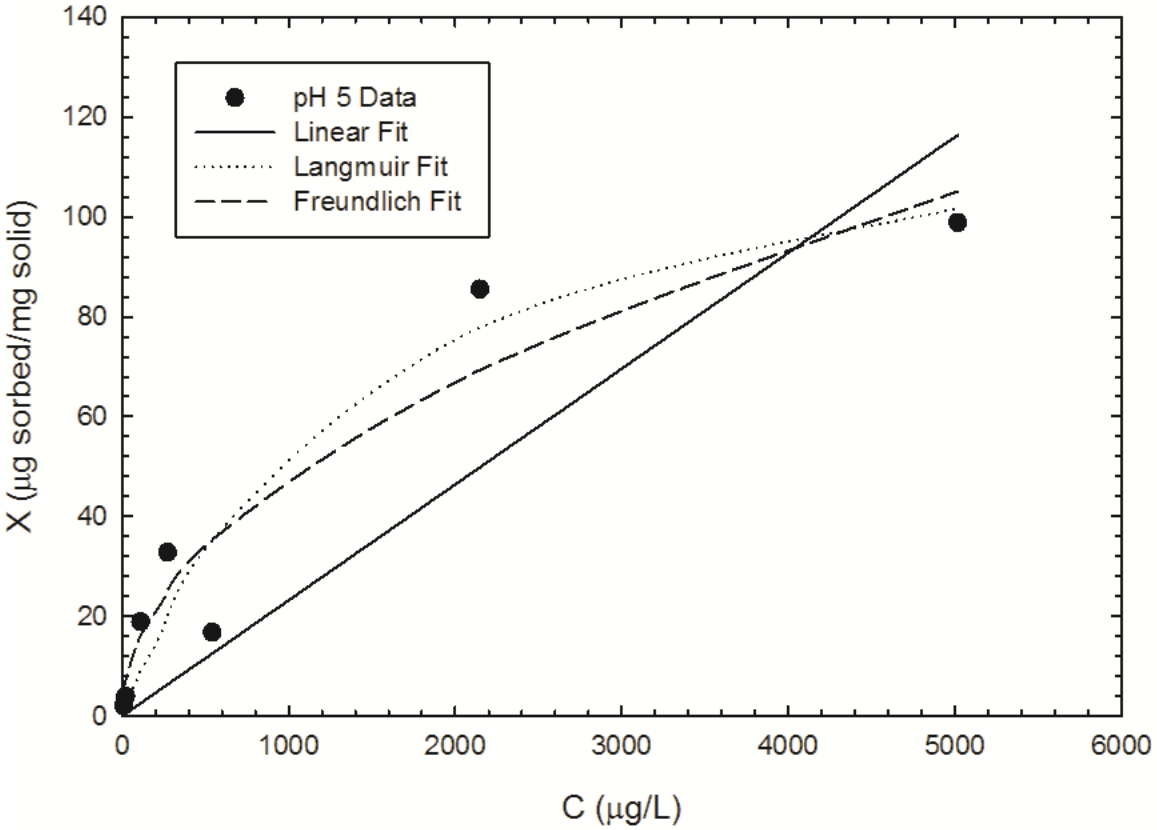

Figure 5.32. Isotherm experimentation results for Soil *B* at initial pH 5. Original concentration, or C_o, values ranged from 30 to 6000 µg/L. The equilibrium concentration, or C, of U, is shown on the x-axis in µg/L, while X represents the maximum U sorption in µg of U sorbed per mg of soil solid.

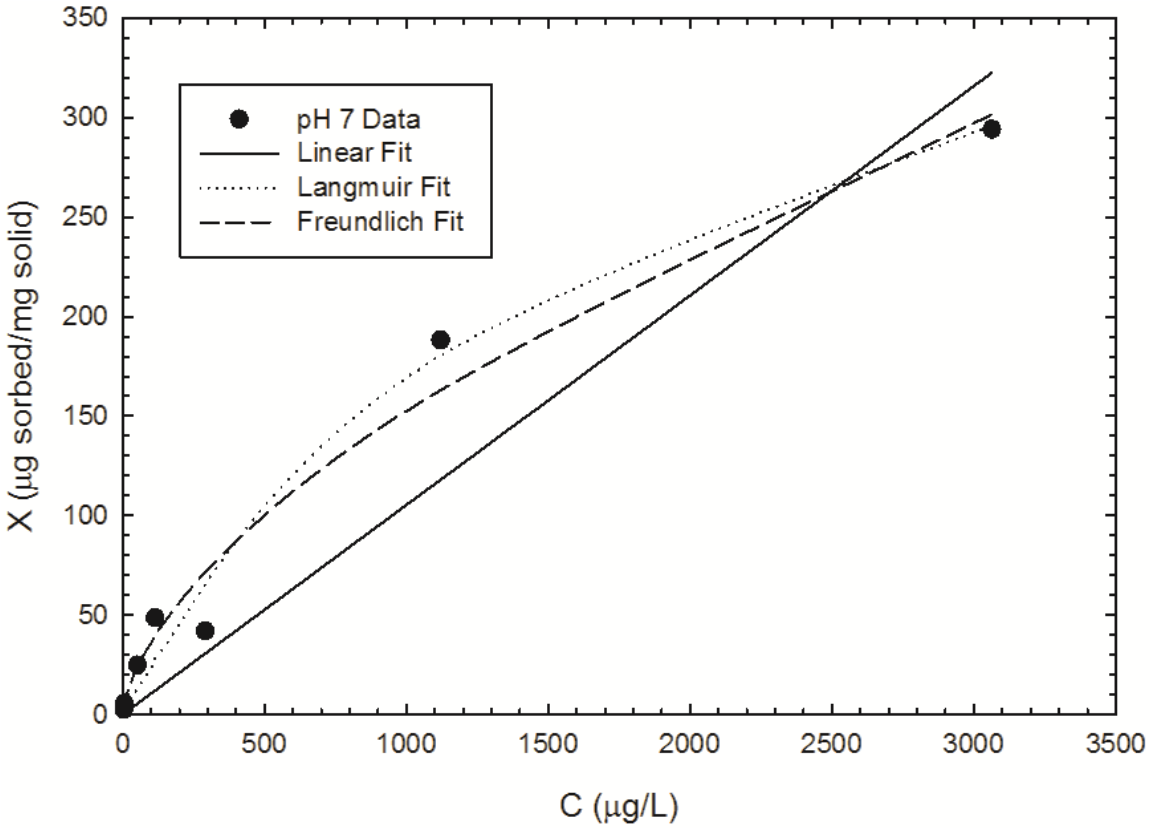

Figure 5.33. Isotherm experimentation results for Soil *B* at initial pH 7. Original concentration, or C_o, values ranged from 30 to 6000 µg/L. The equilibrium concentration, or C, of U, is shown on the x-axis in µg/L, while X represents the maximum U sorption in µg of U sorbed per mg of soil solid.

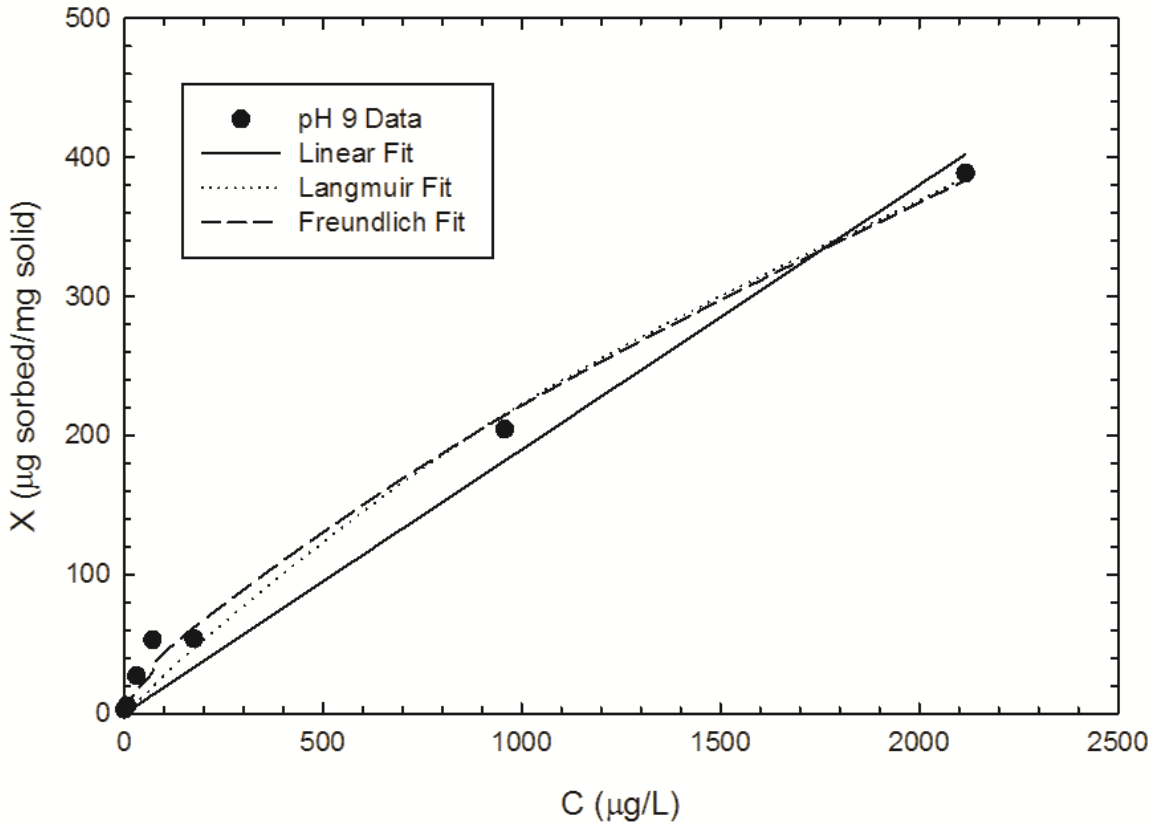

Figure 5.34. Isotherm experimentation results for Soil *B* at initial pH 9. Original concentration, or C_o, values ranged from 30 to 6000 µg/L. The equilibrium concentration, or C, of U, is shown on the x-axis in µg/L, while X represents the maximum U sorption in µg of U sorbed per mg of soil solid.

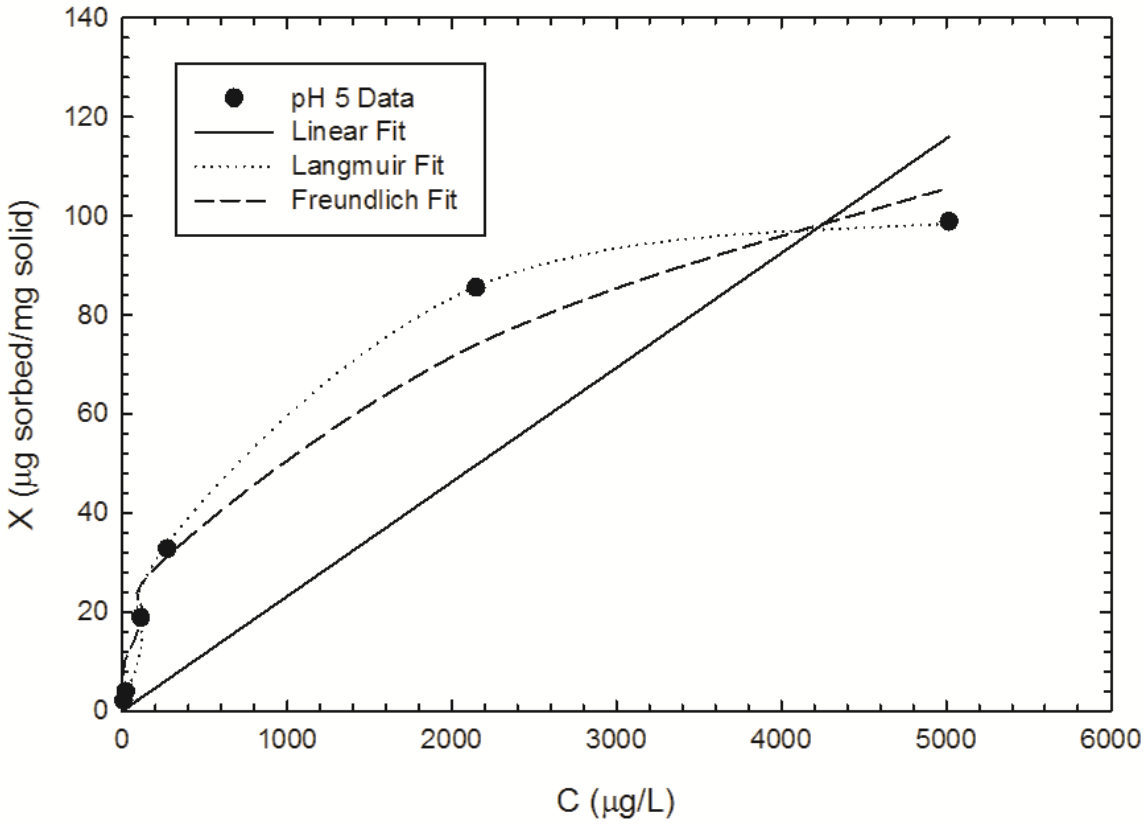

Figure 5.35. Isotherm experimentation results for Soil *B* at initial pH 5 using only data derived from serial dilution. Original concentration, or C_o, values ranged from 30 to 6000 µg/L. The equilibrium concentration, or C, of U, is shown on the x-axis in µg/L, while X represents the maximum U sorption in µg of U sorbed per mg of soil solid.

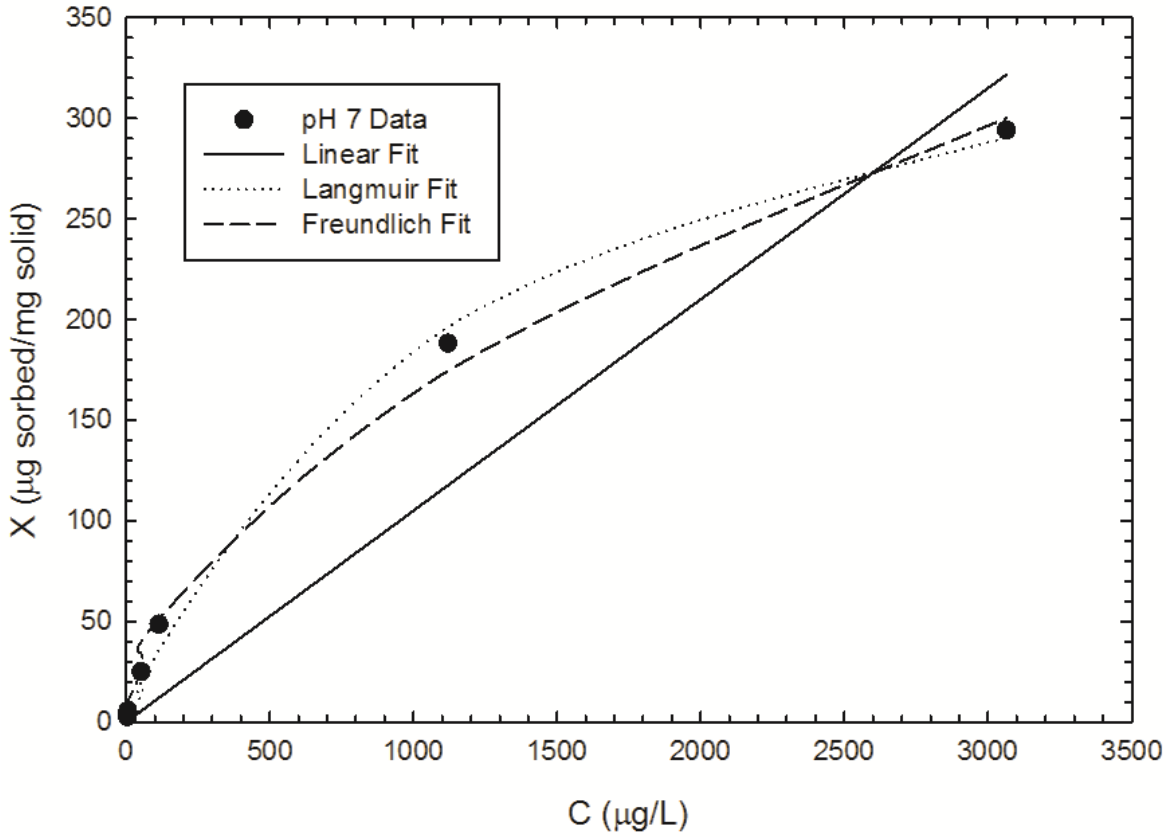

Figure 5.36. Isotherm experimentation results for Soil *B* at initial pH 7 using only data derived from serial dilution. Original concentration, or C_o, values ranged from 30 to 6000 µg/L. The equilibrium concentration, or C, of U, is shown on the x-axis in µg/L, while X represents the maximum U sorption in µg of U sorbed per mg of soil solid.

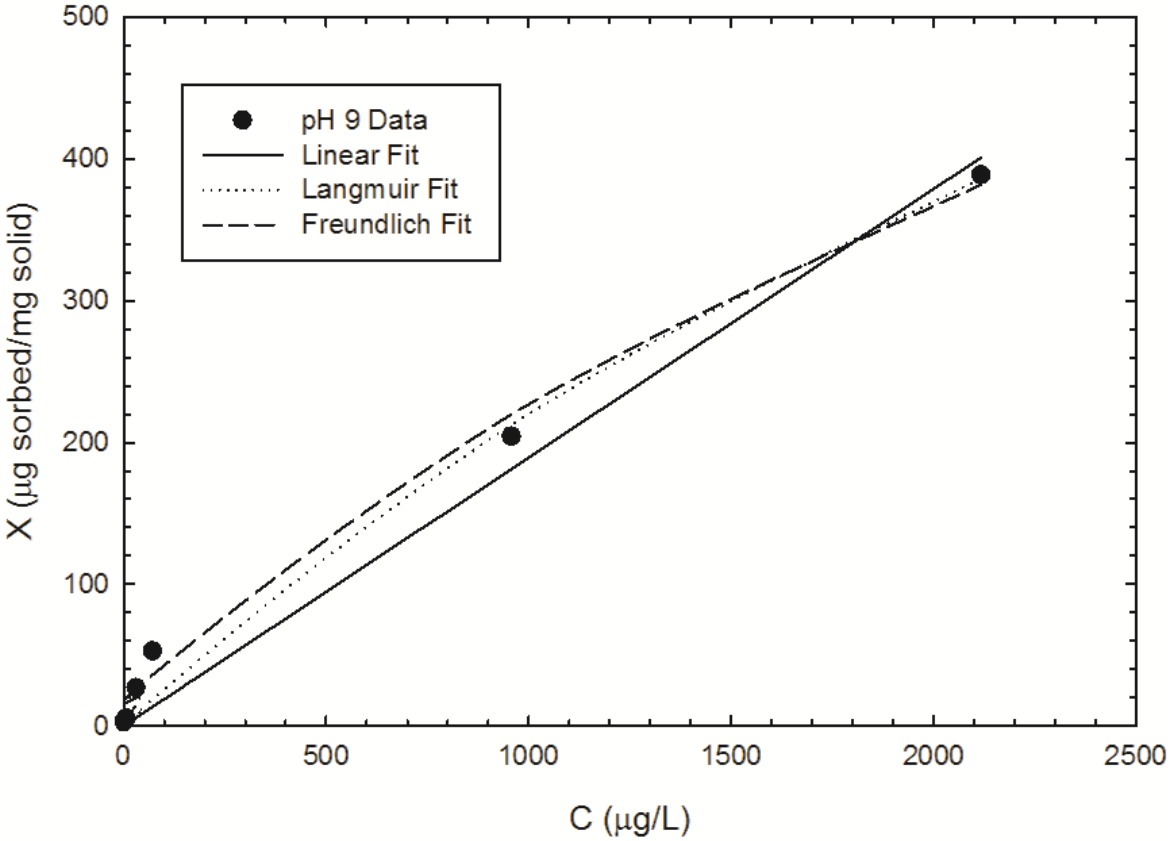

Figure 5.37. Isotherm experimentation results for Soil *B* at initial pH 9 using only data derived from serial dilution. Original concentration, or C_o, values ranged from 30 to 6000 µg/L. The equilibrium concentration, or C, of U, is shown on the x-axis in µg/L, while X represents the maximum U sorption in µg of U sorbed per mg of soil solid.

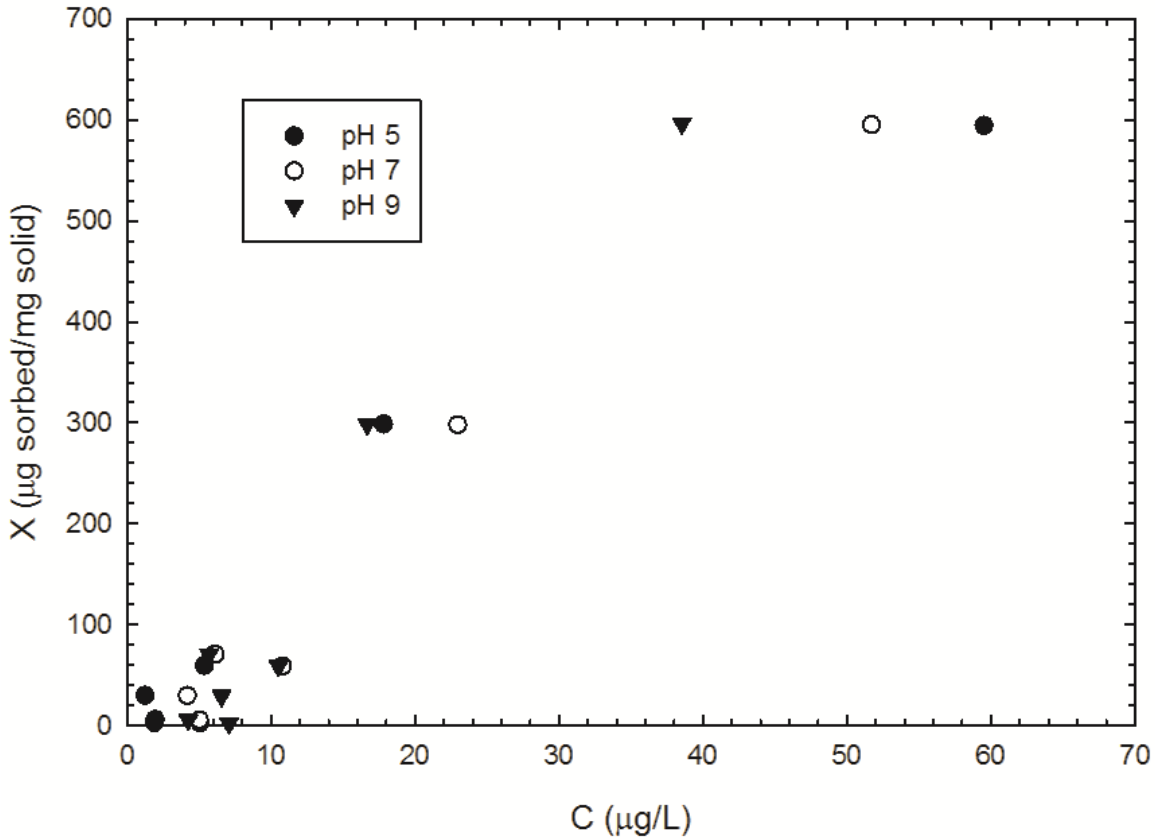

Figure 5.38. Isotherm experimentation results for Soil *C* at initial pH values 5, 7, and 9, respectively. Original concentration, or C_o, values ranged from 30 to 6000 µg/L. The equilibrium concentration, or C, of U, is shown on the x-axis in µg/L, while X represents the maximum U sorption in µg of U sorbed per mg of soil solid.

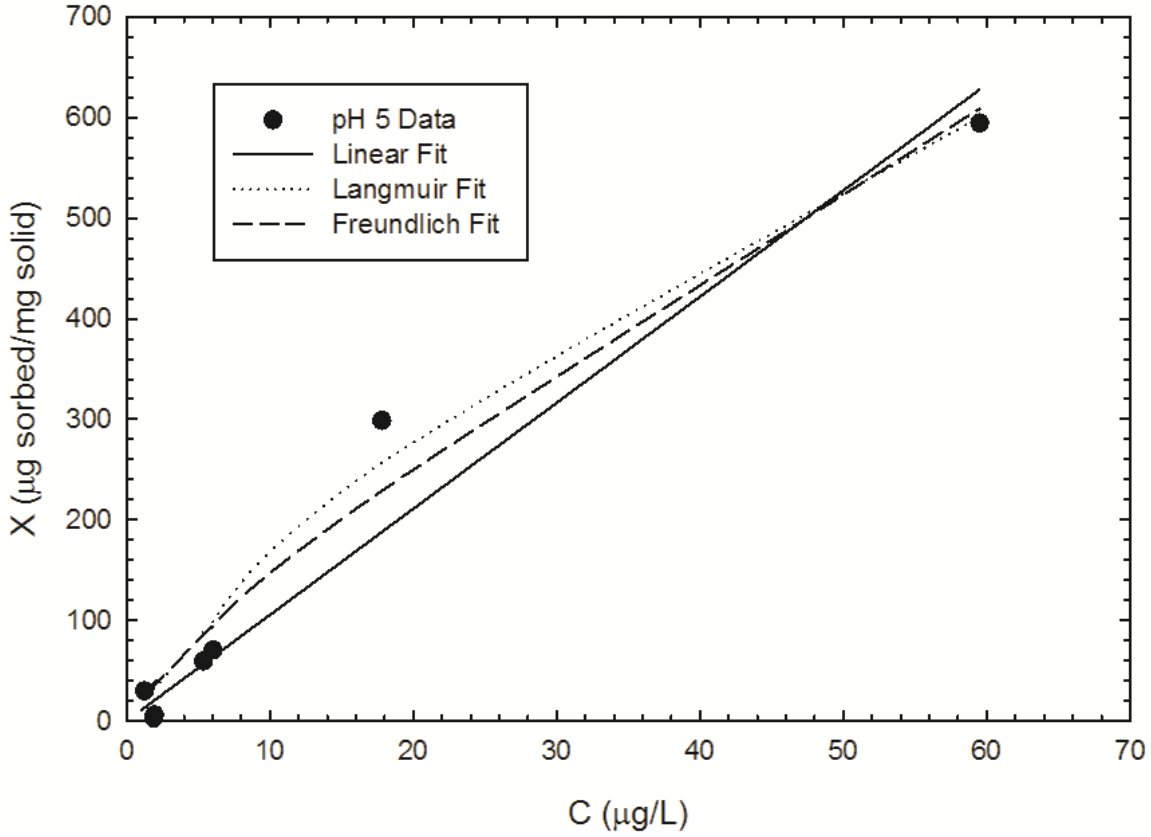

Figure 5.39. Isotherm experimentation results for Soil *C* at initial pH 5. Original concentration, or C_o, values ranged from 30 to 6000 µg/L. The equilibrium concentration, or C, of U, is shown on the x-axis in µg/L, while X represents the maximum U sorption in µg of U sorbed per mg of soil solid.

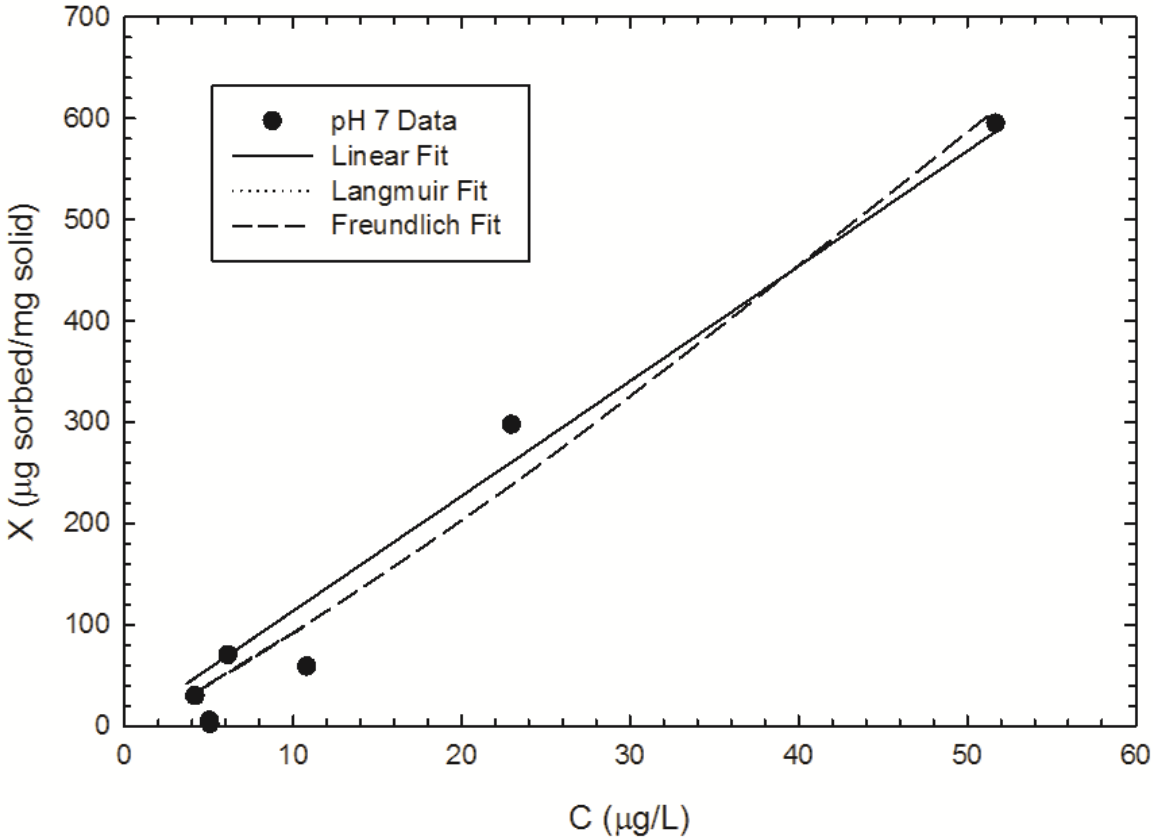

Figure 5.40. Isotherm experimentation results for Soil *C* at initial pH 7. Original concentration, or C_o, values ranged from 30 to 6000 µg/L. The equilibrium concentration, or C, of U, is shown on the x-axis in µg/L, while X represents the maximum U sorption in µg of U sorbed per mg of soil solid.

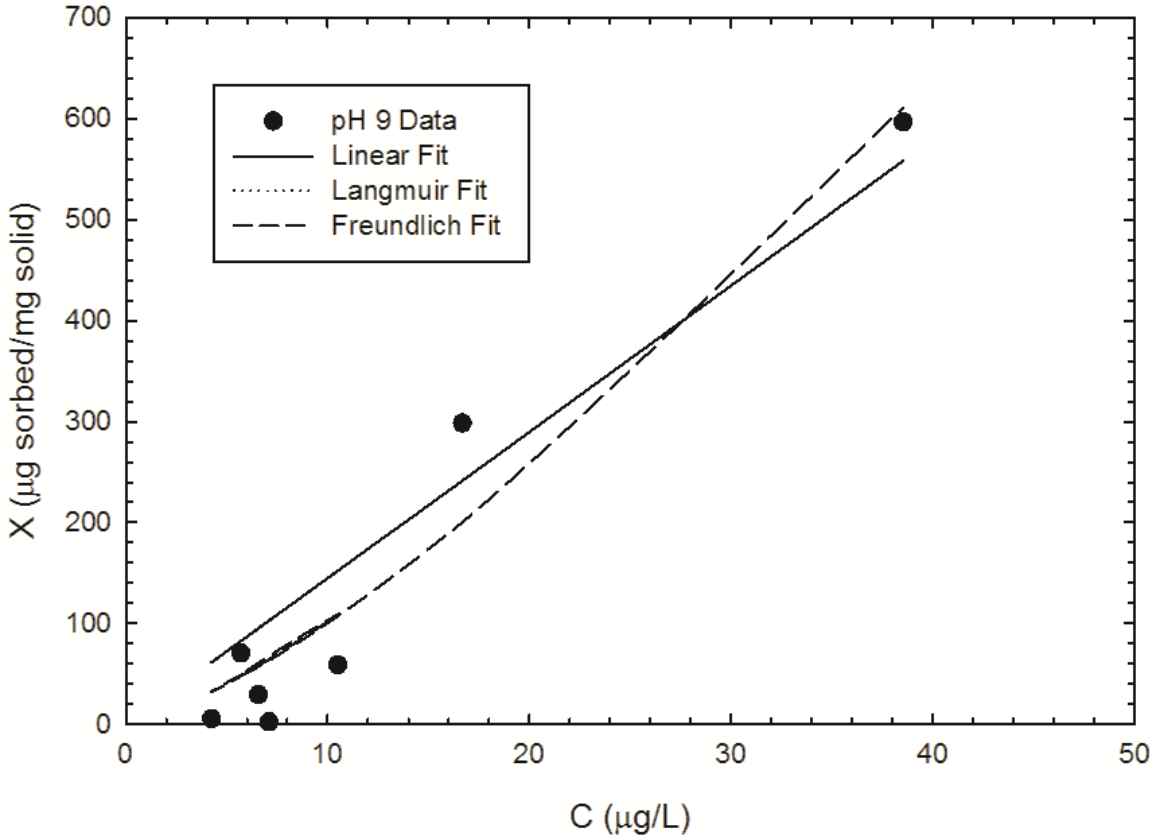

Figure 5.41. Isotherm experimentation results for Soil *C* at initial pH 9. Original concentration, or C_o, values ranged from 30 to 6000 µg/L. The equilibrium concentration, or C, of U, is shown on the x-axis in µg/L, while X represents the maximum U sorption in µg of U sorbed per mg of soil solid.

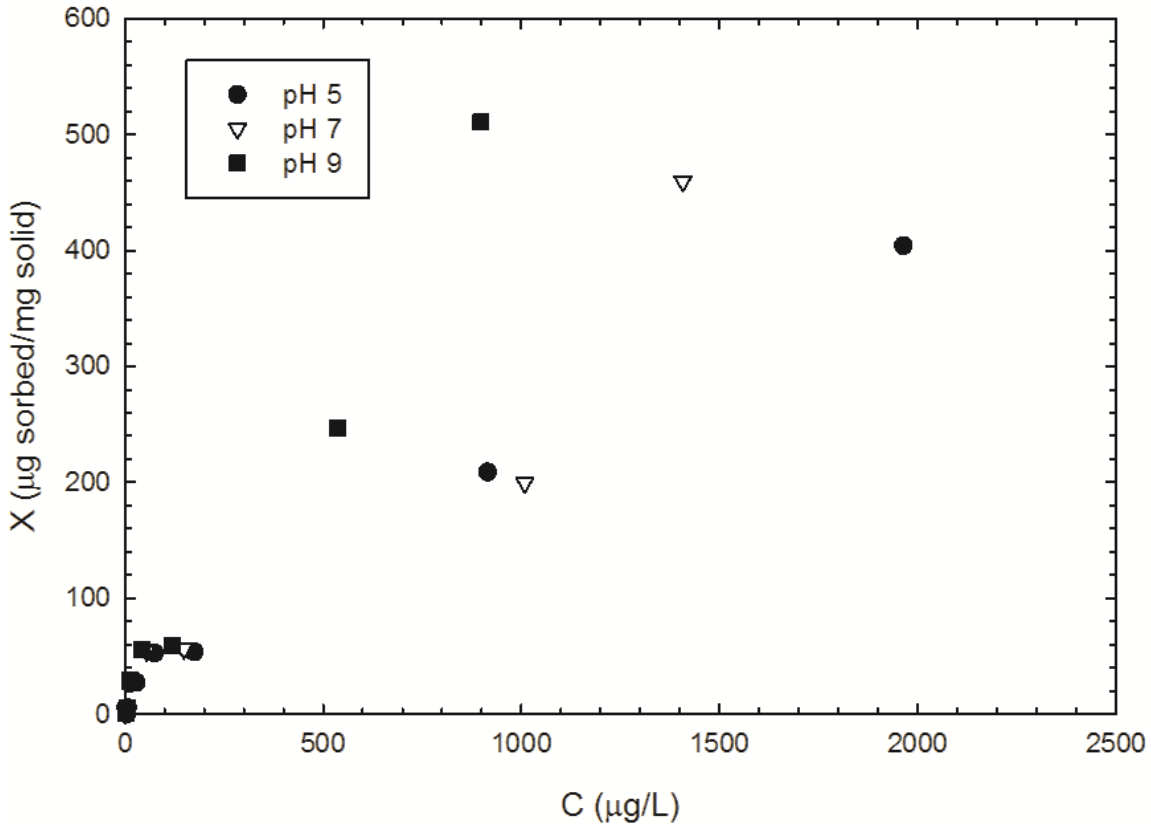

Figure 5.42. Isotherm experimentation results for Soil *D* at initial pH values 5, 7, and 9, respectively. Original concentration, or C_o, values ranged from 6 to 6000 µg/L. The equilibrium concentration, or C, of U, is shown on the x-axis in µg/L, while X represents the maximum U sorption in µg of U sorbed per mg of soil solid.

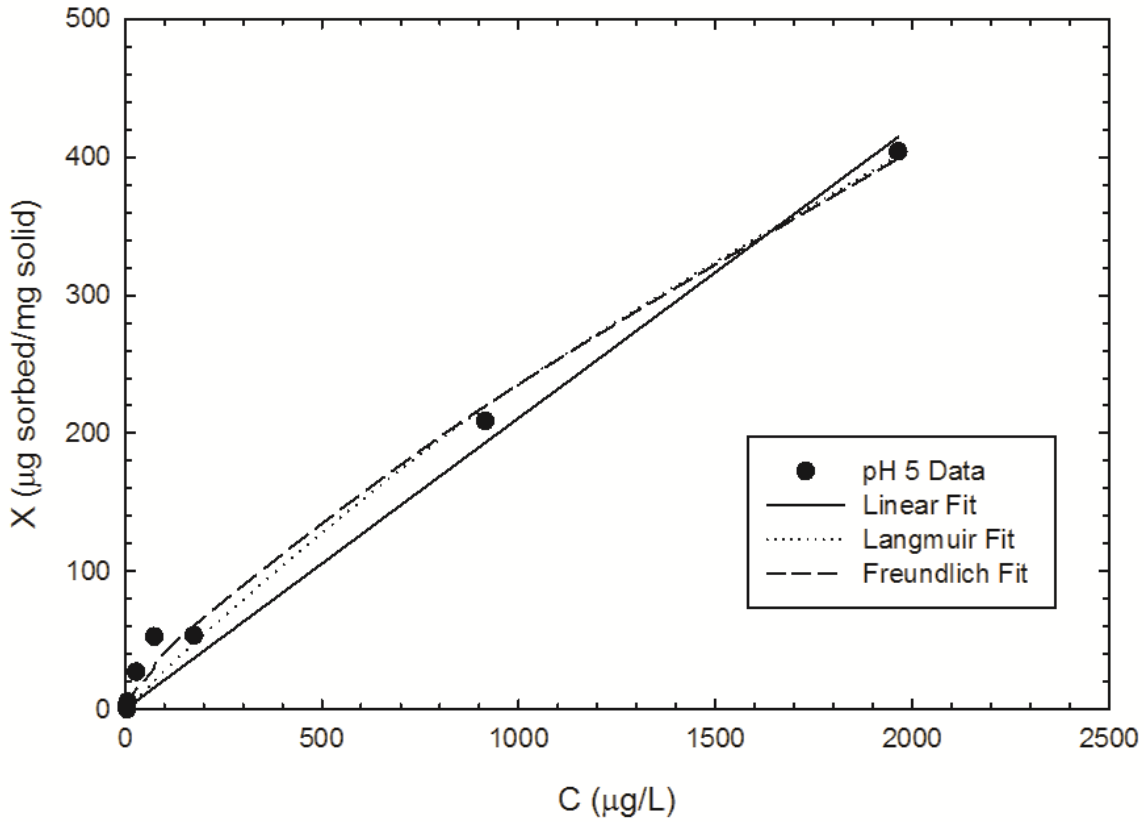

Figure 5.43. Soil *D* isotherm data and fits for initial pH 5, with original U concentration, or C_o, values ranging from 6 to 6000 µg/L. The equilibrium concentration, or C, of U, is shown on the x-axis in µg/L, while X represents the maximum U sorption for the fitting parameters in µg of U sorbed per mg of soil solid.

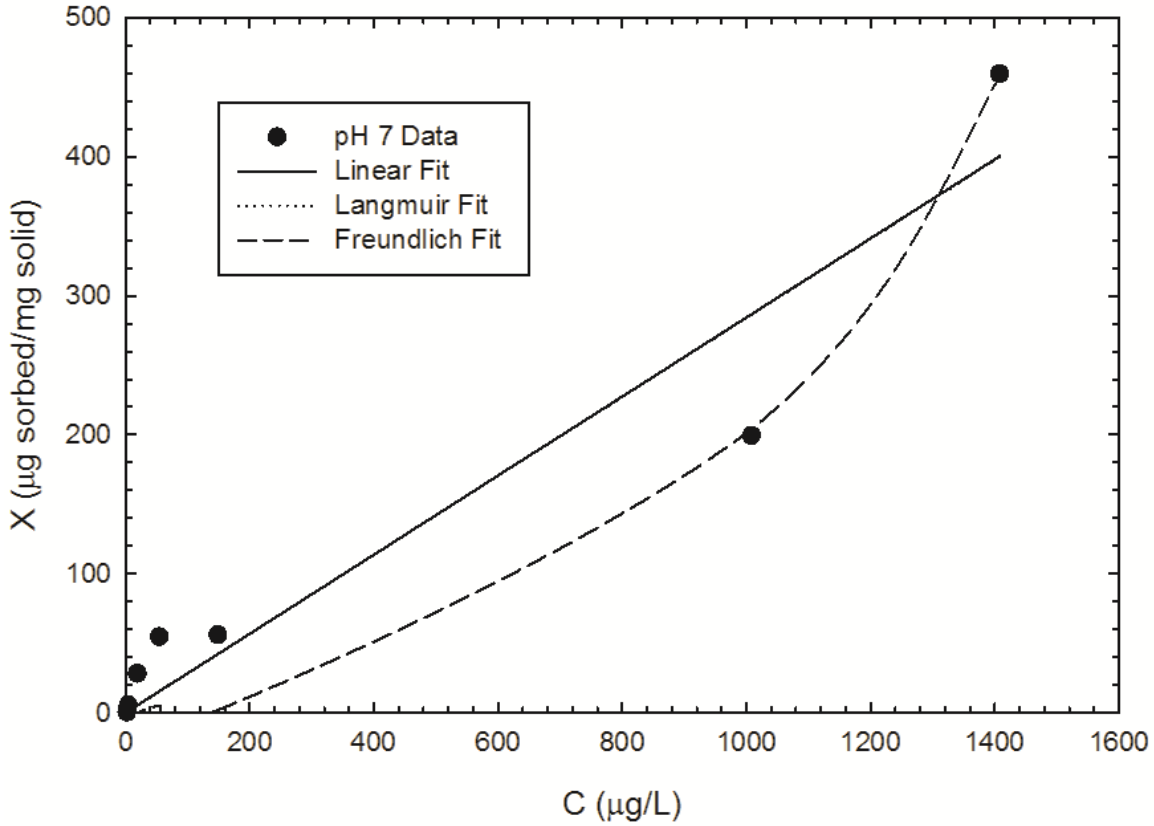

Figure 5.44. Soil *D* isotherm data and fits for initial pH 7, with original U concentration, or C_o, values ranging from 6 to 6000 µg/L. The equilibrium concentration, or C, of U, is shown on the x-axis in µg/L, while X represents the maximum U sorption for the fitting parameters in µg of U sorbed per mg of soil solid. Note that the Langmuir fit directly overlaps the Linear fit.

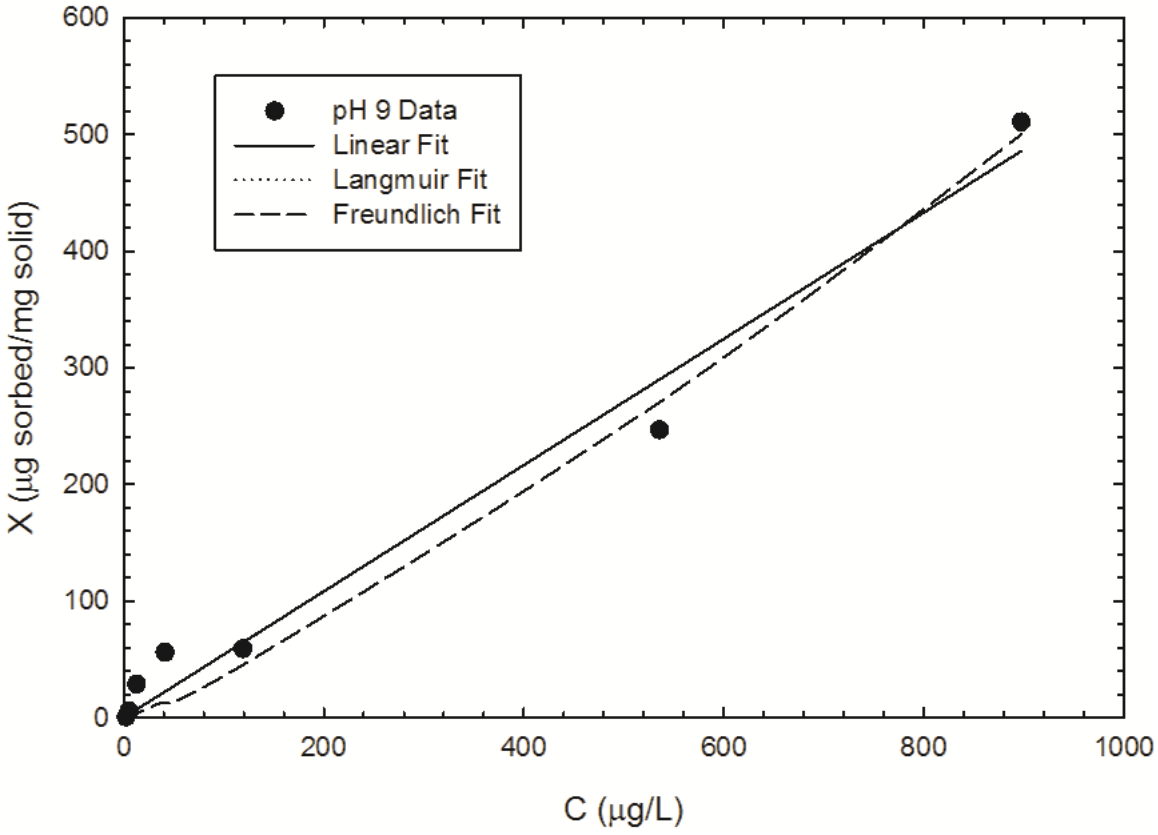

Figure 5.45. Soil *D* isotherm data and fits for initial pH 9, with original U concentration, or Co, values ranging from 6 to 6000 µg/L. The equilibrium concentration, or C, of U, is shown on the x-axis in µg/L, while X represents the maximum U sorption for the fitting parameters in µg of U sorbed per mg of soil solid. Note that all three fits result in nearly identical parameters, with highly similar r^2 values.

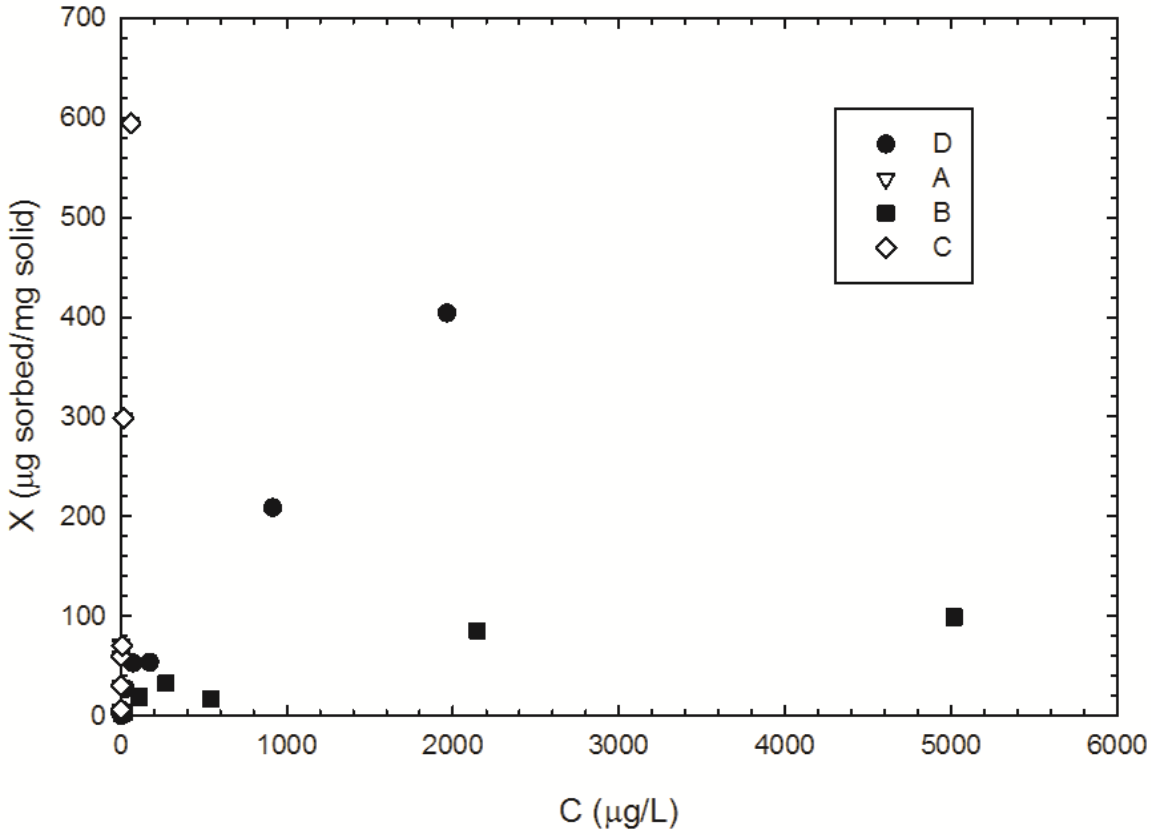

Figure 5.46. Comparison of isotherms for the four study soils at initial pH 5.

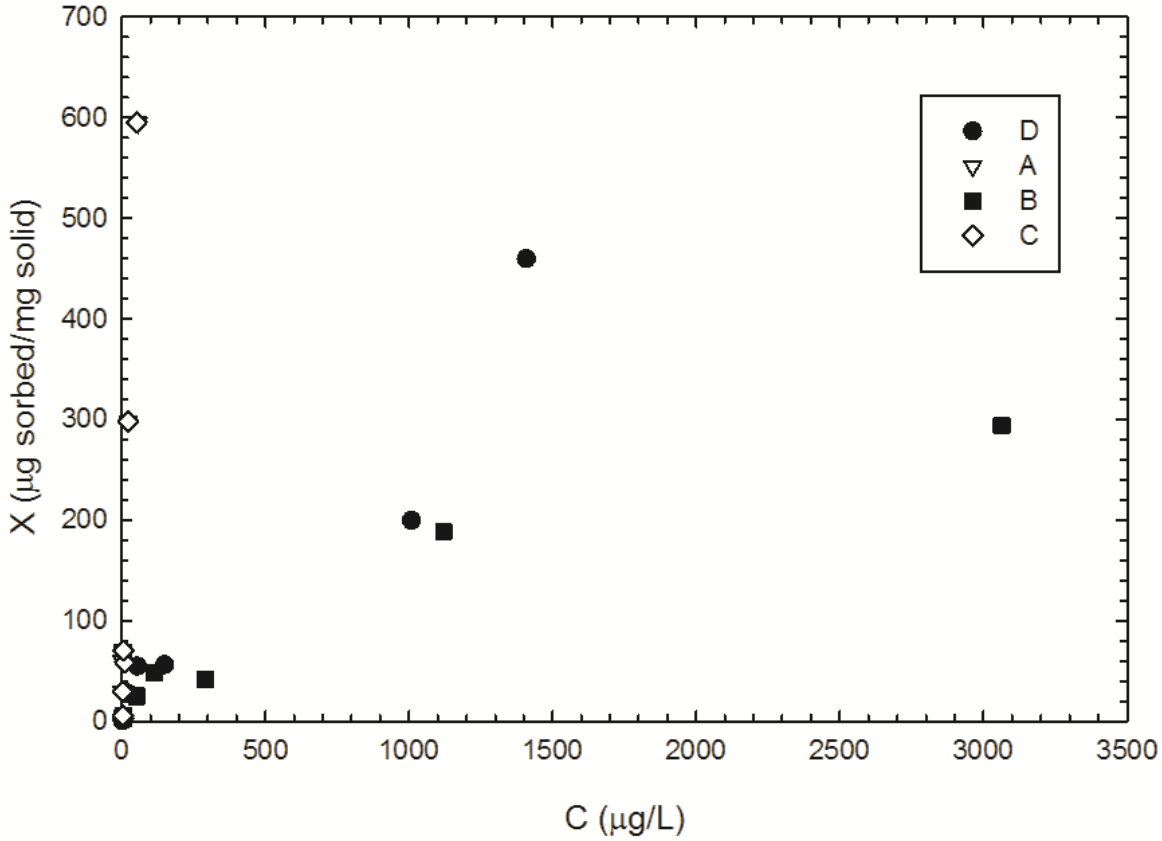

Figure 5.47. Comparison of isotherms for the four study soils at initial pH 7.

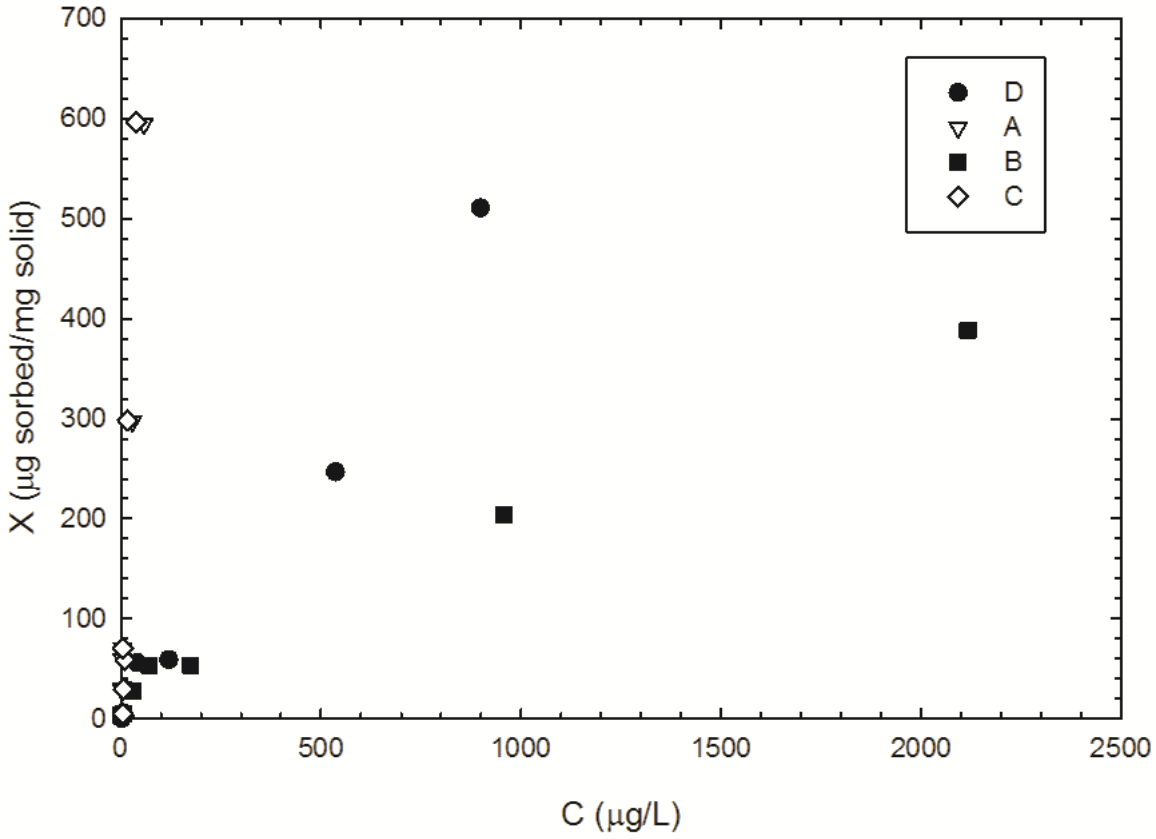

Figure 5.48. Comparison of isotherms for the four study soils at initial pH 9.

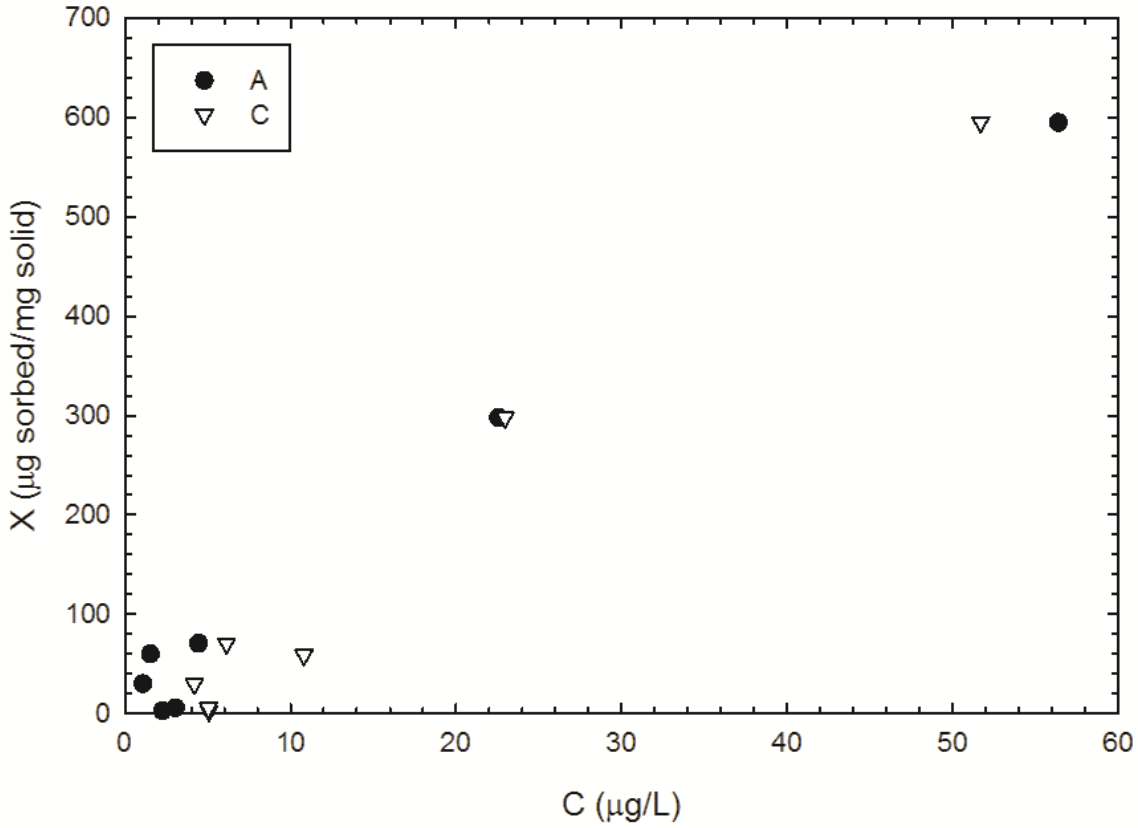

Figure 5.49. Comparison of Soil A and C isotherms at pH 7.90, corresponding to data for the initial pH 7 set.

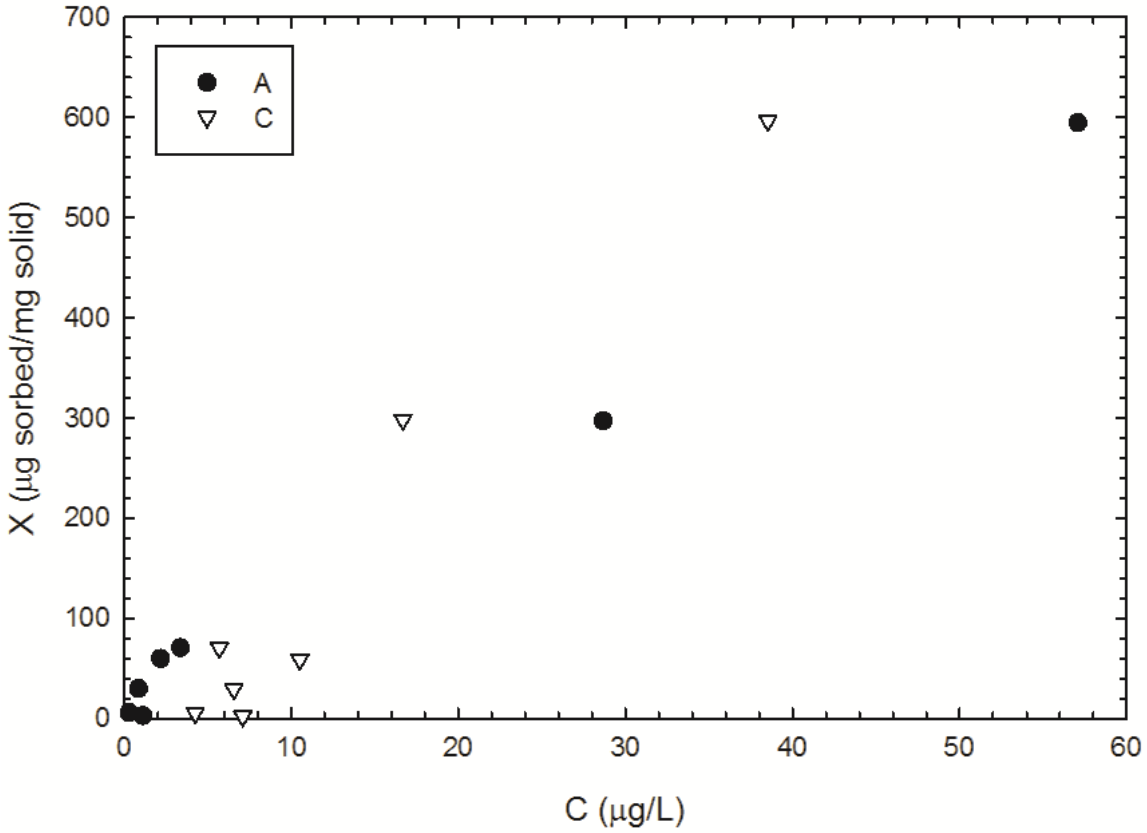

Figure 5.50. Comparison of Soil A and C isotherms at pH 8.50, corresponding to data from the initial pH 9 set.

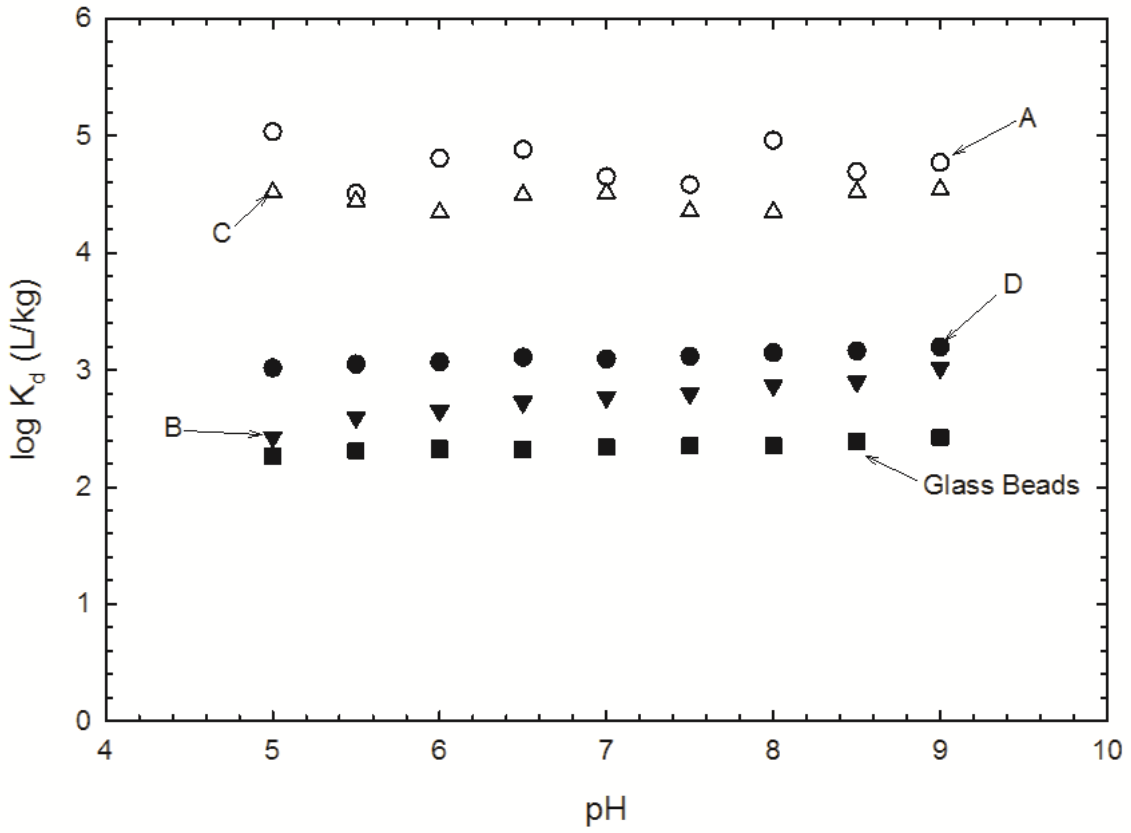

Figure 5.51. Comparison of K_d values to pH for the original poorly buffered system.

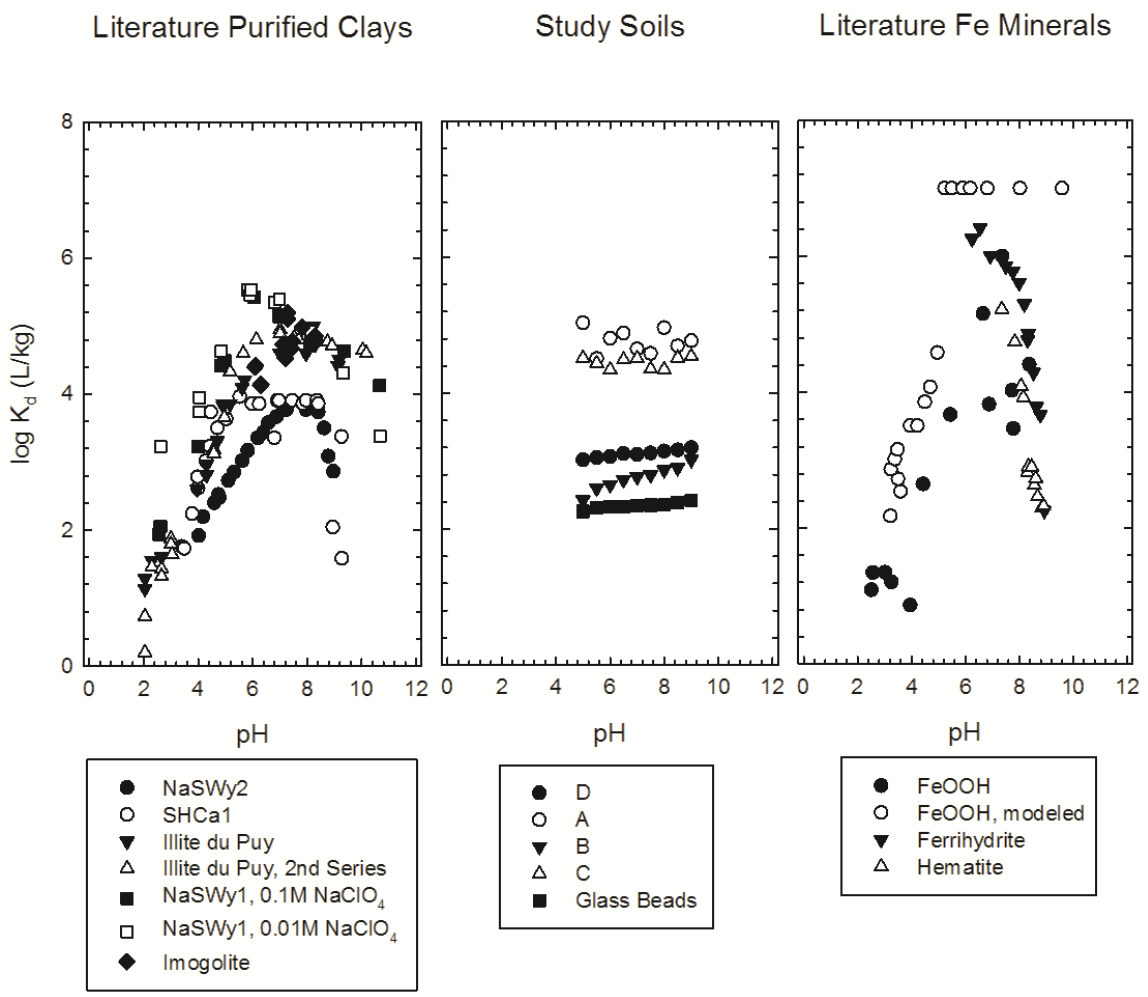

Figure 5.52. Cross-comparison of K_d values for purified clays and iron minerals to the poorly buffered original system.

Section 6 – Sorption of Radioactive Synthetic Leachate to Fine-Grained Barrier Materials

Although single radionuclide experimentation serves an important role in characterizing the interactions of naturally derived barrier soils with LLW, uranium is only one of the many potential components present in LLW systems. Consequently, a second set of experimentation, utilizing solutions built to mimic the behavior and composition of LLW leachate, was used to further characterize potential interactions within the system.

6.1 Materials and Methods

Materials and methods for the second set of experimentation built upon the precedent established both during single radionuclide experimentation and within the literature. The solution chemistry composition used throughout experimentation is discussed in Section 6.1.1 (Radioactive Synthetic Leachate). Paired with the altered solution composition, two sets of soils were used within the expanded sorption experimentation. The first set, comprised of natural barrier soils, was discussed at length in Section 4.1 (Soils) and throughout Section 5. The second set of soil materials, described in Section 6.1.2, was a suite of bentonite-based materials.

6.1.1 Radioactive Synthetic Leachate

As discussed in detail within Section 3, the leachate present at DOE LLW sites can contain a complex and varied mixture of both radioactive and inert components across different sites. To mirror this complexity experimentally, a radioactive synthetic leachate (RSL) was developed for use in a series of projects at the University of Wisconsin–Madison (Tian 2012). Table 6.1 lists the target parameters used in developing the RSL mixture.

The inert inorganic chemical components for RSL were chosen based on the most prevalent species measured at the surveyed DOE LLW sites, as shown in Table

3.3, at concentration levels representative of average values across the four sites. Similarly, the organic content of the mixture, indicated as the Total Organic Content (TOC), and oxidation-reduction potential (ORP) were adjusted to mirror the average values of the DOE LLW sites. As discussed in Section 3, the average values for these parameters are good indicators for the time-dependent behavior of LLW leachate, due to the general consistency with time for many of the components. Additionally, at the time of batch solution creation, the pH was adjusted to the target value of 7.2, indicative of the average pH across the DOE sites. The total ionic strength of the RSL mixture was 0.0436 M, allowing ease of comparison to the 0.05 M $NaClO_4$ ionic basis used during single radionuclide experimentation.

Three radionuclides were chosen for use within RSL – U, as the ^{238}U isotope, ^{99}Tc, and ^{3}H (tritium). The chosen radionuclides represent the species most commonly measured and detected across the four studied DOE LLW sites, as well as those frequently measured in MSW. Concentration levels of the radioactive components were chosen to mirror or slightly exceed the average measured concentrations at ERDF (see Tables 3.3 and 4.7), due to the consistently higher measurements when compared to the other sites.

Table 6.2 presents the inert salts and solutions used in the creation of the RSL mixture, and their accompanying molecular weights. RSL was created in large batches (> 100 L at a time) for use in multiple projects at UW. Despite the large production quantity, a number of the components were added at very small molar concentrations to mirror the composition of the LLW leachate. As such, some variation in the chemical make-up of the measured RSL concentrations is anticipated. Similar to the single radionuclide experimentation, uranium acetate dihydrate (chemical formula: $UO_2(C_2O_2H_3)_2 \bullet 2\ H_2O$; hereafter referred to as uranium acetate) was used as the uranium source for experimentation. Uranium acetate was received in powder form

derived from yellowcake uranium, with a MSDS-listed specific activity of 0.28 μCi/g (SI units: 1.04 x 10^4 Bq/g), from the Office of Radiation Safety at the University of Wisconsin-Madison. The Office of Radiation Safety provided the other radionuclides used within RSL experimentation for use under provisional supervision and use of PPE as discussed in Section 4.

6.1.2 Bentonite Suite

In addition to the importance of natural barrier soils in the creation of traditional compacted clay liners for both MSW and LLW, the use of bentonite both as the primary component of geosynthetic clay liners (GCLs) and as a backfill material for radioactive waste containment has been extensively discussed within the literature (Arcos et al. 2008; Galunin et al. 2009 and 2010; Holmboe et al. 2010; Iijima et al. 2010; Majdan et al. 2010; Missana et al. 2004 and 2008; Sato et al. 1992; Sato and Miyamoto 2004; Sorieul et al. 2008; Wang et al. 2010). To more fully encompass the potential materials used as LLW containment barriers, a suite of GCL-derived bentonites was acquired to provide a counterpoint to the natural barrier soils.

Six GCL-derived bentonites were used within experimentation. Typical GCLs consist of sodium bentonite sandwiched between layers of geotextiles, creating an easy-to-install, self-contained liner system. In order to ascertain the behavior of the bentonites in the presence of RSL and create an experimental program consistent with the natural barrier soils, the GCL components were disassembled to separate the bentonite, which was then ground using a mortar and pestle to pass the US #40 (0.422 mm) sieve but be retained on the US #60 (0.251 mm) sieve, in preparation for separate testing to discern the free swell index of the bentonites as designated by ASTM D5890.

The six GCL-derived bentonites represent products from two different GCL manufacturers (indicated as C and G within the designations for the materials) within

three broader GCL categories. Standard, non-modified, sodium bentonites are indicated with an S as the second letter of their designations (*CS* and *GS*). Bentonites that have been modified through dry mixing of polymers with the bentonite by the manufacturers prior to assembly of the GCL for enhanced chemical resistance are indicated with an R as the second letter of their designations (*CR* and *GR*). GCLs created from bentonite-polymer composites (BPC) are indicated with a T as the second letter of their designation (*CT*). The sixth GCL, *CR+*, is an enhanced version of the original *CR* product created by the manufacturer and indicated by the addition of the plus sign to the designation in text. The alterations to *CR+* regard the process of polymer modification within the bentonite, with a basis in the same bentonite and polymer stock used for the creation of *CR*.

As discussed in Section 2.3.2.3 (Processed Materials – Bentonites), the mineralogy of bentonite dictates its behavior as a sorbent, prior to additions and alterations made for enhancing particular behaviors. Although bentonite has a basis in montmorillonite, bentonite contains multiple minerals of varying percentages depending on location of origin, and therefore does not have a fixed molecular formula. Consequently, differences between both GCL manufacturers and within various GCL product lines are expected. The bulk and clay mineralogy of the 5 primary bentonites was determined using X-Ray Diffraction (XRD) by Mineralogy, Inc., Tulsa, OK. Separate XRD results for *CR+* have not been included, due to its direct derivation from the *CR* material and assumed similarities in general mineralogy. Results of XRD testing are summarized in Table 6.3, and shown graphically in Figure 6.1 for comparison to the natural barrier soils (shown in Figure 4.2).

Similar to the natural barrier soils, characterizations of aspects of the bentonite suite were made for comparison amongst all of the soil materials used. The soluble cation (SC) and bound cation content (BC) and cation exchange capacity (CEC) of the

soils was analyzed using ASTM D 7503 (2010) and is compared graphically in Figure 6.2. Soil pH for the soils was determined using both water and $CaCl_2$-based solutions, as stipulated by ASTM D 4972 (2007), with results tabulated in Table 6.4 and shown for comparison to the natural barrier soils in Figure 6.3.

6.1.3 Methods

Building from the methodology discussed in Section 5.1, batch sorption was used for an initial study on the interactions of RSL with barrier soils. Three sets of experimentation using RSL were conducted: (1) control experimentation, measuring any potential interactions between RSL and the reaction containers; (2) kinetics experimentation, tracking sorption over time for both the initial soil suite and the selected bentonites; and (3) sorption edges and envelopes (E&E) experimentation, investigating the impact of pH on sorption of RSL for otherwise constant system conditions.

Similar to the single radionuclide experimentation discussed in Section 5.1, a 10 g to 1 L solid to solution ratio was used throughout RSL experimentation. As executed experimentally, 40 mL of the RSL mixture was added to 0.4 g of soil, taken from the initial soil suite or the bentonite suite, dependent on the section of experimentation. All RSL experimentation was executed under atmospheric conditions, with exposure to atmospheric levels of pCO_2.

During kinetics experimentation, no adjustments to the system pH were made during batch sorption. The pH of the solutions prior to interaction with the soils was measured and recorded, as well as initial pH of the soil-plus-solution system prior to reaction timing, and final pH at the end of reaction timing. Prior to the start of RSL E&E experimentation, a 2 L aliquot for each of the desired pH levels (pH range: 5 to 9, in 0.5 pH unit increments, for 9 individual solutions) was taken from the total batch of the starting RSL mixture, and adjusted to the desired starting pH using HCl or NaOH,

accordingly. During preparation of the E&E samples, solution pH was measured for maintaining the desired pH level. Initial pH of the soil-plus-solution system was again measured and recorded, followed by adjustment with HCl or NaOH to the desired pH level prior to reaction timing. Following reaction timing, final pH measurements were taken.

Reaction time for experimentation was monitored during end-over-end rotation on ThermoScientific Labquake rotators, with continuous rotation of 8 rpm. Kinetics experimentation used reaction times ranging from 15 min (900 s) to 7 d (604800 s), while E&E experimentation used a 24 h (86400 s) reaction period. Following lab timing, samples were centrifuged at 5000 rpm for 10 min to separate the soil solids from solution. After centrifugation, sample aliquots were filtered below 0.2 μm with polypropylene membrane filters and acidified below pH 2 with HNO_3 for storage prior to further analysis. Following preservation, all batch sorption samples were analyzed via ICP-OES to measure solution concentrations of the following inert elements: Al, As, Ba, Ca, Cu, Fe, K, Li, Mg, Mn, Na, Ni, Si, Sr, and Zn. Additionally, U solution concentrations following sorption experimentation were measured using ICP-OES, with the previously reported MDL of 10 μg/L.

6.2 Geochemical Modeling

In addition to the bench-top batch sorption experimentation used for studying RSL-soil interactions, a series of geochemical models were created for isolating specific behaviors within the system and predicting potential issues with the solution speciation.

6.2.1 Visual MINTEQ Model Parameterization

Visual MINTEQ, a freeware chemical equilibrium model, was used for initial study of the RSL mixture speciation. Speciation was run in the multi-problem sweep mode, where one parameter is varied for the specified number of problems. For the RSL

mixture speciation, pH was the varied parameter, with concentrations and speciation of the specified chemical parameters calculated at 0.10 pH increments from pH 4.5 to pH 10. The chosen pH range encompasses all measurements taken across the four DOE LLW sites, as discussed in Section 3. Table 6.5 provides the initial chemical components, their associated starting concentrations, and the specified valence state for components with multiple potential valences (e.g. UO_2^{2-} as indicative of U(VI), rather than U(IV)) used throughout Visual MINTEQ modeling. Concentrations used within the modeling match those used for the target concentrations during creation of the RSL mixture, as indicated in Table 6.1. DIC, or dissolved inorganic carbon concentration, was used as an indicator for the added alkalinity of the system. Of particular importance is the H^+ concentration, listed as 0 mMol. This H^+ concentration is a product of the sweep parameterization, and indicates that the H^+ concentration is changing with the pH level throughout modeling.

Concurrent to the individual chemical components, Table 6.6 lists the potential species and their related thermodynamic constants at 25 °C as derived from the input parameters listed in Table 6.5 through the standard MINTEQ thermodynamic database. Solution speciation and saturation indices are calculated as a consequence of the changing parameters and associated constants within the framework of the software.

6.2.2 Modeled RSL Solution Issues

Given the variety of species introduced to the RSL mixture, a number of potential solution issues were witnessed both during bench-top experimentation and within speciation modeling. Table 6.7 lists all oversaturated species identified during the Visual MINTEQ pH sweep, along with their concurrent ion activity products (I.A.P.s), the highest saturation index (SI) for each species, and the pH or pH range at which the maximum SI occurred during modeling. An explanation of the equations and formulas

used in calculating mineral solubility can be found in Appendix E, along with a relevant example to the RSL system. During speciation modeling, no species were precipitated across the modeled pH range. However, as shown in Table 6.7, 37 individual species were oversaturated as a consequence of system interactions at various pH levels throughout the modeled sweep. As a likely consequence of the solution behavior of oversaturated systems, precipitation of RSL solution species was routinely witnessed during bench-top experimentation for both the batch sorption experimentation detailed within this section, and for other ongoing laboratory experiments using the RSL mixture. Exact documentation of the chemical composition of the precipitated solution species has not been determined at the point of writing.

6.2.3 RSL Solution Speciation

As discussed in Sections 2.3.3.1 (System pH), 2.3.3.3 (Calcium Content), and 2.3.3.4 (Carbonate Content), speciation of radioactive and inert solution species and the change in speciation with pH have been shown in the literature to directly affect sorption capacity. For direct comparison to the literature and the single radionuclide experimentation, the speciation of some critical components of the RSL mixture is presented.

6.2.3.1 U Speciation in RSL

Figure 6.4 shows the U speciation in RSL as derived from the Visual MINTEQ modeling. A few notable differences are present in comparing the U speciation for the RSL mixture and the speciation models for most of the literature systems (Figure 2.4) and the single radionuclide experimentation (Figure 2.9). As with single radionuclide experimentation, RSL experimentation was open to atmospheric conditions, primarily the inclusion of atmospheric pCO_2 rather than being conducted under glovebox conditions within a N_2-sparged system, and has been modeled to account for these conditions. For

comparison, Figure 2.4 displays U speciation under CO_2-free conditions. Additionally, RSL has added alkalinity, via the direct inclusion of carbonate salts during solution creation. Consequently, uranyl-carbonato species are shown to dominate the RSL system above pH 5. U speciation within single radionuclide experimentation also saw uranyl-carbonato species dominate the system above pH 7. Differences between which uranyl-carbonato species are present result in the shift to dominance under lower pH conditions for the RSL mixture. RSL U speciation shows the ingrowth of U-Ca-CO_3 species, often the dominant solution species for U systems as highlighted by Singer et al. (2012a) and Stewart et al. (2010).

In addition to the dominance of U-Ca-CO_3 in RSL speciation across the upper pH range, the inclusion of SO_4^{2-} alters the speciation at low pH from the other modeled systems. Although UO_2^{2+}, the dominant species at low pH in both the literature and single radionuclide systems, remains a notable species within RSL, UO_2SO_4 (aq) is the majority species. The alteration to speciation dominance within RSL has implications for sorption capacity across the RSL system, due to the switch from the cationic UO_2^{2+} species to the neutral UO_2SO_4 (aq) species, and concurrent potential sorption inhibition with cation exchange sites.

6.2.3.2 Ca and CO_3^{2-} Speciation in RSL

Figures 6.5 and 6.6 show the results of Visual MINTEQ speciation modeling for Ca and CO_3^{2-} based species, respectively. As mentioned in the previous section, the presence of Ca and CO_3^{2-} in solution with U dominates both the speciation and sorption mechanisms for U. However, the corresponding U-Ca-CO_3 complexes, which dominate U speciation, represent an increasingly small fraction of the Ca and CO_3^{2-} speciation, as shown within their respective figures. The significant concentration of Ca within the system could allow for Ca to outcompete U and other species for sorption sites on the

soil surfaces, as expressed within cation replaceability hierarchy described in Section 2.3.3.5 (Interactions with coprecipitants).

6.2.4 The Geochemist's Workbench Models

Figures and tables pertaining to two additional models can be found in Appendix F. These models were created using the SpecE8 application of The Geochemist's Workbench and utilized two thermodynamic databases with varying properties. Comparison to the literature and the Visual MINTEQ modeling showed a departure from expected behavior. The information within Appendix F is provided for comparison.

6.3 Control Experimentation

As discussed in Section 5.2 for the single radionuclide experimentation, control experimentation provides direct comparison between two of the three primary solution components. For RSL experimentation, the components used for comparison are the radionuclides and the basic cations present within the RSL solution that form the ionic basis for the system. In addition to having important implications for the RSL ionic basis, Ca and Na, as two of the primary cations within the solution, are known to influence bentonite behavior. As with single radionuclide experimentation, glass beads (passing the #45 sieve but retained by the #60 sieve) served as a sorption control surface.

Two sets of control experiments were conducted using the RSL mixture to correspond to the two primary sets of experimentation with the soils and bentonites. Both solution control and glass beads control experimentation were run to study the kinetic behavior of the system, while only a set of solution control experimentation was used for comparison with the remainder of the edges and envelopes sorption experimentation. Average concentration and pH values for all experimentation can be found in Appendix G.

6.3.1 U Kinetics Control Experimentation

Figure 6.7 compares the measured solution concentrations of U for both the solution and glass beads kinetics control experimentation for reaction times ranging from 15 min (900 s) to 7 d (604800 s), mirroring the timing used for both single radionuclide and RSL mixture kinetics experimentation with the soil suites. As discussed in Section 6.1.1 (Radioactive Synthetic Leachate), the concentration of U-238, as the specific isotope of U chosen for use within the RSL mixture, was intended to correspond to the measured concentrations at ERDF as the consistently highest DOE LLW leachate U concentrations. The RSL mixture was to include 1500 µg/L of U. Figure 6.7 shows the divergence of the measured concentrations in both the solution control experimentation and the glass beads experimentation from the designated starting concentration of U. Although some variation in the measured U concentration is shown over the given reaction times, both the solution control and glass beads experimentation show a consistently lower U concentration than the intended initial concentration.

Two possible explanations can account for the variation from the intended U concentration. The first potential cause of variation is the human element. As previously expressed in Section 6.1.1 (Radioactive Synthetic Leachate), some variation between the desired RSL mixture and the actual RSL mixture is anticipated due to the small added concentrations of the salts of a number of the included elements, specifically U, to the large (> 100 L) batches of RSL. The second potential cause of variation is the possibility of sorption to precipitated solution species. Due to the variety of oversaturated species (as discussed in Section 6.2.2 – Modeled RSL Solution Issues) and witnessed precipitation within the system during experimentation, removal of U during centrifugation and filtration of precipitated species is possible. As the solids and/or filtrates have not been analyzed during experimentation, exact chemical determination is not available.

Despite the variation from the intended U concentration in the RSL mixture, the measured U concentration within the RSL mixture across both the solution control and glass beads experimentation remains relatively constant across all reaction times used for kinetic comparison (Figure 6.7). Consequently, using the measured experimental data as the basis, 1330 µg/L was the concentration value chosen to represent the initial concentration value throughout the remainder of RSL kinetics experimentation, as compared to the theoretical added concentration of 1500 µg/L. The chosen value encompasses all measured values within the solution control experimentation at a concentration slightly higher than the average measured U concentration.

Figures 6.8 to 6.11 look at the specific kinetic time points and variation in measured pH against measured U concentration for solution control and glass beads sorption control experimentation individually. Figure 6.8 tracks changes in U concentration with the kinetic reaction times for the solution control experimentation, while Figure 6.9 compares changes in U concentration to the measured solution pH values. Across the reaction times used for tracking the kinetic behavior of U in RSL, measured U concentration remains constant for the first 6 reaction times (15 min (900 s) to 24 h (86400 s)), suggesting an approach to steady-state behavior. However, at the longest reaction time (7 d (604800 s)) there is a marked decrease in measured U concentration. The alteration of solution behavior at the longest reaction time makes determination steady-state behavior more tenuous. As discussed in Section 5.3 (Kinetics Experimentation), research within the literature has often focused on significantly longer reaction times than those used during the discussed experimentation, with periods of up to 18 weeks (Bai et al. 2009; Missana et al. 2004). Due to the differences between true system equilibrium and the relative “equilibrium” of steady-state behavior described by Bai et al. (2009), consistent behavior suggesting the approach to steady state is ideal for reducing longer laboratory reaction times. The variation at the 7 d reaction time suggests

that steady state may not have been reached. However, the consistency prior to the 7 d reaction time should still allow for direct comparison between the control experimentation and remainder of the RSL sorption experimentation.

Comparing the measured U concentration to the measured solution pH post-reaction timing (Figure 6.9) shows little connection between the variables in association with the reaction timing for the solution control experimentation. As addressed in Section 6.1.3 (Methods), no adjustments were made to the pH of the solutions during kinetics experimentation, including solution control experimentation. Of note is the variation of the measured solution pH values across all reaction times from the initial intended pH of the RSL solution mixture (initial pH = 7.2, shown in Table 6.1). The measured pH of the reacted solutions was approximately 0.9 pH units higher than the intended pH of the system, both before (values can be found in Appendix G – average initial pH value of 8.09) and after (values displayed on secondary y-axis for Figure 6.9, final average pH value of 8.09) reaction timing, suggesting alteration to the steady-state solution chemistry of the RSL, additionally implicated during speciation modeling (Section 6.2 – Geochemical Modeling).

Figure 6.10 and 6.11 provide the glass bead sorption control experimentation counterpoint to the solution control experimentation shown in Figures 6.8 and 6.9 for the measured U concentrations. Similar to the U behavior of the sorption control experimentation, the first 6 reaction times for the glass beads sorption control experimentation show relatively constant U concentrations with the 7^{th} and longest reaction time showing a decrease in the measured U concentration from the other points. Additionally, the measured pH values across the glass beads experimentation are again higher than the anticipated RSL solution pH, although slightly lower than the values for the solution control experimentation at approximately 0.8 pH units higher than the initial pH (initial average pH value of 8.01, final average pH value of 8.03 (with values

shown in Figure 6.11), versus initial RSL solution pH value of 7.2). Most critically, comparison of Figure 6.10 and 6.11 for the glass beads to Figures 6.8 and 6.9 for the solution control experimentation show no additional loss of U from solution to the sorption control surface, suggesting that any changes in measured U concentration during non-control experimentation are a direct result of interactions between the RSL solution and soil suite sorbents.

6.3.2 Ca and Na Kinetics Control Experimentation

Figure 6.12 compares the measured concentrations of Ca for the solution control and glass beads experimentation to the intended added concentrations for the RSL mixture as indicated in Table 6.1. As indicated within Figure 6.12, the measured concentrations of Ca for both sets of kinetics control experimentation were consistently higher than the intended Ca concentration in RSL (160.312 mg/L, shown by the lower dashed line within the figure). Consequently, a revised initial concentration of 164.159 mg/L (indicated by the upper dashed line within the figure) was chosen to represent the initial concentration value throughout the remainder of RSL experimentation. Similar to the value chosen for U, the Ca value is the average of the measured Ca concentrations within the solution control experimentation. Similar values are shown for the glass beads experimentation, again suggesting no loss to the sorption control surface and indicating changes in solution concentrations during reaction with the soil sorbents are a direct result of the sorbent mineralogy and behavior.

Similar to Figure 6.12, Figure 6.13 compares the solution concentrations of Na for both the solution control and glass beads sorption control kinetics experimentation. Similar to both the measured U and Ca concentrations, the measured Na concentrations varied from the intended concentration of 160.929 mg/L (indicated in Table 6.1). The chosen concentration value of 176.183 mg/L, indicated by the dashed line in Figure

6.13, represents the average measured Na concentration within the solution control experimentation and was chosen to represent the initial concentration value throughout the remainder of RSL experimentation. Values for the Na concentration measured in the glass beads experimentation closely mirror those for the solution control experimentation, again serving as an appropriate indication of changes occurring within measurements of the sorbent and RSL solution interactions being a direct consequence of the sorbents.

6.3.3 U Sorption Edges and Envelopes Control Experimentation

Coupled with the U solution control experimentation for the kinetics experimentation, a set of solution control experiments was run to mirror each of the chosen pH levels for the RSL sorption edges and envelopes experimentation. Figure 6.14 shows the measured U solution concentration for all control experimentation at the final measured pH of each triplicated reaction tube. The dashed line within Figure 6.14 notes the standardized U concentration of 1330 µg/L, chosen from the kinetics solution control experimentation. As indicated previously within Section 6.3.1 (U Kinetics Control Experimentation), the system concentration varied from the intended experimental U concentration of 1500 µg/L. However, as displayed in Figure 6.14, although all solutions were created from the same initial bulk stock solution, the alteration of the pH within each of the individual pH-specific stock solutions resulted in a variation in the measured U. The alteration across the pH range is potentially a consequence of the changes occurring within the U RSL solution speciation, as discussed in Section 6.2.3.1 (U Speciation in RSL). Due to the U concentration changes, comparison of the amount of U sorbed in the RSL-soil sorbent system should ideally be based on the measured concentrations at each specific pH level.

6.3.4 Ca and Na Sorption Edges and Envelopes Control Experimentation

Figures 6.15 and 6.16 compare the measured concentrations of Ca and Na in the RSL solution across the tested pH range. Similar to the U solution control experimentation, both Ca and Na show a direct dependence on the pH of the system. However, across most of the tested pH range, the chosen concentrations discussed in Section 6.3.2 (164.159 mg/L for Ca and 176.183 mg/L for Na) remain an accurate representation of the solution concentration.

6.4 Kinetics Experimentation

The impact of time on both radioactive and inert waste components has important implications for the long-term effectiveness of LLW disposal scenarios. As such, an understanding of the sorption kinetics to barrier soils helps to ascertain the steady-state behavior of LLW. Kinetics experimentation, measuring the impact of time on sorption capacity, was executed in batch experimentation over 7 time steps ranging from 15 min (900 s) to 7 d (604800 s). Two sets of soils were used as sorbents for the RSL solution: the original barrier soil suite used throughout single radionuclide experimentation, and the bentonites chosen for RSL experimentation. Tables of the pH values and average concentrations of the analytes across the triplicated experimentation can be found in Appendix G.

6.4.1 Original Soil Suite RSL Kinetics

Figure 6.17 compares kinetic behavior of U in RSL across the entire original soil suite. Cross-comparing behavior across the four soils shows similar trends to the U sorption behavior shown during single radionuclide experimentation. Soils *A* and *C* show increased U removal from RSL as compared to Soils *B* and *D*. All four soils show less total removal of U from the RSL solution, on the basis of percentage removed, as compared to the single radionuclide experimentation. The difference in sorption is likely

a consequence of increased competition between the solution components due to the increased complexity of the RSL solution versus the uranium acetate-sodium perchlorate solution.

Figures 6.18 through 6.25 show the individual measured concentrations of U for RSL in contact with Soils *A*, *B*, *C*, and *D* in relation to both the individual reaction times and the final pH of each of the experiments. Figures 6.18 and 6.19 show the measured concentrations of U in the RSL solution following kinetics experimentation with Soil *A*. As shown for the single radionuclide U experimentation, Soil *A* was the best sorbent amongst the original soil suite, with between approximately 150 and 350 µg/L of U removed from solution over the increasing reaction times. Soil *A* shows continued increased U sorption across all seven reaction times, with the most U sorption occurring at the 7 d (604800 s) reaction time, as shown in Figure 6.18. Further, in contrast to the single radionuclide experimentation (Figure 5.8), sorption of U from within the RSL solution to Soil *A* shows a strong dependence on solution pH (Figure 6.19).

Figures 6.20 and 6.21 compare measured concentrations of U in the RSL solution and the final measured solution pH values following interaction with Soil *B* across the reaction times. Similar to Soil *A*, Soil *B* also shows increased U sorption as the reaction time increases. However, over the experimental reaction times Soil *B* sorbed approximately 50 to 120 µg/L of U, for less total sorption than Soil *A* across all of the reaction times, but most specifically at the longest reaction time. As discussed at various points throughout Section 5, Soil *B* contains calcite, which directly impacted the soil buffering capacity and the final pH of the single radionuclide kinetics experimentation (Figure 5.10). While the inclusion of calcite in Soil *B*'s mineralogy is also likely to influence behavior in the more complex RSL sorption system, during kinetics experimentation the final measured pH of the Soil *B* experimentation (shown in Figure

6.21) more closely resembled the behavior of Soil *A* in RSL than the single radionuclide experimentation behavior using Soil *B*.

The measured U remaining in the RSL solution following interaction with Soil *C* during reaction timing is shown in Figures 6.22 and 6.23. Although Soil *C* showed similar U sorption capacity to Soil *A* during single radionuclide experimentation, within the more complex RSL solution Soil *A* outperforms Soil *C*, which removed between 110 and 190 µg/L of U across the reaction times. Soil *C* showed the same trends for increasing U sorption capacity with time and pH dependence as the other natural soils.

Figures 6.24 and 6.25 show the U remaining in solution following the Soil *D* kinetics experimentation. Amongst the soils within the natural soil suite, Soil *D* sorbs the least U from the RSL solution, removing approximately 10 to 90 µg/L of U across the measured reaction times. Additionally, while measured U concentrations for both single radionuclide (Figure 5.14) and RSL kinetics experimentation (Figure 6.25) with Soil *D* show a dependence on the pH of the system, the two systems have opposing trends with increasing time. Single radionuclide experimentation with Soil *D* shows an increase in pH and the U remaining in solution with increasing reaction time, while the Soil *D*-RSL system follows the opposite trend, echoing the behavior of the other natural soils.

Figures 6.26 and 6.27 compare the measured Ca and Na concentrations in the RSL solution (in mg/L) following interaction with the four soils of the original soil suite during kinetics experimentation. Across all reaction times, more Ca was measured in solution after interaction with the soils than in the initial solution (Figure 6.26). Similarly, for the first 5 reaction times, more Na was measured in solution than in the starting RSL solution mixture (Figure 6.27). The concentration of Na in solution decreases for all 4 soils during the 24 h (86400 s) and the 7 d (604800 s) reaction times, falling below the initial solution concentration at the longest reaction time. The measured concentrations of Ca and Na suggest an exchange of the cations satisfying the exchange capacity

within the soils for other components within the RSL solution. Additionally, the decrease in the Na concentration towards the starting concentration with increasing time further suggests the approach to a steady state within the four individual soil-RSL systems, with the Na concentration equilibrating between the solution and sorbent.

6.4.2 Bentonite RSL Kinetics

Figure 6.28 shows measured U remaining in the RSL solution following interaction with each of the 6 bentonites within the bentonite suite during kinetics experimentation. Looking at the behavior of the entire suite, the measured U removal by many of the bentonites is similar, with overlapping data points. For ease of comparison for both the kinetics and E&E experimentation amongst the bentonites, the bentonite suite has been divided into two categories: the standard, non-modified GCL bentonites and the polymer-modified GCL bentonites in all variations (as described within the context of this work within Section 6.1.2).

Figure 6.29 compares the U remaining in the RSL solution following interaction with the two standard bentonites, *CS* and *GS*. Both of the standard bentonites show comparable U removal through the first 6 tested reaction times, with *GS* showing increased slightly increased sorption at the 7 d (604800 s) reaction time. Figures 6.30 and 6.31 compare the U concentrations and final pH measurements following interaction with *CS* during kinetics experimentation, while Figures 6.32 and 6.33 show similar data following interaction with *GS*. Over the course of reaction timing, both *CS* show a modest increase in U removal between the 15 min (900 s) and 7 d (604800 s) experimentations, with *CS* sorbing between approximately 130 and 230 µg/L and *GS* sorbing between 130 and 260 µg/L of U. *CS* and *GS* each show a decreasing pH with increasing reaction time with the RSL mixture (Figures 6.31 and 6.33, respectively). For *CS* (Figure 6.31), across the first 6 reaction times the final measured experimental pH is

more basic than the pH of the RSL solution (see Figure 6.11 for comparison). By the longest reaction time, the measured pH of the *CS*-RSL solution mixture begins to approach to a steady state with the pH of the RSL solution. The final measured pH values of the *GS*-RSL experimentation (Figure 6.33) show similar behavior to the *CS*-RSL experimentation, but remains more basic than the RSL solution across the entire reaction time frame. For both standard bentonites, the measured pH behavior is likely a consequence of the buffering capacity and soil pH of the bentonites themselves, shown in Figure 6.3 and Table 6.4.

Figure 6.34 compares the U removal behavior of the polymer-modified GCL bentonites during kinetics experimentation. As discussed briefly in Section 6.1.2, polymer modification is intended to increase the chemical resistance of the GCLs to non-compatible leachate mixtures, such as the diverse chemical system found in LLW leachate. Consequently, prior to the start of experimentation using the RSL solution, the chemically resistant GCLs were anticipated to have greater sorption capacity than the standard GCLs when in contact with the same leachate mixtures. Looking back to Figure 6.28, which showed results for all of the GCLs, the standard bentonites fell within the middle of the suite, with greater sorption capacity for U than some of the polymer modified bentonites (specifically, *CR*+) and less sorption capacity than others (*CT* across all time frames, and *GR* at the longest reaction periods). As such, the variations in the polymer modification processes result in differences amongst the GCLs sorption capacity that do not uniformly meet the prior hypothesis. These differences are further highlighted within Figure 6.34, where the behavior of the four polymer-modified bentonites are compared as a set.

Within the set, each of the four polymer-modified bentonites displays slightly different behaviors. Figures 6.35 and 6.36 show the U remaining in solution and final measured pH values for the RSL solution in contact with bentonite *CR* during kinetics

experimentation. Accounting for standard deviation, the U removal by *CR* most closely resembles traditional kinetics experimentation, approaching a steady-state solution concentration of U approximately 1160 µg/L, or 170 µg/L U sorbed, across the final 4 reaction times. Figure 6.36 shows that at the same time that the U concentration of the *CR*-GSL system approaches a steady state, the measured pH of the system continues to decrease, falling below the pH of the GSL solution.

Measured solution U concentrations and final system pH values following interaction with *CT* are found in Figure 6.37 and 6.38. Over the first 6 reaction times, removal of U from the RSL solution by *CT* is relatively constant within the range of the experimental standard deviation, ranging from 190 to 230 µg/L of U sorbed. The 7 d (604800 s) time frame shows a sharp increase in removal to approximately 290 µg/L of U sorbed. This change in removal may be a directly related to the system pH, as shown in Figure 6.38. Following an identical trend to the U concentration, the pH of the system remains relatively constant across the first 6 reaction times, becoming more acidic at the longest time frame. The soil pH of *CT* is significantly lower than that of the other bentonites (see Table 6.4 and Figure 6.3), resulting in a lower *CT*-RSL solution pH than what was seen for the rest of the suite. While the shift to a slightly more acidic pH is not significant enough to change the U speciation in RSL to dominance by the more favorable cationic U species (see Figure 6.4), the decreasing pH in combination with the increased reaction time may allow for greater exchange between surface species on the CT material and the RSL solution, freeing locations for increased U uptake to occur.

Figures 6.39 and 6.40 compare measured U concentrations in the RSL solution and final pH values for kinetics experimentation using the *CR+* bentonite. Based on the manufacturer's specifications, the *CR+* GCL is intended as an enhanced version of the *CR* GCL, using the same bentonite and polymer stocks for the creation of the material, as discussed in Section 6.1.2. As such, *CR+* ideally would perform either comparably to

CR or with increased sorption capacity as a consequence of the changes to the chemically resistant behavior. However, the two sister bentonites show differing U removal from one another during kinetics experimentation. While *CR* displays a relatively smooth, asymptotic approach to a steady-state solution concentration of U (see Figure 6.35), *CR*+ removes U from the RSL solution at a more erratic pace, easily shown in three distinct time frames (Figure 6.39). Over the course of the first 3 reaction times (from 15 min (900 s) to 1 h (3600 s)), *CR*+ averages only 80 µg/L of U removed from solution. Between the 2 h (7200 s) and 24 h (86400 s) reaction times, the average sorbed U increases to 120 µg/L, before jumping to approximately 170 µg/L U sorbed during the 7 d (604800 s) reaction time. The overall U sorption capacity of *CR*+ at the longest time frame is similar to the average shown within the asymptotic steady state region for *CR*. The three regions of U removal over the reaction times are not mirrored by the solution pH (Figure 6.40). Instead the solution pH is relatively consistent across the first 5 reaction times when accounting for standard deviation, before decreasing at each of the final reaction times. The pH behavior for *CR*+ closely resembles that of *CR* (Figure 6.36), suggesting that either the bentonite or polymer used in both materials directly influences the solution pH, despite slightly different soil pH values measured for the originating materials (see Table 6.4 and Figure 6.3).

U solution concentrations in RSL measured following reaction with *GR* are shown in Figures 6.41 and 6.42. *GR* shows increasing sorption of U from the RSL solution, removing approximately 110 µg/L U removed at the 15 min (900 s) reaction time and increasing to 330 µg/L U removed at the 7 d (604800 s) reaction time. As such, at the two longest reaction times *GR* sorbed the most U from the RSL solution of all of the tested bentonites, while for the shorter reaction periods *CT* acted as the best sorbent (refer back to Figure 6.34 for the comparison of all polymer-modified bentonite U sorption behavior). Figure 6.42 shows the similar behavior of the *GR*-RSL system

measured U concentrations and the final pH, with the pH decreasing steadily at the same rate that the amount of U removed solution increases. The final measured pH of much of the *GR*-RSL system remains higher than that of the other polymer-modified bentonites, showing measured pH values more similar to those of the two standard bentonites (*CS* in Figure 6.31 and *GS* in Figure 6.33). The similarity in solution pH may be influenced by the slightly higher soil pH of *CS*, *GS*, and *GR* in comparison to the other bentonites (see Table 6.4 and Figure 6.3).

Figures 6.43 and 6.44 compare the measured Ca and Na concentrations in the RSL solution (in mg/L) following interaction with the entire bentonite suite during kinetics experimentation. Comparing the conglomerate bentonite Ca and Na solution concentrations to those of the original soil suite (Figures 6.26 and 6.27) show opposing behaviors. While the four original soils show a modest increase in both the Ca and Na solution concentrations over the course of reaction timing, the bentonites display preferential behavior for sorbing Ca in exchange for releasing Na into solution. This behavior is anticipated as GCL bentonites are primarily mineralogically composed of Na-rich montmorillonite as shown specifically for the chosen bentonite suite via the XRD analysis found in Figure 6.1. Heavily clay-rich bentonite more closely adheres to the behavior associated with cation replaceability of clays, with divalent cations, like Ca^{2+}, being more heavily favored than monovalent cations, like Na^{+} (Sposito 1989 pg. 155). Consequently, when placed in contact with the RSL solution containing similar concentrations of both Ca and Na, the bentonites preferentially exchange Na present within the soil structure for Ca in order to satisfy negative surface charge with fewer ions.

Figures 6.45 and 6.46 display the Ca and Na solution concentrations (in mg/L) for the standard bentonites. Despite having similar Ca and Na BC fractions and total CECs (see Figure 6.2), *CS* and *GS* show differing behavior in the exchange of the cations within the RSL solution. While the measured Ca and Na concentrations from the

GS-RSL interactions remain relatively constant across the reaction periods, *CS* shows decreasing Ca and increasing Na concentrations with increasing reaction times. The difference between the processes for *GS* and *CS* suggest that most cation exchange occurs quickly for *GS*, while *CS* exhibits a slower exchange process. The Ca and Na exchange processes of *CS* and *GS* have implications for both the U uptake within the systems and the long-term performance of the bentonites. The increased Ca removal in the *CS* system could result in the difference in U uptake between *CS* and *GS*. Further, exchange of Na for Ca within multi-species ionic systems, like the RSL, results in changes to the swelling mechanisms of the bentonite both within the laboratory and installed as GCLs in the field (Kolstad et al. 2004).

Concurrent to the standard bentonites, Figures 6.47 and 6.48 give the Ca and Na solution concentrations for the polymer-modified bentonites. Within the set, *CT* releases significantly more Na into solution while removing more Ca than the other polymer-modified bentonites. As shown in Figure 6.2, CT has a higher BC fraction of Na than the other bentonites, as a consequence of the use of Na-polyacrylate as the polymer within the creation of the BPC mixture, allowing for a greater initial Na concentration to exchange for Ca within the RSL mixture. Of the other 3 bentonites, *CR+* and *GR* show a slight decrease in Ca concentration and increase in Na concentration with time, while for *CR* both cations remain relatively constant over the tested reaction periods.

6.5 Sorption Edge and Envelope Experimentation

In natural geochemical systems, the soil-water interface is frequently influenced by changes to the pH caused by increases in acidity or basicity. Man-made geochemical systems, like the soil-based barrier systems used for LLW, are similarly influenced. Consequently, understanding how alterations to solution pH of the RSL impact sorption

capacity for both radionuclides and inert components is critical for determination of the long-term behavior of installed barriers.

Complimenting the kinetics experimentation aimed at determination of temporally influenced sorption behavior, a series of experiments were used to investigate the impact of system pH on sorption to a subset of the selected sorbents. Sorption experiments looking at system pH impact are often referred to as Edge and Envelope experimentation (hereafter: E&E) due to the characteristic shapes taken by the classical results of the experiments. Soils *A* and *C* were used from the original barrier soil suite due to their demonstrated sorption capacity for U during both single radionuclide experimentation and RSL kinetics experimentation. Additionally, the entire GCL-derived bentonite suite was used to act as a complimentary set of data to ongoing hydraulic conductivity testing with the RSL mixture. As discussed in Section 6.1.3, initial pH of the RSL solutions was adjusted in batch portions to pH 5 to 9, in 0.5 pH unit increments. The chosen pH range mirrors the expected pH range of the collected DOE LLW leachate data range, shown in Figure 3.2.

The behavior of three species are highlighted within this section: U, as the primary radionuclide for comparison to both the single radionuclide experimentation and the literature; and Ca and Na, for their importance as two of the primary cationic species within the RSL mixture. Figure 6.49 shows U remaining in solution (in µg/L) for all the soils, while Figures 6.50 and 6.51 show the corresponding results for all of the soils for Ca and Na (in mg/L), respectively. The average concentrations and pH values of the triplicated experiments can be found in Appendix G.

As discussed in Section 6.3.3, variation occurred in the measured U solution concentration over the experimental pH range. Consequently, comparison of the amount of U sorbed in the RSL-soil sorbent system should ideally be based on the measured concentrations at each specific pH level. U sorption for each of the soils was made at

both the constant 1330 µg/L concentration level taken from kinetics experimentation and at the variable concentrations resulting from pH changes in the E&E solution control experimentation. However, the some of the resulting sorbed concentrations of U showed negative values, suggesting an increase of U within the system. As such, the U concentration of 1330 µg/L was used throughout this section. Appendix H contains figures comparing sorbed U values at both the 1330 µg/L and pH-variable concentrations for the studied soils.

6.5.1 U in RSL E&E Experimentation

As discussed in Section 6.2.3.1, the speciation of U within RSL is directly connected to the pH of the system. Within the literature, many connections have been drawn between the ingrowth of anionic and neutral U-based species at higher pH and the associated decrease in sorbed U to minerals, highlighted in the collected literature findings shown in Figure 2.4. Of particular note is the turning point of pH 8.5 documented by Schlegel and Descostes (2009), above which U sorption to hectorite and montmorillonite begins to decrease. The pH range of the collected DOE LLW leachates extends beyond pH 8.5. Consequently, determination of U sorption behavior in RSL to barrier soils must also look to this range.

Figure 6.49 showcased the combined behavior of the all of the tested materials across the entire pH range used for E&E experimentation at the final measured pH values. While the solutions for experimentation were adjusted to the targeted pH levels prior to combination with the sorbents as well as individually readjusted to each pH within the reaction tubes, some pH drift still occurred. The difference in pH between the start and end of experimentation and the impact on the measured U remaining in solution is shown in Figure 6.52. For most of the tested soil sorbents, the final measured pH trended towards a compressed pH range when compared to the initial

measurements and targeted values. Although the final solution pH range differed for each soil, influenced in part by the individual soil pH values and associated buffering capacities, a similar pH compression for the upper pH range (pH values 8, 8.5, and 9) occurred during E&E solution control experimentation for the RSL mixture, as shown in Figure 6.14. The reduction in pH range displayed throughout experimentation is likely a consequence of both the speciation of the system and the oversaturation within the RSL solution. Within oversaturated systems like the RSL, precipitation often results in associated pH drift, as species are pulled from solution to the solid phase, altering the solution composition.

Turning from the overall system behavior, discussion of results from E&E experimentation is broken down into three groups that mirror those used within Section 6.4 for the RSL kinetics experimentation. For ease of comparison, the natural barrier soils, standard bentonites, and polymer-modified bentonites are each discussed as a separate soil category.

6.5.1.1 Natural Barrier Soils

Stemming from the results of the single-radionuclide experimentation and RSL kinetics experimentation, the natural barrier soils used for the final set of batch sorption experiments was narrowed to focus solely on the best sorbents identified within the group. For this set of experiments, Soils *A* and *C* were chosen due to their previously demonstrated sorption capacity for U in both the sodium perchlorate solution and within the RSL mixture. Figure 6.53 directly compares the measured U concentration for Soils *A* and *C* following E&E experimentation, while Figures 6.54 and 6.55 look at the U sorbed for each soil individually. The results from the RSL E&E experimentation using the natural barrier soils as sorbents show well-defined behavior with limited deviation between triplicated results, beginning with significant sorption of U at the lowest tested

pH levels. As pH increases, the amount of sorbed U decreases. The documented U behavior is similar to the literature in overall trend, but differs in the pH range at which the shift to decreased sorption occurs. Within the literature, a sorption plateau has been frequently documented in the circa-neutral pH range for CO_2-free U systems (exact range has varied with sorbents; generally pH 6 to 8.5 – see Figure 2.4), with a sharp decline in sorption capacity as pH increases. Further impacting sorption at higher pH levels are the formation and speciation dominance of uranyl-calcium-carbonato complexes. As noted by Singer et al. (2012a), formation of these tripartite species in systems with atmospheric pCO_2 can impact U sorption at lower pHs than those in CO_2-free U systems. The inclusion of Ca and CO_3^{2-} within RSL, as well as experimental work occurring under standard atmospheric pCO_2 conditions, can account for the shift to decreased U sorption at lower pH levels within the tested system.

Within the scope of the experimentation, Soil *A* outperformed Soil *C* under similar system conditions on the basis of U sorption in RSL at the higher system pH levels. The two soils have differing mineralogies, as discussed in Section 5.6, which may influence the soils overall sorption capacity within the RSL solution. Soil *A*'s larger fraction of crystalline Fe minerals and smaller cation exchange capacity may contribute to the increase in U sorption. As discussed in Section 5.6, any increase in the presence of Fe can impact U sorption capacity, particularly the presence of crystalline Fe phases like the goethite in Soil *A*. Additionally, while having greater overall sorption capacity in the context of having a smaller CEC may sound counterintuitive, the decrease in competition for preferred cations in solution over bound surface cations could allow for more initial access to available surface sites, resulting in increased sorption for non-preferred species, like U.

6.5.1.2 Standard Bentonites

Turning attention to the GCL-derived bentonites, Figure 6.56 compares the solution concentration of U following E&E experimentation for the two standard bentonites, while Figures 6.57 and 6.58 look at the U sorption behavior of *CS* and *GS* individually. Similar to the natural barrier soils, *CS* and *GS* show their highest U sorption at the lowest tested pH levels, with decreasing U sorption as pH increases. Although displaying similar trends to the natural barrier soils and the literature foundation, *CS* and *GS* show a more pronounced increase in U sorption at the highest tested pH levels than the other materials. In the context of the U speciation in RSL, no alterations occur to suggest this change in behavior. However, as pH increases, the surface charge of the bentonite will attempt to become less electronegative, allowing further potential binding of solution species and exchange with neutral species.

6.5.1.3 Polymer-modified Bentonites

Similar to the natural barrier soils and the standard bentonites, Figure 6.59 compares the solution concentrations of U following E&E experimentation for the set of polymer-modified bentonites. Figures 6.60, 6.61, 6.62, and 6.63 show the solution concentrations in comparison to the sorbed U for *CR*, *CT*, *CR+*, and *GR*, respectively. As a group, the polymer-modified bentonites showed more distinct changes between the initial and final pH measurements. Further, across all of the tested pH levels, no single bentonite served as having better U sorption capacity within the group. While *CT* sorbed the most U at the low end of the tested pH spectrum with 95% or better sorption of the U from solution, the same product was the worst performer at high pH values, with approximately 90% of the U remaining in solution. Concurrently, *GR* had the least uptake at lower pH values, but consequently had the least difference in sorption between

various pH levels, averaging removal of approximately 30% of the initial U solution concentration across all pHs. *CR* and *CR*+ performed comparably to one another, as would be suggested by *CR*+'s basis in the same bentonite and polymer as *CR*, but not shown during kinetics experimentation.

6.5.2 Ca and Na RSL E&E Experimentation

As mentioned previously, Figures 6.50 and 6.51 compare the Ca and Na concentrations remaining in solution for all of the soil sorbents. Ca and Na are both base cations typically viewed as fundamental in determination of cation exchange capacity as well as representing significant fractions of the DOE LLW leachates and the RSL mixture. Due to its impact on U speciation, changes in Ca concentrations in solution can indicate changes to U sorption. Additionally, as discussed in the context of kinetics experimentation within Section 6.4, preferential exchange of surface-bound Na for Ca has implications for bentonite system performance.

Within Figure 6.50, most of the tested sorbents show a generalized trend of relatively steady Ca concentration across most of the tested pH, with *CR*+ as the notable exception. Breaking down the data set into the individual barrier soil groupings, Figure 6.64 compares solution Ca concentrations for the natural barrier soils. Across the tested pH range, Soil *C* has a slightly greater concentration of Ca remaining in solution than Soil *A*. As indicated by Stewart et al. (2010), an increase in Ca concentration can lead to a decrease in U sorption, while Galunin et al. (2009) noted the tendency for Ca to dominate interlayer sites within clays, reducing the total number of specific sorption sites available to other species. These differences could help to further explain the differences shown between sorption capacity for Soils *A* and *C* in the context of the RSL system not seen in the single radionuclide, sodium perchlorate system, where the lack of system Ca resulted in less competition between ions.

Figure 6.65 compares solution Ca concentrations across the entire bentonite suite, while Figures 6.66 and 6.67 look at Ca concentrations following E&E experimentation with the standard and polymer-modified bentonites, respectively. Major differences in the overall concentrations between the *CS* and *CR* and the *GS* and *GR* groupings are likely a consequence of both refreshment of the overall batch of leachate between experiments and calibration issues sustained while analyzing the samples on the ICP-AES. For the bentonites, discussion is focused on general trends displayed by the materials, rather than overall concentrations, as some differences between Ca concentrations can be anticipated from the other portions of experimentation, but not to the extent displayed.

As shown in Figure 6.66, *CS* and *GS* follow the same general trend of decreasing solution Ca concentration above neutral pH. For the polymer-modified bentonites in Figure 6.67, *CR* and *GR* show similar behavior to the standard bentonites. *CT* and *CR+* have slightly different trends than the other materials. The Ca concentration for *CT* remains relatively constant until pH 8, at which point the concentration begins to decrease, similar to the behavior shown by the rest of the bentonites. As noted earlier, *CR+* is the notable exception within the suite of materials, with an increase in solution concentration above pH 7. The behavior displayed by *CR+* shows no influence on the system, as *CR+* also shows an increase in U sorption above pH 8, typically shown to be opposing behaviors within the literature.

The measured Na concentrations following interactions with all of the sorbents within the E&E experimentation are found in Figure 6.51. Figure 6.68 shows the Na solution concentration for the natural barrier soils. Both Soils *A* and *C* have an increase in Na above pH 8, corresponding directly to the decrease in Ca concentration shown for the two soils. The correlation is likely a direct consequence of preferential cation exchange by the soils.

Figure 6.69 displays the measured Na concentrations across the tested pH range for the entire suite of bentonites. As with the Ca concentrations, differences in the overall concentrations between the bentonite samples are likely a consequence of both refreshment of the overall batch of leachate between experiments and calibration issues sustained while analyzing the samples on the ICP-AES. Discussion for the bentonites is focused on general trends displayed by the materials, rather than overall concentrations, as some differences between Na concentrations can be anticipated from the other portions of experimentation, but not to the extent displayed, particularly in the extremely high Na concentrations for *CR*+, *GS*, and *GR*. In order to simplify discussion of trends, Figure 6.70 separates the data into two panels – one at high concentration and one at lower concentration – in order to allow behavior across the tested pH range to be more readily compared.

Comparing the behavior of the standard bentonites, both *CS* and *GS* follow a generally similar trend to the natural barrier soils, with an increase in Na concentration at the highest tested pH. As with the natural barrier soils, the increase in Na concentration corresponds to the decrease in Ca concentration, suggesting the potential occurrence of preferential exchange occurring between the cations. Of note for *GS* is the significantly sharper increase in solution concentration when compared to either *GS* or the rest of the bentonites. The reason for this change is unclear.

Within the set of polymer-modified bentonites, *CR*, *CT*, and *CR*+ each show a slight increase in Na concentration at the highest pH, while the concentration is relatively constant over the rest of the tested pH range. *GR* shows unique behavior, with decreasing solution concentrations below pH 7 and increasing solution concentrations above pH 7. The increase in solution concentration at basic pH levels mirrors the decrease in Ca concentration for *GR*, while no connections are drawn to the lower pH values.

6.6 Implications of RSL Sorption Experimentation

The sorption performance of the various CCL and GCL components tested provides some perspective on the intrinsic complications present in designing systems for long-term waste containment. To provide a direct comparison to the literature, U sorption in RSL following E&E experimentation is provided in terms of K_d, the distribution coefficient, for final measured pH values in Figure 6.71 and for initial pH values in Figure 6.72. An explanation of the K_d calculation can be found in Appendix C. Comparisons to other K_d values within the literature for U can be found in Figures 2.4 and 2.5 for purified clays and Fe minerals, respectively.

As shown through the results of the kinetics and E&E experimentation, while many of the soils perform well under certain system conditions, none of the tested materials is adept at U retention across all tested situations. This caveat is especially relevant in the context of Soils *A* and *C* and Bentonite *CT*, which each outperformed the other materials in terms of U sorption at the lowest tested pH ranges, but allowed nearly 100% of the U to remain in solution at the higher pH levels. However, as anticipated by the literature results for similarly speciated systems (Galunin et al. 2009, 2010; Stewart et al. 2010), U sorption is hindered by the presence of Ca and CO_3^{2-} within the RSL system. Due to the basis for RSL creation from within the DOE LLW data sets (Tian et al. 2014; Section 3), the current experimental system conditions are an accurate representation of those that are occurring at LLW sites in the U.S. Consequently, the types of materials readily available and frequently installed as barriers within LLW systems are unlikely to perform as desired, particularly in the face of long-term regulations.

In the context of the original experimental hypotheses for this study, the chosen barrier materials were shown to rely heavily on their inherent mineralogies, with the Fe fractions dominating sorption capacity for the natural barrier soils, and differences in

cation exchange capacity due to both clay and polymer behavior influencing the bentonites. Competition between solution species, particularly in terms of preferential cation replacability, dominated solution behavior within the RSL system. The presence of Ca and CO_3^{2-} in the RSL solution altered both speciation and sorption behavior for U on all tested sorbents. While the demonstrated sorption behaviors differed slightly from those shown within the literature, the complexity of the both the natural soils used within experimentation and the RSL mixture itself lend explanations to those differences. Finally, the measured concentrations of many of the solution species could be directly correlated to their equilibrium geochemical behaviors as modeled through speciation and oversaturation calculations.

Table 6.1. Parameters used in radioactive synthetic leachate (RSL). Concentrations of inorganic components are in millimoles per liter, while concentrations for other components are listed individually. Notes: TOC – Total Organic Carbon; ORP – Oxidation Reduction Potential.

Inorganic Components (mM)			
Ca	4	As	0.001
Mg	6	Ba	0.002
Na	7	Cu	0.0002
K	0.7	Fe	0.04
SO_4^{2-}	7.5	Li	0.02
Cl	8	Mn	0.01
NO_2^-/NO_3^-	1.5	Ni	0.0003
Alkalinity	3.5	Sr	0.02
Al	0.03	Zn	0.0005
Radionuclides		**Chemical Characteristics**	
^{238}U (µg/L)	1500	TOC	5 mg/L surfactant and 3 mg/L acetic acid
^{3}H (pCi/L)	120000	ORP	120
^{99}Tc (pCi/L)	800	pH	7.2

Table 6.2. Chemical components used in creation of RSL.

Component	Concentration used in RSL (mmol/L)	Molecular Weight (g/mol)
$CaCl_2 \cdot 2\ H_2O$	4	147.01
$MgSO_4 \cdot 7\ H_2O$	6	246.47
$NaNO_3$	1.5	84.99
$NaHCO_3$	2.8	84.01
Na_2SO_4	1.35	142.04
$KHCO_3$	0.7	100.12
$Al_2(SO_4)_3 \cdot 16\ H_2O$	0.015	630.4
As (aqueous)	0.002	74.9216
$CuSO_4 \cdot 5\ H_2O$	0.002	249.69
$FeSO_4 \cdot 7\ H_2O$	0.05	278.01
LiCl	0.02	42.39
$MnSO_4 \cdot H_2O$	0.01	169.02
$SrCl_2 \cdot 6\ H_2O$	0.02	266.62
$ZnSO_4 \cdot 7\ H_2O$	0.002	287.56
$NiSO_4 \cdot 6\ H_2O$	0.002	262.85
$BaCl_2 \cdot 2\ H_2O$	0.002	244.26

Table 6.3. Soil mineralogy of the project bentonites as determined by XRD.

	Quartz (%)	Cristobalite (%)	Plagioclase Feldspar - Oligoclase (%)	K-Feldspar - Orthoclase (%)	Calcite (%)	Siderite (%)	Gypsum (%)	Augite (%)	Clinoptilolite (%)	Kaolinite (%)	Illite/Mica (%)	Montmorillonite (%)	Total (%)
CS	9		3	Trc.	1		Trc.		2	Trc.	1	84	100
CR	8		3	1	Trc.				1	Trc.	1	86	100
CT	8		5	1					1	Trc.	7	78	100
GS	5	3	3	Trc.				2	1			86	100
GR	6	4	2	1	Trc.	1			Trc.		1	85	100

Note: Trc. indicates trace levels measured.

Table 6.4. Soil pH values for the tested bentonites.

Bentonite	DI Water	0.01 M $CaCl_2$
CR	8.64	8.34
CS	9.32	8.95
CT	6.97	6.81
CR+	8.51	8.22
GS	8.77	8.29
GR	8.86	8.67

Table 6.5. List of components used in RSL Visual MINTEQ speciation modeling.

Component Name (as listed)	Total concentration (millimolal)
H+1	0
Ca+2	4
Mg+2	6
Na+1	7
K+1	0.7
S (SO42-)	7.5
Cl-1	8
N (NO2-)	1.5
Al+3	0.03
As(V)	0.001
Ba+2	0.002
Cu+2	0.0002
Fe+3	0.04
Li+1	0.02
Mn+3	0.01
Ni+2	0.0003
Sr+2	0.02
Zn+2	0.005
UO2+2	0.00630176
DIC	3.5

Table 6.6. List of species and thermodynamic constants used for RSL Visual MINTEQ Speciation modeling at 25 °C.

Species	log K	delta Hr (kJ/mol)		Species	log K	delta Hr (kJ/mol)
(UO2)2(OH)2+2	-5.62	48.9		CuCl2 (aq)	-0.26	44.183
(UO2)2OH+3	-2.7	0		CuCl3-	-2.29	57.279
(UO2)3(CO3)6-6	54	-62.7		CuCl4-2	-4.59	32.5515
(UO2)3(OH)4+2	-11.9	0		CuCO3 (aq)	6.77	0
(UO2)3(OH)5+	-15.55	123		CuHCO3+	12.129	0
(UO2)3(OH)7-	-32.2	0		CuHSO4+	2.34	0
(UO2)4(OH)7+	-21.9	0		CuNO2+	2.02	0
Al(OH)2+	-10.294	122.5		CuOH+	-7.497	35.81
Al(OH)3 (aq)	-16.691	176.3		CuSO4 (aq)	2.36	8.7
Al(OH)4-	-23	183		Fe(NO2)2+	4.72	0
Al(SO4)2-	5.58	11.9		Fe(NO2)3 (aq)	6.78	0
Al2(OH)2+4	-7.694	74.62		Fe(OH)2+	-5.75	37.7
Al2(OH)2CO3+2	4.31	0		Fe(OH)3 (aq)	-15	75.3
Al3(OH)4+5	-13.888	140.24		Fe(OH)4-	-22.7	154.8
AlCl+2	-0.39	0		Fe(SO4)2-	5.38	19.2
AlOH+2	-4.997	47.81		Fe2(OH)2+4	-2.894	56.42
AlSO4+	3.84	9		Fe3(OH)4+5	-6.288	65.24
BaCl+	-0.03	12		FeCl+2	1.48	23
BaCO3 (aq)	2.71	14		FeNO2+2	3.2	0
BaHCO3+	11.309	8.4		FeOH+2	-2.02	25.1
BaOH+	-13.357	60.81		FeSO4+	4.25	25
BaSO4 (aq)	2.13	0		H2AsO4-	18.79	-21.22
Ca2UO2(CO3)3 (aq)	30.7	0		H2CO3* (aq)	16.681	-32
CaCl+	0.4	4		H3AsO4	21.09	-13.25
CaCO3 (aq)	3.22	16		HAsO4-2	11.8	-18.2
CaHCO3+	11.434	0		HCO3-	10.329	-14.6
CaOH+	-12.697	64.11		HNO2 (aq)	3.15	0
CaSO4 (aq)	2.36	7.1		HSO4-	1.99	22
CaUO2(CO3)3-2	27.18	0		KCl (aq)	-0.3	-4
Cu(CO3)2-2	10.2	0		KOH (aq)	-13.757	55.81
Cu(NO2)2 (aq)	3.03	0		KSO4-	0.85	4.1
Cu(OH)2 (aq)	-16.23	93.1		LiCl (aq)	-0.16	0
Cu(OH)3-	-26.64	0		LiOH (aq)	-13.637	55.81
Cu(OH)4-2	-39.73	178.5		LiSO4-	0.64	0
Cu2(OH)2+2	-10.494	76.62		Mg2CO3+2	3.59	0
Cu2OH+3	-6.71	27		MgCl+	0.6	4
Cu3(OH)4+2	-20.788	106.24		MgCO3 (aq)	2.92	10
CuCl+	0.3	8.3		MgHCO3+	11.34	-9.6

Table 6.6. Continued.

Species	log K	delta Hr (kJ/mol)		Species	log K	delta Hr (kJ/mol)
MgOH+	-11.417	67.81		UO2(OH)2 (aq)	-12.15	0
MgSO4 (aq)	2.26	5.8		UO2(OH)3-	-20.25	0
NaCl (aq)	-0.3	-8		UO2(OH)4-2	-32.4	0
NaCO3-	1.27	-20.35		UO2(SO4)2-2	4.14	35.1
NaHCO3 (aq)	10.029	-28.3301		UO2Cl+	0.17	8
NaOH (aq)	-13.897	59.81		UO2Cl2 (aq)	-1.1	15
NaSO4-	0.74	1		UO2CO3 (aq)	9.94	5
Ni(NO2)2 (aq)	1.79	0		UO2OH+	-5.25	0.9
Ni(OH)2 (aq)	-18.994	0		UO2SO4 (aq)	3.15	19.5
Ni(OH)3-	-29.991	0		Zn(CO3)2-2	7.3	0
Ni(SO4)2-2	0.82	0		Zn(NO2)2 (aq)	1.2	0
NiCl+	-0.43	2		Zn(OH)2 (aq)	-16.894	0
NiCl2 (aq)	-1.89	0		Zn(OH)3-	-28.391	0
NiCO3 (aq)	4.57	0		Zn(OH)4-2	-41.188	0
NiHCO3+	12.42	0		Zn(SO4)2-2	3.28	0
NiNO2+	1.38	0		Zn2OH+3	-8.997	63.81
NiOH+	-9.897	51.81		ZnCl+	0.46	5.4
NiSO4 (aq)	2.3	5.8		ZnCl2 (aq)	0.45	35.6
OH-	-13.997	55.81		ZnCl3-	0.5	40
SrCl+	0.19	8		ZnCl4-2	0.2	45.9
SrCO3 (aq)	2.81	21		ZnCO3 (aq)	4.76	0
SrHCO3+	11.539	10.4		ZnHCO3+	11.829	0
SrOH+	-13.177	60.81		ZnNO2+	0.78	0
SrSO4 (aq)	2.3	8		ZnOH+	-8.997	55.81
UO2(CO3)2-2	16.61	18.5		ZnSO4 (aq)	2.34	6.2
UO2(CO3)3-4	21.84	-39.2				

Table 6.7. Oversaturated species in RSL based on Visual MINTEQ modeling.

Mineral	Chemical Formula	Log I.A.P.	Highest SI	pH of Highest SI
Al(OH)3 (Soil)	$Al(OH)_3$	11.435	3.145	6.7
Al2O3 (s)	Al_2O_3	22.871	3.218	6.7
Al4(OH)10SO4 (s)	$Al_4(OH)_{10}SO_4$	29.887	7.187	6.6
Alunite	$KAl_3(SO_4)_2(OH)_6$	6.279	7.679	6.3
Aragonite	$CaCO_3$	-6.309	2.027	10
Artinite	$Mg_2(CO_3)(OH)_2{:}3H_2O$	11.232	1.632	10
BaHAsO4:H2O (s)	$BaHAsO_4{:}H_2O$	-24.198	0.442	8.6-8.9
Barite	$BaSO_4$	-8.649	1.331	4.8-5.0
Bixbyite	$(Mn,Fe)_2O_3$	48.645	49.289	10
Boehmite	γ-AlOOH	11.435	2.857	6.7
Brucite	$Mg(OH)_2$	17.308	0.208	10
CaCO3xH2O (s)	$CaCO_3{:}H_2O$	-6.309	0.835	10
Calcite	$CaCO_3$	-6.309	2.171	10
Cupric Ferrite	$CuFe_2O_4$	26.75	20.762	8.7
Diaspore	α-AlOOH	11.435	4.562	6.7
Dolomite (disordered)	$CaMg(CO_3)_2$	-12.384	4.156	10
Dolomite (ordered)	$CaMg(CO_3)_2$	-12.384	4.706	10
Fe(OH)2.7Cl.3 (s)	$Fe(OH)_{2.7}Cl_{0.3}(s)$	6.24	9.284	8.4
Ferrihydrite	$Fe(OH)_3$	9.42	6.22	8.5
Ferrihydrite (aged)	$Fe(OH)_3$	9.42	6.73	8.5
Gibbsite (C)	$Al(OH)_3$	11.435	3.695	6.7
Goethite	α-FeOOH	9.42	8.929	8.5
Hematite	Fe_2O_3	18.84	20.258	8.5
Huntite	$CaMg_3(CO_3)_4$	-24.536	5.432	10
Hydromagnesite	$Mg_5(CO_3)_4(OH)_2{:}4H_2O$	-6.995	1.771	10
K-Jarosite	$KFe^{3+}{}_3(SO_4)_2(OH)_6$	-4.569	6.431	6.4-6.6
Lepidocrocite	γ-FeOOH	9.42	8.049	8.5
Maghemite	$Fe^{3+}{}_2O_3$	18.84	12.454	8.5
Magnesioferrite	$MgFe^{3+}{}_2O_4$	33.77	16.911	9.6
Magnesite	$MgCO_3$	-6.076	1.384	10
Malachite	$Cu_2(CO_3)(OH)_2$	-5.231	0.238	10
Na-Jarosite	$NaFe^{3+}{}_3(SO_4)_2(OH)_6$	-3.568	1.752	6.3-6.7
Ni(OH)2 (c)	$Ni(OH)_2$ (c)	11.99	1.200	10
Strontianite	$SrCO_3$	-8.538	0.732	10
Tenorite (am)	CuO	9.077	0.587	10
Tenorite (c)	CuO	9.077	1.437	10
Vaterite	$CaCO_3$	-6.309	1.605	10

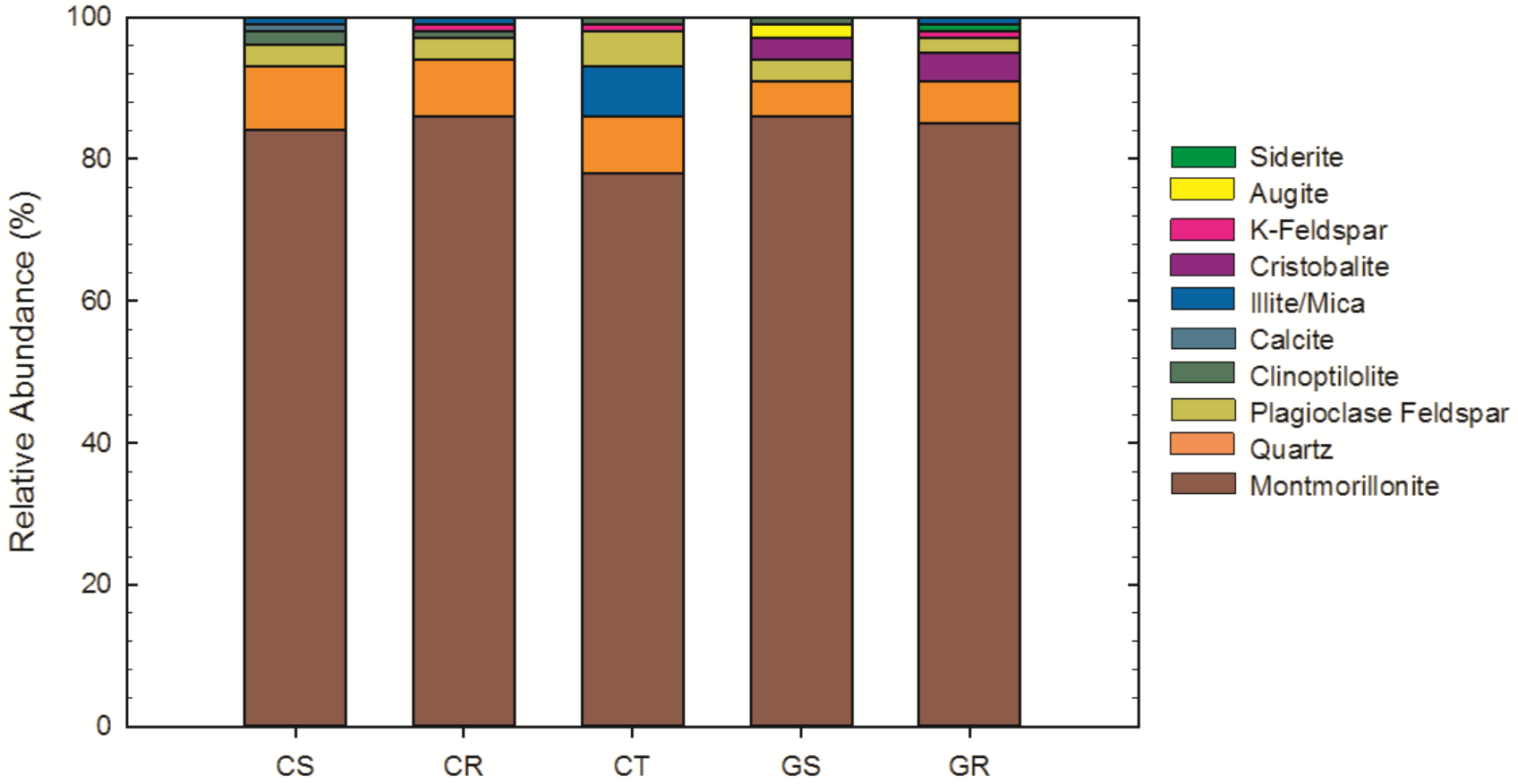

Figure 6.1. Comparison of the crystalline mineralogical content of the study bentonites as analyzed by XRD testing.

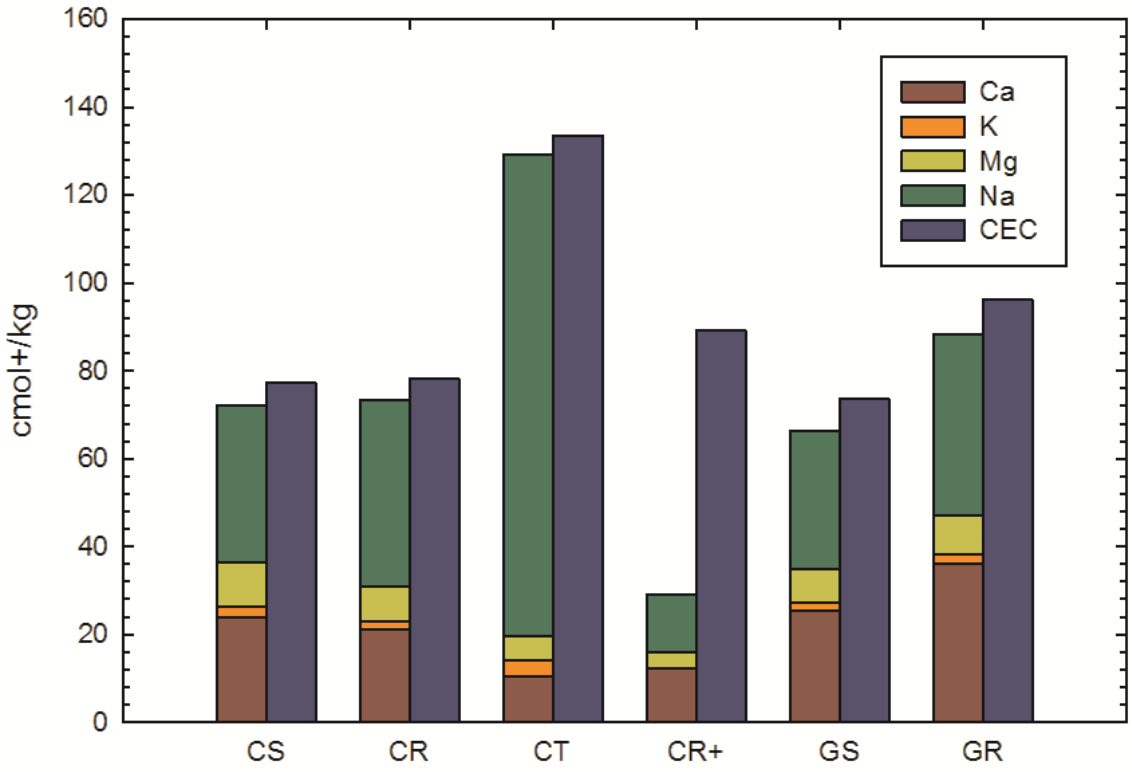

Figure 6.2. Comparison of bound cations and cation exchange capacity measurements for the studied bentonites.

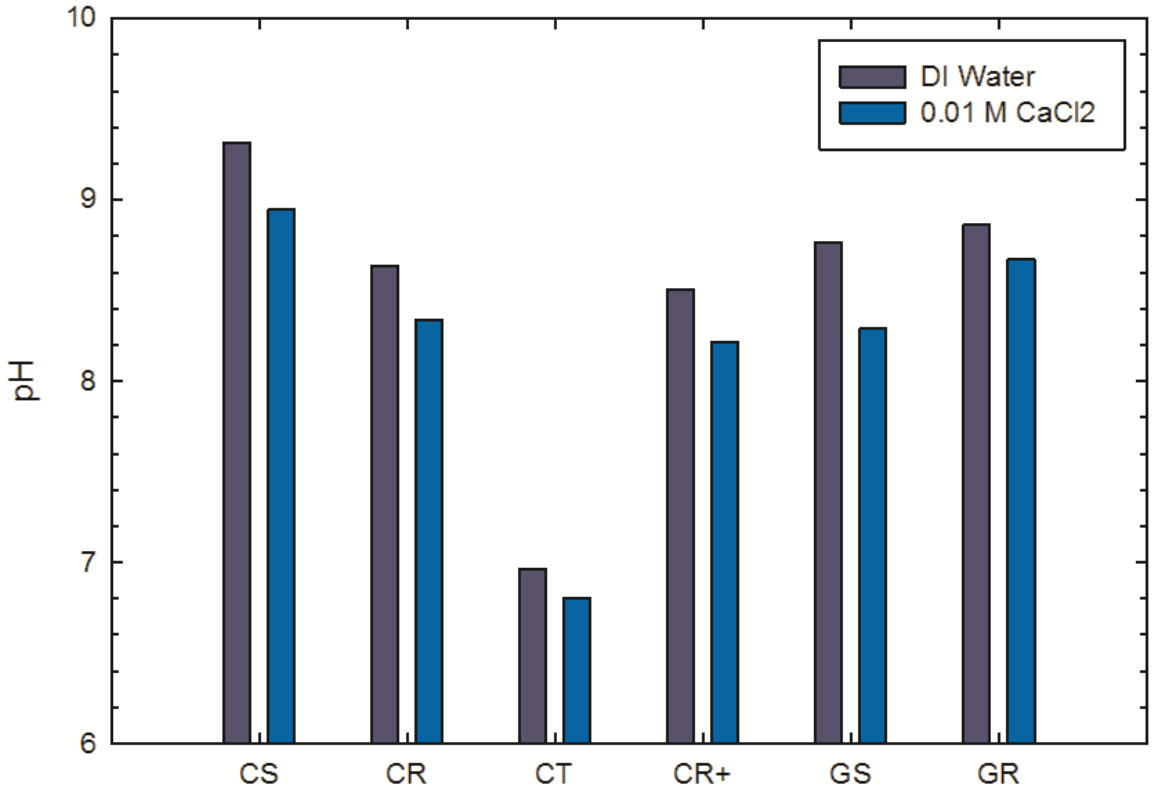

Figure 6.3. Comparison of measured pH values for the bentonite suite from both solutions used for soil pH measurement as indicated by ASTM D 4972.

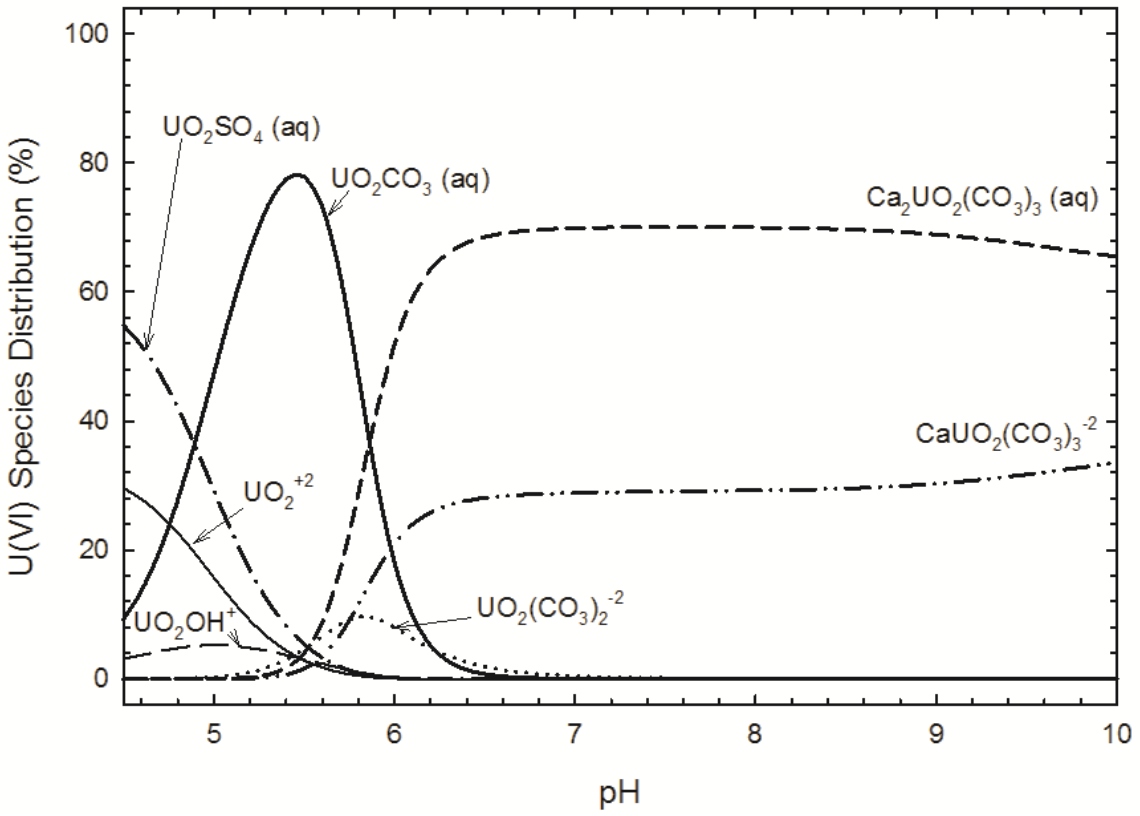

Figure 6.4. U(VI) species distribution in the RSL mixture across the tested pH range. In addition to the species shown on the graph, six additional species are expected at concentrations of less than 3% of the total speciation: $(UO_2)(OH)_2^{2+}$, $(UO_2)_3(OH)_5^{+}$, $UO_2(OH)_2$ (aq), UO_2Cl^{+}, $UO_2(CO_3)_3^{4-}$, and $UO_2(SO_4)_2^{2-}$.

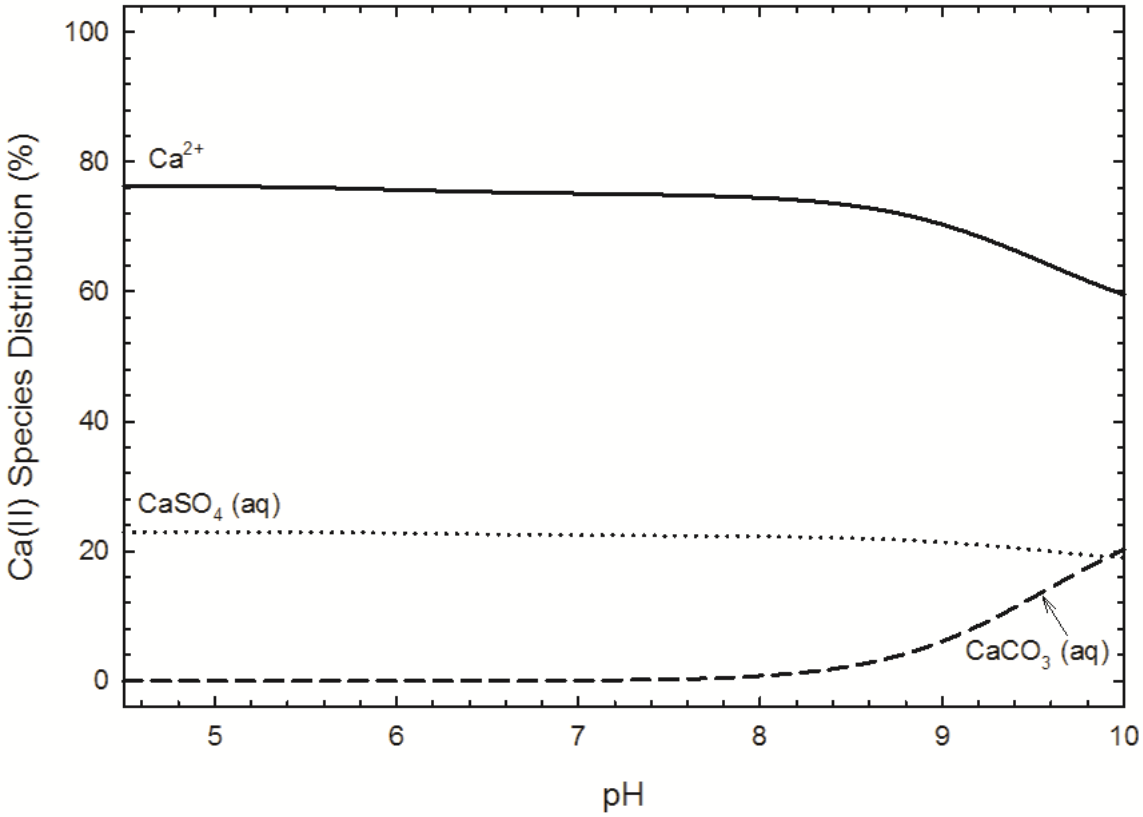

Figure 6.5. Ca speciation in RSL. In addition to the three primary species indicated on the graph, 5 additional species are expected at concentrations of less than 2% of the total species distribution: $CaOH^+$, $CaCl^+$, $Ca_2UO_2(CO_3)_3$ (aq), $CaUO_2(CO_3)_3^{2-}$, and $CaHCO_3^+$.

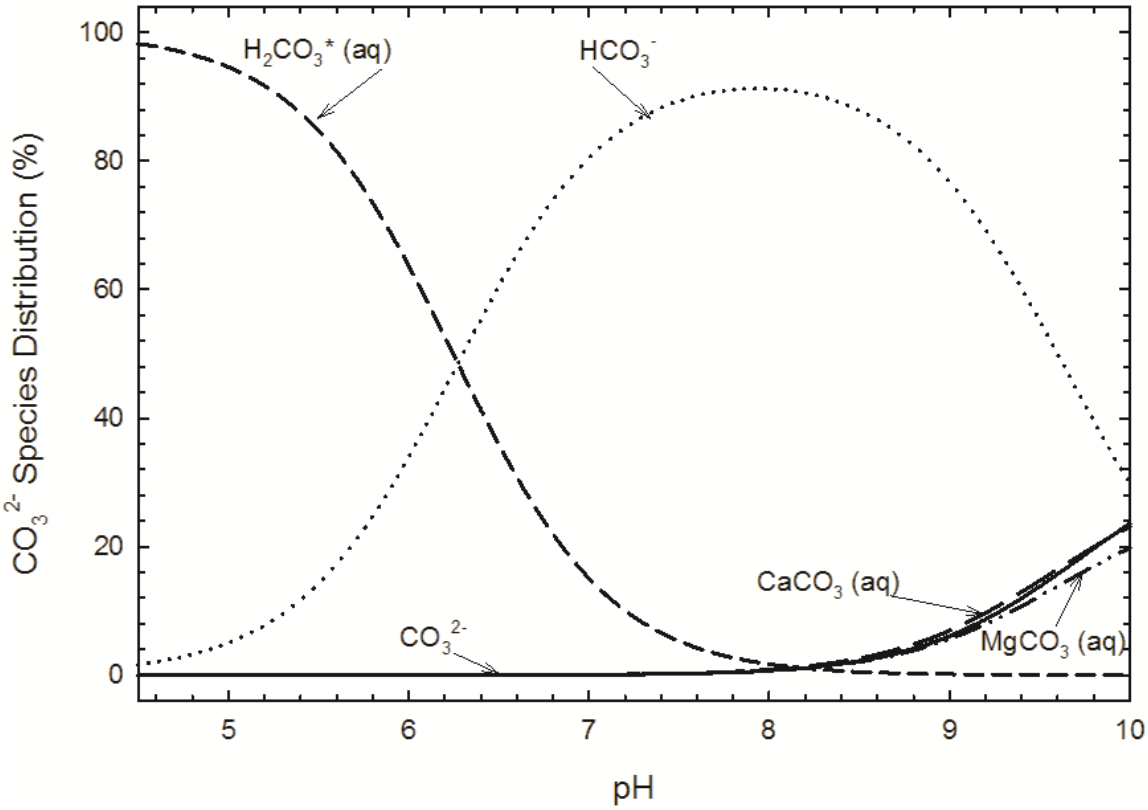

Figure 6.6. Carbonate (CO_3^{2-}) species distribution in RSL mixture across the tested pH range. In addition to the species presented in the graph, 12 additional species are anticipated at maximum concentrations of less than 2% of the total speciation: $Mg_2CO_3^{2+}$, $Ca_2UO_2(CO_3)_3$ (aq), $CaUO_2(CO_3)_3^{2-}$, UO_2CO_3 (aq), $UO_2(CO_3)_2^{2-}$, $MgHCO_3^+$, $CaHCO_3^+$, $SrHCO_3^+$, $SrCO_3$ (aq), $NaCO_3^-$, $NaHCO_3$ (aq), and $Al_2(OH)_2CO_3^{2+}$.

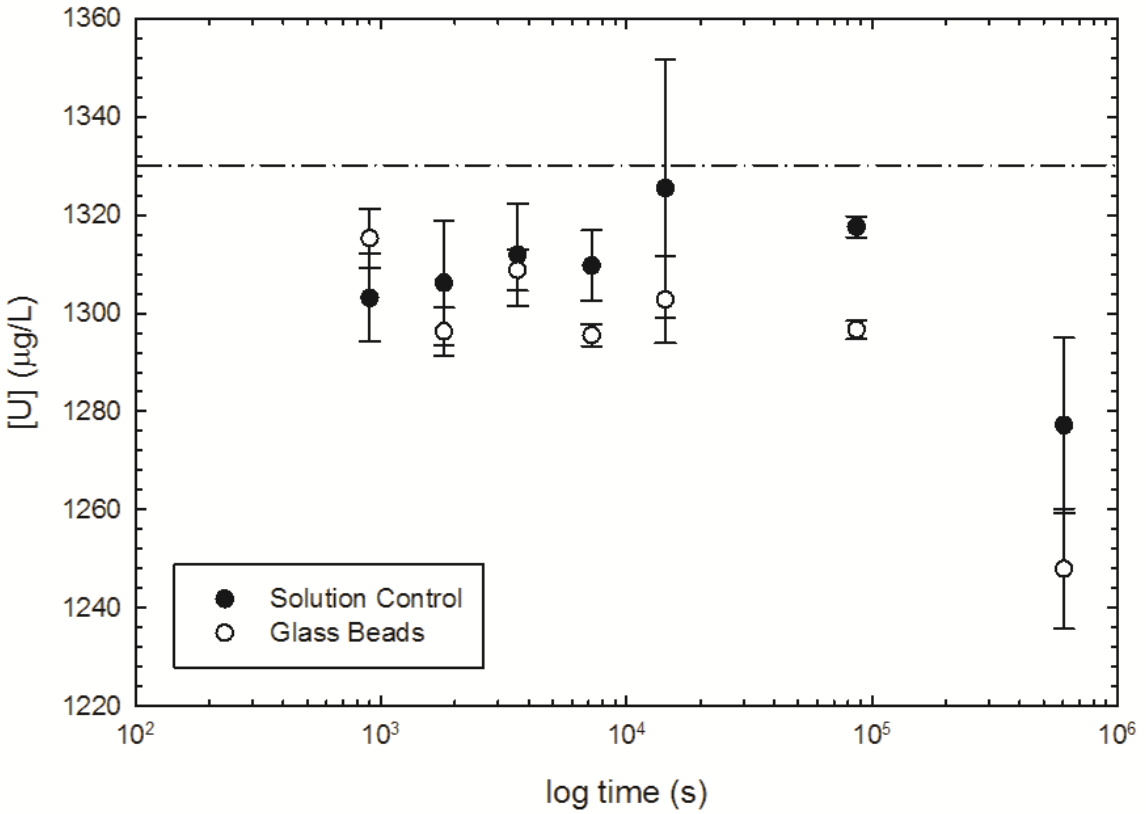

Figure 6.7. Measured U concentrations, [U], in µg/L, for LLW kinetics solution control experimentation and glass bead sorption controls. Measured time frames ranged from 15 min (900 s) to 7 d (604800 s). The dashed line indicates 1330 µg/L, the concentration value chosen to represent the initial concentration value throughout the remainder of LLW experimentation, as compared to the theoretical added concentration of 1500 µg/L.

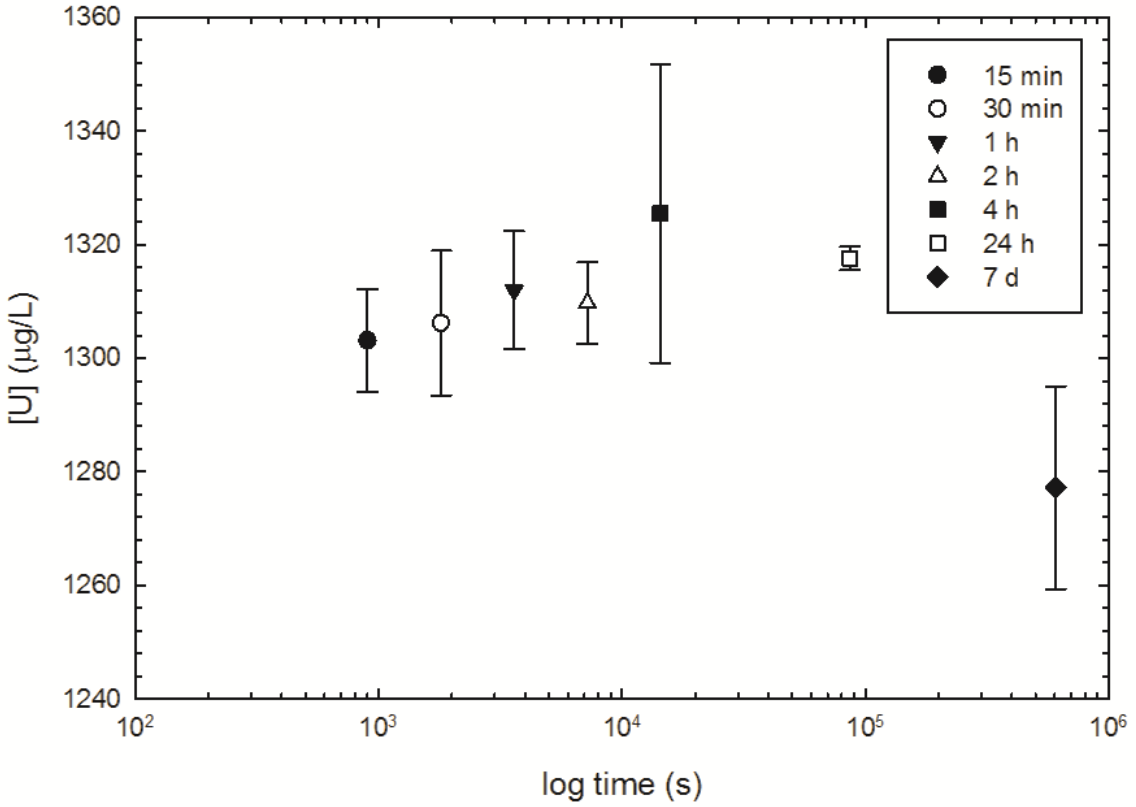

Figure 6.8. Comparison of U concentrations measured in solution during solution control kinetics experimentation. Measured time frames ranged from 15 min (900 s) to 7 d (604800 s). The initial U concentration across all experimentation was averaged to 1330 µg/L.

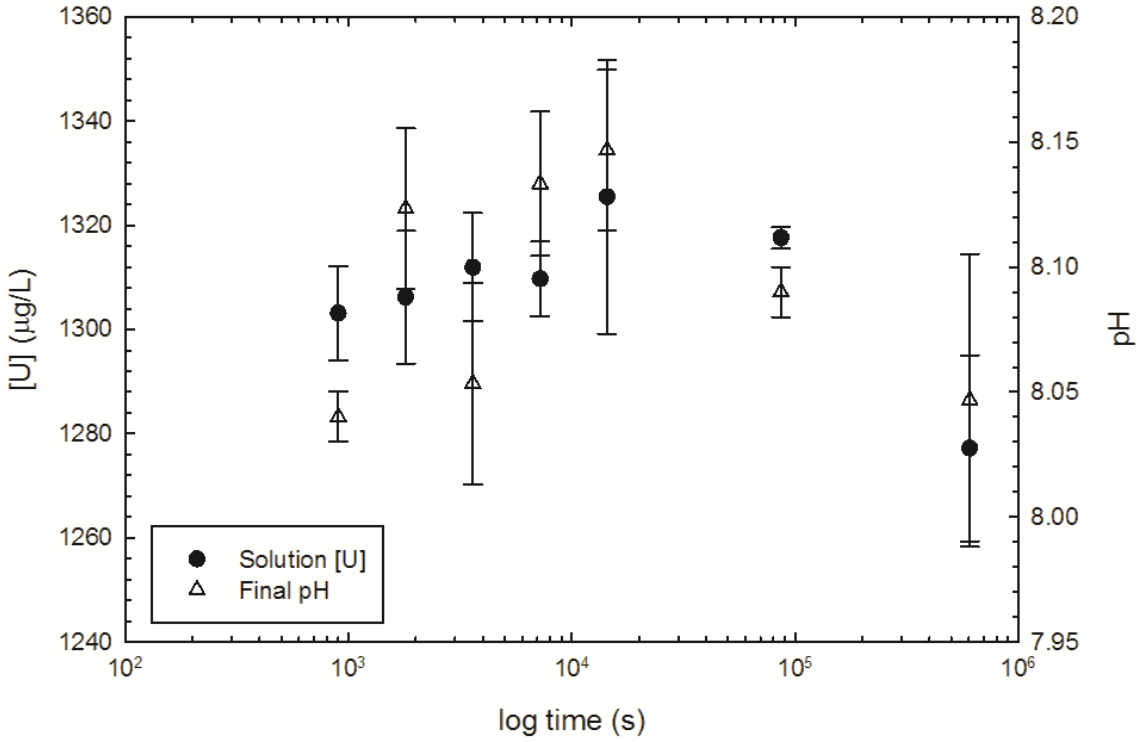

Figure 6.9. Comparison of U concentrations to final pH during LLW kinetics experimentation for the solution control experimentation. The initial U concentration across all experimentation was averaged to 1330 µg/L.

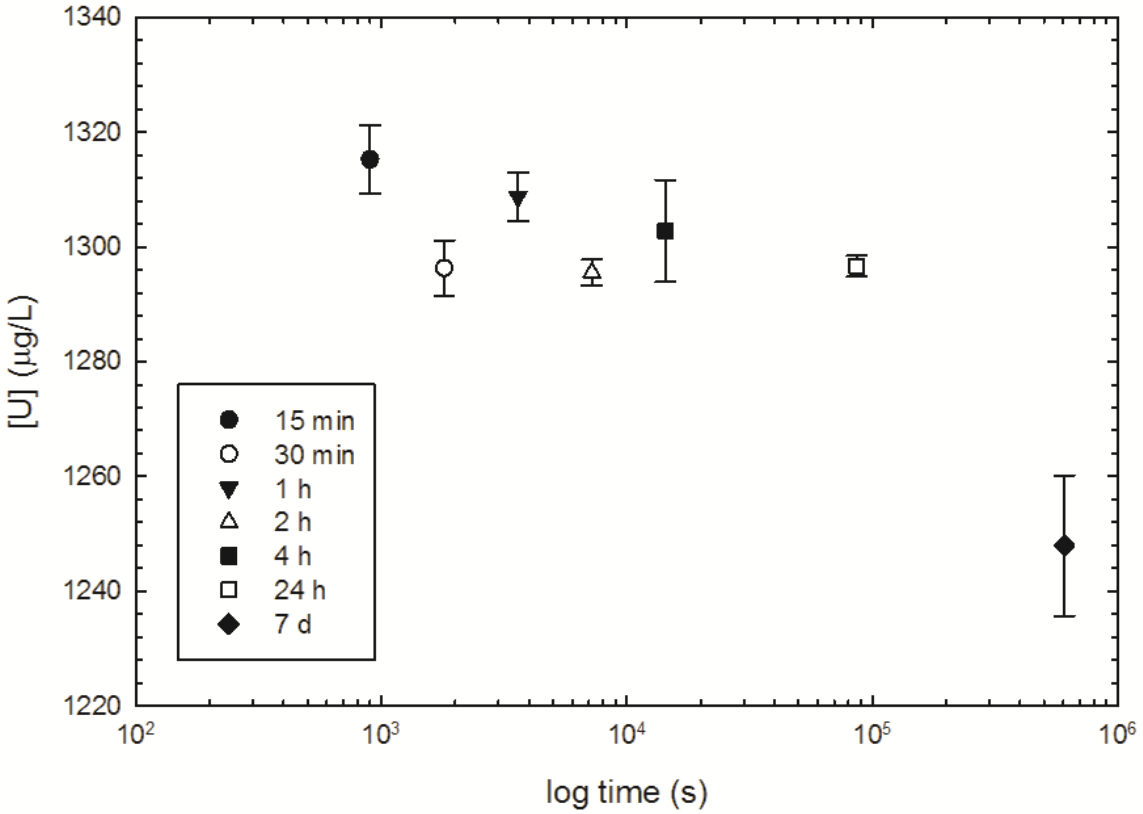

Figure 6.10. Comparison of U concentrations measured in solution during glass beads kinetics experimentation. Measured time frames ranged from 15 min (900 s) to 7 d (604800 s). The initial U concentration across all experimentation was 1330 µg/L.

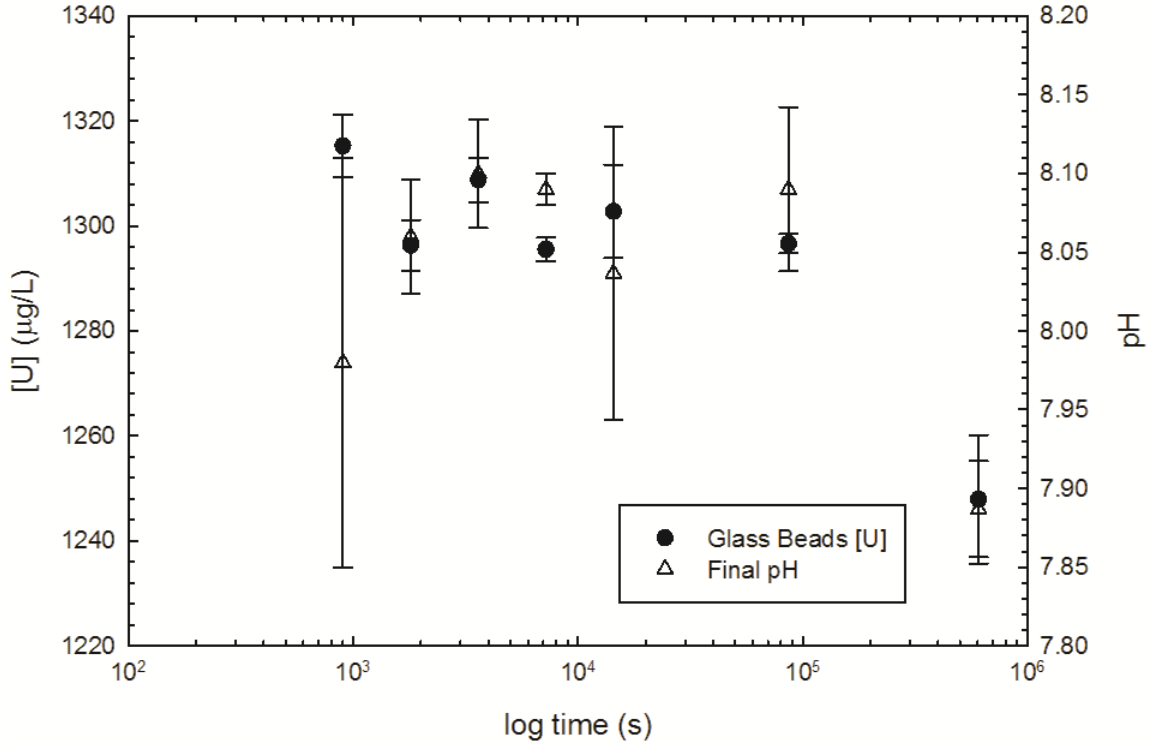

Figure 6.11. Comparison of U concentrations to final pH during LLW kinetics experimentation for the glass bead sorption control experimentation. The initial U concentration across all experimentation was 1330 µg/L.

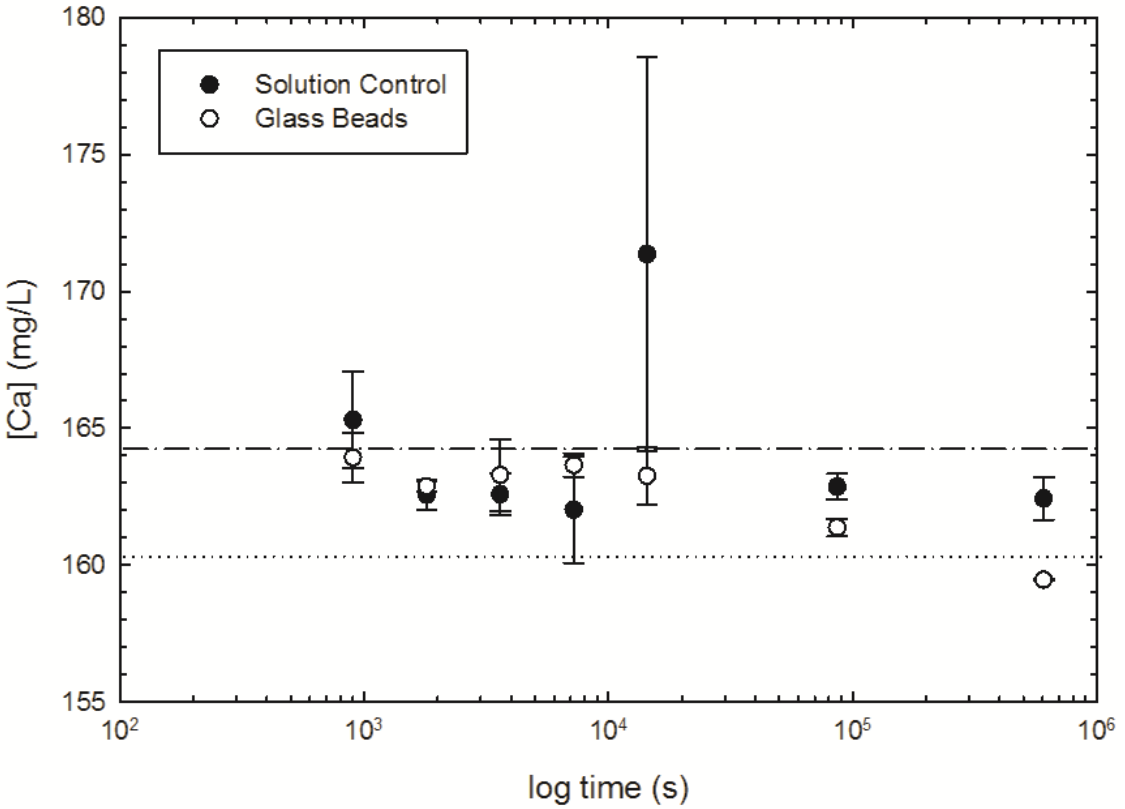

Figure 6.12. Measured Ca concentrations, [Ca], in mg/L, for LLW kinetics solution control experimentation and glass bead sorption controls. Measured time frames ranged from 15 min (900 s) to 7 d (604800 s). The upper dashed line indicates 164.159 mg/L, the concentration value chosen to represent the initial concentration value throughout the remainder of LLW experimentation, as compared to the lower dashed line at 160.312 mg/L, the theoretical added concentration.

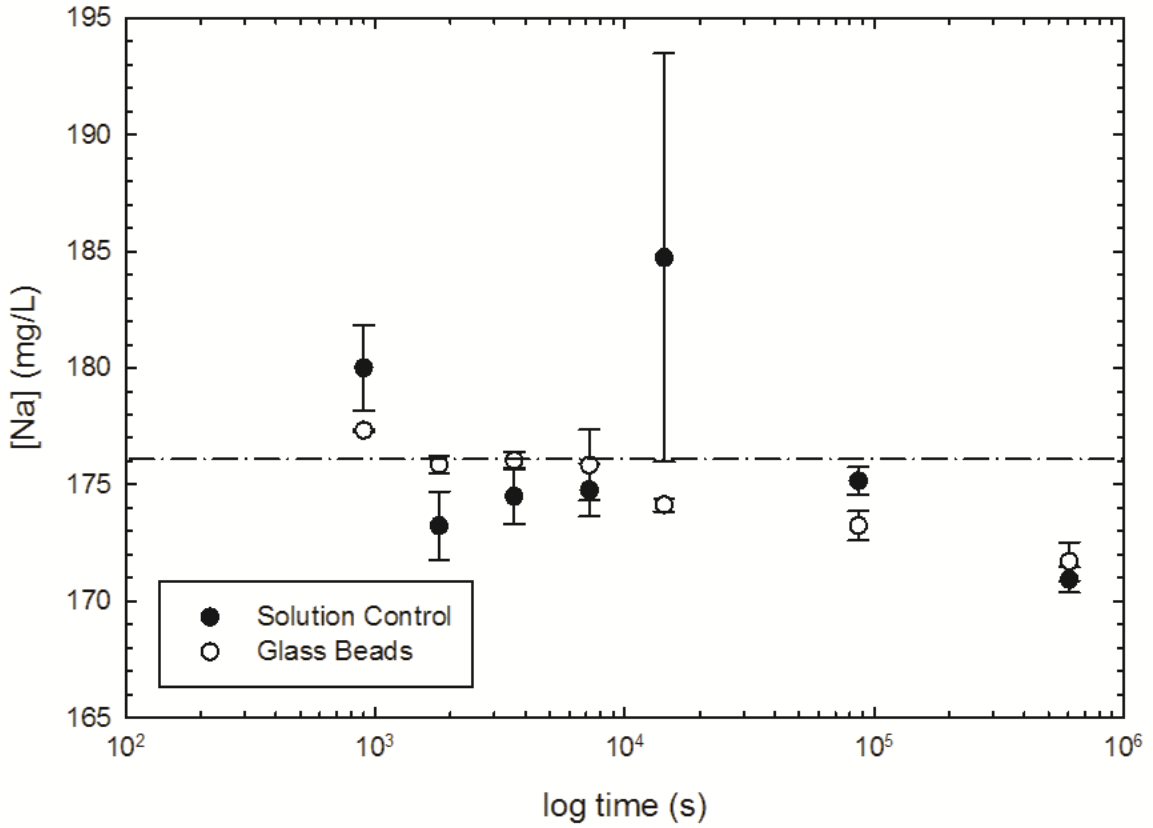

Figure 6.13. Measured Na concentrations, [Na], in mg/L, for LLW RSL kinetics solution control experimentation and glass bead sorption controls. Measured time frames ranged from 15 min (900 s) to 7 d (604800 s). The dashed line indicates 176.183 mg/L, the concentration value chosen to represent the initial concentration value throughout the remainder of RSL experimentation, as compared to 160.929 mg/L, the theoretical added concentration, which falls below the shown y-axis.

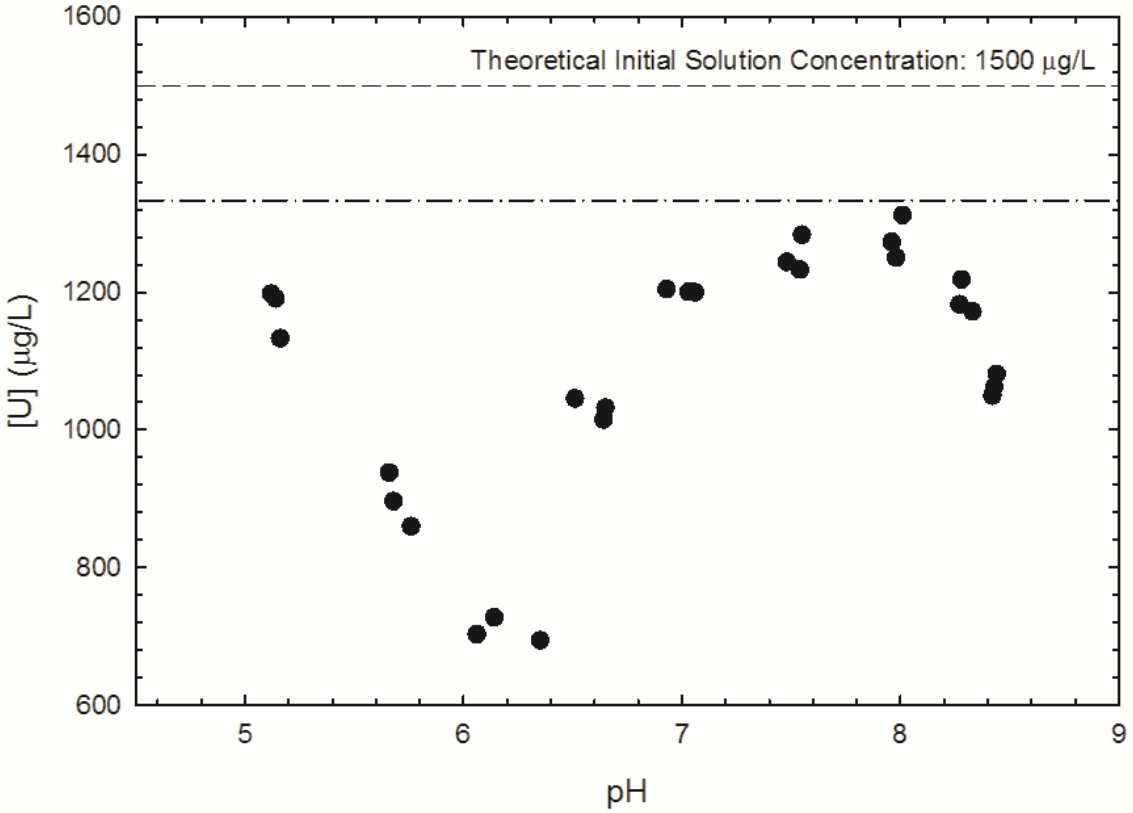

Figure 6.14. Measured concentration of U (in µg/L) for sorption edge solution control experimentation with the RSL mixture. The upper dashed line indicates the theoretical initial RSL solution concentration of 1500 µg/L, while the lower dashed line shows the initial solution concentration, 1330 µg/L, identified during the kinetics control experimentation.

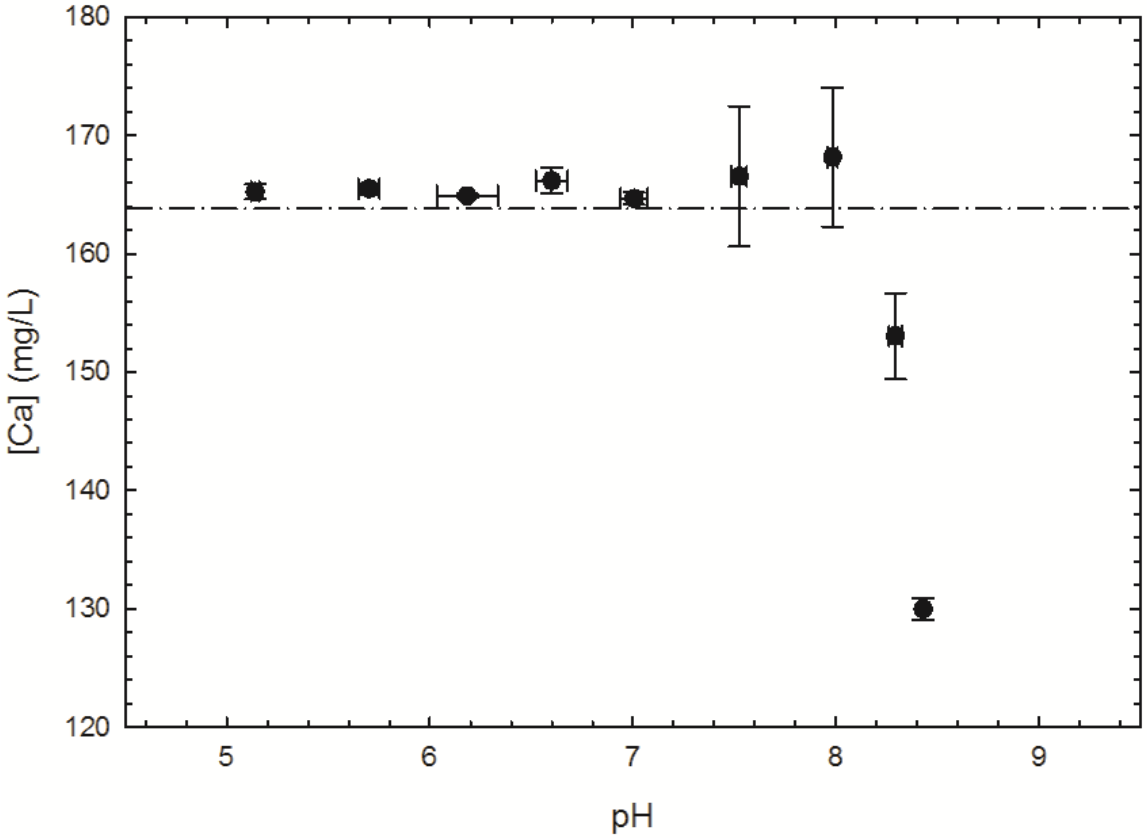

Figure 6.15. Measured concentration of Ca (in mg/L) in RSL for sorption edge and envelope solution control experimentation. The dashed line indicates 164.159 mg/L Ca, the average solution concentration derived from RSL kinetics solution control experimentation.

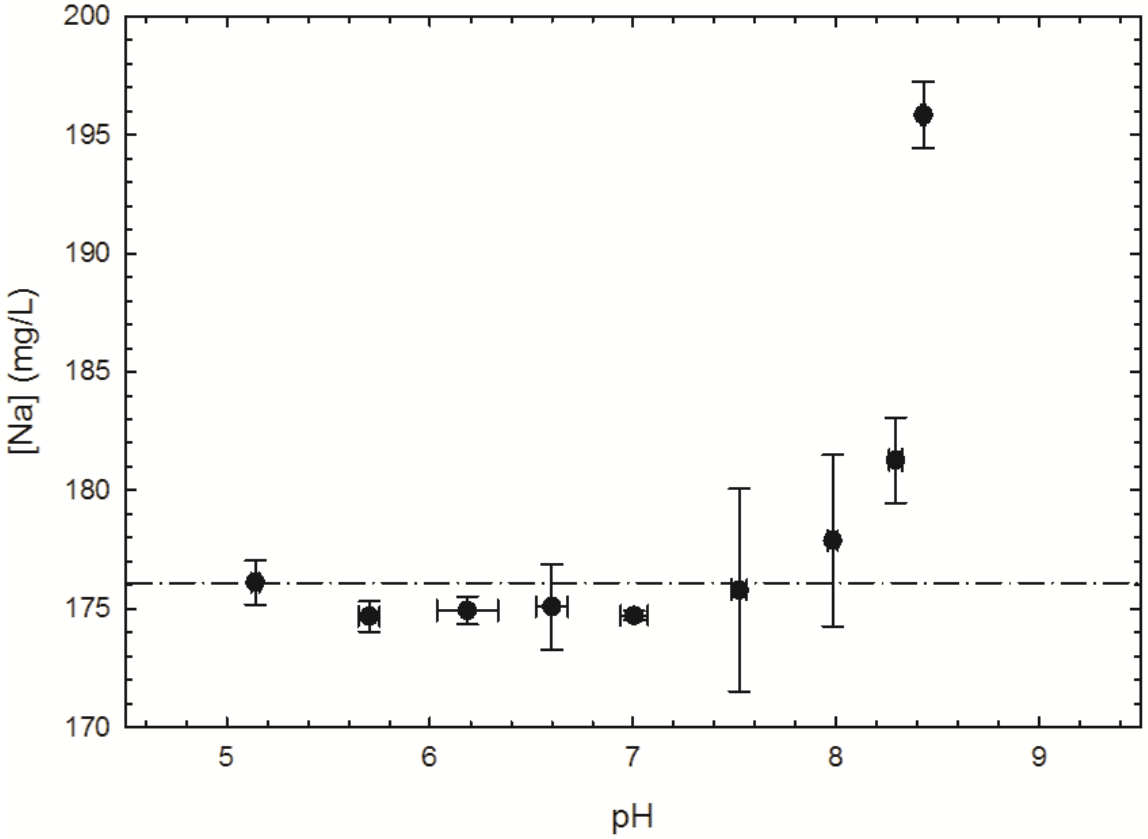

Figure 6.16. Measured Na concentration (in mg/L) in RSL for sorption edge and envelope solution control experimentation. The dashed line indicates 176.183 mg/L Na, the average solution concentration derived from RSL kinetics solution control experimentation.

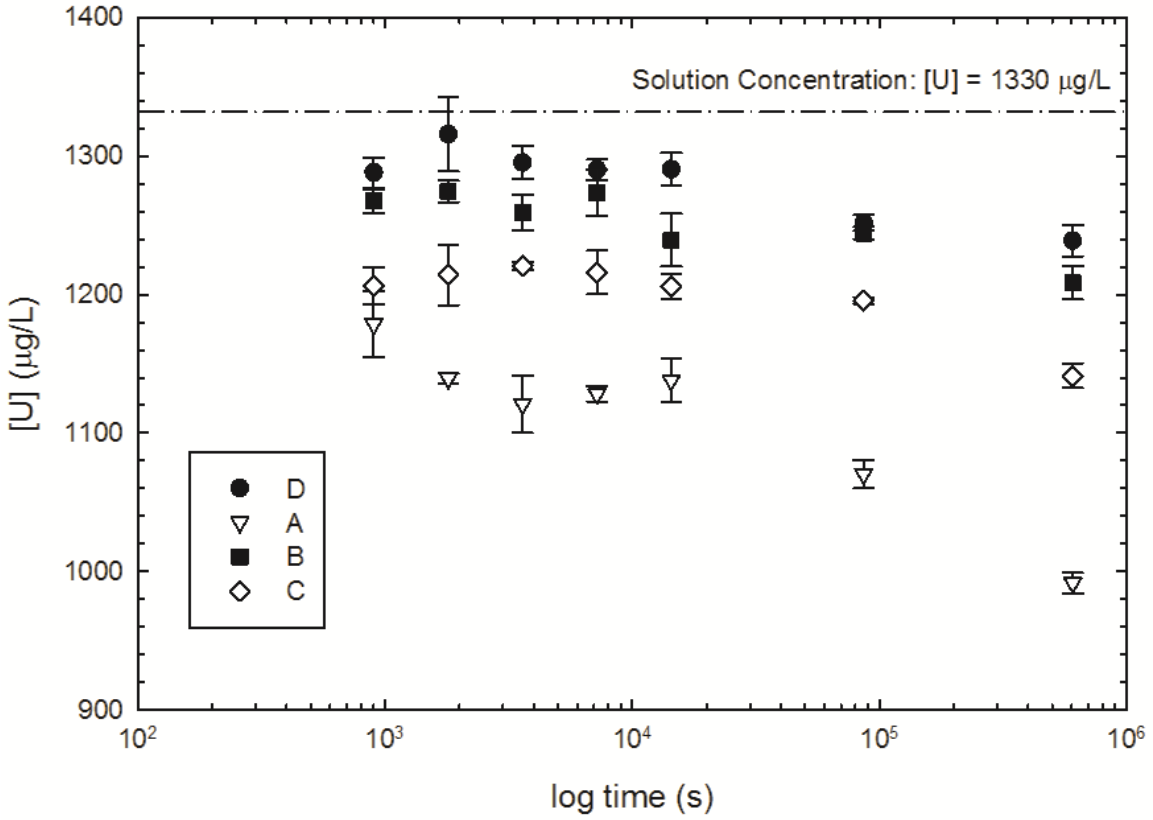

Figure 6.17. Comparison of U concentrations measured in solution during LLW kinetics experimentation for the initial soil suite used during single radionuclide experimentation. Measured time frames ranged from 15 min (900 s) to 7 d (604800 s). Initial U concentration across all experimentation was 1330 µg/L, as indicated by the dotted line.

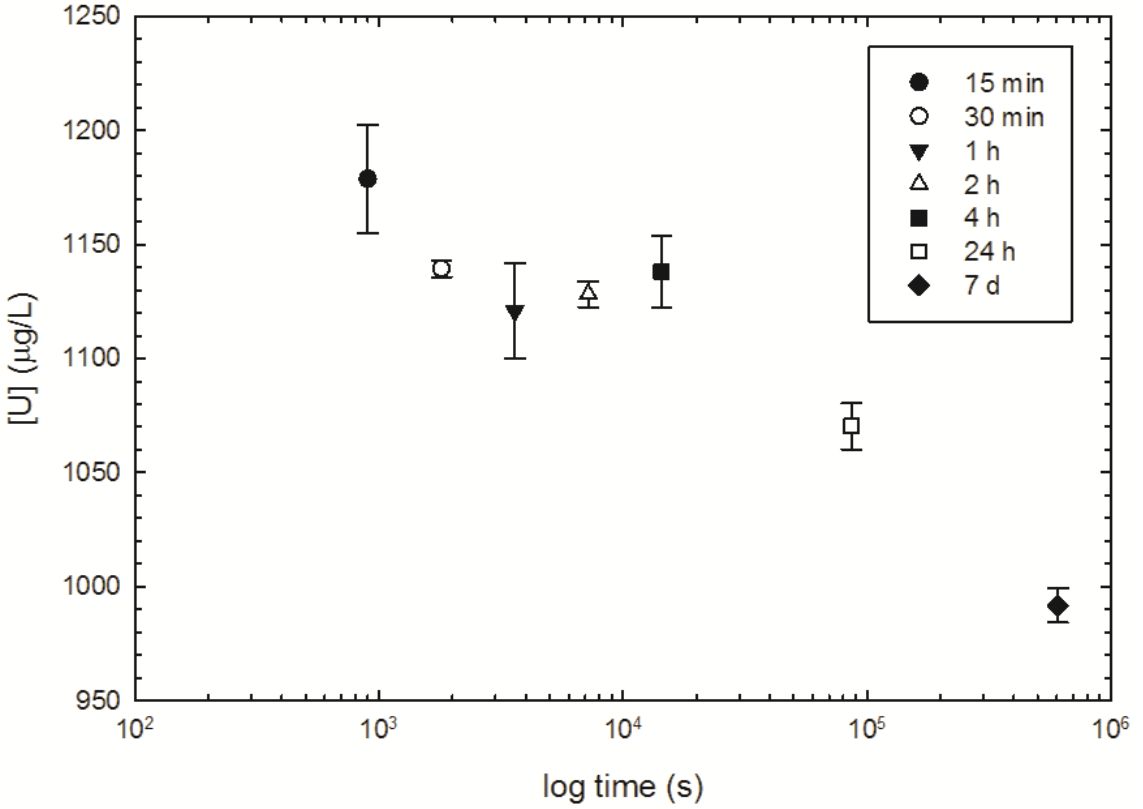

Figure 6.18. Comparison of U concentrations measured in solution for Soil *A* during kinetics experimentation. Measured time frames ranged from 15 min (900 s) to 7 d (604800 s). The initial U concentration across all experimentation was 1330 µg/L.

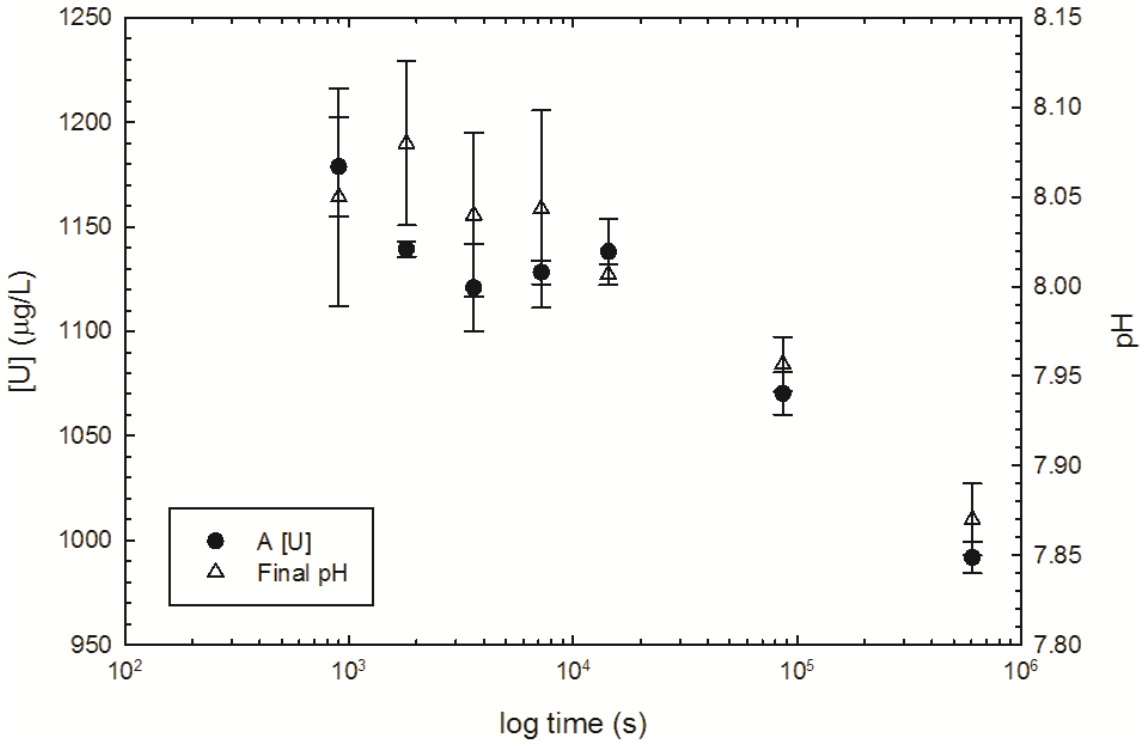

Figure 6.19. Comparison of U concentrations to final pH during LLW kinetics experimentation for Soil *A*. The initial U concentration across all experimentation was 1330 µg/L.

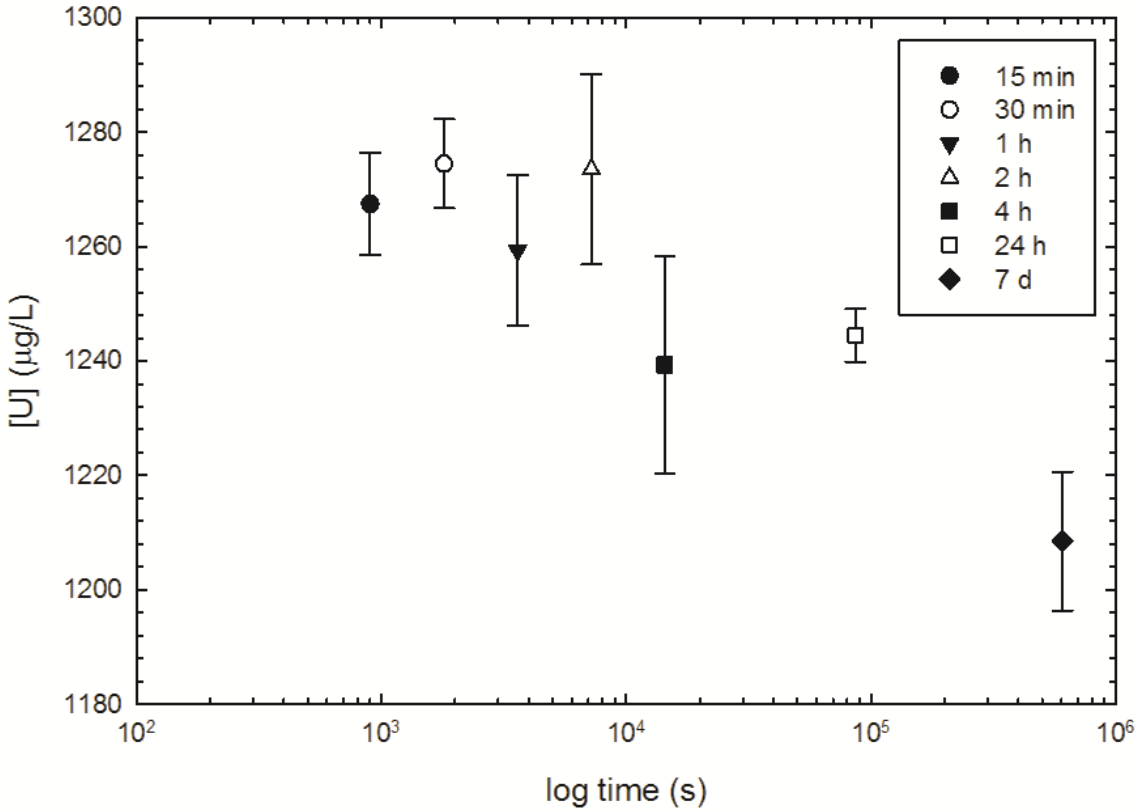

Figure 6.20. Comparison of U concentrations measured in solution for Soil *B* during kinetics experimentation. Measured time frames ranged from 15 min (900 s) to 7 d (604800 s). The initial U concentration across all experimentation was 1330 µg/L.

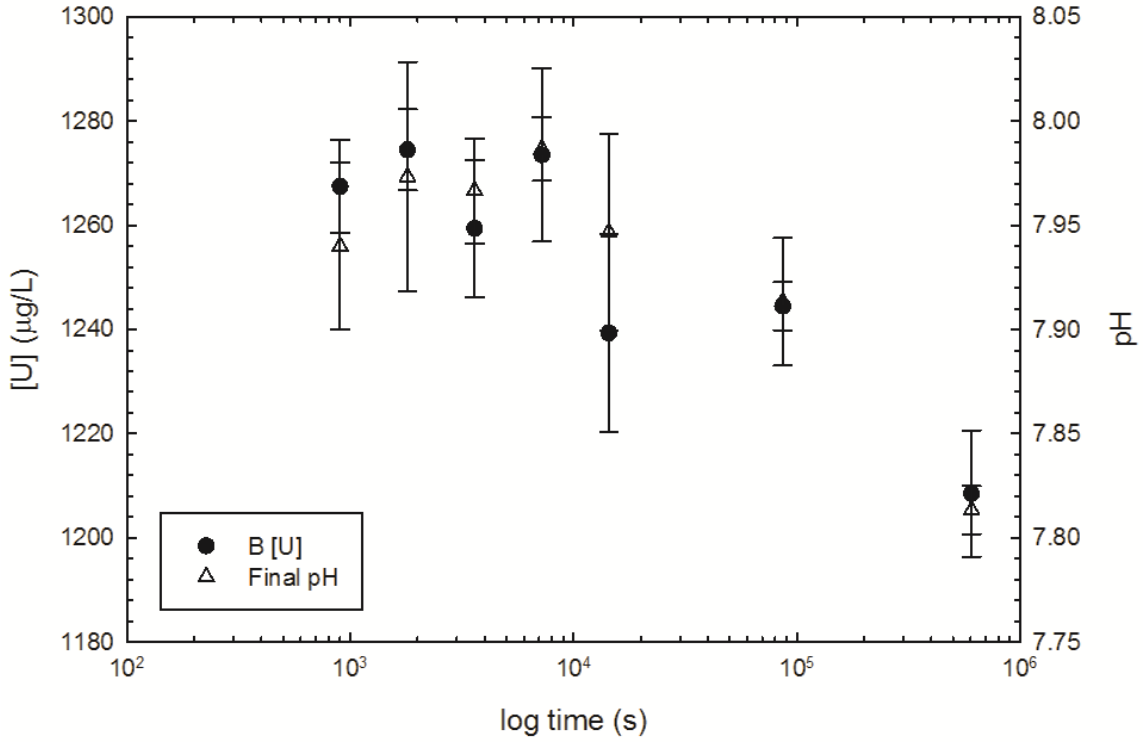

Figure 6.21. Comparison of U concentrations to final pH during LLW kinetics experimentation for Soil *B*. The initial U concentration across all experimentation was 1330 µg/L.

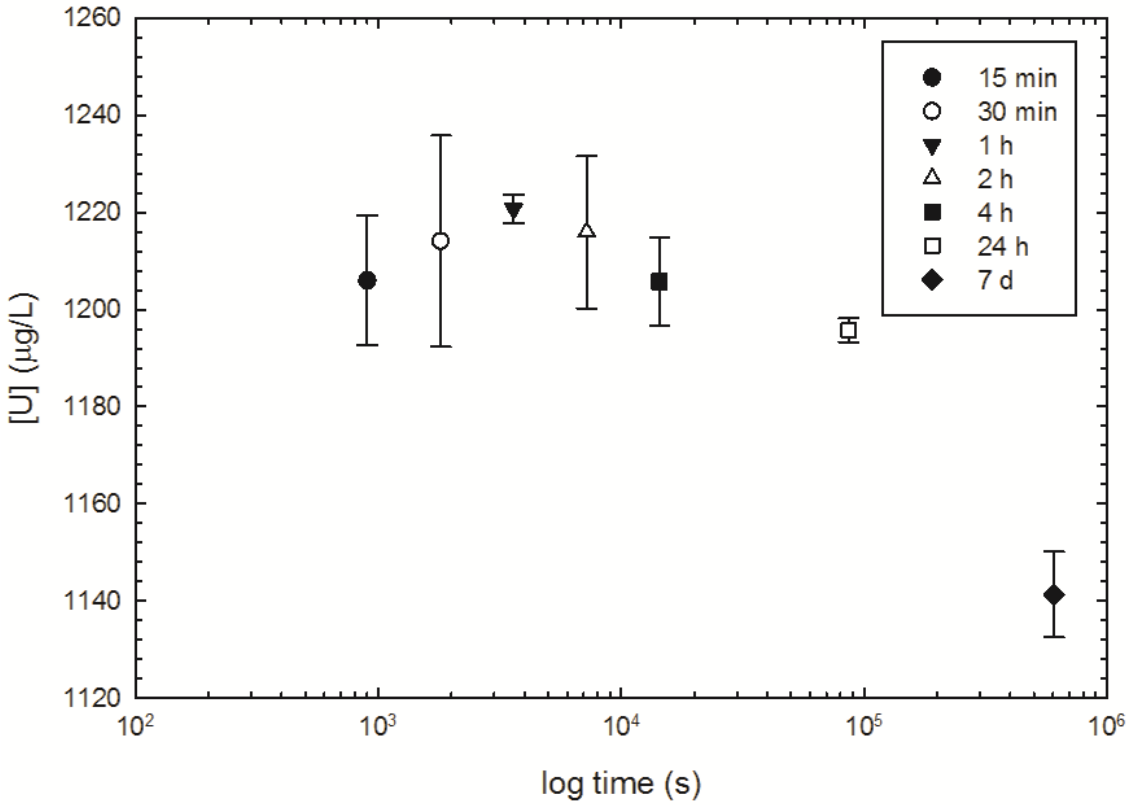

Figure 6.22. Comparison of U concentrations measured in solution for Soil *C* during kinetics experimentation. Measured time frames ranged from 15 min (900 s) to 7 d (604800 s). The initial U concentration across all experimentation was 1330 µg/L.

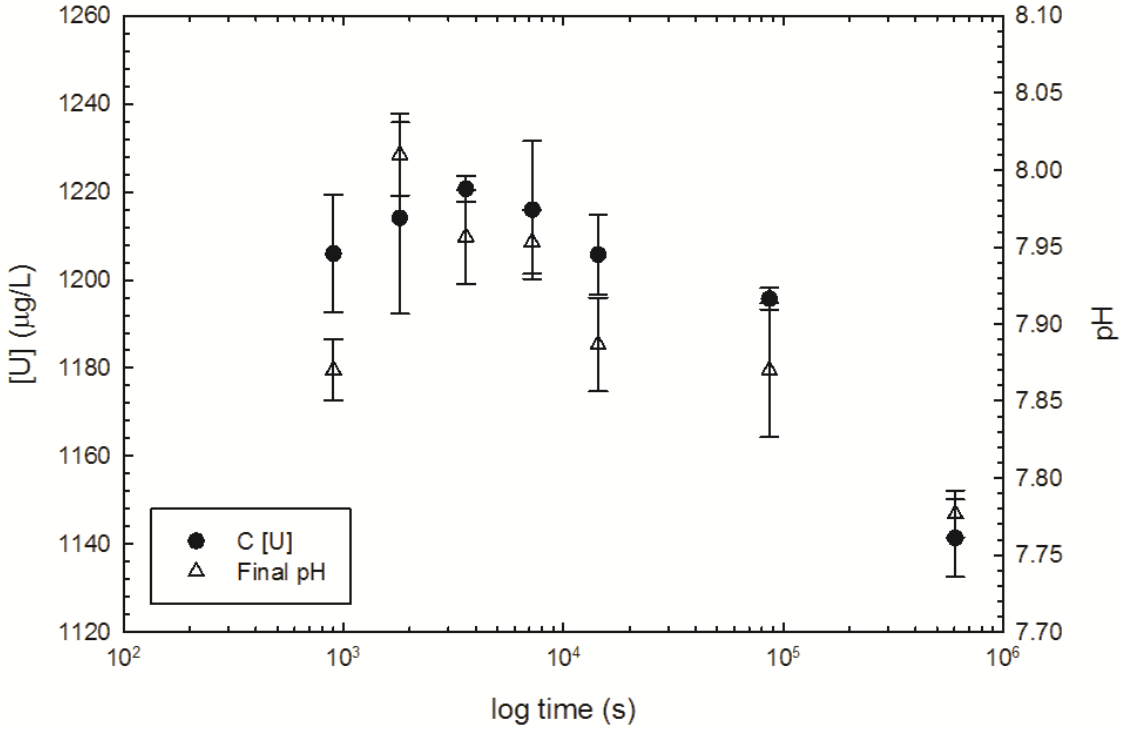

Figure 6.23. Comparison of U concentrations to final pH during LLW kinetics experimentation for Soil *C*. The initial U concentration across all experimentation was 1330 µg/L.

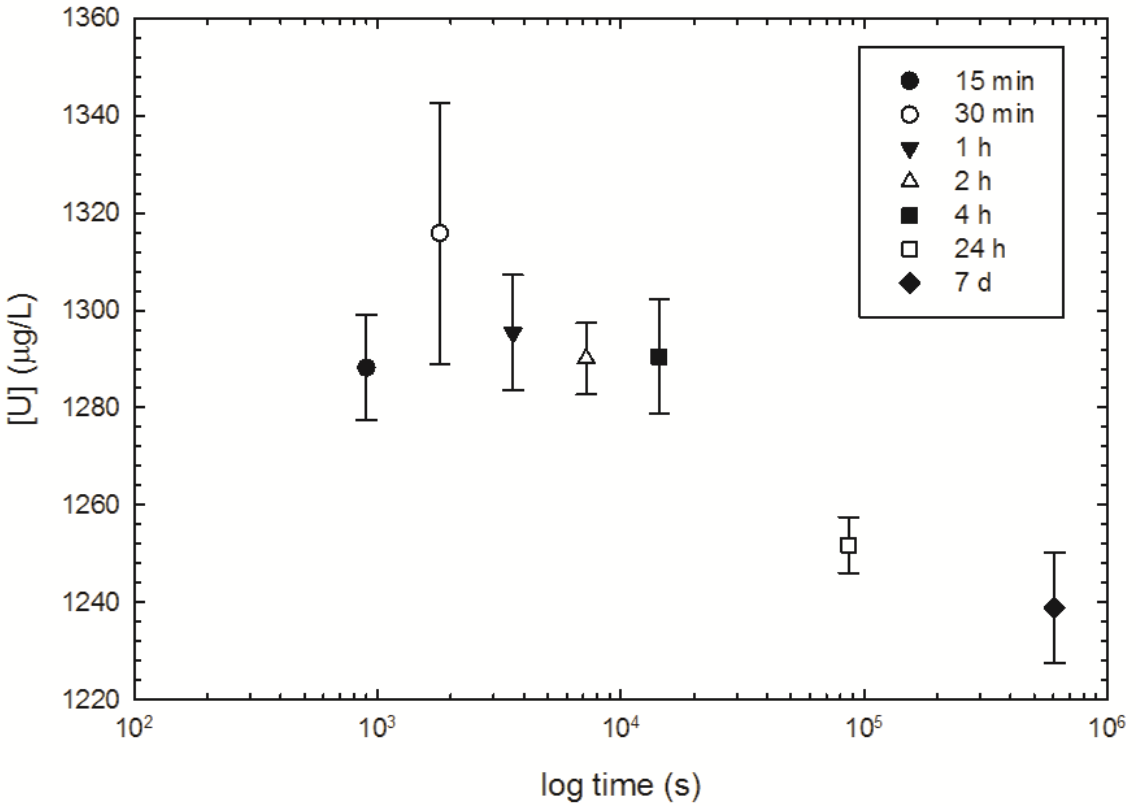

Figure 6.24. Comparison of U concentrations measured in solution for Soil *D* during kinetics experimentation. Measured time frames ranged from 15 min (900 s) to 7 d (604800 s). The initial U concentration across all experimentation was 1330 µg/L.

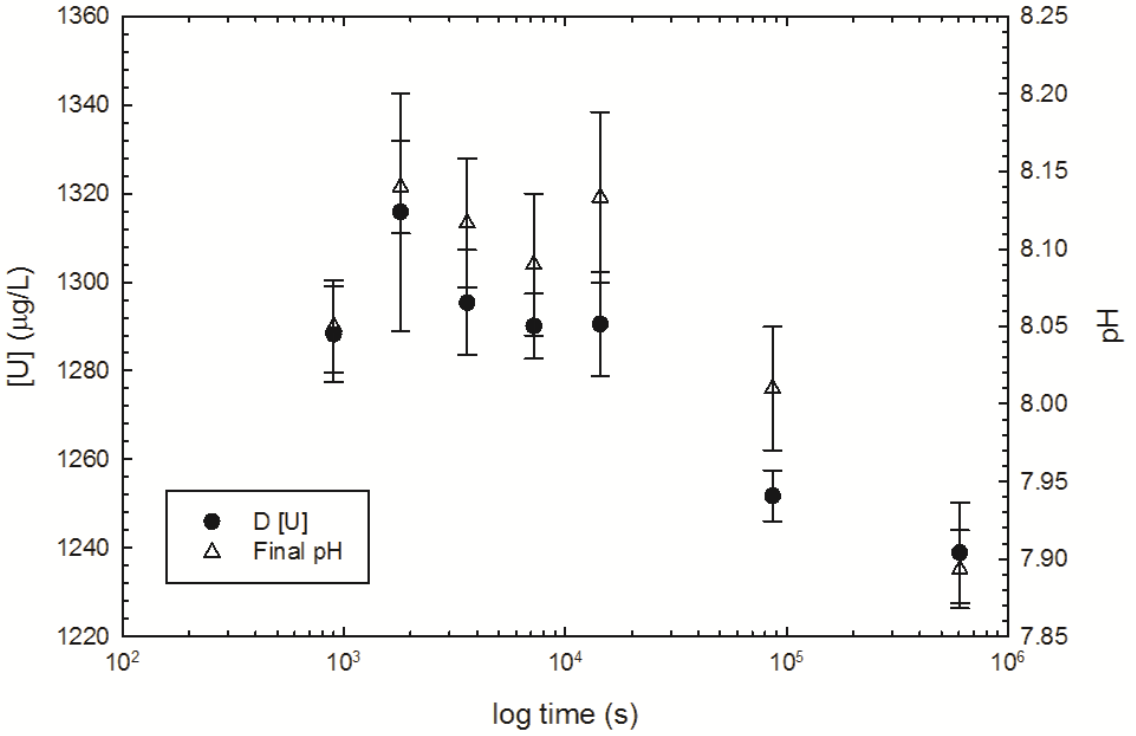

Figure 6.25. Comparison of U concentrations to final pH during LLW kinetics experimentation for Soil *D*. The initial U concentration across all experimentation was 1330 µg/L.

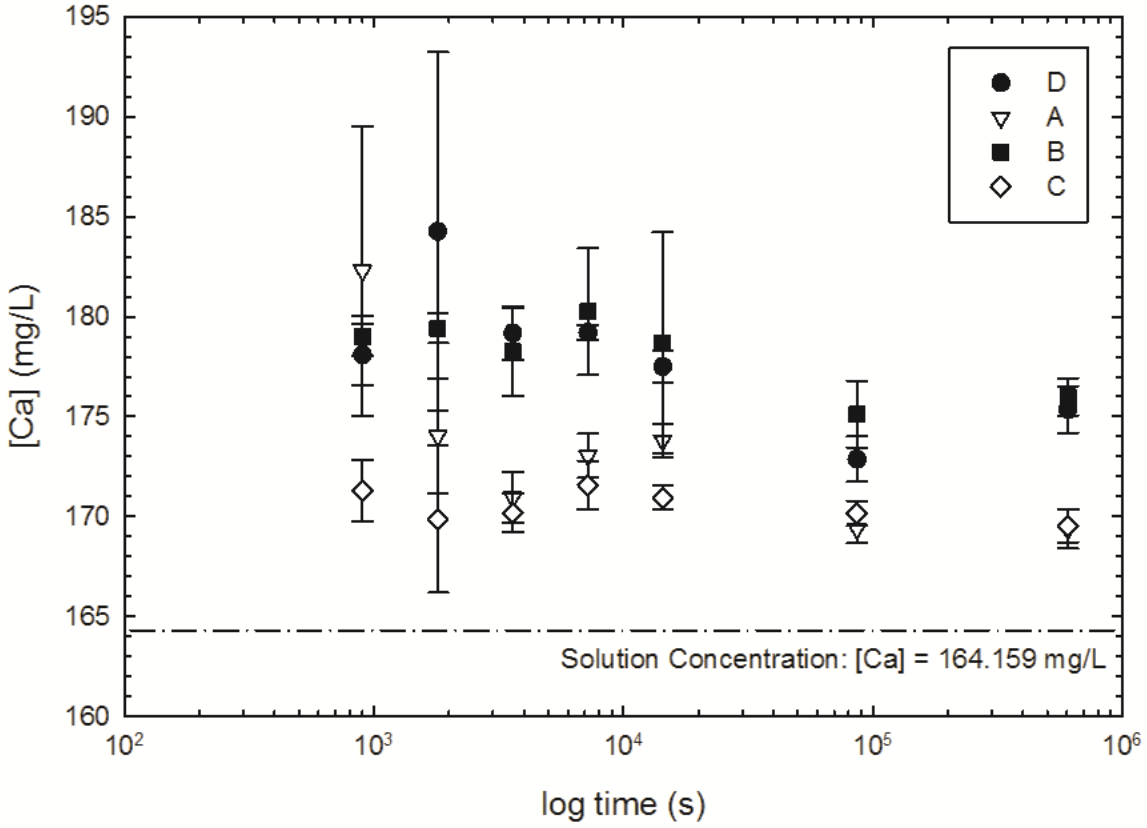

Figure 6.26. Comparison of Ca concentrations measured in solution during LLW kinetics experimentation for the initial soil suite used during single radionuclide experimentation. Measured time frames ranged from 15 min (900 s) to 7 d (604800 s). Initial Ca concentration across all experimentation was 164.159 mg/L, as indicated by the dotted line.

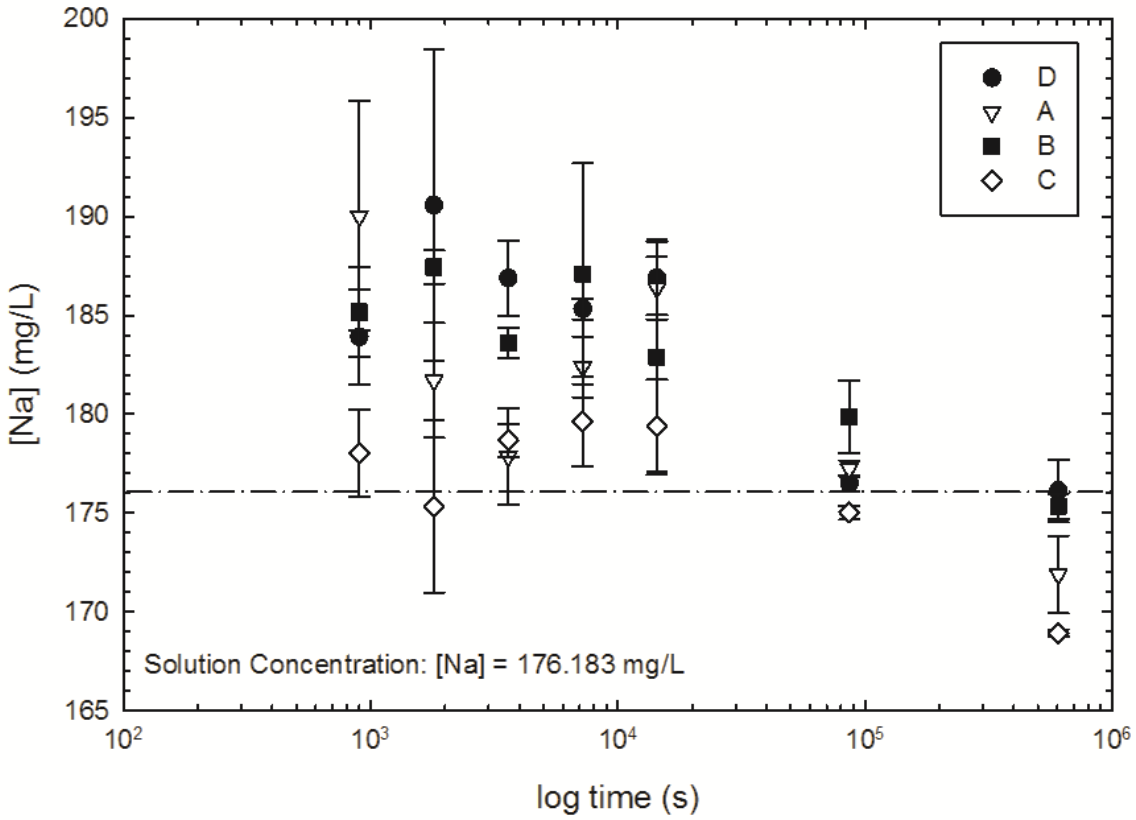

Figure 6.27. Comparison of Na concentrations measured in solution during LLW kinetics experimentation for the initial soil suite used during single radionuclide experimentation. Measured time frames ranged from 15 min (900 s) to 7 d (604800 s). Initial Na concentration across all experimentation was 176.183 mg/L, as indicated by the dotted line.

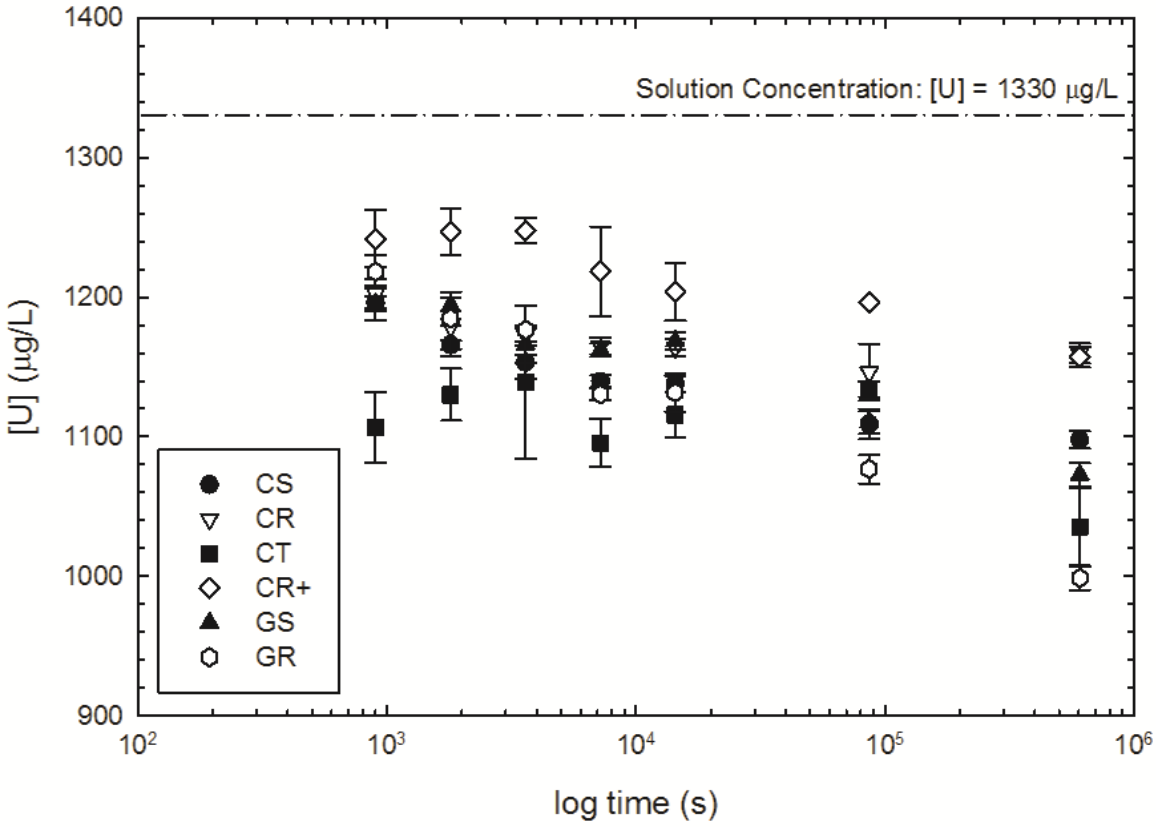

Figure 6.28. Comparison of U concentrations measured in solution during LLW kinetics experimentation for the entire bentonite suite. Measured time frames ranged from 15 min (900 s) to 7 d (604800 s). Initial U concentration across all experimentation was 1330 µg/L, as indicated by the dotted line.

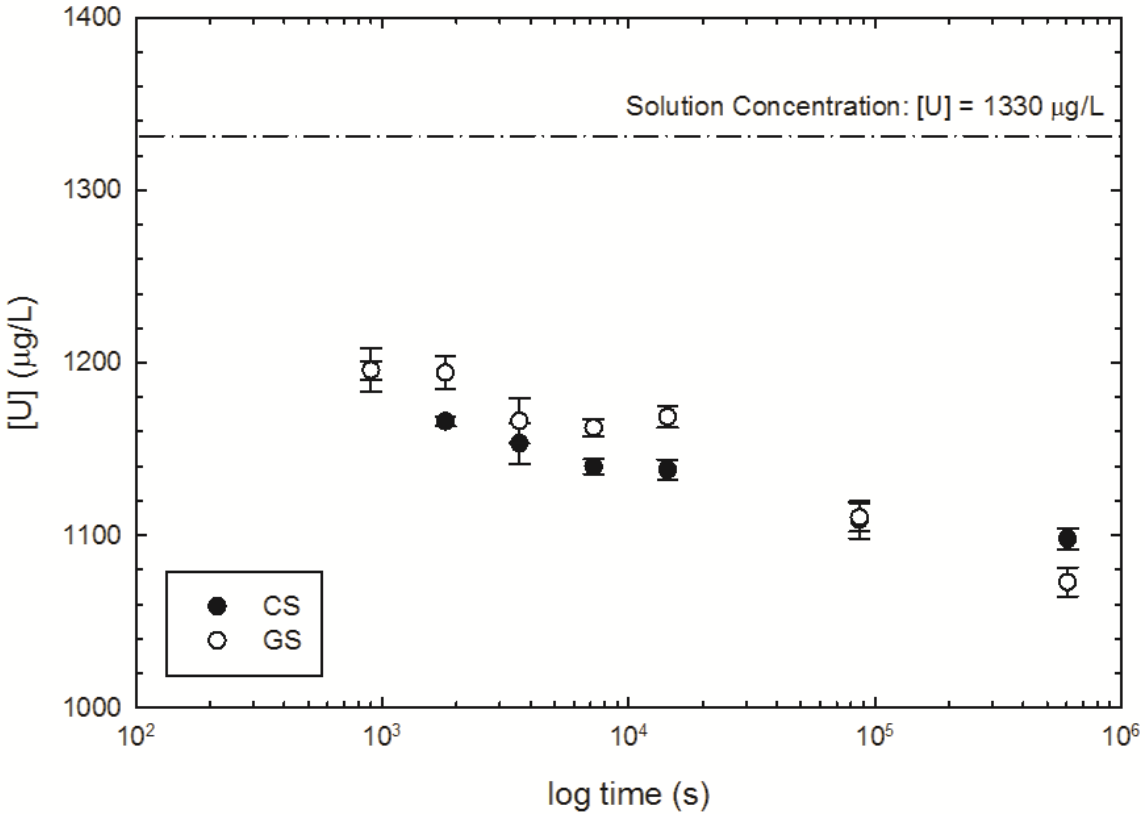

Figure 6.29. Comparison of U concentrations measured in solution during LLW kinetics experimentation for the bentonites derived from standard, non-polymer-modified GCLs. Measured time frames ranged from 15 min (900 s) to 7 d (604800 s). Initial U concentration across all experimentation was 1330 µg/L, as indicated by the dotted line.

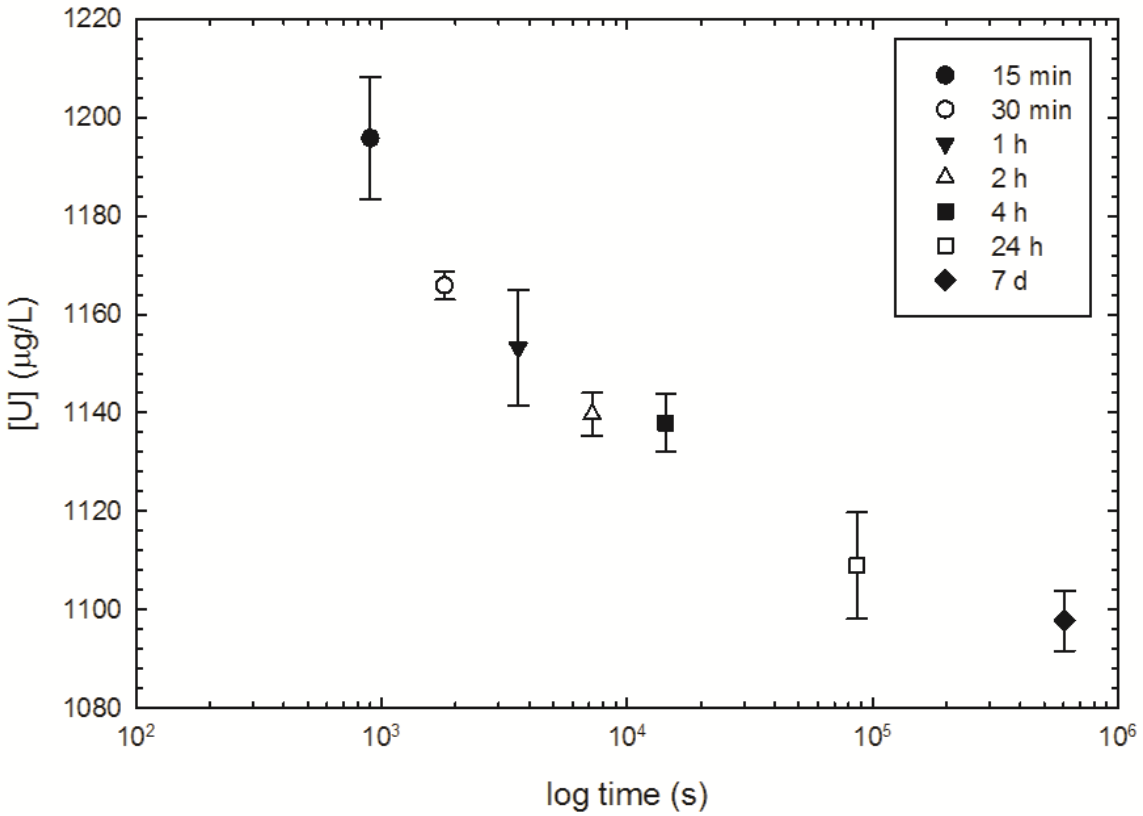

Figure 6.30. Comparison of U concentrations measured in solution for Bentonite *CS* during kinetics experimentation. Measured time frames ranged from 15 min (900 s) to 7 d (604800 s). The initial U concentration across all experimentation was 1330 µg/L.

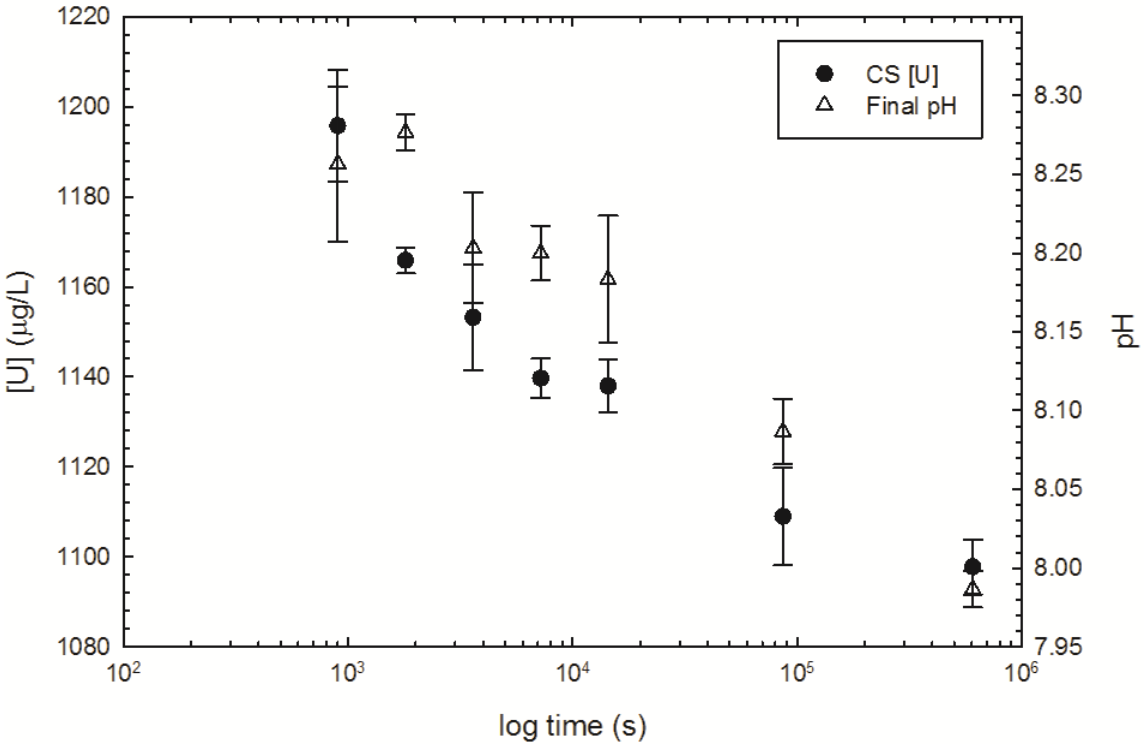

Figure 6.31. Comparison of U concentrations to final pH during LLW kinetics experimentation for Bentonite *CS*. The initial U concentration across all experimentation was 1330 µg/L.

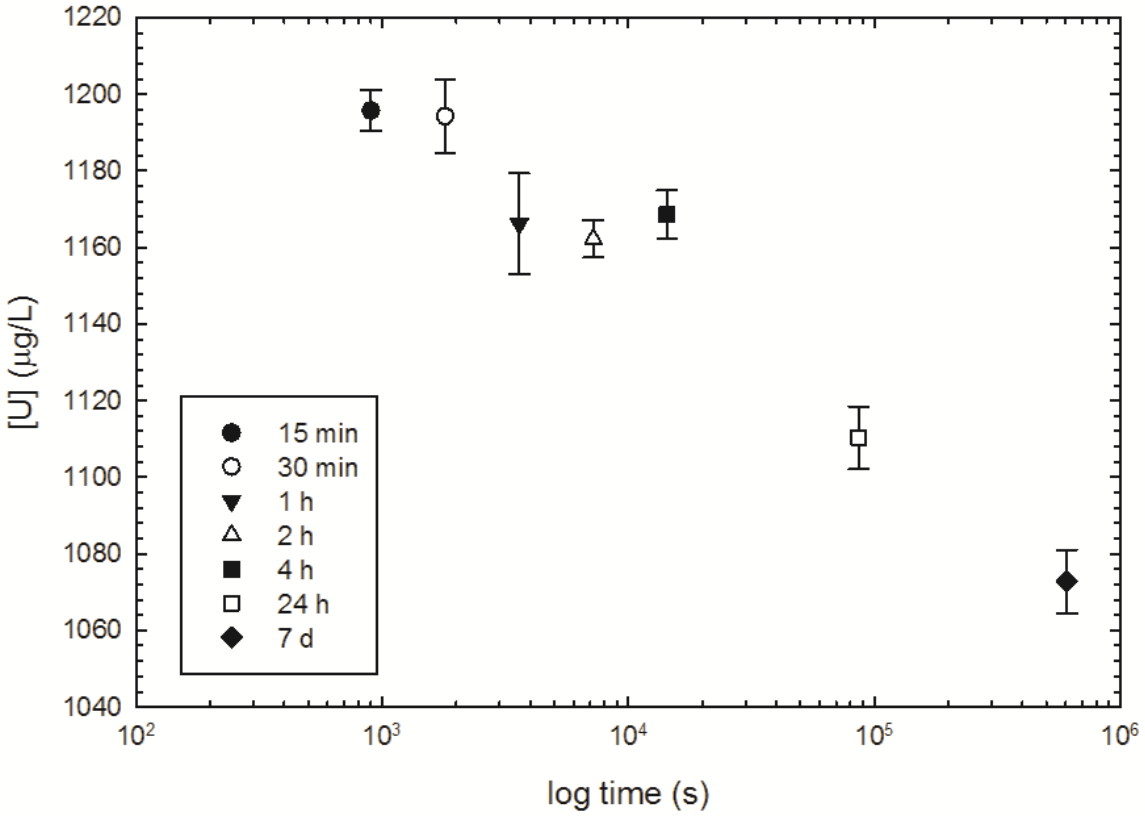

Figure 6.32. Comparison of U concentrations measured in solution for Bentonite *GS* during kinetics experimentation. Measured time frames ranged from 15 min (900 s) to 7 d (604800 s). The initial U concentration across all experimentation was 1330 µg/L.

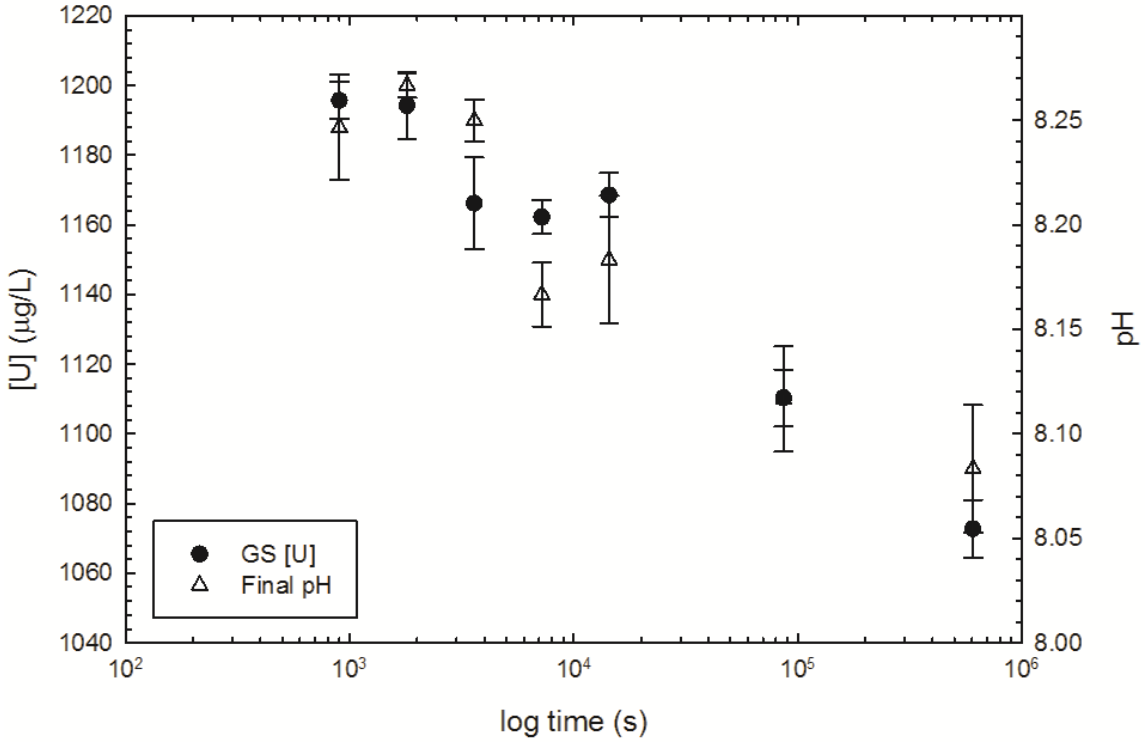

Figure 6.33. Comparison of U concentrations to final pH during LLW kinetics experimentation for Bentonite *GS*. The initial U concentration across all experimentation was 1330 µg/L.

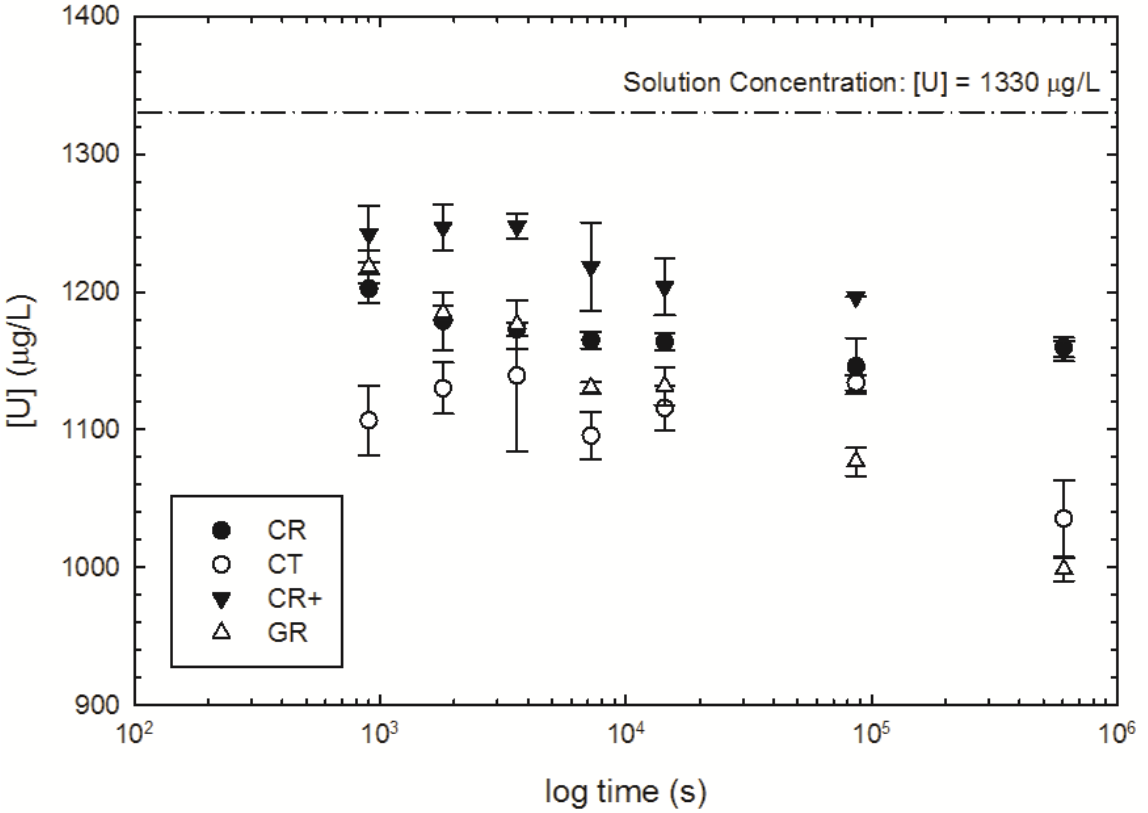

Figure 6.34. Comparison of U concentrations measured in solution during LLW kinetics experimentation for the bentonites derived from polymer-modified GCLs. Measured time frames ranged from 15 min (900 s) to 7 d (604800 s). Initial U concentration across all experimentation was 1330 µg/L, as indicated by the dotted line.

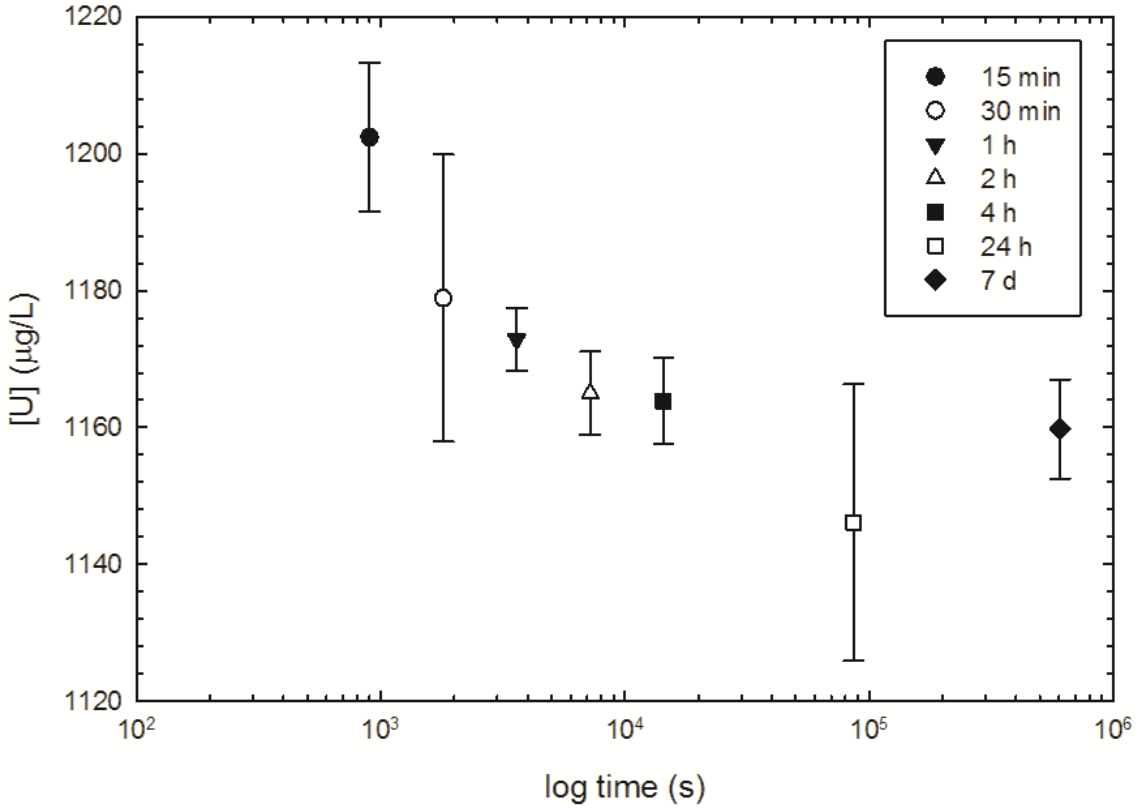

Figure 6.35. Comparison of U concentrations measured in solution for Bentonite *CR* during kinetics experimentation. Measured time frames ranged from 15 min (900 s) to 7 d (604800 s). The initial U concentration across all experimentation was 1330 µg/L.

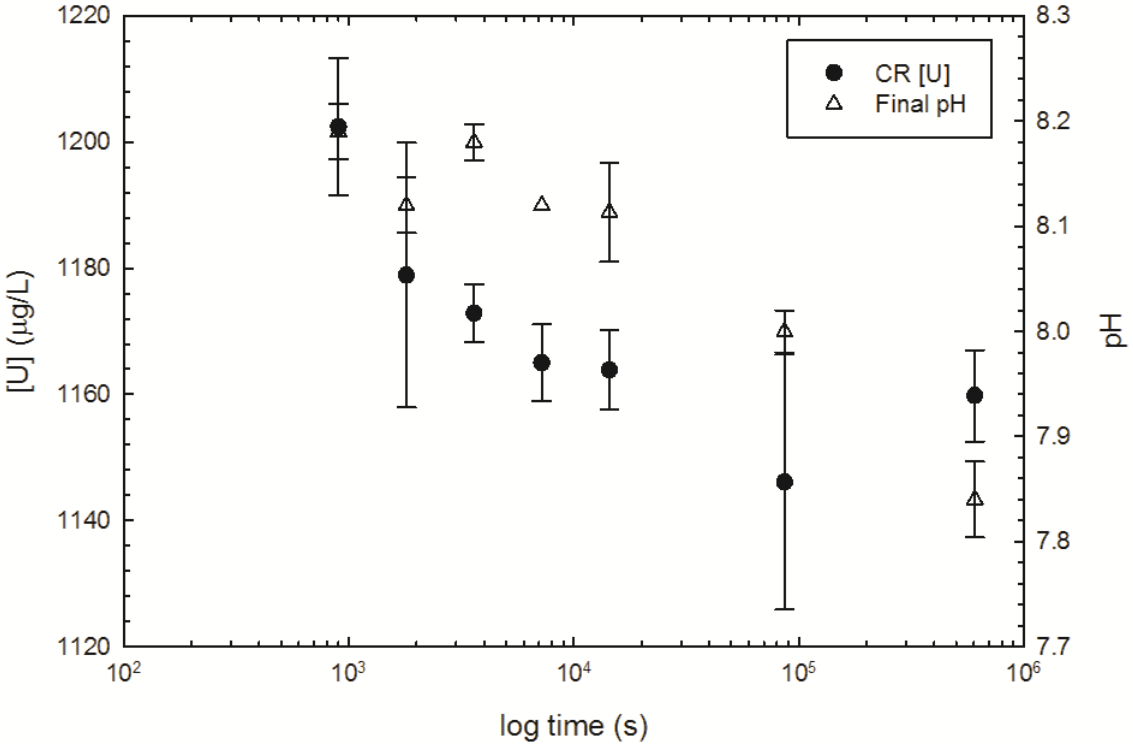

Figure 6.36. Comparison of U concentrations to final pH during LLW kinetics experimentation for Bentonite *CR*. The initial U concentration across all experimentation was 1330 µg/L.

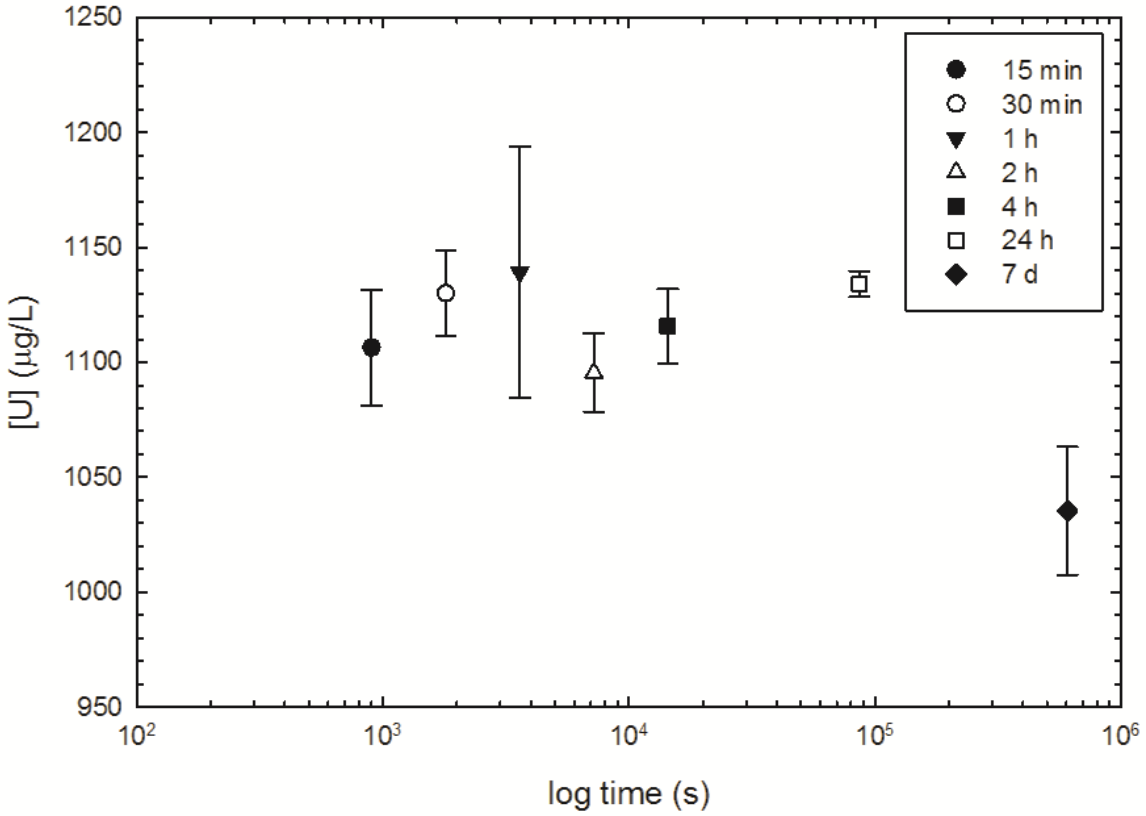

Figure 6.37. Comparison of U concentrations measured in solution for Bentonite *CT* during kinetics experimentation. Measured time frames ranged from 15 min (900 s) to 7 d (604800 s). The initial U concentration across all experimentation was 1330 µg/L.

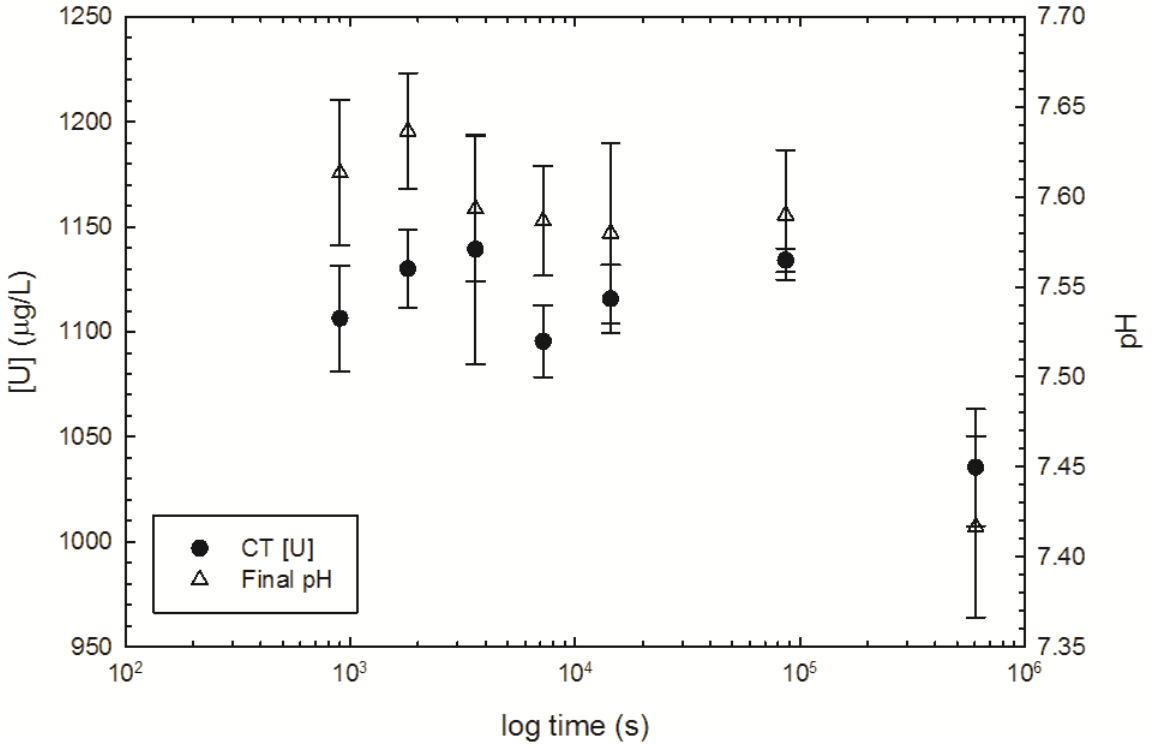

Figure 6.38. Comparison of U concentrations to final pH during LLW kinetics experimentation for Bentonite *CT*. The initial U concentration across all experimentation was 1330 µg/L.

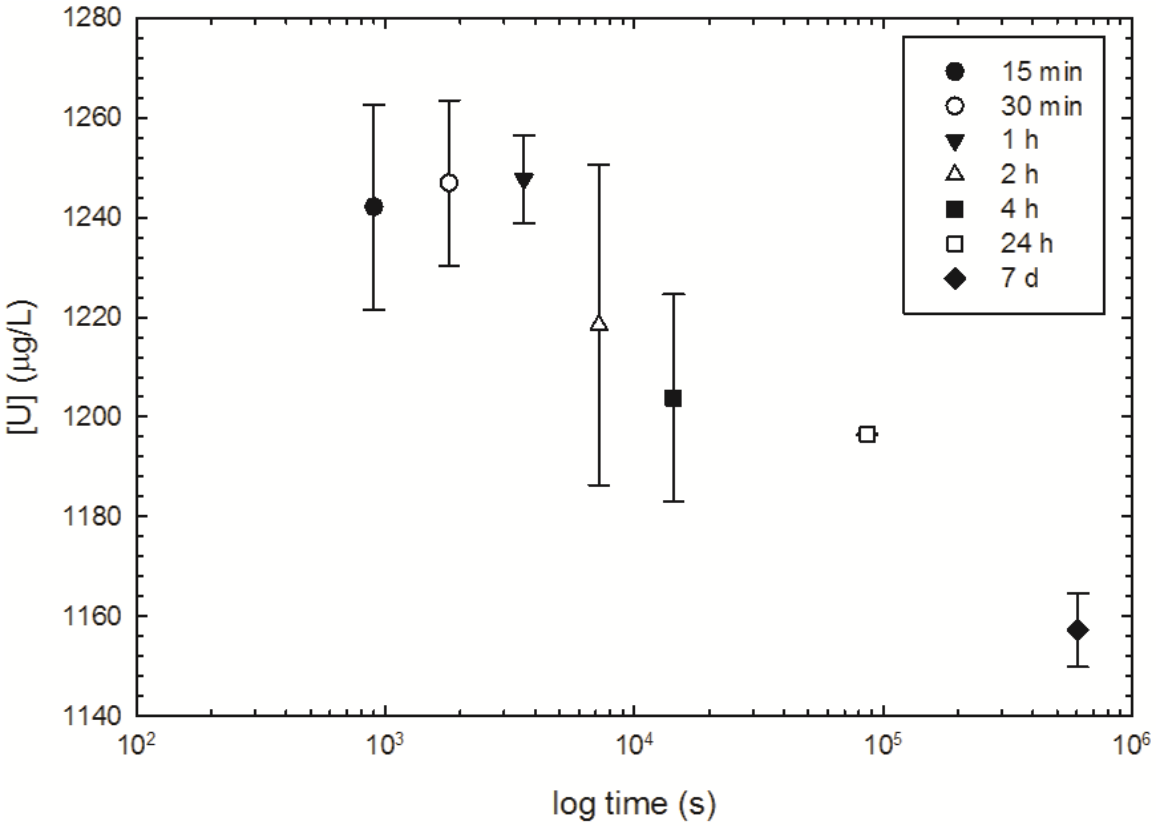

Figure 6.39. Comparison of U concentrations measured in solution for Bentonite *CR+* during kinetics experimentation. Measured time frames ranged from 15 min (900 s) to 7 d (604800 s). The initial U concentration across all experimentation was 1330 µg/L.

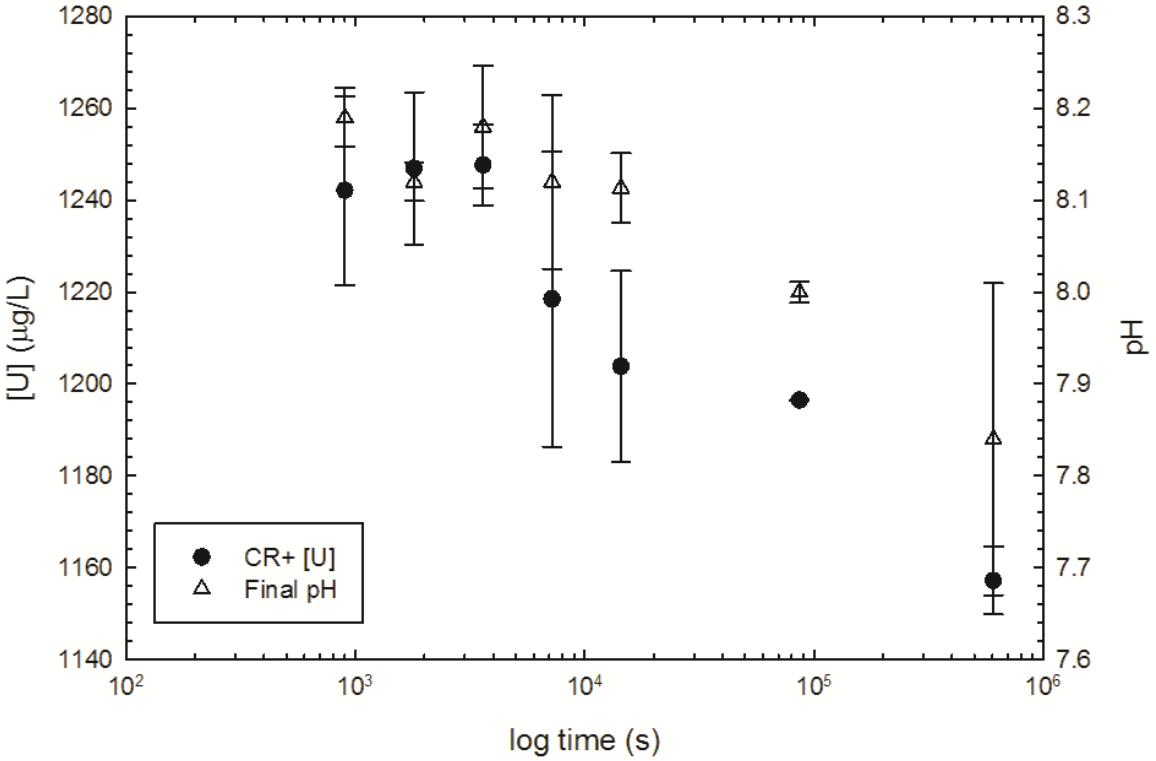

Figure 6.40. Comparison of U concentrations to final pH during LLW kinetics experimentation for Bentonite *CR+*. The initial U concentration across all experimentation was 1330 µg/L.

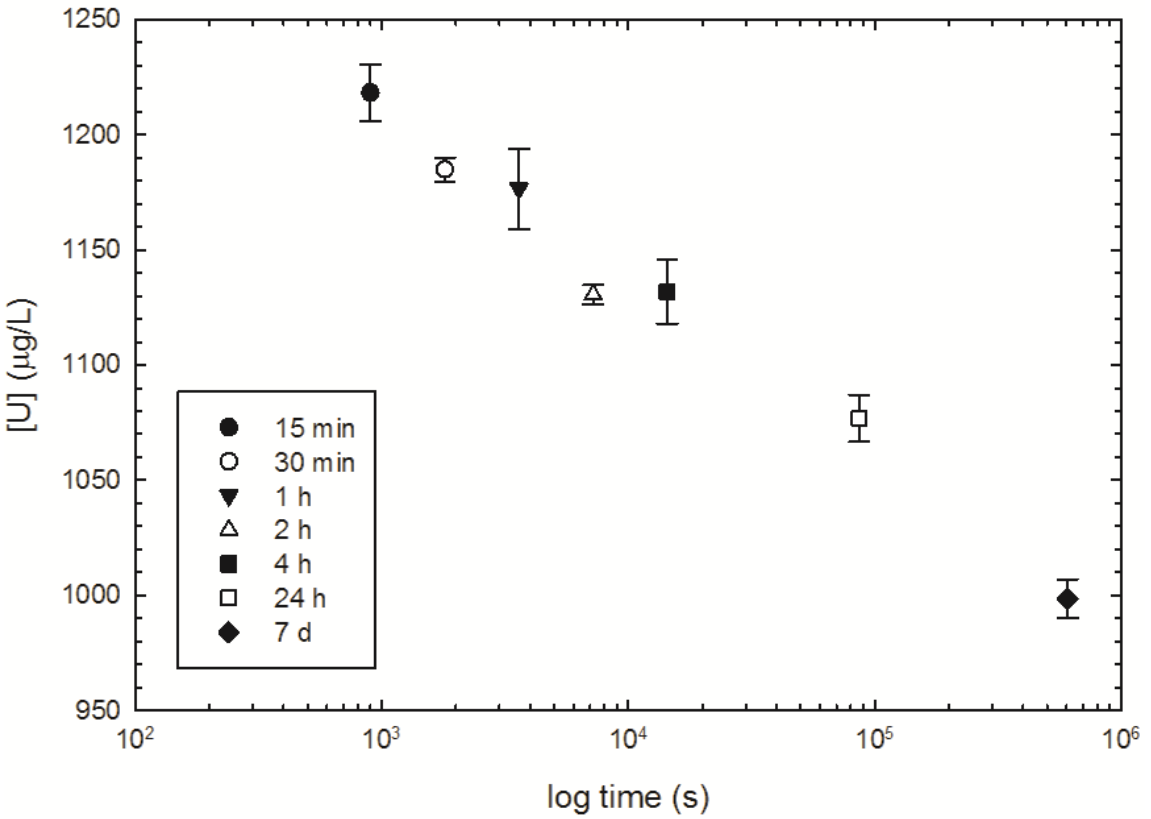

Figure 6.41. Comparison of U concentrations measured in solution for Bentonite *GR* during kinetics experimentation. Measured time frames ranged from 15 min (900 s) to 7 d (604800 s). The initial U concentration across all experimentation was 1330 µg/L.

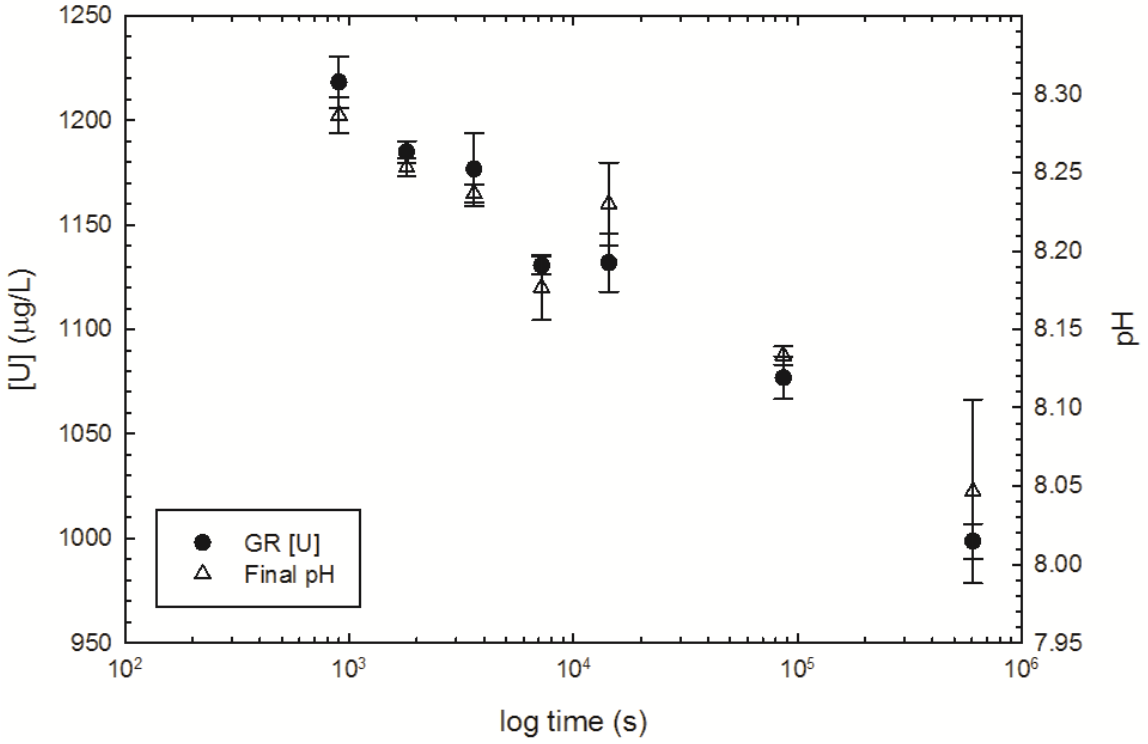

Figure 6.42. Comparison of U concentrations to final pH during LLW kinetics experimentation for Bentonite *GR*. The initial U concentration across all experimentation was 1330 µg/L.

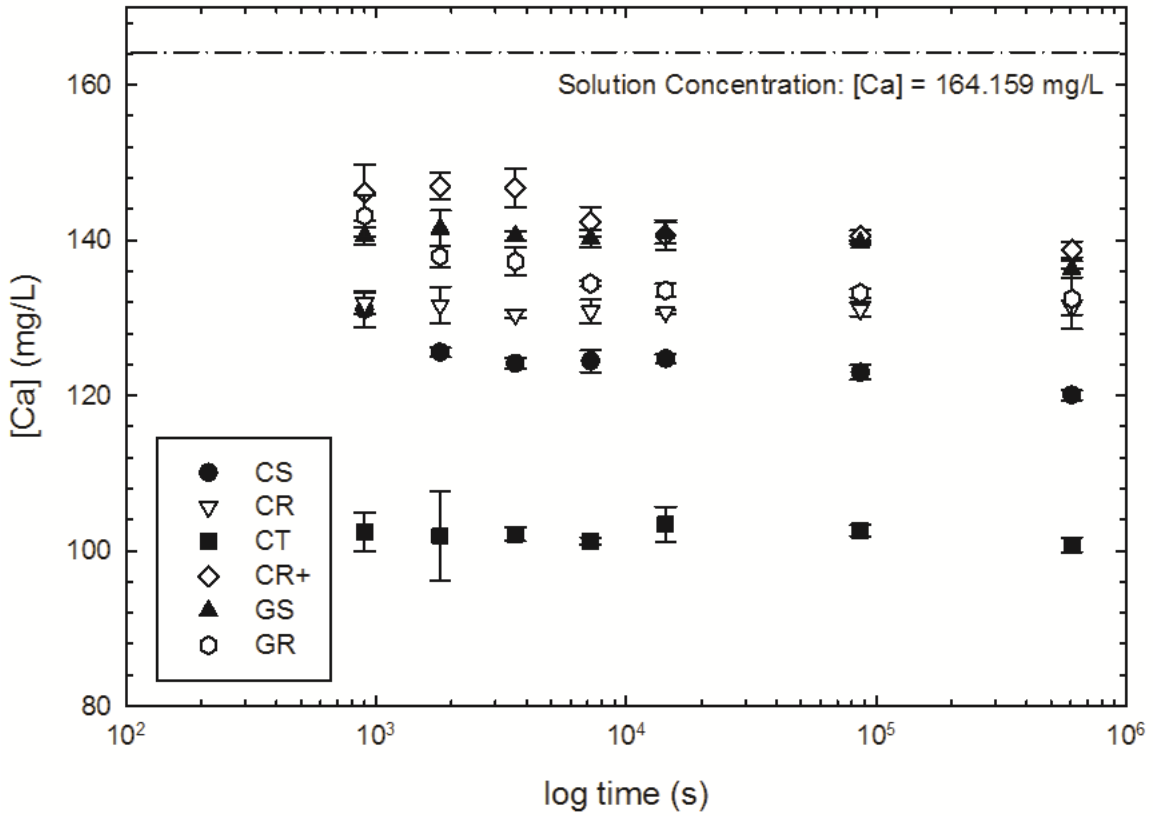

Figure 6.43. Comparison of Ca concentrations measured in solution during LLW kinetics experimentation for the entire bentonite suite. Measured time frames ranged from 15 min (900 s) to 7 d (604800 s). Initial Ca concentration across all experimentation was 164.159 mg/L, as indicated by the dotted line.

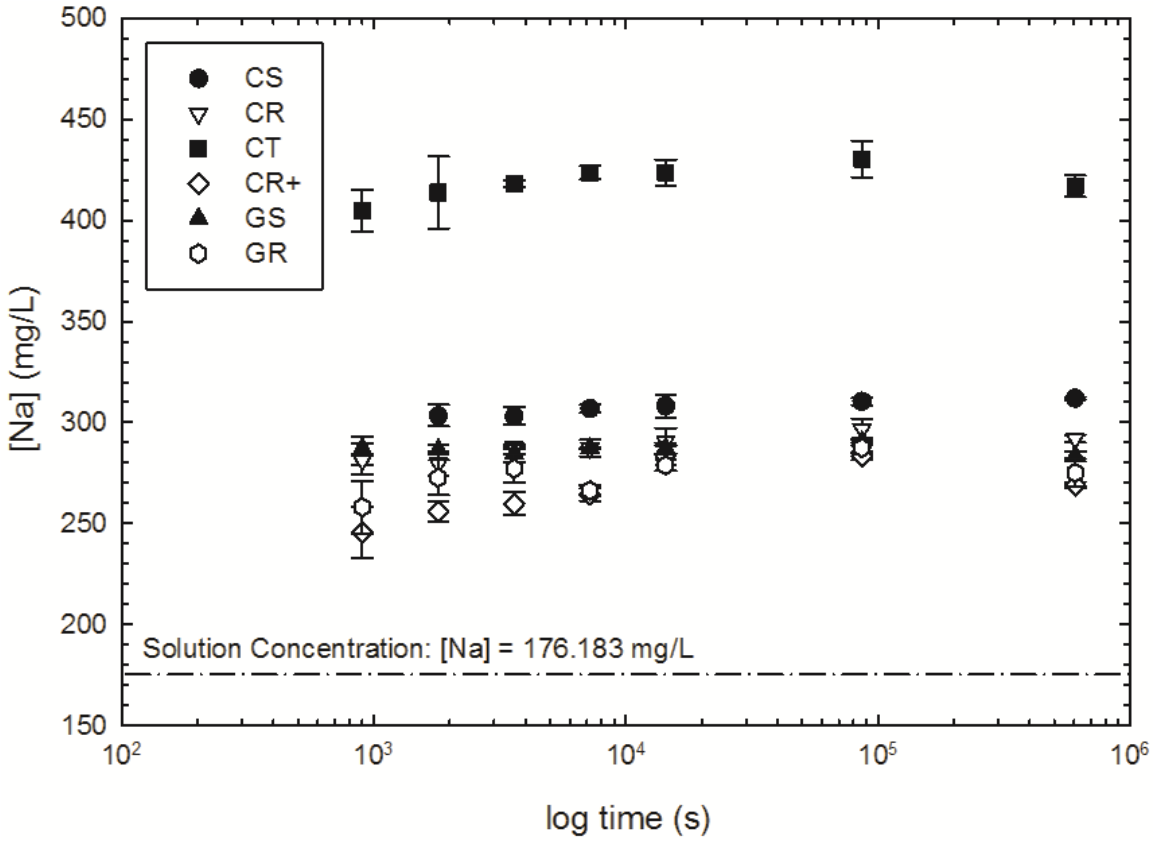

Figure 6.44. Comparison of Na concentrations measured in solution during LLW kinetics experimentation for the entire bentonite suite. Measured time frames ranged from 15 min (900 s) to 7 d (604800 s). Initial Na concentration across all experimentation was 176.183 mg/L, as indicated by the dotted line.

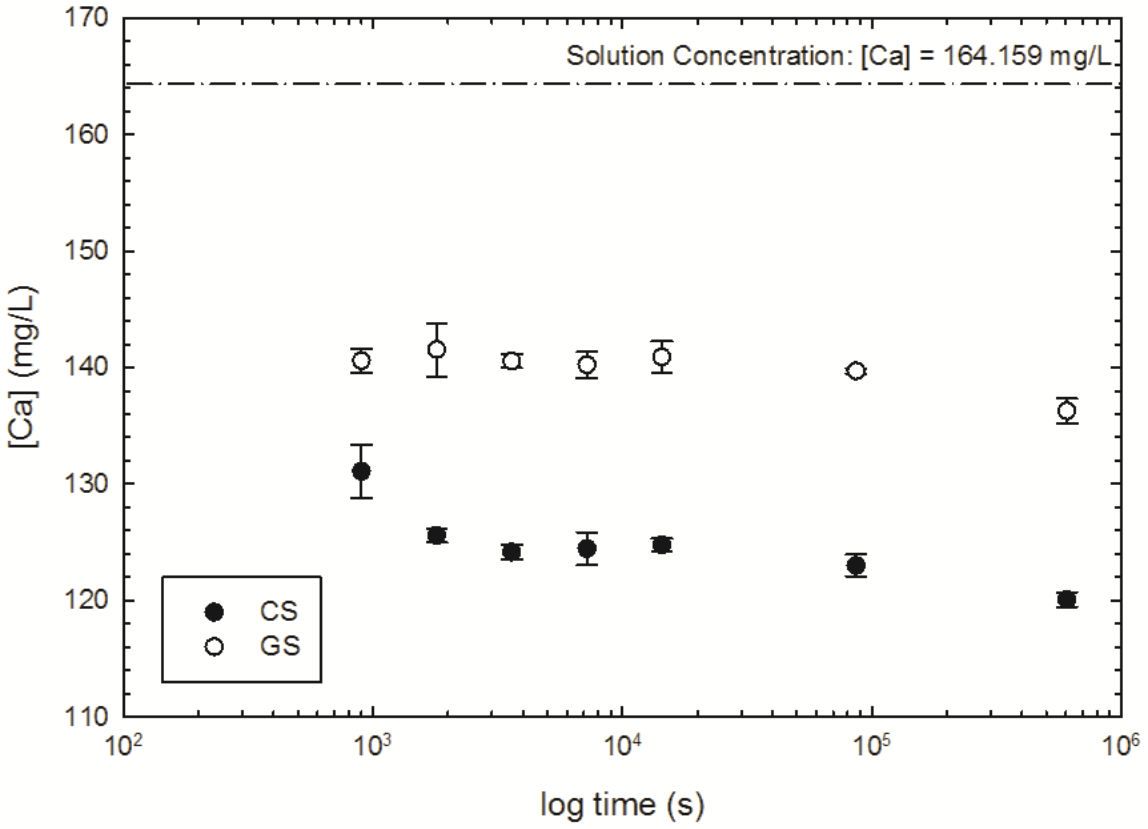

Figure 6.45. Comparison of Ca concentrations measured in solution during LLW kinetics experimentation for the bentonites derived from standard, non-polymer-modified GCLs. Measured time frames ranged from 15 min (900 s) to 7 d (604800 s). Initial Ca concentration across all experimentation was 164.159 mg/L, as indicated by the dotted line.

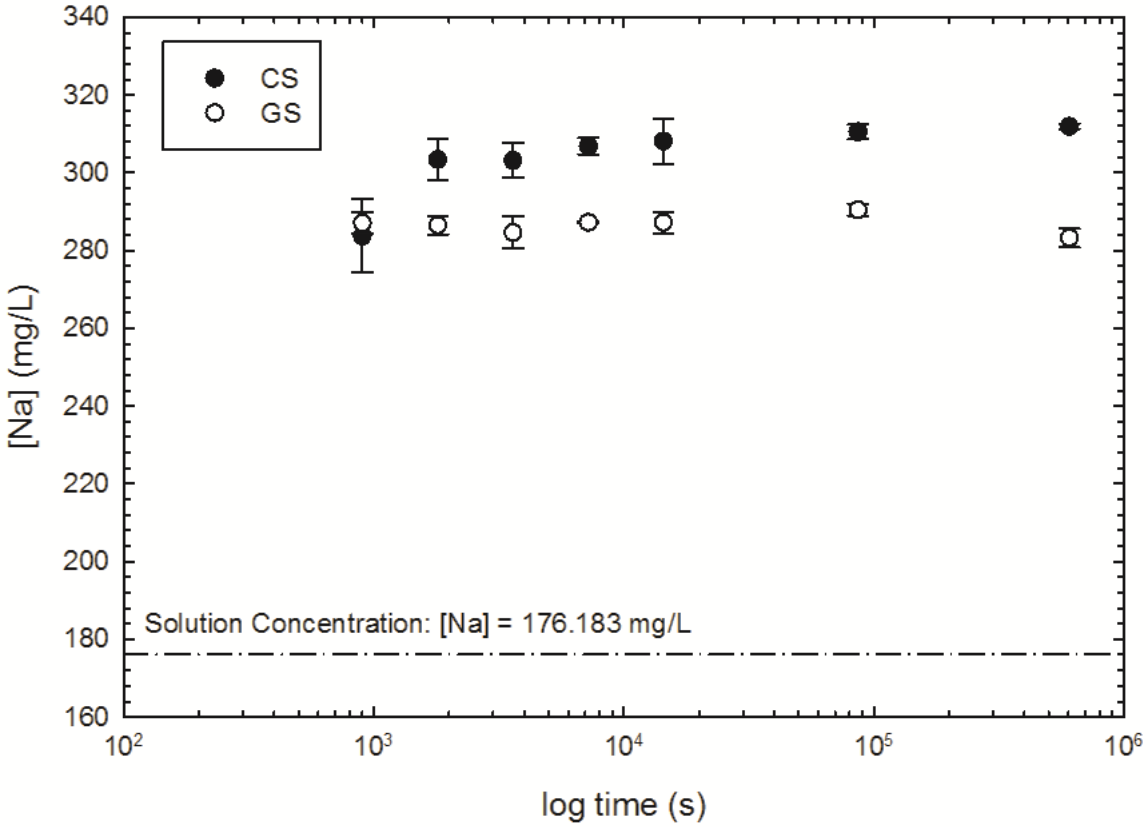

Figure 6.46. Comparison of Na concentrations measured in solution during LLW kinetics experimentation for the bentonites derived from standard, non-polymer-modified GCLs. Measured time frames ranged from 15 min (900 s) to 7 d (604800 s). Initial Na concentration across all experimentation was 176.183 mg/L, as indicated by the dotted line.

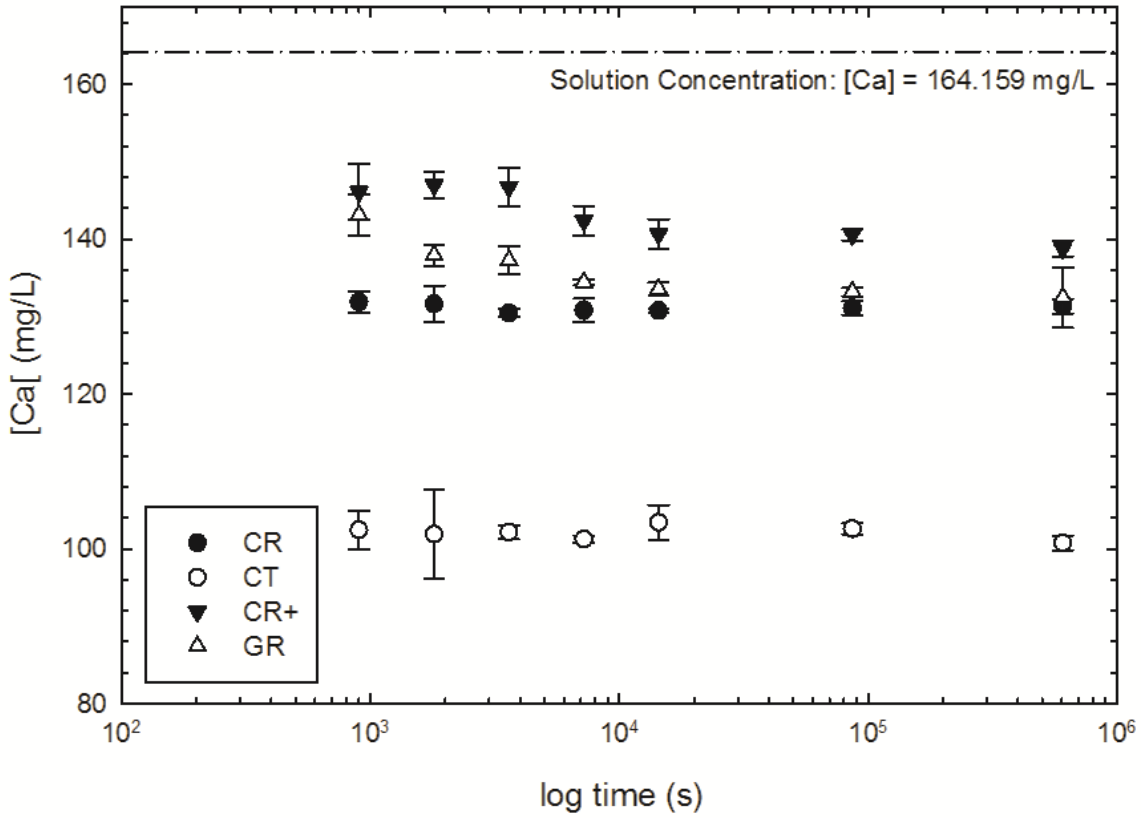

Figure 6.47. Comparison of Ca concentrations measured in solution during LLW kinetics experimentation for the bentonites derived from polymer-modified GCLs. Measured time frames ranged from 15 min (900 s) to 7 d (604800 s). Initial Ca concentration across all experimentation was 164.159 mg/L, as indicated by the dotted line.

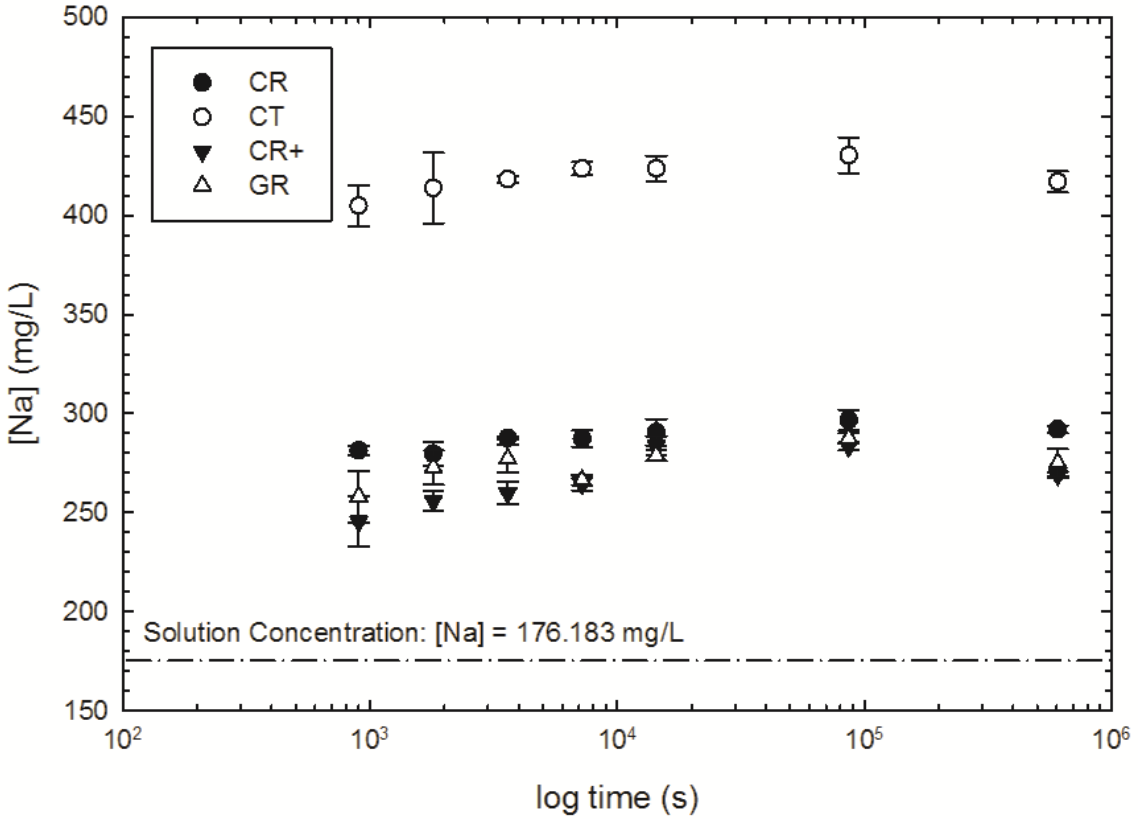

Figure 6.48. Comparison of Na concentrations measured in solution during LLW kinetics experimentation for the bentonites derived from polymer-modified GCLs. Measured time frames ranged from 15 min (900 s) to 7 d (604800 s). Initial Na concentration across all experimentation was 176.183 mg/L, as indicated by the dotted line.

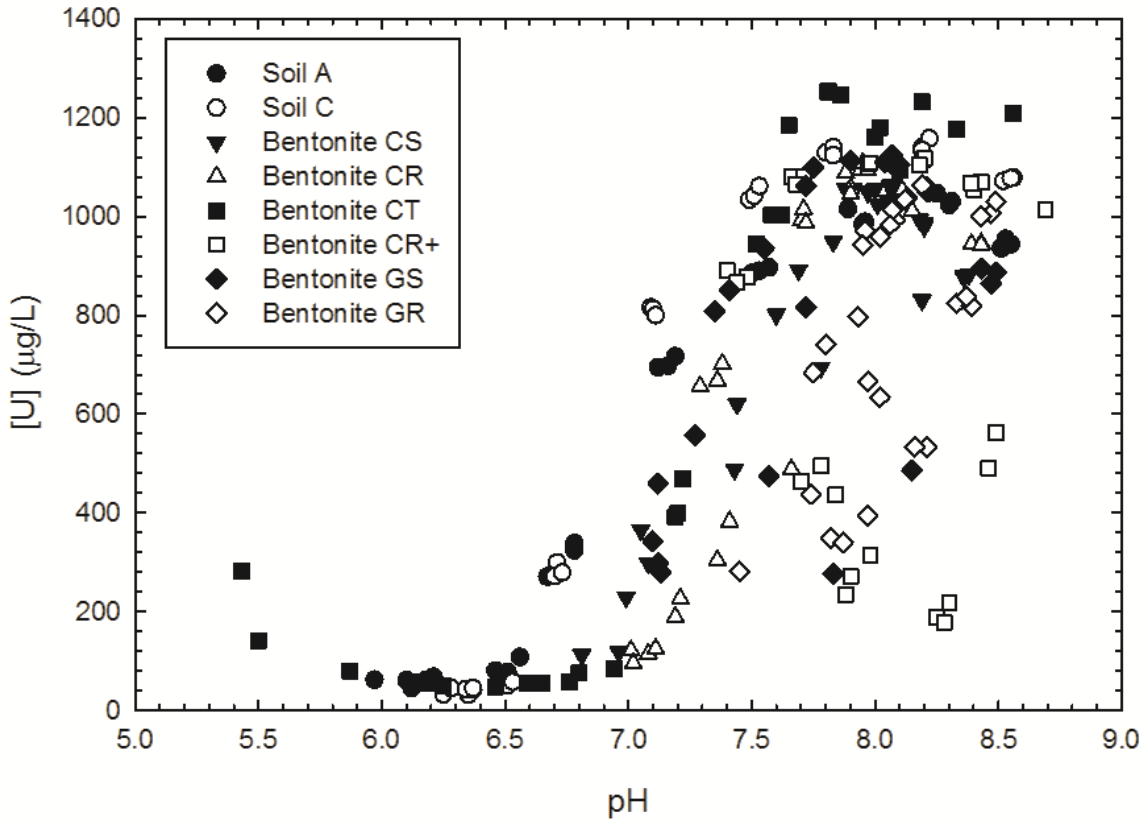

Figure 6.49. Measured concentration of U (in µg/L) during LLW sorption edge and envelope experimentation across the experimental pH range of experimentation for all tested natural soils and bentonites. Initial solution concentration of U was 1330 µg/L.

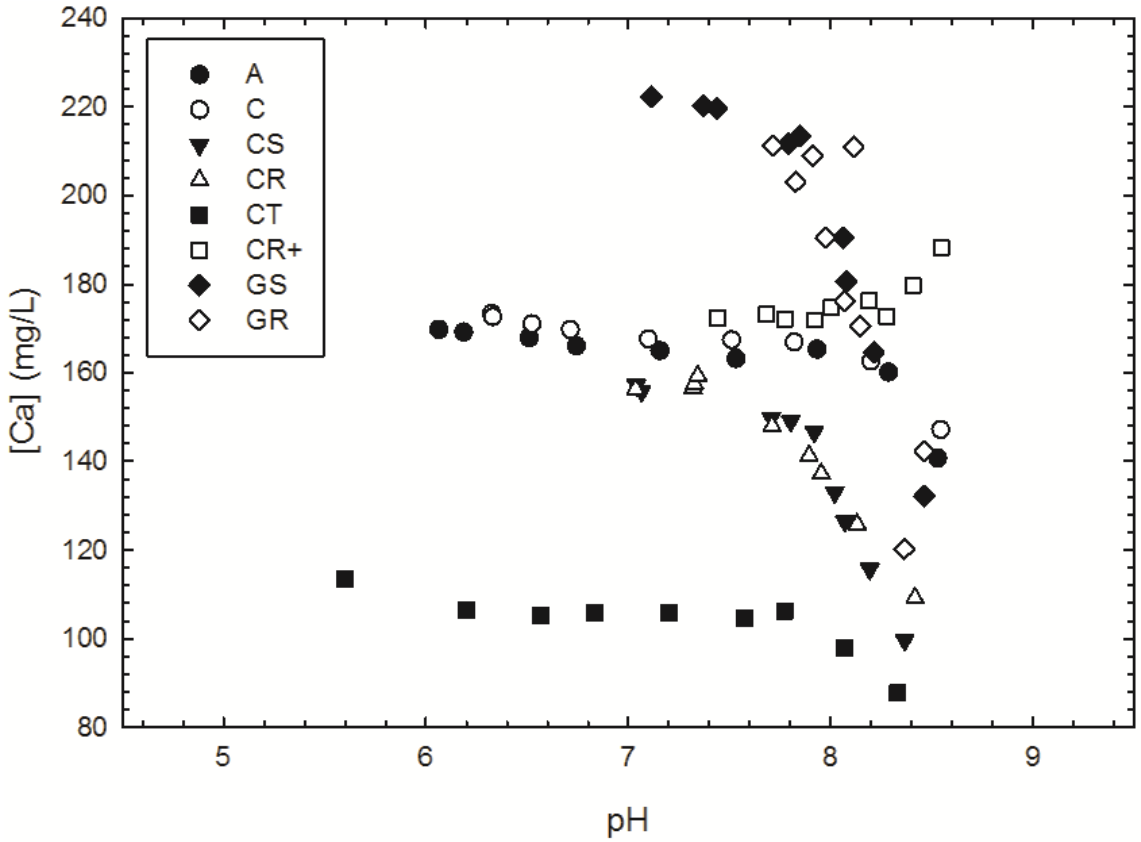

Figure 6.50. Ca concentrations (in mg/L) measured in RSL solution following E&E experimentation for all tested soils. Average solution control concentration across most of the tested pH range was 164.159 mg/L for Ca.

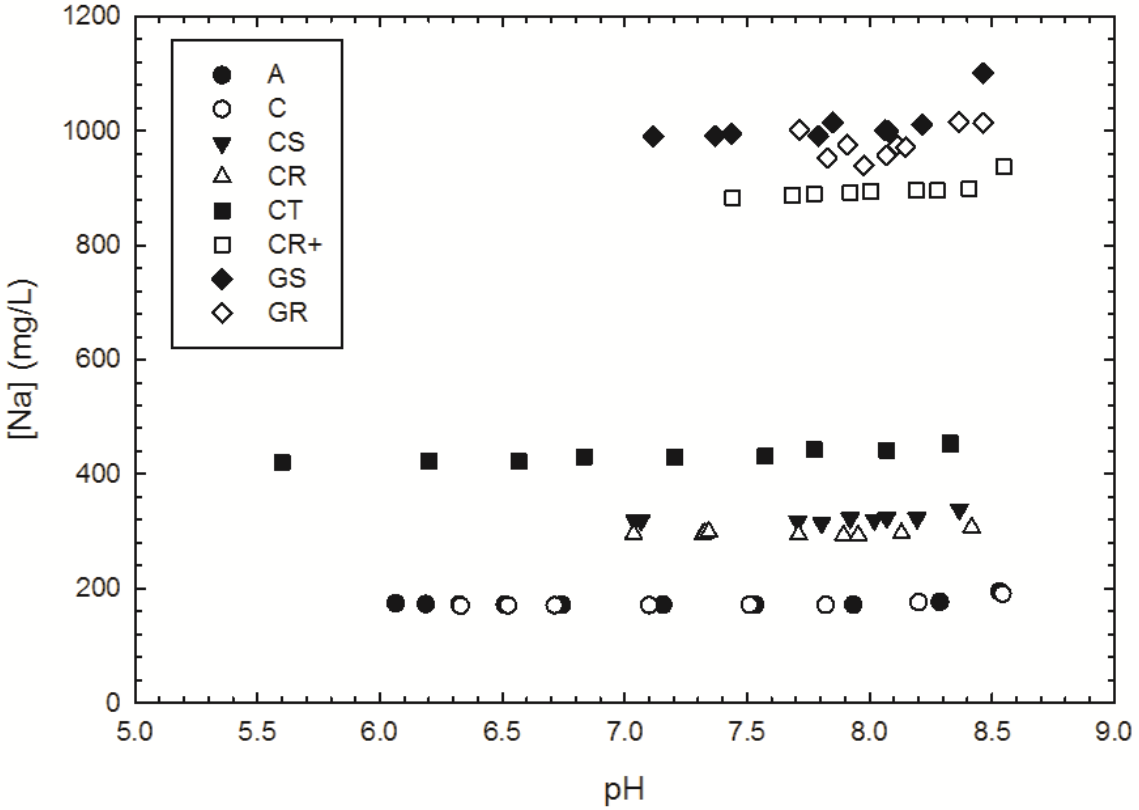

Figure 6.51. Na concentrations (in mg/L) remaining in solution following E&E experimentation for all soils used during experimentation. Average solution control concentration across most of the tested pH range was 176.183 mg/L for Na.

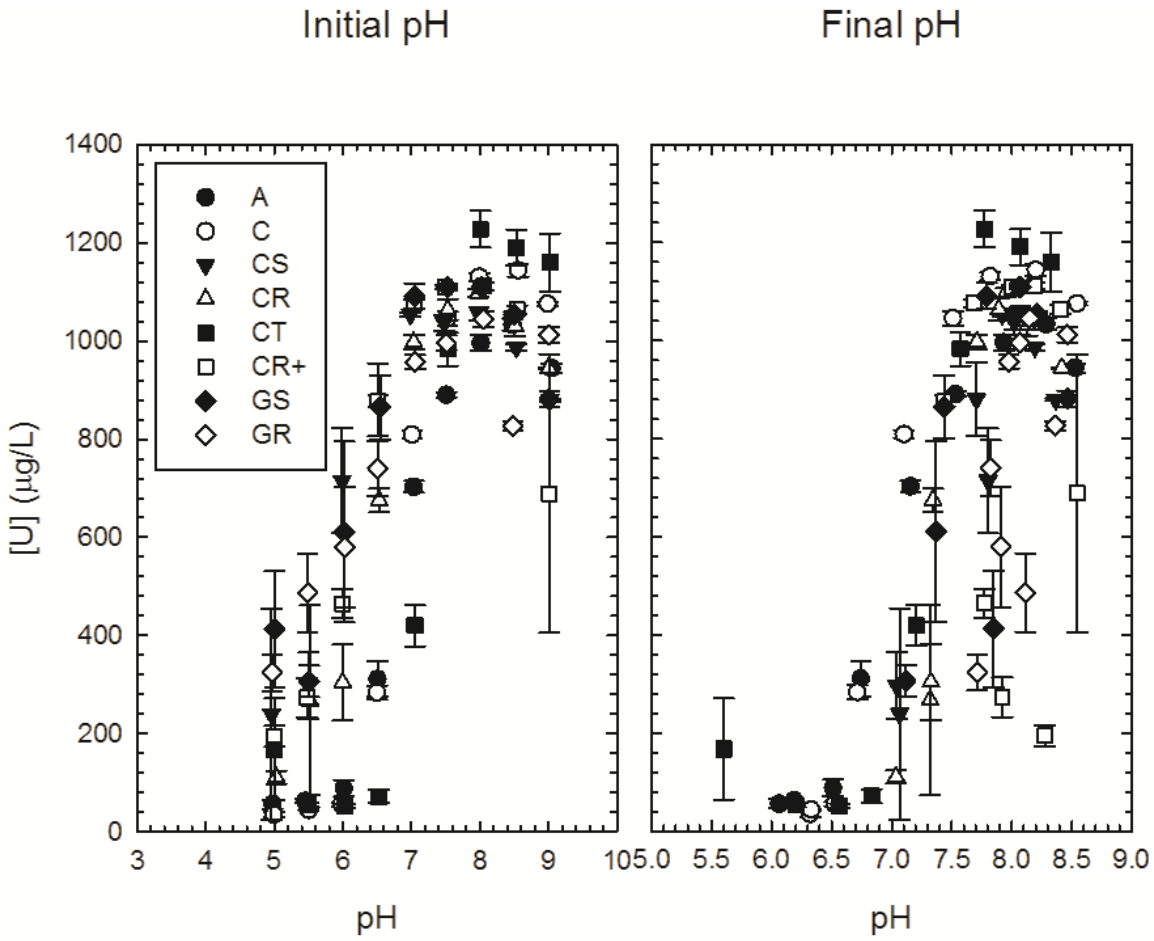

Figure 6.52. Comparison of initial and final pH measurements for natural soils and bentonites during LLW sorption edge and envelope experimentation. Initial U concentration across experimentation was 1330 µg/L.

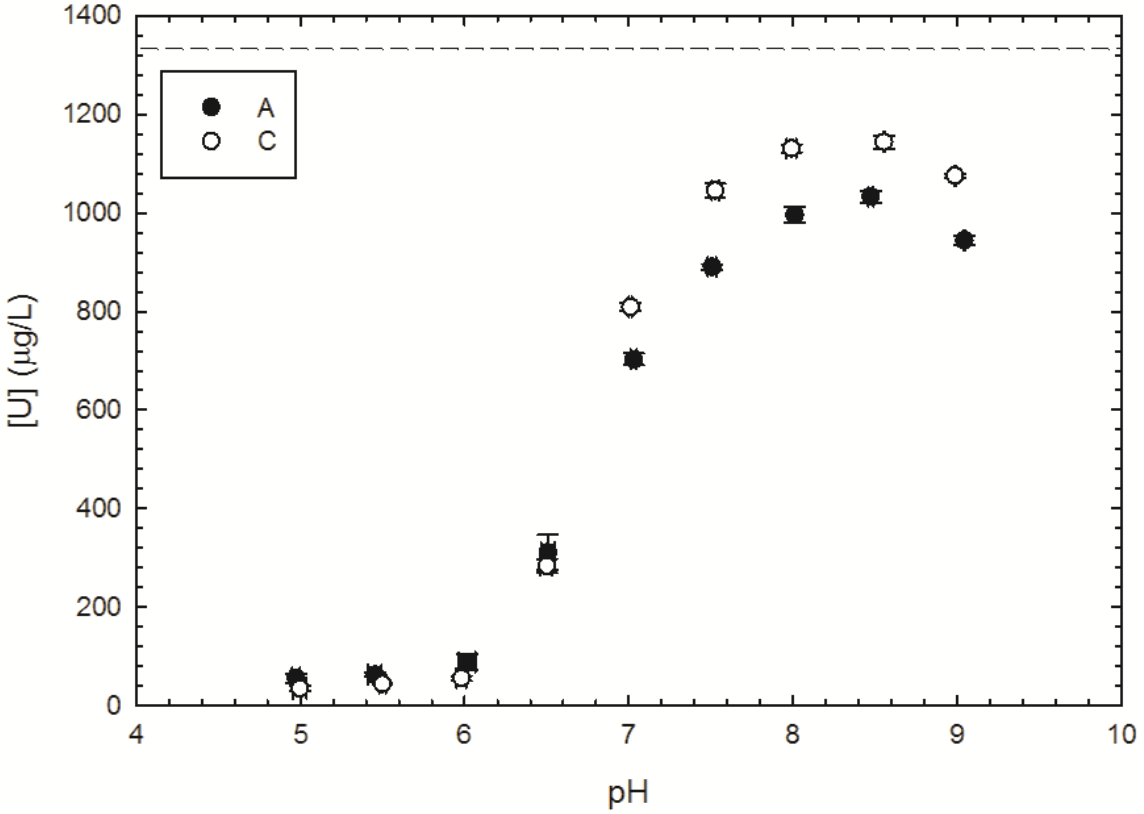

Figure 6.53. Comparison of measured U concentrations remaining in solution (in µg/L) across the experimental pH range for the natural barrier soils. Initial solution concentration was 1330 µg/L of U.

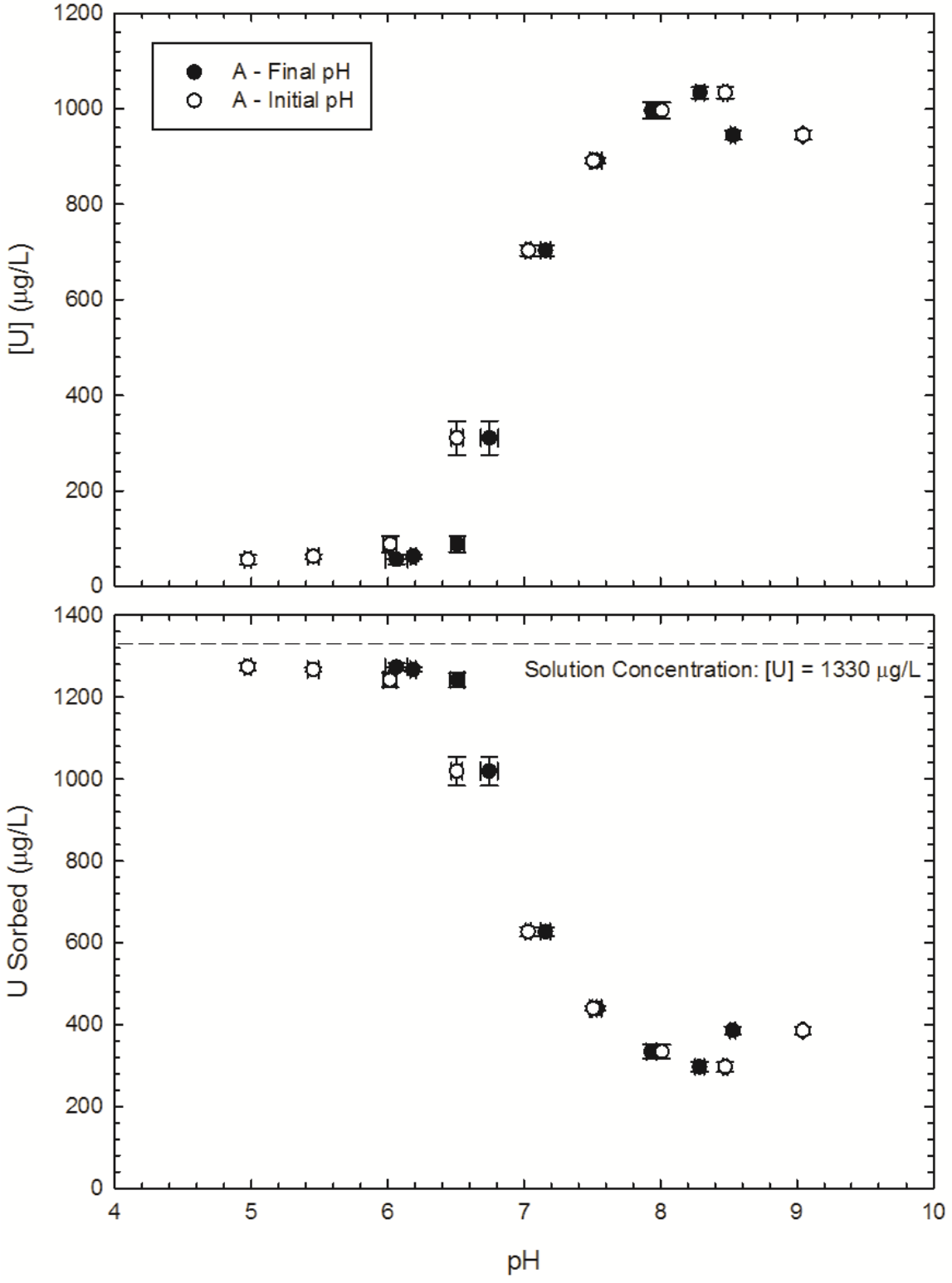

Figure 6.54. Comparison of measured U concentration to sorbed quantity for Soil *A* during RSL E&E experimentation.

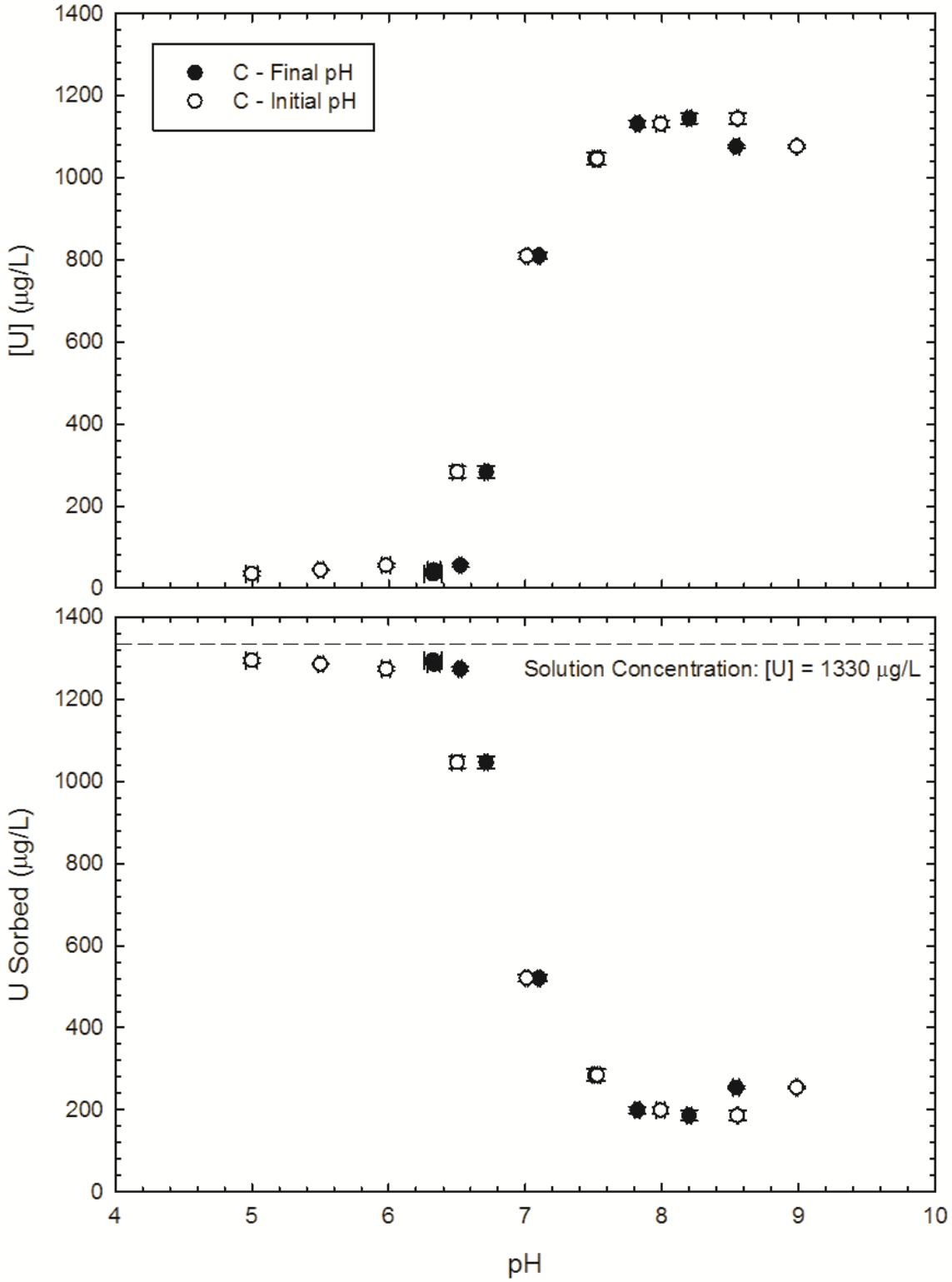

Figure 6.55. Comparison of measured U concentration to sorbed quantity for Soil *C* during RSL E&E experimentation.

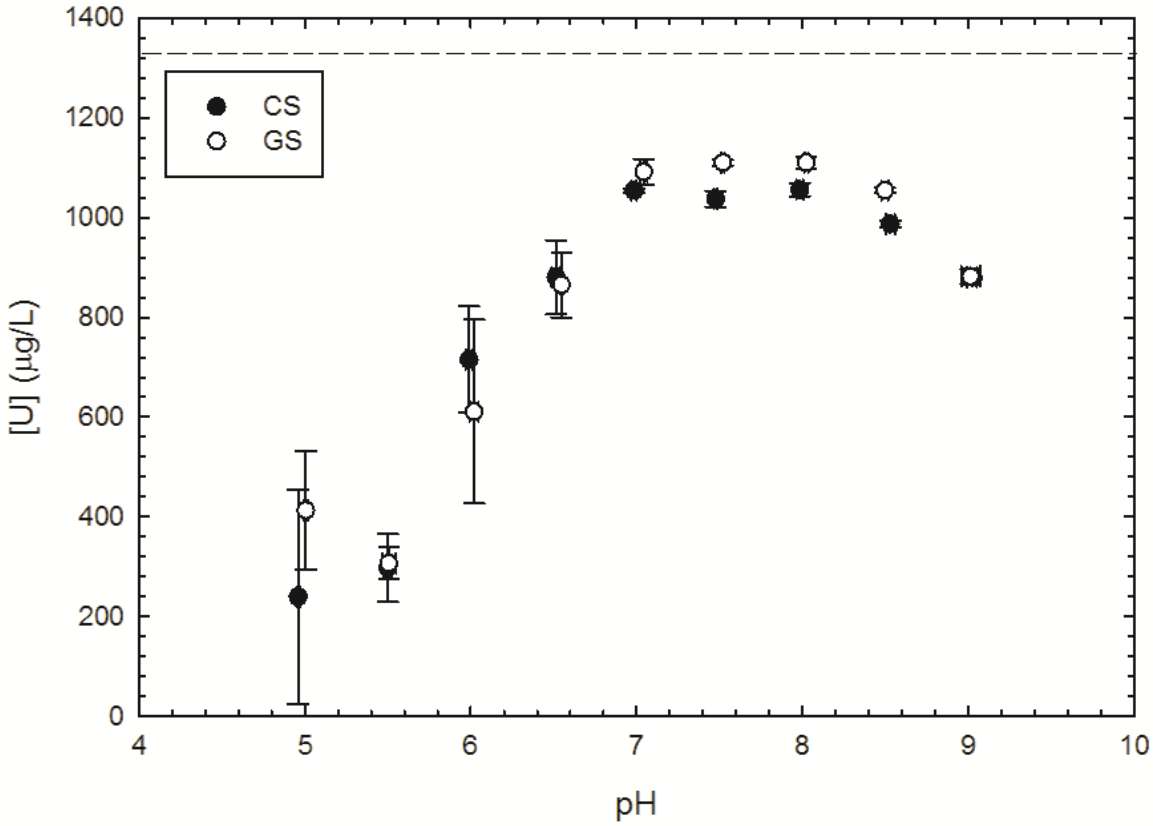

Figure 6.56. Comparison of measured U concentrations remaining in solution (in µg/L) across the experimental pH range for the standard, non-modified bentonites. Initial solution concentration was 1330 µg/L of U.

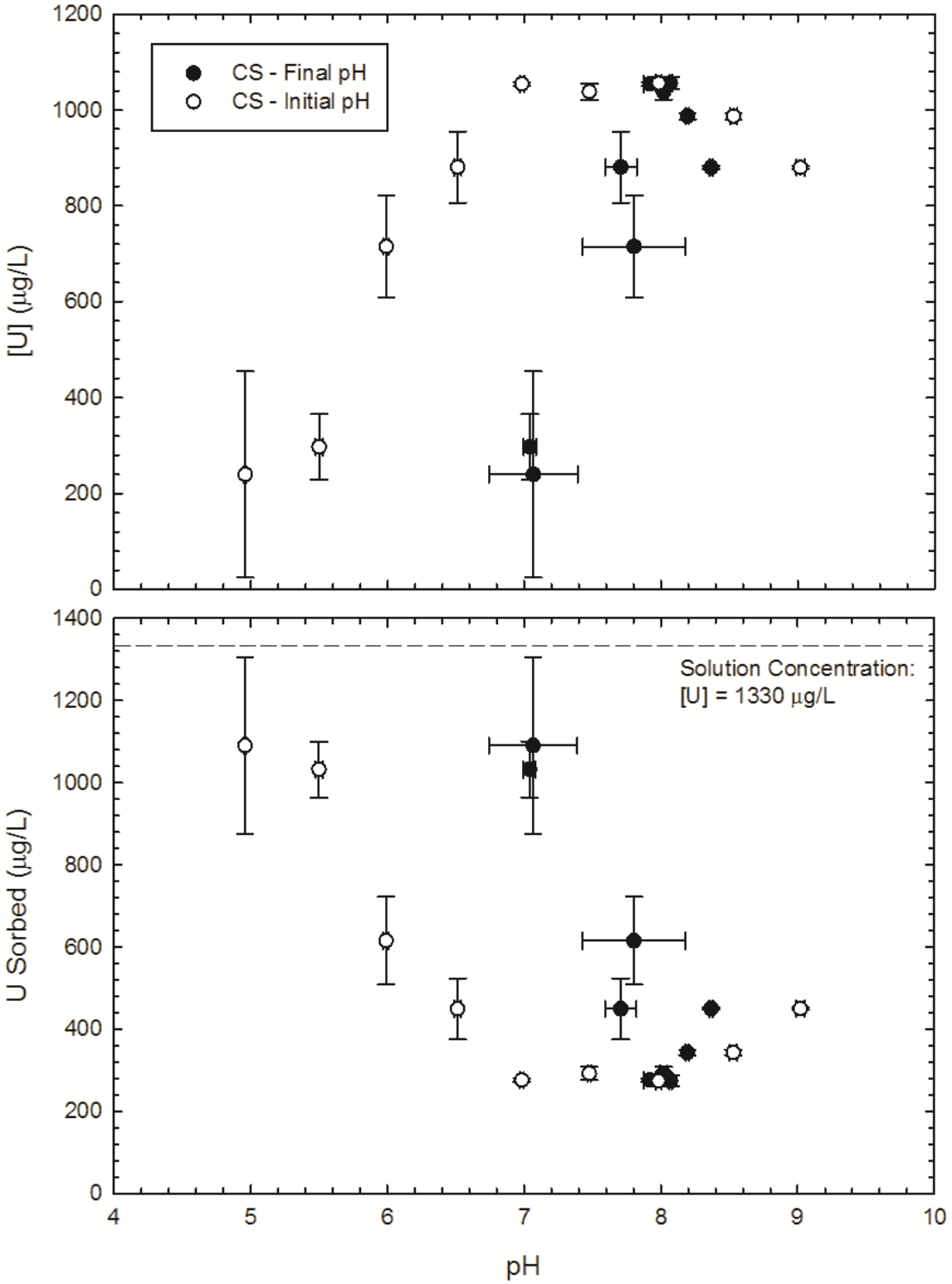

Figure 6.57. Comparison of measured U concentration to sorbed quantity for Bentonite *CS* during LLW sorption edge and envelope experimentation.

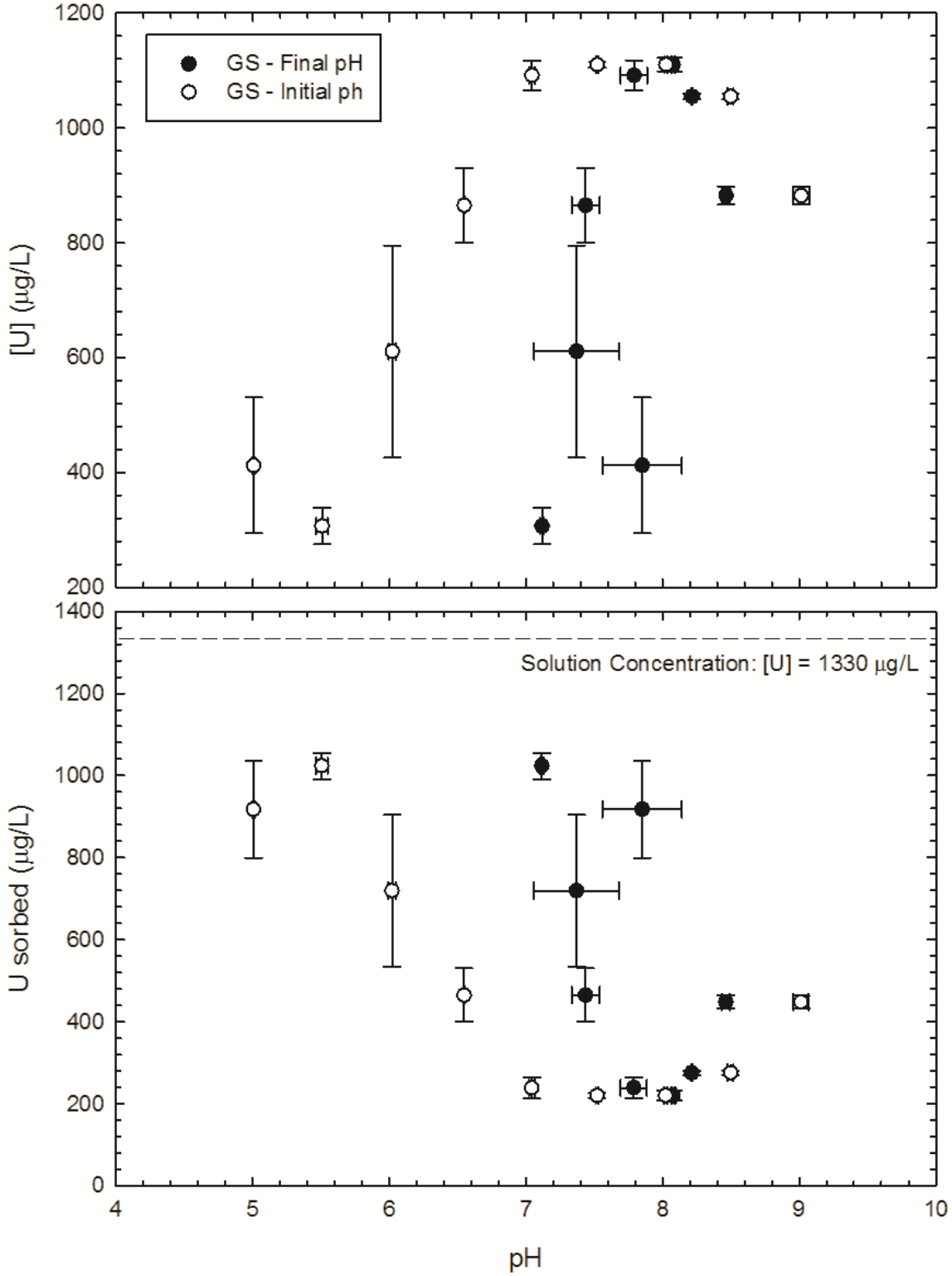

Figure 6.58. Comparison of measured U concentration to sorbed quantity for Bentonite *GS* during LLW sorption edge and envelope experimentation.

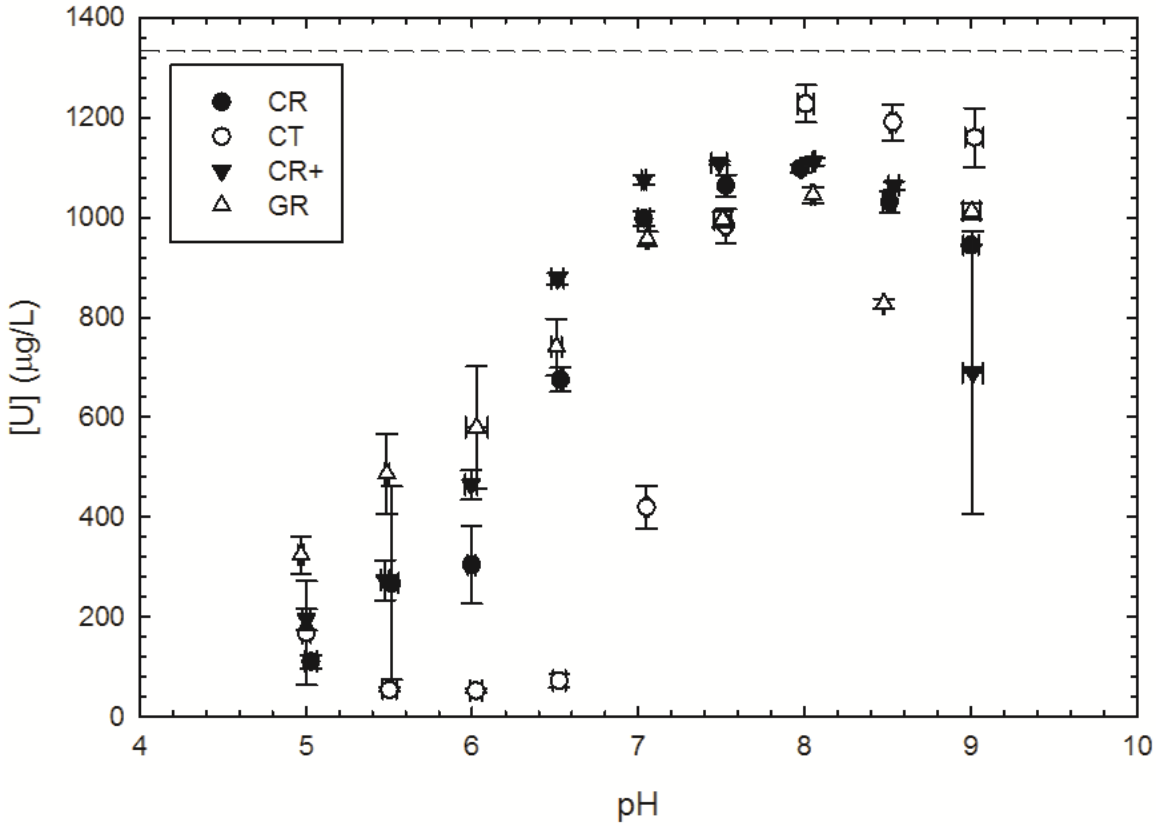

Figure 6.59. Comparison of measured U concentrations remaining in solution (in µg/L) across the experimental pH range for the polymer-modified bentonites. Initial solution concentration was 1330 µg/L of U.

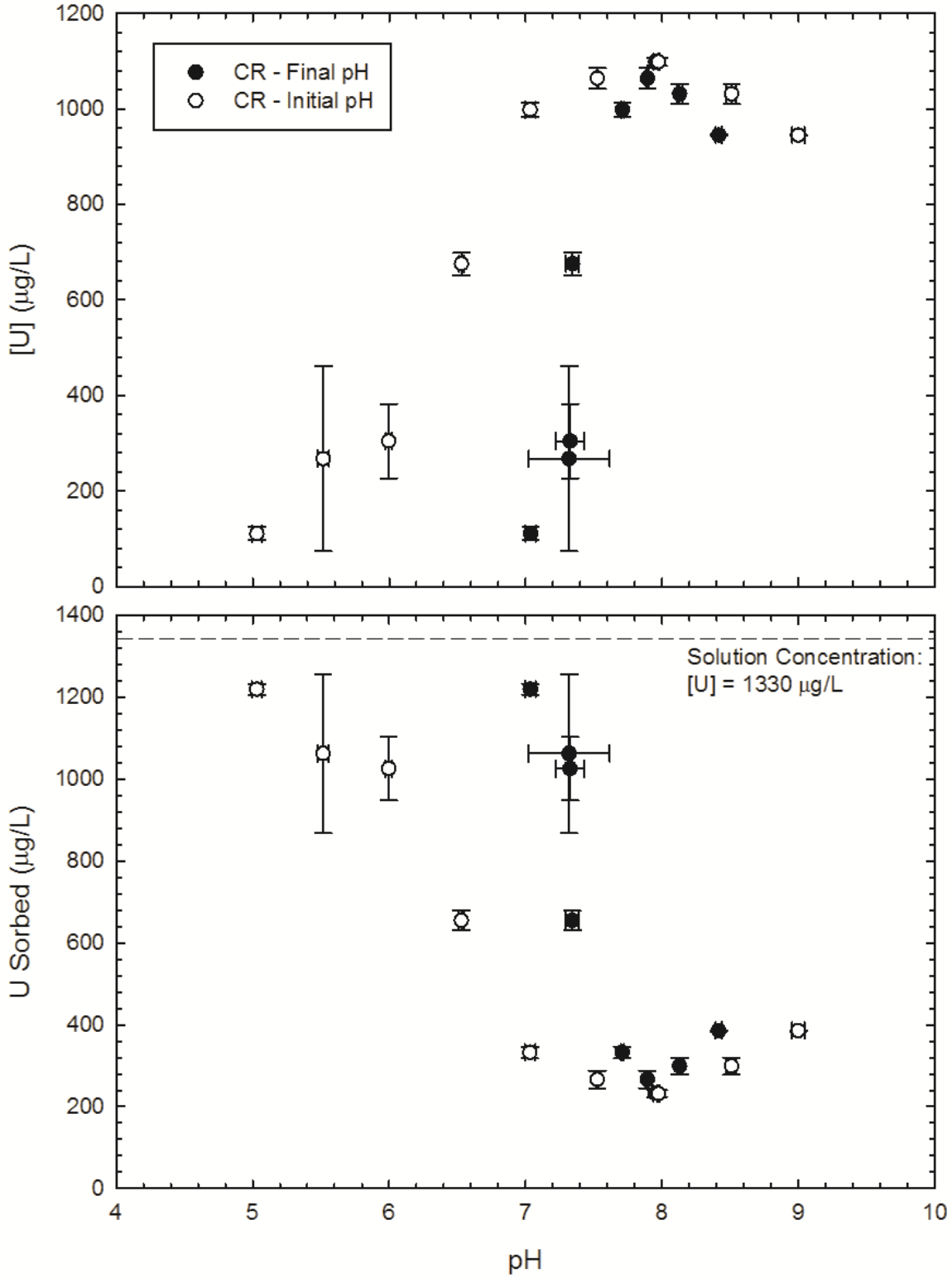

Figure 6.60. Comparison of measured U concentration to sorbed quantity for Bentonite *CR* during LLW sorption edge and envelope experimentation.

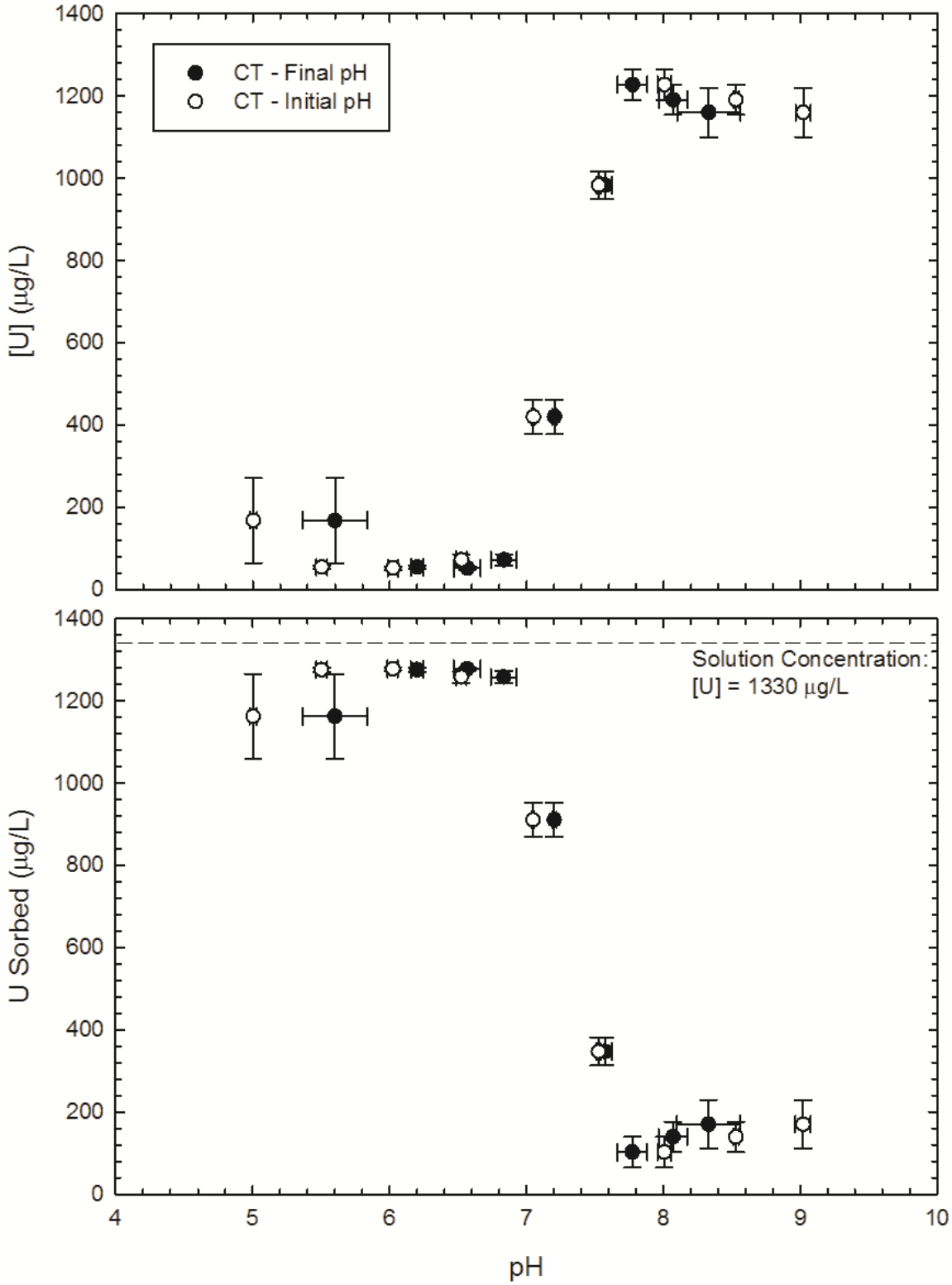

Figure 6.61. Comparison of measured U concentration to sorbed quantity for Bentonite *CT* during LLW sorption edge and envelope experimentation.

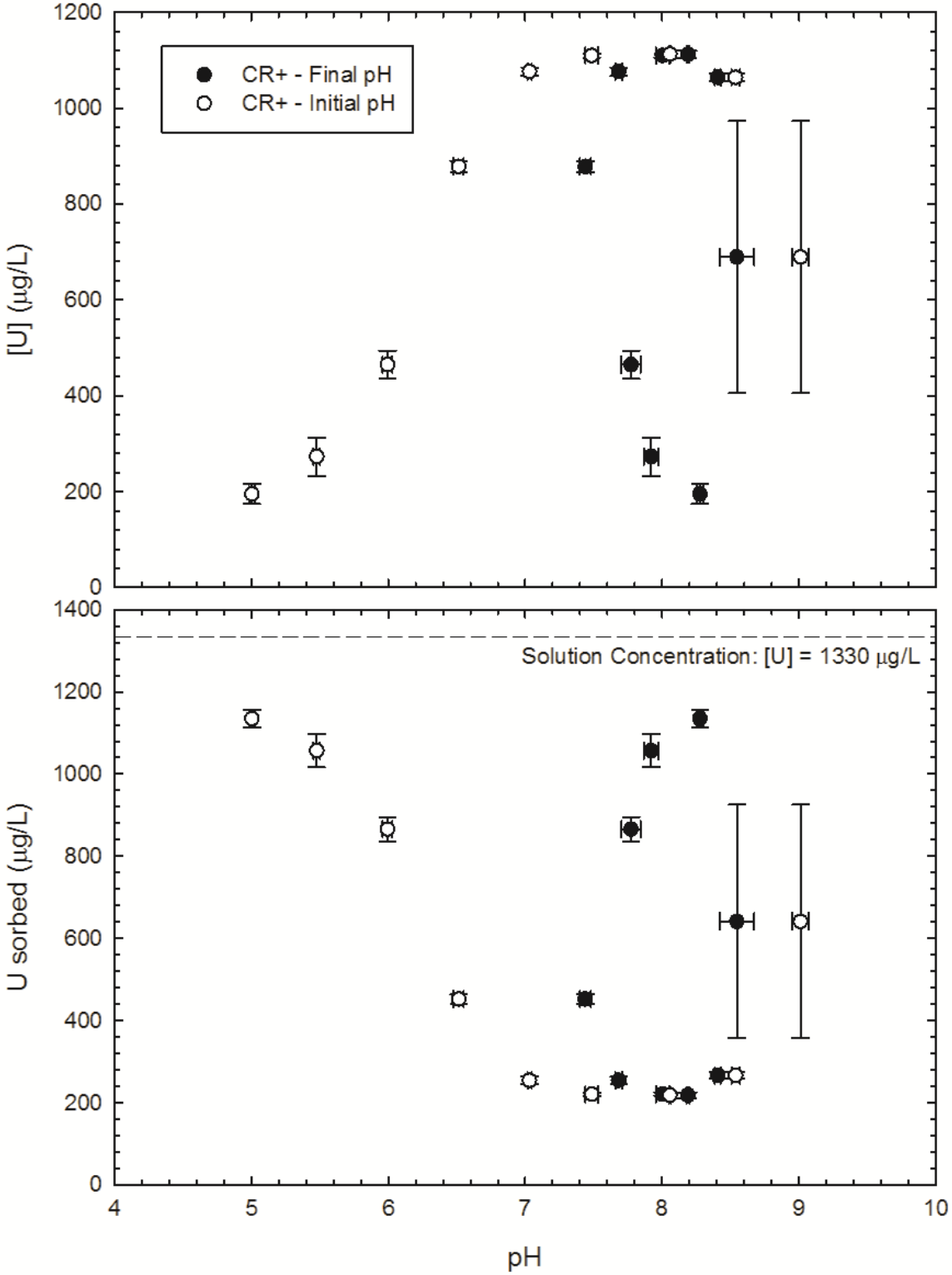

Figure 6.62. Comparison of measured U concentration to sorbed quantity for Bentonite *CR+* during LLW sorption edge and envelope experimentation.

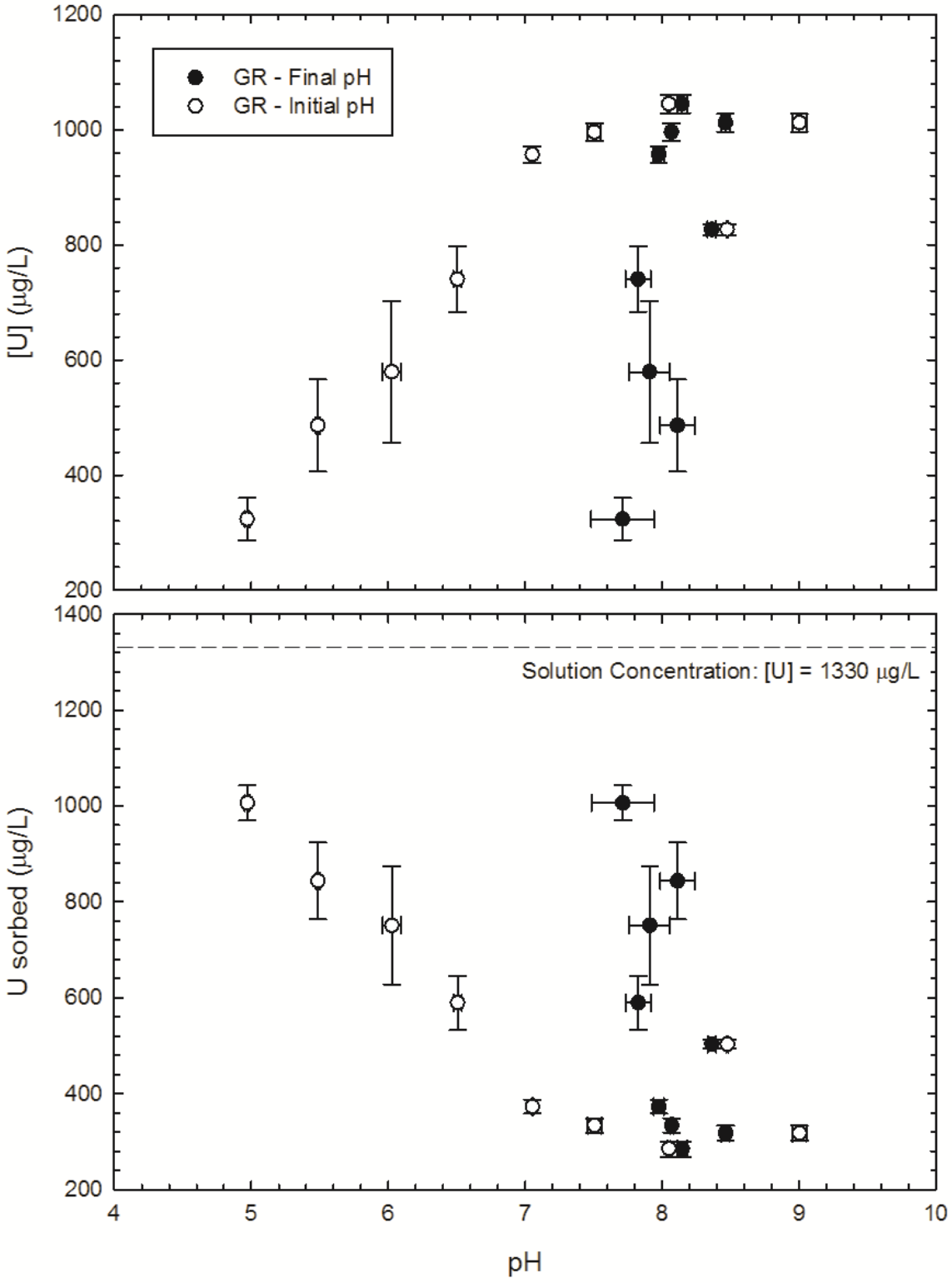

Figure 6.63. Comparison of measured U concentration to sorbed quantity for Bentonite *GR* during LLW sorption edge and envelope experimentation.

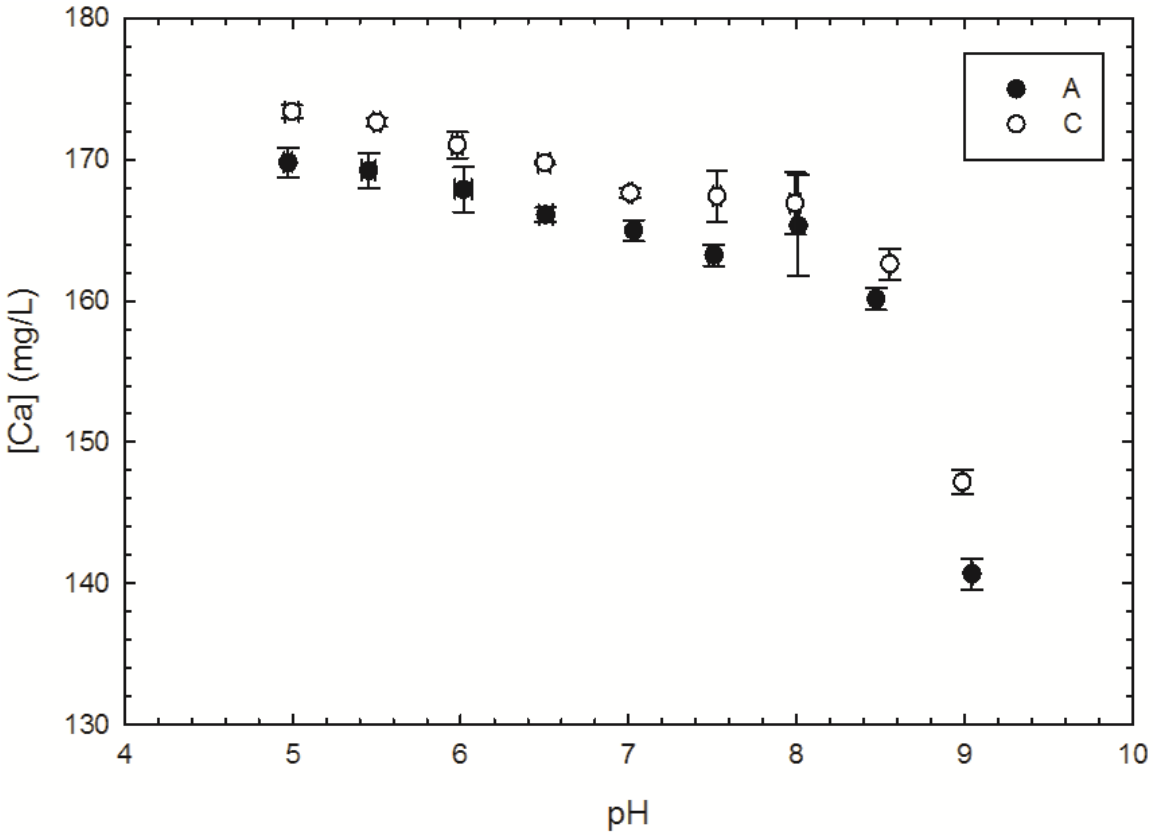

Figure 6.64. Solution concentrations of Ca (in mg/L) across the tested pH range following E&E experimentation with the natural barrier soils.

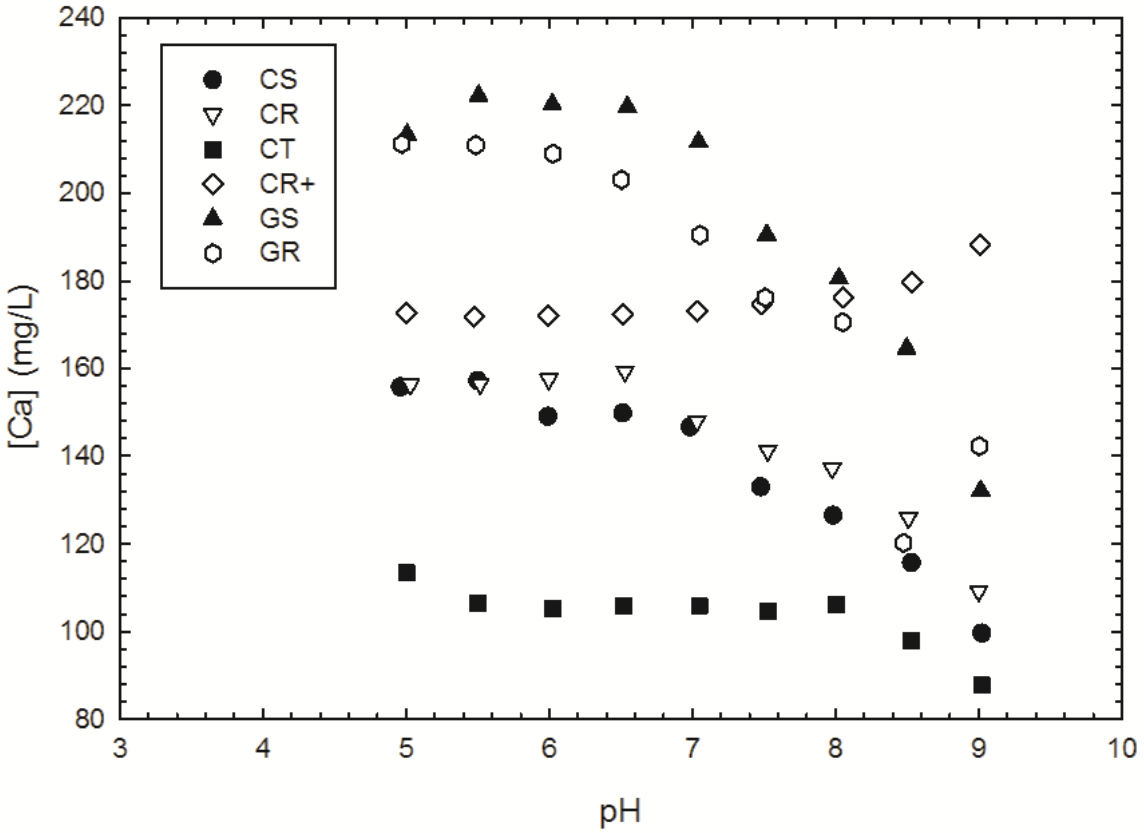

Figure 6.65. Solution concentrations of Ca (in mg/L) across the tested pH range following E&E experimentation with the bentonite suite.

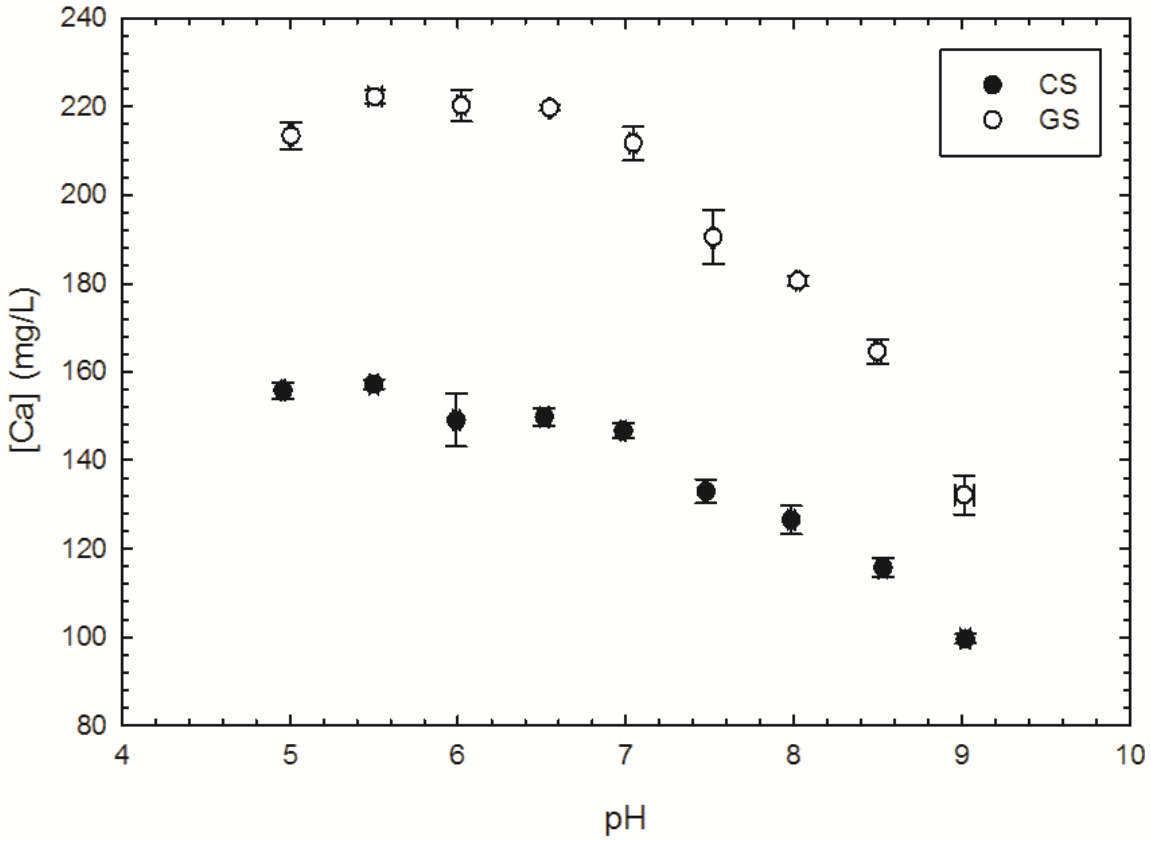

Figure 6.66. Solution concentrations of Ca (in mg/L) across the tested pH range following E&E experimentation with the standard bentonites.

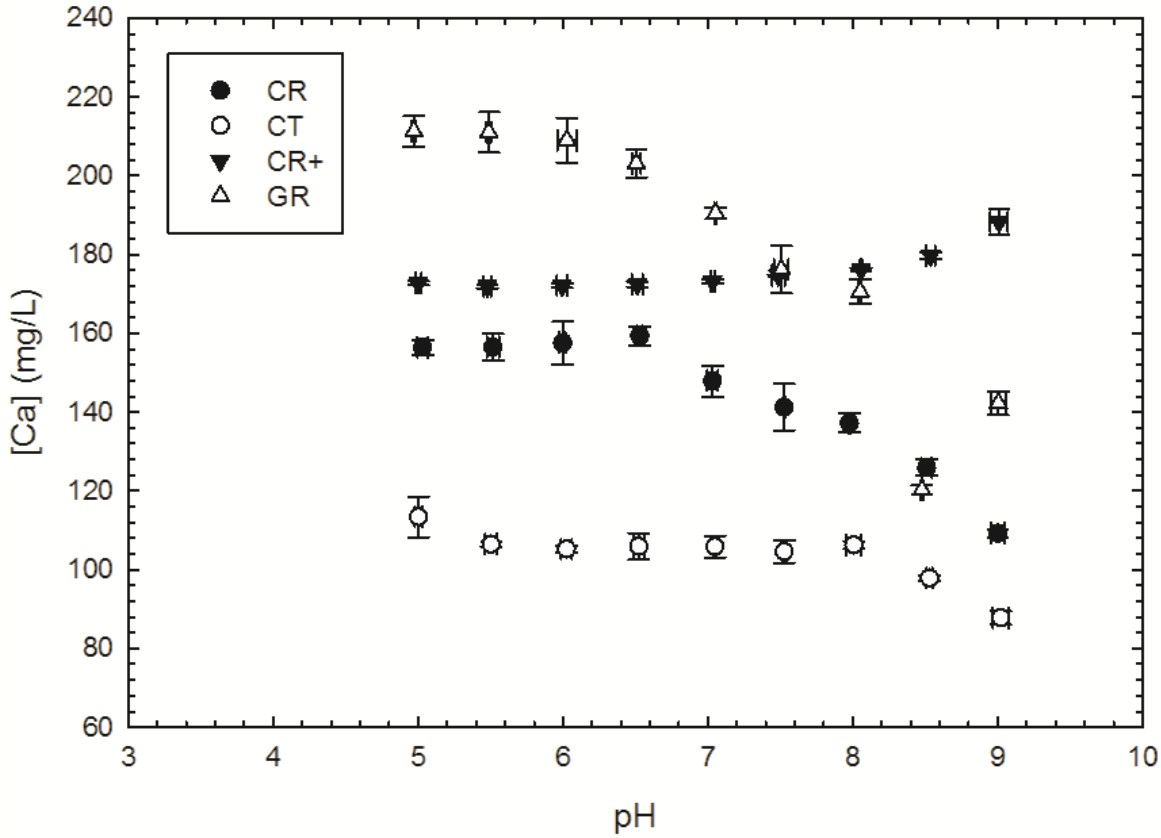

Figure 6.67. Solution concentrations of Ca (in mg/L) across the tested pH range following E&E experimentation with the polymer-modified bentonites.

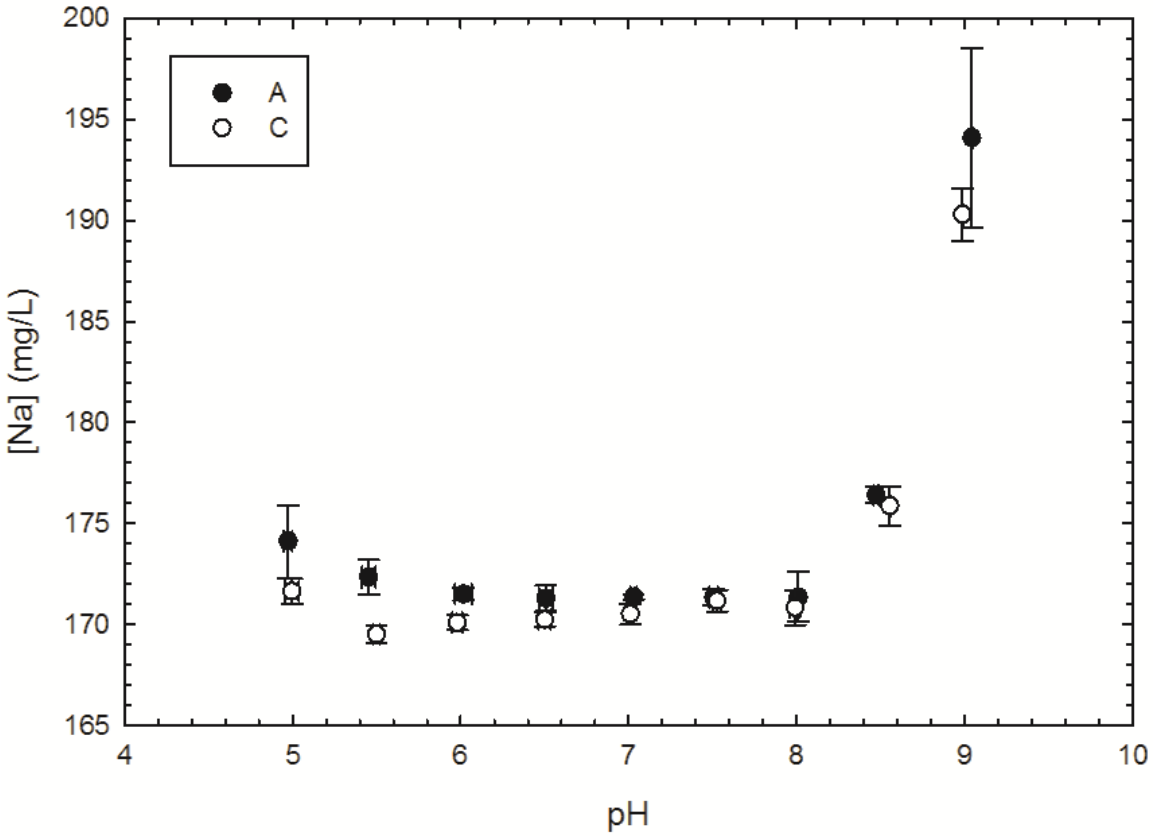

Figure 6.68. Solution concentrations of Na (in mg/L) across the tested pH range following E&E experimentation with the natural barrier soils.

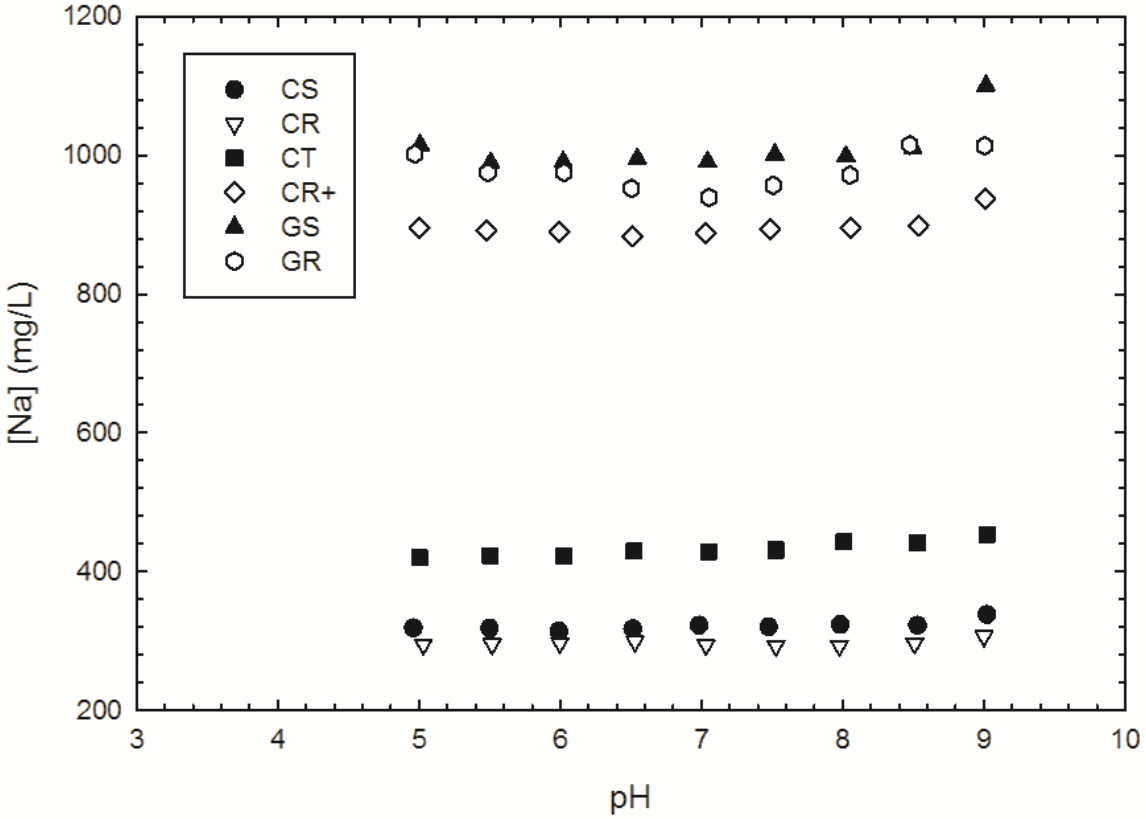

Figure 6.69. Solution concentrations of Na (in mg/L) across the tested pH range following E&E experimentation with the entire bentonite suite.

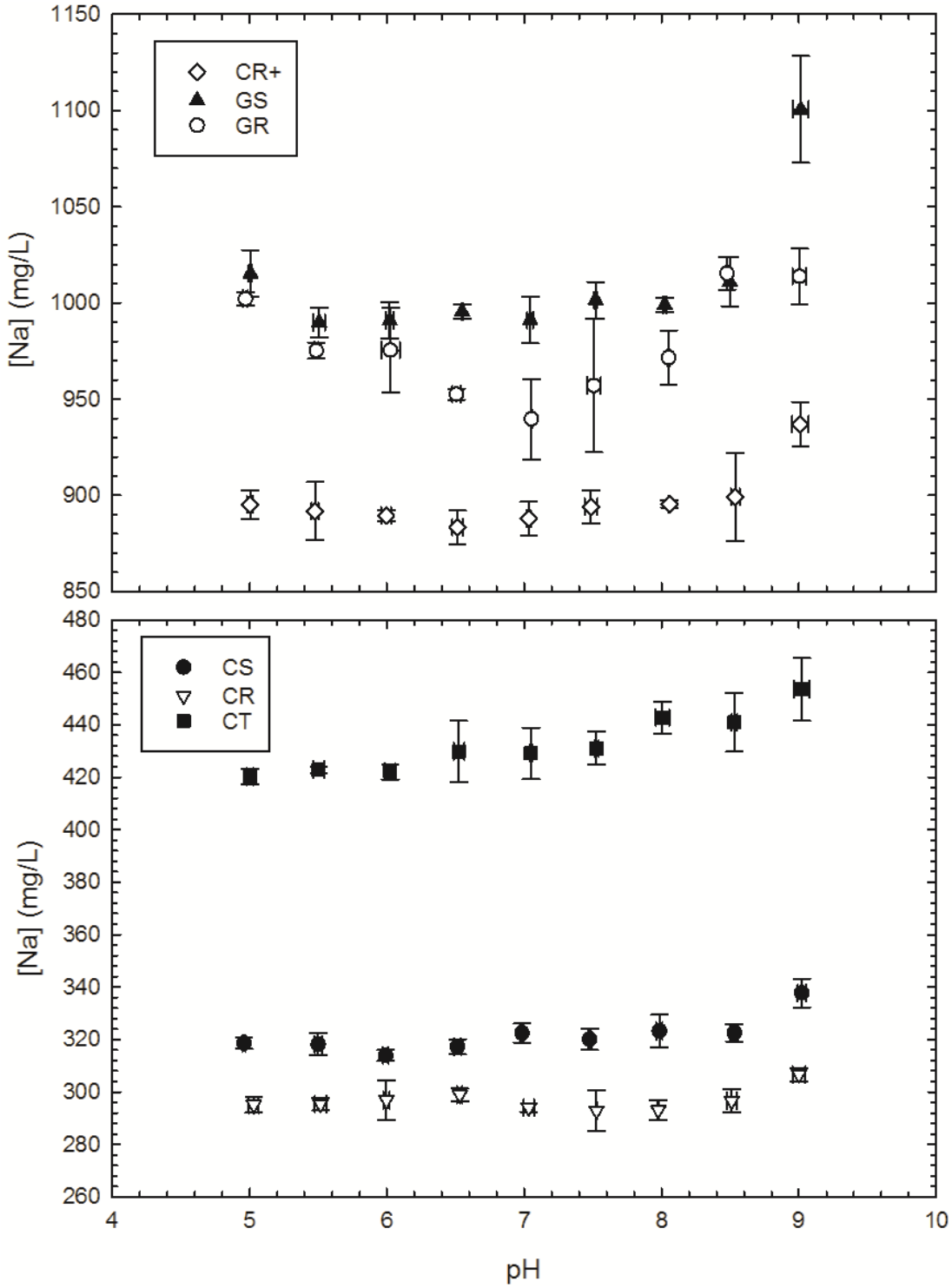

Figure 6.70. Solution concentrations of Na (in mg/L) across the tested pH range following E&E experimentation with the entire bentonite suite. For ease of comparison between the general trends of the standard and polymer-modified bentonites, the upper panel focuses on the high concentration values (850-1150 mg/L), while the lower panel shifts to the lower concentration range (260-480 mg/L). Symbols and colors correspond to those used in Figure 6.69.

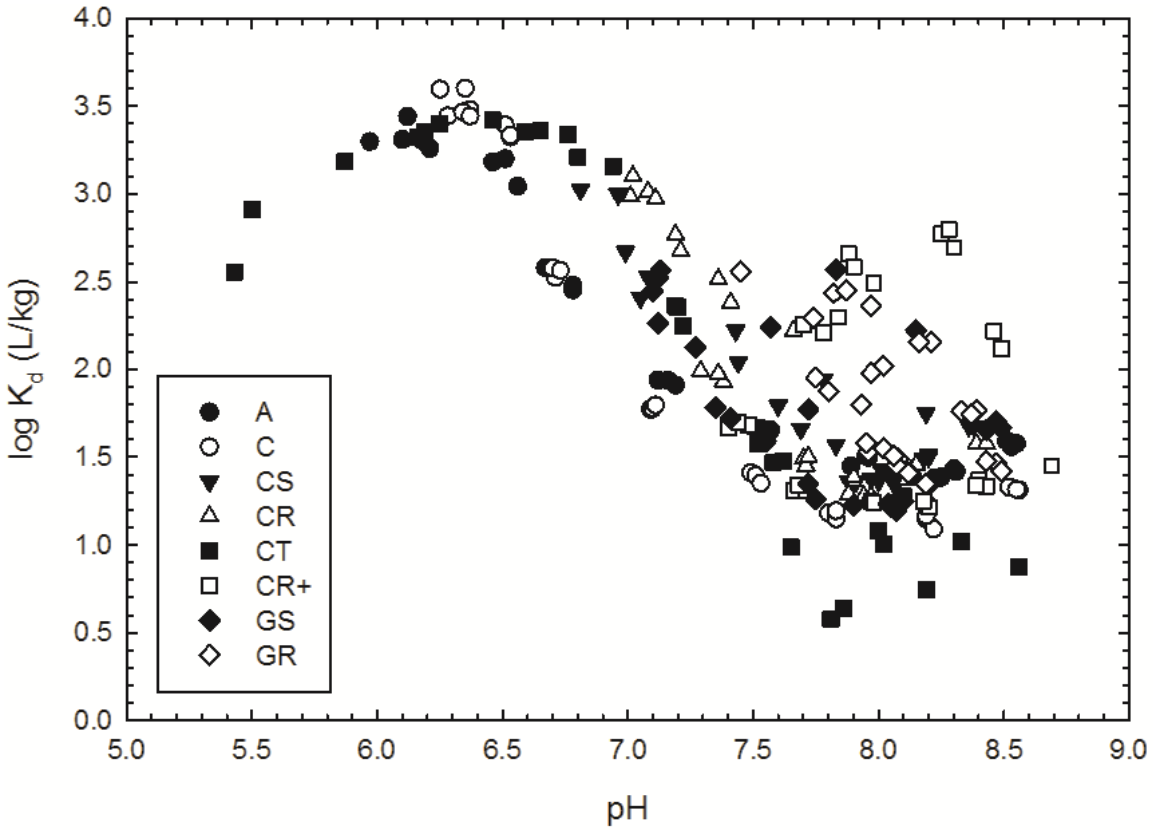

Figure 6.71. Comparison of calculated distribution coefficients (K_d, in L/kg) to final measured pH during LLW sorption edge and envelope experimentation for the tested natural study soils and bentonites.

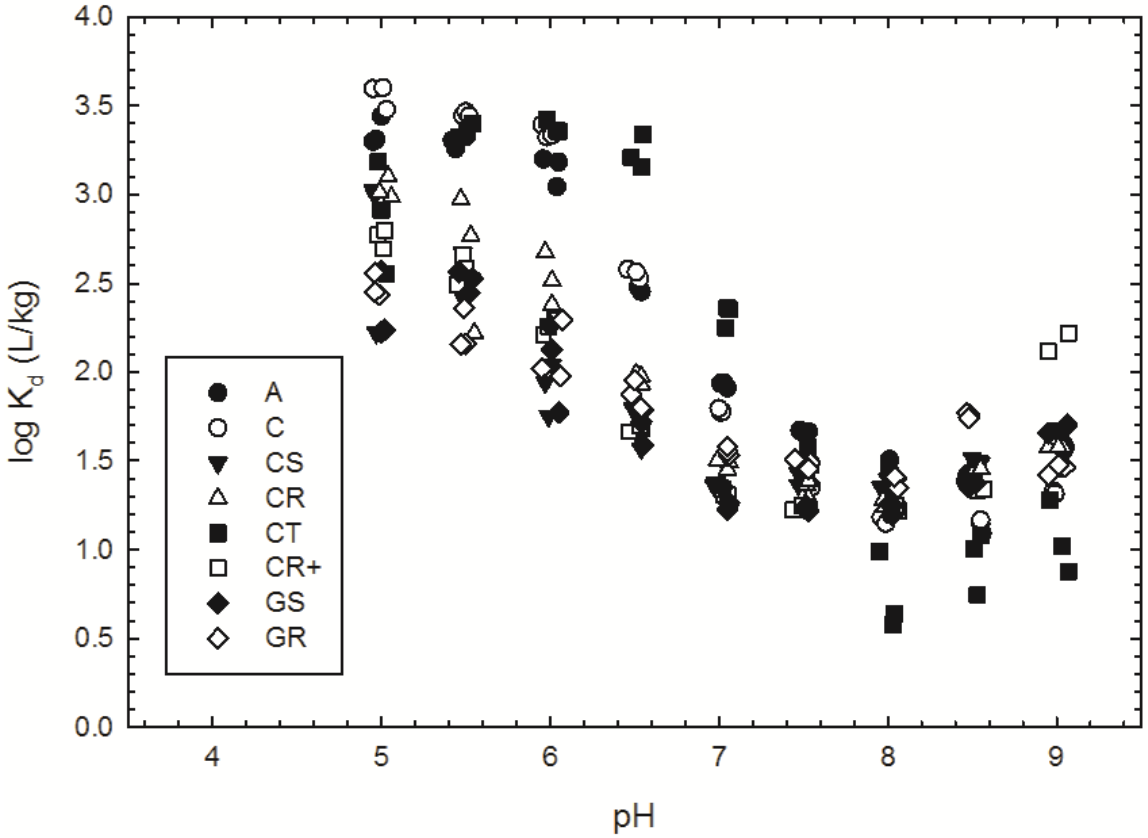

Figure 6.72. Comparison of log K_d values (in L/kg) for all soils at initial experimental pH levels during LLW sorption edge and envelope experimentation for the tested natural study soils and bentonites.

Section 7 – References

10 CFR pt.61.55. (2001). Waste classification. *Code of Federal Regulations* Title 10, Pt. 61.55, 2001 ed.

40 CFR pt.136. (2003). Guidelines establishing test procedures for the analysis of pollutants. *Code of Federal Regulations* Title 40, Pt. 136, 2003 ed.

Abollino, O., Aceto, M., Malandrino, M., Sarzanini, C., & Mentasti, E. (2003). Adsorption of heavy metals on Na-montmorillonite. Effect of pH and organic substances. *Water Research, 37*, 1619-1627.

Abollino, O., Giacomino, A., Malandrino, M., & Mentasti, E. (2008). Interaction of metal ions with montmorillonite and vermiculite. *Applied Clay Science, 38*, 227-236.

Allard, Th. and Galas, C. (2009). Radiation effects on clay mineral properties. *Applied Clay Science* **43**, 143-149.

Altmann, S. (2008). 'Geo'chemical research: A key building block for nuclear waste disposal. *Journal of Contaminant Hydrology* **102**, 174-179.

Arcos, D., Grandia, F., Domenech, C., Fernandez, A.M., Villar, M.V., Muurinen, A., Carlsson, T., Sellin, P., and Hernan, P. (2008). Long-term geochemical evolution of the near field repository: Insights from reactive transport modeling and experimental evidences. *Journal of Contaminant Hydrology* **102**, 196-209.

ASTM D 2487. (2006). "Standard Practice for Classification of Soils for Engineering Purposes (Unified Soil Classification System)," *Annual Book of ASTM Standards*, Vol. 04.08, ASTM International, West Conshohocken, PA.

ASTM D 422. (2007). "Standard Test Method for Particle-Size Analysis of Soils," *Annual Book of ASTM Standards*, Vol. 04.08, ASTM International, West Conshohocken, PA.

ASTM D 4318. (2010). “Standard Test Methods for Liquid Limit, Plastic Limit, and Plasticity Index of Soil.” ASTM International, West Conshohocken, PA, 2010. DOI: 10.1520/D4318-10. www.astm.org

ASTM D 4373. (2007). “Standard Test Method for Rapid Determination of Carbonate Content of Soils.”

ASTM D 4972. (2007). “Standard Test Method for pH of Soils.” *Annual Book of ASTM Standards*, Vol. 04.09, ASTM International, West Conshohocken, PA.

ASTM D 6239. (2009). “Standard Test Method for Uranium in Drinking Water by High-Resolution Alpha-Liquid-Scintillation Spectrometry.” ASTM International, West Conshohocken, PA, 2009. DOI: 10.1520/D6239-09. www.astm.org

ASTM D 7503. (2010). “Standard Test Method for Measuring Exchangeable Cations and Cation Exchange Capacity of Bentonite,” *Annual Book of ASTM Standards*, Vol. 04.09, ASTM International, West Conshohocken, PA.

ASTM D 854. (2010). “Standard Test Methods for Specific Gravity of Soil Solids by Water Pycnometer.” ASTM International, West Conshohocken, PA, 2010. DOI: 10.1520/DO854-10. www.astm.org

Bacaç, M., and Kumru, M.N. (2000). Uranium, radium and field measurements in the water of Gediz river. *Turkish Journal of Engineering and Environmental Sciences* **24**, 229-236.

Baeyens, B. and Bradbury, M.H. (1997). A mechanistic description of Ni and Zn sorption on Na-montmorillonite, Part I: Titration and sorption measurements. *Journal of Contaminant Hydrology* **27**, 199-222.

Bai, J., Liu, C., and Ball, W.P. (2009). Study of sorption-retarded U(VI) diffusion in Hanford silt/clay material. *Environmental Science and Technology* **43**, 7706-7711.

Barger, M. and Koretsky, C.M. (2011). The influence of citric acid, EDTA, and fulvic acid on U(VI) sorption onto kaolinite. *Applied Geochemistry* **26**, S158-S161.

Barnett, M.O., Jardine, P.M., Brooks, S.C., and Selim, H.M. (2000). Adsorption and transport of uranium(VI) in subsurface media. *Soil Science Society of America Journal* **64**, 908-917.

Benson, C.H. and Trast, J.M. (1995). Hydraulic conductivity of thirteen compacted clays. *Clays and Clay Minerals* **43**(6), 669-681.

Benson, C.H., Albright, W.H., Ray, D,P., and Smegal, J. (2007). "Review of the Idaho CERCLA Disposal Facility (ICDF) at Idaho National Laboratory, Independent Technical Review Report: Idaho Operations." Office of Engineering and Technology (EM-20), U.S. Department of Energy, Washington, DC, 5 December 2007.

Benson, C.H., Wang, X., Gassner, F.W., and Foo, D.C.F. (2008a). "Hydraulic conductivity of two geosynthetic clay liners permeated with an aluminum residue leachate." *GeoAmericas 2008 – The First Pan American Geosynthetics Conference and Exhibition*, Industrial Fabrics Association International (IFAI), Roseville, MN, 94–101.

Benson, C.H., Albright, W.H., Ray, D.P., and Smegal, J. (2008b). "Review of the Environmental Management Waste Management Facility (EMWMF) at Oak Ridge, Independent Technical Review Report: Oak Ridge Reservation." Office of Engineering and Technology (EM-20), U.S. Department of Energy, Washington, DC, 1 February 2008.

Bostick, B.C., Fendorf, S., Barnett, M.O., Jardine, P.M., and Brooks, S.C. (2002). Uranyl surface complexes formed on subsurface media from DOE facilities. *Soil Science Society of America Journal* **66**, 99-108.

Bradbury, M.H. and Baeyens, B. (1997). A mechanistic description of Ni and Zn sorption on Na-montmorillonite – Part II: Modelling. *Journal of Contaminant Hydrology* **27**, 223-248.

Bradbury, M.H. and Baeyens, B. (1999). Modelling the sorption of Zn and Ni on Ca-montmorillonite. *Geochimica et Cosmochimica Acta* **63** (3/4), 325-336.

Bradbury, M.H. and Baeyens, B. (2005a). Modelling the sorption of Mn(II), Co(II), Ni(II), Zn(II), Cd(II), Eu(III), Am(III), Sn(IV), Th(IV), Np(V), and U(VI) on montmorillonite: Linear free energy relationships and estimates of surface binding constants for some selected heavy metals and actinides. *Geochimica et Cosmochimica Acta* **69**, 875-892.

Bradbury, M.H. and Baeyens, B. (2005b). Experimental measurements and modeling of sorption competition on montmorillonite. *Geochimica et Cosmochimica Acta* **69**, 4187-4197.

Bradbury, M.H. and Baeyens, B. (2009a). Sorption modelling on illite. Part I: Titration measurements and the sorption of Ni, Co, Eu and Sn. *Geochimica et Cosmochimica Acta* **73** 990-1003.

Bradbury, M.H. and Baeyens, B. (2009b). Sorption modelling on illite. Part II: Actinide sorption and linear free energy relationships. *Geochimica et Cosmochimica Acta* **73** 1004-1013.

Breynaert, E., Scheinost, A.C., Dom, D., Rossberg, A., Vancluysen, J., Gobechiya, E., Kirschhock, C.E.A., and Maes, A. (2010). Reduction of Se(IV) in Boom Clay: XAS solid phase speciation. *Environmental Science and Technology* **44**, 6649-6655.

Brown, G.W., and Parks, G.A. (2001). Sorption of trace elements on mineral surfaces: Modern perspectives from spectroscopic studies, and comments on sorption in the marine environment. *International Geology Review* **43**, 963-1073.

Buesseler, K.O., Kaplan, D.I., Dai, M., and Pike, S. (2009). Source-dependent and source-independent controls on plutonium oxidation state and colloid associations in groundwater. *Environmental Science and Technology* **43**, 1322-1328.

Carter, D.L., Mortland, M.M., and Kemper, W.D. (1986). "Specific surface." *Methods of soil analysis – Part 1: Physical and mineralogical methods*, A. Klute, ed., Soil Science Society of America, Madison, WI, 413-423.

Chawla, F., Steinmann, P., Loizeau, J.-L., Hassouna, M., and Froidevaux, P. (2010). Binding of ^{239}Pu and ^{90}Sr to organic colloids in soil solutions: Evidence from a field experiment. *Environmental Science and Technology* **44**, 8509-8514.

Chen, L. and Lu, S. (2008). Sorption and desorption of radiocobalt on montmorillonite – Effects of pH, ionic strength and fulvic acid. *Applied Radiation and Isotopes* **66**, 288-294.

Cheng, T. and Saiers, J.E. (2010). Colloid-facilitated transport of cesium in vadose-zone sediments: The importance of flow transients. *Environmental Science and Technology* **44**, 7443-7449.

Chian, E.S.K., and DeWalle, F.B. (1977). Characterization of soluble organic matter in leachate. *Environmental Science and Technology* **11**, 158-163.

Christensen, J. B., Jensen, D. L., Gron, C., Filip, Z. and Christensen, T. H. (1998). Characterization of the dissolved organic carbon in landfill leachate-polluted groundwater. *Water Research* **32**, 125–135.

Christensen, T. H. and Kjeldsen, P. (1989). "Basic biochemical processes in landfills." *Sanitary Landfilling: Process, Technology and Environmental Impact,* T.H. Christensen, R. Cossu, and R. Stegmann, eds. Academic Press, London, UK, Chap 2.1, 29-49.

Christensen, T. H. , and Kjeldsen, P. (1995). “Landfill emissions and environmental impact: An introduction.” *Proceedings of Sardinia ‘95 - Fifth International Landfill Symposium, CISA.,* T.H. Christensen, R. Cossu, and R. Stegmann, eds*.,* Cagliari: Environmental Sanitary Engineering Centre, Cagliari, Italy, vol. III, 3-12.

Christensen, T.H., Kjeldsen, P., Bjerg, P.L., Jensen, D.L., Christensen, J.B., Baun, A., Albrechtsen, H.-J., and Heron, G., (2001). Biogeochemistry of landfill leachate plumes. *Applied Geochemistry* **16**, 659-718.

Cornell, R.M. (1993). Adsorption of cesium on minerals: A review. *Journal of Radioanalytical and Nuclear Chemistry* **171**, 483-500.

Curtis, G.P., Fox, P., Kohler, M., and Davis, J.A. (2004). Comparison of in situ uranium K_D values with a laboratory determined surface complexation model. *Applied Geochemistry* **19**, 1643-1653.

Darban, A.K., Yong, R.N., and Ravaj, S. (2010). Coupled chemical speciation-solute transport model for prediction of solute transport in clay buffers. *Applied Clay Science* **47**, 127-132.

Daniel, D.E. (1987). Earthen liners for land disposal facilities. *Geotechnical Practice for Waste Disposal ’87, GSP No. 13*, R.D. Woods, ed. ASCE, New York, NY, 21-39.

Daskalopoulos, E., Bader, O., and Probert, S.D. (1998). Municipal solid waste: a prediction methodology for the generation rate and composition in the European Union countries and the United States of America. *Resources, Conservation and Recycling* **24**, 155–166.

Davis, J.A., Meece, D.E., Kohler, M., and Curtis, G.P. (2004). Approaches to surface complexation modeling of uranium(VI) adsorption on aquifer sediments. *Geochimica et Cosmochimica Acta* **68** (18), 3621-3641.

Dong, W., Ball, W. P., Liu, C., Wang, Z., Stone, A. T., Bai, J., and Zachara, J. M. (2005). Influence of calcite and dissolved calcium on uranium(VI) sorption to a Hanford subsurface sediment. *Environmental Science and Technology* **39**, 7949-7955.

Dos Reis, E.L.T., Scapin, M., Cotrim, M.E.B., Salvador, V.L., and Pires, M.A.F. (2009). Impurities determination on nuclear fuel element components for the IEA-RI Research Reactor by analytical methods based on ED-XRF and ICP-OES. *2009 International Nuclear Atlantic Conference*, INAC 2009, Associação Brasileira de Energia Nuclear – ABEN, Rio de Janeiro, RJ, Brazil.

Ehrig, H.J. (1988). "Water and element balances of landfills." *Lecture Notes in Earth Sciences 20: The landfill - reactor and final storage*, P. Baccini, ed., Springer-Verlag, Berlin, Germany, 83-115.

El Himri, H., Pastor, A., and de la Guardia, M. (2000). Determination of uranium in tap water by ICP-MS. *Fresenius' Journal of Analytical Chemistry* **367**, 151-156.

Emsley, John. (2011). "Uranium." *Nature's Building Blocks: An A-to-Z Guide to the Elements.* Oxford: Oxford University Press, 594-602.

EPA (1994). "Method 200.8: Determination of Trace Elements in Waters and Wastes by Inductively Coupled Plasma-Mass Spectrometry," Revision 5.4. http://www.epa.gov/sam/pdfs/EPA-200.8.pdf

Fan, Q.H., Tan, X.L., Li, J.X., Wang, X.K., Wu, W.S., and Montavon, G. (2009). Sorption of Eu(III) on attapulgite studied by batch, XPS, and EXAFS techniques. *Environmental Science and Technology* **43**, 5776-5782.

Farquhar C.J. and Rovers, F.A. (1973). Gas production during refuse decomposition. *Water, Air, and Soil Pollution* **2**, 483-495.

Fatta D., Papadopoulos, A., and Loizidou, M. (1999). A study on the landfill leachate and its impact on the groundwater quality of the greater area. *Environmental Geochemistry and Health* **21**(2), 175–190.

Faure, G. (2001). “Chemical properties of Rb and Sr.” *Origin of igneous rocks: The isotopic evidence*, Springer, New York, NY, 1-2.

Fernandes, M.M., Baeyens, B., and Bradbury, M.H. (2008). The influence of carbonate complexation on lanthanide/actinide sorption on montmorillonite. *Radiochimica Acta* **96**, 691-697.

Fernandes, M.M., Stumpf, T., Baeyens, B., Walther, C., and Bradbury, M.H. (2010). Spectroscopic identification of ternary Cm-carbonate surface complexes. *Environmental Science and Technology* **44**, 921-927.

Fernandes, M.M., Baeyans, B., Dähn, R., Scheinost, A.L., and Bradbury, M.H. (2012). U(VI) sorption on montmorillonite in the absence and presence of carbonate: A macroscopic and microscopic study. *Geochimica et Cosmochimica Acta* **93**, 262-277.

Foo, K.Y. and Hameed, B.H. (2010). Insights into the modeling of adsorption isotherm systems. *Chemical Engineering Journal* **156**, 2-10.

Fox, P.M., Davis, J.A., and Zachara, J.M. (2006). The effect of calcium on aqueous uranium(VI) speciation and adsorption to ferrihydrite and quartz. *Geochimica et Cosmochimica Acta* **70**, 1379-1387.

Galunin, E., Alba, M.D., Mviles, M.A., Santos, M.J., and Vidal, M (2009). Reversibility of La and Lu sorption onto smectites: Implications for the design of engineered barriers in deep geological repositories *Journal of Hazardous Materials* **172**, 1198-1205.

Galunin, E., Alba, M.D., Santos, M.J., Abrao, T., and Vidal, M. (2010). Lanthanide sorption on smectitic clays in presence of cement leachates. *Geochimica et Cosmochimica Acta* **74**, 862-875.

Gaona, X., Montoya, V., Colas, E., Grive, M., and Duro, L. (2008). Review of the complexation of tetravalent actinides by ISA and gluconate under alkaline to hyperalkaline conditions. *Journal of Contaminant Hydrology* **102**, 217-227.

Gates, W.P. and Bouazza, A. (2010). Bentonite transformations in strongly alkaline solutions. *Geotextiles and Geomembranes* **28** (2), 219–225.

Gates, W.P., Bouazza, A., and Churchman, G.J. (2009). Bentonite clay keeps pollutants at bay. *Elements* **5** (April), 105-110.

Geckeis, H. and Rabing, T. (2008). Actinide geochemistry: From the molecular level to the real system. *Journal of Contaminant Hydrology* **102**, 187-195.

Goldstein, S.J., Abdel-Fattah, A.I., Murrell, M.T., Dobson, P.F., Norman, D.E., Amato, R.S., and Nunn, A.J. (2010). Uranium-series constraints on radionuclide transport and groundwater flow at the Nopal I Uranium Deposit, Sierra Pena Blanca, Mexico. *Environmental Science and Technology* **44**, 1579-1586.

Grambow, B. (2008). Mobile fission and activation products in nuclear waste disposal. *Journal of Contaminant Hydrology* **102**, 180-186.

Gray, T. (2007a). “Isotope Data for Curium 244.” *Periodic Table* <periodictable.com/isotopes/096.244/index.full.html> (June 11, 2012).

Gray, T. (2007b). “Isotope Data for Uranium 238.” *Periodic Table* <periodictable.com/isotopes/092.238/index.full.html> (June 13, 2012).

Gulec, S.B., Edil, T.B., and Benson, C.H. (2004). Effect of acidic mine drainage on the polymer properties of an HDPE geomembrane. *Geosynthetics International* **11** (2), 60–72.

Gurdal, T., Benson, C.H., and Albright, W. (2003). Hydrologic properties of final cover

soils from the Alternative Cover Assessment Program. Geo Engineering Report No. 03-02, Geo Engineering Program, University of Wisconsin-Madison Madison, Wisconsin 53706 USA, February 5, 2003.

Hartmann, E., Baeyens, B., Bradbury, M.H., Geckeis, H., and Stumpf, T. (2008). A spectroscopic characterization and quantification of M(III)/clay mineral outer-sphere complexes. *Environmental Science and Technology* **42**, 7601-7606.

Hammond, G.E., Lichtner, P.C., and Rockhold, M.L. (2011). Stochastic simulation of uranium migration at the Hanford 300 area. *Journal of Contaminant Hydrology* **120-121**, 115-128.

Heberling, F., Brendebach, B., and Bosbach, D. (2008). Neptunium(V) adsorption to calcite. *Journal of Contaminant Hydrology* **102** 246-252.

Holmboe, M., Wold, S., and Jonsson, M. (2010). Colloid diffusion in compacted bentonite: Microstructural constraints. *Clays and Clay Minerals* **58**(4), 531-541.

Holtz, R.D., Kovacs, W.D., and Sheahan, T.C. (2011). "4.6.2 Exchangeable cations and cation exchange capacity (CEC)." *An introduction to geotechnical engineering, second edition,* Pearson Education, Inc., Upper Saddle River, NJ, 136-138.

Humelnicu, D., Dinu, M.V., and Drăgan, E.S. (2011). Adsorption characteristics of UO_2^{2+} and Th^{4+} ions from simulated radioactive solutions onto chitosan/clinoptilolite sorbents. *Journal of Hazardous Materials* **185**, 447-455.

Hyun, S.P., Fox, P.M., Davis, J.A., Campbell, K.M., Hayes, K.F., and Long, P.E. (2009). Surface complexation modeling of U(VI) adsorption by aquifer sediments from a former mill tailings site at Rifle, Colorado. *Environmental Science and Technology* **43**, 9368-9373.

Iijima, K., Tomura, T., and Shoji, Y. (2010). Reversibility and modeling of adsorption behavior of cesium ions on colloidal montmorillonite particles. *Applied Clay Science* **49**, 262-268.

International Atomic Energy Agency (IAEA). (2009). IAEA Safety Standards Series No. GSG-1: Classification of radioactive waste – General safety guide. International Atomic Energy Agency, Vienna, Austria, November 2009. Accessible via: http://www-pub.iaea.org/MTCD/publications/PDF/Pub1419_web.pdf

Inyang, H.I., Wachsmuth, P.R. and Menezes, G.B. (2009a). Georadiological barrier gamma attenuation model for waste containment. I: Model formulation. *Journal of Environmental Engineering* **April**, 225-233.

Inyang, H.I., Wachsmuth, P.R., and Menezes, G.B. (2009b). Georadiological barrier gamma attenuation model for waste containment. II: Model implementation. *Journal of Environmental Engineering* **April**, 234-242.

Jackson, M.L., Lim, C.H., and Zelazny, L.W. (1986). "Oxides, hydroxides, and aluminosilicates." *Methods of soil analysis – Part 1: Physical and mineralogical methods*, A. Klute, ed., Soil Science Society of America, Madison, WI, 113-119.

Jo, H.Y., Benson, C.H., Shackelford, C.D., Lee, J.-M., and Edil, T.B. (2005). Long-term hydraulic conductivity of a geosynthetic clay liner (GCL) permeated with inorganic salt solutions. *Journal of Geotechnical and Geoenvironmental Engineering* **131** (4), 405–417.

Kaplan, D.I., Parker, K.E., and Ritter, J.C. (1998). "Effects of aging quartz sand and Hanford sediment with sodium hydroxide on radionuclide sorption coefficients and sediment physical and hydrologic properties: Final report for Subtask 2a." Pacific Northwest National Laboratory, PNNL-11965, Richland, Washington.

Kautenburger, R. and Beck, H.P. (2010). Influence of geochemical parameters on the sorption and desorption behaviour of europium and gadolinium onto kaolinite. *Journal of Environmental Monitoring* **12**, 1295-1301.

Kim, Y. and Kirkpatrick, R.J. (1997). ^{23}Na and ^{133}Cs NMR study of cation adsorption on mineral surface: Local environments, dynamics, and effects of mixed cations. *Geochimica et Cosmochimica Acta* **61-24**, 5199-5208.

Kjeldsen, P., Morton, A. B., Rooker A. P., Baun A., Ledin A., and Christensen, T. H. (2002). Present and long-term composition of MSW landfill leachate: A review. *Critical Reviews in Environmental Science and Technology* **32**(4), 297-336.

Kolstad, D., Benson, C., and Edil, T. (2004). Hydraulic conductivity and swell of nonprehydrated GCLs permeated with multi-species inorganic solutions. *Journal of Geotechnical and Geoenvironmental Engineering* **130**(12), 1236–1249.

Kremleva, A., Kruger, S., and Rosch, N. (2011). Uranyl adsorption at (0 1 0) edge surfaces of kaolinite: A density functional study. *Geochimica et Cosmochimica Acta* **75**, 706-718.

Krumhansl, J.L., Brady, P.V., and Anderson, H.L. (2001). Reactive barriers for ^{137}Cs retention. *Journal of Contaminant Hydrology* **47**, 233-240.

Langmuir, D. (1997). “Aqueous geochemistry of uranium.” *Aqueous environmental geochemistry*, Prentice Hall, Upper Saddle River, NJ, 495-501.

Law, G.T.W., Geissler, A., Lloyd, J.R., Livens, F.R., Boothman, C., Begg, J.D.C., Denecke, M.A., Rothe, J., Dardenne, K., Burke, I.T., Charnock, J.M., and Morris, K. (2010). Geomicrobiological redox cycling of the transuranic element neptunium. *Environmental Science and Technology* **44**, 8924-8929.

Liu, C., Shi, Z., and Zachara, J.M. (2009). Kinetics of uranium(VI) desorption from contaminated sediments: Effect of geochemical conditions and model evaluation. *Environmental Science and Technology* **43**, 6560-6566.

Limousin, G., Gaudet, J.-P., Charlet, L. Szenknect, S., Barthès, V., and Krimissa, M. (2007). Sorption isotherms: A review on physical bases, modeling and measurement. *Applied Geochemistry* **22**, 249-275.

Lujaniene, G., Motiejunas, S., and Sapolaite, J. (2007). Sorption of Cs, Pu and Am on clay minerals. *Journal of Radioanalytical and Nuclear Chemistry* **274**(2), 345-353.

Luo, W. and Gu, B. (2009). Dissolution and mobilization of uranium in a reduced sediment by natural humic substances under anaerobic conditions. *Environmental Science and Technology* **43**, 152-156.

Majdan, M., Pikus, S., Gajowiak, A., Sternik, D., and Zieba, E. (2010). Uranium sorption on bentonite modified by octadecyltrimethylammonium bromide. *Journal of Hazardous Materials* **184**, 662-670.

Miller, A.W., Rodriguez, D.R., and Honeyman, B.D. (2010). Upscaling sorption/desorption processes in reactive transport models to describe metal/radionuclide transport: A critical review. *Environmental Science and Technology* **44**, 7996-8007.

Missana, T., Garcia-Gutierrez, M., and Alonso, U. (2004). Kinetics and irreversibility of cesium and uranium sorption onto bentonite colloids in a deep granitic environment. *Applied Clay Science* **26**, 137-150.

Missana, T., Alonso, U., Garcia-Gutierrez, M., and Mingarro, M. (2008). Role of bentonite colloids on europium and plutonium migration in a granite fracture. *Applied Geochemistry* **23**, 1484-1497.

Mor, S., Ravindra, K., Dahiya, R.P., and Chandra, A. (2006). Leachate characterization and assessment of groundwater pollution near municipal solid waste landfill site. *Environmental Monitoring and Assessment* **118**, 435–456.

Morrison, S.J. and Spangler, R.R. (1992). Extraction of uranium and molybdenum from aqueous solutions: A survey of industrial materials for use in chemical barriers for

uranium mill tailings remediation. *Environmental Science and Technology* **26**, 1922-1931.

Morrison, S.J., Metzler, D.R., and Carpenter, C.E. (2001). Uranium precipitation in a permeable reactive barrier by progressive irreversible dissolution of zerovalent iron. *Environmental Science and Technology* **35**, 385-390.

Morrison, S.J. (2003). Performance evaluation of a permeable reactive barrier using reaction products as tracers. *Environmental Science and Technology* **37**, 2302-2309.

Moturi, M. C. Z., Rawat, M. and Subramanian, V. (2004). Distribution and fractionation of heavy metals in solid waste from selected sites in the industrial belt of Delhi, India. *Environmental Monitoring and Assessment* **95**, 183–199.

Omar, H., Arida, H., and Daifullah, A. (2009). Adsorption of ^{60}Co radionuclides from aqueous solution by raw and modified bentonite. *Applied Clay Science* **44**, 21-26.

Øygard, J. K. and Gjengedal, E. (2009). Uranium in municipal solid waste landfill leachate. *International Journal of Environmental Research* **3**(1), 61-68.

Park, M.G., Edil, T.B., and Benson, C.H. (2011). Modeling volatile organic compound transport in composite liners. *Journal of Geotechnical and Geoenvironmental Engineering* doi:10.1061/(ASCE)GT.1943-5606.0000630

Poinssot, C., Baeyens, B., and Bradbury, M.H. (1999). Experimental and modelling studies of caesium sorption on illite. *Geochimica et Cosmochimica Acta* **63** (19/20), 3217-3227.

Powell, B.A., Fjeld, R.A., Kaplan, D.I., Coates, J.T., and Serkiz, S.M. (2004). Pu(V)O2+ adsorption and reduction by synthetic magnetite (Fe3O4). *Environmental Science and Technology* **38**, 6016-6024.

Powell, J., Abitz, R.J., Broberg, K.A., Hertel, W.A., and Johnston, F. (2011). “Status and performance of the On-Site Disposal Facility Fernald Preserve, Cincinnati, Ohio.”

Proceedings, Waste Management Symposia 2011, WM Symposia, Ref. 11137, accessed via: http://www.wmsym.org/archives/2011/papers/11137.pdf

Reimann, C., Banks, D., Bogatyrev, I., de Caritat, P., Kashulina G., and Niskavaara, H. (1999). Lake water geochemistry on the western Kola Peninsula, northwest Russia. *Applied Geochemistry* **14**, 787-805.

Rimstidt, J.D., Balog, A., and Webb, J. (1998). Distribution of trace elements between carbonate minerals and aqueous solutions. *Geochimica et Cosmochimica Acta* **62**, 1851–1863.

Rod, K.A., Um, W., and Flury, M. (2010). Transport of strontium and cesium in simulated Hanford tank waste leachate through quartz sand under saturated and unsaturated flow. *Environmental Science and Technology* **44**, 8089-8094.

Rosin-Paumier, S. and Touze-Foltz, N. (2012). Hydraulic and chemical evolution of GCLs during filter press and oedopermeametric tests performed with real leachate. *Geotextiles and Geomembranes* **33**, 15-24.

Rowe, R.K. (2005). Long-term performance of containment barrier systems. *Géotechnique* **55**(9), 631-678.

Rowe, R.K., Rimal, S., and Sangam, H. (2009). Ageing of HDPE geomembrane exposed to air, water and leachate at different temperatures. *Geotextiles and Geomembranes* **27**(2), 137-151.

Saarela, J. (2003). Pilot investigations of surface parts of three closed landfills and factors affecting them. *Environmental Monitoring and Assessment* **84**, 183–192.

Sato, H., Ashida, T., Kohara, Y., Yui, M., and Sasaki, N. (1992). Effect of dry density on diffusion of some radionuclides in compacted sodium bentonite. *Journal of Nuclear Science and Technology* **29**(9), 873-882.

Sato, H. and Miyamoto, S. (2004). Diffusion behavior of selenite and hydroselenide in compacted bentonite. *Applied Clay Science* **26**, 47-55.

Schlegel, M.L. and Descostes, M. (2009). Uranium uptake by hectorite and montmorillonite: A solution chemistry and polarized EXAFS study. *Environmental Science and Technology* **43**, 8593-8598.

Shackelford, C.D. (1991). Laboratory diffusion testing for waste disposal – A review. *Journal of Contaminant Hydrology* **7**, 177-217.

Singer, D.M., Maher, K., and Brown, G.E. Jr. (2009). Uranyl-chlorite sorption/desorption: Evaluation of different U(VI) sequestration processes. *Geochimica et Cosmochimica Acta* **73**, 5989-6001.

Singer, D.M., Chatman, S.M., Ilton, E.S., Rosso, K.M. Banfield, J.F., and Waychunas, G.A. (2012 a). Identification of simultaneous U(VI) sorption complexes and U(IV) nanoprecipitates on the magnetite (1 1 1) surface. *Environmental Science and Technology* **46**, 3811-3820.

Singer, D.M., Chatman, S.M., Ilton, E.S., Rosso, K.M., Banfield, J.F., and Waychunas, G.A. (2012 b). U(VI) sorption and reduction kinetics on the magnetite (1 1 1) surface. *Environmental Science and Technology* **46**, 3821-3830.

Singh, A., Ulrich, K.-U., and Giammar, D.E. (2010). Impact of phosphate on U(VI) immobilization in the presence of goethite. *Geochimica et Cosmochimica Acta* **74**, 6324-6343.

Singh, A., Catalano, J.G., Ulrich, K.-U., and Giammar, D.E. (2012). Molecular-scale structure of uranium(VI) immobilized with goethite and phosphate. *Environmental Science and Technology* **46**, 6594-6603.

Singh, B.K., Jain, A., Kumar, S., Tomar, B.S., Tomar, R., Manchanda, V.K., and Ramanathan, S. (2009). Role of magnetite and humic acid in radionuclide migration in the environment. *Journal of Contaminant Hydrology* **106**, 144-149.

Skempton, A.W. (1953). “The colloidal activity of clays.” *Proceedings of the Third International Conference on Soil Mechanics and Foundation Engineering*, Swiss Society for Soil Mechanics and Foundation Engineering, Zurich, Switzerland, Vol. I, p. 57-61.

Sorieul, S., Allard, T., Wanh, L.M., Grambin-Lapeyre, C., Lian, J., Calas, G., and Ewing, R.C. (2008). Radiation-stability of smectite. *Environmental Science and Technology* **42**, 8407-8411.

Sposito, G. (1989). *The chemistry of soils,* Oxford University Press, New York, NY.

Stewart, B.D., Mayes, M.A., and Fendorf, S. (2010). Impact of uranyl-calcium-carbonato complexes on uranium(VI) adsorption to synthetic and natural sediments. *Environmental Science and Technology* **44**, 928-934.

Stravato, M. (2014). “Rodney A. Baltzer, president of Waste Control Specialists, showing a model of the engineered bed that containers of radioactive waste sit on. There is a base layer of nearly waterproof clay, a layer of concrete reinforced with steel and three layers of plastic.” Photograph. *The New York Times,* January 20, 2014, <http://www.nytimes.com/2014/01/21/business/energy-environment/texas-company-alone-in-us-cashes-in-on-nuclear-waste.html> (Jan. 29, 2014).

Strawn, D.G. and Sparks, D.L. (1999). The use of XAFS to distinguish between inner- and outer-sphere lead adsorption complexes on montmorillonite. *Journal of Colloid and Interface Science* **216**, 257-269.

Tian, K. (2012). “Durability of high density polyethylene geomembrane in low-level radioactive waste leachate.” M.S. thesis, University of Wisconsin – Madison, Madison, WI.

Tian, K., Hunter, E.L., Tinjum, J.M., and Benson, C.H. (2014, forthcoming). Chemical characteristics of leachate in low-level radioactive waste disposal facilities.

Tsai, S-C., Wang, T-H., Li, M-H., Wei, Y-Y., and Teng, S-P.(2009). Cesium adsorption and distribution onto crushed granite under different physicochemical conditions. *Journal of Hazardous Materials* **161**, 854-861.

Um, W. and Serne R.J. (2005). Sorption and transport behavior of radionuclides in the proposed low-level radioactive waste disposal facility at the Hanford site, Washington. *Radiochimica Acta* **93**(1), 57–63.

Um, W., Serne R.J., and Krupka, K.M. (2007). Surface complexation modeling of U(VI) sorption to Hanford sediment with varying geochemical conditions. *Environmental Science and Technology* **41**(10), 3587–3592.

Um, W., Wang, Z., Serne, R.J., Williams, B.D., Brown, C.F., Dodge, C.J., and Francis, A.J. (2009a). Uranium phases in contaminated sediments below Hanford's U Tank Farm. *Environmental Science and Technology* **43**, 4280-4286.

Um, W., Serne, R.J., Vast, G.V., Clayton, R.E., and Glossbrenner, E.T. (2009b). The effect of gravel size fraction on the distribution coefficients of selected radionuclides. *Journal of Contaminant Hydrology* **107**, 82-90.

Um, W., Icenhower, J.P., Brown, C.F., Serne, R.J., Wang, Z., Dodge, C.J., and Francis, A.J. (2010a). Characterization of uranium-contaminated sediments from beneath a nuclear waste storage tank from Hanford, Washington: Implications for contaminant transport and fate. *Geochimica et Cosmochimica Acta* **74**, 1363-1380.

Um, W., Zachara, J.M., Liu, C., Moore, D.A., and Rod, K.A. (2010b). Resupply mechanism to a contaminated aquifer: A laboratory study of U(VI) desorption from capillary fringe sediments. *Geochimica et Cosmochimica Acta* **74**, 5155-5170.

U.S. Department of Energy (U.S. DOE). (1999). Implementation guide for use with DOE M 435.1-1, *Radioactive waste management manual,* Chapter 1. Office of Environmental Management, U.S. Department of Energy, Washington, D.C., 09 June 1999. Available via: <https://www.directives.doe.gov/directives/0435.1-EGuide-1ch1/view>.

U.S. Department of Energy (U.S. DOE). (2012). "Environmental Restoration Disposal Facility." *Hanford*, <www.hanford.gov/page.cfm/erdf> (Oct. 29, 2013).

U.S. Department of Energy Office of Environmental Management (U.S. DOE OEM). (2000). "The current and planned low-level waste disposal capacity report revision 2." Office of Environmental Management, U.S. Department of Energy, Washington, DC. Available via: <http://energy.gov/sites/prod/files/em/llwrev2.pdf>

U.S. Department of Energy Office of Legacy Management (U.S. DOE OLM) (2008). "Fernald Site: Evaluation of aqueous ions in the monitoring systems of the On-site Disposal Facility." DOE-LM/1591-2008. Office of Legacy Management, U.S. Department of Energy, Grand Junction, Colorado, March 2008.

U.S. Nuclear Regulatory Commission (U.S. NRC). (2002). "Radioactive Waste: Production, Storage, Disposal (NUREG/BR-0216, Revision 2)." Office of Public Affairs, U.S. Nuclear Regulatory Commission, Washington DC, 20555-0001. Available via: <http://www.nrc.gov/reading-rm/doc-collections/nuregs/brochures/br0216/>.

Utsunomiya, S., Kersting, A.B, and Ewing, R.C. (2009). Groundwater nanoparticles in the far-field at the Nevada Test Site: Mechanism for radionuclide transport. *Environmental Science and Technology* **43**, 1293-1298.

Van Loon, L.R., Baeyens, B., and Bradbury, M.H. (2009). The sorption behaviour of caesium on Opalinus Clay: A comparison between intact and crushed material. *Applied Geochemistry* **24**, 999-1004.

Volchek, K. Miah, M.F., Kuang, W., DeMaleki, Z., and Tezel, F.H. (2011). Adsorption of cesium on cement mortar from aqueous solutions. *Journal of Hazardous Materials* **194**, 331-337.

Waite, T.D., Davis, J.A., Payne, T.E., Waychunas, G.A., and Xu, N. (1994). Uranium(VI) adsorption to ferrihydrite: Application of a surface complexation model. *Geochimica et Cosmochimica Acta* **58**(24), 5465-5478.

Wan, J., Kim, Y., Tokunaga, T.K., Wang, Z., Dixit, S., Steefel, C.I., Saiz, E., Kunz, M., and Tamura, N. (2009). Spatially resolved U(VI) partitioning and speciation: Implications for plume scale behavior of contaminant U in the Hanford vadose zone. *Environmental Science and Technology* **43**, 2247-2253.

Wang, T-H., Hsieh, C-J., Lin, S-M., Wu, D-C., Li, M-H., and Teng, S-P. (2010). Effect of alkyl properties and head groups of cationic surfactants on retention of cesium by organoclays. *Environmental Science and Technology* **44**, 5142-5147.

Wellman, D.M., Zachara, J.M., Liu, C., Qafoku, N.P., Smith, S.C., and Forrester, S.W. (2008). Advective desorption of uranium(VI) from contaminated Hanford vadose zone sediments under saturated and unsaturated conditions. *Vadose Zone Journal* **44**, 2911-2917.

Wu, T., Amayri, S., Drebert, J., Van Loon, L.R., and Reich, T. (2009). Neptunium(V) sorption and desorption in Opalinus Clay. *Environmental Science and Technology* **43**, 6567-6571.

Yan, S., Hua, B., Bao, Z., Yang, J., Liu, C., and Deng, B. (2010). Uranium(VI) removal by nanoscale zerovalent iron in anoxic batch systems. *Environmental Science and Technology* **44**, 7783-7789.

Zachara, J.M., Serne, J., Freshley, M., Mann, F., Anderson, F., Wood, M., Jones, T., and Myers, D. (2007a). Geochemical processes controlling migration of tank wastes in Hanford's vadose zone. *Vadose Zone Journal* **6**(4), 985-1003.

Zachara, J.M., Brown, C., Christensen J., Davis, J.A., Dresel, E., Liu, C., Kelly, S., McKinley, J., Serne, J., and Um, W. (2007b). *A site-wide perspective on uranium geochemistry at the Hanford Site*. Pacific Northwest National Laboratory Report PNNL-17031, US Department of Energy Publications, Richland, WA.

Appendix A

Abbreviations used within the text.

Abbreviation	Meaning
2 SPNE SC/CE	Two Site Protolysis Non-Electrostatic Surface Complexation and Cation Exchange Model
CEC	Cation Exchange Capacity
DOE	U.S. Department of Energy
GRBGAM	Geo-Radiological Barrier Gamma Attenuation Model
HLW	High-Level Radioactive Waste
IAEA	International Atomic Energy Association
LLW	Low-Level Radioactive Waste
NRC	U.S. Nuclear Regulatory Commission
pCO_2	Partial pressure of carbon dioxide
PRB	Permeable Reactive Barrier
ZVI / Fe(0)	Zero-Valent Iron

Appendix B

Elements referenced in text.

Symbol	Name	Atomic Number	Symbol	Name	Atomic Number
Ac	Actinium	89	Mo	Molybdenum	42
Al	Aluminum	13	N	Nitrogen	7
Am	Americium	95	Na	Sodium	11
At	Astatine	85	Nb	Niobium	41
Au	Gold	79	Nd	Neodymium	60
Ba	Barium	56	Ne	Neon	10
Bi	Bismuth	83	Ni	Nickel	28
C	Carbon	6	Np	Neptunium	93
Ca	Calcium	20	O	Oxygen	8
Cd	Cadmium	48	Os	Osmium	76
Ce	Cerium	58	Pa	Protactinium	91
Cl	Chlorine	17	Pb	Lead	46
Cm	Curium	96	Pm	Promethium	61
Co	Cobalt	27	Po	Polonium	84
Cr	Chromium	24	Pt	Platinum	78
Cs	Cesium	55	Pu	Plutonium	94
Cu	Copper	29	Ra	Radium	88
Dy	Dysprosium	66	Rb	Rubidium	37
Er	Erbium	68	Re	Rhenium	75
Eu	Europium	63	Rn	Radon	86
Fe	Iron	26	Se	Selenium	34
Gd	Gadolinium	64	Si	Silicon	14
H	Hydrogen	1	Sm	Samarium	62
^{3}H	Tritium	1	Sr	Strontium	38
He	Helium	2	Ta	Tantalum	73
Hf	Hafnium	72	Tb	Terbium	65
Hg	Mercury	80	Tc	Technetium	43
Ho	Holmium	67	Te	Tellurium	52
I	Iodine	53	Th	Thorium	90
Ir	Iridium	77	Tl	Thallium	81
K	Potassium	19	Tm	Thulium	69
La	Lanthanum	57	U	Uranium	92
Li	Lithium	3	V	Vanadium	23
Lu	Lutetium	71	W	Tungsten	74
Mg	Magnesium	12	Yb	Ytterbium	70
Mn	Manganese	25	Zn	Zinc	30

Appendix C

Distribution Coefficient (K_d) Calculations and Example

The solid-liquid distribution coefficient, K_d, is defined as:

$$K_d = \frac{c_{sorb}}{c_{eq}} = \frac{(c_{init} - c_{eq})}{c_{eq}} \times \frac{V}{m}$$

Where:

c_{sorb} = total sorbed nuclide concentration (Mol/L or mg/L)
c_{init} = total initial aqueous nuclide concentration (Mol/L or mg/L)
c_{eq} = total equilibrium aqueous nuclide concentration (Mol/L or mg/L)
V = volume of liquid phase (L or mL)
m = mass of solid phase (kg or g)

K_d is traditionally reported with units of L/kg or mL/g, stemming from the volume and mass terms. Note that any concentration units can be used for c_{sorb}, c_{init}, and c_{eq}, as long as the same units are used for all of the concentration variables to allow for cancellation of units.

As an example from the single radionuclide portion of experimentation, the following parameters were used for calculating the K_d for U at initial pH 7 for Soil A:

c_{init} = 710 µg/L
c_{eq} = 4.43 µg/L
V = 40 mL = 0.04 L
m = 0.40 g = 0.004 kg

$$K_d = \frac{\left(710\,\frac{\mu g}{L} - 4.43\,\frac{\mu g}{L}\right)}{\left(4.43\,\frac{\mu g}{L}\right)} \times \frac{(0.04\ L)}{(0.004\ kg)} = 4.20\,\frac{L}{kg}$$

Appendix D

Sorption Isotherm Fitting Parameters

- Linear Isotherm Equation
  - $X=K_dC$
  - $K_d=\frac{X}{C}$
  - Where:
    - X is the concentration per mass adsorbed to solid
    - C is the concentration per volume remaining in solution
    - K_d is the distribution coefficient
- Freundlich Isotherm Equation
  - $X=K_fC^n$
  - Where:
    - X is the concentration per mass adsorbed to the solid
    - C is the concentration per volume remaining in solution
    - K_f is the Freundlich distribution coefficient, similar to K_d
    - n is a constant, usually < 1
- Langmuir Isotherm Equation
  - $X=\frac{X_{(max)}K_LC}{1+K_LC}$
  - Where:
    - X is the concentration per mass adsorbed to the solid
    - C is the concentration per volume remaining in solution
    - $X_{(max)}$ is the maximum amount of adsorption
    - K_L is the Langmuir distribution coefficient, accounting for the plateau is sorption

Appendix E

Mineral Solubility Formulas and Example

Using ferric hydroxide ($Fe(OH)_3$) as an example to demonstrate the relationship between solubility products and saturation indices:

$$Fe(OH)_3 \overset{K_{so}}{\leftrightarrow} Fe^{3+} + 3OH^-$$

$$^cK_{so} = \frac{[Fe^{3+}][OH^-]^3}{[Fe(OH)_{3\,(s)}]} = [Fe^{3+}][OH^-]^3 = I.A.P.$$

- $^cK_{so}$ is the conditional solubility (as compared to K_{eq}, the equilibrium solubility), which relates to the concentrations of an ion that is present at any given solid/solution composition.
    - $^cK_{so}$ is a function of pH, additional ligands present in the solution, ionic strength, temperature, solid composition, size, and other potential solution parameters.
- I.A.P. is the Ion Activity Product, and is used to compare the solubility of a given solution to the theoretical equilibrium conditions.
- Note that within the given example for ferric hydroxide, for any given dissolved Fe^{3+} concentrations, there will be a pH for which the product of $[Fe^{3+}][OH^-]^3$ will be greater than $^cK_{so}$.

Conditions regarding the solution solubility:

1. If I.A.P. > K_{eq}, precipitation should occur within the solution.
2. If I.A.P. = K_{eq}, equilibrium has been achieved within the solution.
    a. Note that equilibrium rarely occurs, as many solids are metastable or have difficult-to-define K_{eq} values.
3. If I.A.P. < K_{eq}, the solution is undersaturated with respect to the species of interest.

Comparing the log of the activity of any species with that at the hypothetical solubility equilibrium provides a determination of the system Saturation Index (SI).

$$\log {}^cK_{so} - \log K_{eq} = SI$$

Conditions regarding the SI (based on the comparison of the log activity values):

1. SI > 0, the system is oversaturated.
2. SI = 0, the system is at equilibrium.
3. SI < 0, the system is undersaturated.

Appendix F

RSL Modeling in The Geochemist's Workbench

As discussed in Section 6.2.4, two additional geochemical speciation models were created using the SpecE8 application of The Geochemist's Workbench (GWB). GWB is a suite of geochemical software applications for modeling various reaction processes. Specifically, the SpecE8 application allows calculation of speciation behavior in solution. GWB and SpecE8 include multiple thermodynamic databases for use in providing contextual chemical properties for solution species and minerals for calculating behavior. For the included figures and tables, two of the available databases were used, with varying results: the Lawrence Livermore National Laboratory (LLNL) thermodynamic database (the default database within GWB) and Visual MINTEQ's thermodynamic database, identical in version to that used within the Visual MINTEQ software and modeling. Based on the species found in the overall RSL mixture, both databases in their initial states provide benefits and drawbacks. The LLNL database includes Tc and Tc-based species, but only provides thermodynamic data for U-CO_3 and U-OH polymeric species, excluding Ca-U-CO_3 species. In opposition, the Visual MINTEQ database includes thermodynamic data for Ca-U-CO_3 species, but does not include Tc in the list of elements included within the database. Ideally, a database incorporating both of these aspects would have been created for modeling this system within GWB, but in the interest of time only calculations using the readily available databases have been executed.

Table F.1 provides a list of the components and molar concentrations used for speciation modeling in SpecE8 with the LLNL database. Note that values for H^+ varied as pH was varied from 4.5 to 10 to simulate system conditions and were calculated by SpecE8 based on the input pH value. The H^+ value within the table is the concentration

for pH 4.5. Table F.2 lists the species and thermodynamic constants extracted by SpecE8 from the LLNL database for use within the RSL system calculations at 25 °C. Table F.3 shows oversaturated species in the RSL solution as calculated within SpecE8 using the LLNL database. Given the current limitations, U speciation from the LLNL database excludes the critical Ca-U-CO_3 components, showing preferential speciation of U-OH polymeric species at higher pH levels (Figure F.1). Figure F.2 shows the predominance of TcO_4^- across all the entire pH range, implicating the expected lack of sorption due to anionic behavior as indicated within the literature.

Table F.4 lists the components and molar concentrations used for speciation modeling in SpecE8 with the Visual MINTEQ thermodynamic database. As with the LLNL thermodynamic database modeling, values for H^+ varied as pH was varied from 4.5 to 10 to simulate system condition. H^+ values were calculated by SpecE8 based on the input pH value, with the H^+ value within the table representing the concentration for pH 4.5. Table F.5 lists the species and thermodynamic constants used by SpecE8 from the Visual MINTEQ thermodynamic database for the RSL solution at 25 °C. Table F.6 provides oversaturated species in the RSL solution as calculated within SpecE8 using the Visual MINTEQ database. Despite ostensibly using the same thermodynamic parameters as the Visual MINTEQ software, calculations in SpecE8 yielded a different speciation for U (Figure F.3). The differences between the two resultant models are not readily apparent based on the input parameterization.

Table F.1. List of components used in RSL SpecE8 speciation modeling using the LLNL thermodynamic database.

Original basis	Total moles
Al+++	3.00E-05
As(OH)4-	1.00E-06
Ba++	2.00E-06
Ca++	0.004
Cl-	0.008
Cu+	2.00E-07
Fe++	4.00E-05
H+	7.30E-05
H2O	55.5
HCO3-	7.85E-05
K+	0.0007
Li+	2.00E-05
Mg++	0.006
Mn++	1.00E-05
NO3-	0.0015
Na+	0.007
Ni++	3.00E-07
O2(aq)	0.000264
SO4--	0.0075
Sr++	2.00E-05
TcO4-	2.97E-10
U++++	6.30E-06
Zn++	5.00E-07

Table F.2. List of species and thermodynamic constants used for SpecE8 speciation modeling using the LLNL thermodynamic database.

Species	log K
(UO2)2(CO3)(OH)3	11.524
(UO2)2(OH)2++	5.6799
(UO2)3(OH)4++	11.8794
(UO2)3(OH)5+	15.8192
(UO2)3(OH)7-	28.3379
(UO2)4(OH)7+	21.8987
[TcO(OH)2]2	0.909
Al(O-phth)+	-4.7996
Al(O-phth)2-	-8.4792
Al(OH)2+	10.1035
Al(OH)3	16.1667
Al(OH)4-	22.1567
Al(SO4)2-	-4.9029
Al13O4(OH)24(7+)	98.7072
Al2(OH)2++++	7.6743
Al3(OH)4(5+)	13.8614
AlCH3COO++	-2.8616
AlOH++	4.9345
AlSO4+	-3.0096
As(OH)3	-9.2327
AsO2OH--	11.0123
AsS2-	-26.8053
Ba(O-phth)	-2.3294
BaCH3COO+	-1.0724
BaCl+	0.1246
BaCO3	10.3512
BaNO3+	-0.9016
BaOH+	13.396
BaSO4	-2.6996
Ca(O-phth)	-2.4196
CaCH3COO+	1.1816
CaCl+	-0.7
CaCO3	7.128
CaHCO3+	-1.222
CaNO3+	-0.9016
CaOH+	12.6887
CaSO4	-2.3199
Cu(NH3)2+	2.9554
Cu(NH3)2++	11.835
Cu(NH3)3++	17.5638
Cu(NO2)2	2.6166
CuCl+	-0.01
CuCl2	0.69
CuCl2-	-4.94
CuCl3-	2.29
CuCl3--	-5.14
CuCl4--	4.59
CuNH3+	3.3475
CuNH3++	5.2408
CuNO2+	-2.0194
CuOH+	6.66
CuSO4	2.26
Fe(CH3COO)2+	-7.5989
Fe(CH3COO)3	-9.5984
Fe(OH)2	21.4222
Fe(OH)2+	5.6689
Fe(OH)3	12.018
Fe(OH)3-	34.2245
Fe(OH)4-	21.6458
Fe(SO4)2-	-5.3852
Fe2(OH)2++++	2.9495
Fe3(OH)4(5+)	6.2993
FeCH3COO+	-2.3587
FeCH3COO++	-3.7998
FeCl+	-0.3797
FeCl++	-1.4799

Table F.2. Continued.

Species	log K	Species	log K
FeCl2	-0.0997	MgCl+	-0.1503
FeCl2+	-2.1301	MgCO3	7.4266
FeCl3	-1.1295	MgHCO3+	-1.0101
FeCl4-	0.7902	MgOH+	11.7908
FeCO3	6.6636	MgSO4	-2.2275
FeCO3+	0.6252	Mn(NH3)2++	17.014
FeHCO3+	-1.2996	Mn(NH3)3++	26.1331
FeHSO4++	-3.703	Mn(NO3)2	-0.601
FeNO2++	-3.1518	Mn(OH)2	22.1962
FeNO3++	-0.9998	Mn(OH)3-	34.2142
FeOH+	10.179	Mn(OH)4--	48.292
FeOH++	2.1894	Mn2(OH)3+	23.8953
FeSO4	-2.1997	Mn2OH+++	10.555
FeSO4+	-4.1113	MnCl+	0.1979
H(O-phth)-	-5.4072	MnCl2	-0.2529
H2(O-phth)	-8.3568	MnCl3-	0.3152
H2AsO4-	-18.3539	MnCO3	6.8255
H2S(aq)	-6.95	MnHCO3+	-1.2666
H2SO4	1.0122	MnNH3++	8.2761
H3AsO4	-20.6042	MnNO3+	-0.1979
HAsO4--	-11.5958	MnOH+	10.5887
HAsS2	-30.5068	MnSO4	-2.2862
HCH3COO	-4.7563	Na(O-phth)-	-0.7
HCl	6.1	NaCH3COO	0.1825
HNO2	-3.2207	NaCl	1.5994
HSO4-	-1.993	NaCO3-	9.8396
KCl	1.5876	NaHCO3	-0.129
KOH	14.4852	NaOH	14.1891
KSO4-	-0.8525	NaSO4-	-0.6938
LiOH	13.6269	NH3	9.2774
LiSO4-	-0.7696	NH4SO4-	-0.9397
Mg2CO3++	6.8842	Ni(NH3)2++	13.4224
Mg2OH+++	13.3652	Ni(NH3)6++	46.7138
Mg4(OH)4++++	39.65	Ni(NO3)2	0.7476
MgCH3COO+	-1.2703	Ni(OH)2	19.5751

Table F.2. Continued.

Species	log K
Ni(OH)3-	30.9627
Ni(OH)4--	43.9908
Ni2OH+++	10.6979
Ni4(OH)4++++	28.4764
NiNO3+	-0.3262
NiOH+	9.6659
NiSO4	-2.111
OH-	13.9868
S--	13.9032
S2--	2.396
S3--	-8.5513
S4--	-22.0517
S5--	-32.686
S6--	-43.0029
SrCH3COO+	-1.1383
SrCO3	7.5366
SrHCO3+	-1.1786
SrNO3+	-0.7997
SrOH+	13.2766
SrSO4	-2.2994
TcO(OH)2	3.3072
TcOOH+	1.1185
U(OH)2++	2.2517

Species	log K
U(OH)3+	4.8802
U(OH)4	8.5349
U(OH)5-	16.4987
U(SO4)2	-9.7472
U6(OH)15(9+)	17.2179
UCl+++	-1.334
UCl4	0.0147
UO2(CO3)2--	3.6085
UO2(CO3)3----	9.3331
UO2(NO3)2	0.088
UO2(SO4)2--	-4.2498
UO2Cl+	-0.2346
UO2CO3	0.6941
UO2OH+	5.0913
UO2SO4	-2.748
UOH+++	0.6494
USO4++	-5.46
ZnCl+	-0.43
ZnCl2	-0.61
ZnCl3-	-0.53
ZnCl4--	-0.2
ZnSO4	-2.37

Table F.3. Oversaturated species in RSL based on SpecE8 speciation modeling in GWB using the LLNL thermodynamic database.

Mineral	Chemical Formula	Highest SI	pH of Highest SI
Alunite	$KAl_3(SO_4)_2(OH)_6$	4.5229	5.1
Aragonite	$CaCO_3$	0.5799	10
Artinite	$Mg_2(CO_3)(OH)_2{:}3H_2O$	0.1609	10
Ba3(AsO4)2(c)	$Ba_3(AsO_4)_2(c)$	15.605	10
Barite	$BaSO_4$	1.1689	10
Birnessite	$Na_{0.3}Ca_{0.1}K_{0.1}Mn^{4+}Mn^{3+}O_4{:}1.5H_2O$	66.0774	8.5
Bixbyite	$(Mn,Fe)_2O_3$	13.1448	8.5
Boehmite	γ-AlOOH	0.8325	7.1
Brucite	$Mg(OH)_2$	0.9813	10
Calcite	$CaCO_3$	0.7448	10
CuFeO2(c)	$CuFeO_2(c)$	5.7815	10
Diaspore	α-AlOOH	1.6769	7.1
Dolomite	$CaMg(CO_3)_2$	2.6132	10
Dolomite-dis	$CaMg(CO_3)_2$	1.0688	10
Dolomite-ord	$CaMg(CO_3)_2$	2.6132	10
Fe(OH)3(ppd)	$Fe(OH)_3$	2.708	8
Ferrite-Ca	$CaFe_2O_4$	9.7331	10
Ferrite-Cu	$CuFe_2O_4$	13.8095	9.6
Ferrite-Mg	$MgFe_2O_4$	10.3868	10
Ferrite-Zn	$Zn_xFe_{3-x}O_4$	15.718	10
Gibbsite	$Al(OH)_3$	2.4682	7.1
Goethite	α-FeOOH	7.0972	8
Hausmannite	$Mn^{2+}Mn^{3+}{}_2O_4$	13.0899	8.5
Hematite	Fe_2O_3	15.151	8
Jarosite-K	$KFe^{3+}{}_3(SO_4)_2(OH)_6$	3.9657	5.1
Jarosite-Na	$NaFe^{3+}{}_3(SO_4)_2(OH)_6$	0.9546	5.1
Magnesite	$MgCO_3$	0.2396	10
Magnetite	Fe_3O_4	4.9092	8
Manganite	MnO(OH)	6.255	8.5
NiFe2O4	$NiFe_2O_4$	17.0192	9.8
NiO	NiO	0.1456	10
Pyrolusite	MnO_2	10.7076	8.5
Strontianite	$SrCO_3$	1.2434	10
Tenorite	CuO	2.2131	10
Todorokite	$Na_{0.2}Ca_{0.05}K_{0.02}Mn^{4+}{}_4Mn^{3+}{}_2O_{12}{:}3H_2O$	57.4239	8.5
Witherite	$BaCO_3$	2.0428	10

Table F.4. List of components used in RSL SpecE8 speciation modeling using the Visual MINTEQ thermodynamic database.

Original basis	Total moles
Acetate-	1.26E-05
Al+++	3.00E-05
AsO4---	1.00E-06
Ba++	2.00E-06
CO3--	7.85E-05
Ca++	0.004
Cl-	0.008
Cu++	2.00E-07
Fe+++	4.00E-05
H+	0.000131
H2O	55.5
K+	0.0007
Li+	2.00E-05
Mg++	0.006
Mn+++	1.00E-05
NO3-	0.0015
Na+	0.007
Ni++	3.00E-07
O2(aq)	0.000213
SO4--	0.0075
Sr++	2.00E-05
UO2++	6.30E-06
Zn++	5.00E-07

Table F.5. List of species and thermodynamic constants used for RSL Speciation Modeling in SpecE8, using the Visual MINTEQ Thermodynamic database.

Species	log K	delta Hr (kJ/mol)		Species	log K	delta Hr (kJ/mol)
(UO2)2(OH)2++	5.62	-48.9		CaCl+	-0.4	-4
(UO2)2CO3(OH)3-	0.861	0		CaCO3 (aq)	-3.22	-16
(UO2)2OH+++	2.7	0		CaHCO3+	-11.434	0
(UO2)3(CO3)6----	-54	62.7		CaNO3+	-0.5	5.4
(UO2)3(OH)4++	11.9	0		CaOH+	12.697	-64.11
(UO2)3(OH)5+	15.55	-123		CaSO4 (aq)	-2.36	-7.1
(UO2)3(OH)7-	32.2	0		CaUO2(CO3)3--	-25.4	0
(UO2)3CO3(OH)3+	-0.649	0		Cu-(Acetate)2 (aq)	-3.4	-11
(UO2)4(OH)7+	21.9	0		Cu-(Acetate)3-	-3.94	-6.2
Al-(Acetate)2+	-4.6	-41		Cu-Acetate+	-2.21	-7.1
Al-Acetate++	-2.75	-16		Cu(CO3)2--	-10.2	0
Al(OH)2+	10.294	-122.5		Cu(NO3)2 (aq)	0.4	0
Al(OH)3 (aq)	16.691	-176.3		Cu(OH)2 (aq)	16.23	-93.1
Al(OH)4-	23	-183		Cu(OH)3-	26.64	0
Al(SO4)2-	-5.58	-11.9		Cu(OH)4--	39.73	-178.5
Al2(OH)2-Acetate	2.414	0		Cu+	18.83	-147.984693
Al2(OH)2++++	7.694	-74.62		Cu2(OH)2++	10.494	-76.62
Al2(OH)2CO3++	-4.31	0		Cu2OH+++	6.71	-27
Al3(OH)4+++++	13.888	-140.24		Cu2S3--	2.45	0
AlCl++	0.39	0		Cu3(OH)4++	20.788	-106.24
AlOH-Acetate+	0.147	0		CuCl (aq)	-3.1	0
AlOH++	4.997	-47.81		CuCl+	-0.3	-8.3
AlSO4+	-3.84	-9		CuCl2 (aq)	0.26	-44.183
As3S4(HS)-	-72.314	0		CuCl2-	-5.42	1.7573
AsS(OH)HS-	-18.038	0		CuCl3-	2.29	-57.279
Ba-Acetate+	-1.07	0		CuCl3--	-4.75	20
BaCl+	0.03	-12		CuCl4--	4.59	-32.5515
BaCO3 (aq)	-2.71	-14		CuCO3 (aq)	-6.77	0
BaHCO3+	-11.309	-8.4		CuHCO3+	-12.129	0
BaNO3+	-0.7	13		CuHSO4+	-2.34	0
BaOH+	13.357	-60.81		CuNO3+	-0.5	4.1
BaSO4 (aq)	-2.13	0		CuOH+	7.497	-35.81
Ca-Acetate+	-1.18	-4		CuS(aq)	2.8	0
Ca2UO2(CO3)3 (aq	-30.55	0		CuSO4 (aq)	-2.36	-8.7

Table F.5. Continued.

Species	log K	delta Hr (kJ/mol)		Species	log K	delta Hr (kJ/mol)
Fe-(Acetate)2+	-7.57	0		KOH (aq)	13.757	-55.81
Fe-(Acetate)3 (aq)	-9.5867	0		KSO4-	-0.85	-4.1
Fe-Acetate+	-1.4	0		Li-Acetate (aq)	-0.28	0
Fe-Acetate++	-4.24	-25		LiCl (aq)	0.16	0
Fe(OH)2 (aq)	20.494	-119.62		LiOH (aq)	13.637	-55.81
Fe(OH)2+	5.75	-37.7		LiSO4-	-0.64	0
Fe(OH)3 (aq)	15	-75.3		Mg-Acetate+	-1.26	0
Fe(OH)3-	30.991	-126.43		Mg2CO3++	-3.59	0
Fe(OH)4-	22.7	-154.8		MgCl+	-0.6	-4
Fe(SO4)2-	-5.38	-19.2		MgCO3 (aq)	-2.92	-10
Fe++	8.488	-98.384693		MgHCO3+	-11.34	9.6
Fe2(OH)2++++	2.894	-56.42		MgOH+	11.417	-67.81
Fe3(OH)4+++++	6.288	-65.24		MgSO4 (aq)	-2.26	-5.8
FeCl+	0.2	0		Mn-Acetate+	-1.4	0
FeCl++	-1.48	-23		Mn(NO3)2 (aq)	-0.6	1.6569
FeHCO3+	-11.429	0		Mn(OH)4--	48.288	0
FeHS+	-5.62	0		Mn++	-3.83	-33.284693
FeOH+	9.397	-55.81		Mn2(OH)3+	23.891	0
FeOH++	2.02	-25.1		Mn2OH+++	10.597	0
FeSO4 (aq)	-2.39	-8		MnCl+	0	0
FeSO4+	-4.25	-25		MnCl2 (aq)	-0.25	0
H-Acetate (aq)	-4.757	-0.41		MnCl3-	0.31	0
H2AsO3-	9.17	-27.62		MnCO3 (aq)	-4.7	0
H2AsO4-	-18.79	21.22		MnHCO3+	-11.629	10.6
H2CO3* (aq)	-16.681	32		MnHS+	-5.14	0
H2S (aq)	-7.02	22		MnNO3+	-0.2	0
H3AsO3	3.053	-143.319386		MnO4-	20.1945	-117.246435
H3AsO4	-21.09	13.25		MnO4--	32.3418	-146.731128
HAsO3--	23.27	-59.4086		MnOH+	10.597	-59.81
HAsO4--	-11.8	18.2		MnSO4 (aq)	-2.25	-8.7
HCO3-	-10.329	14.6		Na-Acetate (aq)	0.12	-8
HS-	138.5	-1068.537544		NaCl (aq)	0.3	8
HSO4-	-1.99	-22		NaCO3-	-1.27	20.35
K-Acetate (aq)	0.27	-4		NaHCO3 (aq)	-10.029	28.3301
KCl (aq)	0.3	4		NaNO3 (aq)	0.55	0
KNO3 (aq)	0.19	12		NaOH (aq)	13.897	-59.81

Table F.5. Continued.

Species	log K	delta Hr (kJ/mol)		Species	log K	delta Hr (kJ/mol)
NaSO4-	-0.74	-1		UO2(CO3)3----	-21.84	39.2
Ni-(Acetate)2 (aq)	-2.4	-10		UO2(OH)2 (aq)	12.15	0
Ni-Acetate+	-1.44	-8.7		UO2(OH)3-	20.25	0
Ni(OH)2 (aq)	18.994	0		UO2(OH)4--	32.4	0
Ni(OH)3-	29.991	0		UO2(SO4)2--	-4.14	-35.1
Ni(SO4)2--	-0.82	0		UO2Cl+	-0.17	-8
NiCl+	0.43	-2		UO2Cl2 (aq)	1.1	-15
NiCl2 (aq)	1.89	0		UO2CO3 (aq)	-9.94	-5
NiCO3 (aq)	-4.57	0		UO2NO3+	-0.3	12
NiHCO3+	-12.42	0		UO2OH+	5.25	-0.9
NiHS+	-5.49	0		UO2SO4 (aq)	-3.15	-19.5
NiNO3+	-0.4	0		UOH+++	0.597	-47.81
NiOH+	9.897	-51.81		USO4++	-6.58	-8
NiSO4 (aq)	-2.3	-5.8		Zn-(Acetate)2 (aq)	-1.91	-22
OH-	13.997	-55.81		Zn-Acetate+	-1.57	-8.3
S--	17.4	-49.4		Zn(CO3)2--	-7.3	0
Sr-Acetate+	-1.12	0		Zn(NO3)2 (aq)	0.3	0
SrCl+	-0.19	-8		Zn(OH)2 (aq)	16.894	0
SrCO3 (aq)	-281	-21		Zn(OH)3-	28.391	0
SrHCO3+	-11.539	-10.4		Zn(OH)4--	41.188	0
SrNO3+	-0.6	10		Zn(SO4)2--	-3.28	0
SrOH+	13.177	-60.81		Zn2OH+++	8.997	-63.81
SrSO4 (aq)	-2.3	-8		Zn2S3--	-0.35	0
U(CO3)5------	-34	20		Zn4S6----	-1.93	0
U(NO3)2++	-2.3	0		ZnCl+	-0.46	-5.4
U(OH)4 (aq)	10	0		ZnCl2 (aq)	-0.45	-35.6
U(SO4)2 (aq)	-10.51	-32.7		ZnCl3-	-0.5	-40
U++++	33.824	-138.069386		ZnCl4--	-0.2	-45.9
UCl+++	-1.72	19		ZnCO3 (aq)	-4.76	0
UNO3+++	-1.47	0		ZnHCO3+	-11.829	0
UO2-(Acetate)2 (aq)	-5.04	-18		ZnNO3+	-0.4	4.6
UO2-(Acetate)3-	-7.06	-16		ZnOH+	8.997	-55.81
UO2-Acetate+	-3.11	-21		ZnS (aq)	1.43	0
UO2(CO3)2--	-16.61	-18.5		ZnSO4 (aq)	-2.34	-6.2

Table F.6. Oversaturated species in RSL based on SpecE8 speciation modeling in GWB using the Visual MINTEQ thermodynamic database.

Mineral	Chemical Formula	Highest SI	pH of Highest SI
Al(OH)3 (am)	$Al(OH)_3$ (am)	0.7617	6.5
Al(OH)3 (Soil)	$Al(OH)_3$	3.2717	6.5
Al2O3	Al_2O_3	3.4716	6.5
Al4(OH)10SO4	$Al_4(OH)_{10}SO_4$	8.2188	6.3
AlOHSO4	$AlOHSO_4$	0.0292	5.7
Alunite	$KAl_3(SO_4)_2(OH)_6$	8.8392	6.1
Aragonite	$CaCO_3$	0.484	10
Artinite	$Mg_2(CO_3)(OH)_2{:}3H_2O$	0.1126	10
BaHAsO4:H2O	$BaHAsO_4{:}H_2O$	0.4615	9.1
Barite	$BaSO_4$	1.3314	8.5-9.7
Birnessite	$Na_{0.3}Ca_{0.1}K_{0.1}Mn^{4+}Mn^{3+}O_4{:}1.5H_2O$	8.8292	8.5
Bixbyite	$(Mn,Fe)_2O_3$	13.2896	8.5
Boehmite	γ-AlOOH	2.9839	6.5
Brochantite	$Cu_4(SO_4)(OH)_6$	1.1761	9
Brucite	$Mg(OH)_2$	0.273	10
Calcite	$CaCO_3$	0.6277	10
Cu(OH)2	$Cu(OH)_2$	0.1019	9.6
Cupric Ferrite	$CuFe_2O_4$	21.8121	8.7
Cuprous Ferrite	$CuFeO_2$	9.4563	8.8
Diaspore	α-AlOOH	4.6889	6.5
Dolomite (disordered)	$CaMg(CO_3)_2$	1.0282	10
Dolomite (ordered)	$CaMg(CO_3)_2$	1.5782	10
Fe(OH)2.7Cl.3	$Fe(OH)_{2.7}Cl_{0.3}$	9.2856	8.3
Fe3(OH)8	$Fe_3(OH)_8$	0.4751	8.5
Ferrihydrite	$Fe(OH)_3$	6.2208	8.5
Ferrihydrite (aged)	$Fe(OH)_3$	6.7308	8.5
Gibbsite (C)	$Al(OH)_3$	3.8217	6.5
Goethite	α-FeOOH	8.9301	8.5
Hausmannite	$Mn^{2+}Mn^{3+}{}_2O_4$	13.39	8.5
Hematite	Fe_2O_3	20.2604	8.5
Hercynite	$FeAl_2O_4$	0.5289	6.7
K-Jarosite	$KFe^{3+}{}_3(SO_4)_2(OH)_6$	6.4352	6.6
Lepidocrocite	γ-FeOOH	8.0501	8.5

Table F.6. Continued.

Mineral	Chemical Formula	Highest SI	pH of Highest SI
Maghemite	$Fe^{3+}_2O_3$	12.4564	8.5
Magnesioferrite	$MgFe^{3+}_2O_4$	16.9642	10
Magnetite	Fe_3O_4	17.2952	8.5
Malachite	$Cu_2(CO_3)(OH)_2$	0.2857	8.9
Manganite	MnO(OH)	6.3324	8.5
Na-Jarosite	$NaFe^{3+}_3(SO_4)_2(OH)_6$	1.7571	6.6
Ni(OH)2 (c)	$Ni(OH)_2$ (c)	1.4924	10
Nsutite	$(Mn^{4+},Mn^{2+}(O,OH)_2$	9.4162	8.5
Pyrolusite	MnO_2	10.8902	8.5
Tenorite(am)	CuO (am)	0.9022	9.6
Tenorite(c)	CuO (c)	1.7522	9.6
Vaterite	$CaCO_3$	0.0613	10

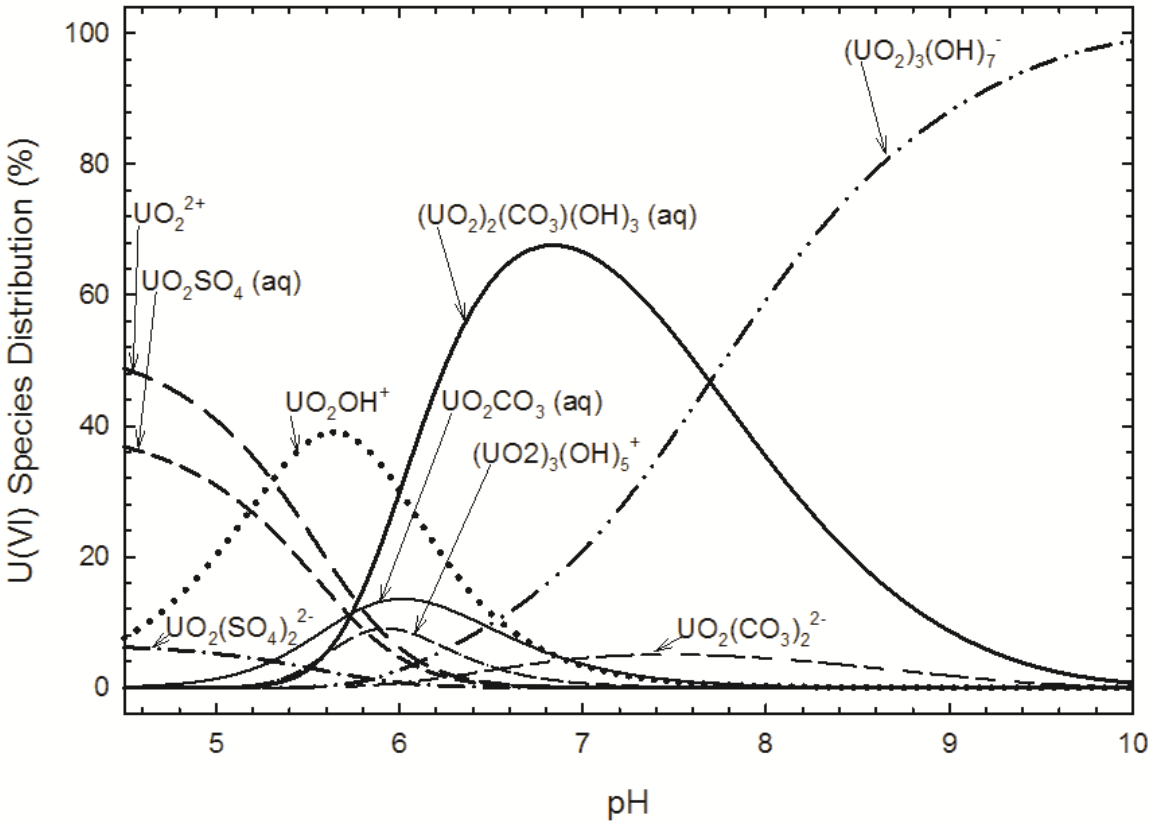

Figure F.1. U(VI) species distribution in the RSL mixture across the tested pH range as found using the SpecE8 module within GWB coupled with the LNNL thermodynamic database. The following species were also present at levels of less than 3.5% of the total distribution: $(UO_2)_2(OH)_2^{2+}$, $(UO_2)_3(OH)_4^{2+}$, $(UO_2)_4(OH)_7^+$, $UO_2(CO_3)_3^{4-}$, and UO_2Cl^+. In addition to the 9 graphed species and 5 additional species, a further 14 species were used with speciation modeling, each at concentrations representing less than 0.01% of the total distribution.

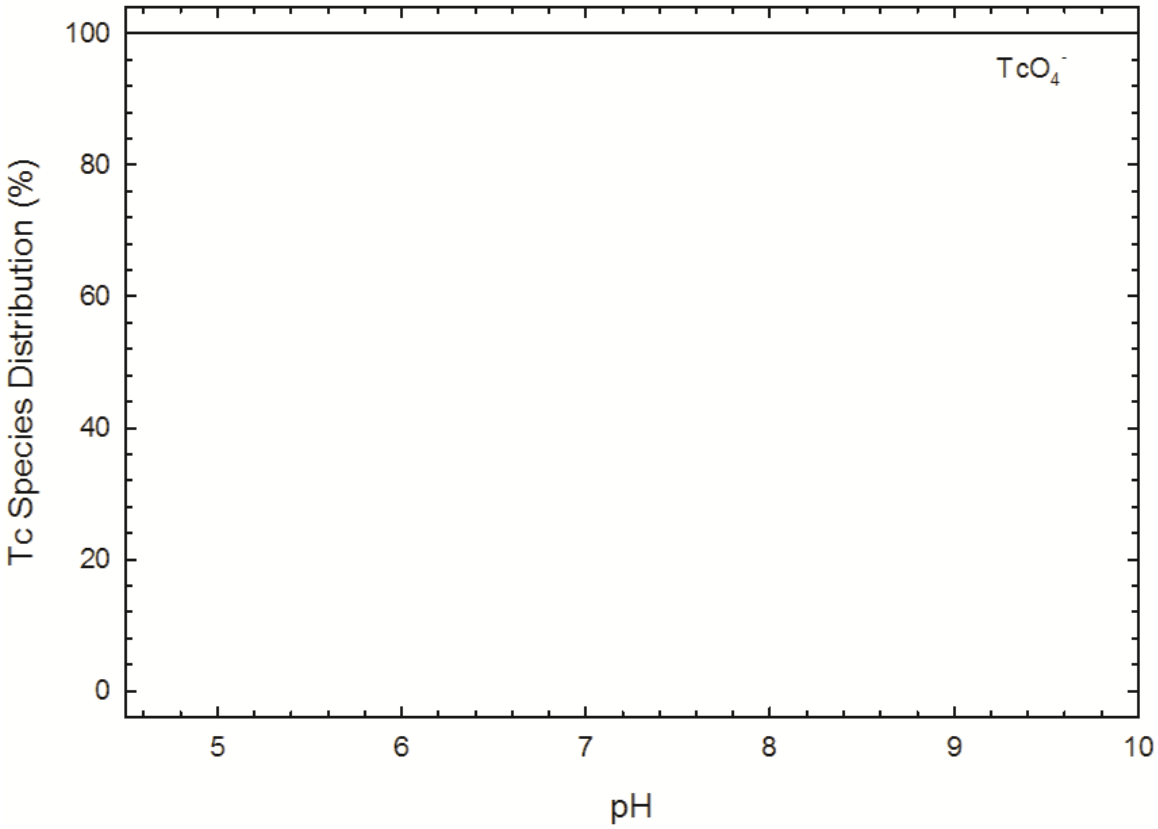

Figure F.2. Tc species distribution in the RSL mixture across the tested pH range as found using the SpecE8 module within GWB coupled with the LNNL thermodynamic database. In addition to TcO_4^-, which dominates speciation across the entire pH range, four additional species were used within speciation modeling, each at concentrations representing less than 0.01% of the total distribution.

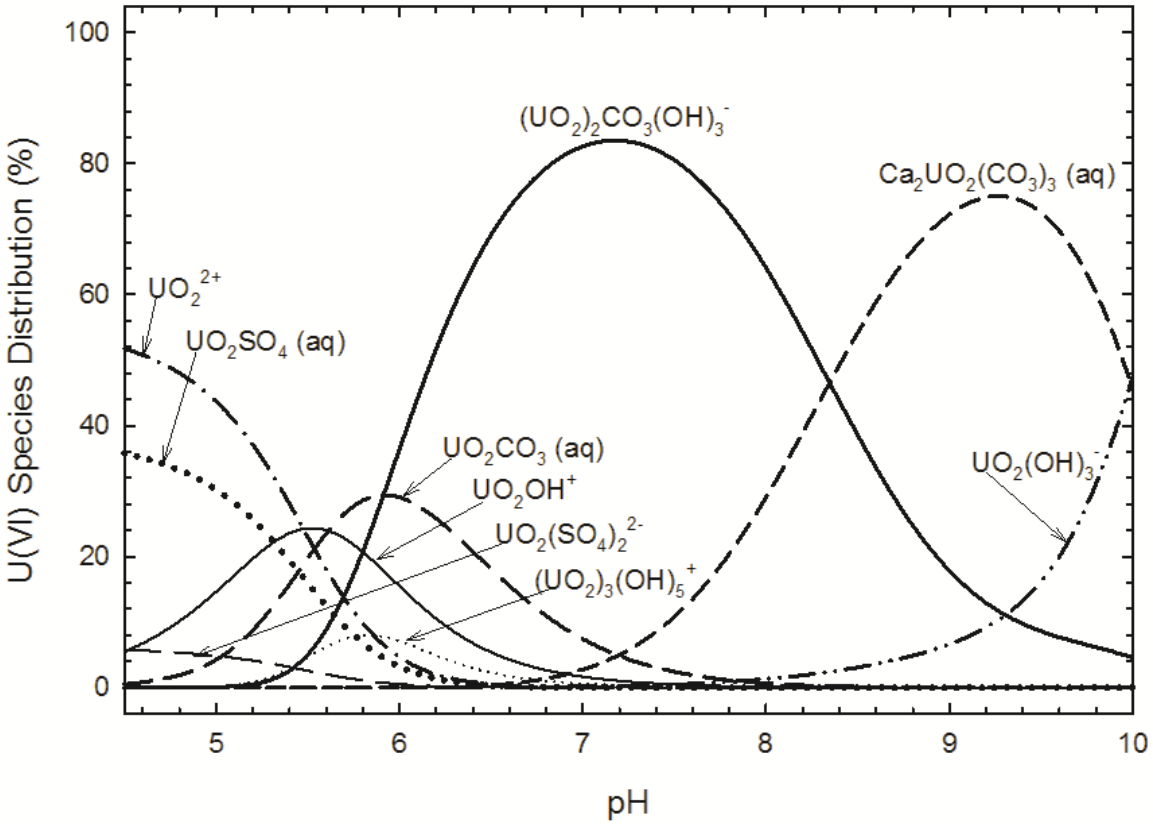

Figure F.3. U(VI) species distribution in the RSL mixture across the tested pH range as found using the SpecE8 module within GWB coupled with the Visual MINTEQ Thermodynamic database. The following species were also present at levels of less than 3.5% of the total distribution: $(UO_2)_2(OH)_2^{2+}$, $(UO_2)_2OH^{3+}$, $(UO_2)_3(OH)_4^{2+}$, $(UO_2)_3(OH)_7^-$, $(UO_2)_4(OH)_7^+$, $CaUO_2(CO_3)_3^{2-}$, UO_2-Acetate$^+$, $UO_2(CO_3)_2^{2-}$, $UO_2(CO_3)_3^{4-}$, $UO_2(OH)_2$ (aq), $UO_2(OH)_4^{2-}$, UO_2Cl^+, and $UO_2NO_3^+$. In addition to the 9 graphed species and 13 additional species, a further 14 species were used with speciation modeling, each at concentrations representing less than 0.01% of the total distribution.

Appendix G

Additional Data Tables for Radioactive Synthetic Leachate Experimentation (Section 6)

Table G.1. RSL Kinetics pH values.

		Reaction Time						
	pH	**15 min**	**30 min**	**1 h**	**2 h**	**4 h**	**24 h**	**7 d**
RSL Solution	Final	8.04	8.12	8.05	8.13	8.15	8.09	8.05
	Std. dev	*0.01*	*0.03*	*0.04*	*0.03*	*0.03*	*0.01*	*0.06*
Glass Beads	Final	7.98	8.06	8.10	8.09	8.04	8.09	7.89
	Std. dev	*0.13*	*0.04*	*0.03*	*0.01*	*0.09*	*0.05*	*0.03*
A	Final	8.05	8.08	8.04	8.04	8.01	7.96	7.87
	Std. dev	*0.06*	*0.05*	*0.05*	*0.06*	*0.01*	*0.02*	*0.02*
B	Final	7.94	7.97	7.97	7.99	7.95	7.91	7.81
	Std. dev	*0.04*	*0.05*	*0.03*	*0.02*	*0.05*	*0.03*	*0.01*
C	Final	7.87	8.01	7.96	7.95	7.89	7.87	7.78
	Std. dev	*0.02*	*0.03*	*0.03*	*0.02*	*0.03*	*0.04*	*0.02*
D	Final	8.05	8.14	8.12	8.09	8.13	8.01	7.89
	Std. dev	*0.03*	*0.03*	*0.04*	*0.05*	*0.06*	*0.04*	*0.03*
CS	Final	8.26	8.28	8.20	8.20	8.18	8.09	7.99
	Std. dev	*0.05*	*0.01*	*0.04*	*0.02*	*0.04*	*0.02*	*0.01*
CR	Final	8.19	8.12	8.18	8.12	8.11	8.00	7.84
	Std. dev	*0.03*	*0.03*	*0.02*	*0.00*	*0.05*	*0.02*	*0.04*
CT	Final	7.61	7.64	7.59	7.59	7.58	7.59	7.42
	Std. dev	*0.04*	*0.03*	*0.04*	*0.03*	*0.05*	*0.04*	*0.05*
CR+	Final	8.19	8.12	8.18	8.12	8.11	8.00	7.84
	Std. dev	*0.03*	*0.02*	*0.07*	*0.09*	*0.04*	*0.01*	*0.17*
GS	Final	8.25	8.27	9.25	8.17	8.18	8.12	8.08
	Std. dev	*0.03*	*0.01*	*0.01*	*0.02*	*0.03*	*0.03*	*0.03*
GR	Final	8.29	8.25	8.24	8.18	8.23	8.13	8.05
	Std. dev	*0.01*	*0.01*	*0.01*	*0.02*	*0.03*	*0.01*	*0.06*

Table G.2. RSL Kinetics Solution Control analytes, reported in mg/L except where noted.

		Reaction Time						
	Analyte	**15 min**	**30 min**	**1 h**	**2 h**	**4 h**	**24 h**	**7 d**
RSL Solution	U 263.553 (µg/L)	1300	1310	1310	1310	1330	1320	1280
	Al 396.152	0.052	0.059	0.058	0.059	0.073	0.056	0.060
	As 228.812	0.002	0.003	0.003	0.002	0.001	0.003	0.003
	Ba 455.403	-0.011	0.000	-0.001	-0.001	-0.011	-0.001	-0.001
	Ca 422.673	165	163	163	162	171	163	162
	Cu 321.754	-0.018	-0.061	-0.061	-0.057	-0.018	-0.060	-0.339
	Fe 234.350	0.001	0.002	0.001	0.001	-0.003	0.002	0.000
	K 769.897	35.8	34.5	34.7	34.7	37.8	34.2	36.5
	Li 670.783	0.122	0.120	0.120	0.121	0.125	0.121	0.118
	Mg 285.213	143	144	143	143	147	143	143
	Mn 257.610	0.523	0.510	0.508	0.508	0.525	0.512	0.480
	Na 568.821	180	173	174	175	186	175	171
	Ni 231.604	0.048	0.040	0.038	0.038	0.043	0.040	0.033
	Sr 421.552	1.82	1.78	1.78	1.79	1.88	1.80	1.76
	Zn 213.857	0.036	-0.119	-0.118	-0.112	0.030	-0.117	-0.285
Glass Beads	U 263.553 (µg/L)	1320	1300	1320	1300	1300	1300	1250
	Al 396.152	0.040	0.040	0.041	0.044	0.040	0.040	0.033
	As 228.812	0.003	0.003	0.001	0.002	0.002	0.002	0.000
	Ba 455.403	0.003	-0.001	-0.001	-0.001	-0.001	-0.001	0.001
	Ca 422.673	164	163	163	164	163	161	159
	Cu 321.754	-0.060	-0.060	-0.060	-0.060	-0.061	-0.061	-0.338
	Fe 234.350	0.001	0.001	0.001	0.000	0.000	0.000	0.000
	K 769.897	35.0	34.4	34.5	35.1	34.6	34.9	36.3
	Li 670.783	0.121	0.120	0.121	0.120	0.120	0.119	0.119
	Mg 285.213	143	142	142	142	142	142	144
	Mn 257.610	0.515	0.512	0.511	0.511	0.510	0.505	0.481
	Na 568.821	177	176	176	176	174	173	172
	Ni 231.604	0.043	0.042	0.041	0.042	0.041	0.039	0.037
	Sr 421.552	1.81	1.79	1.80	1.79	1.79	1.78	1.70
	Zn 213.857	-0.122	-0.124	-0.127	-0.126	-0.129	-0.136	-0.289

Table G.3. RSL Kinetics analytes for Soils *A* and *B* in mg/L, except where noted.

		Reaction Time						
	Analyte	**15 min**	**30 min**	**1 h**	**2 h**	**4 h**	**24 h**	**7 d**
A	U 263.553 (µg/L)	1180	1140	1120	1130	1140	1070	992
	Al 396.152	0.020	0.020	0.018	0.020	0.020	0.022	0.023
	As 228.812	0.001	0.001	0.000	0.001	0.001	0.002	0.001
	Ba 455.403	-0.007	-0.007	-0.005	-0.004	-0.003	0.015	0.018
	Ca 422.673	182	174	171	173	173	169	169
	Cu 321.754	-0.022	-0.022	-0.022	-0.022	-0.021	-0.064	-0.342
	Fe 234.350	-0.005	-0.006	-0.006	-0.006	-0.006	0.000	0.000
	K 769.897	38.5	35.9	34.9	36.3	37.4	34.2	37.2
	Li 670.783	0.108	0.100	0.096	0.092	0.088	0.064	0.030
	Mg 285.213	146	142	141	141	141	140	142
	Mn 257.610	0.344	0.320	0.320	0.306	0.303	0.299	0.248
	Na 568.821	190	182	178	182	186	177	172
	Ni 231.604	0.002	-0.002	-0.003	-0.004	-0.006	-0.010	-0.013
	Sr 421.552	1.87	1.79	1.75	1.79	1.81	1.76	1.74
	Zn 213.857	0.004	0.004	0.004	0.004	0.006	-0.143	-0.309
B	U 263.553 (µg/L)	1270	1270	1260	1270	1240	1240	1210
	Al 396.152	0.015	0.015	0.014	0.014	0.014	0.018	0.019
	As 228.812	0.002	0.001	0.001	0.000	0.000	0.002	0.001
	Ba 455.403	0.227	0.235	0.213	0.205	0.164	0.123	0.078
	Ca 422.673	179	179	178	180	179	175	176
	Cu 321.754	-0.023	-0.023	-0.023	-0.023	-0.023	-0.065	-0.343
	Fe 234.350	-0.006	-0.006	-0.006	-0.006	-0.005	0.001	0.000
	K 769.897	30.6	31.2	30.1	31.4	30.5	29.2	32.0
	Li 670.783	0.123	0.124	0.122	0.122	0.119	0.119	0.115
	Mg 285.213	137	137	137	138	139	136	139
	Mn 257.610	0.347	0.337	0.317	0.303	0.285	0.228	0.133
	Na 568.821	185	187	184	187	183	180	175
	Ni 231.604	-0.007	-0.009	-0.012	-0.013	-0.014	-0.002	-0.005
	Sr 421.552	1.77	1.79	1.76	1.80	1.77	1.73	1.71
	Zn 213.857	0.005	0.007	0.006	0.006	0.006	-0.143	-0.309

Table G.4. RSL Kinetics analytes for Soils *C* and *D* in mg/L, except where noted.

	Analyte	Reaction Time						
		15 min	30 min	1 h	2 h	4 h	24 h	7 d
C	U 263.553 (µg/L)	1210	1210	1220	1220	1210	1200	1140
	Al 396.152	0.020	0.017	0.016	0.017	0.017	0.035	0.020
	As 228.812	0.000	0.001	0.001	0.001	0.001	0.002	0.000
	Ba 455.403	0.201	0.026	0.206	0.208	0.197	0.235	0.230
	Ca 422.673	171	170	170	172	171	170	170
	Cu 321.754	-0.023	-0.023	-0.023	-0.023	-0.023	-0.064	-0.343
	Fe 234.350	-0.005	-0.006	-0.006	-0.006	-0.006	0.001	0.000
	K 769.897	31.0	30.5	31.3	31.3	30.7	29.6	30.7
	Li 670.783	0.117	0.117	0.117	0.118	0.117	0.114	0.107
	Mg 285.213	141	140	140	141	141	140	141
	Mn 257.610	0.323	0.288	0.278	0.270	0.268	0.233	0.209
	Na 568.821	178	175	179	180	179	175	169
	Ni 231.604	0.001	0.005	0.002	0.002	0.001	-0.006	-0.009
	Sr 421.552	1.65	1.65	1.66	1.67	1.66	1.64	1.61
	Zn 213.857	0.008	0.005	0.005	0.004	0.004	-0.144	-0.310
D	U 263.553 (µg/L)	1290	1320	1300	1290	1290	1250	1240
	Al 396.152	0.017	0.017	0.015	0.017	0.018	0.018	0.017
	As 228.812	0.000	0.002	0.000	0.001	0.002	0.002	0.001
	Ba 455.403	-0.003	-0.005	-0.004	-0.003	-0.001	0.015	0.018
	Ca 422.673	178	184	179	179	177	173	175
	Cu 321.754	-0.023	-0.022	-0.022	-0.022	-0.022	-0.064	-0.331
	Fe 234.350	-0.004	-0.005	-0.005	-0.006	-0.006	0.001	0.001
	K 769.897	36.7	38.2	37.1	36.6	36.9	34.1	38.2
	Li 670.783	0.124	0.127	0.126	0.125	0.126	0.120	0.121
	Mg 285.213	139	143	139	139	139	138	142
	Mn 257.610	0.374	0.374	0.359	0.353	0.346	0.351	0.308
	Na 568.821	184	190	187	185	187	176	176
	Ni 231.604	0.009	0.007	0.004	0.003	0.001	0.000	0.001
	Sr 421.552	2.16	2.22	2.17	2.15	2.16	2.13	2.21
	Zn 213.857	0.005	0.007	0.003	0.003	0.004	-0.143	-0.305

Table G.5. RSL Kinetics analytes for Bentonites *CS* and *CR* in mg/L, except where noted.

		Reaction Time						
	Analyte	**15 min**	**30 min**	**1 h**	**2 h**	**4 h**	**24 h**	**7 d**
CS	U 263.553 (µg/L)	1200	1170	1150	1140	1140	1110	1100
	Al 396.152	0.016	0.014	0.014	0.014	0.013	0.015	0.015
	As 228.812	0.002	0.002	0.003	0.003	0.003	0.002	0.001
	Ba 455.403	0.016	0.017	0.017	0.017	0.017	0.016	0.012
	Ca 422.673	131	126	124	124	125	123	120
	Cu 321.754	-0.064	-0.064	-0.064	-0.064	-0.064	-0.064	-0.342
	Fe 234.350	0.000	0.000	0.000	0.000	0.000	0.000	0.000
	K 769.897	27.5	26.5	25.4	25.9	25.5	26.4	28.8
	Li 670.783	0.119	0.120	0.120	0.122	0.123	0.124	0.125
	Mg 285.213	114	109	108	107	107	106	108
	Mn 257.610	0.239	0.196	0.187	0.174	0.162	0.124	0.087
	Na 568.821	284	303	303	307	308	310	312
	Ni 231.604	0.011	0.005	0.005	0.002	0.001	-0.004	-0.007
	Sr 421.552	1.52	1.48	1.48	1.51	1.50	1.52	1.51
	Zn 213.857	-0.351	-0.350	-0.350	-0.350	-0.352	-0.352	-0.510
CR	U 263.553 (µg/L)	1200	1180	1170	1160	1160	1150	1160
	Al 396.152	0.014	0.014	0.014	0.014	0.014	0.013	0.016
	As 228.812	0.002	0.003	0.003	0.003	0.002	0.003	0.002
	Ba 455.403	0.023	0.026	0.025	0.025	0.025	0.022	0.017
	Ca 422.673	132	132	130	131	131	131	131
	Cu 321.754	-0.061	-0.061	-0.060	-0.061	-0.060	-0.061	-0.339
	Fe 234.350	0.000	0.000	0.000	0.000	0.000	0.000	0.000
	K 769.897	32.4	28.1	27.3	27.8	27.6	28.0	30.9
	Li 670.783	0.128	0.127	0.128	0.128	0.129	0.132	0.134
	Mg 285.213	112	112	110	111	110	110	112
	Mn 257.610	0.261	0.248	0.231	0.230	0.217	0.181	0.172
	Na 568.821	281	280	288	287	290	297	292
	Ni 231.604	0.012	0.010	0.008	0.008	0.006	0.001	-0.001
	Sr 421.552	1.74	1.75	1.75	1.77	1.79	1.80	1.86
	Zn 213.857	-0.301	-0.299	-0.300	-0.298	-0.301	-0.299	-0.466

Table G.6. RSL Kinetics analytes for Bentonites *CT* and *CR+* in mg/L, except where noted.

		Reaction Time						
	Analyte	**15 min**	**30 min**	**1 h**	**2 h**	**4 h**	**24 h**	**7 d**
CT	U 263.553 (µg/L)	1110	1130	1140	1100	1120	1130	1040
	Al 396.152	0.014	0.014	0.015	0.014	0.015	0.015	0.016
	As 228.812	0.001	0.001	0.001	0.001	0.001	0.001	0.003
	Ba 455.403	0.001	0.000	0.002	0.002	0.002	0.004	0.004
	Ca 422.673	102	102	102	101	103	103	101
	Cu 321.754	-0.328	-0.329	-0.328	-0.328	-0.328	-0.329	-0.339
	Fe 234.350	0.004	0.003	0.003	0.002	0.002	0.002	0.002
	K 769.897	32.6	33.2	29.0	29.1	28.8	29.6	31.3
	Li 670.783	0.120	0.122	0.122	0.122	0.123	0.124	0.121
	Mg 285.213	95.4	95.7	94.6	93.6	95.1	94.1	92.5
	Mn 257.610	0.298	0.271	0.291	0.282	0.291	0.277	0.276
	Na 568.821	405	414	418	424	424	430	417
	Ni 231.604	-0.003	-0.007	-0.006	-0.008	-0.006	-0.011	-0.002
	Sr 421.552	1.15	1.16	1.17	1.16	1.17	1.17	1.15
	Zn 213.857	-0.429	-0.43	-0.428	-0.427	-0.428	-0.427	-0.474
CR+	U 263.553 (µg/L)	1240	1250	1250	1220	1200	1200	1160
	Al 396.152	0.018	0.016	0.016	0.016	0.015	0.015	0.016
	As 228.812	0.001	0.001	0.001	0.001	0.001	0.000	0.002
	Ba 455.403	0.004	0.008	0.007	0.010	0.015	0.026	0.032
	Ca 422.673	146	147	147	142	141	141	139
	Cu 321.754	-0.329	-0.327	-0.328	-0.327	-0.327	-0.331	-0.341
	Fe 234.350	-0.002	-0.001	-0.002	-0.002	-0.003	-0.003	0.000
	K 769.897	36.9	37.0	37.1	36.5	38.2	38.3	39.3
	Li 670.783	0.122	0.125	0.126	0.123	0.128	0.129	0.126
	Mg 285.213	121	121	121	116	110	108	109
	Mn 257.610	0.326	0.318	0.316	0.288	0.236	0.185	0.191
	Na 568.821	245	256	260	264	284	283	269
	Ni 231.604	0.007	0.006	0.007	0.004	-0.001	-0.005	0.007
	Sr 421.552	1.94	1.96	1.96	1.95	2.08	2.24	2.23
	Zn 213.857	-0.365	-0.361	-0.373	-0.375	-0.380	-0.383	-0.421

Table G.7. RSL Kinetics analytes for Bentonites *GS* and *GR* in mg/L, except where noted.

		Reaction Time						
	Analyte	**15 min**	**30 min**	**1 h**	**2 h**	**4 h**	**24 h**	**7 d**
GS	U 263.553 (µg/L)	1200	1190	1170	1160	1170	1110	1070
	Al 396.152	0.015	0.014	0.013	0.014	0.014	0.014	0.015
	As 228.812	0.001	0.000	0.001	0.002	0.001	0.001	0.002
	Ba 455.403	0.038	0.040	0.041	0.042	0.040	0.035	0.026
	Ca 422.673	141	142	141	140	141	140	136
	Cu 321.754	-0.331	-0.331	-0.331	-0.331	-0.331	-0.332	-0.343
	Fe 234.350	-0.003	-0.003	-0.002	-0.003	-0.003	-0.002	0.000
	K 769.897	32.2	33.0	32.0	32.0	28.8	29.1	32.7
	Li 670.783	0.133	0.133	0.132	0.133	0.133	0.136	0.137
	Mg 285.213	115	115	114	114	114	113	114
	Mn 257.610	0.188	0.163	0.133	0.100	0.085	0.071	0.062
	Na 568.821	287	286	285	287	287	290	283
	Ni 231.604	-0.006	-0.009	-0.011	-0.014	-0.014	-0.018	-0.009
	Sr 421.552	2.27	2.27	2.27	2.27	2.27	2.27	2.20
	Zn 213.857	-0.298	-0.298	-0.298	-0.298	-0.297	-0.296	-0.345
GR	U 263.553 (µg/L)	1220	1180	1180	1130	1130	1080	1000
	Al 396.152	0.015	0.015	0.016	0.016	0.015	0.015	0.018
	As 228.812	0.001	0.001	0.000	0.001	0.002	0.001	0.003
	Ba 455.403	0.032	0.039	0.042	0.043	0.048	0.061	0.058
	Ca 422.673	143	138	137	134	134	133	132
	Cu 321.754	-0.331	-0.331	-0.331	-0.330	-0.331	-0.331	-0.343
	Fe 234.350	-0.002	-0.003	-0.002	-0.002	-0.002	-0.003	0.000
	K 769.897	33.8	35.6	36.2	34.0	31.8	33.0	34.7
	Li 670.783	0.123	0.124	0.124	0.119	0.122	0.125	0.123
	Mg 285.213	122	117	115	113	111	110	111
	Mn 257.610	0.251	0.197	0.176	0.158	0.118	0.063	0.073
	Na 568.821	258	273	277	266	279	287	275
	Ni 231.604	0.002	-0.003	-0.005	-0.006	-0.008	-0.017	-0.008
	Sr 421.552	1.94	1.93	1.94	1.88	1.96	2.06	1.99
	Zn 213.857	-0.299	-0.296	-0.297	-0.295	-0.302	-0.303	-0.346

Table G.8. RSL Edges pH values.

	Target pH	5	5.5	6	6.5	7	7.5	8	8.5	9
RSL Solution	Initial	5.00	5.49	5.97	6.51	7.03	7.53	8.03	8.50	9.04
	Std. dev.	*0.04*	*0.04*	*0.03*	*0.04*	*0.01*	*0.01*	*0.02*	*0.05*	*0.03*
	Final	5.14	5.70	6.18	6.60	7.01	7.52	7.98	8.29	8.43
	Std. dev.	*0.02*	*0.05*	*0.15*	*0.08*	*0.07*	*0.04*	*0.03*	*0.03*	*0.01*
A	Initial	4.97	5.45	6.02	6.51	7.03	7.51	8.01	8.47	9.04
	Std. dev.	*0.03*	*0.04*	*0.05*	*0.04*	*0.02*	*0.03*	*0.00*	*0.02*	*0.01*
	Final	6.06	6.19	6.51	6.74	7.16	7.53	7.93	8.29	8.53
	Std. dev.	*0.08*	*0.02*	*0.04*	*0.06*	*0.04*	*0.04*	*0.04*	*0.03*	*0.02*
C	Initial	5.00	5.50	5.98	6.50	7.01	7.53	7.99	8.55	8.99
	Std. dev.	*0.04*	*0.02*	*0.04*	*0.05*	*0.01*	*0.02*	*0.03*	*0.01*	*0.01*
	Final	6.32	6.33	6.52	6.71	7.10	7.51	7.82	8.20	8.54
	Std. dev.	*0.06*	*0.05*	*0.01*	*0.02*	*0.01*	*0.02*	*0.02*	*0.02*	*0.02*
CS	Initial	4.96	5.50	5.99	6.51	6.98	7.48	7.98	8.53	9.02
	Std. dev.	*0.01*	*0.03*	*0.02*	*0.03*	*0.02*	*0.01*	*0.02*	*0.03*	*0.03*
	Final	7.07	7.04	7.80	7.71	7.92	8.02	8.07	8.19	8.36
	Std. dev.	*0.32*	*0.05*	*0.38*	*0.12*	*0.05*	*0.03*	*0.01*	*0.01*	*0.01*
CR	Initial	5.03	5.52	6.00	6.53	7.03	7.53	7.98	8.51	9.00
	Std. dev.	*0.04*	*0.04*	*0.02*	*0.02*	*0.04*	*0.01*	*0.01*	*0.04*	*0.05*
	Final	7.04	7.32	7.33	7.34	7.71	7.89	7.95	8.13	8.42
	Std. dev.	*0.04*	*0.30*	*0.10*	*0.05*	*0.01*	*0.01*	*0.02*	*0.02*	*0.02*
CT	Initial	5.00	5.50	6.02	6.52	7.05	7.53	8.01	8.53	9.02
	Std. dev.	*0.03*	*0.04*	*0.04*	*0.04*	*0.01*	*0.02*	*0.05*	*0.02*	*0.06*
	Final	5.60	6.20	6.57	6.83	7.20	7.57	7.77	8.07	8.33
	Std. dev.	*0.24*	*0.05*	*0.10*	*0.09*	*0.02*	*0.05*	*0.11*	*0.10*	*0.23*
CR+	Initial	5.00	5.48	5.99	6.51	7.03	7.49	8.06	8.54	9.01
	Std. dev.	*0.02*	*0.03*	*0.04*	*0.04*	*0.02*	*0.05*	*0.01*	*0.03*	*0.06*
	Final	8.28	7.92	7.77	7.44	7.68	8.00	8.19	8.41	8.55
	Std. dev.	*0.03*	*0.05*	*0.07*	*0.04*	*0.03*	*0.05*	*0.01*	*0.02*	*0.13*
GS	Initial	5.01	5.51	6.02	6.55	7.04	7.52	8.02	8.50	9.01
	Std. dev.	*0.01*	*0.04*	*0.03*	*0.01*	*0.02*	*0.01*	*0.01*	*0.02*	*0.06*
	Final	7.85	7.12	7.37	7.44	7.79	8.06	8.08	8.21	8.46
	Std. dev.	*0.29*	*0.02*	*0.31*	*0.10*	*0.10*	*0.03*	*0.01*	*0.01*	*0.03*
GR	Initial	4.97	5.49	6.03	6.51	7.05	7.51	8.05	8.48	9.00
	Std. dev.	*0.02*	*0.02*	*0.07*	*0.03*	*0.01*	*0.05*	*0.01*	*0.01*	*0.05*
	Final	7.71	8.11	7.91	7.83	7.98	8.07	8.15	8.36	8.46
	Std. dev.	*0.23*	*0.13*	*0.15*	*0.09*	*0.04*	*0.01*	*0.04*	*0.03*	*0.03*

Table G.9. RSL Edges analytes for the solution control in mg/L, except where noted.

		Target pH								
	Analyte	**5**	**5.5**	**6**	**6.5**	**7**	**7.5**	**8**	**8.5**	**9**
RSL Solution	U 263.553 (µg/L)	1170	898	708	1030	1200	1250	1280	1190	1060
	Al 396.152	0.039	0.004	0.000	0.001	0.005	0.022	0.048	0.051	0.057
	As 228.812	0.000	0.001	0.001	0.001	0.000	0.001	0.001	0.001	0.000
	Ba 455.403	-0.002	-0.002	-0.002	-0.002	-0.002	-0.002	-0.002	-0.003	-0.003
	Ca 422.673	165	165	165	166	165	167	168	153	130
	Cu 321.754	0.049	0.018	-0.021	-0.041	-0.048	-0.051	-0.052	-0.054	-0.055
	Fe 234.350	0.009	0.005	0.004	0.004	0.004	0.004	0.004	0.032	0.016
	K 769.897	46.6	44.7	43.3	42.4	39.0	39.2	39.2	37.0	38.5
	Li 670.783	0.127	0.127	0.126	0.127	0.127	0.128	0.128	0.125	0.124
	Mg 285.213	143	141	140	141	139	139	140	137	135
	Mn 257.610	0.521	0.515	0.508	0.506	0.493	0.484	0.423	0.416	0.100
	Na 568.821	176	175	175	175	175	176	178	181	196
	Ni 231.604	0.077	0.072	0.070	0.066	0.059	0.051	0.039	0.027	0.012
	Sr 421.552	1.79	1.78	1.78	1.79	1.78	1.81	1.82	1.56	1.31
	Zn 213.857	0.084	0.077	0.067	0.054	0.033	0.010	-0.007	-0.015	-0.025

Table G.10. RSL Edge Analytes for Soil *A* in mg/L, except where noted.

		Target pH								
	Analyte	**5**	**5.5**	**6**	**6.5**	**7**	**7.5**	**8**	**8.5**	**9**
A	U 263.553 (µg/L)	56.1	62.6	88.2	311	703	891	996	1030	945
	Al 396.152	0.017	0.016	0.016	0.016	0.017	0.019	0.021	0.026	0.031
	As 228.812	-0.001	0.000	0.001	0.000	0.001	0.002	0.000	-0.001	0.001
	Ba 455.403	0.009	0.008	0.008	0.008	0.008	0.007	0.007	0.060	0.006
	Ca 422.673	170	169	168	166	165	163	165	160	141
	Cu 321.754	-0.157	-0.162	-0.163	-0.163	-0.163	-0.163	-0.162	-0.162	-0.162
	Fe 234.350	0.030	0.003	0.002	0.003	0.004	0.004	0.004	0.005	0.040
	K 769.897	44.4	41.0	38.0	39.4	37.0	37.0	36.8	37.5	38.2
	Li 670.783	0.099	0.097	0.091	0.086	0.079	0.073	0.063	0.057	0.051
	Mg 285.213	143	142	140	138	138	137	137	135	134
	Mn 257.610	0.501	0.483	0.448	0.421	0.379	0.337	0.280	0.197	0.038
	Na 568.821	174	172	172	171	171	171	171	176	194
	Ni 231.604	0.049	0.043	0.033	0.026	0.016	0.005	-0.002	-0.007	-0.010
	Sr 421.552	1.75	1.75	1.73	1.72	1.71	1.71	1.72	1.66	1.50
	Zn 213.857	-0.041	-0.061	-0.082	-0.092	-0.103	-0.107	-0.110	-0.111	-0.112

Table G.11. RSL Edges analytes for Soil *C* in mg/L, except where noted.

		Target pH								
	Analyte	**5**	**5.5**	**6**	**6.5**	**7**	**7.5**	**8**	**8.5**	**9**
C	U 263.553 (µg/L)	35.2	44.3	55.6	283	810	1050	1130	1140	1080
	Al 396.152	0.001	0.000	0.000	0.001	0.002	0.003	0.005	0.011	0.017
	As 228.812	0.003	0.002	0.003	0.002	0.003	0.001	0.001	0.003	0.003
	Ba 455.403	0.301	0.304	0.298	0.290	0.263	0.247	0.233	0.211	0.191
	Ca 422.673	173	173	171	170	168	167	167	163	147
	Cu 321.754	-0.055	-0.056	-0.056	-0.056	-0.056	-0.056	-0.055	-0.055	-0.055
	Fe 234.350	0.003	0.002	0.002	0.002	0.003	0.004	0.004	0.028	0.012
	K 769.897	36.6	34.3	34.7	34.3	33.3	33.0	31.8	31.5	31.9
	Li 670.783	0.118	0.117	0.116	0.116	0.115	0.114	0.113	0.110	0.109
	Mg 285.213	143	142	140	138	137	136	135	134	133
	Mn 257.610	0.502	0.492	0.451	0.420	0.362	0.287	0.223	0.125	0.014
	Na 568.821	172	170	170	170	171	171	171	176	190
	Ni 231.604	0.045	0.044	0.037	0.033	0.024	0.014	0.008	0.020	-0.002
	Sr 421.552	1.65	1.65	1.63	1.62	1.62	1.61	1.60	1.52	1.37
	Zn 213.857	-0.015	-0.016	-0.020	-0.023	-0.026	-0.028	-0.029	-0.030	-0.029

Table G.12. RSL Edges analytes for Bentonite *CS* in mg/L, except where noted.

		Target pH								
	Analyte	**5**	**5.5**	**6**	**6.5**	**7**	**7.5**	**8**	**8.5**	**9**
CS	U 263.553 (µg/L)	240	297	715	881	1050	1040	1060	987	880
	Al 396.152	0.000	0.000	-0.001	-0.001	-0.001	-0.001	-0.001	-0.002	-0.001
	As 228.812	0.002	0.003	0.001	0.002	0.002	0.001	0.002	0.001	0.001
	Ba 455.403	0.021	0.020	0.017	0.018	0.018	0.015	0.014	0.012	0.011
	Ca 422.673	156	157	149	150	147	133	126	116	99.6
	Cu 321.754	-0.055	-0.055	-0.055	-0.055	-0.055	-0.055	-0.055	-0.055	-0.055
	Fe 234.350	0.010	0.007	0.007	0.007	0.008	0.027	0.012	0.009	0.009
	K 769.897	40.6	36.8	33.7	33.1	32.1	32.3	31.2	29.6	28.9
	Li 670.783	0.131	0.130	0.127	0.127	0.128	0.126	0.126	0.124	0.124
	Mg 285.213	110	110	108	107	109	106	105	101	98.8
	Mn 257.610	0.537	0.502	0.291	0.282	0.222	0.165	0.131	0.085	0.021
	Na 568.821	319	318	314	317	322	320	323	323	338
	Ni 231.604	0.036	0.033	0.018	0.019	0.014	0.012	0.011	0.008	0.004
	Sr 421.552	2.22	2.27	2.11	2.16	2.03	1.72	1.55	1.36	1.21
	Zn 213.857	-0.223	-0.232	-0.235	-0.236	-0.237	-0.237	-0.236	-0.236	-0.236

Table G.13. RSL Edges analytes for Bentonite *CR* in mg/L, except where noted.

		Target pH								
	Analyte	**5**	**5.5**	**6**	**6.5**	**7**	**7.5**	**8**	**8.5**	**9**
CR	U 263.553 (µg/L)	110	267	304	675	998	1060	1100	1030	945
	Al 396.152	-0.001	-0.001	-0.001	-0.001	-0.001	0.000	-0.002	-0.002	-0.001
	As 228.812	0.002	0.002	0.001	0.001	0.002	0.001	0.001	0.001	0.001
	Ba 455.403	0.027	0.027	0.027	0.026	0.026	0.025	0.026	0.023	0.021
	Ca 422.673	156	157	158	159	148	141	137	126	109
	Cu 321.754	-0.051	-0.051	-0.052	-0.052	-0.052	-0.052	-0.052	-0.052	-0.053
	Fe 234.350	0.011	0.009	0.008	0.008	0.008	0.031	0.013	0.016	0.008
	K 769.897	34.9	33.2	33.7	33.2	31.1	30.9	30.7	31.0	30.5
	Li 670.783	0.143	0.144	0.145	0.145	0.142	0.141	0.141	0.140	0.138
	Mg 285.213	111	111	112	113	108	108	108	106	103
	Mn 257.610	0.463	0.415	0.415	0.390	0.291	0.233	0.183	0.129	0.027
	Na 568.821	295	295	297	299	294	292	293	297	307
	Ni 231.604	0.035	0.030	0.029	0.027	0.019	0.017	0.014	0.010	0.006
	Sr 421.552	2.20	2.21	2.21	2.25	2.11	2.00	1.95	1.73	1.58
	Zn 213.857	-0.178	-0.180	-0.181	-0.182	-0.183	-0.183	-0.183	-0.183	-0.183

Table G.14. RSL Edges analytes for Bentonite *CT* in mg/L, except where noted.

		Target pH								
	Analyte	**5**	**5.5**	**6**	**6.5**	**7**	**7.5**	**8**	**8.5**	**9**
CT	U 263.553 (µg/L)	168	54.4	52.2	72.3	420	983	1230	1190	1160
	Al 396.152	0.188	0.024	0.005	0.003	0.003	0.002	0.002	0.004	0.004
	As 228.812	0.005	0.005	0.005	0.004	0.004	0.005	0.040	0.002	0.004
	Ba 455.403	0.017	0.005	0.004	0.004	0.004	0.004	0.004	0.004	0.003
	Ca 422.673	113	106	105	106	106	105	106	97.8	87.8
	Cu 321.754	-0.039	-0.051	-0.052	-0.053	-0.054	-0.055	-0.055	-0.056	-0.056
	Fe 234.350	0.020	-0.054	-0.062	-0.065	-0.065	-0.065	-0.065	-0.061	-0.066
	K 769.897	38.8	35.7	34.5	34.3	33.3	34.1	35.7	33.8	34.6
	Li 670.783	0.128	0.128	0.129	0.131	0.131	0.130	0.132	0.130	0.130
	Mg 285.213	99.9	96	96.3	97.8	97.3	96.3	98.6	94.7	93.3
	Mn 257.610	0.492	0.376	0.348	0.339	0.318	0.290	0.256	0.232	0.125
	Na 568.821	420	423	422	430	429	431	443	441	453
	Ni 231.604	0.035	0.026	0.024	0.021	0.017	0.013	0.009	0.006	0.001
	Sr 421.552	1.25	1.20	1.19	1.20	1.20	1.19	1.21	1.06	0.97
	Zn 213.857	-0.150	-0.180	-0.187	-0.193	-0.199	-0.205	-0.207	-0.208	-0.210

Table G.15. RSL Edges analytes for Bentonite *CR+* in mg/L, except where noted.

		Target pH								
	Analyte	**5**	**5.5**	**6**	**6.5**	**7**	**7.5**	**8**	**8.5**	**9**
CR+	U 263.553 (µg/L)	195	273	465	878	1080	1110	1110	1060	689
	Al 396.152	-0.003	-0.005	-0.006	-0.005	-0.005	-0.005	-0.005	-0.004	-0.006
	As 228.812	0.003	0.002	0.002	0.002	0.001	0.002	0.002	0.002	0.002
	Ba 455.403	0.021	0.021	0.021	0.021	0.020	0.021	0.020	0.018	0.014
	Ca 422.673	173	172	172	172	173	175	186	180	188
	Cu 321.754	-0.048	-0.054	-0.054	-0.054	-0.054	-0.053	-0.053	-0.052	-0.051
	Fe 234.350	-0.027	-0.028	-0.028	-0.028	-0.028	-0.027	-0.028	-0.027	-0.028
	K 769.897	51.0	49.5	50.5	49.5	48.5	49.2	48.8	47.9	46.4
	Li 670.783	0.115	0.116	0.115	0.115	0.115	0.115	0.115	0.113	0.112
	Mg 285.213	105	105	104	105	104	103	102	102	95.9
	Mn 257.610	0.183	0.200	0.211	0.241	0.208	0.175	0.124	0.135	0.022
	Na 568.821	895	892	889	883	888	894	895	899	937
	Ni 231.604	0.021	0.019	0.019	0.021	0.017	0.013	0.012	0.010	0.005
	Sr 421.552	2.08	2.10	2.09	2.10	2.06	2.05	1.95	1.77	1.65
	Zn 213.857	-0.137	-0.146	-0.149	-0.146	-0.149	-0.149	-0.149	-0.150	-0.150

Table G.16. RSL Edges analytes for Bentonite *GS* in mg/L, except where noted.

		Target pH								
	Analyte	**5**	**5.5**	**6**	**6.5**	**7**	**7.5**	**8**	**8.5**	**9**
GS	U 263.553 (µg/L)	412	307	611	865	1090	1110	1110	1050	882
	Al 396.152	0.013	0.011	0.011	0.013	0.013	0.011	0.012	0.012	0.010
	As 228.812	0.001	0.001	0.000	0.000	0.000	0.000	0.000	0.000	0.000
	Ba 455.403	0.038	0.044	0.045	0.045	0.046	0.045	0.046	0.041	0.035
	Ca 422.673	213	222	220	220	212	191	181	165	132
	Cu 321.754	0.001	0.000	0.000	0.000	0.000	0.000	0.000	0.000	0.000
	Fe 234.350	-0.058	-0.059	-0.059	-0.059	-0.059	-0.059	-0.059	-0.057	-0.058
	K 769.897	64.6	56.2	50.6	48.5	43.4	42.4	39.7	42.3	45.3
	Li 670.783	0.123	0.131	0.131	0.130	0.130	0.130	0.133	0.128	0.124
	Mg 285.213	113	116	114	114	113	110	109	109	108
	Mn 257.610	0.155	0.343	0.281	0.260	0.157	0.084	0.075	0.052	0.013
	Na 568.821	1020	990	991	996	991	1000	999	1010	1100
	Ni 231.604	0.018	0.015	0.012	0.011	0.008	0.005	0.003	0.005	0.005
	Sr 421.552	2.25	2.29	2.27	2.30	2.23	2.12	2.06	1.95	1.77
	Zn 213.857	-0.017	-0.018	-0.018	-0.018	-0.018	-0.019	-0.019	-0.019	-0.018

Table G.17. RSL Edges analytes for Bentonite *GR* in mg/L, except where noted.

		Target pH								
	Analyte	**5**	**5.5**	**6**	**6.5**	**7**	**7.5**	**8**	**8.5**	**9**
GR	U 263.553 (µg/L)	324	487	579	741	957	996	1045	827	1010
	Al 396.152	0.007	0.007	0.033	0.008	0.009	0.007	0.008	0.007	0.006
	As 228.812	0.001	0.001	0.000	0.000	0.000	0.001	0.000	0.001	0.000
	Ba 455.403	0.063	0.076	0.078	0.075	0.074	0.072	0.077	0.056	0.066
	Ca 422.673	211	211	209	203	191	176	171	120	142
	Cu 321.754	0.001	0.000	0.000	0.000	0.000	0.000	0.000	0.000	0.000
	Fe 234.350	-0.057	-0.058	-0.051	-0.058	-0.058	-0.056	-0.058	-0.058	-0.058
	K 769.897	55.2	51.9	49.9	44.5	41.6	42.6	45.3	44.0	42.7
	Li 670.783	0.114	0.120	0.120	0.117	0.115	0.116	0.121	0.111	0.119
	Mg 285.213	110	109	110	108	106	107	106	103	104
	Mn 257.610	0.175	0.108	0.155	0.163	0.108	0.078	0.064	0.017	0.018
	Na 568.821	1000	975	975	953	940	957	972	1020	1010
	Ni 231.604	0.022	0.008	0.009	0.009	0.006	0.006	0.004	0.006	0.004
	Sr 421.552	2.28	2.27	2.28	2.20	2.10	1.94	1.86	1.52	1.68
	Zn 213.857	-0.021	-0.023	-0.023	-0.023	-0.024	-0.024	-0.024	-0.024	-0.025

Appendix H

Figures for pH-variable U Concentrations for RSL E&E Experimentation

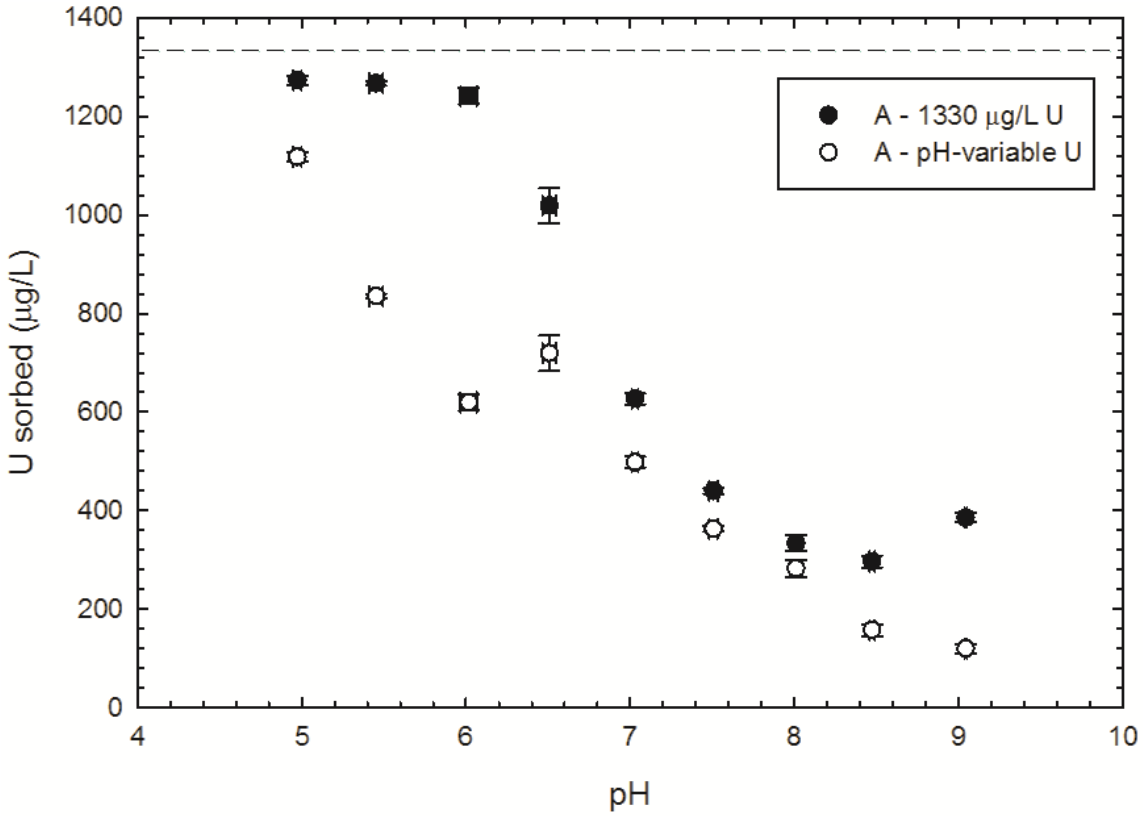

Figure H.1. Comparison sorbed U (in µg/L) as based on a constant solution concentration of U and pH-variable U concentrations derived from solution control experimentation for Soil *A*.

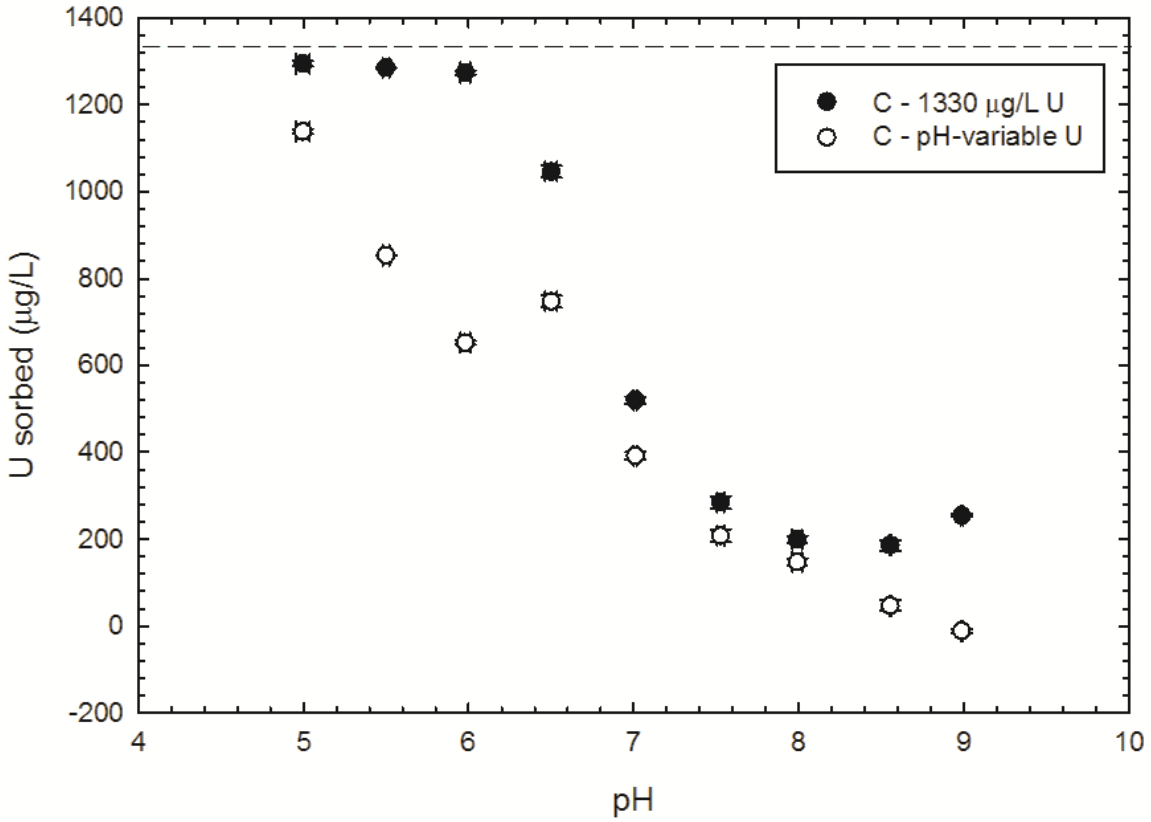

Figure H.2. Comparison sorbed U (in µg/L) as based on a constant solution concentration of U and pH-variable U concentrations derived from solution control experimentation for Soil *C*.

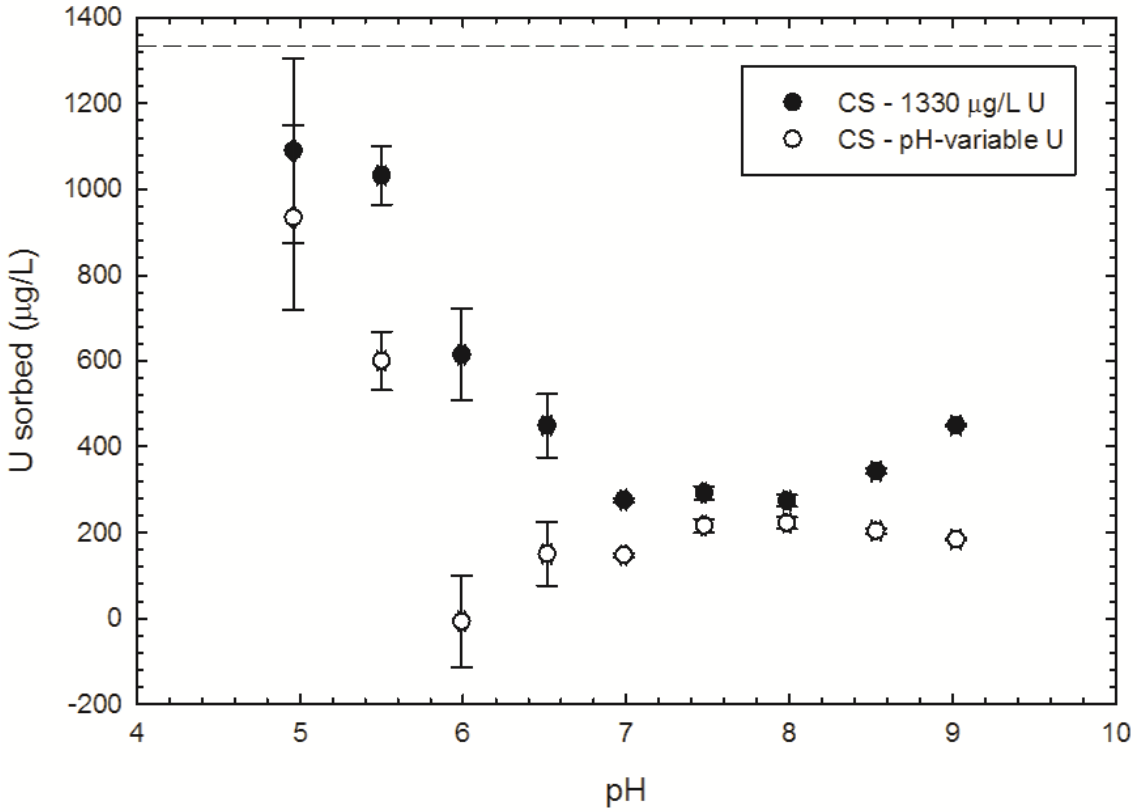

Figure H.3. Comparison sorbed U (in µg/L) as based on a constant solution concentration of U and pH-variable U concentrations derived from solution control experimentation for Bentonite *CS*.

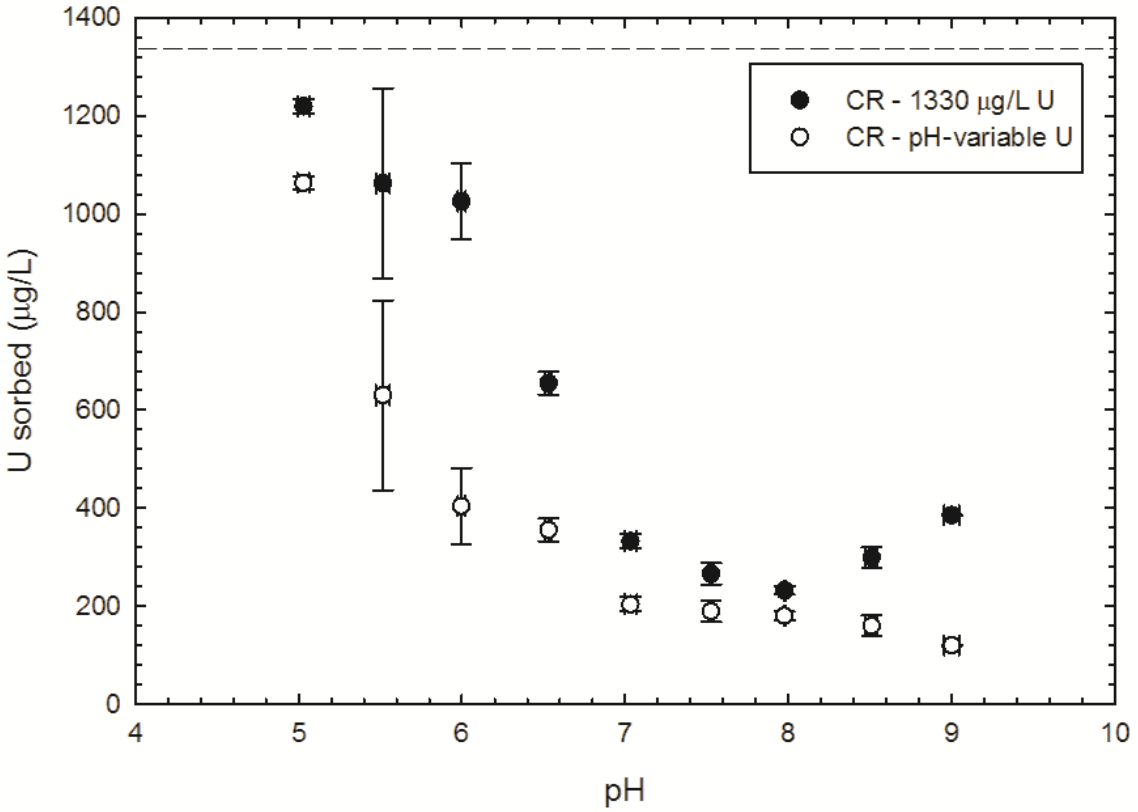

Figure H.4. Comparison sorbed U (in µg/L) as based on a constant solution concentration of U and pH-variable U concentrations derived from solution control experimentation for Bentonite *CR*.

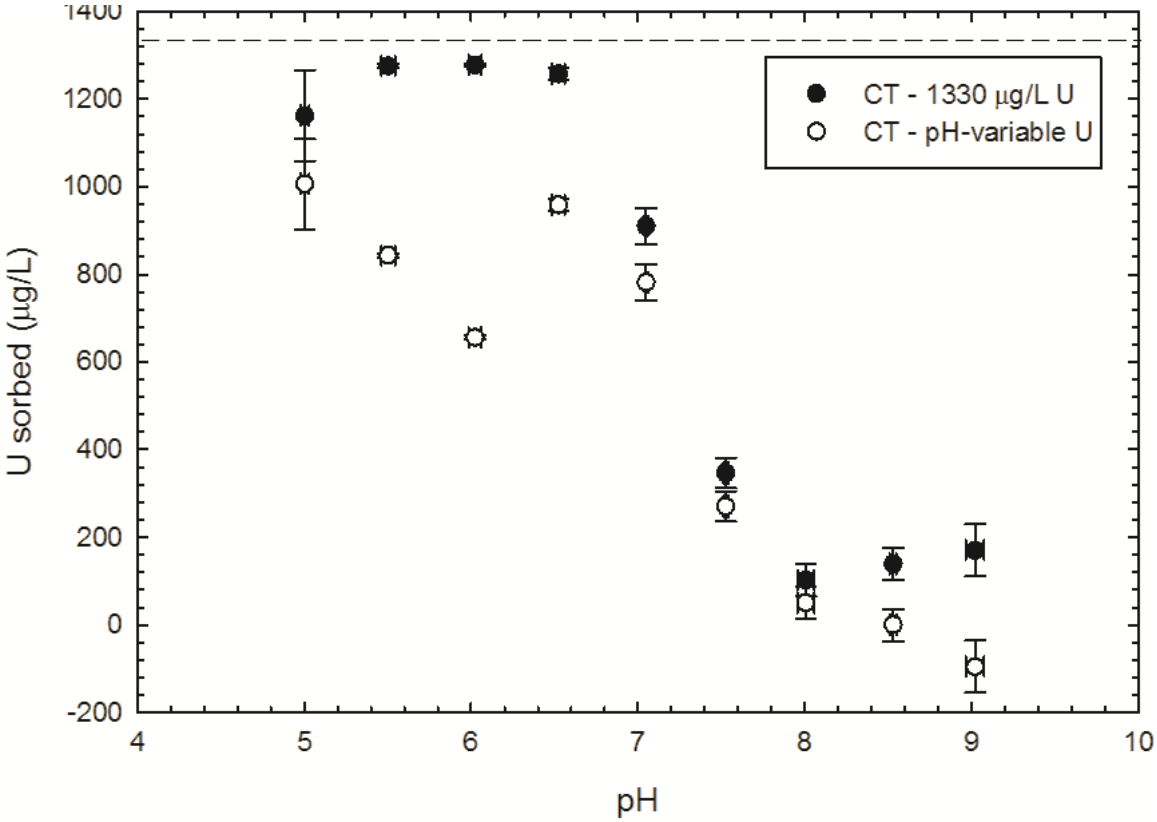

Figure H.5. Comparison sorbed U (in µg/L) as based on a constant solution concentration of U and pH-variable U concentrations derived from solution control experimentation for Bentonite *CT*.

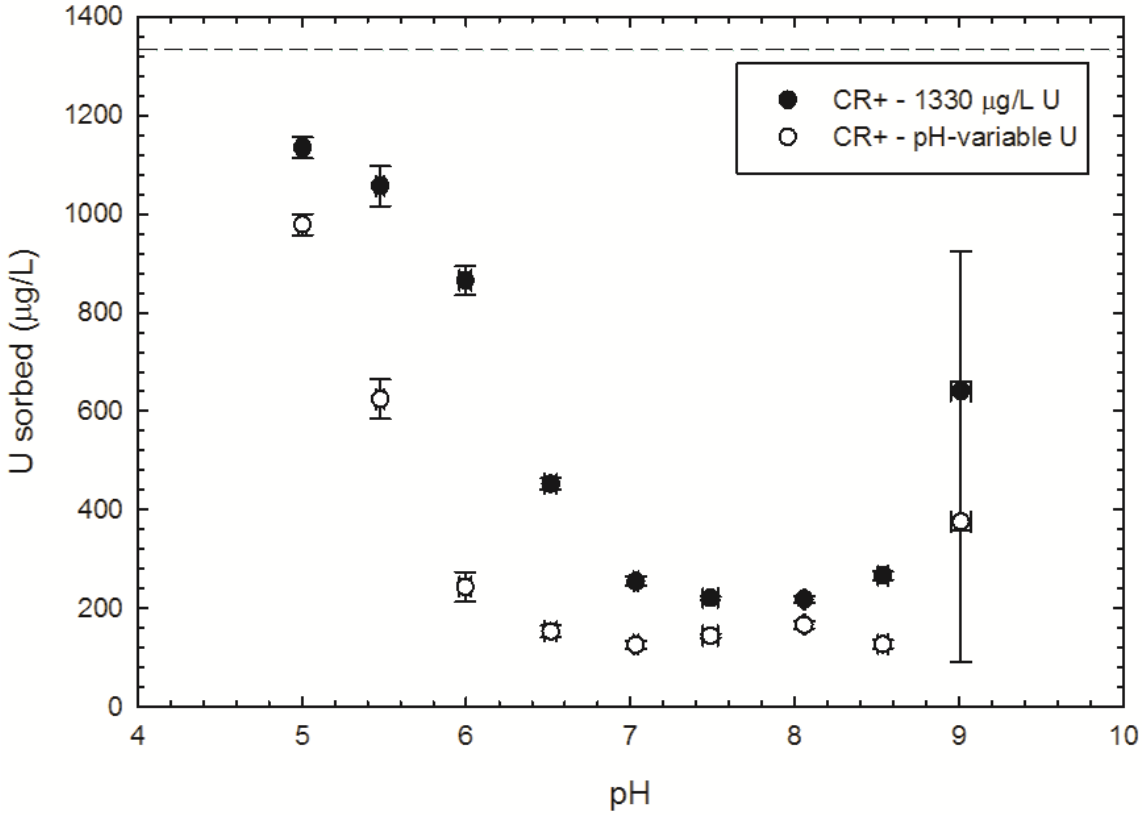

Figure H.6. Comparison sorbed U (in µg/L) as based on a constant solution concentration of U and pH-variable U concentrations derived from solution control experimentation for Bentonite *CR+*.

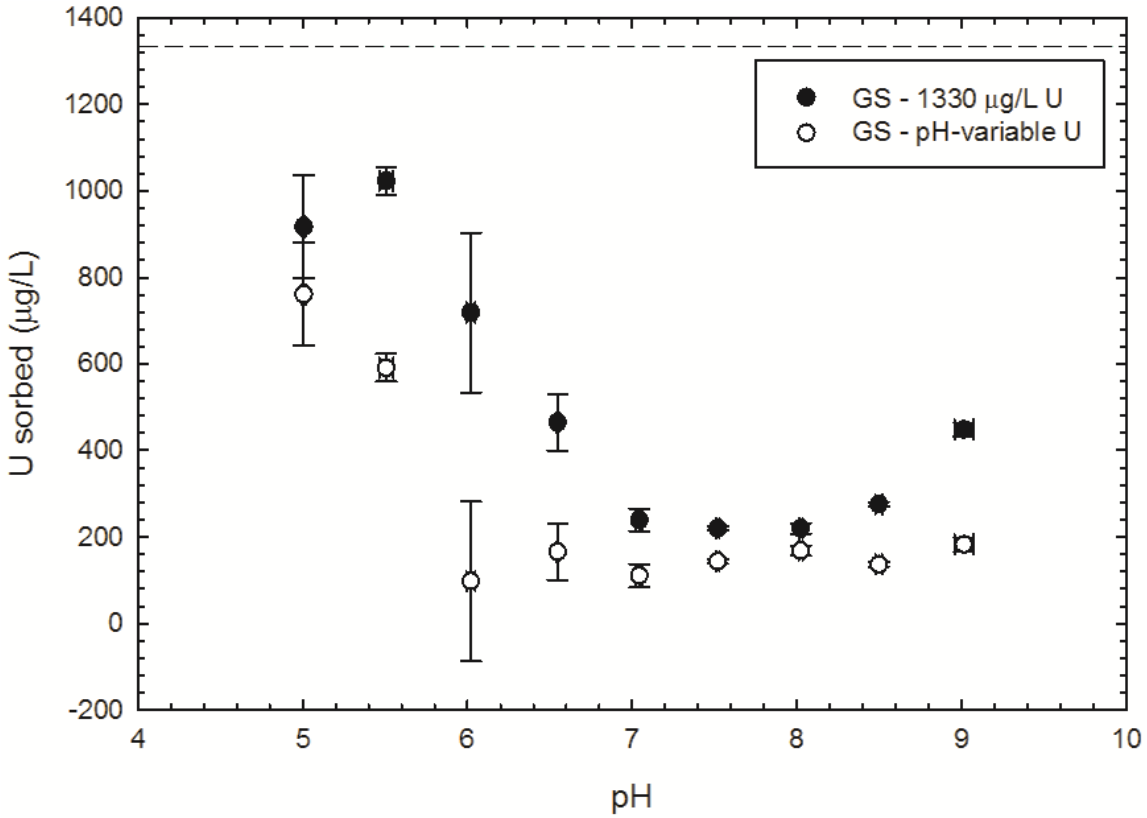

Figure H.7. Comparison sorbed U (in µg/L) as based on a constant solution concentration of U and pH-variable U concentrations derived from solution control experimentation for Bentonite *GS*.

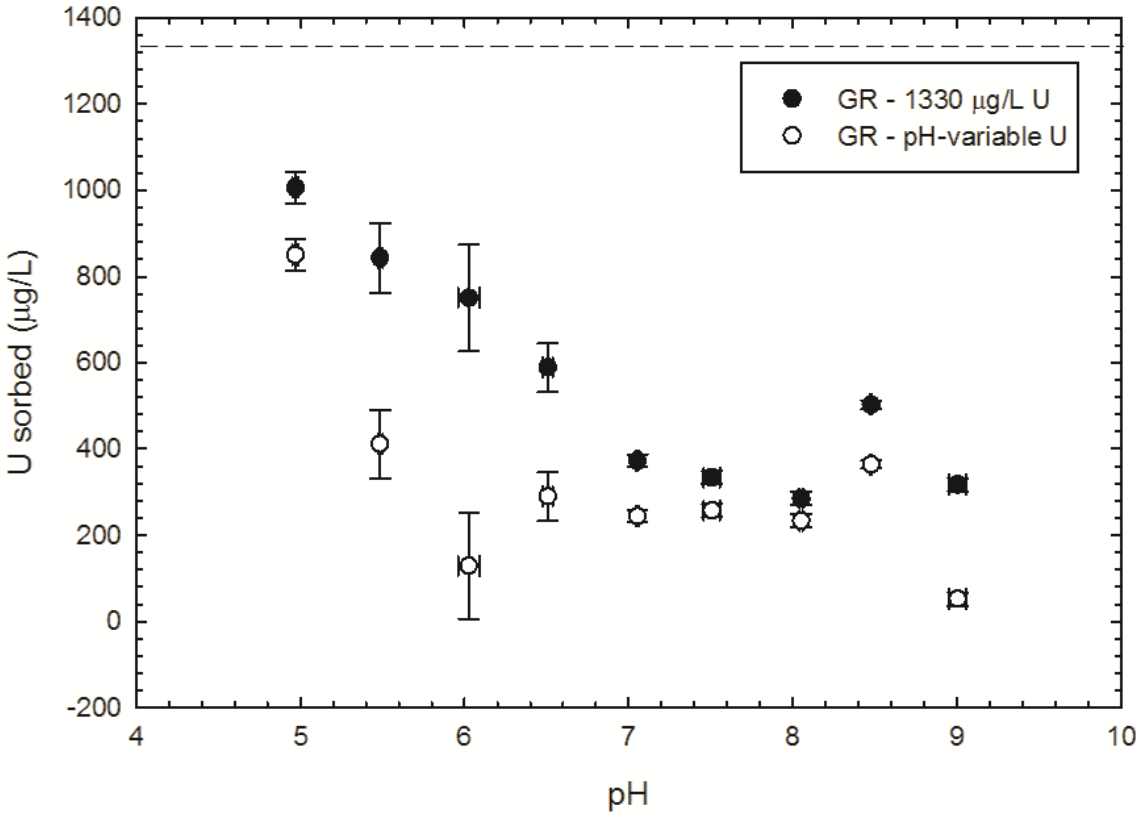

Figure H.8. Comparison sorbed U (in µg/L) as based on a constant solution concentration of U and pH-variable U concentrations derived from solution control experimentation for Bentonite *GR*.

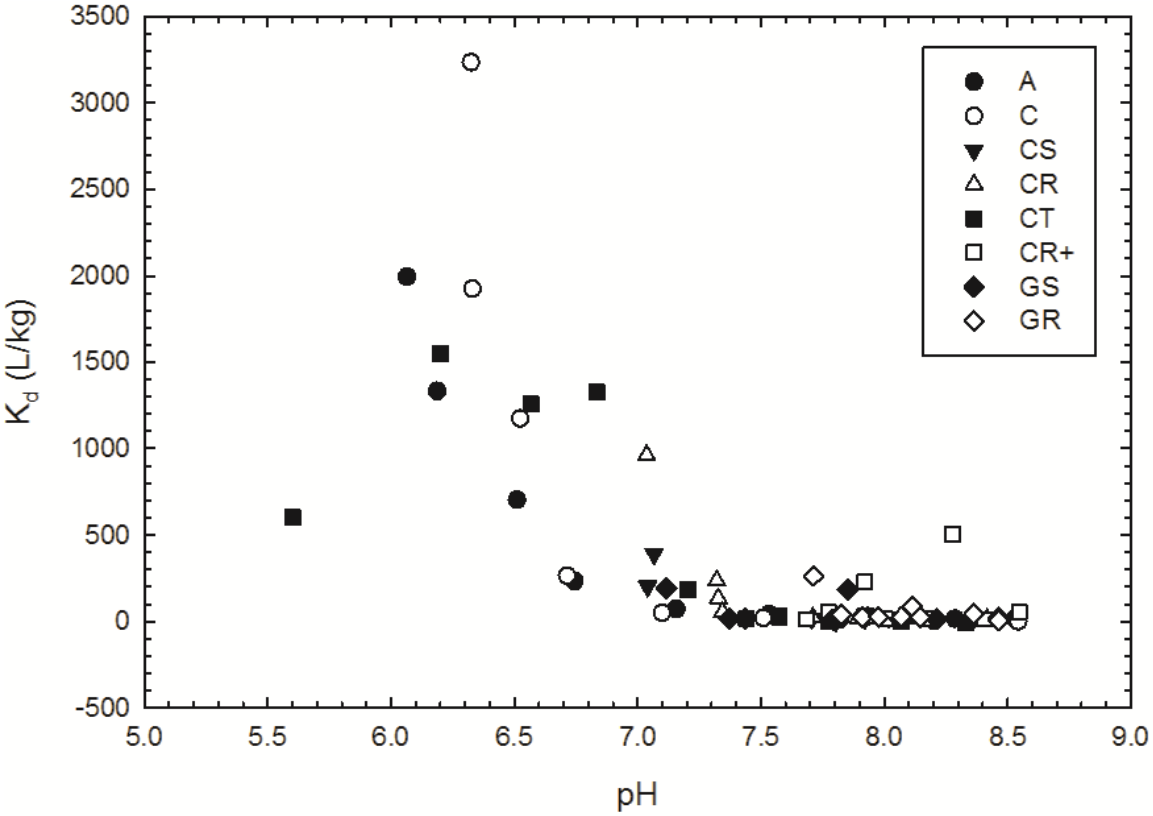

Figure H.9. Comparison of K_d values (in L/kg) for all soils across the tested pH levels derived from pH-variable U concentrations. Note that at some points the K_d values are negative.

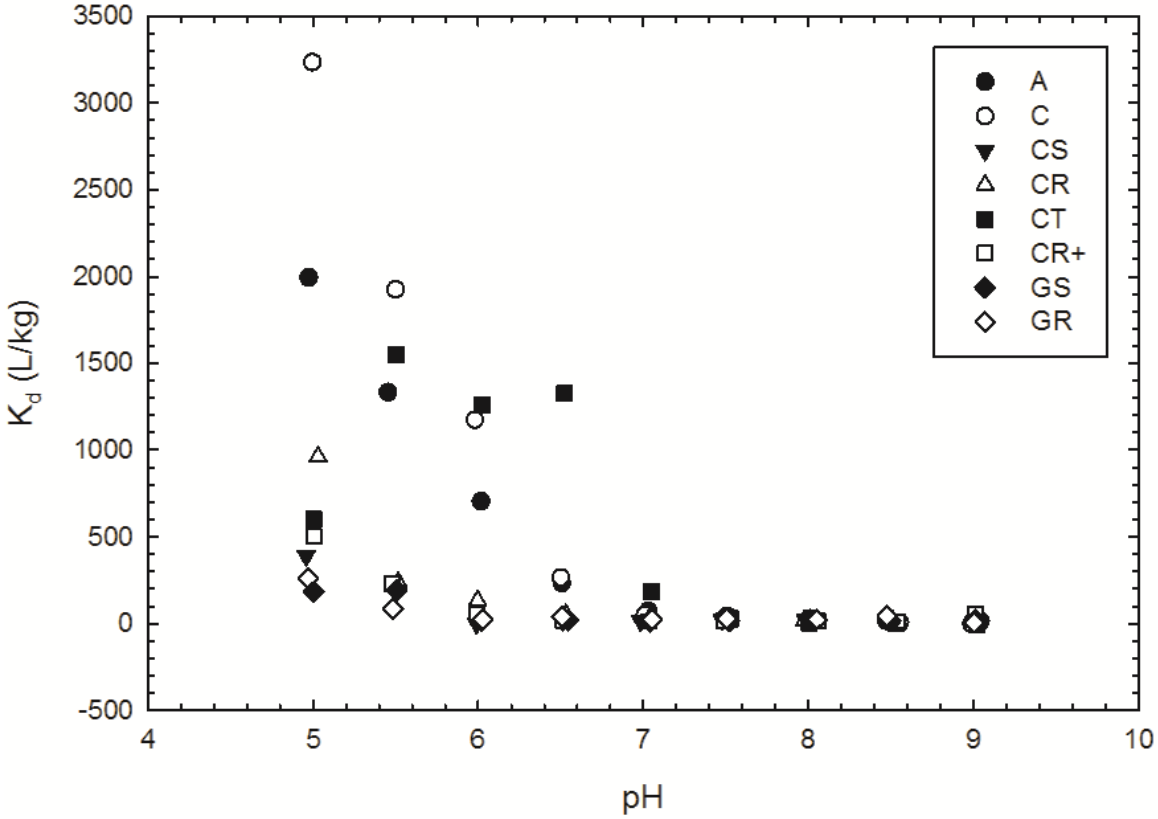

Figure H.10. Comparison of K_d values (in L/kg) for all soils at initial experimental pH levels derived from pH-variable U concentrations. Note that at some points the K_d values are negative.